TEXTBOOK

Christopher S. Cronan

Ecosystem Biogeochemistry

Element Cycling in the Forest Landscape

Springer

Springer Textbooks in Earth Sciences, Geography and Environment

More information about this series at http://www.springer.com/series/15201

Christopher S. Cronan

Ecosystem Biogeochemistry

Element Cycling in the Forest Landscape

Springer

Christopher S. Cronan
School of Biology and Ecology
University of Maine
Orono, ME, USA

ISSN 2510-1307 ISSN 2510-1315 (electronic)
Springer Textbooks in Earth Sciences, Geography and Environment
ISBN 978-3-319-66443-9 ISBN 978-3-319-66444-6 (eBook)
DOI 10.1007/978-3-319-66444-6

Library of Congress Control Number: 2017950665

Printed on acid-free paper

This Springer imprint is published by Springer Nature
The registered company is Springer International Publishing AG
The registered company address is: Gewerbestrasse 11, 6330 Cham, Switzerland

Preface

Ecological surprises are not that uncommon – they often emerge when we overlook the subtle signs of cascading causes and effects from seemingly inconsequential perturbations in our surroundings. Take an example of a corn chip that you might dip into your salsa sauce. Who would guess that the corn chip can be linked to shrimp mortality in the Gulf of Mexico and global warming? The surprising interconnections can be traced back to a cornfield along the Mississippi River, where a farmer growing a crop destined for corn chip production may routinely add more fertilizer than is required by the corn plants. From that simple initial action, at least two unintended consequences may follow. First off, the addition of excess nitrogen fertilizer to the soil is likely to stimulate increased microbial production of the greenhouse gas N_2O that contributes to increased warming potential of the atmosphere. A second major outcome occurs when the excess fertilizer is transported by drainage waters into the nearby river system and is ultimately delivered downstream to coastal waters in the Gulf of Mexico. There, the farmer's fertilizer contributes to a process of nutrient enrichment and eutrophication that transforms the Gulf waters into a massive "dead zone" where dissolved oxygen levels are too low to sustain shellfish and other marine organisms.

The anoxic Gulf coast waters are a symbol of the adverse environmental externalities that often accompany human activities. Many of the current and emerging issues regarding water quality, food production, deforestation, climate change, atmospheric pollution, and human health are linked inextricably to humans and their influence on the cycles of nutrients and contaminants in the biosphere. As we confront the challenges of sustaining environmental quality in the twenty-first century, our progress will depend in part on our ability to understand the intricate and diverse interactions of global chemical cycles with living systems. It is those cycles, processes, and feedbacks that are the focus of this textbook on the subject of biogeochemistry.

Biogeochemistry is an interdisciplinary science that integrates the study of biological, ecological, geochemical, and hydrologic patterns and processes in an effort to understand how biologically active elements and compounds interact with living organisms. The goal of this book is to provide a learning tool that will allow readers to gain biogeochemical insights and critical thinking skills that can be applied to careers in watershed science, ecosystems analysis, ecology, global change science, and environmental science.

This textbook presents a comprehensive process-oriented approach to biogeochemistry that is intended to appeal to readers who want to go beyond a general exposure to topics in biogeochemistry, and instead are seeking a holistic understanding of the interplay of biotic and environmental drivers in the cycling of elements in forested watersheds. The book is organized around a core set of **ecosystem** processes and attributes that collectively help to generate the whole-system structure and function of a terrestrial ecosystem. In the first nine chapters, a conceptual framework is developed based on distinct soil, microbial, plant, atmospheric, hydrologic, and geochemical processes that are integrated in the element cycling behavior of watershed ecosystems. With that conceptual foundation in place, readers then proceed to the final three chapters where they are challenged to think critically about integrated element cycling patterns; biogeochemical models; the impacts of disturbance, stress, and management on watershed biogeochemistry; and linkages among patterns and processes in watersheds experiencing environmental changes.

The organization and content of this biogeochemistry text are intended to provide an engaging and fresh alternative to existing references on this topic. Many of the well-known books on biogeochemistry focus on nutrient cycling patterns in specific local long-term watershed study sites such as Hubbard Brook Experimental Forest in New Hampshire (Likens et al. 1977, 2013; Bormann and Likens 1996) and the Walker Branch Watershed in Tennessee (Johnson and Van Hook 1989). The current alternative to those books is the widely-adopted *Biogeochemistry: An Analysis of Global Change* by Schlesinger and Bernhardt (2013) that offers a global-scale overview of major element cycles in terrestrial, freshwater, marine, atmospheric, and wetland sectors of the earth. There are thus several more narrowly focused case studies at one end of the spectrum, compared with a global-scale overview of biogeochemistry at the opposite end of the spectrum.

In comparison with those existing instructional resources, this biogeochemistry textbook is distinctive in two key respects: (a) it provides a unified emphasis on forested watershed ecosystems that is more process-oriented, detailed, and pedagogical than the single watershed case studies; and (b) unlike the broader, global scope of the reference by Schlesinger and Bernhardt, this book specifically delivers a coherent synthesis of biogeochemistry at the watershed ecosystem scale – the most common landscape unit for current research and resource management. Using this text as an introduction to biogeochemistry, students will achieve a level of subject mastery and disciplinary perspective that will permit them to see and to interpret the individual components, interactions, and synergies that are represented in the dynamic element cycling patterns of watershed ecosystems. In many respects, this book is intended to serve as an operational manual that examines how forested watersheds work with respect to fundamental parts, processes, interrelationships, whole-system behavior, and responses to changing conditions.

The text that follows provides an introduction to the biogeochemistry of terrestrial watershed ecosystems, with a major emphasis on forested systems. The subject treatment emphasizes concepts, principles, and patterns, and includes selected examples from the literature. The intent of the illustrations and tables is to provide visual examples of biogeochemical observations, rather than a comprehensive comparison of data from different ecosystems. A number of the examples of data are based on research by the author and his colleagues, because those research results provide simple illustrations for points that are emphasized by the author in his graduate class. To complement those specific regional examples, the author requires students in his class to read and to discuss a broad range of other research studies from the primary literature.

It is hoped that this book will provide readers with a clear and meaningful introductory framework for understanding biogeochemical principles and processes that apply to pristine or human-dominated watershed ecosystems. The goal of this textbook is to present the fundamental biogeochemical patterns and processes common to forested watershed ecosystems and to examine how biogeochemistry varies in response to changing environmental conditions in the landscape.

Note: Words printed in **bold print** within the text are defined in the glossary at the end of this book.

Orono, ME, USA Christopher S. Cronan

Acknowledgements

I thank the many teachers, mentors, colleagues, and friends who helped to make this book possible. I have learned so much from all of them and appreciate their willingness to share their wisdom and knowledge with me. Bill Reiners and Bob Reynolds helped to cultivate my early interest in biogeochemistry at Dartmouth College and for that, I am truly grateful. My colleagues on the ILWAS, RILWAS, and ALBIOS investigations were a great source of inspiration and insights. I owe a special measure of gratitude to Joe Yavitt at Cornell University and Myron Mitchell at SUNY-ESF for their kindness in reviewing an earlier draft of this textbook. Finally, I thank the great staff and my faculty peers at the University of Maine for their support and good cheer!

Contents

General Chemical Concepts

1

Introduction

In the chapters that follow, a framework will be developed for understanding and interpreting biogeochemical patterns and processes in terrestrial ecosystems. Our analysis of biogeochemistry will require a basic working knowledge of general chemical concepts covered in this initial review chapter. Readers are encouraged to use this chapter as a means of refreshing the terms and topics in introductory chemistry that are especially relevant to our discussion of chemical cycling in living systems.

Periodic Table and Element Groups

The **periodic table** is arranged so that elements with similar properties appear in the same column of the table. As shown in Table 1.1, the first column of elements contains monovalent **alkali metals** such as lithium (Li), sodium (Na), and potassium (K) that have one unpaired electron in the outermost *s* orbital. These metals combine readily with halogens in the second to last column to form familiar salts such as NaCl and KI. Elements in the second column include the divalent **alkaline earth metals** such as magnesium (Mg), calcium (Ca), and strontium (Sr), which readily form oxides (e.g., CaO and MgO). To the right of these familiar elements, columns 3 through 12 (and parts of 13 through 16) contain a range of elements referred to as the transition metals. Biogeochemical analysis of transition metals often focuses on two specific subsets of these elements: (i) **trace metals** such as Mn, Fe, Co, Ni, Cu, Zn, Al, and Mo, and (ii) **heavy metals** such as Cd, Hg, and Pb. At the right side of the periodic table, we observe the core nutrient elements C, N, O, P, and S, and the final two columns of halogens and noble gases.

It is important to note that the elements in the upper right hand corner of the periodic table – oxygen, sulfur, fluorine, and chlorine – are the most **electronegative** elements in the periodic table. Thus, they are most likely to attract bonding electrons and to form polar or ionic bonds with other elements that are less electronegative. We should also recognize that some of the elements in the periodic table exist in multiple valence states. For example, iron may occur in the ferrous state as Fe (II) or in the ferric form as Fe (III). Similarly, Mn, Cr, and numerous other transition metals have more than one oxidation state.

Another useful concept to consider regarding the periodic table is the **atomic radius** of an atom. Atomic radii generally (i) decrease from left to right across a row of the periodic table, and (ii) increase from the top to the bottom of a column in the periodic table. In later portions of this text, we shall encounter a discussion of the term **charge density** of ions in solution. Charge density is a measure of the ionic charge relative to the radius of a given ion. As an example, sodium ion (Na^+) has a low charge density in comparison with trivalent aluminum ion (Al^{3+}) that has a high charge, coupled with a small ionic radius.

Chemical Bonding

We are all familiar with the general principles of atomic bond formation involving ionic and covalent bonding. In a **covalent bond**, electrons are shared between nuclei of adjacent atoms. Examples of molecules with covalent bonding are H_2, N_2, and CH_4. Under some circumstances, the shared electrons may be preferentially attracted toward a more electronegative atom, resulting in a **polar covalent bond**.

C.S. Cronan, *Ecosystem Biogeochemistry*, Springer Textbooks in Earth Sciences, Geography and Environment, DOI 10.1007/978-3-319-66444-6_1

Table 1.1 Periodic table of elements showing atomic masses in superscript notation

1	2	3	4	5	6	7	8	9	10	11	12	13	14	15	16	17	18
^{1}H																	^{4}He
^{7}Li	^{9}Be											^{11}B	^{12}C	^{14}N	^{16}O	^{19}F	^{20}Ne
^{23}Na	^{24}Mg											^{27}Al	^{28}Si	^{31}P	^{32}S	^{35}Cl	^{40}Ar
^{39}K	^{40}Ca	^{45}Sc	^{48}Ti	^{51}V	^{52}Cr	^{55}Mn	^{56}Fe	^{59}Co	^{59}Ni	^{64}Cu	^{65}Zn	^{70}Ga	^{73}Ge	^{75}As	^{79}Se	^{80}Br	^{84}Kr
^{85}Rb	^{88}Sr	^{89}Y	^{91}Zr	^{93}Nb	^{96}Mo	^{98}Tc	^{101}Ru	^{103}Rh	^{106}Pd	^{108}Ag	^{112}Cd	^{115}In	^{119}Sn	^{122}Sb	^{128}Te	^{127}I	^{131}Xe
^{133}Cs	^{137}Ba	$^{139}La*$	^{178}Hf	^{181}Ta	^{184}W	^{186}Re	^{190}Os	^{192}Ir	^{195}Pt	^{197}Au	^{201}Hg	^{204}TI	^{207}Pb	^{209}Bi	^{209}Po	^{210}At	^{220}Rn
^{223}Fr	^{226}Ra	$^{227}Ac**$															
Lanthanides			*	^{140}Ce	^{141}Pr	^{144}Nd	^{145}Pm	^{150}Sm	^{152}Eu	^{157}Gd	^{159}Tb	^{163}Dy	^{165}Ho	^{167}Er	^{169}Tm	^{173}Yb	^{175}Lu
Actinides			**	^{232}Th	^{231}Pa	^{238}U	^{237}Np	^{244}Pu	^{243}Am	^{247}Cm	^{247}Bk	^{251}Cf	^{252}Es	^{257}Fm	^{258}Md	^{259}No	^{262}Lr

For example, hydrofluoric acid has a localized electron density around the fluorine atom, creating a polar covalent bond in the HF molecule. Other molecules that form polar covalent bonds include nitric oxide (NO), sulfur dioxide (SO_2), and silicon dioxide (SiO_2). In an **ionic bond**, there is a **coulombic attraction** between oppositely charged ions that occurs when a metal loses electrons to a paired nonmetal with a high electron affinity. Two examples of compounds that contain ionic bonds are the salts $MgCl_2$ and KI.

The biogeochemistry of metals is often affected by the formation of metal-ligand **coordination complexes** that influence the solubility, bioavailability, and potential toxicity of the element. Complex formation occurs in solution when an electron-deficient metallic ion binds to one or more anionic **ligands** that donate pairs of electrons to the formation of covalent coordinate bonds with the metal. The simplest **monodentate** ligands coordinate to a metal ion through a single donor atom such as N, O, S, P, or C. For example, acetate anion forms metal-ligand complexes through a coordinate bond between the carboxyl group (COO^-) of the acetate molecule and the metallic **cation**. Cations can also bind to **multidentate** ligands containing two or more sites with donor atoms, resulting in the formation of a more stable type of complex known as a **chelate**. For instance, some isomers of hydroxy-benzoic acid form complexes with cations through coordinate bonds involving both alcoholic-OH and carboxylic-COOH donor groups (Fig. 1.1). Another example of a chelate is the porphyrin ring at the center of a chlorophyll *a* molecule, which contains a magnesium atom coordinated to four donor nitrogen atoms.

Hydrogen bonding is another valuable concept to understand regarding intermolecular attraction mechanisms. Many of the non-polar contaminants such as pesticides and aromatic hydrocarbons in soils and surface waters are strongly affected by interactions with natural organic matter that originate through hydrogen bonding. A hydrogen bond occurs when a highly electronegative atom serves as an electron donor and partially shares its nonbonding electrons with a positively polarized hydrogen atom. In order for hydrogen bond formation to occur, two requirements must be met (Olmsted and Williams 1997). First, there must be an electron-deficient hydrogen atom to act as an electron pair acceptor (hydrogen atoms in O-H, F-H, and N-H bonds meet this requirement). In addition, there must be a highly electronegative donor atom present with at least one lone pair of electrons (three second-row elements – O, N, and F – meet this requirement). An example of a hydrogen bond linking molecules of water and ammonia is shown in Fig. 1.2. Although hydrogen bonds are only about 5–10% as strong as covalent bonds, the simultaneous formation of multiple hydrogen bonds between two different molecules can have a great influence on the biogeochemical fate of certain substances.

Chemical Reactions, Stoichiometry, and Kinetics

Many of the biogeochemical processes that concern us can be represented by chemical reactions. In a chemical reaction such as the one illustrated below, **reactants** are shown on the left side, **products** are depicted on the right hand side, and the reaction can be described thermodynamically in terms of a positive or negative change in free energy. In chemical notation, each reactant or product is preceded by an integer termed a **stoichiometric coefficient** that indicates the relative numbers of moles of each molecule involved in the reaction. The stoichiometry of the reaction must account for conservation of mass and balanced ionic charges on both sides of the chemical reaction.

$$N_2 + 3H_2 \leftrightarrow 2NH_3 \quad \Delta G^\circ = \quad 34\text{kJ}$$

$$K_{eq} = [NH_3]^2 / [N_2] \times [H_2]^3$$

At equilibrium, the rates of forward and backward reactions are equal and the reaction can be described by an **equilibrium constant**, K_{eq}. An equilibrium constant is defined as the value of the ratio of equilibrium concentrations of products to equilibrium concentrations of reactants, each raised to the power equal to its stoichiometric coefficient. In the

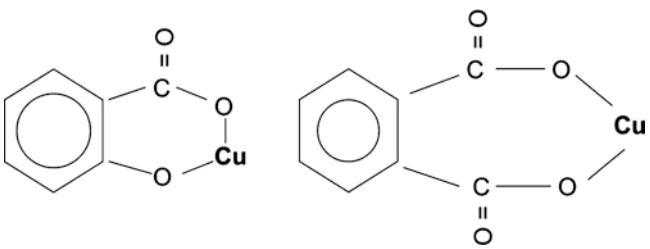

Fig. 1.1 Examples of metal chelation in two multi-dentate complexes involving salicylic acid and copper (*left*) and phthalic acid and copper (*right*)

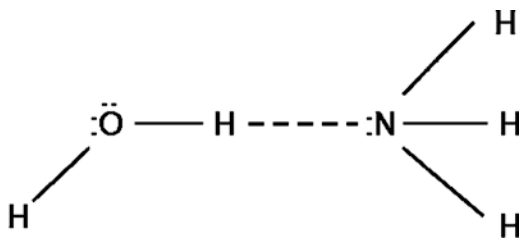

Fig. 1.2 Hydrogen bonding between a molecule of ammonia (NH_3) and water; *the dashed line* represents the bond linking hydrogen (H) with the electron donor (N)

example illustrated above, the equilibrium constant, K_{eq} = [products]/[reactants] = 5.6 x 10^5.

The equilibrium solubility of gases in water can be computed using a **Henry's Law constant**, K_H, for specific gases and solvents of interest (Daniels and Alberty 1975). This equilibrium constant describes the ratio of dissolved gas divided by the partial pressure of the gas at a specified temperature. As an example, the K_H for carbon dioxide is 7.8×10^{-2} at 0 °C and 3.4×10^{-2} at 25 °C; thus, this gas is twice as soluble at the lower temperature.

One can also discuss the proton dissociation behavior and equilibria of acids using **acid ionization constants**, K_a. For example, the dissociation reaction of acetic acid in water to form acetate and free H^+ ion can be expressed with the following equilibrium (where H^+ ion is represented as hydronium ion H_3O^+ and the solvent water or H_2O is by definition left out of the denominator in writing the equilibrium expression):

$$CH_3COOH + H_2O \leftrightarrow CH_3COO^- + H_3O^+$$

$$K_a = \left[CH_3COO^-\right] \times \left[H_3O^+\right] / \left[CH_3COOH\right]$$

Some chemical reactions approach equilibrium very slowly; in such cases, it is useful to describe the reaction in **kinetic** terms expressed as a **reaction rate** or a rate constant. Rate-limited reactions can be influenced by temperature, concentrations of reactants, and background chemical conditions. In the case of a dissolution reaction, the rate may also be greatly affected by the surface area of the solid phase. The effect of concentration on the rate of a specific chemical reaction can be described using an algebraic expression known as a rate law. Although each reaction has its own unique rate law, many rate laws have the following general form: Rate = $k[A]^y[B]^z$. Rate laws contain a proportionality constant (k) and one or more concentrations, each raised to some power (y and z). The exponents in the rate expression are the orders of the reaction – when the value of y is 1, the reaction is called **first order** in A and when the value of z is 2, the reaction is called **second order** in B, and so on. Figure 1.3 illustrates an example of a rate-limited process of radioactive decay, showing that it takes 19,000 years for 90% of the unstable ^{14}C atoms to decompose into the stable isotope ^{14}N.

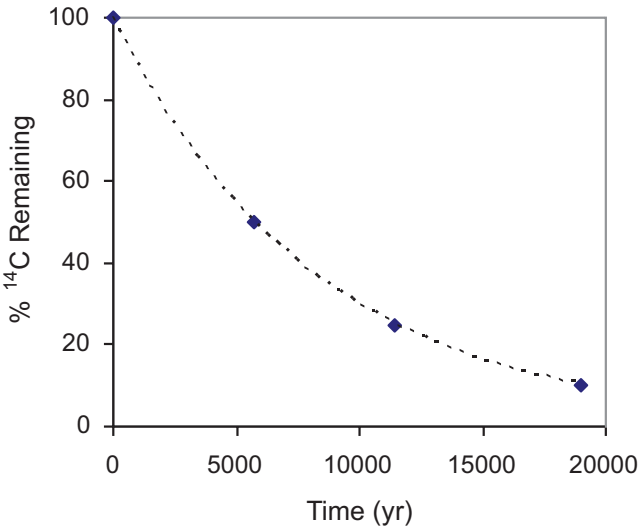

Fig. 1.3 Kinetic decay curve showing the percent of original radioactive ^{14}C remaining versus time. The isotope ^{14}C decays to ^{14}N with a mean half-life of 5730 years

Equilibrium, Steady-State, and Residence Time

It is important to note here a distinction between two terms. In biogeochemistry, the familiar term ***equilibrium*** is sometimes confused with the term **steady-state,** which is often used to describe element pools and fluxes. In a steady-state condition, the concentration or pool size of an element or compound remains relatively stable, because inputs and outputs of that element or compound to the system are approximately equal. Thus, a steady-state is characterized by balanced inputs and outputs of a given substance, whereas an equilibrium condition is defined as having equivalent forward and backward rates of reaction. A final term that will be encountered in subsequent chapters is the concept of **residence time**. In a system with inputs and outputs, the pool size of a given element or substance divided by the input rate gives an estimate of the average time period that an atom or molecule of that material resides in the system before being replaced, transformed, or decomposed.

General Concepts of Organic Chemistry

Organic chemistry is often described as the analysis of carbon compounds. In biogeochemistry and ecology, much of what we study is related directly or indirectly to the formation and circulation of organic carbon in the biosphere. Consequently, it is helpful to have a working vocabulary of the terms that are used to describe different aspects of carbon-based substances. Hydrocarbons generally can be separated into three large structural groups: (i) **aliphatic** compounds composed of chains of carbon, (ii) **alicyclic** molecules in which carbon chains link to form rings, and (iii) **aromatic** hydrocarbons that contain 6-membered rings with three carbon-carbon double bonds.

Carbon forms a large number of **binary compounds** with hydrogen, and these C-H compounds can be divided into three categories: alkanes, alkenes, and alkynes. An **alkane** such as ethane or propane contains only single bonds between

carbon atoms. An **alkene** such as ethylene is a binary C-H compound with one or more double bonds between carbon atoms. Finally, an **alkyne** such as acetylene contains one or more triple bonds between carbon atoms.

The chemical behavior of organic compounds is strongly influenced by the presence or absence of **functional groups**. Organic substances that contain **hydroxyl** (−OH) functional groups or **carboxyl** groups (−COOH) are able to act as weak acids and to participate in complexation reactions with metals. Examples of two organic acids that contain functional groups are oxaloacetic acid (a dicarboxylic acid) and salicylic acid (an aromatic compound that contains one carboxyl group and one phenolic-OH group) (Fig. 1.4).

Other important classes of organic compounds besides organic acids are illustrated in Fig. 1.5 below, including sugars, starches, amino acids, phenols (e.g., catechol), lipids, polysaccharides, esters, ketones (e.g., quinone), and nucleic acids. Note that organic compounds may contain different functional groups such as amino (NH_2) or sulfhydryl (HS) structures, or a carbon backbone symbolized by "R".

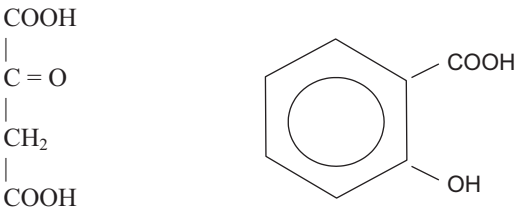

oxaloacetic acid *salicylic acid*

Fig. 1.4 Structures of two organic acids containing carboxylic acid groups

Aqueous Solubility and Polarity

The terms **hydrophilic** and **hydrophobic** are often used in reference to the solubility of organic substances. A hydrophilic substance is compatible with water and is soluble in an aqueous solvent, whereas a hydrophobic compound has **nonpolar** characteristics that make it less soluble or poorly soluble in water. A given molecule may be either hydrophobic or hydrophilic; for instance, glucose and citric acid are hydrophilic, whereas a lipid is hydrophobic. Alternatively, a single organic molecule may contain both hydrophilic and hydrophobic regions within its molecular structure. As an example, portions of natural humic acids contain hydrophilic carboxylic functional groups, whereas the bulk of the **humic acid** structure may be dominated by hydrophobic aromatic rings. Similarly, a compound such as lecithin, which occurs in the lipid bilayers of membranes, contains a hydrophilic head and a hydrophobic tail (Fig. 1.6). In the lab, hydrophobic compounds can be isolated from hydrophilic substances by adsorption on a non-polar C_{18} chromatographic column, followed by elution with a non-aqueous solvent such as methanol. Looking at Fig. 1.7, can you predict which of the vitamins are likely to be water or fat soluble based on structure? As a clue, vitamin C contains many hydroxyl groups that help to make the molecule more hydrophilic.

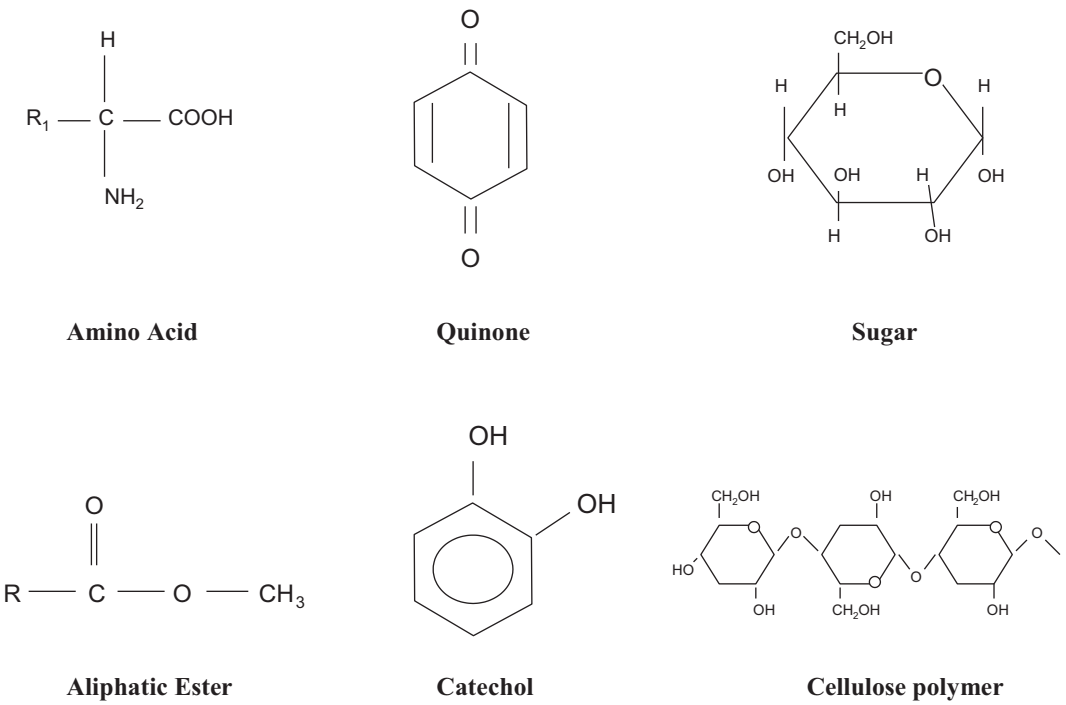

Amino Acid **Quinone** **Sugar**

Aliphatic Ester **Catechol** **Cellulose polymer**

Fig. 1.5 Examples of chemical structures in different organic compounds

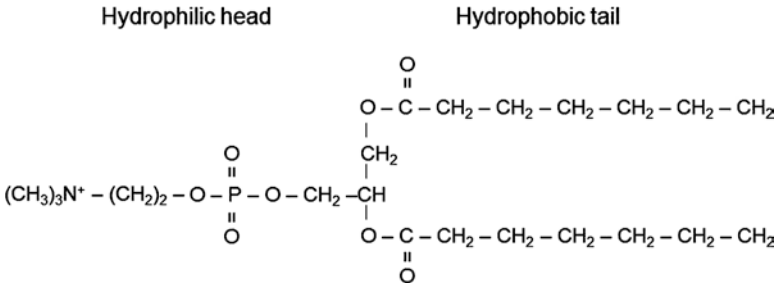

Fig. 1.6 Structure of lecithin containing hydrophilic and hydrophobic regions

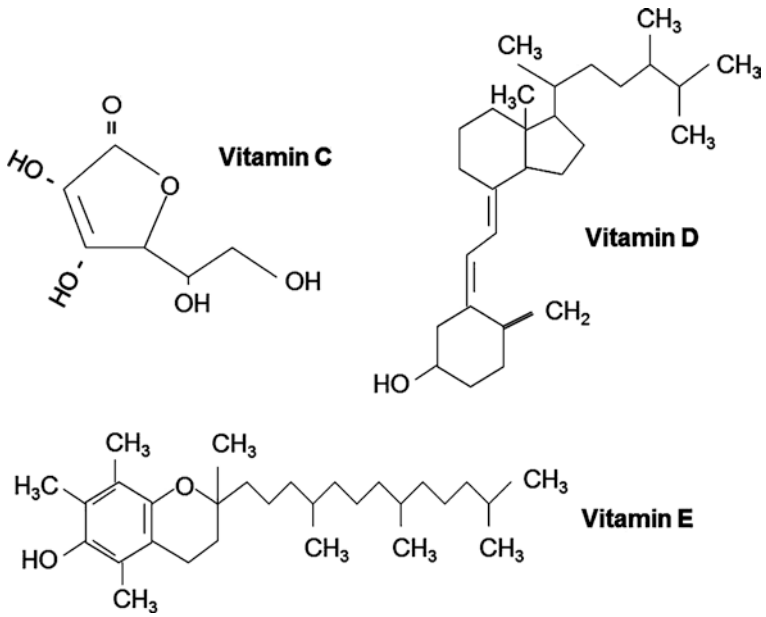

Fig. 1.7 Vitamins C, D, and E differ in water solubility based on chemical structures

Diffusion and Osmotic Potential

Diffusion is the movement of gas molecules or solutes from an area of higher concentration to a region of lower concentration. In comparison, **osmosis** refers to the movement or diffusion of water across a semi-permeable membrane such as a cell membrane. When solutes accumulate inside a semi-permeable membrane in biological systems, there is an associated increase in the **osmotic potential**. Water responds to that osmotic potential by flowing toward the region of higher solute concentration. This process can contribute to cell expansion during growth of living organisms, and water absorption by roots.

Freezing Exclusion and Concentration of Solutes

Have you ever frozen a bottle of pond or bog water and noticed a blob of brown color in the ice? This phenomenon is an example of the freezing exclusion that occurs in natural waters during ice formation and in snow that has re-crystallized. As water freezes, solutes are excluded from the ice crystals, so that the initial ice is nearly pure water and the last ice to form contains the concentrated solutes from the original volume of water. In the frozen bottle of bog water, the brown blob is the concentrated dissolved organic matter and other solutes that were originally mixed throughout the water sample. When snow melts and then refreezes, the re-crystallization process forms nearly pure ice crystals and excludes most solutes to the exterior boundary or interstitial spaces of the crystals. This has implications for the chemistry of meltwater released during subsequent snowmelt events.

Defining Dissolved and Particulate Phases

Biogeochemical analysis often focuses on elements that occur in natural waters in a continuum of states from dissolved ions or solutes to **colloidal** substances and on up to particles of various sizes. Because there are no distinct and universally-accepted definitions for these size classes, researchers use **operational definitions** for the fractions or

phases that they are studying. Thus, the dissolved elements in a given water sample may be defined by the filter pore size through which a water sample is passed. For example, dissolved organic carbon (DOC) may be defined as the filtrate from a glass fiber filter with a nominal pore size of 0.45 μm, or the dissolved metals in a water sample may be defined as those passing through a filter with a pore size of 0.2 μm. It is important to be aware of accepted operational definitions when conducting research or comparing published studies concerning dissolved, colloidal, or particulate phases of elements.

SI Units and Concentrations

As one reads the biogeochemical literature, it becomes apparent that element cycling and chemical data are expressed with a variety of unit notations, some of which are derived from the International System of SI Units. In reports of aqueous chemistry, the more common units of concentration are ppm (parts per million) or ppb (parts per billion), mg L^{-1} or μg L^{-1}, and mmol L^{-1} or μmol L^{-1}. Perhaps less familiar are units that represent ***ionic charge equivalents***, including μeq L^{-1}, $\mu mol_c\ L^{-1}$, or $mmol_c\ L^{-1}$.

Substances do not react with each other on a gram for gram basis, but rather on a stoichiometric basis in proportion to their separate equivalent weights. The chemical definition of an **equivalent weight** is the mass of an element or substance that will displace or otherwise react with one mole (1.008 g) of hydrogen or one-half mole (8.00 g) of oxygen. As one example, the formula for ammonium sulfate, $(NH_4)_2SO_4$, contains two moles of monovalent ammonium to balance one mole of divalent sulfate (which contains two moles of negative or anionic charge). Being able to express ions in terms of electrical charge equivalents provides important insights in a variety of applications.

The equivalent weight of a substance is calculated by dividing the atomic weight or molar mass by its valence (absolute value of its charge). For a monovalent ion such as Na^+, the equivalent weight is 22.98 g divided by 1 or 22.98 g, whereas a divalent cation such as Ca^{2+} has an equivalent weight of 40.08 g divided by its valence of 2, giving a value of 20.04 g per equivalent. Another way of looking at this is that a mole of calcium contains two moles of charge equivalents, so it only takes one half of molar mass (e.g., 20.04 g) to provide a mole of charge equivalents. At a smaller scale, a milli-equivalent of calcium ion would be 1/1000th of 20.04 g or 20.0 mg, and a micro-equivalent of calcium ion would be 20.04 g × 10^{-6} or 20.0 μg.

In the current biogeochemical literature, ionic charges are often expressed in terms of moles of charge using $\mu mol_c\ L^{-1}$, $mmol_c\ L^{-1}$, or $mmol_c\ kg^{-1}$, where the subscript "c" indicates charge units. Thus, for example, 2.0 mg of Ca^{2+} per liter of water is equivalent to 0.1 $mmol_c\ L^{-1}$. Similarly, we can express charge equivalents for sulfate anion, which has a formula weight of 96 g, a charge of −2, and an equivalent weight of 48 g per mole of charge. For practice, consider a solution containing 2.4 mg L^{-1} of sulfate ion and calculate the concentration in $mmol_c\ L^{-1}$. A mmol is 1/1000th of a mole, so a $mmol_c$ of sulfate ion is equal to 48 g / 1000 = 0.048 g. This value can be converted to mg by multiplying 0.048 g × 1000 mg g^{-1}, which is equal to 48 mg per $mmol_c$ of sulfate. Next, it is a matter of expressing 2.4 mg of sulfate as a fraction of 48 mg (i.e., 2.4 / 48), which equals 0.05. Thus, 2.4 mg L^{-1} sulfate equals 0.05 $mmol_c\ L^{-1}$. Table 1.2 provides additional examples of conversions between moles and moles of charge.

Table 1.2 Examples of conversions from moles to mol_c for different elements (values are rounded to whole numbers)

Ion	Atomic mass	Equivalent weight (= mass/valence)
Ca^{2+}	40 g	40/2 = 20 g per mol_c (or 20 mg $mmol_c^{-1}$)
Mg^{2+}	24 g	24/2 = 12 g
K^+	39 g	39/1 = 39 g
SO_4^{2-}	96 g	96/2 = 48 g
Al^{3+}	27 g	27/3 = 9 g

Ionic Charge Balance

The preceding discussion provides an opportunity to introduce and to emphasize a principle that is central to biogeochemical analysis. Wherever ions occur – in a cell, in solution, in a soil – we expect that the sum of positive and negative charges will balance. Thus, a solution containing a mixture of chloride and nitrate ions with 100 $mmol_c\ L^{-1}$ of anionic charge will inevitably contain 100 $mmol_c\ L^{-1}$ of positive charge. This principle of **charge balance** will be discussed in a variety of contexts in subsequent chapters.

Stable Isotope Chemistry

Stable isotopes provide a powerful tool for tracing and quantifying biogeochemical patterns and processes (Lajtha and Michener 1994). Elemental stable isotopes can be briefly defined in the following terms. For any given element, the atomic mass is the sum of the number of positively charged protons and uncharged neutrons. Within limits imposed by physical-chemical constraints, atoms of any element may include isotopes with different numbers of neutrons and corresponding atomic masses. Each of these isotopes can be represented in chemical notation by writing its chemical symbol, preceded by a superscript that specifies isotopic mass. For example, an oxygen **nuclide** composed of 8 protons and

8 neutrons is written as ^{16}O, whereas an oxygen isotope composed of 8 protons plus 10 neutrons is represented as ^{18}O. Out of a total of 1700 known nuclides, roughly 260 of these are stable isotopes; the remaining isotopes are unstable nuclides that are subject to spontaneous disintegration over time (Richardson and McSween 1989). As an illustration, the element carbon occurs in two stable isotopic forms (^{12}C and ^{13}C), as well as the radioactive isotope ^{14}C. Stable isotopes that are commonly used in biogeochemical and geochemical studies include: ^{1}H, ^{2}H, ^{12}C, ^{13}C, ^{14}N, ^{15}N, ^{16}O, ^{18}O, ^{32}S, ^{34}S, ^{40}Ca, ^{44}Ca, ^{86}Sr, ^{87}Sr, ^{54}Fe, and ^{56}Fe.

Under field conditions, various biotic and abiotic processes separate light and heavy isotopes of a particular element. For example, evaporation of water favors enrichment of the vapor phase with the light isotopes of hydrogen and oxygen, leaving the residual liquid water somewhat enriched in heavier isotopes. This **mass fractionation** of light and heavy isotopes permits biogeochemical tracing of the pathways and processes of element cycling (by tracking changes in the ratio of heavy to light isotopes for a given element). Isotope fractionation largely occurs through either equilibrium effects – where a larger activation energy is required to dissociate an isotopically heavy chemical species – or kinetic effects, which occur because heavier molecules or ions react or diffuse more slowly than lighter isotopic analogs. All other factors being equal, fractionation of heavy and light isotopes is greatest between phases that have markedly different bond types or bond strengths. The vibrational frequency is greater in bonds associated with a lighter versus a heavier isotope, resulting in bonds that tend to be less stable or weaker.

Mass fractionation is generally expressed with delta (δ) notation in which the isotopic ratio (R) of the heavy to light isotope in a sample (e.g., ^{13}C / ^{12}C) is compared to the same ratio in a standard reference material:

$$\delta = \left(\left(R_{sample} - R_{standard}\right) / R_{standard}\right) \times 1000$$

where R is the ratio of the heavy to the light isotope

With this convention, the value of δ is a measure of the deviation of R in parts per thousand or *permil* (‰). If a sample (R_{sample}) contains proportionately more of the heavy isotope than the reference standard, a positive delta value is observed. Thus, samples with positive values of δ are isotopically heavy or **enriched**, whereas samples with negative values of δ are isotopically light or **depleted** in the heavy isotope, compared to the standard.

For perspective, it is important to note that heavy isotopes represent a small percentage of the isotopic pool for a given element. In terms of **natural abundance**, the heavy isotope ^{13}C represents 1.1% of the carbon pool, ^{15}N is roughly 0.37% of the nitrogen pool, and ^{18}O is approximately 0.2% of the oxygen pool. Using a sensitive mass spectrometer, small fractional changes in abundances of these relatively rare heavy isotopes can be detected and used to trace biogeochemical patterns and processes.

What patterns of fractionation are observed in the hydrologic cycle? Because isotopically light water molecules escape more readily from a body of water into the atmosphere than do molecules of "heavy" water, atmospheric water vapor always has negative δD (deuterium) and δ ^{18}O values relative to ocean water. In contrast, vapor condensation into rain and snow occurs with little discrimination between light and heavy water molecules. Thus, the first rain to fall from a "new" cloud over the ocean has values of δD (deuterium) and δ ^{18}O that are close to 0‰. Water vapor remaining in the atmosphere is systematically depleted in deuterium and ^{18}O by this process, because each heavy water molecule that condenses removes heavy isotopes from a comparatively small pool, whereas light water molecules remove atoms from a large pool of light isotopes. Subsequent precipitation is derived from a vapor reservoir that has δ ^{18}O and δD values even more negative than freshly evaporated sea water. With continued precipitation, rainwater becomes progressively lighter. The isotopic ratio (R) in the remaining vapor is given by the *Rayleigh distillation equation*:

$$R = R_0 f^{(\alpha - 1)}$$

where R_0 is the initial $^{18}O/^{16}O$ value in the vapor, *f* is the fraction of vapor remaining, and α is the fractionation factor (Richardson and McSween 1989).

The preceding relationships can be used to illustrate how isotopic ratios change in response to rainfall processes. Suppose rain begins to fall from an air mass whose initial $\delta^{18}O$ value is −9.0‰, and whose fractionation factor ($\alpha_{liquid\text{-}vapor}$) is 1.0092 at the condensation temperature. When we apply the Raleigh Distillation Equation to compute the isotopic composition of the air mass after 60% of the water vapor has condensed, we find that the air mass has been depleted to a new $\delta^{18}O$ value of −17.32‰. If we also compute the isotopic composition of the resulting rainwater, we estimate a $\delta^{18}O$ value of –8.28‰. Thus, the rainwater $\delta^{18}O$ value (−8.28‰.) is slightly heavier than the source air mass (−9.0‰), but is depleted in ^{18}O relative to earlier rainfall and freshly evaporated sea water. [See Problem Sets for derivation and solution of this isotope problem].

Because of fractionation processes, (i) the separation between rainwater and seawater becomes more pronounced as air masses move further inland or are lifted to higher elevations, and (ii) δ ^{18}O values for freshwater are always negative compared to seawater. Since the fractionation factors for both oxygen and hydrogen isotopes become larger with decreasing temperature, the difference between seawater and precipitation increases toward the poles (Fig. 1.8).

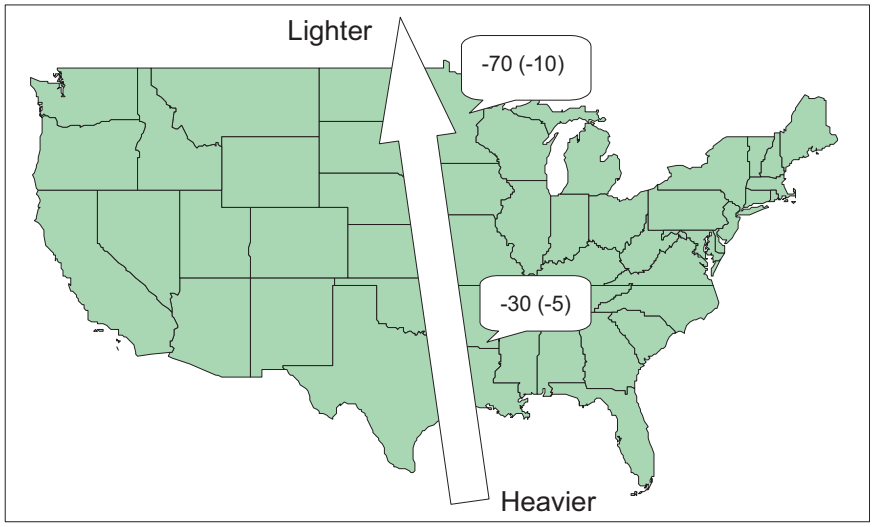

Fig. 1.8 Isotopic signatures of δ D and δ ^{18}O (in parenthesis) in wet precipitation decrease moving northward across North America as air masses become depleted in heavy isotopes of hydrogen and oxygen (data from Richardson and McSween 1989)

Continental rainfall and freshwaters are generally depleted in both heavy isotopes contained in water molecules.

Patterns of isotopic fractionation in carbon compounds have also been extensively investigated, and δ ^{13}C values have been reported to range from about −30‰ to +25‰. In general, carbon in the reduced biogenic compounds found in living and fossil organisms is isotopically light (negative values of δ), whereas inorganic carbonate minerals (especially in marine environments) are isotopically heavy. During photosynthesis, green plants fractionate carbon isotopes in at least three metabolic steps, favoring the retention of ^{12}C rather than ^{13}C (Werner et al. 2012). However, terrestrial **C_3** versus **C_4** plants discriminate carbon isotopes to different degrees, because of differences in their initial enzymatic pathways for CO_2 uptake and fixation. C_3 woody plants and grains have δ ^{13}C values ranging from about −22‰ to −33‰, while C_4 grasses range from −9‰ to −16‰. In the oceans, marine plants have $^{13}C/^{12}C$ ratios that are about 7.5‰ less negative than C_3 terrestrial plants, possibly because the marine plants assimilate carbon from marine HCO_3^- (0‰), rather than atmospheric CO_2 (−7‰).

Bashkin and Binkley (1998) relied on natural abundances of carbon isotopes in soil organic matter to examine changes in carbon storage associated with land conversion in Hawaii. Their results indicated that conversion of wild land to sugar cane, a **C_4 plant**, produced a δ ^{13}C signal in surface soil organic matter that was heavier than the signal associated with native forest cover (dominated by **C_3 plants**). As shown in Fig. 1.9, soils supporting native Hawaiian forest exhibited a relatively consistent depth profile of soil organic matter characterized by isotopic ratios around −26‰. In comparison, soils supporting cane fields exhibited heavier isotopic ratios in surface horizons, averaging around −20‰ (Fig. 1.9). Yet, deeper portions of the same cultivated soils exhibited lighter isotopic ratios of −22 to −24‰, reflecting the influence of previous forest cover. In plots where cane fields were converted back to forest cover, surface soil organic matter reverted to a lighter δ ^{13}C value (see forest plantation soil profile in Fig. 1.9).

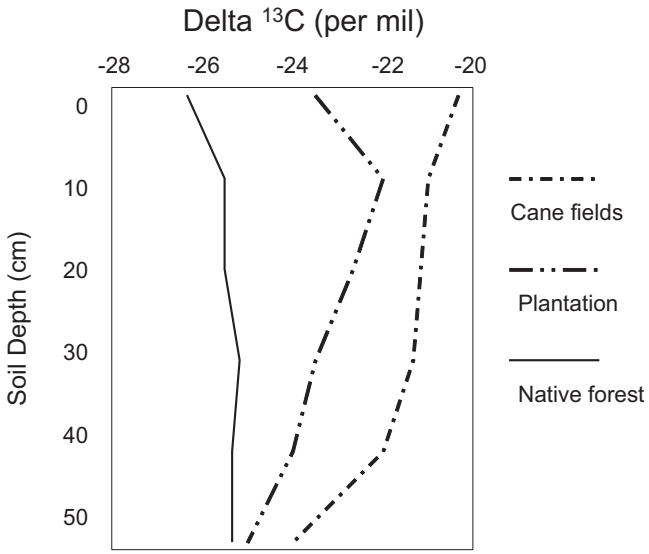

Fig. 1.9 Carbon isotopes in Hawaiian soils. From Bashkin, M.A. and D. Binkley. 1998. Changes in soil carbon following afforestation in Hawaii. Ecology 79:828–833. © 1998 by the Ecological Society of America

In another example, Ehleringer et al. (2000) investigated forest carbon cycling in the western U.S. and reported that δ ^{13}C values generally increase from lighter to heavier ratios moving from leaves, to litter, and into soil organic matter (SOM) in forest ecosystems (Fig. 1.10). It is generally assumed that these changes reflect isotopic discrimination or fractionation by plants and decomposers in the forest carbon cycle. However, Kohl et al. (2015) suggested that because phospholipid fatty acids (PLFA) in soil fungi are relatively depleted in ^{13}C, increased proportions of soil bacterial relative to fungal biomass with soil depth may represent an important mechanism contributing to the pattern illustrated in Fig. 1.10.

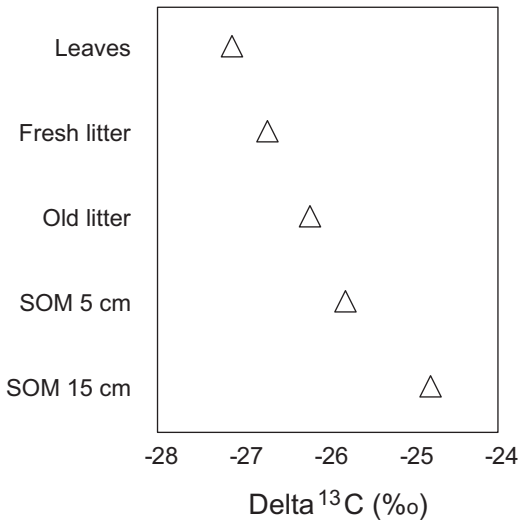

Fig. 1.10 Patterns of $\partial^{13}C$ in a forest stand moving from fresh leaves, to litter, to soil organic matter at two depths (data from Ehleringer et al. 2000)

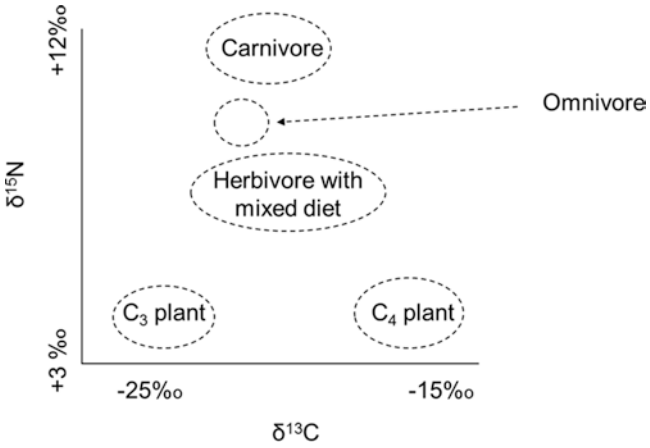

Fig. 1.11 Comparison of $\delta^{15}N$ and $\delta^{13}C$ values in plants, herbivores, and carnivores in a simple food web. The carnivore exhibits considerable ^{15}N enrichment and has a $\delta^{13}C$ signal that reflects likely inputs from both C_3 and C_4 plants

Isotopes of nitrogen are fractionated in a number of distinctive ways by organisms in the biosphere (Lajtha and Michener 1994). Legumes that assimilate atmospheric N_2 directly tend to have $\delta^{15}N$ values near 0‰, whereas nonleguminous plants tend to have delta values that are positive (on the order of +9‰). With each step up a food chain, consumer organisms tend to concentrate more ^{15}N; as a consequence, carnivores or predators tend to have $\delta^{15}N$ values about 3‰ more positive than herbivores, which also are enriched in ^{15}N compared to their own food source. The process of tissue ^{15}N enrichment among consumer organisms is thought to occur in part because of isotopic fractionation during excretion, with preferential retention of ^{15}N and loss of ^{14}N. Figure 1.11 illustrates how a simple food web may contain organisms with distinctive $\delta^{15}N$ and $\delta^{13}C$ isotopic ratios reflecting the types of plants at the base of the food web and the trophic position of each consumer.

Several research investigators have reported evidence that $\delta^{15}N$ values in plants vary in relation to site fertility and N availability. Martinelli et al. (1999) reported that mean foliar $\delta^{15}N$ values were 6.5‰ higher in tropical forests compared to temperate forests. They also found that tropical forest ecosystems with relatively low N availability were significantly more depleted in ^{15}N than other tropical forests. In a related study, Hobbie and Colpaert (2003) reported evidence that fungal biomass and N retention increased at low N supply, whereas needle $\delta^{15}N$ decreased, and there was an inverse relation between needle $\delta^{15}N$ and biomass of mycorrhizal hyphae. Overall, their data and models suggested that low values of plant $\delta^{15}N$ in unproductive N-limited environments result partly from high retention of ^{15}N by mycorrhizal fungi. As a consequence, mycorrhizal plants in N-limited sites became more depleted in ^{15}N than sites where N was more available and mycorrhizal fungal biomass was lower.

Samples enriched with heavy isotopes are often used as tracers of cycling pathways and indicators of reaction rates in field or laboratory experiments. Davidson et al. (1992) enriched soils with concentrated pulses of ^{15}N–labelled nitrate and ammonium salts and used the technique of **isotope dilution** to estimate rates of gross N cycling in two comparative California forest soils. Barnes et al. (2008) used a dual isotope approach with $\partial^{15}N$ and $\partial^{18}O$ to compare the relative importance of atmospheric and microbial sources of nitrate in stream runoff from forested watersheds in Connecticut. Nadelhoffer et al. (1999) used ^{15}N–labelled ammonium and nitrate as tracers to determine fates of added nitrogen amendments to forest plots at Harvard Forest, MA. They found that less than 25% of the added ^{15}N tracer accumulated in plant biomass within the forest; the remaining ^{15}N tracer cycled into decomposing litter and soil organic matter. In each of these cases, the ^{15}N tracers provided invaluable insights regarding rates of processes and key sources and sinks in the nitrogen cycle.

Soil Biogeochemistry

2

Introduction

If you consider all the ways in which soils influence element cycling, hydrologic cycling, species diversity, biotic growth, productivity, and global carbon storage, it is clear that soils have a profound effect on ecological relationships. Soils are a primary determinant of **site quality** and environmental conditions in terrestrial ecosystems, providing water, nutrients, acid neutralizing capacity, shelter, and anchorage for terrestrial life forms. Beyond these essential functions in terrestrial ecosystems, soils also exert a strong influence on aquatic systems through effects on the chemistry and hydrologic routing of drainage water inputs to lakes and streams. Depending upon (i) the hydrologic flow path of water movement into aquatic systems, (ii) the characteristics of soils and **surficial materials** contacted by drainage water, and (iii) the degree of chemical reaction between aqueous and solid phases, soils in a watershed may serve as a source or sink for acidity, alkalinity, nutrients, dissolved organic matter, or toxic pollutants in waters draining to nearby aquatic receptor systems.

Soil Formation and Pedogenesis

Soils and their life support characteristics vary across the biosphere, with examples ranging from deeply weathered tropical Oxisols of the Amazon Basin, to fertile prairie Mollisols of the U.S. Midwest, and extending to acidic forest Spodosols of New England. Major differences among soils originate through variations in one or more of the following five soil forming factors described by soil scientist Hans Jenny: (i) nature of the **parent material**; (ii) climatic conditions; (iii) age of the **soil profile**; (iv) soil topographic position and drainage conditions; and (v) influence of biological soil-forming agents.

In comparing soils, it is clear that one of the primary reasons for distinct differences among soils is the strong influence of geologic conditions and soil parent materials on **pedogenesis** or soil formation. At a given location, soil parent material may consist of a coarse textured sandy glacial deposit versus a volcanic ash deposit, or fertile alluvial floodplain sediments versus an ancient weathered granite bedrock **saprolite** or residuum. Each initial substrate may give rise to differing physical and chemical characteristics over the time course of soil formation. Examples of major types of soil parent materials are shown in Table 2.1.

A second major influence on soil characteristics is the climatic regime in which soil development occurs. Is the climate seasonal, wetter, drier, cooler, or warmer? How would you expect soil formation to compare in the cool humid climate of New England versus the warm humid climate of North Carolina or the warm arid conditions of Arizona and New Mexico? In general, we would expect greater soil development in warmer and wetter climates where favorable drainage conditions have permitted long-term leaching by large amounts of infiltrating precipitation.

Because soil formation is a relatively slow process, soil age is also a strong determinant of soil conditions. In glaciated regions, soils may have experienced less than 10,000–12,000 yr. of pedogenesis since the last glacial retreat; as a result, the soil profile may extend <1 m below the surface. In contrast, many sub-tropical and tropical soils are much older (i.e., > > 10,000 years old); consequently, profile development may extend tens of meters below the soil surface at these sites (Richter and Markewitz 1995).

C.S. Cronan, *Ecosystem Biogeochemistry*, Springer Textbooks in Earth Sciences, Geography and Environment, DOI 10.1007/978-3-319-66444-6_2

Table 2.1 Examples of different parent materials that act as substrates for soil formation

Surficial geologic deposits	Bedrock geology
Alluvial floodplain sediments	Granitic saprolite or residuum
Glacial till or outwash	Limestone or dolomitic residuum
Aeolian (wind-blown) silt	Sandstone residuum
Volcanic ash	Metamorphic schist residuum
Lacustrine (lake) sediments	Volcanic lava
Marine sediments	Basalt

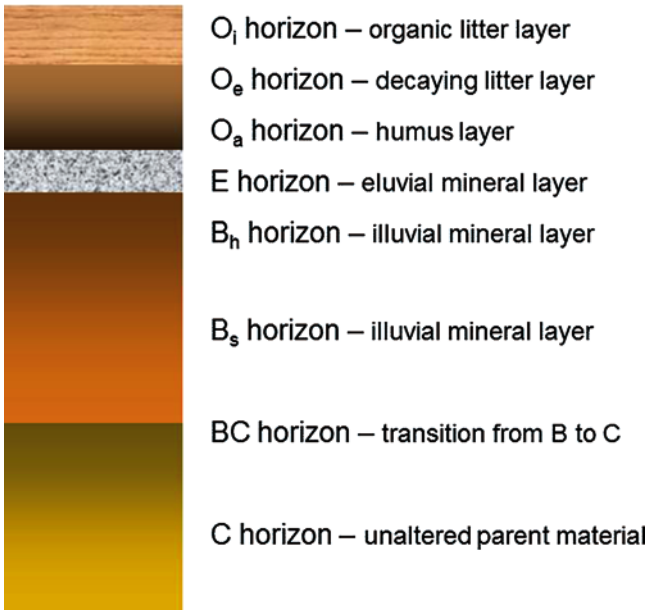

Fig. 2.1 Idealized soil profile showing vertical zonation of a northern well-drained forest soil. The combined O horizon layers are often referred to as the forest floor, and the uppermost mineral horizon is usually either an A or E horizon

Yet a fourth factor affecting pedogenesis is the topographic location of a soil. If a soil is well-drained, it will have a very different profile development compared to a lowland soil that is waterlogged or poorly-drained. In a soil with high permeability, a deeper water-table, and a mesic climate with adequate annual precipitation, the cumulative effects of water infiltration through the soil parent material promote gradual development of distinctive soil horizons. However, when water infiltration and drainage are impeded by topographic position or physical barriers in the parent material, pedogenesis is inhibited and soil horizon differentiation occurs only very slowly.

The fifth and final major influence on soil development is biological activity in the form of soil invertebrates, plants, burrowing mammals, and microbes. Respiration and metabolic activities by these organisms generate the carbonic and organic acids that promote mineral weathering and soil leaching. In addition, the life processes and organic matter derived from living organisms help to build up the structure, exchange capacity, porosity, and soil moisture storage capacity of the soil.

During pedogenesis, soils gradually develop a vertical zonation composed of various layers or **soil horizons**, each with particular properties. Soil formation is largely driven by (i) the percolation of water and acids through the soil profile, (ii) subsequent **weathering** and **leaching** of soil minerals exposed to acid attack, and (iii) differential mobilization, transport, and deposition of soluble organic matter and metals in the soil profile. Over time, forest soil development generally leads to the formation of a surficial O horizon composed of the detrital organic remains of plants and other organisms; beneath that uppermost organic horizon, soils typically contain several distinctive **mineral soil** layers such as the A, E, B, and C horizons.

In the example shown in Fig. 2.1, the soil horizons of this well-drained, cool temperate forest **Spodosol** have developed under the influence of a process termed **podzolization**. This process begins when precipitation moisture infiltrates the O horizon and leaches organic acids from the decaying litter and **humus**. As the drainage water percolates through the underlying mineral soil, the acidic water attacks the mineral soil particles through acid weathering, ion exchange, and organic complexation. This **cheluviation** process strips cations from the A or E horizon, leaching them to the underlying B horizon. One of the key features of this process is the mobilization or **eluviation** of iron (Fe) and aluminum (Al) from the A or E horizon as soluble organic complexes, followed by vertical transport of the metal-organic complexes to the B horizon. In the mineral B horizon, the dissolved Fe, Al, and organic carbon are removed from solution through precipitation and/or adsorption reactions. This soil **illuviation** process leads to the accumulation of iron and aluminum oxides and **humic** coatings in the soil matrix of the upper B horizon. It should be noted that if we examined soil formation under different environmental conditions than this, a number of other possible pedogenetic processes and outcomes could be expected (Brady 1984).

Evidence of the dynamic processes of podzolization in cool temperate forest soils can be observed with examples of soil and solution chemistry data from two different field investigations. Figure 2.2 shows a vertical gradient of water samples collected as precipitation inputs**, throughfall** solutions sampled beneath the tree canopy, and soil moisture in the upper and lower soil horizons of a forest ecosystem in the Cascade Mountains of Washington. As expected, solutions in the upper mineral soil profile (E horizon) contain the highest concentrations of acidity, organic acids (**fulvic acids**), and soluble Fe and Al. This pattern occurs because the O horizon is the location where organic acids are being released by decomposition processes, causing intense weathering and metal cheluviation in the adjacent uppermost mineral soil horizon. Moving downward in the soil through the B horizons, concentrations of acidity, organic acids, and soluble Fe and

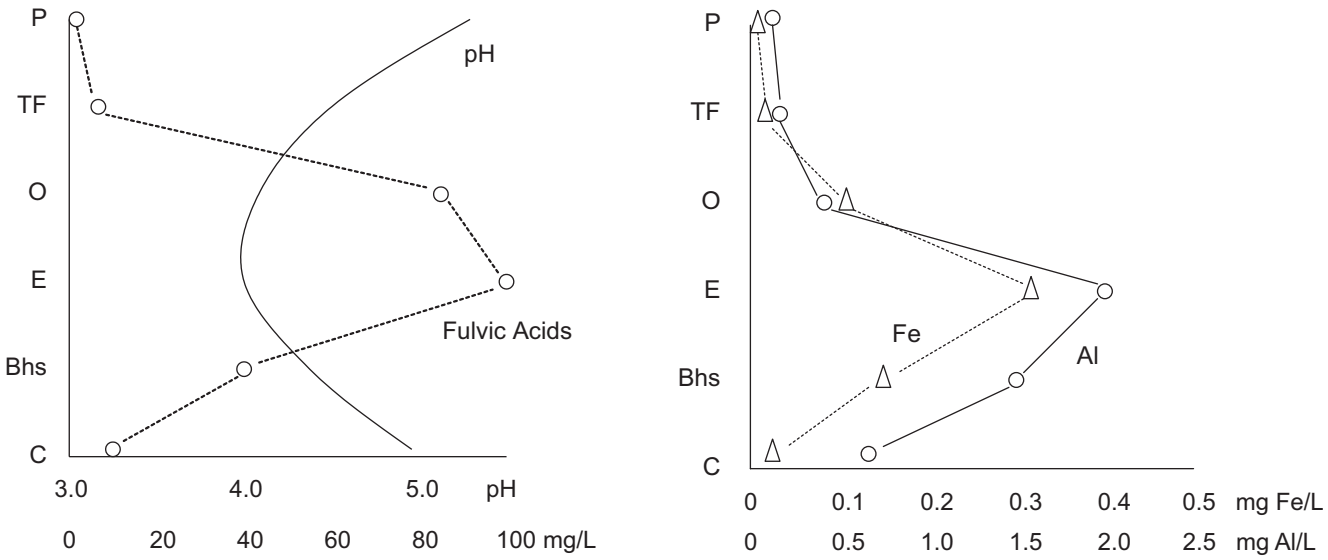

Fig. 2.2 Vertical gradients of water chemistry in a western conifer forest at Findley Lake, WA sampled as precipitation, throughfall (TF), and soil solutions in the O, E, B, and C horizons (Data used by permission from Ugolini and Dahlgren 1987)

Table 2.2 Concentrations of extractable soil aluminum fractions in the vertical profile of a northern forest Spodosol in New York (Cronan et al. 1990)

Soil horizon	Organic Al[a]	Amorphous hydroxy Al[a]
O	3.0	11.0
E	2.4	9.1
Bhs	11.7	42.7
Bs2	24.1	153.4
C	2.7	72.1

[a]Units in $cmol_c\ kg^{-1}$. Organic Al was estimated by extraction with copper acetate, while amorphous hydroxy Al was extracted with ammonium oxalate

Al all decline as a result of further weathering, ion exchange, and illuviation processes (Fig. 2.2).

As a result of these processes, we would expect that concentrations of extractable Fe and Al oxides and metal-organic complexes in the soil profile would be highest in the B horizons where these metals are accumulating through illuviation processes. Indeed, the data in Table 2.2 from a northern temperate forest ecosystem illustrate that concentrations of extractable organic Al and extractable amorphous Al oxides are five to ten-fold higher for soil particles within illuvial B horizons compared to other horizons. In summary, soluble Al leaches from the upper mineral horizons and accumulates as solid phase Al oxides in B horizons.

Soil Classification

There are many different types of soils besides the forest Spodosol depicted in Fig. 2.1. In Table 2.3, world soils are listed taxonomically by major **soil orders** that reflect the degree of vertical stratification and the nature of soil forming processes and factors at a given site or regional location (Fig. 2.3). Where time and climatic conditions have allowed long-term leaching of the mineral soil profile, one generally finds a strongly developed soil profile such as a northern **Spodosol**, a warm temperate or subtropical **Ultisol**, or a tropical **Oxisol**. A Spodosol is characterized by an intensely leached whitish or gray E horizon and a dark brown to chestnut brown B_s or B_2 horizon that is enriched with Fe, Al, and organic C. In contrast, older more highly weathered Ultisols and Oxisols typically exhibit a deep B horizon with abundant accumulation of red iron oxide. Sites with younger parent material, a drier or colder climate, or waterlogged conditions may have soils such as **Inceptisols**, **Aridisols**, or **Histosols** that lack obvious mineral soil horizons.

It should be noted that when soils are classified and their horizons are described, soil scientists use various subordinate horizon abbreviations to convey information about the characteristics of each horizon. These abbreviations, which are placed beside the master horizon designation as a subscript letter (e.g., B_s), include the following designators: (a) highly decomposed organic matter; (c) concretions; (e) partially decomposed organic matter; (g) gleyed and saturated; (h) accumulation of illuvial organic matter; (i) slightly decomposed organic matter; (m) cementation; (p) plowed; (r) soft or weathered rock; (s) accumulation of metal sesquioxides; (t) accumulation of silicate clay; and (x) **fragipan** character.

Soil Texture and Coarse Fragments

Soil texture is an important soil physical property defined in terms of the relative proportions of three size classes of soil particles: **sand** (diameter = 0.05–2.0 mm), **silt** (0.002–0.05 mm),

Table 2.3 Major soil orders defined in the taxonomy of the Soil Conservation Service (USDA Soil Conservation Service 1975; Singer and Munns 1996)

Order name	Distinctive features
Alfisol	Soils have accumulations of illuviated clay in subsoil, moderate to high base saturation, and low organic matter in upper soil
Andisol	Soils are formed on volcanic parent materials, have a low bulk density, and the clay fraction is poorly crystallized or amorphous
Aridisol	Soils are found in arid regions where moisture is limiting; upper horizons may be enriched in sodium, carbonates, or gypsum
Entisol	Soils generally lack distinctive pedogenetic horizons as a result of inadequate time for soil formation, inert parent material, steep slopes, a weatherable parent material that leaves no residue, or profile mixing
Histosol	Soils are primarily composed of organic matter (e.g., peaty soil)
Inceptisol	Soils tend to form in fine-textured parent material where annual rainfall is moderate, but leaching and translocation are insufficient to create distinctive subsurface horizons and strong profile differentiation.
Mollisol	Soils form under grassland conditions and have a thick dark brown to black surface horizon that is high in organic matter and base cations.
Oxisol	Soils develop in humid tropical and subtropical regions where leaching and weathering are intense, creating a thick subsurface accumulation of iron and aluminum oxides.
Spodosol	Soils tend to form in cool humid climates on coarser parent materials and exhibit a diagnostic subsurface "spodic" B horizon containing translocated metal oxides and humic substances; the spodic B horizon is often found beneath an "albic" E horizon that is white to light grey.
Ultisol	Soils form in warm humid climates, have a subsurface accumulation of translocated clays, have a lower base saturation than Alfisols, and often exhibit more of a red iron oxide appearance than do Alfisols.
Vertisol	Soils form in clay-textured parent material in dry or seasonally dry climates; the clays swell with moisture and shrink upon drying, causing the formation of cracks in the soil surface.

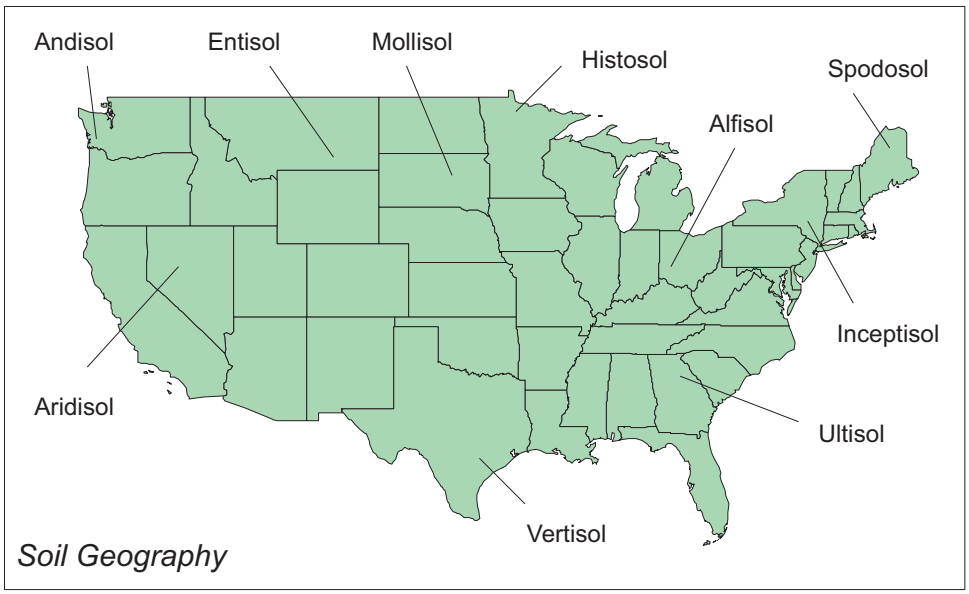

Fig. 2.3 Examples of geographic locations where specific soil orders are common in North America

and **clay** (< 0.002 mm or <2.0 μm). These primary soil particles typically aggregate into larger structural units resembling plates, blocks, or crumbs that may be bound together by **soil organic matter**. In many soils, coarse particles or fragments larger than sand also occur in the form of pebbles, cobbles, and boulders.

Soil textural classes based on particles ≤2 mm in size are commonly described using the soil textural triangle shown in Fig. 2.4. This conceptual model allows us to describe the texture of a soil as a function of the percent sand, silt, and clay. For a soil developed from silty **lacustrine** or lake sediments, the textural class would likely fall near the silt loam category at the lower right corner of the triangle in Fig. 2.4. In contrast, a soil developed from coarse glacial outwash material might plot in the lower left corner as a sand or loamy sand.

The illustration in Fig. 2.5 provides a comparison of texture for two contrasting mineral soil profiles in North America – a forest Ultisol in central Tennessee versus a forest Spodosol in the Adirondack Mountains of New York State. For the southern Ultisol, the upper mineral soil profile is dominated by sand and silt, with a small percentage of clay. Yet, with increasing depth, the soil texture shifts to a finer texture, reaching 60% silt and 30% clay at a depth of 60 cm. In contrast, the northern soil (formed in glacial till) is virtually uniform from 0 to 60 cm depth, with >60% sand, > 25% silt, and <5% clay (Cronan et al. 1990).

Comparison of soil textures for three northern soils

Soil Series	Parent Material	Sand	(%) Silt	Clay
Adams	Outwash	92.6	6.2	1.2
Becket	Till	62.2	31.3	6.5
Unadilla	Lacustrine	14.7	79.2	6.1

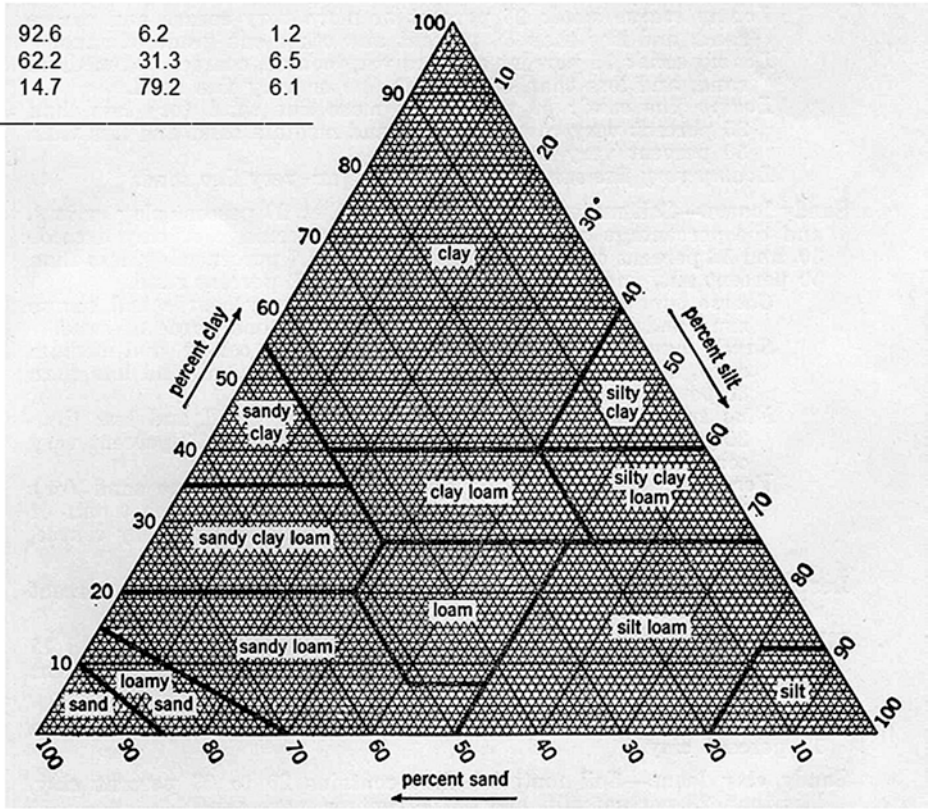

Fig. 2.4 Soil texture classes delineated as a function of the percent sand, silt, and clay. Use the insert data table to place the Adams, Becket, and Unadilla soils in the triangle (Source: USDA 1951)

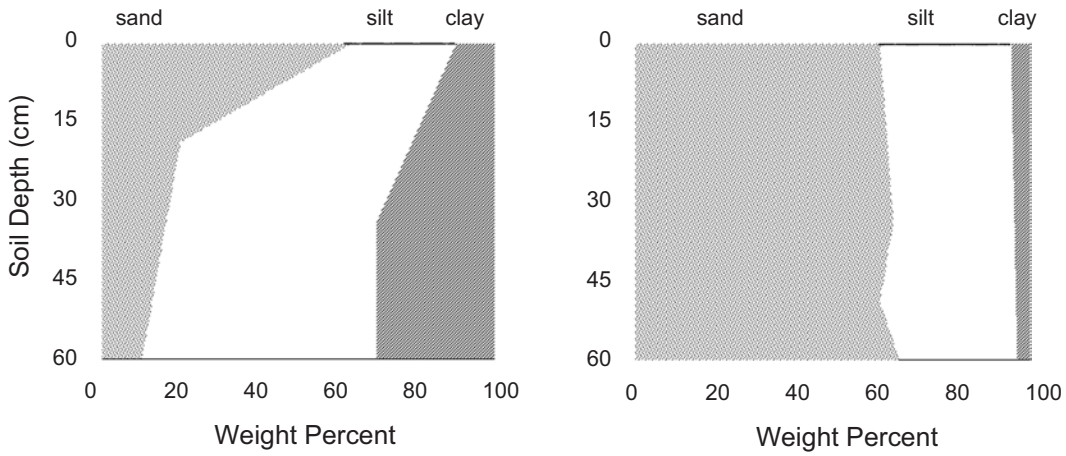

Fig. 2.5 Comparison of soil textural changes through a vertical soil profile in a contrasting southern Ultisol (*left*) and northern Spodosol (*right*)

Soil Moisture

The water infiltration and moisture retention characteristics of a soil are largely controlled by the combined influence of soil texture, aggregate structure, and organic matter content. These master variables determine whether water drains rapidly through the soil profile, puddles up on the soil surface, or is absorbed and retained by sponge-like **soil colloids**. In a soil with favorable texture, structure, and organic matter content, water drains from larger pores and is retained in the smaller pores, giving a proper balance of water availability and aeration.

The moisture supply characteristics of different soils can be compared if we know the amount of water held by the soils at **field capacity** and at the **wilting point** (Fig. 2.6)**.** The difference between these two measurements is the quantity of **available water** that can potentially be used by plants and other organisms during drying intervals between precipitation events. As shown in Fig. 2.7, the retention and availability of moisture can vary considerably among soils with different textures. For example, sandy soils tend to exhibit low field capacities and limited amounts of available water, producing droughty conditions and more frequent **water stress** in plants. In contrast, silty loams have much more optimal soil moisture conditions, with higher field capacities and reservoirs of available water. Clay soils generally have a high water holding capacity, but exhibit lower permeability for water infiltration and gaseous diffusion.

Another important physical feature of soils is water-table depth and its influence on soil moisture conditions. In lowland and wetland habitats, a high water-table can produce seasonal or chronic water-logging or **gleying** of the soil profile. The resulting saturated conditions can decrease aeration of the soil, inhibit aerobic processes in plants and microbes, and affect nutrient uptake and leaching processes. In soils that experience seasonal waterlogging, one can often detect rusty iron oxide mottles in the soil matrix near the uppermost extent of the seasonal water-table.

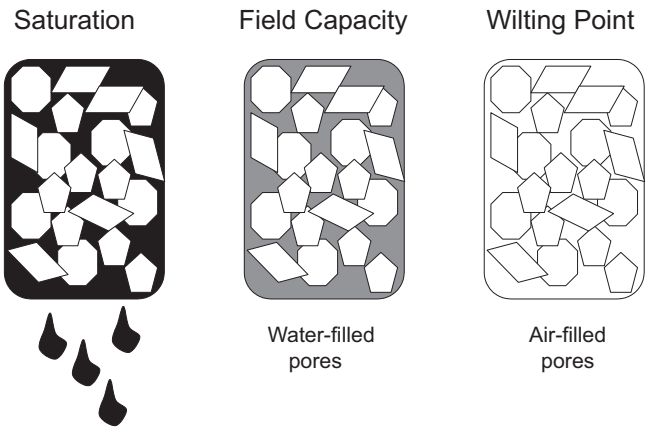

Fig. 2.6 Amounts of soil moisture at saturation, field capacity, and wilting point

Mineralogy

Differences in soil mineralogy are important in determining the kinds of weathering reactions that occur in the soil, release rates for various elements, patterns of alkalinity and acidity generation in the soil profile, and the nature and extent of **secondary mineral** formation in soils. If one soil is predominantly glacial outwash sand composed of SiO_2, whereas another soil contains fluvial sediments composed of multiple minerals, these mineralogical differences can translate into marked contrasts in soil fertility and chemistry.

The potential influence of mineralogical differences on soil conditions can be illustrated by looking at an example from the field. In their analysis of soil mineralogy in a forested watershed located in the Adirondack Mountains of New York, April and Newton (1985) reported that soil parent material in the C horizon at a depth of 60–90 cm was composed of 38% quartz, 50% feldspars, 2% hornblende, and various minor minerals. Further analysis of mineral chemistry indicated substantial differences in the elemental composition of these soil particles (Table 2.4). For example, hornblende was identified as a potentially rich source of calcium, magnesium, and iron, whereas plagioclase was an important source of sodium and calcium. K-feldspar was an important source of potassium, but otherwise contained negligible amounts of other nutrients besides small amounts of sodium.

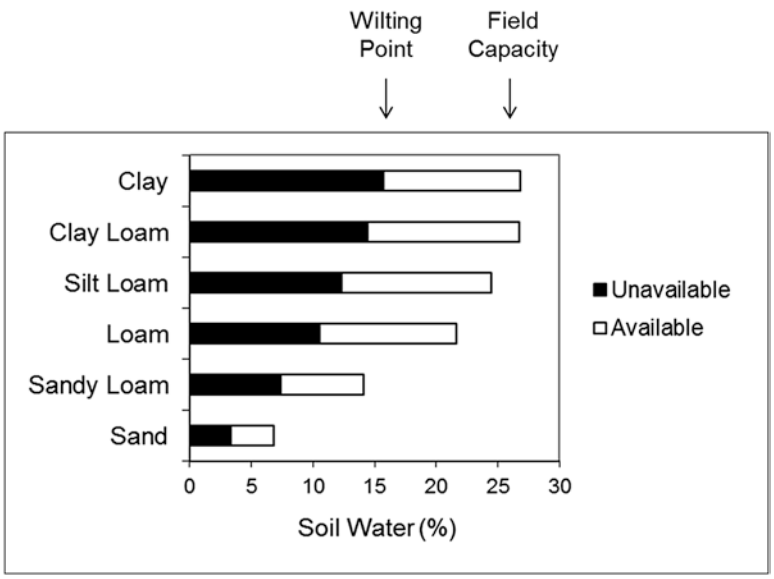

Fig. 2.7 Comparative availability of water in soils with different textures. Water held at soil tensions greater than the wilting point (*black bars - left side*) is not readily available to plants

Physical-Chemical Features of Clays and Other Soil Colloids

The chemical behavior of soils is intimately linked with the physical-chemistry of soil colloids and ion exchange processes in the soil matrix. Soil **colloids**, consisting of clay-sized mineral particles <2 μm in diameter and microscopic **humic colloids**, are crucial in storing and controlling the availability of many elements in soils. Mineral colloids include metal oxides such as Fe_2O_3 and Al_2O_3, as well as different layer silicate clays, including kaolinite and vermiculite (Table 2.5). Both types of mineral colloids are termed **secondary minerals**, because they result from the breakdown of **primary minerals** such as feldspars, micas, and pyroxenes. As a general rule, soil colloids are characterized by enormous surface areas and often exhibit large ion exchange capacities (Table 2.5).

Table 2.4 Comparative chemical composition of different minerals sampled in the C horizon of Panther Lake Watershed, Old Forge, NY (Data from April and Newton 1985)

Weight % oxide	Quartz	Plagioclase	K-feldspar	Hornblende
SiO_2	>99	64	64	40
MgO	0	0	0	6
CaO	0	3	0	11
Na_2O	0	10	1	2
K_2O	0	0.1	15	2
FeO	0	0	0	24

Table 2.5 Comparison of properties of clay minerals and organic soil colloids

Colloid	Mineral type	Surface area ($m^2\ g^{-1}$)	Cation exchange capacity* (cmol (+) kg^{-1})
Kaolinite	1:1 aluminosilicate	10–20	1–10
Montmorillonite	2:1 aluminosilicate	600–800	80–120
Vermiculite	2:1 aluminosilicate	600–800	120–150
Mica	2:1 aluminosilicate	70–120	20–40
Chlorite	2:1:1 aluminosilicate	70–150	20–40
Humic acid	Aromatic polycarboxylic organic colloid	800–900	100–300

*cmol represents a centimole or 0.01 mole

Clay Colloids

A typical layer silicate clay is a combination of two structural units: (i) sheets of silicon-oxygen (Si-O) tetrahedra and (ii) octahedral sheets containing a central atom of aluminum (Al), magnesium (Mg), or iron (Fe) surrounded by oxygen atoms (Fig. 2.8). In **1:1 clays** such as kaolinite, the basic clay structural unit contains one tetrahedral Si-O sheet plus one Al-O octahedral sheet, giving a stoichiometric formula of $Al_2Si_2O_5(OH)_4$. By comparison, **2:1 clays** such as vermiculite and montmorillonite exhibit a colloidal clay structural unit composed of two tetrahedral Si-O sheets plus one octahedral sheet containing a mixture of Al-O and Mg-O octahedra (Fig. 2.8). In the case of vermiculite, the clay composition can be represented by the following formula: $Na_x[(Mg_3)(Si_{4-x}Al_x)O_{10}(OH)_2]$.

The functional importance of clays as chemical storehouses and regulators of nutrients in the soil environment results from two special features of these colloids: (i) their tremendous surface area (up to 600–800 $m^2\ g^{-1}$) and (ii) the unsatisfied electrical charges in clay lattices that attract oppositely charged ions. The enigmatic electrical charges in clays arise from three key processes – **isomorphic substitution**, ionization, and edge breakage – that can be explained as follows. In 2:1 layer silicates (e.g., vermiculite), a relatively large **permanent charge** originates during clay formation or weathering as a result of isomorphic substitution of lower valence cations for higher valence cations in the tetrahedral and octahedral sheets. For example, Mg^{2+} ions may replace some of the Al^{3+} ions in an Al-O octahedral sheet or Al^{3+} may replace or substitute for some of the Si^{4+} ions in a Si-O tetrahedral sheet. In each case, the substitution results in unsatisfied negative charges in the clay lattice, because of the introduction of a cation with lower valence.

Ionization and edge breakage are the major sources of negative charge in 1:1 clays such as kaolinite and are a secondary source of charge in 2:1 clays. Above a certain pH defined as the **isoelectric point**, some OH groups in the clay structure ionize, releasing an H^+ ion and exposing a negatively charged oxygen atom. The resulting charge is **pH-dependent** and increases as the soil pH rises above roughly 4.5. There is also evidence that clays develop negative charges through physical

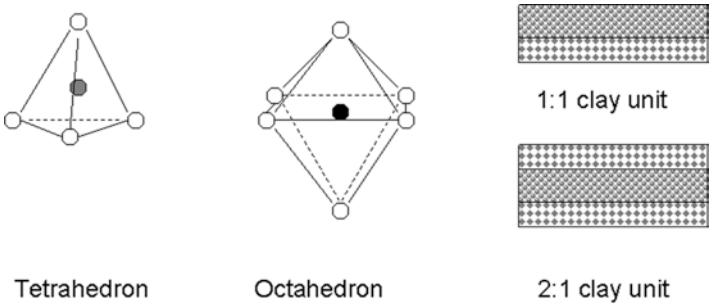

Fig. 2.8 Structure of 1:1 layer silicate and 2:1 layer silicate clays, along with enlarged views of the tetrahedral and octahedral crystal units

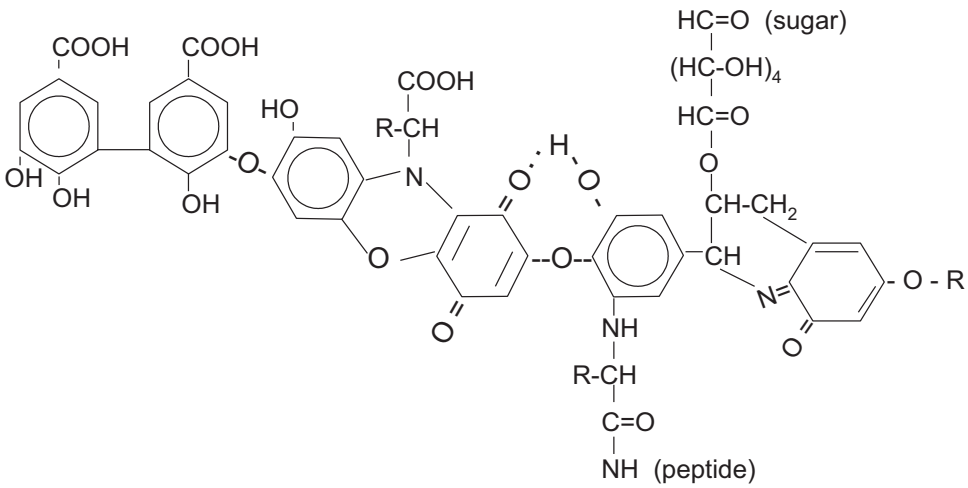

Fig. 2.9 Theoretical partial structure of a humic acid colloid found in soils (Republished with permission of John Wiley and Sons Inc. from Stevenson, F.J. 1982. Humus chemistry: genesis, composition, reactions. Permission conveyed through Copyright Clearance Center Inc.)

edge breakage that exposes electronegative oxygen atoms at the perimeter of a clay lattice.

It is important to note here that soil mineral colloids can acquire a positive charge under acidic soil conditions. As soil pH declines below the isoelectric point of a mineral colloid, the increasing H^+ ion activity in the soil solution shifts thermodynamic conditions toward protonation of pH-dependent oxygen groups, creating a net positive charge on parts of the clay or oxide surface. This process will be more fully developed later in this chapter.

Humic Colloids

Humic colloids occur in soils as a mixture of aromatic and aliphatic organic molecules enriched with carboxylic acid and phenolic hydroxyl functional groups (Fig. 2.9). Because of their low density in g cm^{-3} and complex physical structure, soil humic substances have a tremendous surface area per unit mass. Likewise, humic colloids have an enormous pH-dependent negative charge that results from ionization of oxygen-containing COOH and OH functional groups. With increasing pH above ~4.0, the negative charge or **cation exchange capacity** of soil humus increases significantly as these groups progressively ionize.

Soil chemists often focus on two major classes of soil humic substances – **humic acid** and **fulvic acid** – that are defined operationally by accepted laboratory extraction procedures. Both of these are poorly characterized mixtures of aromatic polycarboxylic organic acids. By definition, humic acids (HA) are soluble in dilute NaOH, are insoluble at pH < 1, and have average molecular weights greater than ~2000 daltons. Fulvic acids (FA), on the other hand, are soluble in acid and base, and typically have molecular weights <2000 daltons.

Chemical Processes in Soils

Ion Exchange and Adsorption in Soils

Cations (e.g., Ca^{2+}) and anions (e.g., SO_4^{2-}) are retained and conserved to varying degrees in the soil environment through the processes of **cation** and **anion adsorption** on soil colloids. The mechanism of retention generally involves a dynamic electrostatic attraction between a charged ion and a colloid surface with an opposite electrical charge. After adsorption, ions may subsequently be subject to reversible **ion exchange**, a competitive process that acts to buffer soil solution chemistry through exchanges of ions in soil solution for adsorbed ions at the colloid surface (Fig. 2.10). As one example, when acidic precipitation containing dilute sulfuric acid leaches through a mineral soil horizon, cation exchange processes occur, resulting in adsorption and retention of exchangeable H^+ ions on soil colloids and a corresponding release of previously adsorbed or exchangeable cations such as Ca^{2+} and Mg^{2+} (Fig. 2.10). This process helps to neutralize the H^+ ions entering the soil solution from atmospheric inputs of acidic precipitation.

Cation exchange in soils can be described in terms of a general chemical equilibrium expression of the following form: $Ca•X + 2NH_4^+ \leftrightarrow (NH_4)_2•X + Ca^{2+}$, where X is the soil colloid exchanger, Ca•X is the adsorbed calcium, and NH_4^+ is ammonium ion in solution. This reaction can be rearranged to provide an equilibrium constant, K, as follows: $K_{eq} = [(NH_4)_2•X][Ca^{2+}] / [Ca•X][NH_4^+]^2$, which can be estimated with laboratory measurements of the amounts of adsorbed calcium, adsorbed ammonium, free calcium, and free ammonium ion at equilibrium. The implication of the reaction illustrated above is that ion exchange processes can potentially control the concentration of an ion in solution.

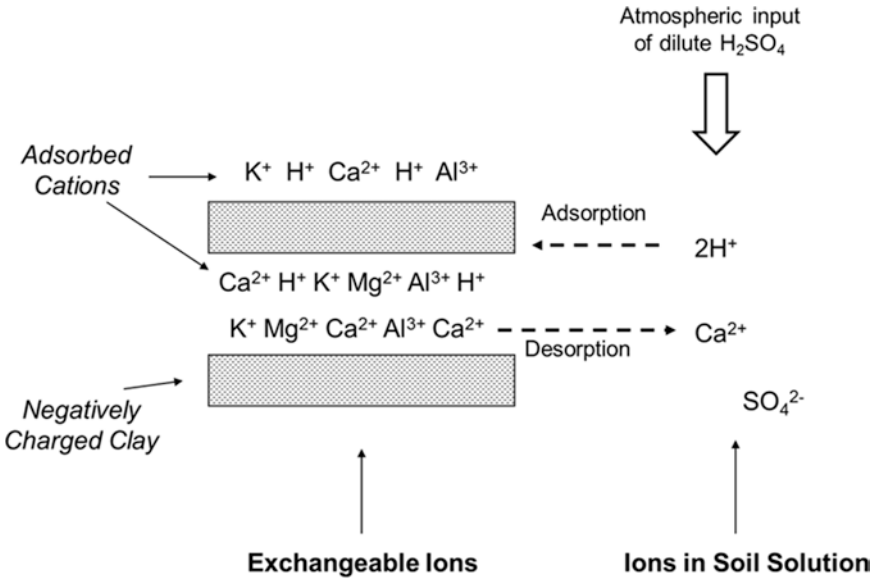

Fig. 2.10 Conceptual representation of ion exchange in the soil environment. In this example, cation leaching through the soil occurs in response to acidic precipitation inputs containing dilute H_2SO_4

It should be noted, however, that there are innumerable possible exchange reactions involving different soil colloids and cations that may help to determine the chemistry of the soil solution (Reuss 1983; Reuss and Walthall 1990).

Cation exchange processes in soils are characterized by a number of important chemical features. The rate of cation exchange is rapid, so that equilibrium is reached in a matter of seconds after the addition or removal of a cation from the system. The exchange process is also influenced by mass action, so that when the concentration of a cation in solution increases, the exchange reaction is pushed to the right, and there is an increase in the amount of the added cation that is adsorbed. Another aspect of cation exchange is that soil colloids exhibit differential selectivity toward cations, largely as a result of cation differences in **charge density** (the ratio of ionic charge to ionic radius). Thus, a highly charged ion that is relatively small will be more strongly attracted to an exchange surface than one that has a low charge density. Selectivity for exchangeable cation adsorption to clay minerals is described by the Lyotropic series shown below, and ranges from the weaker binding of some monovalent cations to the stronger binding of cations such as H^+ and Al^{3+}. It should be noted that cation selectivities may differ between clay minerals versus humic colloids.

Likelihood of replacement by another cation higher on the Lyotropic series

$$Li^+ \sim Na^+ > K^+ \sim NH_4^+ > Mg^{2+} > Ca^{2+} > Sr^{2+} \sim Ba^{2+} > H^+ > Al^{3+}$$

Lower charge density ---------- >> Higher charge density

Least affinity for *exchanger* *Greatest affinity* for *exchanger*

Anion adsorption commonly occurs in soils containing net positive surface charges on metal hydroxides, oxides, and **sesquioxides** such as $Fe(OH)_3$, Fe_2O_3, and Al_2O_3. The charge on these soil colloids originates when soil pH drops below the **zero point of charge** (ZPC) or isoelectric point for the metal colloid (Fig. 2.11); as a result, the surfaces become protonated. The impact of anion adsorption can be very dramatic – in one of our soil column leaching experiments, sulfate inputs of >300 $\mu mol_c\ L^{-1}$ were depleted by sulfate adsorption to less than 20 $\mu mol_c\ L^{-1}$ during infiltration through 50 cm of a sandy Adams soil from New Hampshire (Cronan 1985b).

The affinity of anions for positively charged soil surfaces varies, with stronger adsorption by phosphate and humic ligands, intermediate adsorption by sulfate and chloride, and lower adsorption affinity for nitrate and bicarbonate. In northern soils, much of the potential anion adsorption capacity may be masked by organic matter coatings originating from pedogenetic leaching of dissolved organic matter from the forest floor, followed by accumulation of **organo-metallic complexes** in the mineral soil. The presence of organic matter coatings can markedly diminish the effective anion adsorption capacity of a soil.

Investigators have found that the mobility of sulfate ion derived from acidic precipitation can be limited in forest soil solutions by pH-dependent sulfate adsorption processes. In soils where this occurs, leaching export of sulfate ions below the rooting zone is generally less than sulfate inputs from atmospheric deposition. An example of a sulfate adsorption isotherm is illustrated in Fig. 2.12 for a soil supporting mature Douglas-fir forest in Washington. The graph illustrates that as the soil is exposed to increasing concentrations of sulfate ion in solution, there is increased adsorption of sulfate by soil solid phase colloids such as Fe and Al oxides. It is also apparent that the B horizon in this soil profile adsorbs more sulfate than the A horizon, presumably because of illuvial accumulation of metal sesquioxides in this horizon.

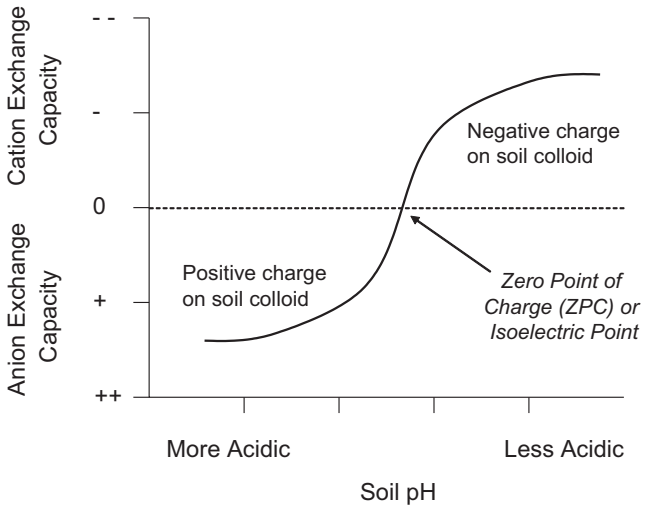

Fig. 2.11 Influence of pH and isoelectric point (zero point of charge) on cation and anion adsorption by soil colloids. Above the isoelectric point pH, the colloid becomes negatively charged and contributes to CEC

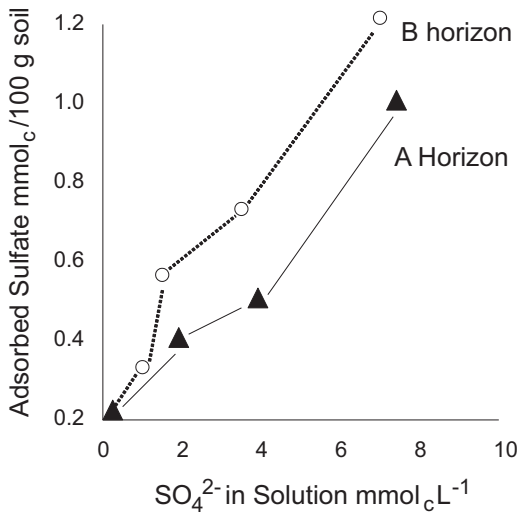

Fig. 2.12 Sulfate adsorption by an Everett soil in Washington as a function of equilibrium sulfate concentration (Reproduced with permission of Springer with data from Johnson DW, Cole DW (1977) Sulfate mobility in an outwash soil in western Washington. Water Air Soil Pollut 7:489–495. © 1977 by D. Reidel Publishing Company)

It is important to note that cation and anion adsorption processes are not mutually exclusive in the soil environment. In soils containing suitable mineral colloids where the pH is below about 5.0–5.5, anion adsorption sites can coexist with cation adsorption sites. Generally, the pH-dependent anion adsorption capacity will increase as a soil becomes more acidic; conversely, pH-dependent cation adsorption capacity increases as soil acidity decreases through liming or base addition.

Soil Ion Exchange Chemistry and Base Saturation

In evaluating a soil, it is important to determine the size of the cation or anion exchange capacities (CEC or AEC) and the composition of adsorbed ions on soil exchange sites. Soil **CEC** values are typically larger in neutral or slightly acidic soils with abundant clay or humus, whereas AEC values are generally higher in acidic soils with abundant Fe and Al oxides and limited organic matter coatings.

Soil CEC can be viewed as a "serving table" filled with a mixture of desirable nutrient cations and less desirable acidic cations. The percentage of CEC filled with nutrient **base cations** (Ca + Mg + K + Na) is referred to as the **base saturation** (% B.S.). Better soils are usually characterized by larger CEC values and higher percent base saturation levels (Fig. 2.13). Because base saturation is expressed as the ratio of the sum of base cations (in **charge equivalents**) divided by the CEC, it is important to specify whether the CEC term represents the ideal CEC estimated at pH 7.0 or the **effective CEC** estimated as the sum of total extractable cations at field pH. As implied in Fig. 2.13 and shown in Fig. 2.14, soil % B.S. exhibits a positive relationship with soil pH, although the relationships for organic O horizons and mineral horizons are offset considerably from each other. At the same base saturation, O horizons generally exhibit a much lower pH than mineral soil horizons from the same profile.

Figure 2.15 illustrates that cation exchange capacity (CEC) and base saturation (% B.S.) can change markedly moving vertically through a soil profile. In this example from a northern Spodosol, the highest CEC occurs in the organic O horizon, and this horizon also exhibits the highest concentrations of exchangeable nutrient cations. The next highest CEC occurs in the illuvial zone of the Bhs horizon where metals, organic matter, and clays have accumulated. This subsoil horizon is dominated by exchangeable acidity (H^+ and Al^{3+}), and contains very low concentrations of

exchangeable base cations. The other horizons illustrated in the figure – E, Bs1, Bs2, and C – all have much lower CEC values, are dominated by exchangeable acidity, and contain extremely low stores of exchangeable base cations.

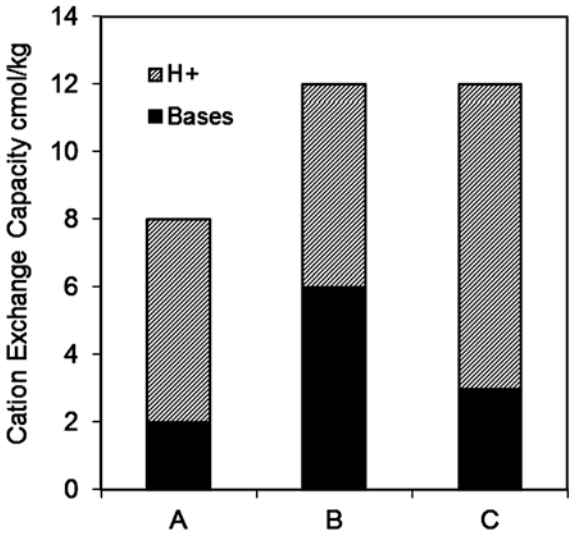

Soil	pH	CEC	% B.S.
A	4.8	8.0	25
B	5.8	12.0	50
C	5.0	12.0	25

Fig. 2.13 Comparison of soil pH, cation exchange capacity (CEC), and base saturation (% B.S.) for three contrasting theoretical soil samples. For any given CEC, soil pH tends to rise with increasing base saturation

Acidification

Soil acidification is an ongoing process that results from the acid attack of natural carbonic and organic acids released by plant and microbial metabolism, from hydrogen ions produced by plant roots, and from **strong acids** derived from either atmospheric pollution (acidic deposition) or microbial oxidative breakdown of reduced sulfur and nitrogen compounds in decaying organic matter. As soils acidify, exchangeable nutrient base cations (e.g., Ca^{2+}, Mg^{2+}, and K^{+}) are lost from the soil and are replaced by **exchangeable acidity** (measured as H^{+} and Al^{3+} ions extracted with 1 M KCl). The decline in soil base saturation over time makes it increasingly difficult for plants to acquire essential nutrients. Acidification processes may be counterbalanced to varying degrees by neutralization from rock weathering processes, by plant cycling of nutrients from less acidic to more acidic soil horizons, by atmospheric inputs of base cations, and by human applications of lime to a soil.

In a study of biogeochemical changes associated with stand development of loblolly pine on an old-field site in North Carolina, Richter et al. (1994) provided a striking example of rapid soil acidification and base depletion within a successional time frame. During the first three decades of pine growth, KCl-exchangeable acidity increased by 37 $kmol_c\ ha^{-1}$ in the upper 0.6 m of soil and exchangeable Ca and Mg decreased by 35 and 9 $kmol_c\ ha^{-1}$, respectively. In the uppermost 7.5 cm of soil, percent base saturation declined from ~70% to ~10% over the 30 yr time period.

Acidic deposition and intensive forest harvesting are two important anthropogenic processes that contribute to biotic stress in forest ecosystems by promoting soil acidification, depleting soil nutrients, and increasing the concentration of ionic aluminum in the soil solution. The resulting decline in

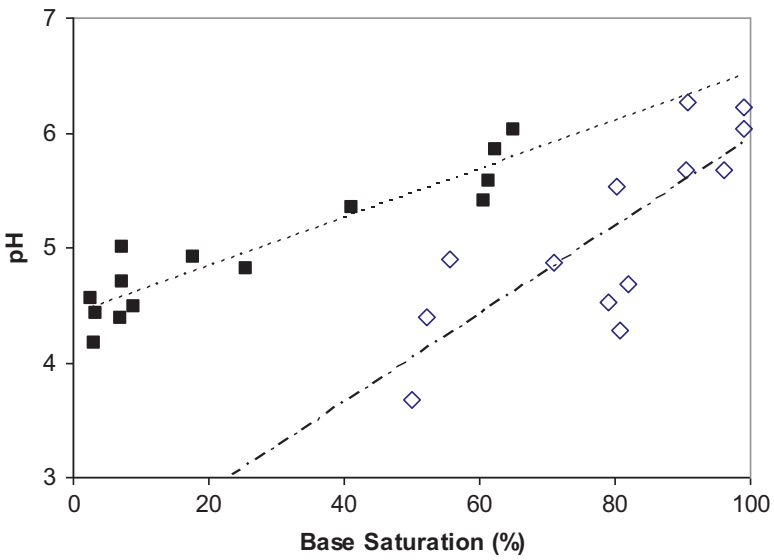

Fig. 2.14 Comparison of base saturation versus soil pH for O horizons (*open boxes*) and B horizons (*black boxes*) in a range of forest ecosystems. Note that O and B horizons both exhibit increasing pH as base saturation increases (Data from Cronan 1994)

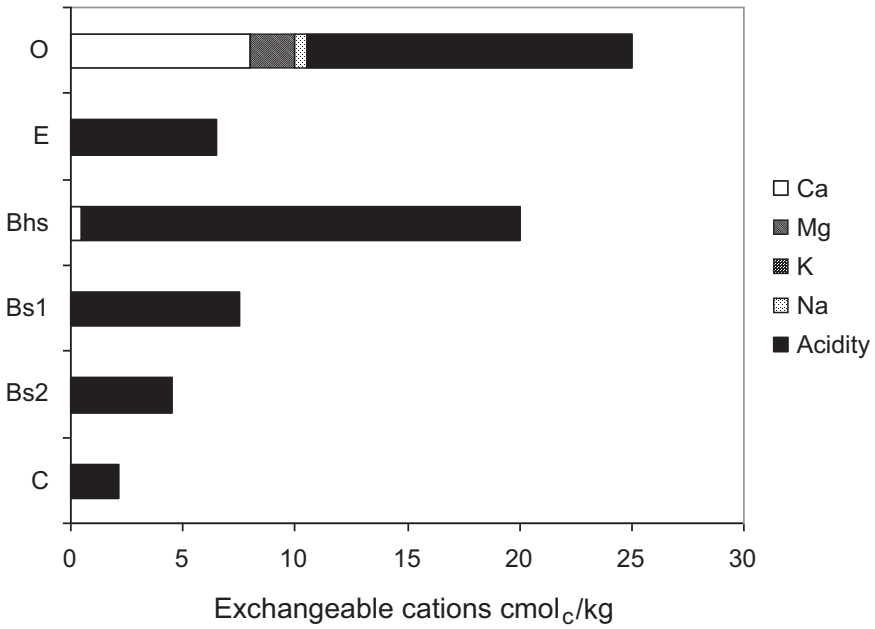

Fig. 2.15 Vertical soil profile showing CEC and relative proportions of exchangeable acidity and base cations for an Adirondack forest Spodosol (Cronan 1985a)

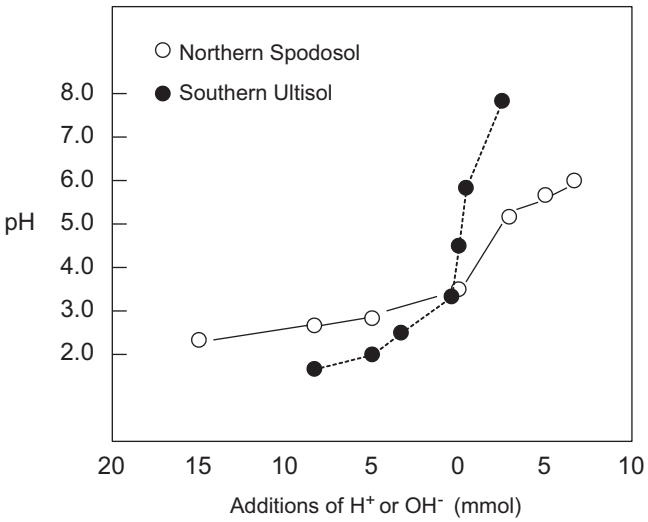

Fig. 2.16 Buffer capacity curves for mineral B horizons in a northern Spodosol from Big Moose, NY and a southern Ultisol from Camp Branch, TN (Data from Cronan et al. 1990)

the Ca/Al and Mg/Al ion ratios in the soil rhizosphere can impair plant community productivity through aluminum toxicity or as a result of calcium and magnesium deficiencies (Cronan and Grigal 1995).

Soil buffer capacity curves can be used to compare the resistance of different soils or horizons to pH changes or acidification. In Fig. 2.16, the much flatter response of the northern Spodosol B horizon to additions of strong acid or strong base indicates that it has a greater buffer capacity than the southern Ultisol B horizon. In other words, as a result of inherent organic and mineral proton buffering systems, the northern soil horizon exhibits much less change in pH in response to acidic or basic inputs.

Complexation

Dissolution and aqueous transport of metals in soils can be enhanced through **complexation** processes involving binding of an electronegative **ligand** with a metallic cation (see Chap. 1). Formation of soluble complexes containing single **coordinate bonds** results when the proton of an acidic functional group such as a carboxylic group is replaced by a metal ion, forming an organo-metallic complex. Simple complexes can also be formed between metals and inorganic anions such as F^- and SO_4^{2-}; in fact, acidic streams often contain inorganic complexes of aluminum fluoride and aluminum sulfate ($Al\text{-}F^{2+}$ and $AlSO_4^+$). Formation of a more stable **multi-dentate complex** or **chelate** is possible when an organic ligand provides two or more adjacent functional groups capable of bonding coordinately to a central metallic atom or ion (see Fig. 1.1). This can happen most readily when the organic ligand contains adjacent carboxyl groups (e.g., oxalic acid) or adjacent carboxyl and phenolic-OH groups (e.g., trihydroxybenzoic acid).

Complexation reactions are important in soil environments because they (i) increase the solubility and mobility of otherwise poorly soluble metals, and (ii) diminish the toxicity of metals such as aluminum and copper. Processes of eluviation and metal leaching in soils are often dominated by complexation reactions involving organic acids generated and released in the O horizon. Plants and microbes benefit

from complexation reactions, and are known to release organic ligands into the **rhizosphere** to improve availability of certain metals. Once formed, metal complexes may be subject to transport, transformation, and degradation.

Leaching

Soil leaching is a key process for element transport through the soil profile and into groundwater and surface waters. Leaching occurs when soluble ions or other solutes are removed from a substrate or soil micro-zone under the influence of water. The amounts and kinds of nutrients and other elements that move through this cycling pathway are determined by the interaction of a number of geochemical, biological, physical, and hydrologic factors. For example, the **mobile anion** nitrate may easily leach through soils and into streams during April snowmelt. However, once plant nutrient uptake resumes in the spring, nitrate leaching may cease completely, because of the efficient removal of nitrate from the soil solution by plant absorption and microbial immobilization. In contrast, chloride that enters an ecosystem from atmospheric deposition or road salting may freely leach through soils and into stream water year-round with minimal biological retention. The diagram in Fig. 2.10 provides a visual example showing the leaching of Ca^{2+} ion that results when inputs of acidic deposition to a soil displace exchangeable calcium from clays and humus, promoting transport or leaching of the soluble cation out of the rooting zone. In that illustration, we would expect increased cation leaching in response to increased inputs of acidic deposition.

Investigators have described three major soil leaching paradigms that predominate under different environmental conditions in the biosphere: (i) **carbonic acid leaching**; (ii) **organic acid leaching**; and (iii) **strong acid leaching** (Cronan et al. 1978; Johnson and Cole 1980). Each of these major types of acids has different characteristics, sources, sinks, and potential consequences for soil formation and ion transport through the soil profile. Carbonic acid leaching occurs in soils with pH greater than about 4.5–5.0, and involves relatively weak acid conditions with little complexation of trace metals such as iron and aluminum. Organic acid leaching often predominates in cool temperate, boreal, and montane forest soils and peats containing large amounts of decaying organic matter. The high concentrations of organic acids in these soils enhance the leaching of iron and aluminum through complexation reactions. A third group of soils includes those that are affected by strong acid leaching by sulfuric and nitric acids derived from anthropogenic pollution or natural sources of strong acids. Strong acid leaching can accelerate the losses of nutrient cations and the mobilization of trace elements such as aluminum in soils.

For each of these leaching regimes, it is important to recognize that the principles of ionic charge balance mentioned in Chap. 1 are observed. Molecules of each acid contain equivalent charges of H^+ and acid anions and as these acids react and interact with soil materials, cation and anion charge equivalents are maintained. Thus, adsorption of a mole of acid protons by soil colloids is balanced by a quantitative release of other cations from soil sources and/or a loss of anions to soil or biotic sinks.

Dissolution and Precipitation Reactions

Solute concentrations in a soil profile are controlled to varying degrees by solubility relationships involving **dissolution** and **precipitation** reactions. As an example, aluminum occurs abundantly in many soils as an insoluble aluminosilicate framework in primary minerals and clays. Under favorable acidic conditions, particularly when complexing organic acids are present, dissolution and complexation reactions can release aluminum into solution as a free ion (e.g., trivalent Al^{3+}) or complex. However, if the chemical activity of free aluminum increases enough or the solution pH rises and lowers the solubility of aluminum, then aluminum may precipitate from solution as a solid aluminum trihydroxide mineral such as gibbsite, $Al(OH)_3$. Similarly, in an arid soil, calcium dissolution and transport may occur in surface soil horizons during moist seasons, but Ca^{2+} ions may be removed from soil solutions during dry periods through precipitation of calcium carbonate, $CaCO_3$. Soil chemists often express the potential for precipitation or dissolution of a mineral in a given soil environment using a **saturation index**, which is based on the ion activity product of the aqueous **counter ions** of interest divided by the solubility constant of the solid mineral formed from those ions.

Lithic elements such as Ca, Mg, K, Na, Al, Si, Fe, and Mn that originate from primary minerals are strongly dependent on dissolution and weathering processes for their release into circulation within the biosphere. Each of these elements has a distinctive geochemical solubility that is differentially sensitive to changes in concentration, pH, and **redox** status. At one extreme, sodium ion is exceedingly soluble under a wide range of soil conditions. In contrast, iron solubility decreases as pH and pO_2 (partial pressure of oxygen) increase (e.g., as solution acidity decreases and the micro-environment becomes more oxidizing). Aluminum is distinctive in other ways, because it exhibits a parabolic pattern of pH-dependent solubility, with minimum solubility around pH 7 and exponential increases in Al solubility above and below pH 7. Consider how these differences in aqueous solubility might affect the mobilization, immobilization, and distribution of metals in a soil profile!

Besides metals described above, several other elements are strongly influenced by solubility relationships in soil environments. Phosphorus (P), as an example, forms relatively insoluble solid-phase precipitates with iron and aluminum. There is evidence that microbes and plants release organic acids into the rhizosphere in an effort to solubilize iron and/or aluminum from these precipitates, thereby enhancing bioavailability of P. In some soils, aluminum sulfate minerals are found, suggesting that these precipitates help to control the solubility of aluminum and sulfate. Anaerobic wetland soils may contain insoluble iron sulfide (FeS) that forms through precipitation of ferrous iron with sulfide derived from microbial sulfate reduction. The insoluble sulfur can eventually be mobilized if the soil is aerated and becomes oxidized in the presence of water.

Carbon is also affected by dissolution-precipitation reactions in the soil environment. In soils containing calcite ($CaCO_3$) or dolomite (Ca/Mg carbonate), dissolution processes can release inorganic carbonate species into solution. Likewise the precipitation of metal carbonate solid phases in the soil can remove inorganic carbon from solution. Soluble **humic substances** occur at high concentrations in surface horizons of many soils, but are stripped from solution in lower mineral soil horizons by both adsorption processes and precipitation reactions that generate insoluble metal-organic complexes and organo-mineral clay aggregates (Mayer and Xing 2001). Thus, both inorganic and organic carbon compounds can be influenced by precipitation reactions in soils.

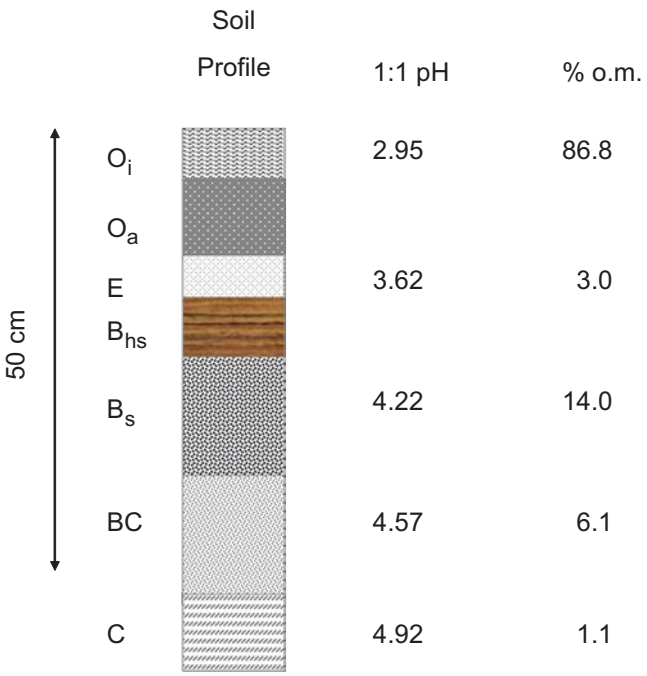

Fig. 2.17 Soil profile patterns for pH (1:1 soil and water) and organic matter in a northern Spodosol. For reference, the E horizon is 4 cm thick. (Cronan 1985a)

Comparative Analysis of Soil Chemical Properties

There are many lessons to be learned and insights to be gained by examining comparative soil data and trying to interpret the observed patterns and differences among contrasting soils and soil horizons. As an example, Fig. 2.17 illustrates the striking vertical profile development of a northern Spodosol, showing the distinctive changes in soil pH (1:1 in water) and soil organic matter content with depth. In this forest soil, pH rises two full units from the surface O horizon (at pH 2.95) to the subsurface C horizon (pH 4.92 at a depth of 50 cm below the surface). Presumably, this acidity gradient reflects the fact that acidic inputs to the O horizon are much greater than inputs of **acid neutralizing capacity** (ANC), whereas the C horizon is a zone with lower inputs of acidity relative to the generation of ANC. We also observe in this soil profile that organic matter concentration drops from 87% in the O horizon, to 3% in the eluvial E horizon, rises again to 14% in the upper B horizon, and declines to 1% in the parent material of the C horizon. How can we account for this pattern? In the O horizon, there are large annual inputs of organic detritus in the form of aboveground litter and fine roots that help to maintain a high concentration of organic matter. In the illuvial B horizon, organic matter enrichment results from two major processes: accumulation of soluble organic matter leached from the O horizon and death and turnover of fine roots within the B horizon.

Soil Exchange Chemistry

How do soils and horizons compare in terms of concentrations of exchangeable cations and other chemical parameters? For perspective, let's examine the inter-horizon differences in soil chemistry for a northern forest Spodosol from New York versus a southern Ultisol from a forest in Tennessee (Table 2.6). In both soils, there are striking contrasts in exchangeable cation concentrations, CEC, and percent base saturation between the surface O horizon and the subsoil B horizons. For example, exchangeable Ca is two orders of magnitude higher in the O horizon compared to the B2 horizon. Whereas O horizons from both forest ecosystems have base saturation values ranging from 50% to 85%, the mineral B2 horizons have base saturation values <10%. There is also an interesting contrast in cation stoichiometries between the northern and southern soils. In the B2t horizon of the southern Ultisol, exchangeable Ca is roughly one fifth as large as exchangeable Mg; in contrast, exchangeable Ca in the Bs2 horizon of the northern Spodosol is ten times larger than exchangeable Mg. Can you detect other interesting patterns of soil properties in Table 2.6?

Table 2.6 Comparison of soil chemical properties for a northern Spodosol at Big Moose, NY versus a southern Ultisol at Camp Branch, TN (Data from Cronan et al. 1990). Soil pH in water is abbreviated pH_w; CEC refers to soil cation exchange capacity; and % BS is percent base saturation

				Exchangeable cations in cmol(+)/kg							
	pH_w	%C	%N	Ca	Mg	K	Na	Al	H^+	CEC	%BS
Southern Soil horizon											
Oa	4.68	36.9	1.27	13.13	2.35	1.96	0.05	2.44	2.94	22.87	76
A1	4.11	11.4	0.48	1.52	0.53	0.85	0.02	3.01	2.18	8.11	35
E	4.53	1.1	0.05	0.03	0.03	0.09	0.005	2.93	1.29	4.375	4
B21	4.51	0.5	0.03	0.03	0.07	0.1	0.005	6.76	0.78	7.745	3
B2t	4.71	0.4	0.04	0.09	0.46	0.13	0.01	7.29	2.31	10.29	7
C	4.71	0.2	0.04	0.02	0.31	0.08	0.01	7.22	3	10.64	4
Northern Soil horizon											
Oi	4.84	46.9	2.13	27.9	2.81	1.79	0.05	2.65	2.97	38.17	85
Oa	3.68	46.3	2.02	13.99	1.45	0.61	0.04	3.62	12.33	32.04	50
E	3.97	2.6	0.15	0.43	0.05	0.05	0.01	1.99	0.63	3.16	17
Bhs	3.79	6.9	0.32	0.92	0.08	0.06	0.03	7.14	1.08	9.31	12
Bs2	4.38	6.2	0.26	0.29	0.02	0.02	0.01	4.25	0.42	5.01	7
C	4.82	0.8	0.03	0.02	0.002	0.007	0.002	0.69	0.001	0.722	5

Additional insights emerge if we expand our comparison to a range of soils from different regions. Figure 2.18 presents an interregional survey of soil exchange chemistry in a mildly acidic forest Inceptisol in North Carolina, an acidic Ultisol in Tennessee, and two acidic Spodosols from New York and Germany. As shown by the data, O horizons tend to exhibit high concentrations of exchangeable base cations and large CEC values; yet, organic horizons in different soils can vary greatly in relative proportions of acidity and base cations. The data in Fig. 2.18 also suggest that CEC values in mineral B horizons tend to be much lower compared to O horizons, and are typically dominated by exchangeable acidity (mostly in the form of exchangeable Al).

Soil Distributions of Aluminum

Depending upon the focus of a given biogeochemical investigation, it is sometimes important to develop more detailed information about specific forms of elements distributed through a soil profile. For example, a study of soil aluminum biogeochemistry might require an analysis of extractable soil aluminum pools in each soil horizon. As shown in Fig. 2.19, pools of exchangeable Al, organically bound Al, and amorphous Al hydroxides differ greatly among soil horizons and different soil types. Exchangeable Al, the most reactive form of soil Al, tends to comprise a small portion of the total soil storehouse of Al, whereas amorphous forms of Al oxides and hydroxides tend to be the largest pool of soil Al. In forest soils such as the two Spodosols in Fig. 2.19, total Al concentrations tend to reach maximum values in the B2 horizons, reflecting the influence of podzolization and illuviation processes on levels of soil Al in northern forest ecosystems. Given the contrasting patterns of soil Al distribution, we could explore a number of intriguing questions regarding Al biogeochemistry. How does the distribution of soil Al affect cycles of other elements and how stable are the distribution patterns? What are the residence times of the different Al fractions and are turnover rates for these forms of soil Al affected by environmental changes and disturbance?

Vertical Distributions of Organic Carbon, Nitrogen, and Phosphorus in Soils

Many soils contain large amounts of detrital and adsorbed carbon, nitrogen, and phosphorus. In previous literature reviews, Jobbagy and Jackson (2000, 2001) analyzed a large interregional data base of soil chemical properties and prepared a broad synthesis of vertical distribution patterns of C, N, and P in the upper 1 m of soil. As illustrated in Fig. 2.20, the investigators found that roughly 50% of soil organic carbon (SOC) in the upper 1 m of forest soils was stored within the uppermost 0–20 cm, with the remaining SOC declining steeply below that depth. Total SOC content in the upper 1 m of forest soils ranged two-fold from 9.3 in boreal forests to 18.6 kg C m^{-2} in tropical evergreen forests, and SOC values generally increased with precipitation amount and soil clay content (Jobbagy and Jackson 2000). Compared with that global data base, Huntington et al. (1988) estimated that total soil profile carbon content in the Becket soil at Hubbard Brook Experimental Forest, NH was approximately 16 kg C m^{-2}.

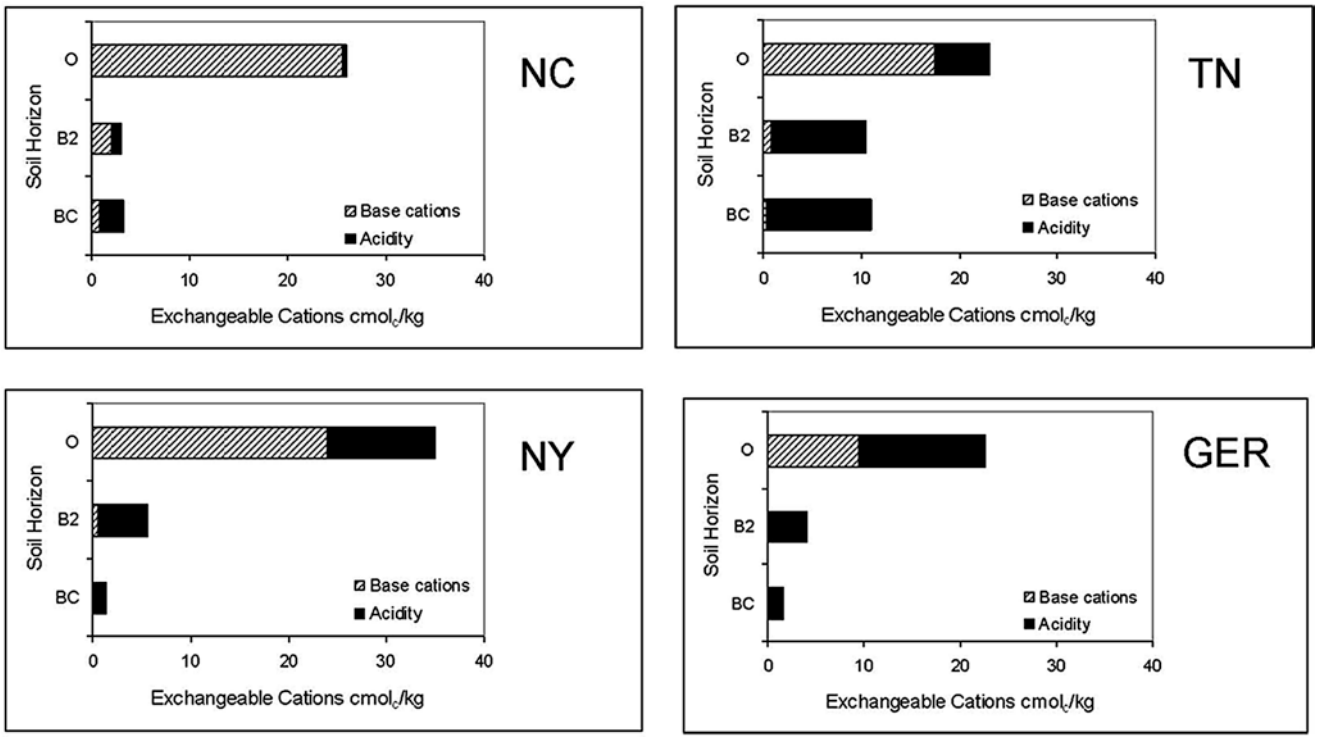

Fig. 2.18 Total exchange capacity and proportions of exchangeable base cations and exchangeable acidity in O and B horizons for a forest Inceptisol in North Carolina, an Ultisol in Tennessee, and forest Spodosols in New York and western Germany (Data from Cronan 1994)

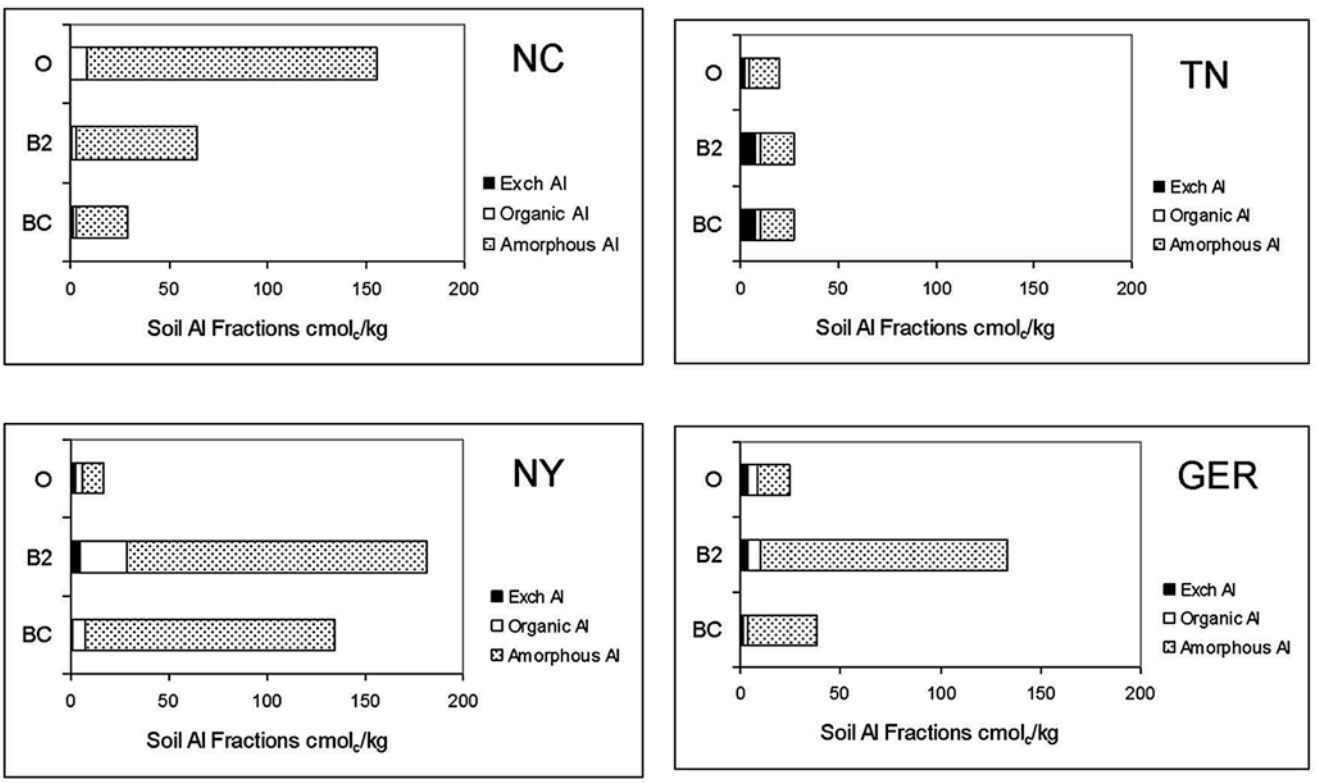

Fig. 2.19 Comparison of soil aluminum fractions by depth for organic and mineral soil horizons in a southern Inceptisol (NC), a southern Ultisol (TN), and two northern forest Spodosols (NY and GER). Stacked bars show concentrations of exchangeable Al, organically bound Al, and amorphous hydroxy Al in each horizon (From Cronan 1994)

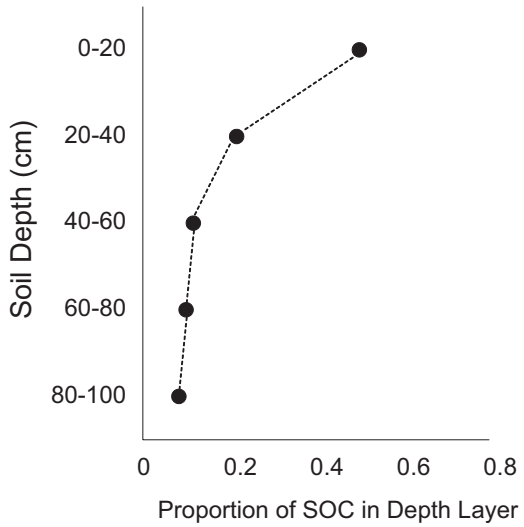

Fig. 2.20 Generalized vertical profile of soil organic carbon (SOC) content in the upper 1 m of a forest soil. Values are expressed as a fraction of the SOC pool in the entire 1 m depth (Data from Jobbagy and Jackson 2000)

In their examination of vertical depth profiles of other soil nutrients, Jobbagy and Jackson (2001) reported that roughly 40% of the N and P content of the top meter of soil was concentrated in the 0–20 cm depth for a wide range of soil series. A comparison of grassland Mollisols and warm temperate Ultisols indicated that extractable P in the upper 1 m of soil averaged 7.4 and 2.5 g m^{-2} for the two respective soils, whereas mean total N content was 1227 and 542 g m^{-2} in the two soils. For perspective, Huntington et al. (1988) estimated a total soil profile nitrogen content of 720 g N m^{-2} at Hubbard Brook Experimental Forest, NH.

Forms of Organic Nitrogen in Soils

There is broad research interest in the biogeochemical patterns of N distribution and turnover in soils. Unfortunately, many soil data sets in the literature include only estimates of total soil N concentration or total organic N concentration in a given soil horizon. How much soil N occurs in more versus less labile forms and how rapidly do these pools turnover? In their biogeochemical study of specific forms of organic N in the O_a horizon of a Swedish forest Spodosol, Johnsson et al. (1999) found that roughly 40% of the N was associated with amino acids + amino sugars, whereas most of the remaining soil N pool consisted of uncharacterized non-amino forms of N (Table 2.7). A related study of soil amino acid abundance along a forest fertility gradient in Michigan by Rothstein (2009) indicated that free amino acid N represented 2–39% of the total potentially plant-available N.

Table 2.7 Chemical characterization of O_a horizon organic matter from a Norway spruce (*Picea abies*) stand in Sweden (Data from Johnsson et al. 1999)

Parameter	Concentration (mg kg^{-1})
Total C	344,000
Total N	9970 ± 1130
Extractable NH_4^+	113 ± 9
Extractable NO_3^-	0.45 + 0.06
Total organic N	9860 ± 1124
Amino acid N	3540 ± 451
Amino sugar N	469 ± 77
Glucosamine	374 ± 61
Other forms of N	> 5137

Patterns of Soil Solution Chemistry

In addition to having variable patterns of solid phase chemistry, soil profiles also reveal striking differences in soil solution chemistry sampled with **lysimeters** or aqueous extraction. Figure 2.21 presents a comparison of solution chemistry sampled in the O and B horizons of the New York Spodosol shown in Fig. 2.18, along with stream water chemistry draining the same watershed. To the left of the figure, the flow diagram depicts the spatial sampling context for the three water samples. Each stacked bar provides a composite chemical description and proportions of ionic charge equivalents contributed by different soluble cations and anions in the O horizon, B horizon, and stream samples. It is clear that dynamic changes are observed moving through the vertical sampling gradient. For example, H^+ ion and nitrate concentrations decrease substantially from O horizon to stream runoff, whereas soluble Al peaks in the B horizon and declines in transit to the stream. What other changes do you see and how might you account for them?

If we next compare the B horizon solution from Fig. 2.21 with two contrasting B horizons from other geographic locations, it is possible to glimpse the range of biogeochemical differences that can be observed among soils in different environmental settings. In Fig. 2.22, the three soil solutions from B horizons in New York, Tennessee, and Germany vary in ionic concentrations by a factor of ten and exhibit considerable variation in chemical composition. How can we account for these differences?

As it turns out, the contrasting chemistries for soil solutions at the three sites depicted in Fig. 2.22 are largely the result of differences in soil solid phase chemistry, atmospheric inputs of sulfuric and nitric acids, and ion exchange and adsorption processes in each soil. For example, there is relatively little ionic leaching at the Tennessee watershed, because of the strong influence of plant nitrate absorption and soil sulfate adsorption in this southern Ultisol. When nitrate and sulfate ions are removed from infiltrating

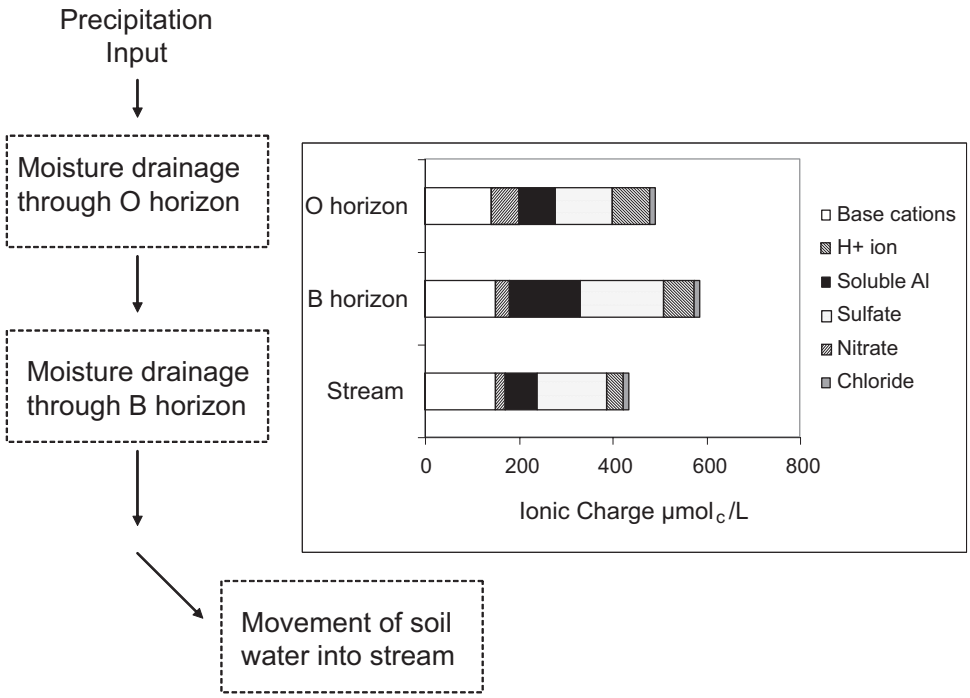

Fig. 2.21 Charge balance relationships for major cations and anions in soil solutions and stream water at Big Moose watershed, NY (Data from Cronan et al. 1990)

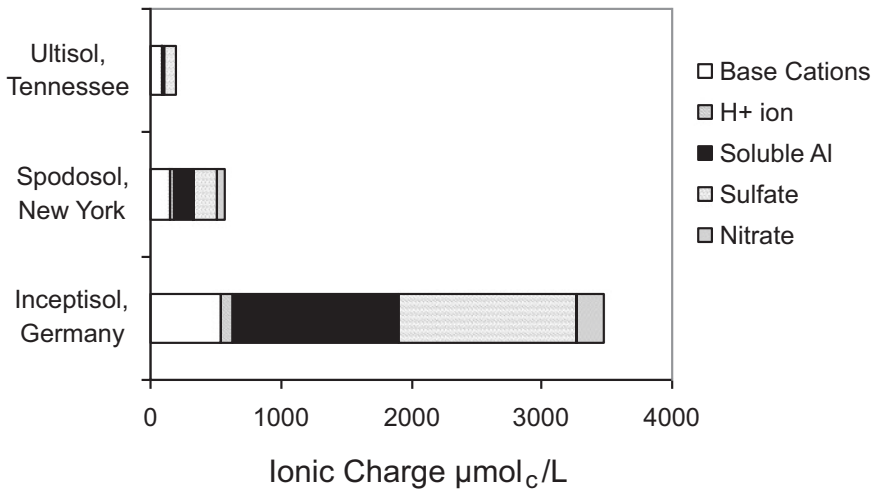

Fig. 2.22 Comparison of soil solution chemistries for acidic B horizons from a Tennessee Ultisol, a New York Spodosol, and a German Inceptisol exposed to respective sulfur deposition inputs of 20, 18, and 88 kg S ha^{-1} yr^{-1} (Data from Cronan 1994)

precipitation moisture, charge balance principles mandate a corresponding decrease in leaching of soluble cations derived from atmospheric deposition or soil cation exchange reactions. At the other extreme, the German site is a location with very large inputs of atmospheric sulfate (H_2SO_4) and nitrate (HNO_3) and limited retention of those mobile anions by soil adsorption and plant absorption processes. As a consequence, sulfuric and nitric acid inputs to the German forest soil generate substantial leaching of exchangeable soil cations released by H^+ exchange.

Note: Concepts of soil solution chemistry introduced in this chapter will be examined in further detail in Chap. 9.

Integrated Processes of Nutrient Supply and Storage in Soils

In concluding this chapter, we can note that soils provide a remarkable system of nutrient supply and storage based on integrated contributions from geologic and organic source materials. As depicted in Fig. 2.23, geologic materials serve both as a source of soluble nutrients and a substrate for the formation of clay minerals that contribute to ion exchange capacity. Likewise, detrital organic matter in the soil environment decomposes to release soluble nutrients, accompanied by the generation of soil humus that enriches the ion exchange capacity of the soil. As a whole, these processes and properties provide the basis for soil fertility and biological productivity.

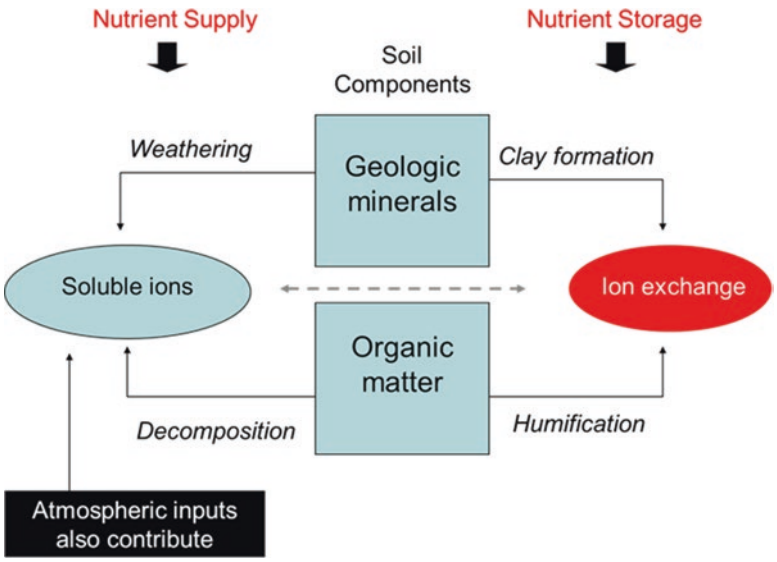

Fig. 2.23 A conceptual diagram illustrating how geologic and organic materials contribute to nutrient supply and nutrient storage in soils

Microbial Biogeochemistry

3

Introduction

The biogeochemical cycles of carbon, nitrogen, and sulfur are characterized by important gaseous pathways, biochemical transformations, **immobilization** processes, and **mineralization** reactions associated with microbial metabolism. Microbial organisms are thus important regulators of the source-sink behavior and cycling rates of these key elements in terrestrial and aquatic ecosystems. In addition, numerous other elements such as mercury, iron, and even phosphorus are affected either directly or indirectly by microbial exudation, respiration, assimilation, oxidation-reduction, methylation, and acidification processes. Taken as a whole, microscopic bacteria and fungi have critical roles in controlling element cycles in the biosphere.

The variable patterns of microbial biogeochemistry in the landscape are a reflection of complex microbial assemblages responding to distinctive environmental conditions. Communities of microbes in an ecosystem may include heterotrophic micro-organisms that use organic substrates for both their carbon and energy sources or **chemoautotrophic** organisms that utilize carbon dioxide as a carbon source and reduced inorganic substrates as an energy source. Whereas some microbes function as **obligate aerobes**, others may be **facultative** or strictly **anaerobic** organisms capable of exploiting **anoxic** conditions. In many cases, microbial biogeochemistry occurs in the context of a heterogeneous landscape mosaic containing a diversity of habitat conditions including uplands, lowlands, riparian zones, wetlands, and various aquatic systems. At any given location in the landscape, environmental conditions can vary in terms of temperature, moisture, aeration, oxidation-reduction status, metabolic substrates, local inorganic chemistry, and nutrient status. Microbial biogeochemical processes are sensitive to these environmental variations and may be restricted to specific habitats or micro-sites in the landscape. For example, microbes capable of producing methane (CH_4), hydrogen sulfide (H_2S), and nitrous oxide (N_2O) occur almost exclusively in wet anoxic soils; yet, the relative amounts of each gas released from anaerobic soils can vary considerably as a function of sulfate and nitrate availability, soil oxidation-reduction potential, iron availability, and the abundances of suitable metabolic carbon substrates. In the following chapter, we shall examine the roles of microbial processes in watershed biogeochemistry.

Redox Conditions

One of the major environmental constraints on microbial gas exchanges and transformations is the oxidation-reduction or **redox** potential of a substrate or micro-habitat. In chemical terms, oxidation is the donation of an electron, whereas reduction is electron reception. Substances that are oxidized become more deficient in electrons, and reduced substances become more electron rich. Theoretically, a reduced system will tend to lose electrons to an inert **platinum electrode** which will take on a negative charge. The redox potential

C.S. Cronan, *Ecosystem Biogeochemistry*, Springer Textbooks in Earth Sciences, Geography and Environment, DOI 10.1007/978-3-319-66444-6_3

Table 3.1 Variations in oxidation-reduction status of soils and sediments

Process	E_h (mV)	Microbes
Disappearance of O_2	400–800	Aerobic
Disappearance of NO_3^-	420	
Reduction of Mn^{4+}	400	Facultative anaerobic
Reduction of Fe^{3+}	−180	
Reduction of SO_4^{2-}	−215	Obligate anaerobic
Formation of H_2 and CH_4	−240	

Adapted from Stevenson (1986)

and measured $\mathbf{E_h}$ will consequently be low. If a system becomes more oxidized, electron activity will be lower, the charge on a platinum electrode will be more positive, and the estimated E_h will be higher.

As shown in Table 3.1, the redox potential, E_h, can range from aerobic or oxidizing conditions characterized by a positive E_h of several hundred millivolts to anoxic or reducing conditions characterized by an E_h as low as −240 mV. In aerated soils and sediments, oxygen is abundant and serves as the dominant oxidizer and terminal electron acceptor. When O_2 becomes depleted, electrons are passed to progressively weaker oxidizing agents such as nitrate (which is reduced to NO, N_2O, or N_2), ferric iron (which is reduced to ferrous iron), sulfate (which is reduced to sulfide), and carbon dioxide (which is reduced to methane). An example of a redox half reaction involving Fe can be illustrated as follows:

$$Fe^{3+} + e^- \leftrightarrow Fe^{2+}$$

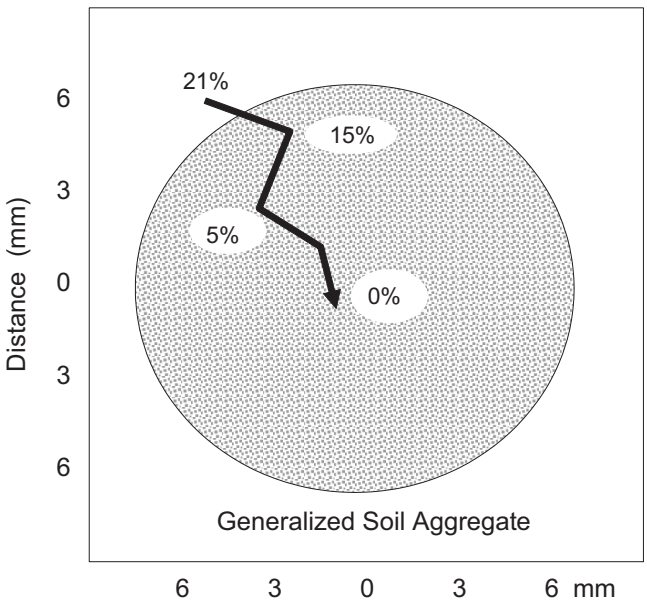

Fig. 3.1 Generalized cross section of oxygen concentrations within a saturated soil aggregate (Based on data from Sexstone et al. 1985)

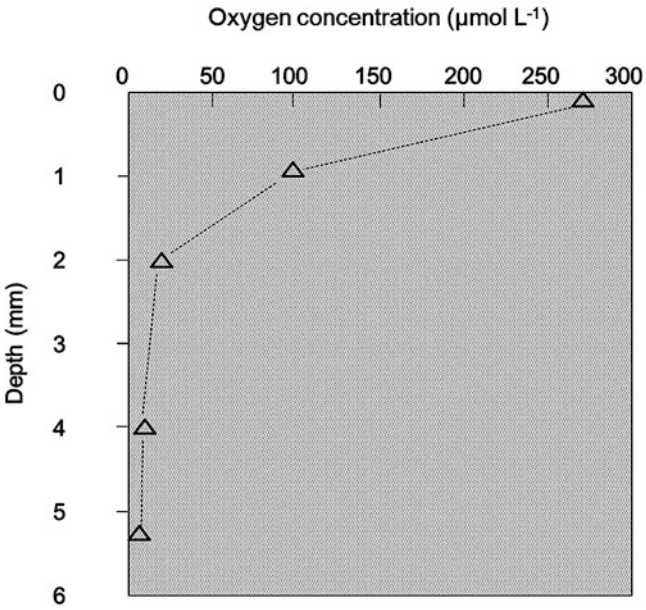

Fig. 3.2 Attenuation of O_2 with depth in a wetland soil (King 1996)

In general, anaerobic or reducing conditions occur in soils that are saturated with water and are deficient in oxygen. Such conditions are commonly observed in forested wetlands, bogs, marshes, and fens, and may also occur seasonally in lowland forests and fields. In addition, there is evidence that aerobic soils containing larger-sized soil aggregates can develop internal anaerobic micro-sites during wetter periods, permitting initiation of reducing processes within an otherwise well-drained, aerated soil. As an example, Sexstone et al. (1985) detected a pO_2 gradient ranging from 21% at the exterior to 0% at the interior of a soil aggregate measuring roughly 1 cm in diameter (Fig. 3.1). King (1996) examined a vertical gradient or micro-profile of O_2 concentrations in a saturated wetland soil and found that pO_2 declined exponentially within the upper 1–3 mm of peat (Fig. 3.2).

Microbial Nitrogen Transformations

The diagram in Fig. 3.3 illustrates the primary pathways and processes by which microbes participate in nitrogen cycling within a watershed ecosystem. In the next section, we shall examine how each of these processes contributes to the biogeochemistry of N.

Nitrogen Fixation

Atmospheric **nitrogen fixation** by symbiotic *Rhizobium* bacteria, the actinomycete genus *Frankia*, and blue-green

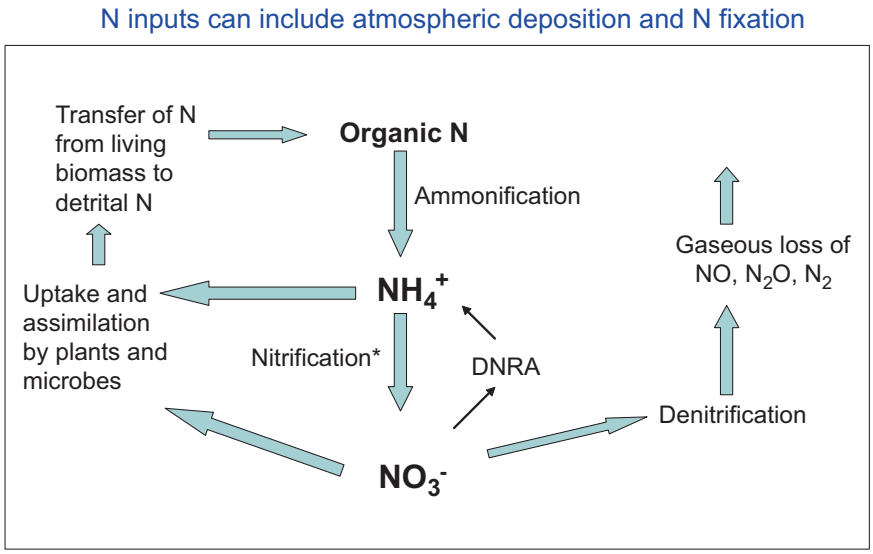

Fig. 3.3 Conceptual diagram of N cycling processes associated with soil microbes

Cyanobacteria (e.g., *Trichodesmium*) contributes substantial amounts of reduced nitrogen to the global nitrogen cycle (Vitousek et al. 1997), with local N fixation rates by free-living or symbiotic microbes ranging up to 150 kg N ha^{-1} yr^{-1} or more. Although legumes such as clover and soybeans are well-known as hosts for N fixation activities, less well recognized are the N-fixing lichens (e.g., *Lobaria* and *Peltigera*) and the N-fixing woody shrubs and trees such as *Casuarina*, *Alnus* (alder), and *Myrica* (bayberry) that serve as hosts for **actinorhizal** *Frankia*, a bacterial genus characterized by filamentous mycelia and tolerance to acidic soils.

The basic overall reaction for biological fixation of atmospheric dinitrogen is shown below:

$$N_2 + 8e^- + 8H^+ + 16\,ATP \xrightarrow[+Mg^{2+}]{} 2NH_3 + H_2 + 16\,ADP + 16\,P_i$$

where ATP is adenosine triphosphate, P_i is inorganic phosphate, and Mg^{2+} ion is required as a co-factor. The ammonia resulting from N fixation is typically incorporated into glutamine or glutamate, which serve as a precursor for numerous secondary pathways leading to the synthesis of enzymes and proteins.

The energy-intensive process of N fixation is catalyzed by the enzyme **nitrogenase**, which has two component proteins: protein I, an iron-molybdenum protein, and protein II, an iron protein. We thus see that magnesium and two trace metals - iron and molybdenum - play an indispensable role in facilitating N fixation. Because the enzyme nitrogenase is inactivated or destroyed by oxygen, the process of N fixation requires a mechanism for limiting oxygen penetration to the reaction center. N fixation is also sensitive to external concentrations of inorganic N; rates of this process decline when ammonium concentrations in the **rhizosphere** increase to levels that are sufficient for normal plant nutrition.

Investigators have estimated rates of N-fixation in the field using a chamber incubation technique in which soil microbes are exposed to acetylene gas, which diffuses to the N-fixation reaction sites and is reduced to ethylene in the presence of the nitrogenase enzyme. The resulting ethylene is then quantified by gas chromatography to provide an estimate of the potential *in situ* rate of N-fixation, assuming a theoretical conversion ratio of 4 C_2H_4: 1 N_2 (Schwintzer and Tjepkema 1994). Field studies in the Pacific Northwest using acetylene reduction assays have estimated N fixation rates ranging from 17 kg N ha^{-1} yr^{-1} in mixed stands of alder and Douglas-fir to 150 kg N ha^{-1} yr^{-1} in pure stands of alder (Binkley 1981; Heilman and Ekuan 1982). In contrast, Barkmann and Schwintzer (1998) found that N-fixation rates in pine forests in Maine were <0.1 kg N ha^{-1} yr^{-1}, and Roskowski (1975) reported that microbial N-fixation in decaying woody litter in a New Hampshire northern hardwood forest was 1 kg N ha^{-1} yr^{-1} or less. In Costa Rica, rates of N-fixation ranged from mean values of 1.2 kg N ha^{-1} yr^{-1} in primary tropical rain forests to 14.2 kg N ha^{-1} yr^{-1} in secondary rain forest habitats (Sullivan et al. 2014).

Vitousek and Walker (1989) studied forest stands at Hawaiian Volcanoes National Park to determine whether invasion by an exotic actinorhizal N-fixing tree (*Myrica faya*) changes the availability of nitrogen in young volcanic sites, thereby altering ecosystem conditions and future suc-

cessional patterns and processes. Their results indicated that low N availability normally limits plant growth at volcanic early successional sites, but that N-fixation by *Myrica faya* greatly increases overall N inputs to these forest stands. At sites with native vegetation, annual N inputs from atmospheric deposition and minor amounts of N fixation amount to 4–5 kg N ha^{-1} yr^{-1}. By comparison, stands with *Myrica* exhibit annual N inputs of roughly 18 kg N ha^{-1} yr^{-1} from N fixation plus 4–5 kg N ha^{-1} yr^{-1} from atmospheric deposition. Thus, invasion by the N-fixing tree species causes a four to five-fold increase in annual inputs of N that enhances biological availability of N and site productivity. The authors concluded that these changes in N cycling alter ecosystem-level properties and subsequent ecosystem development at these Hawaiian volcanic sites.

Mineralization or Ammonification

Mineralization is broadly defined as a microbial decomposition process in which organically bound elements in detritus are converted to soluble inorganic ions. In the nitrogen cycle, the initial stage of mineralization is termed **ammonification**. This is a microbial process in which amino N groups ($-NH_2$) in decaying organic matter are subjected to enzymatic hydrolysis, releasing ammonia (which is quickly converted to ammonium in acidic soils). The fate of the free ammonium ion may include uptake by plants, utilization by microbes, adsorption onto cation exchange sites, or leaching transport through the soil profile. Where soil conditions are not acidic, emissions of volatile ammonia gas can result from N mineralization.

$$\underset{\textit{Organic amino N}}{R-NH_2}+H_2O \xrightarrow[\text{enzymatic hydrolysis}]{} R-OH+NH_3+\text{energy} \qquad (3.1)$$

$$NH_3+H^+ \leftrightarrow NH_4^+ \quad (\text{favored at pH} < 7) \qquad (3.2)$$

Rates of soil ammonification have been estimated in the field and laboratory using stable isotope tracers for **gross mineralization** patterns (Davidson et al. 1992) and sequential extraction of soils with KCl to determine **net mineralization** rates (Strader et al. 1989), where gross mineralization – **immobilization** = net mineralization. Net mineralization is operationally defined as the increase in KCl-extractable NH_4-N over a fixed time period, plus any net increase in extractable NO_3-N. Studies of forests in the Sierra Nevada Mts. of California indicated that rates of net N mineralization ranged from 16 to 37 kg N ha^{-1} yr^{-1}, whereas gross N mineralization rates were roughly 7 times higher (Hart and Firestone 1989; Davidson et al. 1992). As such, these data imply that microbial immobilization of mineralized N is very substantial. Rates of net N mineralization in spruce-fir forests of the southern Appalachian Mts. ranged from 26 to 180 kg N ha^{-1} yr^{-1} (Strader et al. 1989), compared with rates of 143 kg N ha^{-1} yr^{-1} in northern hardwood forest plots in Michigan (Holmes and Zak 1994) and rates of 121 kg N ha^{-1} yr^{-1} in black cherry-sugar maple forest plots in Pennsylvania (Bowden et al. 2000). Net N mineralization in well-decayed downed tree boles in old-growth Douglas-fir/western hemlock/western red cedar stands in the Oregon Cascades contributed up to 2.5 kg N ha^{-1} yr^{-1} to the soil pool of available inorganic N (Hart 1999).

Given the wide range of estimates noted above, one might ask if there is evidence that observed variations in N mineralization rates are related to measurable environmental variables. Reich et al. (1997) reported that N mineralization rates in 27 hardwood and conifer stands in Wisconsin and Minnesota were significantly correlated with soil texture (percent silt + clay), total litterfall N, and mean annual temperature. Booth et al. (2005) examined N cycling results from 100 different terrestrial studies and concluded that gross N mineralization is positively correlated with microbial biomass and soil C and N concentrations, and is inversely related to soil C:N ratio (after correction for differences in soil C).

Nitrogen Immobilization

Whereas mineralization refers to microbial release of inorganic N from organically-bound detrital N, immobilization is the incorporation of nitrate-N and ammonium-N into microbial biomass. When soil microbes immobilize N, it is unavailable for plants and other microbial competitors. As we shall see later, the term immobilization can be applied more broadly to other elements assimilated into microbial biomass.

Patterns of microbial N immobilization have been examined under a range of conditions. Perakis and Hedin (2001) found that efficient long-term retention of N in unpolluted old-growth forests in southern Chile is promoted by rapid assimilation and turnover of NH_4^+ and NO_3^- through microbial biomass in the short term, followed by transfer from microbial biomass into plant and soil organic matter pools. Similar results were reported by Zogg et al. (2000), who found that cycling of N through microorganisms appears to be the major short-term factor influencing patterns of nitrate retention in a Michigan northern hardwoods forest. Holmes and Zak (1999) compared northern hardwood forest stands in Michigan, and reported rates of microbial immobilization ranging from ~0.05 to 0.4 kg NH_4-N ha^{-1} d^{-1} and 0.02 to 0.7 kg NO_3-N ha^{-1} d^{-1}. By comparison, gross mineralization rates in the same study ranged from about 0.5 to 1.8 kg N ha^{-1} d^{-1}. Bardgett et al. (2003) used ^{15}N amendments to compare microbial and plant competition for inorganic and organic N substrates in temperate grasslands. In low pro-

ductivity grasslands, the bulk of the added ^{15}N was immobilized by microbial biomass, and was not immediately available to plants.

Nitrification

Once ammonium ion is released or is added to the soil rhizosphere, there is vigorous competition among plants and microbes for the NH_4^+ substrate. Chemoautotrophic bacteria (e.g., *Nitrosomonas* and *Nitrobacter*), heterotrophic bacteria, and fungi are able to oxidize ammonium to nitrate through the process of **nitrification** illustrated at the end of this paragraph (Santoro 2016). Chemoautotrophic nitrifiers tend to predominate in managed agricultural soils with pH values >6.0, whereas heterotrophic microbes (especially fungi such as *Aspergillus*) appear to be the dominant microorganisms responsible for nitrification in acidic forest soils. It should be noted, however, that some investigators have found that chemoautotrophic nitrifiers are more common in acidic soils than previously reported (DeBoer and Kowalchuck 2001). All groups of nitrifying microbes require adequate oxygen and ammonium substrate for efficient nitrification; even when these conditions are met, some soils contain soluble phenolic compounds that inhibit nitrification (Olson and Reiners 1983).

$$NH_4^+ + 1.5O_2 \xrightarrow[\text{enzymatic oxidation}]{} NO_2^- + H_2O + 2H^+ + \text{energy} \quad (3.3)$$

$$NO_2^- + 0.5O_2 \xrightarrow[\text{enzymatic oxidation}]{} NO_3^- + \text{energy} \quad (3.4)$$

Nitrification is a key biogeochemical process that not only serves as a potentially large source of acidity, but also mediates the conversion of a **conservative** cation, NH_4^+, into a mobile anion, NO_3^-, that readily leaches through soils in the absence of plant uptake or denitrification. As an example, in the aftermath of a clear-cut logging experiment at Hubbard Brook Experimental Forest, NH, soil nitrification rates increased dramatically, causing a large pulse of soil and stream acidification and nitrate leaching (Bormann et al. 1974). This response was apparently caused by an accumulation of ammonium substrate in the absence of plant uptake, thus providing a **priming effect** for nitrifying microbes.

Many investigators have examined *in situ* nitrification processes in terrestrial ecosystems. Rates of net nitrification in conifer forests of the Sierra Nevada Mts. in California ranged from 5 to 42 kg N ha^{-1} yr^{-1} in a study by Hart and Firestone (1989), and gross nitrification rates were as much as 10–20 times greater at the same sites (Davidson et al. 1992). Strader et al. (1989) reported net soil nitrification rates in spruce-fir forests of the southern Appalachian Mts. ranging from roughly 8 to 80 kg N ha^{-1} yr^{-1}, compared with rates of 54 to 148 kg NO_3-N ha^{-1} yr^{-1} in northern hardwood

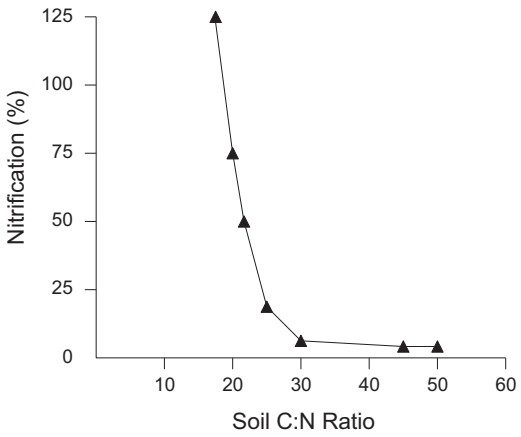

Fig. 3.4 General trend of percent nitrification in combined mineral and organic soils as a function of soil C:N ratio. From Aber, J.D., C.L. Goodale, S.V. Ollinger, M.L. Smith, A.H. Magill, M.E. Martin, R.A. Hallett, and J.L. Stoddard. 2003. Is nitrogen deposition altering the nitrogen status of northeastern forests? BioScience 53:375–389 by permission of the American Institute of Biological Sciences

forest plots in Michigan (Holmes and Zak 1994) and rates of 86 kg NO_3-N ha^{-1} yr^{-1} in black cherry-sugar maple stands in Pennsylvania (Bowden et al. 2000). In an investigation of landscape patterns of net nitrification in a northern hardwood-conifer forest in New Hampshire, Venterea et al. (2003) found that rates varied by a factor of 150 across the forest as a function of biotic and abiotic parameters such as elevation, exposure, and dominant species. When intact forest soil columns were exposed to simulated rainfall inputs, Cronan (1985b) found that net leaching exports of NO_3-N generated by internal nitrification processes reached levels as high as 515 kg N ha^{-1} yr^{-1} (under conditions where plant uptake was zero). Overall, evidence from field and lab investigations indicates that there is a large potential for nitrification by soil microbes in many soils (Barnes et al. 2008).

Efforts to understand environmental variations in nitrification rates have met with mixed success. In reviewing 100 different studies of N cycling, Booth et al. (2005) found that there was no clear effect of pH on soil nitrification and no significant relationship between nitrification and soil C:N ratios. In contrast, studies by Aber et al. (2003) in New England demonstrated a threshold response, with increasing percent nitrification (net nitrification/net mineralization) in forest soils with C:N ratios less than 25 to 30 (Fig. 3.4). The apparent discrepancy between these two reports may perhaps be explained by the use of a ratio of nitrification/mineralization by Aber et al. (2003). Since mineralization tends to be inversely related to C:N ratio (Booth et al. 2005), its use in the denominator by Aber et al. (2003) may have dampened the scatter that would otherwise be found using absolute nitrification rate as the dependent variable.

One of the surprising additional features of microbial nitrification is the fact that this process can also contribute

to the production of nitrous oxide, N_2O (Bremner 1997), and nitric oxide, NO (Davidson et al. 1993) – gases that are normally associated with **denitrification**. As an example, Panek et al. (2000) compared rates of N_2O production from denitrification versus nitrification in a Mexican wheat field, and reported that each process contributed equally to total N_2O gaseous losses over a 4-week period, with nitrification increasing in relative importance as soils drained and became aerated.

As a final note regarding ammonification and nitrification, we should take a moment to explore more fully how the technique of **isotope dilution** provides a tool for elucidating gross versus net rates of mineralization. With the dilution technique, a soil is initially enriched with a concentrated pulse or spike of ^{15}N-labelled nitrate and ammonium salts dissolved in an aqueous medium. After an incubation period, the soil is then sampled to quantify how the finite initial amount of ^{15}N added as nitrate or ammonium has been diluted by subsequent inputs of $^{14}NO_3^-$ and $^{14}NH_4^+$ ions generated *in situ* by microbial mineralization and nitrification of organic matter. The rate of gross mineralization is calculated from the ‰ decline in ^{15}N enrichment of the NH_4^+ pool during an incubation period of 24 hr., whereas gross nitrification is calculated from the ‰ decline in ^{15}N enrichment of the soil NO_3^- pool (Davidson et al. 1991).

Denitrification

In some ecosystems, the annual nitrogen budget of inputs and outputs may include losses of nitrate ions that cannot be fully accounted for in terms of biological assimilation or leaching fluxes. Instead, the apparent imbalance of N inputs and outputs reflects denitrification losses of gaseous N from the system (Morse et al. 2015). **Denitrification** is a microbial process that occurs in poorly aerated and anoxic environments, causing reduction of nitrate ions and evolution of gaseous nitrogen species (Anderson et al. 2015). Estimates of denitrification rates in field soils generally range from roughly 1 to 15 kg N ha^{-1} yr^{-1}. Common microbial denitrifiers include the bacterial genera *Bacillus*, *Pseudomonas,* and *Thiobacillus*. These denitrifying bacteria potentially compete for nitrate substrate with plants, heterotrophic microbes, and fermentative bacteria capable of reducing nitrate to ammonium via dissimilatory nitrate reduction (discussed in the next section). The overall reaction for denitrification can be expressed as follows:

$$2NO_3^- + 12H^+ + 10e^- \rightarrow\rightarrow\rightarrow\rightarrow N_2 + 6H_2O$$

However, that simplified reaction pathway ignores several important intermediates that are illustrated below (where the oxidation state or valence of N is shown in parenthesis):

$$\underset{\text{nitrate}}{\underset{N(+5)}{NO_3^-}} \rightarrow\rightarrow \underset{\text{nitrite}}{\underset{N(+3)}{NO_2^-}} \rightarrow\rightarrow \underset{\text{nitric oxide}}{\underset{N(+2)}{NO}} \rightarrow\rightarrow \underset{\text{nitrous oxide}}{\underset{N(+1)}{N_2O}} \rightarrow\rightarrow \underset{\text{dinitrogen}}{\underset{N(0)}{N_2}}$$

What is apparent in the more detailed pathway is the fact that denitrification not only removes nitrate from solution, but also results in the release of up to three volatile nitrogen species: nitric oxide, nitrous oxide, and dinitrogen. Because nitric oxide and nitrous oxide are active atmospheric trace gases that influence smog formation, ozone depletion, and greenhouse warming potential, there is a great need for quantitative understanding of the rates at which gaseous nitrogen species are generated by denitrification under various environmental conditions (Galloway et al. 2003; Boyer et al. 2006; Weintraub et al. 2014).

Firestone et al. (1980) noted that denitrification can serve as either a major source for N_2O or as a sink for the gas, through reduction of N_2O to N_2. Their experiments showed that increased concentrations of nitrate, nitrite, and molecular oxygen enhanced production of nitrous oxide relative to molecular nitrogen during denitrification in soils. The ratio of nitrous oxide to molecular nitrogen production also increased in acidic soils (pH 4.9 vs. 6.5) amended with added nitrate.

Cultivated ecosystems have been identified as the single most important source of anthropogenic N_2O (IPCC 1992), and some of the highest gaseous fluxes of N_2O to the atmosphere have been measured in irrigated and fertilized agricultural systems. For example, Matson et al. (1998) reported that Mexican wheat fields fertilized with 250 kg N ha^{-1} exhibited annual gaseous emissions of N_2O plus NO amounting to 12 to 16 kg N ha^{-1}. In comparison, Holmes and Zak (1999) examined a northern hardwood forest in Michigan, and reported denitrification rates ranging from 0.6 to 6.5 kg N ha^{-1} yr^{-1} in soils characterized by annual net N mineralization rates of 137 kg N ha^{-1} yr^{-1}. Davidson et al. (1998) estimated that NO emissions resulting from denitrification plus nitrification in the southeastern U.S. were 8.8 kg NO-N ha^{-1} yr^{-1} for cultivated land, compared with <10% that rate for forested and uncultivated land. In the Great Plains of the western U.S., Kaye et al. (2004) estimated that urban lawns occupied 6.4% of their 1578 km^2 study region, but exerted a disproportionate impact on trace gas exchanges, contributing up to 30% of regional N_2O emissions. Aquatic scientists have also found high rates of denitrification in the riparian soil-stream interface where drainage inputs of soluble C and nitrate ions support denitrifying microbes (Hedin et al. 1998; Jacinthe et al. 1998). Methods for estimating denitrification rates have been compared by Kulkarni et al. (2014).

Dissimilatory Nitrate Reduction to Ammonium (DNRA)

As noted in Fig. 3.3, nitrate ions may be reduced to ammonium ions via a **dissimilatory nitrate reduction** pathway (Firestone et al. 1980; Tiedje et al. 1982). Under anaerobic soil conditions, especially with elevated nitrate concentrations and a high ratio of available C relative to electron acceptors, facultative and obligate fermentative bacteria can apparently reduce NO_3^- ions to NH_4^+. Intermediate gaseous products in this process can include N_2O and NO_2 (Firestone et al. 1980; Silver et al. 2001). In a study of tropical soils in Puerto Rico, Silver et al. (2001) found that rates of DNRA averaged 0.6 μg g^{-1} d^{-1} and accounted for 75% of the microbial turnover of the soil nitrate pool. Thus, in that study, the potential daily rate of DNRA was high enough to reduce 0.6 g NO_3-N per 1000 kg of soil. Given that a typical cultivated soil contains roughly 2 million kg in a hectare-furrow slice 15 cm deep (Brady 1984), this DNRA rate translates into a ballpark value of 1.2 kg N ha^{-1} d^{-1}.

Assimilatory Nitrate Reduction

Microbes and other living organisms that absorb nitrate ions as a source of N for metabolism and growth rely on **assimilatory nitrate reduction** in order to generate the reduced amino nitrogen required for protein synthesis. This energy-intensive intracellular process serves not so much as an electron sink, but rather as a source of precursors for amino acid production. In the reaction pathway that follows, we see that (i) nitrogen changes from an oxidation state of +5 in the nitrate reactant to a final oxidation state of −3 in the reaction product; and (ii) the ammonium resulting from assimilatory nitrate reduction is shunted through the glutamine pathway as a point of entry for synthesis of amino acids and proteins.

$$NO_3^- + 8e^- + 10H^+ \xrightarrow[\text{Catalyzed by nitrate reductase}]{} NH_4^+ + 3H_2O \xrightarrow{\text{glutamine synthesis}}$$

Microbial Sulfur Transformations

Mineralization of Organic Sulfur

Sulfur (S) primarily occurs in organic matter as sulfate **esters** (R-O-SO_3) and as **carbon-bonded sulfur** in the form of sulfhydryl groups (-HS) and disulfide bridges (-S-S-). Examples of carbon-bonded sulfur compounds include methionine and cysteine (Fig. 3.5), whereas ester sulfate compounds include examples such as choline sulfate and phenolic sulfate.

During the decomposition of detritus, organic reduced sulfur is mineralized by microbes through an enzymatic oxidation process illustrated below (where R-HS represents a generic organic compound).

$$R - HS + 2O_2 \xrightarrow[\text{enzymatic oxidation}]{} SO_4^{2-} + H^+ + \text{residual detritus} + \text{energy}$$

As indicated on the right side of the unbalanced reaction, the oxidation of reduced organic sulfur yields sulfuric acid that is either assimilated, reacts with soil minerals, or contributes to acidification of the environment. When waterlogged wetland peats are drained, there is often a large pulse of acidity that results from aeration and oxidation of the stored organic sulfur (and iron sulfide compounds).

The hydrolysis of ester sulfates in decomposing organic matter occurs when the O-S bond is split by sulfatase enzymes, resulting in formation of an alcohol plus sulfuric acid. The unbalanced reaction can be briefly summarized as follows:

$$R - O - SO_3^- + H_2O \xrightarrow[\textit{Catalyzed by sulfatase}]{} ROH + H^+ + SO_4^{2-}$$

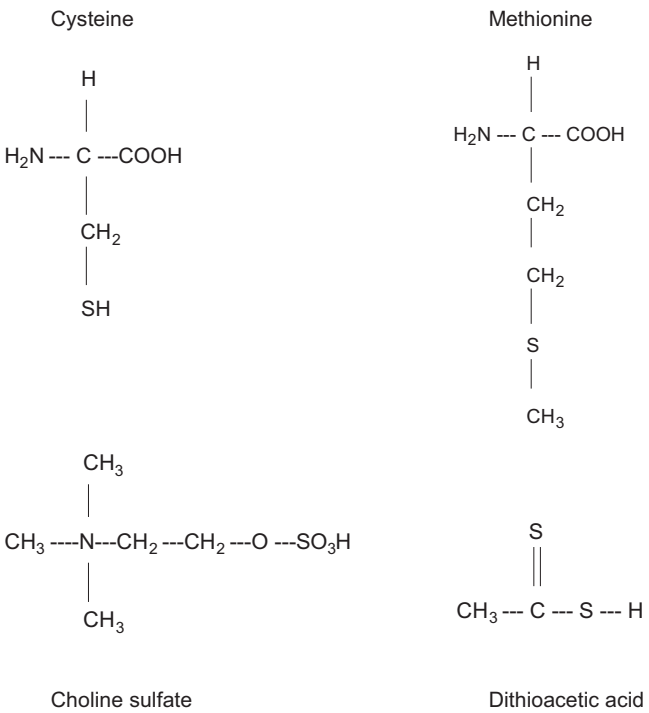

Fig. 3.5 Examples of organic sulfur compounds

Anaerobic Dissimilatory Sulfate Reduction

Sulfate reduction is one of the major microbial processes affecting sulfur cycling in salt marshes and other wetlands. In **dissimilatory sulfate reduction**, major bacterial genera such as *Desulfovibrio* and *Desulfomaculum* use sulfate as an electron acceptor in the metabolism of carbon substrates in anaerobic habitats. Representative reactions are shown below (where R represents a generic hydrocarbon).

$$\underset{\text{Organic alcohol}}{2R-CH_2OH} + SO_4^{2-} \rightarrow\rightarrow\rightarrow\rightarrow \underset{\text{Organic acid}}{2R-COOH} + 2H_2O + \underset{\text{Sulfide}}{S^{2-}} \quad (3.5)$$

$$\underset{\text{Lactic acid}}{2CH_3CHOHCOOH} + SO_4^{2-} \rightarrow\rightarrow\rightarrow$$

$$2CH_3COOH + HS^- + H_2CO_3 + HCO_3^- \quad (3.6)$$

The reduced sulfide that results from microbial sulfate reduction is very reactive and toxic, and may encounter a variety of possible fates. Some of the sulfide may combine with hydrogen to form the volatile gas hydrogen sulfide, H_2S. If and when the hydrogen sulfide reaches an aerobic zone, the sulfur may be oxidized back to sulfuric acid as follows: $H_2S + 2O_2$ ---> H_2SO_4. Alternatively, where there is available ferrous or hydroxy iron (as in a salt marsh), the sulfide can react to form iron sulfide (FeS) or pyrite (FeS_2) as follows:

$$Fe^{2+} + S^{2-} \rightarrow\rightarrow\rightarrow FeS \quad (3.7)$$

$$2FeOOH + 2H_2S + 2H^+ \rightarrow\rightarrow\rightarrow FeS_2 + 4H_2O + Fe^{2+} \quad (3.8)$$

Besides hydrogen sulfide, other important volatile sulfur trace gases that originate from microbial and/or plant metabolism are carbonyl sulfide (COS), dimethyl sulfide (DMS), carbon disulfide (CS_2), and dimethyl disulfide (DMDS).

Assimilatory Sulfate Reduction

Dissimilatory sulfate reduction in wetlands can be contrasted with **assimilatory sulfate reduction**, an essential metabolic process in the sulfur nutrition of microbes and other living organisms. Through this pathway that is illustrated below, organisms obtain the reduced sulfide that is required for the amino acids cysteine and methionine. During this reduction process, sulfur changes from an oxidation state of +6 to a final oxidation state of −2, and is rapidly incorporated into metabolic sulfur compounds.

$$SO_4^{2-} + ATP + 8e^- + 8H^+ \rightarrow\rightarrow S^{2-} + 4H_2O + AMP + \underset{\text{Inorganic P}}{PP_i}$$

Microbial Carbon Transformations

Three of the major microbial carbon transformations are: aerobic respiration, fermentation, and methanogenesis. Respiration is a complex process in which energy and matter move through a stepwise series of oxidation and reduction reactions associated with glycolysis, the Krebs or TCA cycle, and the electron transport system. Along the way, three key events occur: (i) energy-rich ATP is formed; (ii) heat is released; and (iii) carbon skeleton intermediates are provided for other essential metabolic products. The overall reaction for aerobic respiration can be simplified as shown below, where the complete oxidation of one mole of hexose sugar yields 36 moles of ATP and a free energy change of −686 kilocalories per mole.

$$\underset{\text{Hexose sugar}}{C_6H_{12}O_6} + 6O_2 \rightarrow\rightarrow 6CO_2 + 6H_2O + \text{energy}$$

Field estimates of gaseous CO_2 emissions from microbial respiration have been reported for a number of different terrestrial ecosystems. For example, Bowden et al. (1993) estimated that CO_2 emissions from microbial decomposition in a temperate mixed hardwood forest were roughly 2500 kg C ha^{-1} yr^{-1}. In a warm temperate floodplain swamp, Pulliam (1993) estimated that annual total soil CO_2 emissions were 9200 kg C ha^{-1} yr^{-1}, with roughly 4100 kg C ha^{-1} yr^{-1} contributed by aerobic mineralization of detritus by microbes. At Harvard Forest in Massachusetts, Peterjohn et al. (1994) conducted an interesting experiment to examine the response of trace gas fluxes to soil warming. When soil temperature was elevated 5 °C above ambient, soil CO_2 efflux increased by 5380 kg C ha^{-1} yr^{-1}. Unfortunately, it was not possible to determine what percentage of this increase was from microbial versus plant root respiration.

Fermentation

When oxygen is limited in a given environmental setting, aerobic respiration declines or ceases and **fermentation** processes assume increased importance in the overall mix of microbial metabolism. In fermentation, the process of glycolysis terminates in the formation of lactic acid or ethanol as the end-product of pyruvate synthesis.

Methane Production

Methanogenesis is another important microbial carbon cycling process that predominates in many anaerobic organic soils and peats (and in ruminants, sewage digestors, and landfills). On a global basis, microbes produce about 400 million metric tons of methane per year, with much of this gas being rapidly oxidized to CO_2. Microbial production of CH_4 occurs via the two reaction pathways shown below involving either (i) the reduction of CO_2 with electrons from hydrogen or formate or (ii) the splitting of a methyl group from acetic acid. Production of methane is often facilitated by fermentation processes in the local environment. Fermentative microbes such as the anaerobic bacterium *Clostridium pasteurianum* metabolize sugars and utilize an iron-based hydrogenase enzyme to yield three key substrates required by methanogens: acetate, CO_2, and free hydrogen gas (Adams and Stiefel 1998).

$$CO_2 + 8H^+ + 8e^- \rightarrow\rightarrow\rightarrow\rightarrow CH_4 + 2H_2O \quad E_h = -244\,mV \qquad (3.9)$$

$$CH_3COOH \rightarrow\rightarrow\rightarrow\rightarrow\rightarrow\rightarrow\rightarrow CH_4 + CO_2 \qquad (3.10)$$

Net emissions of methane from wetland soils can vary considerably as a function of environmental conditions. In organic soils or peats with elevated concentrations of sulfate (e.g., salt marsh peat), sulfate reducing bacteria typically out-compete methanogens for carbon substrates, resulting in diminished methane production. In waterlogged soils that experience seasonal water-table fluctuations, methane production may be important during wetter periods, but may decline and virtually cease during water-table draw-down. At such times, there may be a large pulse of CO_2 production as the soil dries and the microbial community shifts over to aerobic respiration of stored detritus. Moore and Knowles (1989) conducted experiments showing that the molar ratio of CO_2 to CH_4 emissions from peat may be as low as 10 with standing water above the peat, but can rise to >10,000 when the water-table recedes to −70 cm below the peat surface and soil aeration increases (Fig. 3.6).

A final important influence on net gaseous methane emissions is exerted by **methanotrophs** in the soil environment. Evidence indicates that 10–100% of the methane gas produced by anaerobic microbes is oxidized to CO_2 before it reaches the atmosphere. This consumption of methane can occur if there is an oxidized zone overlying the reducing micro-environment where methane is generated. Methanotrophs also occur in well-drained upland soils and can act as a sink for (i) methane transported into a forest ecosystem from upwind wetland sources or (ii) methane that diffuses upward through the soil from leaky underground natural gas pipelines.

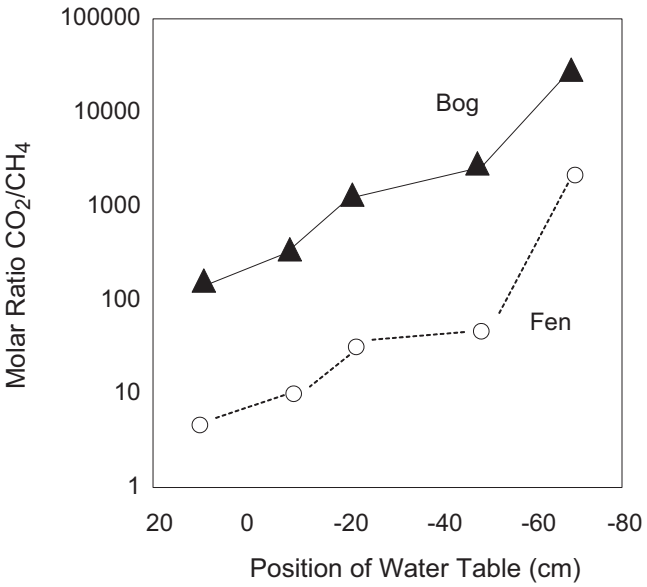

Fig. 3.6 Influence of water table level and associated redox potential on the molar ratio of carbon dioxide to methane in gaseous emissions from peat columns. Data from Moore, T.R. and R. Knowles. 1989. The influence of water table levels on methane and carbon dioxide emissions from peatland soils. Canadian Journal of Soil Science 69:33-38. © Canadian Science Publishing

Crill et al. (1988) compiled estimates from a number of field studies indicating that peak summer carbon fluxes as methane from peatlands in North America ranged from roughly 1 to 1.9 kg CH_4-C ha^{-1} d^{-1}. In another study, Pulliam (1993) compared methane emissions from riparian and other wetland ecosystems. He reported that mean daily year-round emission rates ranged from 0.2 to 2.4 kg CH_4-C ha^{-1} d^{-1}, whereas mean daily summer flooded emission rates ranged from <0.5 to 7.2 kg CH_4-C ha^{-1} d^{-1}. In a study of the Ogeechee River floodplain swamp in Georgia, USA, Pulliam (1993) estimated that annual total fluxes of methane carbon from lowland habitats averaged 170 kg CH_4-C ha^{-1} yr^{-1}. Soils in black cherry-sugar maple forest plots in Pennsylvania studied by Bowden et al. (2000) acted as strong sinks for methane, absorbing 8.9 kg CH_4-C ha^{-1} yr^{-1}.

Organic Acid Synthesis by Microbes

Microbes exert another important influence on environmental conditions through their synthesis and release of soluble organic acids. These acidic compounds range from simple aliphatic carboxylic acids such as malic or oxalic acids to more complex aromatic compounds such as phenolic acids and **fulvic acids**. Whereas aliphatic carboxylic acids (e.g., citric, succinic, and malic acid) are likely to originate in the TCA or Krebs Cycle within microbial cells, the more complex aromatic organic acids may be generated by microbial

metabolism via the Shikimic Acid Pathway or through *in situ* reactions involving extracellular microbial enzymes. After their production and release by microbes, these organic acids act as weathering agents, metal complexing ligands, sources of acidity, and metabolic substrates.

Microbial Processes that Contribute to Bioremediation or Metal Transformations

Before leaving this section on microbial processes, we should note that microbes also participate in a number of important biogeochemical transformations involving toxic chlorinated hydrocarbons (e.g., pesticides) and a variety of toxic and nontoxic metals (e.g., Hg, Fe, and Mn). Certain microbes are able to metabolize directly or to co-metabolize incidentally such compounds as 2,4-D, toxic phenolic substances, and solvents such as trichloroethane (Sun et al. 2002). Microbial metabolism of these industrial chemicals can provide a means of restoring environmental quality through bioremediation.

In contrast to the many examples of microbial bioremediation, microbial **methylation** of mercury (Hg) enhances the biotoxicity of this element. Methylation of Hg by microbes is a complex process that is only partially understood (Gilmour et al. 1992; Rudd 1995). In anaerobic sediments of freshwater lakes, sulfate-reducing bacteria facilitate the methylation of Hg(II), forming soluble monomethyl mercury CH_3Hg^+ or less soluble dimethyl mercury $(CH_3)_2Hg$ (Fig. 3.7). This process seems to require adequate sulfate concentrations to maintain viable populations of sulfate reducing bacteria. Yet, if toxic sulfide accumulates from vigorous sulfate reduction, this may retard the methylation process or increase the production of insoluble HgS. Evidence suggests that acidification of lakes by atmospheric deposition processes tends to increase the potential for microbial methylation of Hg by favoring sulfate reducing bacteria. Recent studies indicate that some iron-reducing bacteria can also promote this methylation process (Kerin et al. 2006).

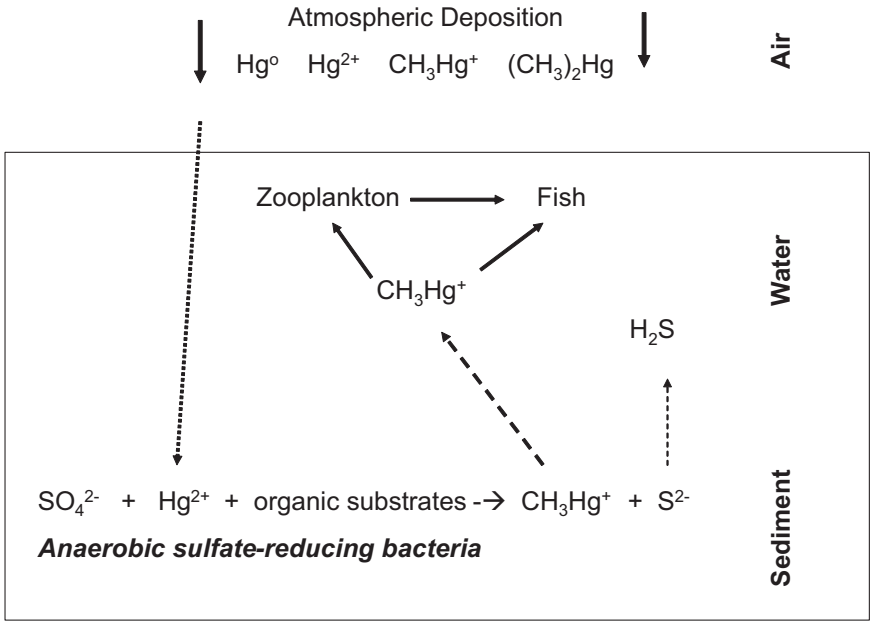

Fig. 3.7 Simple conceptual diagram of mercury cycling in lakes

Plant Biogeochemistry

4

Introduction

Terrestrial plant communities exist at the interface between the atmosphere and the underlying soil and geologic substrate, acting as major regulators of biogeochemical and hydrologic cycling patterns in the biosphere (Fig. 4.1). In the course of their life histories, plants face the challenge of acquiring sufficient energy, water, and nutrient resources to achieve growth, survival, reproductive success, and evolutionary fitness. Because processes of energy flow, water use, and nutrient circulation are closely coupled in plants, this chapter examines the biogeochemistry of plants in the context of energy and water relations in plants.

Whether we begin our analysis at the microscopic scale of a fine root absorbing nutrients from the soil or perhaps at a larger scale focusing on net carbon exchange in a vast forest landscape, it is clear that there are many intriguing questions concerning the biogeochemistry of plants. For example, do plant roots preferentially absorb ammonium, nitrate, or soluble organic N as a nutrient source and are there energetic or biogeochemical consequences associated with using one form or another? In the field, do wild plants compete for nutrients and what strategies are used to maximize acquisition and conservation of essential elements? Why is it that the element potassium cycles 10–100 times faster through the living biomass of a forest ecosystem compared to elements such as nitrogen and calcium? Under what conditions does aluminum in soil mineral phases become toxic to tree roots, thus interfering with plant nutrition and growth? These are just a few examples of the kinds of research questions that have been investigated by scientists trying to understand the role of plants in the biogeochemistry of terrestrial ecosystems.

General Plant Chemistry

An analysis of tissue chemistry indicates that plants contain a mix of **macronutrients** such as nitrogen, calcium, and phosphorus, along with a variety of **micronutrients** or trace elements required for plant growth (Table 4.1). Each nutrient may serve one or more essential structural and/or functional roles in a plant. For example, phosphorus occurs in membrane phospholipids, in nucleic acids involved with gene structure and function, and in ATP molecules essential for energy transfer. In comparison, calcium is well-known for its role as a structural component of cell wall pectins, but has also been recognized as a mediator of cell signaling and stress responses involving calmodulin and protein kinases (Sheen 1996; Putney 1998). Both nitrogen and magnesium are integral parts of chlorophyll, but these two elements otherwise diverge considerably in terms of their other functional roles in plants. Sulfur not only occurs in two amino acids – methionine and cysteine – but also forms part of the iron-sulfur center in the enzyme ferredoxin:thioredoxin reductase, a key mediator of redox signaling in chloroplasts (Dai et al. 2000).

In terrestrial ecosystems analysis, one of our basic objectives is to gain an understanding of the nutrient pools and exchanges of elements in the plant and soil system. Measurements of tissue nutrient concentrations indicate that plant biomass is dominated by oxygen (45%) and carbon (45–48%) on a dry weight basis. Whereas living foliage typically contains 1.0–2.5% nitrogen, live fine roots are about half as concentrated, averaging 1.1% N (Gordon and Jackson

C.S. Cronan, *Ecosystem Biogeochemistry*, Springer Textbooks in Earth Sciences, Geography and Environment, DOI 10.1007/978-3-319-66444-6_4

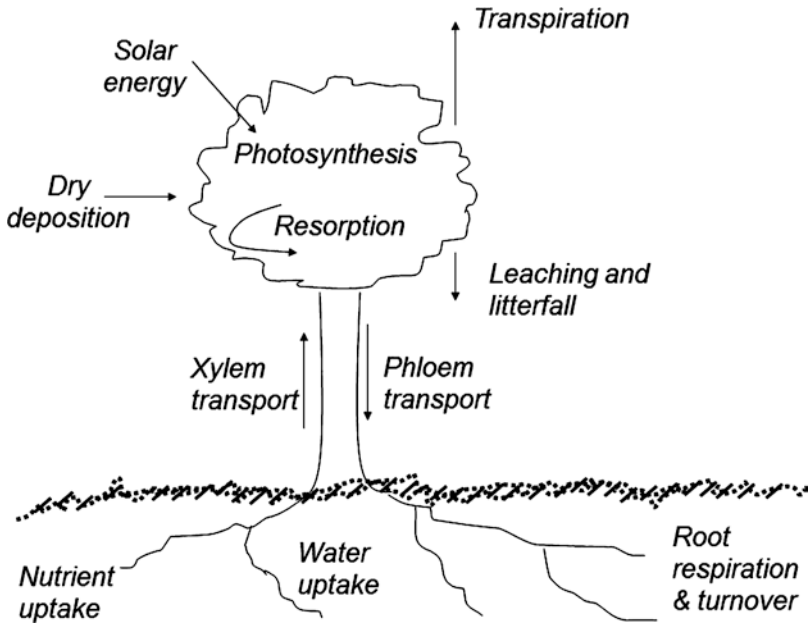

Fig. 4.1 Simple conceptual model of plant biogeochemical processes in a forest ecosystem

Table 4.1 General overview of plant macronutrients and micronutrients

Element	Function or role
Carbon (C)	Structural and functional hydrocarbons
Oxygen (O)	Multiple roles
Hydrogen (H)	Hydrocarbons and proton pumps
Nitrogen (N)	Proteins, enzymes, RNA, DNA, chlorophyll
Phosphorus (P)	RNA, DNA, ATP, phospholipids
Calcium (Ca)	Plant cell walls, membranes, stress signals
Magnesium (Mg)	Enzymes and chlorophyll
Potassium (K)	Electrolytes in plant cells
Sulfur (S)	Amino acids, proteins, coenzyme A
Micronutrients	
Iron (Fe)	Enzymes, ferredoxin
Manganese (Mn)	Enzyme co-factor
Boron (B)	Nucleic acid synthesis, membrane function
Copper (Cu)	Cytochrome oxidase, plastocyanin
Zinc (Zn)	Enzymes
Chlorine (Cl)	Participates in photosynthetic reactions
Molybdenum (Mo)	Nitrate reductase

2000), and sapwood contains only about 0.1–0.2% N (Whittaker et al. 1979; Johnson and Henderson 1989). Phosphorus concentrations average roughly 0.1–0.2% in foliage and fine roots, but are less than one-tenth of that concentration in sapwood. In contrast to these macronutrients, concentrations of micronutrients can be considerably lower. For example, iron concentrations are usually <0.01% in foliage and <0.002% in sapwood. Detailed data summarizing nutrient concentrations in plant tissues can be found in Bowen (1966, 1979) and journal articles from the ecological literature (e.g., Whittaker et al. 1979; Weand et al. 2010).

Table 4.2 Comparison of nutrient concentrations, pools, and stoichiometries in foliage and sapwood of a mature northern hardwood forest (data from Whittaker et al. 1979)

	Foliage	Sapwood
Nitrogen		
Concentration range	1.3–2.8%	0.05–0.1%
Mass (kg/ha)	70	79
Calcium		
Concentration range	0.3–0.9%	0.06–0.1%
Mass (kg/ha)	20	60
C:N elemental mass ratio	20	450
N:P elemental mass ratio	13	10

Although plant tissues vary considerably in terms of nutrient concentrations, ***stoichiometries*** or ratios of essential elements in plants are relatively consistent, reflecting the common biochemical processes and structural chemistry of these organisms (Redfield 1958; Reiners 1986; Elser et al. 1996). For example, carbon:nitrogen (C:N) mass ratios in foliage from diverse forest types range from 20 to 30, whereas C:N ratios in wood are uniformly 10–20 times higher than that, reflecting the dilute nutrient chemistry of woody tissues (Table 4.2). Nitrogen:phosphorus (N:P) mass ratios in plant tissues commonly average ~12–13, although specific molecules such as ATP, phospholipids, and nucleic acids can vary substantially in their N:P ratios (Fig. 4.2). Whenever **element ratios** are used in an analysis, it is important to note whether they are computed using mass units or molar ratios. As an example, an N:P mass ratio of 12:1 is equivalent to a molar N:P ratio of roughly 27:1.

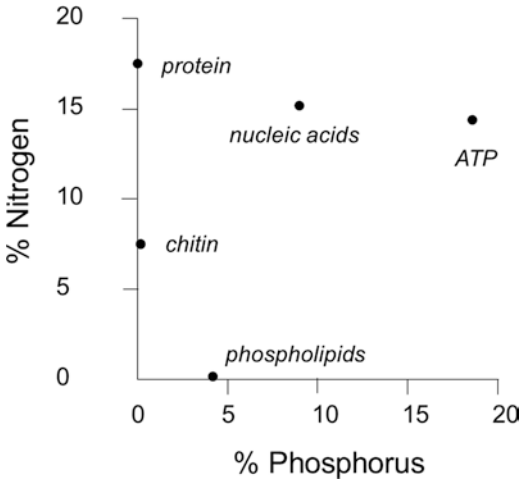

Fig. 4.2 Stoichiometry of N and P in various biomolecules based on weight. From Elser, J.J., D.R. Dobberfuhl, N.A. MacKay, and J.H. Schampel. 1996. Organism size, life history, and N:P stoichiometry. BioScience 46:674–684 by permission of the American Institute of Biological Sciences

Table 4.3 Recommended element ratios for optimum plant nutrition, based on studies with birch seedlings (Ingestad 1971). Proportions are shown in mass units relative to nitrogen; thus, for example, a plant demands 65 mg K and 7 mg Ca for each 100 mg of N

N	100	Fe	0.7	Mo	0.007
K	65	Mn	0.4	Na	0.003
P	13	B	0.2		
S	9	Cu	0.03		
Ca	7	Zn	0.03		
Mg	8.5	Cl	0.03		

Ingestad (1971) used general concepts of element stoichiometry to develop a ***theory of optimum plant nutrition***, proposing that growing plants demand element ratios similar to those summarized in Table 4.3, with large relative requirements for N, K, and P and smaller demands for trace metals. These ratios imply that plants have a proportionately large influence on the cycles of elements such as N and P, versus a smaller direct influence on the cycles of trace elements such as iron and copper.

An interesting question we might ask is how stoichiometric demands change over the course of a growing season as plants proceed through **phenological** development? When growing plants sequentially or simultaneously allocate resources to the production of foliage, roots, and wood (with contrasting nutrient chemistries), are there shifts in the stoichiometry of nutrient demand by the plant community? Are nutrient demands by plants generally in synchrony with patterns of nutrient supply in the **rhizosphere** or are there times when plant growth is limited by competition for nutrients with microbes or by reduced decomposition rates in the microbial community?

Plant Functional Morphology and Growth Allocation

Because plant structure and function are interrelated, it is important to recognize how nutrient cycling processes in plants are influenced by the distinctive morphology of root and shoot systems and by the proportions of energy and growth allocated to above and belowground tissues. In a forest ecosystem, the plant canopy represents the "power station" for energy flow, the major end-user for water, a massive gas exchange system, a primary sink for nutrients, and a multi-dimensional surface exposed to continuous atmospheric interactions. The belowground root system, on the other hand, contains large structural woody roots that anchor a prolific branching system of fine roots that acts as a sink for photosynthate, a nutrient absorption network, a hydrologic connection between the shoot and the soil, and a source of fresh organic matter for the surrounding subsoil environment.

Aboveground Structure and Function

Plant canopy structure is characterized by a high foliar surface area optimized for the capture of solar energy. **Leaf area index** (LAI) is a metric for quantifying and comparing forest canopies in terms of the ratio of foliar surface area relative to ground area. Average projected leaf areas for forests typically range from 4 to 12 m^2 of leaf area per m^2 of ground area (LAI = 4–12). In a study of 28-yr-old hardwood and conifer plantations in Wisconsin, Gower et al. (1993) reported total foliage masses ranging from 300 to 3000 g m^{-2} ground surface and LAI values ranging from 4.5 in red oak to 10.2 in Norway spruce. The large surface area of tree canopies not only facilitates optimal photosynthesis, but also enhances canopy filtration of particulate aerosols and gases from the atmosphere (via **dry deposition**). As shown in Fig. 4.3, the amount of leaf area in a tree is directly related to the sapwood cross-sectional area of the tree (i.e., the tissue that allows water transport to the canopy).

The anatomy of leaves and needles (Fig. 4.4) reflects a structural response to the multiple functional challenges of (i) promoting CO_2 uptake via stomata and carbon fixation by chloroplasts within the mesophyll; (ii) controlling water loss by means of a protective waxy cuticle and stomatal guard cells; (iii) maximizing light capture, while avoiding excess heat gain and (iv) providing vascular tissues for the import of water and nutrients in the xylem and the export of photosynthate in the phloem. Gas exchange in terrestrial plants is dominated by uptake of CO_2 and release of O_2 plus water vapor. However, stomatal pores are also exposed to gaseous air pollutant oxidants such as SO_2 and O_3 that may be readily

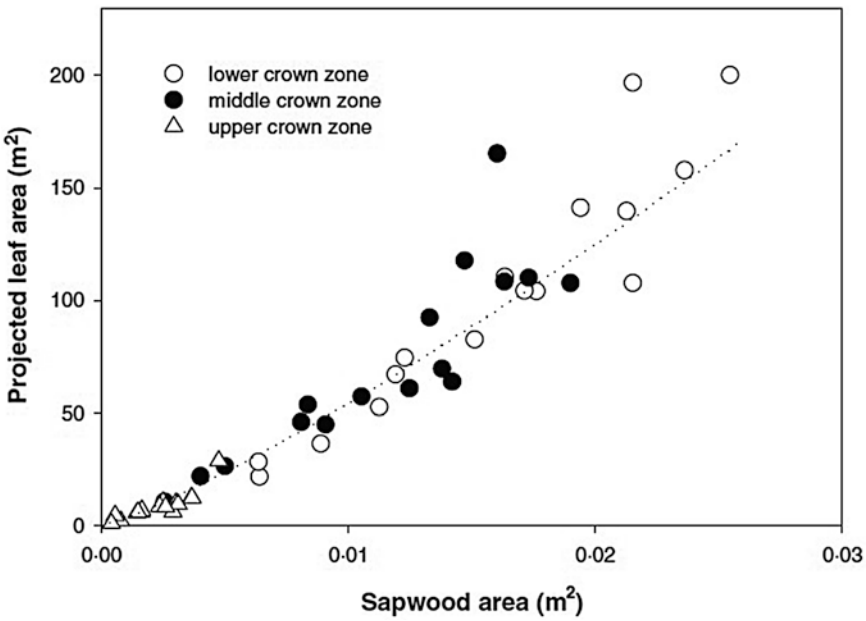

Fig. 4.3 Leaf area as a function of cross-sectional sapwood area in Eucalyptus trees in Australia. From Medhurst, J.L. and C.L. Beadle. Sapwood hydraulic conductivity and leaf area – sapwood area relationships following thinning of a *Eucalyptus nitens* plantation. Plant, Cell, and Environment 25:1011–1019. ©2002 Blackwell Science Ltd

Fig. 4.4 Physical structure of fir (*left*), pine (*middle*), and oak foliage (*right*)

taken up by plant foliage (Taylor et al. 1994). Once inside the plant mesophyll, these substances can damage cells and interfere with normal plant functions (Winner 1994). Plants can also absorb ammonia gas, NH_3, from the atmosphere and may release volatile hydrocarbons such as isoprene and other aromatic compounds from the foliar surface of the plant canopy (Fuentes and Wang 1999).

One of the interesting ecological tradeoffs involving plant structural and physiological traits is the contrast between deciduous and evergreen tree species that retain their foliage for different time spans. In a comparison of five tree species that retain foliage for periods ranging from 5 to 66 months, Gower et al. (1993) reported that foliage mass and LAI were positively correlated with leaf longevity, whereas leaf longevity was inversely correlated with specific leaf area ($cm^2\ g^{-1}$), maximum net photosynthesis per unit mass, and leaf nitrogen per unit mass. Their results indicated that longer-lived evergreen needles tend to be less efficient and productive than shorter-lived deciduous foliage; however, the total mass and longevity of these needles compensate for the diminished photosynthetic efficiency. This trade-off allows needle-leaved evergreen forests to achieve annual rates of aboveground net primary production similar to or greater than comparable deciduous forests. Reich et al. (1992) examined similar relationships between canopy structure and function in a diversity of trees, and demonstrated an inverse relationship between net photosynthesis and leaf longevity (Fig. 4.5).

Belowground Structure and Function of the Root System

Aboveground productivity and nutrient cycling in a forest ecosystem are only possible as a result of crucial belowground processes that occur in the poorly understood and mostly invisible **rhizosphere**. Below the soil surface, the root system of a tree is composed of larger woody roots that anchor the plant, along with various size classes of smaller roots involved in the acquisition of water and nutrient resources (Fig. 4.6). **Fine roots** ≤1–2 mm in diameter dominate water and nutrient uptake by the plant. With their dense branching structure, each dry gram of fine roots provides roughly 10–12 m of root length and a surface area of roughly 10 m^2 for absorption processes (Jackson et al. 1997). In most, if not all, forest ecosystems, the fine root system also hosts a diverse symbiotic community of **mycorrhizal fungi** that serve as functional partners in the uptake of water and nutrients for the forest community, enhancing the growth and nutrition of host trees (Nasto et al. 2014).

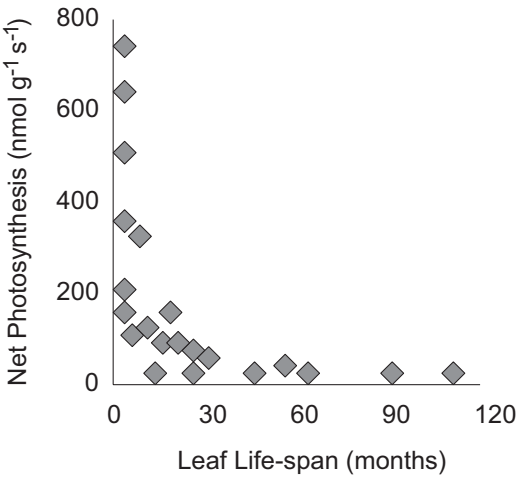

Fig. 4.5 Maximum net photosynthetic rate versus leaf longevity From Reich, P.B., M.B. Walters, and D.S. Ellsworth. Leaf life-span in relation to leaf, plant, and stand characteristics among diverse ecosystems. Ecological Monographs 62:365–392. © 1992 by the Ecological Society of America

Field studies have shown that live fine root biomass in forest ecosystems typically ranges from 200 to 800 g m^{-2} (Jackson et al. 1997; Cronan 2003), with roughly 50% of that biomass concentrated in the upper 10–20 cm of the soil profile (Fig. 4.7). Because fine roots are not particularly long-lived, roughly 50–200% of the fine root live biomass pool turns over each year through new root production, mortality, and decomposition. In one example focused on mature Norway spruce forests in Maine, biomass of fine roots <1 mm in diameter averaged 360 g m^{-2}, whereas annual production of new fine roots was ~300 g m^{-2} yr^{-1} (Cronan 2003). These estimates suggest that the mean lifetime or residence for fine roots in that forest ecosystem is roughly 1.2 years, compared with mean needle longevity of more than 5 years. Other related studies have suggested that fine roots may have longer mean residence times in forest ecosystems – on the order of several years (Trumbore and Gaudinski 2003).

Growth Allocation and Root:Shoot Relationships

Plants face an important ecological challenge in terms of balancing growth allocation to produce (i) sufficient foliage for optimum photosynthesis, and (ii) adequate fine root biomass

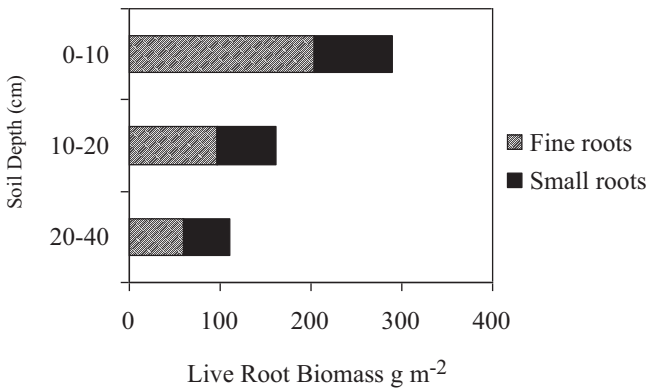

Fig. 4.7 Biomass distribution of fine roots (<1 mm in diameter) and small roots (1–3 mm) for Norway spruce (*Picea abies*) in Maine, USA Data from Cronan (2003)

Fig. 4.6 Overview of root system structure at a range of scales, from the microscopic anatomy of fine root tips containing mycorrhizae to the macroscopic spatial distribution of fine roots in a forest stand. Reproduced from Lyford and Wilson (1964) by permission of Harvard Forest, Petersham, MA

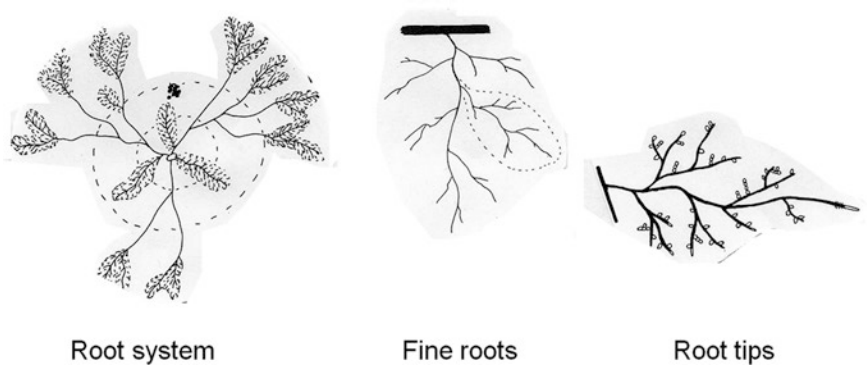

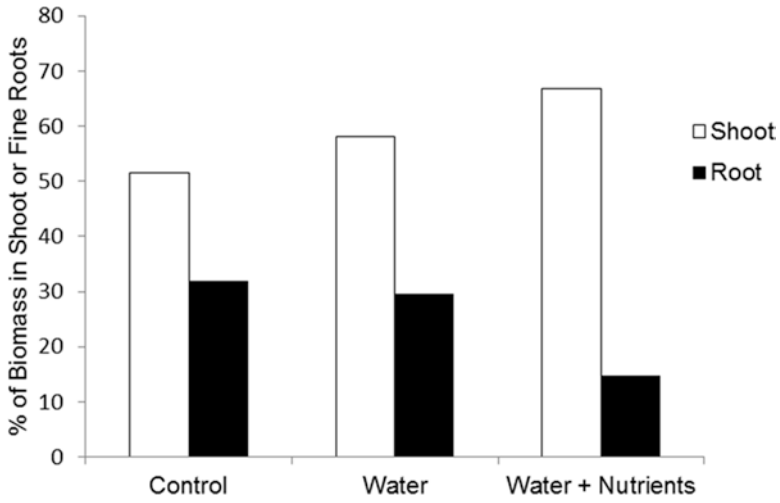

Fig. 4.8 Biomass allocation in response to changing plant resources (Data from Axelsson and Axelsson 1986)

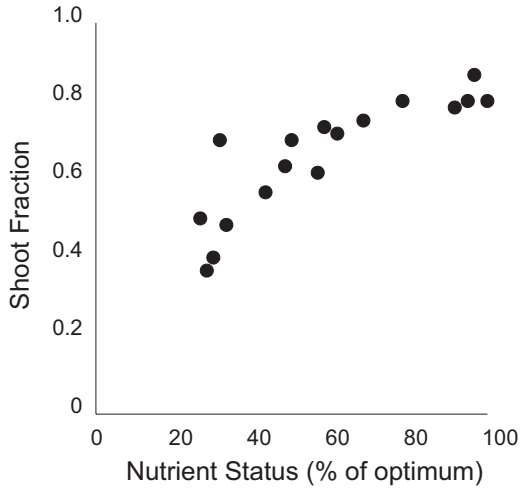

Fig. 4.9 Shoot mass fraction in birch (*Betula pendula*) under different nutrient conditions involving limitation by nitrogen (expressed as a percent of optimum N nutrition). Shoot fraction = shoot mass /total plant biomass. Based on Ingestad, T. and G.I. Agren. The influence of plant nutrition on biomass allocation. Ecological Applications 1:168–174. © 1991 by the Ecological Society of America

to supply water and nutrients under varying environmental conditions. Previous studies have shown that plant nutrition often has a strong effect on the partitioning of dry matter to different plant parts, and that nutrient limitation tends to induce an increased root:shoot ratio to compensate for low nutrient supply (Ingestad and Agren 1991). Based on field studies in Sweden, Axelsson and Axelsson (1986) reported that untreated Scots pine trees (*Pinus sylvestris*) exhibited shoot:fine root ratios of 1.6 expressed as dry matter carbon allocation. In contrast, Scots pine subjected to irrigation, fertilization, or combined irrigation + fertilization decreased their relative carbon allocation to roots, exhibiting respective shoot:root ratios of 2.0 (irrigation), 3.9 (fertilization), and 4.5 (combined water + fertilizer). Study results indicated that Scots pine trees responded to increased soil resource availability by shifting growth allocation away from belowground fine roots to aboveground woody shoots (Fig. 4.8).

In another investigation of tree seedling growth allocation as a function of steady-state nutrition, Ingestad and Agren (1991) showed that allocation of growth to shoots increased as the internal nitrogen status of plants improved from suboptimal to optimal conditions (Fig. 4.9). Keyes and Grier (1981) also reported evidence indicating dynamic shifts in root and shoot allocation as a function of belowground resource availability. The authors found that 40 yr–old Douglas-fir trees on two contrasting sites allocated >80% of total biomass to aboveground shoots, but trees on sites with low nutrient availability invested up to half of annual **net primary production** in belowground roots in order to acquire nutrients.

Carbon Fixation, Metabolism, and Plant Production

Photosynthesis and Nutrients

Energy flow is a central concept in ecology and biogeochemistry that focuses on carbon fixation by photosynthetic plants and the subsequent metabolism, biomass production, and trophic transfers that result from energy inputs to an ecosystem. The overall photosynthetic reaction involves a photochemical oxidation of water and reduction of CO_2 to form carbohydrates (Fig. 4.10). At each step, there are critical reactions involving specific elements that are controlled by different biogeochemical processes.

One of the major pathways in plant photosynthesis is the **Hill Reaction** or Light Reaction. This biochemical process occurs in chloroplasts and involves the capture of light energy by chlorophyll (in Photosystems I and II), photolysis

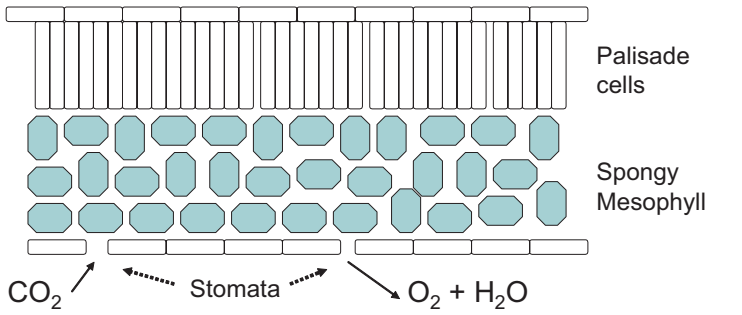

Fig. 4.10 Cross-sectional view of plant leaf showing site of photosynthetic reactions

$$CO_2 + 2H_2O + 12\ photons \rightarrow\rightarrow\rightarrow (CH_2O)_n + O_2 + H_2O$$

of water to release O_2, and production of reducing power in the form of NADPH (a reductant) and ATP (adenosine triphosphate – an energy transfer molecule). A schematic summary of the process is shown below.

Hill Reaction

$$PS\ II \xrightarrow{+\ Light} H_2O \rightarrow 0.5O_2 + 2H^+$$

$$PS\ I \xrightarrow{+\ Light} NADPH + H^+ \quad (NADP^+)$$

$$ADP + P_i \rightarrow ATP \text{ (via electron transport chain)}$$

where P_i represents inorganic phosphate and PS I and PS II are photosystems I and II.

Key compounds required for the Hill Reaction include chlorophyll and associated pigments, $NADP^+$/NADPH, ADP/ATP, CO_2, H_2O, plastocyanin, plastoquinone, ferredoxin, and cytochromes.

Key elements that contribute to the process are H, C, N, P, Mg, Fe, Mn, Cl, Cu, and S.

Coupled with the Hill Reaction is the **Calvin Cycle**, a process of CO_2 fixation that is powered by energy and reducing power generated in the light reaction (see below).

Calvin Cycle

$$3CO_2 + 3H_2O + 9ATP + 6NADPH + 6H^+ \rightarrow \rightarrow \rightarrow$$

$$3\text{-PGald} + 6NADP^+ + 9ADP + 8P_i$$

[where 3-PGald = 3-phosphoglyceraldehyde]

Key compounds required for the Calvin Cycle include 3-PGA (3-phosphoglyceric acid), RuBP (ribulose-1,5-bisphosphate), rubisco (ribulose bisphosphate carboxylase), ADP/ATP, $NADP^+$/NADPH, H_2O, and H^+

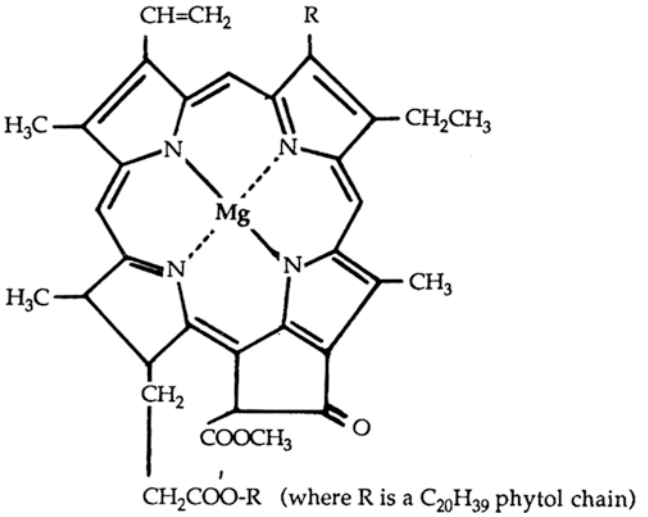

Fig. 4.11 Chlorophyll *a* with its central atom of Mg surrounded by four atoms of N

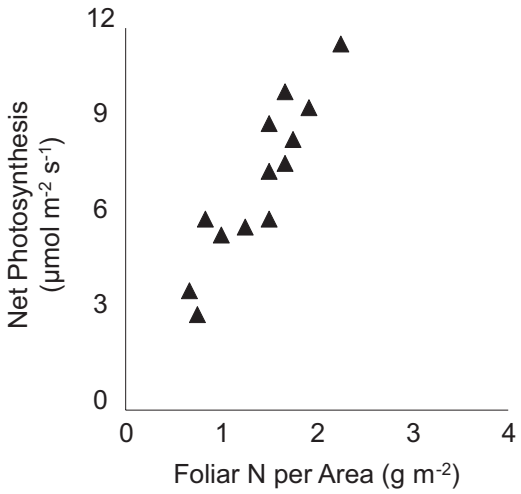

Fig. 4.12 Relationship between foliar N and photosynthesis in sugar maple. (*Acer saccharum*) in Wisconsin (Based on Ellsworth, D.S. and P.B. Reich. Canopy structure and vertical patterns of photosynthesis and related leaf traits in a deciduous forest. Oecologia 96:169–178. ©1993 Springer. With permission of Springer.)

Following the initial process of carbon fixation, plant metabolism draws on photosynthate to produce a wide variety of structural and non-structural carbohydrates, proteins, fats, and the like. Each of these metabolic pathways requires contributions from specific plant nutrients. For example, Mg^{2+} serves an important role as a co-factor in sucrose formation. Likewise, K^+ is required to activate starch synthetase for starch production. Magnesium is also essential in chlorophyll production – a deficiency of this element can deprive a plant of the central atom required for chlorophyll synthesis (Fig. 4.11), resulting in **chlorosis** or yellowing of foliage.

As much as 10–25% of the protein in plant leaves occurs in the form of ribulose bisphosphate carboxylase (**rubisco**), a key enzyme that catalyzes fixation of CO_2 in the Calvin Cycle. Because rubisco, ATP, NADPH, and other key photosynthetic molecules contain nitrogen and phosphorus, rates of photosynthesis and plant growth are influenced by the availability of these elements. When one or both of these critical elements are in short supply, photosynthetic rates decline. By the same token, increases in the supply of these elements can enhance plant productivity, as illustrated by the positive relationship between foliar N concentration and net photosynthesis shown in Fig. 4.12.

Rates of photosynthetic carbon fixation vary among species as a function of resource availability (e.g., light, water, nutrients, and CO_2), environmental conditions, and ecological interactions. Salisbury and Ross (1985) reported that maximum photosynthetic rates in tree species can range from 3 to >12 μmol CO_2 m^{-2} s^{-1}. Variations in photosynthetic performance and productivity among species provide an ecological basis for differential competitive success over time and across spatial scales as resource levels change. Taking light as one key resource, Fig. 4.13a provides an illustration of the contrasting photosynthetic light response curves one might observe comparing a shade adapted plant with species such as aspen or birch that are adapted to high light conditions. Clearly, the sun-adapted aspen can exploit high light levels for a potential competitive advantage. In the companion Fig. 4.13b, the combined interactive effects of light and nitrogen resource availability on photosynthesis are shown.

Photosynthesis and Water

Photosynthesis is also strongly influenced by plant moisture status and soil water resource levels. The ability of plants to absorb and to transport water is determined by a **water potential** gradient linking the *soil-plant-air continuum* from the rooting zone to the atmosphere. The water potential gradient develops in response to the plant water deficit created by water loss to the dry atmosphere, from xylem tension, and from an **osmotic potential** generated by ion and solute accumulation in plant cells. When there is a water potential difference between the plant and the soil, moisture in the soil responds to the water potential gradient like a ball rolling down a hill in response to gravity. In other words, the soil moisture moves from a zone of greater abundance (the soil matrix) to a zone of lesser abundance (inside the plant); ultimately, much of this water is transpired as vapor into the dry atmosphere at the terminus of the water potential gradient.

The process of plant water uptake will continue as long as there is a sufficient water potential gradient to extract water from the soil. If the soil becomes too dry or freezes, or if transpirational water loss ceases, water movement into the

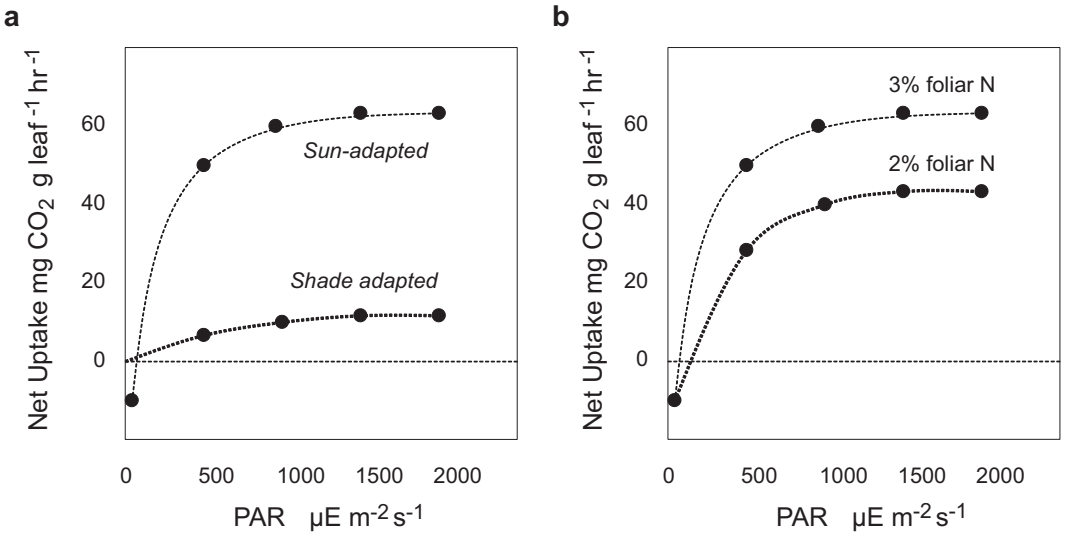

Fig. 4.13 (**a**) Photosynthetic response curves for different plants as a function of photosynthetic active radiation (PAR) and (**b**) interactive effects of light and foliar N on photosynthetic performance in trees

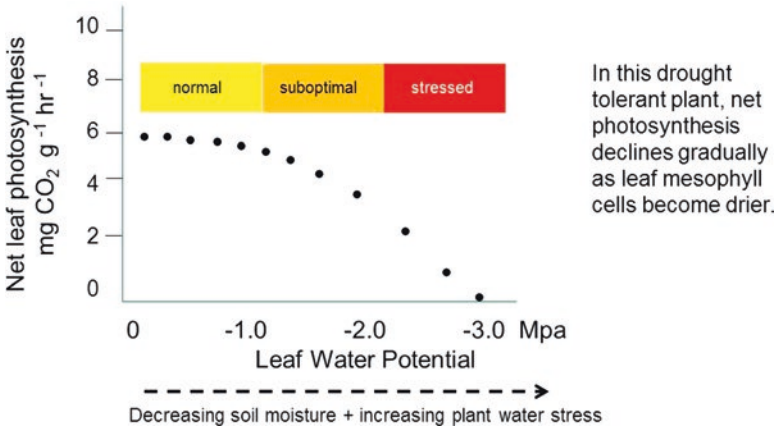

Fig. 4.14 Net carbon uptake by leaves declines at critical thresholds of leaf water potential and water stress. Plant water stress increases as soil and leaf water potentials become more negative

plant will decrease or stop. Water potential is expressed in units of megaPascals (MPa), where 1 MPa is equal to 10^7 dyne cm^{-2}, 10 bars, or 10.13 atm. Trees can generally extract moisture from the soil until the soil water potential drops to approximately −1.5 MPa; for most temperate forest species, plant water potentials below −5.0 MPa are potentially lethal.

In the final analysis, plants must balance transpirational water loss and CO_2 uptake in order to maintain photosynthesis and to permit the flow of water required for nutrient circulation, plant growth, and leaf cooling. Decreases in water availability and plant water potential can lead to stomatal closure as a means of limiting transpirational water loss through leaf pores. This action conserves precious water, but has an important consequence for terrestrial plants – it interrupts uptake of carbon dioxide (Fig. 4.14). Unfortunately, without continuous uptake of carbon dioxide, photosynthesis declines and ultimately stops.

Investigators have shown that **stomatal conductance** generally declines as evaporative demand increases, with the result that plant transpirational water loss usually does not exceed 0.7 mm/hr or 6 mm/day (Waring and Schlesinger 1985). In one example, Day (2000) reported that as the leaf-to-air VPD (**vapor pressure deficit**) increased from ≤1 to ≥4 kPa during mid-summer in a Maine conifer forest, stomatal conductance decreased in red spruce needles, and there was a corresponding decline in net photosynthesis (Fig. 4.15).

Respiration and Metabolism

Respiration is the complex process by which energy captured in photosynthesis is released as heat and work in plants and other organisms. The prime metabolic substrates for this process include starches, sugars, fats, organic acids, and

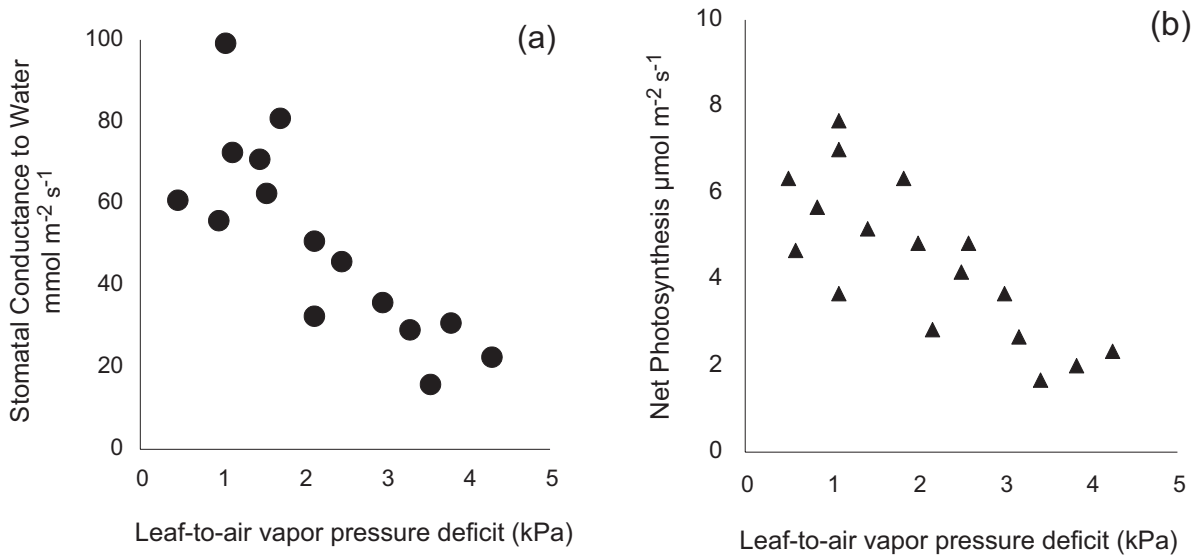

Fig. 4.15 Relationship between vapor pressure deficit (VPD), (**a**) stomatal conductance, and (**b**) net photosynthesis in red spruce, *Picea rubens* From Day, M.E. 2000. Influence of temperature and leaf-to-air vapor pressure deficit on net photosynthesis and stomatal conductance in red spruce (*Picea rubens*). Tree Physiology 20:57–63 by permission of Oxford University Press

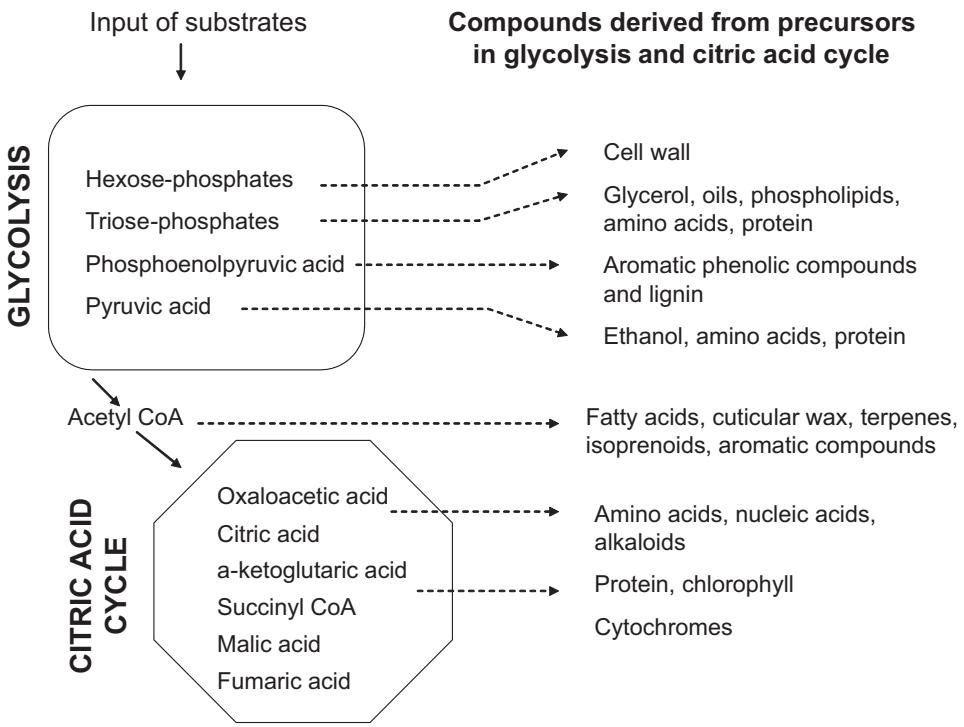

Fig. 4.16 Metabolic pathways derived from precursors in glycolysis and the Krebs Cycle

even some proteins. The overall reaction for aerobic respiration can be viewed as the reverse of the photosynthetic reaction:

$$C_6H_{12}O_6 + 6O_2 \rightarrow\rightarrow 6CO_2 + 6H_2O + \left(energy = 2{,}870 \text{ kJ } or \text{ } 686 \text{ } kcal/mole \text{ } glucose\right)$$

During respiration, three key events occur: (1) energy-rich ATP and reduced NADH are formed; (2) heat is released; and (3) carbon skeleton intermediates are generated for a number of other essential metabolic products and pathways (Fig. 4.16).

Autotrophic plant respiration is generally assumed to be roughly 50–60% of gross photosynthesis for many

species (Ryan 1991). Harris et al. (1975) estimated that total plant respiration in a mixed southern deciduous forest was 14,400 kg C ha^{-1} yr^{-1} or 66% of **gross production**. In an oak-pine forest in New York, Woodwell and Botkin (1970) estimated autotrophic respiration at 6800 kg C ha^{-1} yr^{-1} or 53% of gross production, whereas Bormann and Likens (1979) reported an annual total plant respiration rate of 6100 kg C ha^{-1} yr^{-1} or 55% of gross primary production.

Exchange of Carbon Dioxide in a Forest Ecosystem

One of the important areas of research in ecosystem carbon cycling is the estimation of net rates of gaseous carbon dioxide exchange via photosynthesis and respiration in forest ecosystems (Lindroth et al. 2008). As an example, scientists at Harvard Forest in Massachusetts used a biophysical **eddy-covariance** technique based on measurements of CO_2 concentrations above and below the canopy to estimate exchange of CO_2 between the atmosphere and a deciduous hardwood forest (Goulden et al. 1996). Over a five-year period of study, the forest gained 3–6 g C m^{-2} day^{-1} from net photosynthesis during the growing season and lost 1–2 g C m^{-2} day^{-1} in the dormant winter periods as a result of ecosystem respiration. On an annual basis, net CO_2 uptake by the forest ranged from 1400 to 2800 kg C ha^{-1} yr^{-1}. In a follow-up paper at the same site, Barford et al. (2001) reported that net annual CO_2 uptake averaged 2000 ± 400 kg C ha^{-1} yr^{-1} during 1993–2000, with interannual variations exceeding 50%. Similar studies were conducted by Lindroth et al. (2008) focusing on net ecosystem exchange along a climatic gradient in Sweden.

Energy Budgets and Primary Production

Processes of photosynthesis and respiration can be viewed in the context of an ecosystem energy budget that examines the fate of plant primary production. As illustrated in Fig. 4.17, plant production and energy flow in a beech-maple-birch forest were estimated using energy units of kilocalories per square meter of land surface area. For perspective, there are 686 kcal of energy per mole of glucose (formula weight = 180 g/mole), 1 calorie = 4.19 joules, and 1 calorie cm^{-2} min^{-1} = 697 watts m^{-2}. In this example, annual gross primary production (GPP) in a 55 yr-old northern hardwood forest was estimated to be 10,400 kcal m^{-2}, and roughly half of the annual photosynthetic production was consumed as autotrophic respiration (R1). The difference between GPP – R1 is the net primary production (NPP) of the forest, which averaged 4680 kcal m^{-2} yr^{-1} and is equivalent to roughly 10,000 kg organic matter ha^{-1} yr^{-1} or 5000 kg C ha^{-1} yr^{-1} as NPP. The annual energy budget of this north temperate zone hardwood forest can be summarized with two different expressions. **Production efficiency** of the forest ecosystem (NPP/GPP) is approximately 45%, and annual **net ecosystem production** (GPP-R1-R2) is roughly 1340 kcal m^{-2} (which is close to 2 moles of glucose equivalents per square meter).

Compared to the Hubbard Brook Forest depicted in Fig. 4.17, Waring and Schlesinger (1985) reported that forest net primary production in the biosphere ranges from roughly 1000 to 40,000 kg organic matter ha^{-1} yr^{-1}, with a mean of about 15,000 kg ha^{-1} yr^{-1}. In a separate analysis of net primary production in boreal forest ecosystems, Gower et al. (2001) reported that total above- and belowground NPP ranges from 520 to 8680 kg C ha^{-1} yr^{-1} and averages 4240 kg C ha^{-1} yr^{-1} as NPP.

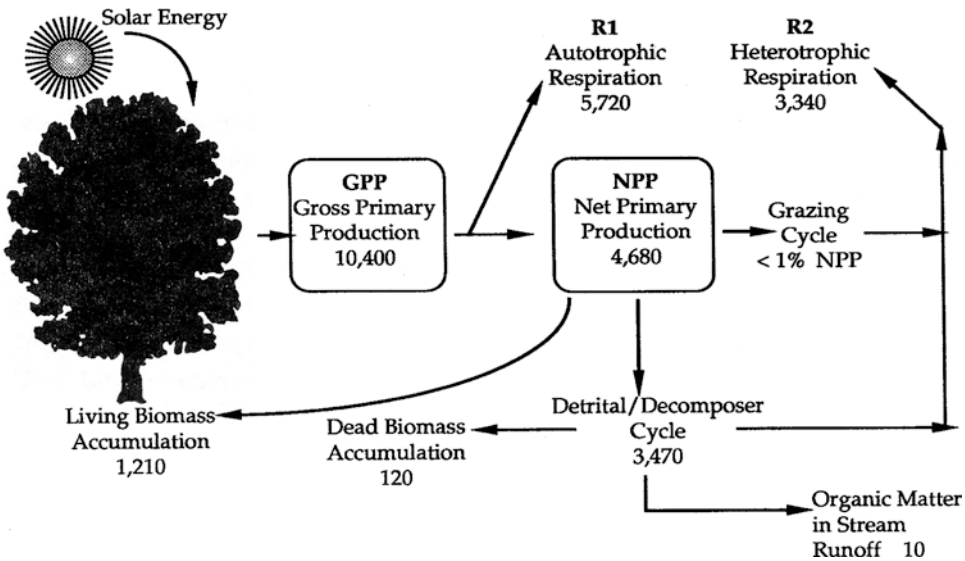

Fig. 4.17 Estimated annual energy budget for a 55 yr old northern hardwood forest at Hubbard Brook Experimental Forest, NH. Units are kcal m^{-2} (Data from Bormann and Likens 1979)

Whole-Plant Carbon Cycling and Allocation

The initial products of photosynthesis contain energy in the form of chemical bonds and carbon skeletons that can be allocated differentially to meet the functional and structural needs of an individual plant. In a given year, the amount of energy captured through photosynthesis will vary with environmental conditions and will be used differentially to meet the needs of growth, tissue maintenance, defense, storage, and reproduction (Fig. 4.18). Sugars derived from photosynthesis may be converted to starches and stored, metabolized into cellulose and lignin for structural growth, respired to produce ATP for energy-dependent processes such as nutrient uptake or flowering, or used in various other metabolic processes. Weinstein et al. (1991) used these concepts in their TREGRO model to predict dynamic changes in carbon allocation patterns for red spruce trees exposed to environmental stresses. One might expect that trees experiencing stress or unpredictable environmental conditions will allocate carbon and energy in ways that permit survival, while perhaps compromising other competing demands such as reproduction or storage.

In a study aimed at tracing the seasonal patterns of photosynthate distribution in 4 yr-old seedlings of red pine (*Pinus resinosa*), Schier (1970) exposed the trees to labeled $^{14}CO_2$ and tracked changes in tissue concentrations of ^{14}C over the growing season. During May–June, rates of shoot and needle growth were high, these tissues acted as the major sinks for ^{14}C, and relatively little photosynthate was transferred to fine roots. In July, when elongated shoots were no longer a strong sink for photosynthate, the proportion of ^{14}C transferred to fine roots increased to more than twice the level observed in May. By autumn, the cessation of shoot and needle elongation and cambial growth resulted in a large transfer of ^{14}C photosynthate to fine roots. The author also observed a massive channeling of ^{14}C into non-cell wall fractions of red pine roots and shoots during autumn, thus indicating that storage of non-structural carbohydrates was occurring prior to winter dormancy. Similar results were reported by Horwath et al. (1994) based on studies with 2 yr old hybrid polar trees. In July, 80% of recovered ^{14}C label was found in aboveground poplar shoots, whereas carbon allocation shifted to belowground sinks in September, with 51% of ^{14}C label recovered from the root system of hybrid poplars.

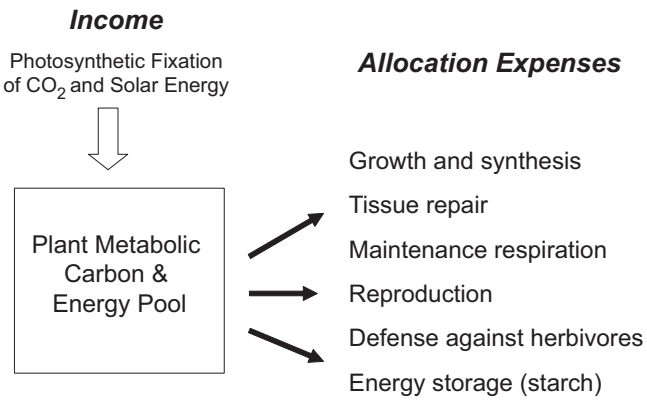

Fig. 4.18 Carbon and energy fixed through plant photosynthesis enter a general metabolic carbon pool that is used in growth, maintenance, and other life processes. Allocation of carbon and energy to various plant processes and sinks can change with conditions and plant phenology

Metabolic Allocation to Plant Defense

Plants are subject to varying intensities of herbivory and insect attack; in response, plants often invest some portion of their energy and carbon budget to biochemical defense (Harborne 1982). The three general classes of plant defensive compounds used against herbivory include: (i) substances that reduce palatability of plant tissues (e.g., cucurbitacins); (ii) plant metabolites that act as toxic deterrents (e.g., alkaloids and cyanogens); and (iii) biochemical products that reduce the nutritional value of plant tissues (e.g., tannins). The synthetic pathways that generate these **secondary compounds** in plants include the Shikimic Acid Pathway, terpenoid pathway, and various reaction pathways involving nitrogen metabolism in plants (Fig. 4.16). The scientific discipline that focuses on the role of these compounds in plant-insect interactions has been termed **ecological biochemistry** or **chemical ecology**.

One intriguing example of a nitrogenous toxin is the class of **cyanogenic glycosides** (including compounds such as linamarin) that are produced by certain plant species. After ingestion by herbivores, cyanogenic glycosides are broken down by enzymes to release hydrogen cyanide (Fig. 4.19).

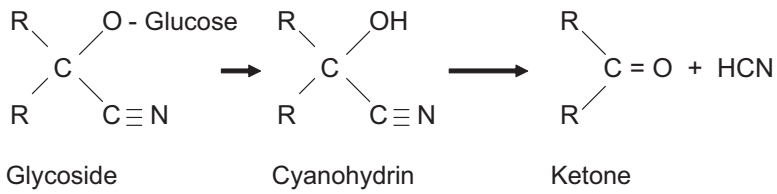

Fig. 4.19 Pathway for release of hydrogen cyanide from cyanogenic glycosides Reprinted from Harborne, J.B. Introduction to Ecological Biochemistry Chapter 3 page 81 ©1982 with permission from Elsevier

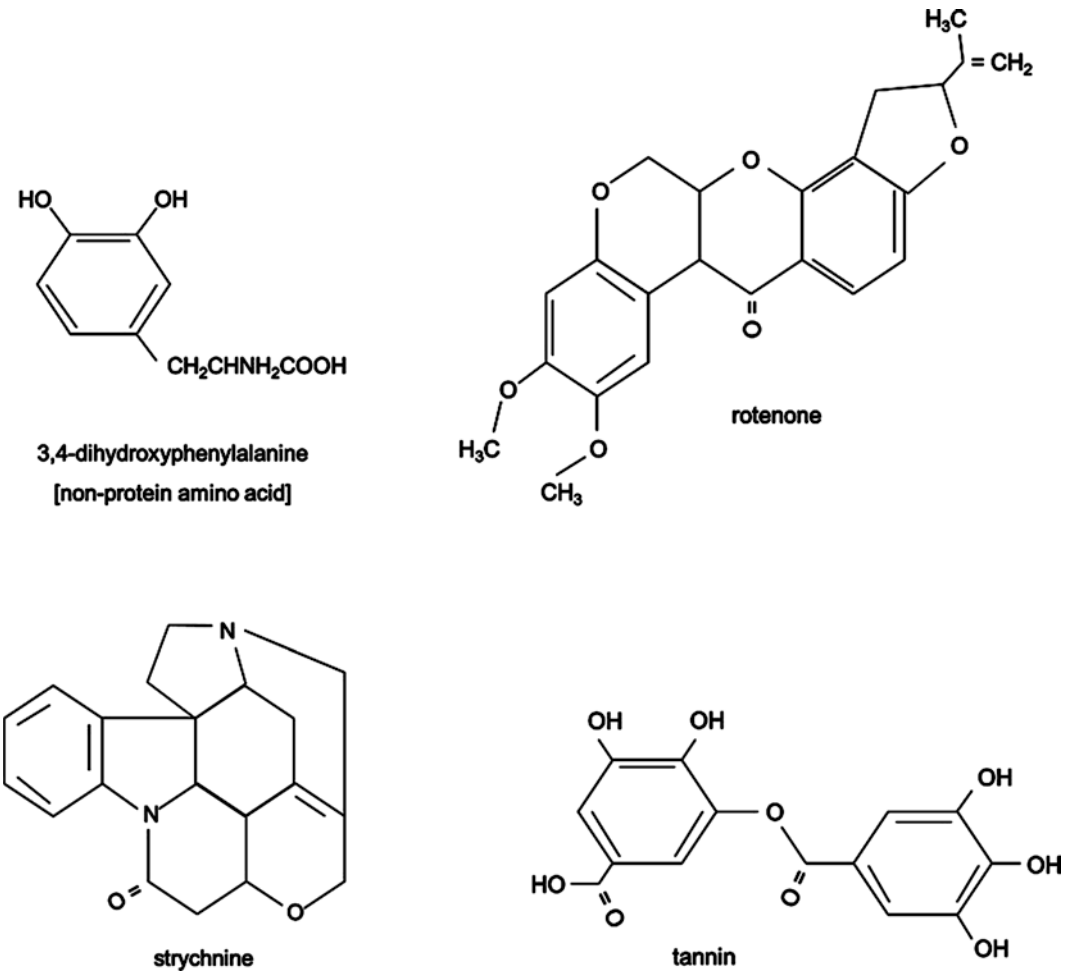

Fig. 4.20 Examples of plant defensive compounds used against insect herbivory

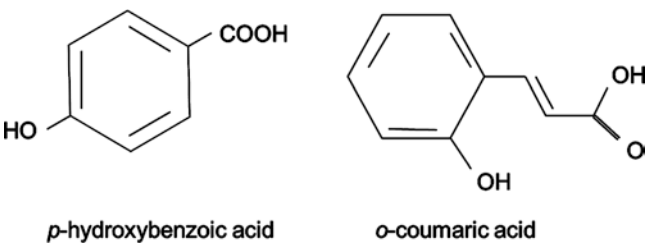

Fig. 4.21 Examples of water soluble allelopathic agents in plants

This compound inhibits cellular respiration by interfering with cytochromes in the electron transport system.

Examples of nitrogen-based plant toxins also include heterocyclic **alkaloids** such atropine and strychnine (Fig. 4.20) that cause mortality or nervous system disorders. In some plants, the production of toxic non-protein amino acids such as 3,4-dihydroxyphenylalanine (Fig. 4.20) interferes with herbivory. When these compounds are mistakenly incorporated into protein synthesis by an insect herbivore, non-functional enzymes are produced that contribute to insect mortality. Other plants rely on polycyclic toxic **flavonoids** such as rotenone (Fig. 4.20), **quinones** such as hypericin, or triterpenoids such as **cucurbitacins** that impart a bitterness to host plants and act as feeding deterrents (Harborne 1982). An example of the tannins found in the foliage of oaks and other plants is also shown in Fig. 4.20. These compounds bind soluble protein in the gut of insects, thus interfering with digestion and assimilation of amino acids necessary for insect nutrition and growth.

Some plants allocate a portion of metabolic output to the production of **allelopathic** substances that are used in competitive interactions among different species (Harborne 1982). Most allelopathic compounds are either volatile terpenes or phenolic substances that are released to inhibit the growth of potential competitors. Examples of water-soluble allelopathic agents generated by plants include *p*-hydroxybenzoic acid and *o*-coumaric acid (Fig. 4.21). Another well-known example is juglone (5-hydroxynapthoquinone), an allelopathic substance produced by black walnut (*Juglans nigra*) trees to suppress understory competitors

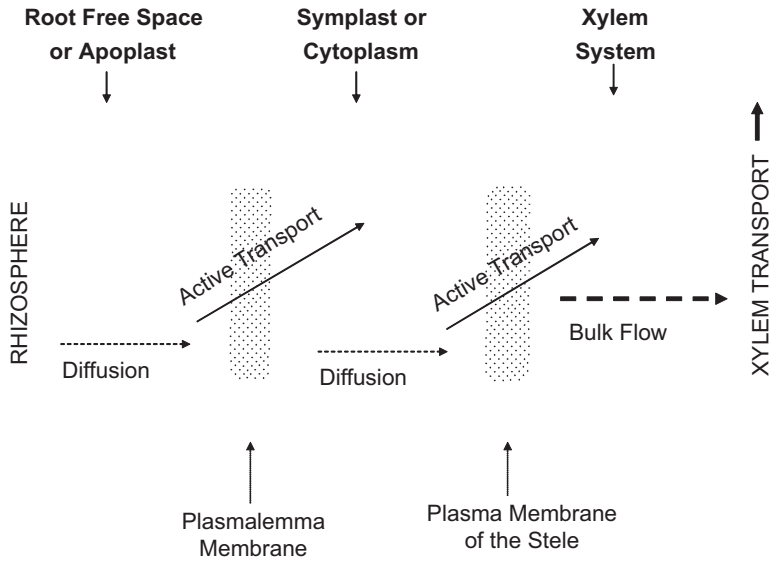

Fig. 4.22 General pathway of ion uptake from the soil rhizosphere into a plant

Plant Nutrient Cycling

Plants act as major nutrient sinks and element cycling pumps in terrestrial ecosystems, and exert a strong influence on the biogeochemistry of many elements. As an example, new foliage production in a mature northern hardwoods forest in New England requires >60 kg N ha^{-1} yr^{-1}, and litterfall recycling of senescent foliage returns roughly 30 kg N ha^{-1} back to the soil each year. By comparison, annual inputs of N in atmospheric deposition in the region are roughly 6 to 8 kg N ha^{-1} yr^{-1}. In the section that follows, we shall examine patterns and processes of plant element cycling, including nutrient absorption, internal nutrient cycling, and element recycling through leaching and turnover of detritus.

Plant Nutrient Absorption

Plant nutrient acquisition is dominated by belowground absorption of solutes by plant fine roots and filamentous **hyphae** of symbiotic mycorrhizal fungi in the soil rhizosphere. Although plant scientists have historically assumed that fine root systems primarily absorb soluble inorganic ions from the soil solution and exchangeable cations from soil colloids, evidence indicates that plants can also absorb simple soluble organic forms of nutrients, including glycine and alanine (Nasholm et al. 1998; Rothstein 2009; Moran-Zuloaga et al. 2015).

Nutrient acquisition by higher plants is a multi-stage process that can be represented in simplified fashion by the diagram in Fig. 4.22. Nutrient ions and solutes in the soil matrix or **rhizosphere** move by diffusion and bulk flow toward the nutrient depletion zone surrounding the fine root tips and associated mycorrhizal hyphae of a plant. Initially, ions or solutes enter the **root free space** or **apoplast** and may adsorb to the cell walls of plant roots. From there, most ions move by active transport mechanisms across the first membrane barrier of the root system, the **plasmalemma**. Ions then diffuse through the cytoplasm within the **symplastic system** of the plant until they encounter the next membrane barrier, the plasma membrane of the stele. After active transport across that membrane, ions move through the xylem via bulk flow until they reach a sink destination where the ions are actively transported into receiving cells or tissues. Along the way, ions may be subject to chromatographic separation and differential transport.

Rates and patterns of nutrient uptake vary considerably and are subject to different physiological and environmental controls. If free diffusion were responsible for uptake, the rate for each ion would be low and essentially proportional to the concentration gradient. Yet, evidence indicates that (i) ion uptake rates are much higher than those accounted for by diffusion, and (ii) plants exhibit ion selectivity and can accumulate ions according to internal demand via **active transport**, independent of external concentration differences. Given the importance of active transport in nutrient uptake processes, one would expect ion uptake to be sensitive to temperature, oxygen availability (for root respiration), and metabolic inhibitors. Indeed, low temperatures or decreased oxygen tensions in the rhizosphere generally tend to inhibit rates of nutrient uptake.

Plants can enhance the availability and uptake of certain elements such as Fe and P through the release or exudation of **siderophores** into the rhizosphere. These soluble organic substances have carboxyl and hydroxyl functional groups capable of complexing and/or reducing ferric iron associated with insoluble iron phosphate salts in the soil matrix, thereby

increasing concentrations of both Fe and P for plant uptake. Burghelea et al. (2015) and others have also shown that plants and associated arbuscular mycorrhizae can promote and accelerate nutrient release from mineral weathering in the rooting zone.

In yet another example, Hamilton and Frank (2001) provided intriguing evidence that plants can stimulate soil microbes to increase decomposition rates that contribute to soil nutrient replenishment. Using a ^{14}C label, the authors found that grazing of the grass *Poa pratensis* promoted root exudation of soluble carbon, which was quickly assimilated into microbial biomass in the soil rhizosphere. This then enhanced microbial mineralization processes contributing to soil nitrogen pools, stimulating plant regrowth in response to improved nutrient availability.

As mentioned earlier, one major mechanism that contributes to plant nutrient acquisition is the mutualism of endomycorrhizal and ectomycorrhizal fungi with plant roots. In exchange for valuable energy and carbon subsidies from their plant hosts, mycorrhizae generate a tremendous surface area of hyphal filaments that increases the nutrient absorption capabilities of the forest community. As a result, plants with mycorrhizal symbionts tend to exhibit higher growth rates and tissue nutrient concentrations as compared with plants that lack this benefit (Table 4.4). In a comparative study of pitch pine (*Pinus rigida* Mill.) seedlings grown with or without symbiotic ectomycorrhizal fungi, Cumming (1993) found that pine seedlings innoculated with *Pisolithus tinctorius* exhibited superior growth and maintained normal foliar nutrient concentrations under conditions of phosphorus limitation. In contrast, non-mycorrhizal seedlings suffered adverse effects under the same growing conditions.

Table 4.4 White pine (*Pinus strobus*) seedling growth with and without mycorrhizal infection after 1 yr (Hatch 1937)

	Seedling biomass		Leaf (% dry weight)		
Treatment	Dry Wt.	Root/shoot[a]	N	P	K
Mycorrhizal	405 g	0.8	1.24	0.20	0.74
Nonmycorrhizal	321 g	1.1	0.85	0.07	0.43

[a]Ratio of root:shoot biomass

Implications of Nutrient Uptake for Acid-Base Chemistry

Whenever ion uptake occurs, thermodynamic constraints dictate that **charge balance** must be maintained between cations and anions. This can be accomplished by various strategies in order to permit selective uptake of certain ions or preferential uptake of cations in excess of anions (Fig. 4.23). In the simplest case, a plant root might take up both K^+ and Cl^- ions from the external solution, thus maintaining charge balance inside and outside the cell while also meeting an internal demand for both potassium and chloride. Alternatively, a plant might absorb 2 K^+ while expelling two H^+ from inside the cell (Fig. 4.23b) or a plant might take up one K^+ to balance an internal malate anion while releasing one H^+ to balance the residual Cl^- ion in the external solution. In yet another case, a cell exposed to dilute nitric acid in the external solution might take up a molecule of NO_3^- and release a molecule of HCO_3^- to maintain charge balance inside and outside the cell (Fig. 4.23c).

The cumulative impacts of plant nutrient uptake on soil acid-base chemistry can be impressive as a result of the large quantities of H^+ and OH^- ions released to maintain charge balance during nutrient absorption. For example, if a forest absorbs 72 kg NH_4^+ ion ha^{-1} yr^{-1} to meet its N demand, there is a potential release of 4 kmol of H^+ ion ha^{-1} yr^{-1} associated with that N uptake (compared with atmospheric deposition

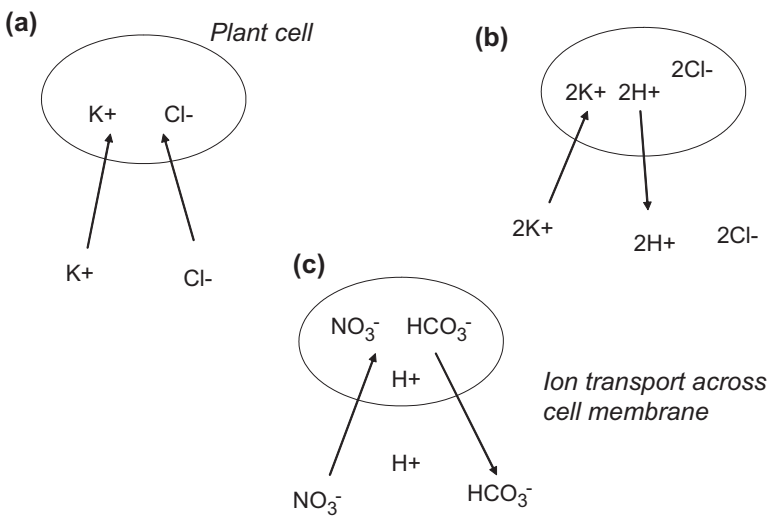

Fig. 4.23 Acid-base chemistry of ion uptake involving charge balance with (**a**) coupled uptake of a cation and anion, (**b**) exchange of protons for other cations, and (**c**) exchange of anions

inputs on the order of 1 kmol). On the other hand, forest absorption of 8 kg S ha^{-1} yr^{-1} as sulfate ion could result in the release of 0.5 kmol **ANC** ha^{-1} yr^{-1}, thus offsetting some of the potential acidification associated with cation uptake. Because woody plants tend to absorb more cations than anions on an annual basis, forest growth generally contributes to long-term acidification of the soil (Binkley and Richter 1987).

Plant Transport or Translocation of Nutrients

Following absorption from the external environment, nutrient solutes move in the xylem stream to internal plant sinks. Some of these nutrients may later be re-mobilized and retranslocated to new locations via the phloem stream. Those "mobile" elements that are subject to **retranslocation** in the phloem include K, Na, Mg, P, N, S, Cl, and soluble C. Much of the re-mobilized N transported within the plant phloem occurs in the form of organic amides such as asparagine and glutamine, whereas transport of P in the phloem occurs principally as inorganic forms of the element (Bloom et al. 1985). In contrast to so-called **mobile** nutrients, the elements Ca, Sr, Ba, B, and structural C (e.g., lignin and cellulose) are relatively **immobile** within the plant, and generally experience little to no retranslocation via the phloem.

Plant Nutrient Resorption

Resorption is an important internal recycling process in perennial terrestrial plants that permits conservation and reuse of essential or critical elements that have been acquired through energy-intensive nutrient uptake processes. Plants initiate resorption just prior to or in the early stages of foliar **senescence**, the programmed aging and deterioration of foliage that precedes leaf fall. In many woody plants, 30–60% of the N and P content of foliage may be resorbed from leaves or needles prior to leaf drop, stored over winter in woody tissues, and reused the following year for the production of new foliage. Extremely **proficient plants** are able to lower nutrient concentrations in senescent foliage to levels of 0.3% N and 0.01% P, thus conserving the vast majority of their foliar nutrient capital for those elements (Killingbeck 1996). In a survey of 77 species of deciduous and evergreen woody perennials, Killingbeck (1996) found that mean nutrient concentrations in senesced leaves of these plants were very low compared to green leaves, averaging 0.87% N and 0.06% P. Figure 4.24 illustrates the seasonal N resorption observed in an oak forest in New York, and a comparison of foliar nutrient levels in green versus senescent leaves.

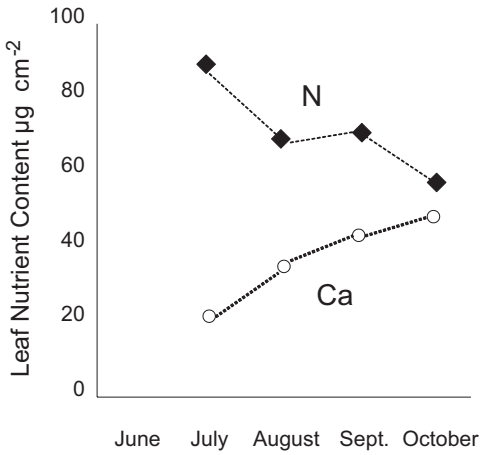

Leaves sampled prior to and after senescence have contrasting levels of nitrogen and phosphorus

Senescing leaves progressively lose N through resorption, where as Ca content increases in aging leaves

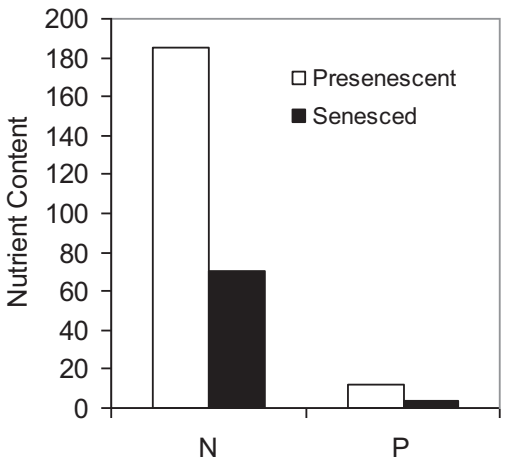

Fig. 4.24 N resorption and Ca accumulation in aging leaves in an oak forest (*left panel*) (Data from Woodwell 1974b); comparison of foliar nutrients (*right panel*) expressed in µg cm^{-2} for green versus senesced leaves (Data from Killingbeck et al. 1990)

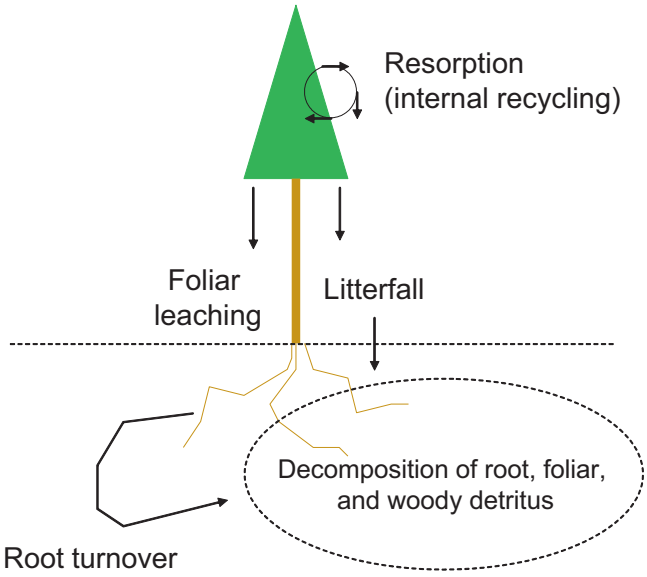

Fig. 4.25 Cycling of plant nutrients in foliar litterfall and organic matter turnover

Detrital Cycling of Plant Nutrients

Plant nutrients are recycled when foliage, branches, roots, and woody stems die and are returned to the soil as **detritus** (Fig. 4.25 and Chap. 5). The annual cycle of aboveground litterfall in forest ecosystems is usually dominated by leaves or needles that have gone through senescence prior to leaf drop. These senescent needles or leaves are typically depleted in N and P (which have been resorbed), depleted in K^+ (which has leached rapidly from the leaky senescent plant cells), and enriched in C and Ca (which have progressively accumulated in the aging foliage). In contrast, green leaves dropped prematurely during the growing season as a result of disturbances tend to have normal concentrations of critical nutrients and low C:N and C:P ratios. Besides the annual cycle of foliar litterfall, forests may experience episodic or stochastic inputs of woody detritus associated with disturbance or forest decline. The chemistry of woody litterfall is usually carbon-rich and nutrient-poor, although bark may contain elevated Ca concentrations.

In the belowground system, **fine root production and turnover** are important nutrient cycling processes that exhibit seasonal cycles related to plant activity and environmental changes. In many forest systems, there is a peak of fine root production and associated nutrient demand in spring, followed by a decline in live root biomass and an increase in fine root **necromass**. Forest ecosystems often exhibit another peak of fine root production in autumn. As live roots die and decompose, there is a fresh input of organic matter and nutrients that can be recycled within the soil by decomposition processes. Although resorption has been clearly demonstrated in the foliage of many woody species, there is conflicting evidence from studies of fine root systems as to whether these tissues undergo senescence and nutrient resorption prior to death.

Plant Canopy Processes Affecting Element Cycling

Element inputs and outputs in the forest plant canopy occur through a variety of mechanisms. Ions and associated solutes can enter the plant canopy in wet precipitation and through **impaction** or condensation of fog water and cloudwater (see Chap. 6). Although much of the moisture input usually passes through the foliage as **canopy throughfall**, 1–2 mm of moisture can be stored on the canopy as **interception**, where it eventually evaporates and leaves behind the dry salt residues formerly dissolved in the precipitation.

Dry deposition is another important pathway for element inputs to the forest canopy. Particles, microscopic aerosols, and gases are filtered or absorbed from the atmosphere through sedimentation, impaction, and dissolution processes on the vast foliar surface of the canopy. Canopy enhancement of dry deposition varies as a function of air chemistry, wind speed, leaf surface area, turbulence, canopy height and roughness, moisture conditions, and elemental chemistry.

Two of the major pathways for element removals from the plant canopy are **crown leaching** and **canopy washout.** Crown or foliar leaching occurs as water films or droplets contact the foliage and remove plant nutrients via diffusion or ion exchange (e.g., H^+ in acidic deposition exchanges for foliar Ca^{2+} adsorbed on plant exchange sites). Foliar leaching may also involve dissolution of plant substances accumulated on the cuticle or exterior of stomatal pores. Canopy leaching is an especially prominent pathway for potassium cycling during the growing season, since K^+ ion occurs as an aqueous electrolyte in plant cells and is readily leached during precipitation events. In contrast to crown leaching, canopy washout refers to the rinsing of accumulated dry deposition from the canopy surface by moisture derived from precipitation, fog water, or cloudwater. **Canopy throughfall** solutions that pass through the foliage and enter the underlying soil carry the combined element chemistry of the original precipitation input plus any solutes derived from crown leaching and canopy washout minus any solutes removed through absorption or adsorption in the canopy. The portion of wet deposition (~0–5%) that runs down branches and flows downward along the stem of a tree and into the soil is termed **stemflow**.

Elements deposited in wet or dry deposition are subject to a variety of potential transformations and transfers in the plant canopy (Table 4.5). Partial evaporation of moisture

Table 4.5 Canopy processes that may potentially contribute to changes in the chemistry of wet deposition passing through a forest canopy. ANC refers to acid neutralizing capacity or alkalinity in a solution

Canopy process	Effect on pH	Change in solution chemistry
1. Neutral salt leaching or washout	No net change	Increase in ion concentrations
2. Washout or leaching of acids	Decrease	Increase in anions and acidity
3. Uptake of NH_4^+ by microflora	Potential decrease	Loss of NH_4^+ and H^+ increase
4. Ion exchange of H^+ on cuticle	Potential increase	Loss of acidity + cation increase
5. Washout or leaching of alkalinity	Potential increase	Loss of acidity + increased ANC
6. Uptake of NO_3^-	Potential increase	Loss of nitrate + free acidity

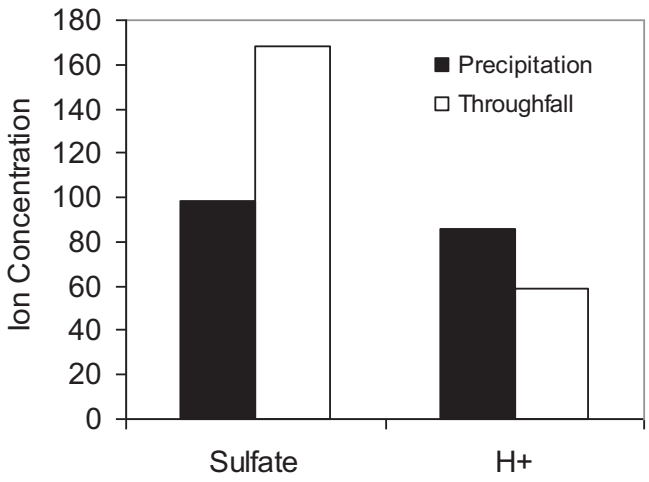

Fig. 4.26 Comparison of ion concentrations ($\mu mol_c\ L^{-1}$) in wet deposition (*dark bars*) versus throughfall (*open bars*) beneath a northern hardwood forest canopy

inputs can concentrate solutes, so that resulting ion concentrations in throughfall are higher than those in incident precipitation. This process can theoretically be checked by converting concentrations to masses and comparing the mass balance of atmospheric deposition versus canopy throughfall. Wet or dry inputs of nitrogen and other critical nutrients may be assimilated by foliage or by canopy epiphytes (e.g., lichens, bromeliads, or algae), rather than washing through the canopy and entering the soil as throughfall. As mentioned above, ion exchange processes can also occur in the canopy as inputs of ions in precipitation or cloudwater adsorb to charged sites on the plant cuticle or epidermis and cause the release of exchangeable ions from the host plant. For example, inputs of acid precipitation are often neutralized in the forest canopy when protons from sulfuric or nitric acid exchange with Ca^{2+} or Mg^{2+} ions on the foliar surface, producing a partially neutralized solution of Ca and Mg salts of sulfate or nitrate in the resulting throughfall solution.

Figure 4.26 illustrates how canopy processes in a forest ecosystem can dramatically transform the chemistry of input solutions of wet deposition. In this example based on data from Cronan and Reiners (1983), the sulfate concentration in throughfall is greatly enriched compared to precipitation (presumably through canopy washout), whereas free H^+ ions are attenuated in transit through the hardwood canopy (presumably through ion exchange for Ca^{2+} and other cations leached from foliage)

NUE as an Index of Plant Nutrition and Nutrient Cycling

The concept of **nutrient use efficiency** (NUE) provides a useful indicator for comparing plant performance and nutrient cycling under various environmental conditions (Vitousek 1982). NUE is commonly defined as the amount of biomass produced per unit of nutrient; as such, it is simply the inverse of nutrient concentration (Chapin and Van Cleve 1989). Efficient plants are able to maximize carbon fixation per unit of nutrient absorbed, and thus have high nutrient use efficiencies. On a whole-plant basis, NUE generally increases under conditions of nutrient stress or limitation, because tissue nutrient concentrations decline and the ratio of root biomass (with low tissue nutrient concentrations) to leaf biomass (with higher tissue nutrient concentrations) increases (Chapin and Van Cleve 1989). In a comparison of five species of shrubs, Field et al. (1983) found more than a two-fold range of variation in the nitrogen use efficiency of these plants.

Nutrient Limitation

In the field, plant growth and performance are strongly influenced by resource availability, and when an essential resource is limited, plants typically respond either with reduced growth or increased resource use efficiency (e.g., NUE). Plant **nutrient limitation** occurs under a variety of conditions in response to sub-optimal supply or outright deficiencies of single or multiple key nutrient elements. Some of the more common elements that limit plant growth in forested ecosystems are N, P, Ca, and Fe, although many other examples are reported in the literature.

Effects of Chemical Stress on Plants

In concluding this chapter, we shall examine ways in which environmental stresses can influence plant functions through a variety of biogeochemical interactions. A **stress** can generally be viewed as any biotic (e.g., pathogen) or abiotic

(e.g., drought) constraint or influence that adversely affects critical life processes for an organism. It is not uncommon for plants to experience multiple stresses that individually exert sub-lethal effects on the target, but which collectively can disrupt normal homeostasis for a plant. In the three examples below, we shall briefly consider how plants respond to exposure to acidic deposition, soil metal toxicity, and oxidant pollution in the form of ozone.

Effects of Acidic Deposition on Plant Membrane-Bound Calcium

One of the interesting biogeochemical interactions in northern forests is the impact of acidic cloud deposition on calcium cycling and biogeochemistry of red spruce trees. Studies in the upper elevations of the Green Mountain National Forest of Vermont have shown that acidic cloud water leaches membrane-bound Ca from red spruce needles. This process disrupts normal membrane function and interferes with the ability of mature red spruce trees to achieve and to maintain winter frost hardiness. Investigators have concluded that loss of membrane-bound Ca predisposes high elevation red spruce trees to increased winter injury and risk of mortality during severe winter cold periods and freeze-thaw cycles (DeHayes et al. 1999; Schaberg et al. 2000). The evidence of this freezing injury is often apparent in springtime, when rusty red dead needles are observed on the tips of high-elevation red spruce trees.

Aluminum Antagonism and Toxicity Stress

Investigators have described a wide range of fascinating environmental conditions where plants are adversely affected by exposure to toxic elements that interfere with normal life processes. For instance, when plant roots growing in acidic soils are exposed to elevated concentrations of ionic aluminum (Al^{3+}), sensitive species may suffer from (i) antagonistic interference with cation uptake or (ii) toxic interactions involving irreversible damage to cells and essential biomolecules (Haug 1984). Symptoms of "aluminum stress" in these sensitive species may result from any of several specific biogeochemical interactions: (i) Al may bind to nucleotides and nucleic acids, inhibiting cell division; (ii) Al can bind to ATP, ADP, or membrane-bound ATPases, interfering with energy transfer; (iii) Al may interfere with enzyme systems such as acid phosphatases; (iv) Al can bind to plant calmodulin, seriously disrupting cellular control, signaling, and contractile processes; (v) Al may bind to phospholipid groups and alter membrane permeability; or (vi) Al can bind to root apoplast surface adsorption sites and interfere with plant uptake or selectivity for nutrient ions such as Ca^{2+} and Mg^{2+} (Cronan and Grigal 1995). In addition, elevated foliar Al, coupled with decreased foliar Ca and Mg, may promote higher rates of dark respiration, adversely affecting the carbon balance of plants (McLaughlin et al. 1990).

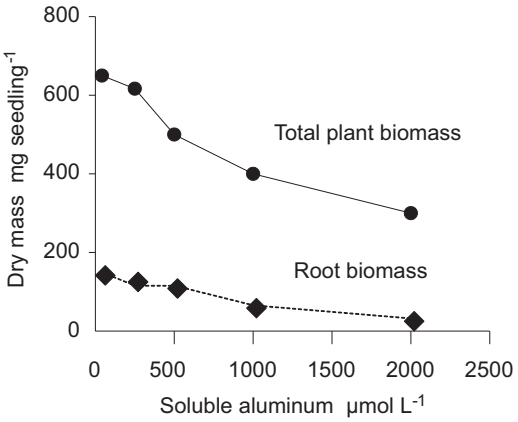

Fig. 4.27 Adverse impact of increasing soluble Al concentration on growth of red spruce (*Picea rubens*) seedlings (Data from Cronan 1994)

In its various manifestations, stress from ionic aluminum in sensitive plants can adversely affect energy transformations, carbon balance, cell division, membrane transport, nutrient accumulation, as well as activities regulated by calmodulin, a multi-functional, Ca-dependent regulatory protein (Sucoff et al. 1990). These responses can translate directly into decreased root and shoot growth in plants exposed to elevated concentrations of ionic Al (Fig. 4.27).

Plant Responses to Ozone Stress

Tropospheric or ground-level ozone (O_3) occurs at concentrations ranging from less than 50 to over 100 ppb in the lower atmosphere. It is a potential health risk and environmental stressor for sensitive forest species at ambient air concentrations below 100 ppb. Visual symptoms of ozone stress include **foliar stipling** (Findley et al. 1996), tip **necrosis** (Wenner and Merrill 1998), bifacial black necrosis and premature leaf abscission (Yun and Laurence 1999), and accelerated cellular senescence (Gunthardt-Goerg et al. 2000). Physiological responses to this oxidant gas can include impaired photosynthetic performance and altered plant carbon cycling.

The threshold for adverse responses to ozone is a function of the sensitivity of individual species or phenotypes to ozone stress, differences in stomatal conductance among species (Kolb et al. 1997), air concentrations of ozone, and cumulative plant exposure to ozone. Black cherry (*Prunus serotina*) exhibited foliar injury from exposure to **ambient ozone** concentrations in the Great Smoky Mts. (Chappelka et al. 1999a), and developed foliar stress symptoms in another study with

cumulative exposures ≥60 ppb ozone (Hildebrand et al. 1996). Trembling aspen (*Populus tremuloides*) and red oak (*Quercus rubra*) seedlings experienced reduced growth and photosynthesis at 95 ppb ozone (Volin et al. 1998). In contrast, red spruce (*Picea rubens*) tolerated 4 seasons of exposure to 2X ambient ozone (Laurence et al. 1997), and red maple (*Acer rubrum*) cultivars tolerated acute exposures of 300 ppb ozone (Findley et al. 1996). Overall, studies using controlled exposures to ozone have demonstrated that sensitive tree species suffer significant adverse effects from ozone stress, whereas other tolerant species are able endure acute and chronic ozone exposures without major repercussions.

Ollinger et al. (1997) combined leaf-level ozone response data from field experiments with a forest simulation model to estimate regional effects of ambient ozone concentrations on mature hardwood forests in the northeastern U.S. Model results suggested that ozone stress could reduce forest net primary production as much as 16% and wood production as much as 22%. Thus, both empirical and modeling studies indicate that the structure and function of forest ecosystems – containing a variable mix of sensitive and tolerant species – can potentially be adversely impacted by stresses associated with ozone air pollution.

Cycling of Organic Matter

5

Introduction

One of the useful ways of integrating concepts of energy flow and nutrient cycling in a terrestrial ecosystem is to focus on the cycling of organic matter. When we consider the chemical energy and nutrients sequestered in terrestrial plant biomass or within a forest soil, it is important to understand that they are part of a larger ecosystem cycle of organic matter characterized by (i) multiple storage pools with different residence times and (ii) multiple component processes, including trophic transfers into consumer organisms, production of **detritus** or **necromass** from senescent or dead life forms, release of elements from organic matter via decomposition and mineralization processes, evolution of gaseous CO_2 through respiration, and recycling of nutrients into new growth of organisms. In this chapter, we examine how organic matter pools are distributed in the landscape, what processes control organic matter cycling, and how organic matter cycling is influenced by environmental and ecological conditions.

Ecosystem Perspective

The primary pools and pathways of organic matter cycling in a terrestrial ecosystem can be illustrated with the organic matter budget of a forest ecosystem from the northeastern U.S. (Fig. 5.1). In this example, the major storage compartments of organic matter include: mineral **soil organic matter** (280,000 kg dry organic matter ha^{-1}), aboveground biomass (189,900 kg ha^{-1}), **forest floor** or O horizon detritus (54,000 kg ha^{-1}), and belowground biomass (50,220 kg ha^{-1}). Transfers of organic matter among compartments and annual changes in storage pools in the forest ecosystem are as follows: net primary production of aboveground + belowground plant biomass (10,700 kg dry organic matter ha^{-1} yr^{-1}), decomposition of forest floor detritus and soil organic matter (9200 kg ha^{-1} yr^{-1}), litterfall return of leaf and woody detritus to the soil (6220 kg ha^{-1} yr^{-1}), inputs from atmospheric deposition (34 kg ha^{-1} yr^{-1}), leaching of dissolved organic matter (**DOM**) from the forest canopy (62 kg ha^{-1} yr^{-1}), and stream hydrologic export of DOM and suspended particulate organic matter or POM (45 kg ha^{-1} yr^{-1}).

In this example, we have an ecosystem where the two largest storage reservoirs of organic matter are living biomass and the combined forest floor and mineral soil pools. Although the forest biomass pool is aggrading, the soil pool of organic matter is relatively stable, with annual inputs of detritus from litterfall and root turnover (6220 + 3620 kg ha^{-1} yr^{-1}) approximately balanced by losses of organic matter through decomposition (9200 kg ha^{-1} yr^{-1}). As you consider the example in Fig. 5.1, it is important to note that this estimate is merely one specific illustration of a terrestrial organic matter budget. Depending upon the composition and structure of a forest community, the nature of previous disturbances, topography, soil conditions, climate, and other environmental factors, the relative and absolute sizes of organic matter pools and transfers can vary enormously among different upland and lowland terrestrial ecosystems.

Storage of Organic Matter in Forest Soils, Biomass, and Woody Debris

On a world-wide basis, the pool of organic carbon in soils amounts to approximately 1500 Pg C of stored detritus and soil organic matter in the upper 1 m of soil (where

C.S. Cronan, *Ecosystem Biogeochemistry*, Springer Textbooks in Earth Sciences, Geography and Environment, DOI 10.1007/978-3-319-66444-6_5

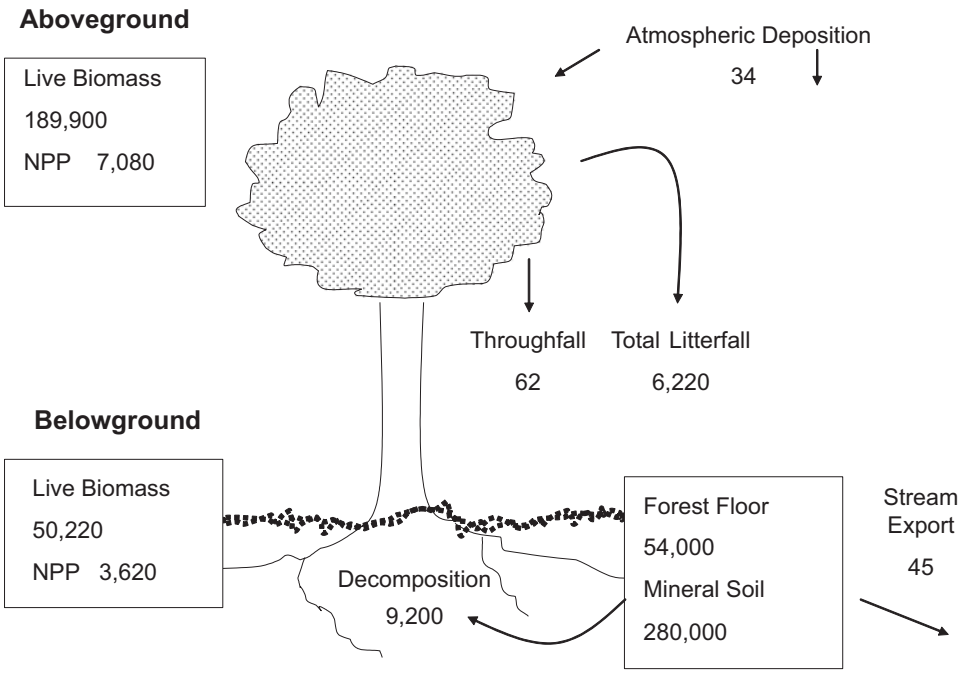

Fig. 5.1 Organic matter budget of an aggrading mid-successional age hardwood forest ecosystem at Hubbard Brook, NH. Units are kg ha^{-1} for masses and kg ha^{-1} yr^{-1} for rates of net primary production (NPP) and other fluxes (Based on data from Fahey et al. 2005)

Pg = 10^{15} g), and 2344 Pg C in the upper 3 m of soil (Jobbagy and Jackson 2000). Organic matter at the soil surface is dominated by litterfall inputs of foliar and woody detritus and dead fine roots located in the surface soil horizon. Subsurface organic matter is derived from root system turnover and decay, vertical infiltration and accumulation of dissolved organic matter (DOM) on soil mineral colloids, mixing of surface litter by soil fauna, and growth and turnover of soil microbial biomass. In wetland ecosystems, organic matter in the form of subsurface peat may accumulate as successive layers of *Sphagnum* moss and plant litter are buried beneath subsequent annual inputs of plant detritus under waterlogged conditions that prevent all but minimal decomposition.

Organic matter in forest soils exists in a continuum of detrital fractions ranging from recognizable litter and woody debris, to humus, to humic coatings on soil minerals, and finally to DOM in the soil solution phase. Some investigators prefer to make a spatial distinction between the litter and humus of the surface O horizon and the soil organic matter (**SOM**) of the subsurface mineral horizons in their analysis of organic matter budgets. Others focus on turnover rates of organic matter, treating soil organic matter as a mixture of two operationally-defined pools: a smaller "labile" pool of carbon and a larger more stable or refractory pool of "protected" carbon. Still other investigators distinguish two different density classes of organic matter: a mineral-free **light fraction**, which includes partly decomposed plant material and microbial biomass, and a denser **heavy fraction** consisting of organic material that is adsorbed onto mineral surfaces or is sequestered within micro-aggregates (Strickland and Sollins 1987; McFarlane et al. 2012). These light and heavy

Table 5.1 Comparison of light and heavy fractions in a range of different soils and soil textures (Strickland and Sollins 1987)

Location	Soil type	% sand	% clay	Heavy fraction %	Light fraction %
Waldo, FL	Spodosol	91.5	3.3	99	1
HJA, OR[a]	Inceptisol	46.3	22.2	94	6
Cascade,OR	Inceptisol	41	14	74	26
Konza, KS	Mollisol	20	20	99.5	0.5
Costa Rica	Inceptisol	9	73	99.75	0.25

[a]HJA = H.J. Andrews Forest

SOM fractions can be separated by flotation in solutions of varying density (e.g., NaI solution with a density of 1.70 g cm^{-3}). In a comparison of soils from North and Central America, Strickland and Sollins (1987) reported that heavy fractions tended to predominate over light fractions (Table 5.1).

Soil Organic Matter and Soil Carbon Storage

In forest ecosystems, the **ash-free** organic matter content of the entire soil profile generally ranges from approximately 100,000 to 500,000 kg SOM ha^{-1}. Jobbagy and Jackson (2000) surveyed the literature and reported that soil organic carbon content (**SOC**) in the upper 3 m of soil averaged 125,000 kg C ha^{-1} in boreal forests, ≥ 200,000 kg C ha^{-1} in temperate forests, and 280,000 kg C ha^{-1} in tropical evergreen forests (note that soil organic matter is roughly 48% carbon by mass). The authors also found that total SOC content generally increased with precipitation and soil clay

Table 5.2 Distribution of soil carbon pools in forest soil profiles at Harvard Forest, MA (Gaudinski et al. 2000) and Hubbard Brook Experimental Forest, NH (Huntington et al. 1988)

Harvard Forest, MA		Hubbard Brook Forest, NH	
Soil horizon	g C kg^{-1} soil	Soil horizon	g C kg^{-1} soil
Oi	450	Oi + Oe	465
Oe + Oa	470	Oa	296
A	270	E	25
Ap	60	Bh	68
Bw1	20	Bs1	63
Bw2	6	Bs2	36

Table 5.3 Comparison of forest floor pools of organic matter and nutrients (kg ha^{-1}) Data from Lang et al. (1981), Turner and Singer (1976), and Gosz et al. (1976)

Site	Ash-free Dry mass	N	P	Ca	Mg	K	C:N
Subalpine fir, NH	92,200	2300	215	165	100	95	19
Northern hardwood, NH[a]	46,800	830	60	195	25	35	23
Pacific silver fir, WA	53,500	650	45	545	45	175	--

[a]More recent data from Huntington et al. (1988) suggest that this forest floor contains 1300 kg N ha^{-1}

content and decreased with temperature. However, the importance of these controls switched with soil depth, so that climate dominated shallow layers and clay content dominated deeper layers. Mueller et al. (2015) examined controls on SOC in a common garden experiment with 14 tree species and reported that total C in the O horizon and upper 20 cm of mineral soil was negatively correlated with earthworm abundance and positively correlated with the abundance of Al, Fe, and protons. In Table 5.2, examples of two soil profiles are shown that illustrate vertical distributions of soil organic carbon in cool temperate forest ecosystems of North America.

Forest Floor Storage

The ash-free dry mass of the forest floor or O horizon can range from <10,000 kg organic matter ha^{-1} to >110,000 kg ha^{-1}, and often represents 15 to 30% of the total soil organic matter reservoir. In a review of literature on organic matter cycling, Vogt et al. (1986) reported that mean forest floor masses ranged from 2200–22,500 kg ha^{-1} in tropical forests, from 11,500–20,000 kg ha^{-1} in warm temperate forests, from 14,000–44,500 kg ha^{-1} in cold temperate forests, and averaged 44,700 kg ha^{-1} in boreal evergreen forests. In the same study, the authors reported that **mean residence times** of forest floor organic matter ranged from <2.5 yr in tropical forests, <5 yr in warm temperate forests, from 4 to 18 yr in cold temperate forests, and averaged 60 yr in boreal evergreen forests. Stored nitrogen and phosphorus pools in the forest floor or O horizon have been reported to range from 35 to >2200 kg N ha^{-1} and from <20 to 220 kg P ha^{-1}. Table 5.3 presents a comparison of forest floor organic matter and nutrients for three forest ecosystems.

Turnover Rates and Age of Soil Organic Matter Reservoirs

How long does organic matter persist in the soil? Studies have shown that the age and turnover rates of soil organic matter can vary widely as a function of site conditions, history, and methods of soil fractionation (McFarlane et al. 2012). In a study of three well-drained soils from boreal, temperate, and tropical forests, Trumbore (2000) reported that mean residence times for soil C in the 0–40 cm depth ranged from 200 to 1300 yr. Yet, >40% of the SOM in those soils cycled on time scales of decades or less, as indicated by analysis of ^{14}C radiocarbon data. The author concluded from this evidence that the bulk soil contained a labile faster-cycling pool of C that turned over much more rapidly than the overall reservoir of humified and protected soil C. In an earlier study conducted in California, Trumbore et al. (1996) reported that the light fraction of SOM in montane forest soils turned over every 6–8 yr at lower elevations and every 53–71 yr in high elevation forests, where cooler climatic conditions inhibited decay. Another study of carbon cycling at Harvard Forest, MA showed that turnover times for SOM increased with soil depth, averaging 2–5 yr for recognizable leaf litter, 5–10 yr for root litter, 40–100 yr or more for low density humified material, and over 100 yr for SOM associated with soil minerals (Gaudinski et al. 2000). In another example from New Zealand, Baisden et al. (2011) estimated mean residence times of 9 to 17 yr for organic matter in the upper 8 cm of soils, based on ^{14}C data.

Influence of Land Management and Disturbance on SOM

Several studies have demonstrated the dynamic responses of soil organic matter to changes in land use activity, vegetation cover, and disturbance. Richter et al. (1999) reported that conversion of a former cotton field in South Carolina to loblolly pine forest resulted in the accumulation of 39,250 kg soil C ha^{-1} over a period of 40 yr, with 96% in the forest floor and 4% in the mineral subsoil. On average, the soil gained roughly 1000 kg C ha^{-1} yr^{-1} during 40 yr of forest growth, but the mineral soil only gained 4% of this new net carbon input, or 40 kg C ha^{-1} yr^{-1}. At Harvard Forest, MA, Gaudinski et al. (2000) estimated that O and A soil horizons beneath a temperate deciduous forest accumulated 44,000 kg C ha^{-1}

above the plow layer during the century following abandonment in the late 1800's. In contrast, Veldekampe (1994) reported that deforestation, followed by 25 yr of pasture cover, caused a net loss of 21,800 kg C ha^{-1} in a forest Andosol in Costa Rica. Another study of harvesting impacts in New England showed that the forest floor can potentially lose 50% of its mass after harvesting, because of decreased annual inputs of litter and increased decomposition (Covington 1981). However, over the next 50–75 yr, the forest floor regains its original mass as a result of increased inputs of woody litter from stand thinning. In a lengthy review of literature on soil C storage, Johnson (1992) found that current evidence supports the following conclusions: cultivation leads to substantial decreases in soil C in almost all instances (see also Cusack et al. 2012); most studies indicate little or no change in forest soil C following harvesting and reforestation; the effects of fire on soil C storage vary as a function of fire intensity; and soil C tends to increase with fertilization. Frey et al. (2014) reported that nitrogen amendments to a temperate forest in central Massachusetts induced soil C accumulation that was attributed to suppression of organic matter decomposition, reduced fungal biomass, and increased lignin accrual in response to fertilization.

Aboveground and Belowground Biomass

Forest ecosystems across the biosphere generally exhibit aboveground biomass values ranging from <100,000 to >500,000 kg organic matter ha^{-1}, depending on the climate, soil fertility, and successional status of a forest. Some of the major differences in forest biomass in a given biome reflect the impacts of stand history and disturbance. As an example, Reiners (1992) documented successional recovery in the aftermath of clear-cut logging at Hubbard Brook Experimental Forest, NH, noting that forest aboveground biomass increased from 7500 kg ha^{-1} at 5 yr to 52,000 kg ha^{-1} at 20 yr after disturbance.

Although many estimates of aboveground biomass exist, estimates of belowground biomass are much less common in the literature. Total fine root biomass typically ranges from 2000 to 10,000 kg ha^{-1}, whereas coarse plus large root biomass can exceed 100,000 kg ha^{-1}. As illustrated in Fig. 5.2, the biomass distribution of roots in the soil profile generally follows an exponential decay curve, with decreasing biomass as a function of soil depth. Death and subsequent turnover of root biomass provide large annual transfers of carbon and other elements to the SOM reservoir.

Coarse Woody Debris

Coarse woody debris is a term that refers to the dead and decaying remains of downed tree boles, standing dead trees, coarse roots, and branches in a forest ecosystem. Some organic matter budgets ignore or under-sample coarse woody debris, others combine it with detritus in the forest floor or soil organic matter compartments, whereas other organic budgets explicitly quantify woody detritus as a separate storage reservoir in a forest ecosystem. Coarse woody debris (CWD) is a carbon-rich substrate that typically averages 44% cellulose, 26% hemicellulose, and 30% lignin (Harmon et al. 1986). In Douglas-fir stands at H.J. Andrews Experimental Forest in Oregon, Grier et al. (1981) reported that standing dead stems plus fallen logs amounted to >200,000 kg ash-free organic matter ha^{-1}, and constituted >15% of the total mass of ecosystem organic matter. Harmon et al. (1986) summarized data indicating that (i) total volumes of CWD in forest ecosystems range from a low of 60 m^3 ha^{-1} in an *Abies balsamea* forest to 1189 m^3 ha^{-1} in a *Pseudotsuga-Tsuga* forest, and (ii) total masses of CWD generally range from 11,000–38,000 kg ha^{-1} in temperate deciduous forests and from 10,000–511,000 kg ha^{-1} in temperate coniferous forests.

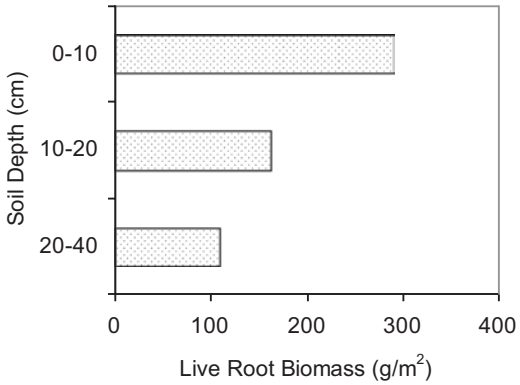

Fig. 5.2 Depth distribution of root biomass (<3 mm diameter) in a Norway spruce stand, Maine, USA (Data from Cronan 2003)

Transfers of Organic Matter in Detritus and Solution

Aboveground Litterfall

Litterfall transfers of organic matter from the aboveground plant community to the soil are one of the major pathways for recycling of nutrients in terrestrial ecosystems. Plant litter can include foliage, flowers, twigs, branches, cones, and stems or boles of woody plants. The flux of litter to the soil surface usually exhibits regular seasonal pulses associated with leaf drop and flowering, episodic inputs of woody litter resulting from windstorm activity and stand mortality, as well as continuous minor background inputs of fine litter over an annual cycle.

Bray and Gorham (1964) compared litter production across multiple international study sites and reported that mean annual leaf litterfall increases along a climatic gradient

Table 5.4 Foliage characteristics of mid-season (L) and senescent (S) leaves (Cromack and Monk 1975)

Species	Location	% N	% P	% Lignin
Chestnut oak (L)	NC	2.0	0.18	12.6
Chestnut oak (S)	NC	1.2	0.12	25.5
Yellow poplar (L)	NC	2.0	0.20	7.2
Yellow poplar (S)	NC	1.0	0.12	14.6
White pine (L)	NC	1.4	0.17	16.4
White pine (S)	NC	0.9	0.11	31.0

from 2500 kg ha^{-1} in cool temperate forests, to 3600 kg ha^{-1} in warm temperate forests, and reaches a peak of 6800 kg ha^{-1} in equatorial tropical forests. Total annual leaf plus woody litter production in the three respective climatic regions was observed to increase from 3500 to 5500 to 10,900 kg ha^{-1}. In comparing evergreen coniferous and deciduous angiosperm forests in the northern hemisphere, the same authors found that conifer forests tended to generate 10– 15% higher litterfall than deciduous forests. When they examined inter-annual variations in litter production, Bray and Gorham (1964) reported that some forests exhibit relatively consistent litterfall amounts (10– 50% differences among years), but litterfall in other forests varies by as much as 2×, 3×, or 5× between minimum and maximum years. Part of the explanation for episodic pulses of litterfall may be the stochastic inputs of CWD (coarse woody debris) that result from disturbance and successional changes in forest ecosystems. Harmon et al. (1986) reported that CWD input rates can range from 120 to 30,000 kg ha^{-1} yr^{-1} as a function of differences in environmental conditions and succession.

Transfers of elements in litterfall are important and are influenced by changes in foliar chemistry during the period of senescence preceding leaf drop. Critical elements such as N and P are resorbed from foliage, while soluble elements such as K^+ are readily leached. As a result, the nutrient content and tissue quality of litterfall can be markedly different from the characteristics of the original live foliage. In their comparative analysis of organic matter quality for mid-season and senescent foliage, Cromack and Monk (1975) demonstrated that leaf senescence is accompanied by declining N and P tissue concentrations and increased % lignin (Table 5.4).

The masses of organic matter and nutrients recycled in aboveground litterfall are a relatively large fraction of net primary production in a forest ecosystem. Vogt et al. (1986) reported that litterfall transfers of N range from 24–55 kg N ha^{-1} yr^{-1} in cold and warm temperate forests, and reach mean values up to 120–200 kg N ha^{-1} yr^{-1} in tropical forests. In comparison, values of litterfall P range from 2–11 kg P ha^{-1} yr^{-1} in temperate and tropical forests surveyed by Vogt et al. (1986). In the same literature review, the authors noted that N:P element ratios in litterfall average from 9:1 to 13:1 in temperate forests and from 22:1 to 27:1 in tropical forests. In Table 5.5, data are presented showing the magnitude of litterfall transfers for northern and southern hardwood ecosystems studied by Gosz et al. (1972) and Cromack and Monk (1975).

Table 5.5 Aboveground litterfall mass and nutrient content for a mature northern hardwoods forest in New Hampshire and a mature southern hardwoods forest in North Carolina[a]

		Mass kg ha^{-1} yr^{-1}				
	Organic matter	N	P	K	Ca	Mg
Northern hardwood						
Leaf litter	2690	30	2	13	23	4
Woody litter	2070	11	1	2	12	1
Southern hardwood						
Leaf litter	2775	24	3.5	13	34	6
Woody litter	1010	5	1	1	7	0.1

[a]Data from Gosz et al. (1972) and Cromack and Monk (1975)

One of the questions we might ask ourselves is how do litterfall transfers of elements compare with other recycling pathways in a forest ecosystem? To address this question, Fig. 5.3 presents a comparison of element recycling patterns from the forest canopy to the soil via leaf litterfall versus canopy leaching. In this example from a mature red spruce forest in Maine, we see that recycling of an electrolyte such as K^+ is dominated by leaching processes, whereas Ca, N, P, Al, Mn, and Fe are predominantly recycled through litterfall. Intermediate between these elements is magnesium, whose recycling transfers are roughly divided between litterfall and leaching (Fig. 5.3).

Belowground Detrital Inputs From Root Mortality and Turnover

How rapidly do roots cycle through life, death, and the production of belowground detritus? Some fine roots in the upper soil profile are probably turned over and are replaced by new growth one or more times per season. However, the total mass of live fine roots in a temperate forest has an average turnover time on the order of 1– 5 yr (Joslin and Henderson 1987; Cronan 2003; Trumbore and Gaudinski 2003). As shown in Fig. 5.4, seasonal variations in fine root biomass suggest that there can be pronounced peaks of root growth and marked declines in root biomass through mortality over the course of a growing season. These periods of **root turnover** result in large inputs of organic matter to the soil reservoir, accompanied by emissions of CO_2 from heterotrophs responding to these new substrates in the soil environment.

Gholz et al. (1986) reported that net annual production for slash pine roots ≤10 mm in diameter in Florida averaged 6000 kg ha^{-1} and that root turnover contributed an average of

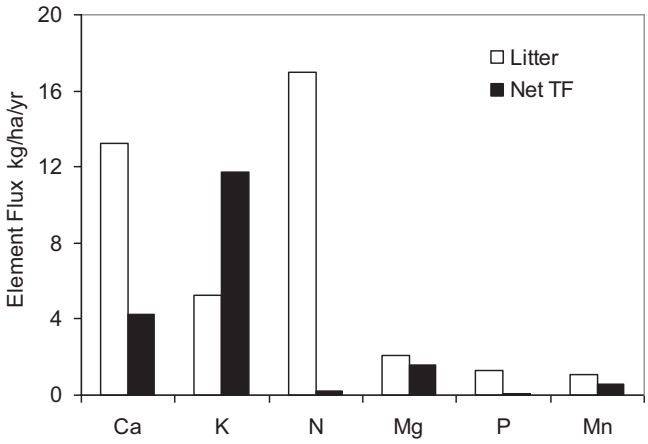

Fig. 5.3 Comparison of relative element transfers in aboveground litterfall versus net canopy leaching (net TF) in a Maine spruce-fir forest (Data from Rustad and Cronan 1988)

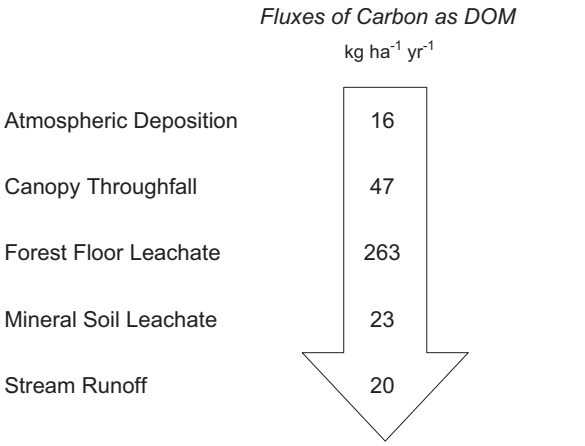

Fig. 5.5 Fluxes of carbon as dissolved organic matter at Hubbard Brook Experimental Forest, NH (Data from McDowell and Likens 1988)

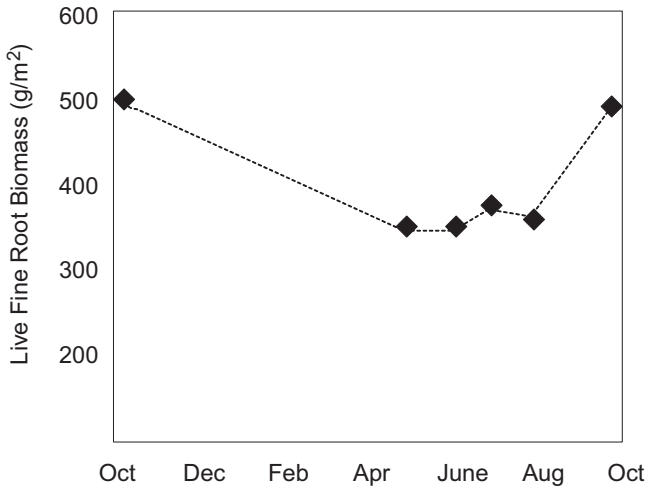

Fig. 5.4 Seasonal variations in fine root biomass in a Norway spruce stand located in Maine, USA. Six replicated sample collections are indicated by the black diamonds (Data from Cronan 2003)

3300 kg organic matter ha^{-1} yr^{-1} to soil detrital pools. In their literature survey, Vogt et al. (1986) reported that inputs of detritus from fine root turnover ranged from 1300 kg ha^{-1} yr^{-1} in a red pine plantation in New England to 7370 kg ha^{-1} yr^{-1} in a Pacific silver fir stand in Washington. They also found that root turnover accounted for 20–77% of total detrital inputs to the forest floor from litterfall plus root turnover. Other studies have indicated that annual detrital inputs to the soil profile from turnover of fine roots are approximately twice the mass of annual inputs of foliar litterfall (Raich and Nadelhoffer 1989; Cronan 2003).

Root turnover processes represent a potentially large transfer of nutrients from living biomass to detrital and SOM pools (McCormack et al. (2015). Because roots do not appear to undergo senescence, it is assumed that fresh fine root detritus has a higher nutritional content (and a lower C:N ratio) than foliar litterfall that has been subjected to resorption prior to leaf abscission. Vogt et al. (1986) reported that root turnover contributed 29– 255 kg N ha^{-1} yr^{-1} to the soil profile across all forest climatic zones; in most regions, more N was added to the soil through annual root turnover than by aboveground litterfall.

Solution Transfers of DOM

Organic matter budgets in terrestrial ecosystems include important transfers of DOM in canopy throughfall, soil drainage water, and streamflow (Neu et al. 2011). McDowell and Likens (1988) estimated that mean annual fluxes of soluble C in DOM at Hubbard Brook Experimental Forest, NH ranged from 16 kg C ha^{-1} yr^{-1} in precipitation, to 263 kg C ha^{-1} yr^{-1} in forest floor leachate, to 20 kg C ha^{-1} yr^{-1} in stream water (Fig. 5.5). Another study estimated that watershed DOM exports of soluble C to streams were approximately 36 kg C ha^{-1} yr^{-1} for hardwood forests and 45 kg C ha^{-1} yr^{-1} for coniferous forests in the Adirondack Mountains, NY (Cronan 1990). Based on work in a southern deciduous forest at Coweeta, NC, Qualls et al. (1991) estimated that annual fluxes of organic C, N, and P in DOM averaged 120, 3.5, and 0.18 kg ha^{-1} $yr^{-1}$for canopy throughfall, compared with 400, 10, and 0.28 kg ha^{-1} yr^{-1}, respectively, for forest floor leachates. C:N ratios for DOM in that study were roughly 35 for canopy throughfall and 40 for forest floor leachate solutions. Currie and Aber (1997) used a mass balance simulation model (DocMod) to estimate that mean fluxes of dissolved organic C and N from forest floors in the White Mountain National Forest, NH are 270 kg C ha^{-1} yr^{-1} and 6.6 kg N ha^{-1} yr^{-1}. Montieth et al. (2015) applied a logistic regression model to describe spatial variations in DOC exports from upland catchments in the United Kingdom.

Decomposition of Organic Matter

General Processes of Decomposition

Decomposition is a critical process that (i) is mediated by soil invertebrates, insects, bacteria, and fungi and (ii) permits the breakdown and recycling of organic matter in terrestrial ecosystems (Fig. 5.6). Melillo et al. (1989) have described decomposition as a continuum, with fresh litter as one end-member and soil organic matter as the other end point. Along this continuum, decay processes transform detritus with divergent initial chemistries and high **C:N ratios** into soil organic matter that is relatively uniform in chemical composition, with a much lower C:N ratio. In addition, decomposition processes generate CO_2 and soluble forms of nutrients that can be recycled into plants and other organisms.

During the early stages of decomposition, there is a rapid loss of mass resulting from leaching of water-soluble compounds derived from fresh litter and microbial breakdown of simple metabolites in the decaying substrate. As decomposition proceeds, there is an increase in the surface area of decayed material as litter and detritus are shredded and fragmented by soil invertebrates and insects. This is accompanied by colonization and degradation of the decaying organic substrates by fungi and soil bacteria that release enzymes such as *b*-1,4-glucosidase, phenol oxidase, and phosphatases to enhance decay (Sinsabaugh and Follstad Shah 2011; Bünemann 2015). After an initial period of exponential mass loss lasting up to 2 years, the decomposition rate declines to a lower level controlled by resistant materials in the organic substrate. At that stage, element ratios gradually converge toward relatively stable **stoichiometries** characteristic of aged soil organic matter.

Much of the weight loss during decomposition occurs as a result of carbon release from the organic substrate. So, what happens to that carbon? A mass balance of original carbon in fresh litter suggests that the fate of initial C at any point in time can be accounted for by summing the carbon released as CO_2 by decomposers, carbon leached as dissolved organic carbon (DOC), carbon immobilized in microbial biomass, and carbon remaining as residual humus or soil organic matter.

Two of the major processes controlling element dynamics during organic matter decomposition are microbial **immoblization** and **mineralization**. In the earlier stages of decomposition, microbes immobilize or sequester limiting nutrients in their biomass to facilitate growth and the metabolism of carbon substrates. As decomposition proceeds, **carbon:element** ratios in detritus gradually decline to critical thresholds where microbial mineralization is favored. At this stage, microbial growth proceeds with the simultaneous release of CO_2 and soluble inorganic nutrients from mineralization processes. As an example, C:N mass ratios typically decline during litter decomposition toward a value of 30:1 or less (Fig. 5.7), a threshold at which both carbon and nitrogen mineralization occur concurrently. Above that approximate C:N threshold, much of the N released from decaying organic matter and gained from the surrounding micro-environment is immobilized in microbial biomass. Conversely, below that critical threshold, there is net mineralization of detrital N that becomes available for general uptake, adsorption, or leaching (Manzoni et al. 2010).

Wood Decay Processes

What are the special characteristics of wood decomposition? In general, decomposition of woody material is a slow process that requires special groups of organisms capable of degrading the cellulose and lignin that dominate the structure of woody tissues. The microbes that decompose wood include two major groups: (i) the molds and staining fungi that feed on sugars and simple carbohydrates in parenchyma tissues and sapwood and (ii) the bacteria and fungi (soft rots, brown rots, and white rots) that degrade cell wall components (Harmon et al. 1986). It is the latter group of microbes that contributes to the major mass losses and structural/chemical changes in decaying wood. In most environments, the processes of wood decay are also strongly influenced by the activities of insects and soil invertebrates. Insects such as carpenter ants reduce CWD to dust and deposit this material outside the branch or log as a substrate for microbial attack. Other forest insects eat wood, reducing the particle size and modifying the wood during digestion. In addition, wood-

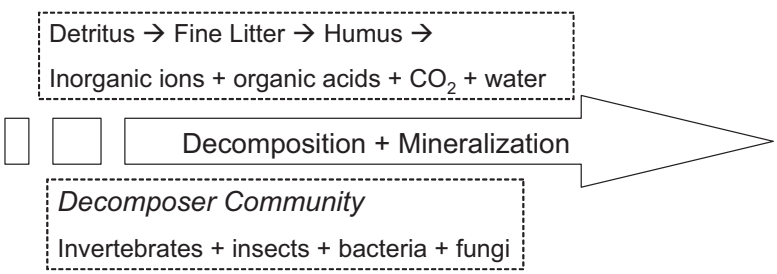

Fig. 5.6 Sequential decay of litter or detrital organic matter into residual soil organic matter, minerals, water, and carbon dioxide

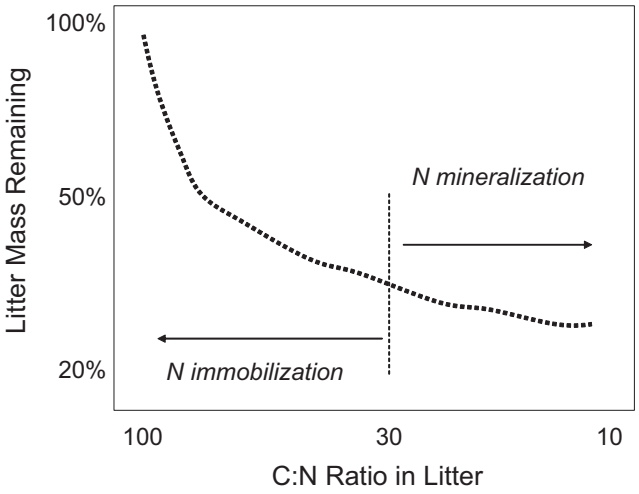

Fig. 5.7 As C/N ratios decline during litter decomposition, microbial communities shift from N immobilization to mineralization of N in substrates

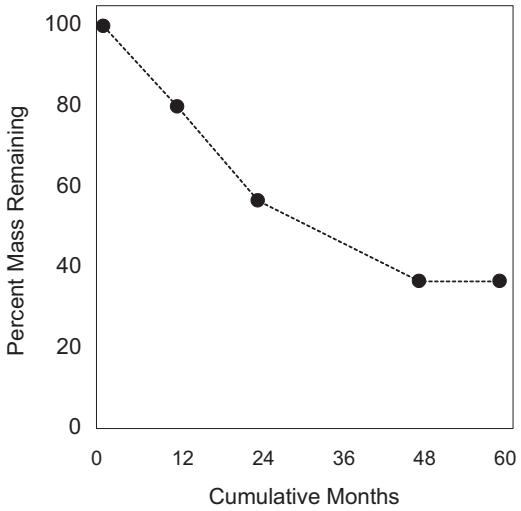

Fig. 5.8 Mass loss of red spruce foliar litter over 60 months in a conifer forest in Maine, USA. From Rustad, L.E. Element dynamics along a decay continuum in a red spruce ecosystem in Maine, USA. Ecology 75:867–879. ©1994 by the Ecological Society of America

boring insects allow non-boring soil invertebrates such as millipedes, centipedes, and wood lice, along with microbial decomposers, to invade CWD, thereby contributing to further decay (Harmon et al. 1986).

Brown rot is a type of wood decay caused exclusively by fungi of the Basidiomycetes, especially taxa in the Polyporaceae family. During brown rot decay, cellulose and hemicelluloses are broken down in the woody substrate, while lignin is largely preserved in a slightly modified form. As a result of the preferential degradation of carbohydrates and cellulosic materials, the decayed wood acquires a brittle consistency, breaks up like cubes, and ultimately crumbles into a powder (Schwarze et al. 1999).

White rot decay processes are caused by Basidiomycete and some types of Ascomycete fungi that are capable of breaking down lignin, cellulose, and hemicelluloses, giving the wood a bleached appearance. In some cases, the process involves *selective delignification* in which lignin is broken down more rapidly than cellulose or hemicellulose. In other instances, the white rot proceeds with simultaneous degradation of all three classes of substrates. Evidence suggests that the white rot fungi break down the lignin by oxidative processes involving phenol oxidases and related compounds (Schwarze et al. 1999; Talbot et al. 2015).

Soft rot refers to the soft consistency of wood that is decayed by Ascomycete and Deuteromycete fungi that break down cell walls, but primarily utilize cellulose and hemicellulose. The characteristic feature of soft rot is the preferred growth of hyphae within the secondary wall, which produces cavities oriented in a longitudinal direction with the cell axis (Schwarze et al. 1999). Evidence indicates that this process is most common in moist wood found in aquatic or riparian environments (Harmon et al. 1986).

Decomposition Rates and Decay Constants

Rates of decomposition vary as a function of the substrate (foliar litter, fine roots, woody detritus, or SOM), environmental conditions, and biological factors. Mass loss of decaying foliar litter often follows a curvilinear negative exponential pattern as illustrated in Fig. 5.8. In long-term studies of decomposing conifer litter, Staaf and Berg (1982) and Rustad (1994) found that needle litter mass declined by 50% or more in the first 24 mo of decomposition, but this rapid rate of decay was not sustained over the next 36 mo. Studies of belowground root decomposition have indicated that mass loss of roots ≤3 mm in diameter ranges from <25% per yr to as much as 50 to 70% per yr (Dornbush et al. 2002; Cronan 2003). Research on the decomposition of woody detritus has indicated that decay rates for CWD are very low, typically ranging from 1 to 3% per yr in temperate regions (Harmon et al. 1986; Foster and Lang 1982; Fahey 1983). However, tree bole mass loss rates as high as 40– 50% per yr have been reported in some rain forest environments and warm temperate forests (Lang and Knight 1979; Lambert 1980). Taken as a whole, estimated residence times for decaying tree boles generally range from decades to centuries, but can be as short as a decade or less.

It is often useful to compare initial rates of litter decay using an empirical **decay constant**, k, based on the following curvilinear weight loss model proposed by Olson (1963): $X_t = X_o\, e^{-kt,}$ where X_t is the mass of litter remaining at time t, X_o is the initial mass of litter, t = time, and k is a litter-specific decay constant. When decay data are analyzed with this model, we find that higher k values correspond with leaves

that decompose more rapidly and have shorter half-lives. As an example, Melillo et al. (1982) reported that northern hardwood leaves exhibited annual decomposition k constants ranging from 0.08 for American beech (with a slow decay rate) to 0.47 for white ash (which lost nearly half its initial mass in 1 year). By comparison, reported annual decay constants for woody stems are primarily in the range of 0.01 to 0.03 (Foster and Lang 1982).

Element Cycling Patterns in Decaying Organic Matter

Studies have shown that litter or detritus can act as a source or a sink for nutrients at various time points during decomposition. As a result, dynamic changes are observed in the patterns of nutrient release and accumulation over the course of litter decay. Elements such as potassium, sodium, and magnesium that occur as soluble ions in biomass are generally leached rapidly from decomposing organic matter, so that <25% of the original element content remains after 12–24 mo (Gosz et al. 1973). In contrast, Ca content in decaying litter tends to decrease at roughly the same rate as mass loss, because Ca primarily occurs as cell wall structural material that requires microbial break down (Fig. 5.9). Other elements such as N, Fe, and Al tend to accumulate in decaying litter for varying periods of time in response to biotic immoblization and abiotic adsorption (Rustad and Cronan 1988). The N content of decaying litter can increase by 50% over original litter N during the first 12–24 mo of decomposition (Berg and Staaf 1981).

Patterns of P immobilization and mineralization during decomposition are varied and complex. In some studies, P and N are both immobilized in the early stages of microbial decomposition (Manzoni et al. 2010), whereas other investigations report that P is released from the beginning of litter decay, while N is immobilized (Rustad 1994; Thompson and Vitousek 1997). This dynamic variation in P biogeochemistry is associated with at least three factors: (i) variable microbial C:P ratios that range from 6 to 60, but include values spanning from 5 to 500; (ii) C:P ratios in detritus that tend to converge around 350, but exhibit large deviations from that value; and (iii) a variable tendency for significant leaching losses of P from decaying litter in some environmental settings (Manzoni et al. 2010; Bünemann 2015).

The changes in tissue chemistry during litter decomposition can be scaled up to an ecosystem-level analysis of nutrient cycling patterns over different periods. As shown in

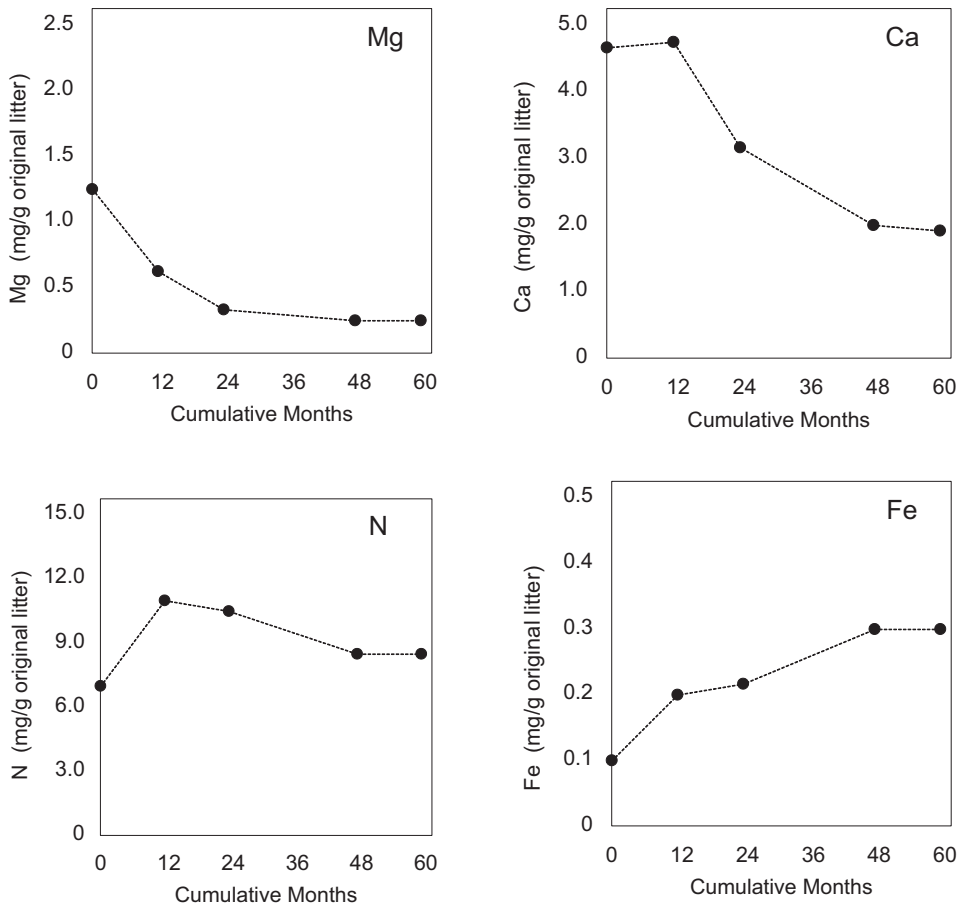

Fig. 5.9 Changes in absolute mass of Mg, Ca, N, and Fe in white pine needles during 57 months of litter decomposition in Maine. From Rustad, L.E. Element dynamics along a decay continuum in a red spruce ecosystem in Maine, USA. Ecology 75:867–879. ©1994 by the Ecological Society of America

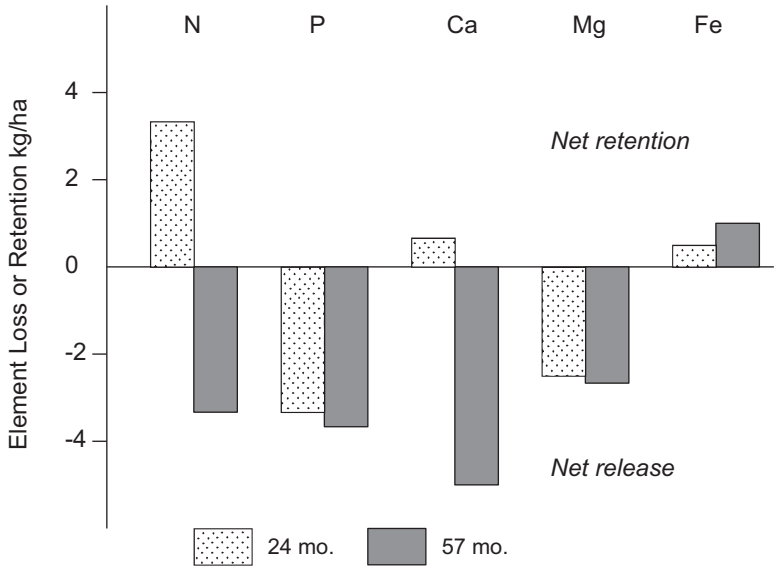

Fig. 5.10 Ecosystem element budgets during decomposition of fine litter in a spruce-fir forest in Maine, USA. From Rustad, L.E. Element dynamics along a decay continuum in a red spruce ecosystem in Maine, USA. Ecology 75:867–879. ©1994 by the Ecological Society of America

Fig. 5.10, decomposing litter in a Maine spruce-fir forest served as a net sink for N, Ca, and Fe during the first 24 mo of decay and as a net source for P and Mg (as well as C) during the same time period (Rustad 1994). However, after nearly 5 yr of decomposition, decaying litter became a net source for all elements measured except Fe and Al. It was noted that the net loss of N from decaying litter amounted to <4 kg N ha^{-1}, which was less than 20–25% of the N contained in the original litterfall material. In contrast, nearly 80% of the original P content in litterfall for that site was released through leaching and mineralization in the first 5 yr of decomposition.

Nutrient dynamics have also been examined in decaying wood at a number of forest ecosystems. In general, logs and woody detritus have been found to act as sinks for N over the course of years to decades, because of the high C:N ratio in wood and the demand of microbial decomposers for N. Woody roots exhibited net accumulation of N and Ca over the course of 7–80 yr of decomposition in a lodgepole pine forest in Wyoming (Yavitt and Fahey 1982). In their study of balsam fir logs in the White Mountains, NH, Lambert et al. (1980) reported that the concentration of N immobilized in well-decayed buried wood was roughly four times higher than the concentration in fresh balsam fir bole wood.

Given enough time, would we expect decaying wood to reach a threshold permitting net microbial mineralization of N? Hart (1999) attempted to answer that question in a study of nitrogen transformations in fallen tree boles at an old-growth conifer stand in Oregon. To his surprise, he found that well-decayed boles exhibited net N mineralization at an elevated C:N ratio of 117 (compared to a ratio of 25– 30 in leaf litter), generating up to 2.5 kg N ha^{-1} yr^{-1} for the ecosystem N budget. His conclusion was that well-decayed boles contribute low but measurable amounts of available N to forest soils; however, the influence of tissue C:N ratios on N mineralization in tree boles was different from the relationships for leaf litter.

Substrate Controls on Decomposition

Detritus contains a mixture of structural and non-structural compounds that vary in their ease of decomposition in the following order: sugars + starches + simple proteins > crude proteins > hemicelluloses > cellulose > lignins + fats + waxes. After the simple carbohydrates and proteins are readily broken down, the decay process slows as microbes encounter the remaining more resistant structural compounds such as cellulose and lignin. Investigators have found that the initial rate of litter decay is inversely correlated with two substrate parameters: (i) % lignin and (ii) the ratio of % lignin: % nitrogen in organic matter. Melillo et al. (1982) reported that the mass of initial litter remaining after 12 months of field incubations with multiple forest species in New Hampshire and North Carolina was highly correlated ($r^2 = 0.90$) with the ratio of initial lignin: initial nitrogen, but that the slopes and intercepts of the regressions varied between the two regions (Fig. 5.11). Murphy et al. (1998) examined rates of litter decomposition along an elevation gradient in Arizona and found that decay rates were inversely correlated with % lignin in the litter substrate. Berg et al. (2010) reported that initial Mn level is an important determinant of limit values, the mass loss at which further decay ceases or becomes minimal. A number of studies have shown that addition of an exogenous C substrate such as root exudates can produce a **priming effect** that increases or decreases the rate of decomposition (Murphy et al. 2015).

One curious observation regarding substrate controls on decay is that the initial concentration of N in litter can influence decomposition in two different ways. Many studies

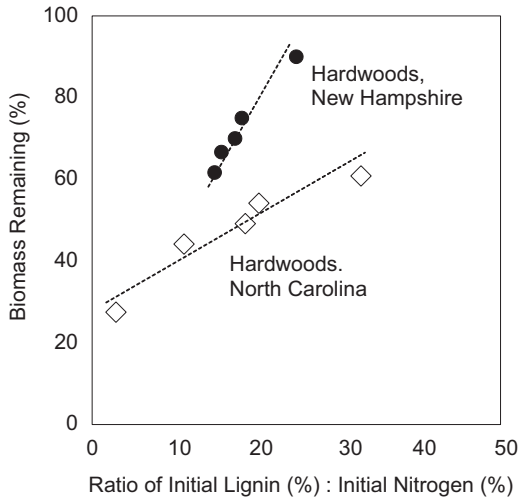

Fig. 5.11 Percent of litter mass remaining after 12 mo. as a function of the ratio of initial lignin to initial nitrogen concentration for northern and southern hardwood species. From Melillo, J.M., J.D. Aber, and J.F. Muratore. Nitrogen and lignin control hardwood leaf litter decomposition dynamics. Ecology 63:621–626. ©1982 by the Ecological Society of America.

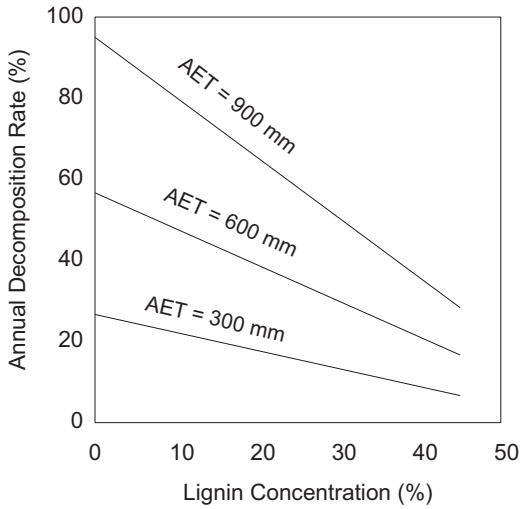

Fig. 5.12 Generalized model showing relationships among decomposition rate, initial lignin concentration of litter, and climatic actual evapo-transpiration (AET) in mm. From Meentenmeyer, V. 1978. Macroclimate and lignin control of litter decomposition rates. Ecology 59:465–472. ©1978 by the Ecological Society of America

have demonstrated that a high N concentration in fresh litter is associated with a faster initial decay rate, which is consistent with Fig. 5.11. However, over a longer time scale of several years, litter at N-enriched sites tends to become stabilized and to decay more slowly than would be expected, which results in SOM accumulation (Frey et al. 2014; Hobbie 2015). Possible explanations for this influence of N enrichment on late-stage decay are that N may induce abiotic formation of compounds that resist microbial attack or N may inhibit oxidative enzymes involved in lignin degradation (Hobbie 2015).

Environmental Controls on Decomposition

Rates of decomposition are strongly controlled by temperature, moisture, and aeration, so that we would expect higher rates of decay in a warm humid ecosystem with well-drained soils. The influence of climate on decomposition is reflected in the offset decay curves of the New Hampshire and North Carolina data sets graphed in Fig. 5.11 and by the decay model of Meentenmeyer (1978) shown in Fig. 5.12. In that decay model, AET (actual evapotranspiration) is used as an integrated proxy of temperature and moisture, and we see that for a given litter substrate and initial lignin concentration, the annual decomposition rate increases with AET. Thus, for example, litter with a lignin concentration of 5% at a site with an annual AET of 900 mm is predicted to lose >80% of its mass in 12 months, whereas litter containing 40% lignin at a site with AET = 300 mm is likely to lose <10% of its mass in the same period.

The influence of temperature on decomposition rate varies and is often tempered by other factors (Hobbie 1996; Prescott 2010). As an example, Murphy et al. (1998) studied litter decomposition along a montane environmental gradient in Arizona where mean annual temperature ranged from 5.5 to 8.5 °C and mean annual precipitation ranged from 32 to 53 cm. The investigators found that decomposition rates were significantly greater at upper elevations, which were colder and wetter. Although this seemed somewhat counterintuitive, the warmer low elevation sites were apparently too dry to permit rapid decay. Melillo et al. (2002) tested the effects of soil warming on decomposition in a Massachusetts hardwood forest and observed only a small, short-lived acceleration of soil organic matter decay in soil warming plots. Their interpretation was that the soil contains a small labile pool of reactive soil carbon compounds such as polysaccharides that are readily used by microbes and a larger pool of carbon compounds characterized by aromatic ring structures that are much more difficult for microbes to metabolize. They concluded that the first pool is very temperature-sensitive, whereas the decay rate of the second pool is not.

Honeycutt et al. (1988) examined the effects of temperature on decomposition and mineralization using concepts of heat units and cumulative **degree days**. Although carbon mineralization rates varied with temperature and apparent substrate complexity, similar amounts of C were respired for the same cumulative heat inputs expressed in degree days. Furthermore, the total number of degree days accumulated until commencement of net N mineralization was also similar for all temperature treatments in their study.

One of the common assumptions concerning global warming is that increases in global temperature will be accompanied by more rapid decomposition of soil organic matter. Yet, Giardina and Ryan (2000) presented evidence from a literature review indicating that decomposition rates of SOM are not well-correlated with changing temperature. According to the authors, this pattern of variation may result because decomposition is performed by enzymes, and enzyme activity is limited by temperature only when the supply rate of substrate exceeds the reaction rate for that substrate. The authors speculated that heterotrophic decomposer microbes in mineral soils survive on a supply of substrate that is sub-optimal for growth, so that there is little apparent influence of temperature on decomposition rates.

Another hypothesis regarding global climate change and organic matter turnover is the prediction that regional warming will decrease winter snow cover, causing increased soil freezing and associated biogeochemical impacts. Mitchell et al. (1996) reported that in the aftermath of a major soil freezing event in December 1989, several watersheds in the northeastern U.S. exhibited elevated concentrations and fluxes of nitrate in spring runoff. This suggested that acute temperature effects such as unusual freezing episodes can influence N turnover and nitrification processes, with consequences for element cycling patterns.

Biological Influences on Decomposition

To what extent are decomposition rates affected by biological influences in terrestrial ecosystems? Coleman and Crossley (1996) suggested that decomposition is primarily the result of microbial activities, but that soil fauna are important in conditioning the litter and in stimulating microbial actions. In an effort to examine the potential impact of soil fauna on decay processes, Gonzalez and Seastedt (2001) examined plant litter decay with faunal exclusion experiments in contrasting tropical and temperate subalpine forests. They found that climate, substrate quality, and soil fauna independently influenced decomposition rates, and that soil fauna had a disproportionately large effect on litter decomposition in tropical wet forests compared to tropical dry and subalpine forests. In tropical wet forests, mean litter decay rates ranged from k = 0.30 to 0.64 in fauna-excluded plots, compared with k = 1.47 to 1.99 in control plots.

Transfers of CO_2 in the Organic Matter Budget of a Forest Ecosystem

Soil respiration provides a major gaseous recycling pathway for the transfer of carbon stored in belowground detrital and biomass pools back into the atmospheric CO_2 reservoir. The magnitude of this transfer can be illustrated with an example from a Norway spruce stand in Maine, where the annual release of C in soil respiration (5200 kg C ha^{-1} yr^{-1}) was almost twice the size of the fine + small root biomass C pool (2700 kg C ha^{-1}) and five times the annual C transfer in foliar litterfall (1000 kg C ha^{-1} yr^{-1}) (Cronan 2003). In that study, it was estimated that 50% of soil respiration was derived from decay of fine roots and fresh litter, 35–40% of the annual CO_2 efflux was derived from root respiration, and the remainder was accounted for by decomposition of SOM and CWD. Other estimates of annual soil respiration have ranged from 4000–6500 kg C ha^{-1} yr^{-1} in red pine stands in Wisconsin (Haynes and Gower 1995), 7100 kg C ha^{-1} yr^{-1} in Norway spruce stands in Germany (Buchmann 2000), 10,650 kg C ha^{-1} yr^{-1} in hardwood stands in Tennessee (Edwards and Harris 1977), and 4450 kg C ha^{-1} yr^{-1} in a mixed hardwood forest located in Massachusetts (Bowden et al. 1993). Schlesinger (1977) examined soil respiration rates from around the world and determined that annual CO_2 effluxes were inversely correlated with latitude, such that CO_2 annual evolution rate = −24.2 (LAT) + 1721.5 with $R^2 = 0.60$.

Atmospheric Deposition

6

Introduction

Biogeochemical processes in watershed ecosystems are closely coupled with dynamic and complex cycling processes and source-sink relationships involving the atmosphere. In some cases, terrestrial systems act as important emission sources contributing to atmospheric chemistry; in other cases, watersheds serve as major **sinks** or receptors for elements and compounds cycling through the atmosphere. There are few terrestrial ecosystems that are not strongly influenced by atmospheric inputs of chemical substances. The atmosphere is the major source for new inputs of nitrogen and sulfur to most terrestrial ecosystems, and is a key transport medium for pollutant contaminants delivered to local and remote watersheds. Atmospheric dust particles provide an important input of calcium for many forested watersheds (Hedin et al. 1994), and dust derived from deserts in northern Africa even serves as an essential source of iron for the Atlantic Ocean (Garrison et al. 2003). Wherever we look, there are fascinating illustrations of the close coupling between terrestrial and atmospheric processes in the biogeochemistry of watershed ecosystems.

Atmospheric deposition refers to the complex processes by which water, particles, gases, and associated elements and chemical compounds are transferred from the atmosphere to vegetation, soil surfaces, lakes, streams, and other receptors at the surface of the Earth (Fig. 6.1). Substances may be deposited from the atmosphere as **wet deposition** (including rain, snow, fog, or cloud water) or as **dry deposition** in the form of dust, particulate **aerosols**, or gases. Wet deposition is defined as the transfer of an element or substance from the atmosphere to the Earth's surface within or on the surface of a hydrometeor (e.g., rain drop). In contrast, dry deposition is the direct transfer of gases and particles to natural surfaces such as vegetation, soil, water, or snow via adsorption or **impaction** processes.

In the chapter that follows, we will focus on the role of atmospheric deposition in ecosystem element budgets and the factors that determine the chemistry and amounts of atmospheric deposition found in different regions and watersheds. We will also examine comparative field data showing the patterns of atmospheric deposition observed at various field sites.

Atmospheric Chemistry

The atmosphere contains a huge inventory of gases, ions, moisture droplets, and particles that generally occur at low concentrations, but which represent enormous absolute quantities of substances on a global scale. For instance, carbon dioxide concentration in the atmosphere is relatively low, averaging roughly 400 ppm in 2015; yet, the total pool of carbon represented by atmospheric CO_2 is approximately 700 billion metric tons. In North America, typical concentrations of common gases and suspended particles regulated by U.S. EPA through the National Ambient Air Quality Standards (NAAQS) are as follows: NO_2 (10–50 ppb), O_3 (20–80 ppb), SO_2 (30–120 ppb), and particulates <10 μm in diameter (50–150 μg/m^3).

Primary sources for elements cycled through atmospheric pathways include the following: (i) marine salts; (ii) dust from agriculture, industrial activities, and roads; (iii) **biogenic** gases such as N_2O (nitrous oxide), H_2S (hydrogen sulfide), NH_3 (ammonia), and volatile plant hydrocarbons (e.g., isoprene); (iv) **anthropogenic gases** such as SO_2 (sulfur dioxide),

C.S. Cronan, *Ecosystem Biogeochemistry*, Springer Textbooks in Earth Sciences, Geography and Environment, DOI 10.1007/978-3-319-66444-6_6

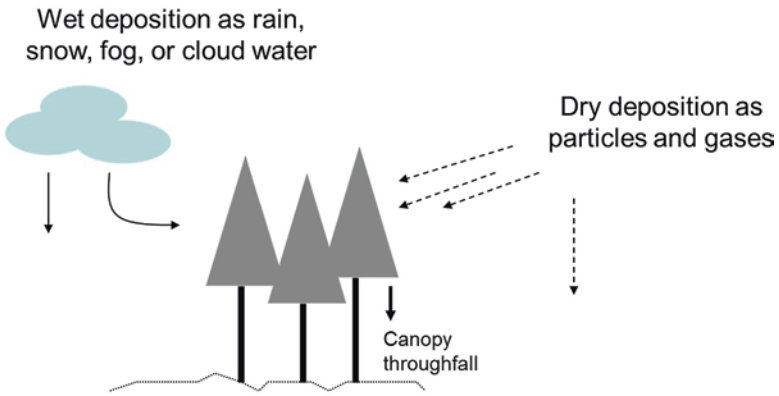

Fig. 6.1 Conceptual diagram of wet and dry deposition processes. The forest canopy can enhance inputs of fog, cloud water, and dry deposition through interactions with foliar surfaces. Throughfall solutions beneath the canopy can be enriched with elements derived from leaching and canopy washout of dry deposition

NO_x (nitrogen oxides), and VOC (volatile organic industrial hydrocarbons such as benzene and methylene chloride); (v) volcanic gases; (vi) ash and soot from fires, volcanic eruptions, and industrial emissions; and (vii) plant pollen. Munger and Eisenreich (1983) suggested that the major elements in precipitation can be separated into three major groups related to sources – elements derived from soil dust and **fly ash** (Ca, Mg, and K), elements associated with marine salt (Na and Cl), and elements such as S, N, and H (as H^+ ion) that originate from anthropogenic combustion. For any terrestrial ecosystem, the contribution of specific natural or anthropogenic sources to atmospheric deposition inputs depends upon such factors as the geographic location of the receptor ecosystem in relation emission sources, prevailing weather patterns, **atmospheric residence times** of elements, and patterns of precipitation washout during **long-range transport.**

On a global basis, the dominant suspended particles in the atmosphere are various forms of sulfur compounds. Toon and Pollock (1976) reported that the troposphere below 3 km contains 50% sulfate particles, 35% soil particles, and 15% sea salt. Above 3 km, the tropospheric particulate phase contains 60% sulfate particles and 40% soil particles. In comparison, the stratosphere is dominated by ammonium sulfate, sulfuric acid, and ammonium persulfate.

Deposition Processes and Patterns

Atmospheric deposition is a major link in a large-scale cycling loop that begins with enrichment of the atmosphere with chemical substances derived from emission sources on Earth or from photochemical and physical-chemical processes within the atmosphere. Examples of enrichment processes that contribute to the chemical composition of the atmosphere include the following: (i) gaseous nitrous oxide emissions released by microbial activities in soils, (ii) generation of gaseous nitric oxide in air masses from oxidation reactions involving atmospheric dinitrogen and lightning, and (iii) formation of ammonium sulfate aerosols in the atmosphere through reactions between gaseous ammonia and sulfuric acid.

As illustrated in Fig. 6.2, chemicals that enter the atmosphere through emissions or *in situ* reaction pathways are potentially subject to long-range transport and chemical transformation reactions occurring within air masses or clouds. As an example, SO_2 released from power plant emissions in the Ohio River valley may be hydrolyzed and oxidized into H_2SO_4 (in the presence of atmospheric water vapor and hydrogen peroxide) during transport toward the northeastern U.S (Driscoll et al. 2001). Another common transformation occurs when limestone dust is blown into the atmosphere and reacts with sulfuric acid droplets to form gypsum particles, $CaSO_4$ (Fig. 6.2). Ultimately, after some finite **residence time** in the atmosphere, many of the chemical substances transported through atmospheric cycling pathways return to Earth through various deposition processes (Figs. 6.1 and 6.2).

There are a number of important processes that contribute to atmospheric deposition of particles, gases, and dissolved solutes. Dry deposition occurs through the combined effects of: (i) **gravitational settling** of heavier particles; (ii) **diffusion** of gases and ions; and (iii) **impaction** and **interception** of wind-entrained aerosols and particles that penetrate the boundary layers of vegetation surfaces or other natural features in the landscape. Processes contributing to chemical enrichment of precipitation and wet deposition include: **gas dissolution** and **oxidation** (e.g., when SO_2 dissolves in a hydrometeor and is oxidized to sulfite or sulfate); **cloud condensation** (which occurs during formation of a rain droplet around a hygroscopic particle); **rainout** (in-cloud removal of gases and particles); and **washout** (below-cloud scavenging of chemical substances).

As shown in Fig. 6.3, particles, aerosols, and gases in the atmosphere are part of a continuum of sizes ranging from sub-micrometer aerosols and gases to large dust particles on the order of 10–100 μm in diameter. From a biogeochemical perspective, there are three important observations that follow from that broad size distribution: (i) element chemistry is not homogeneous across the size spectrum; (ii) the **deposition velocity** (or the rate of transfer of material from the atmosphere to surfaces on Earth) varies non-linearly

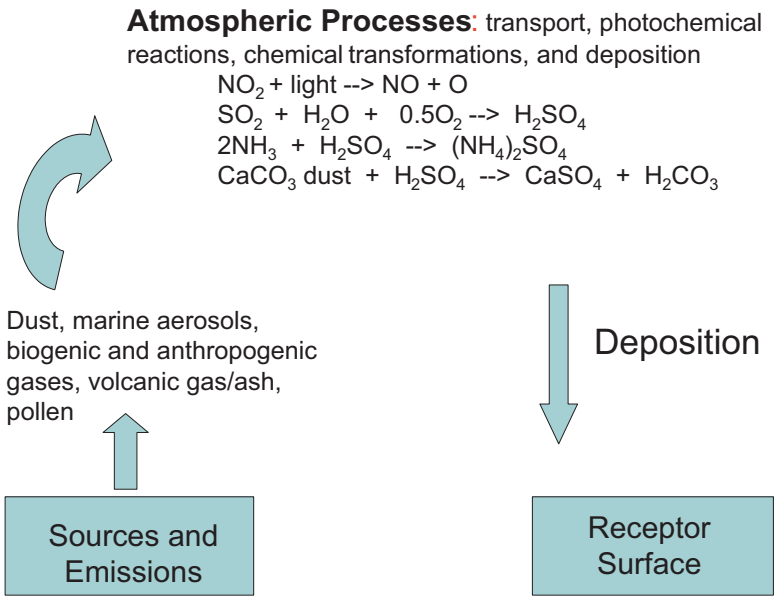

Fig. 6.2 Conceptual illustration of biogeochemical cycling through atmospheric pathways, with examples of atmospheric chemical reactions

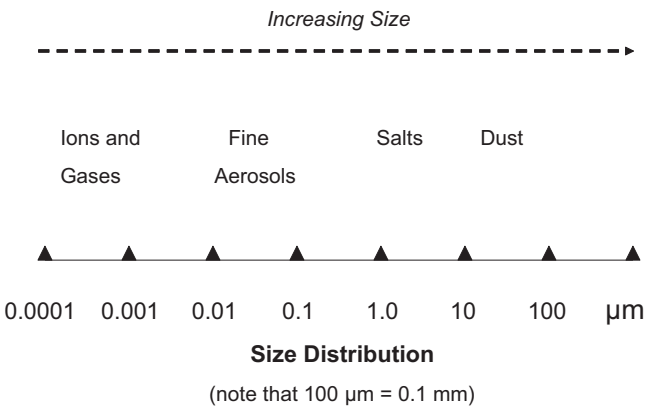

Fig. 6.3 Size distribution of molecules, gases, and particles in the atmosphere

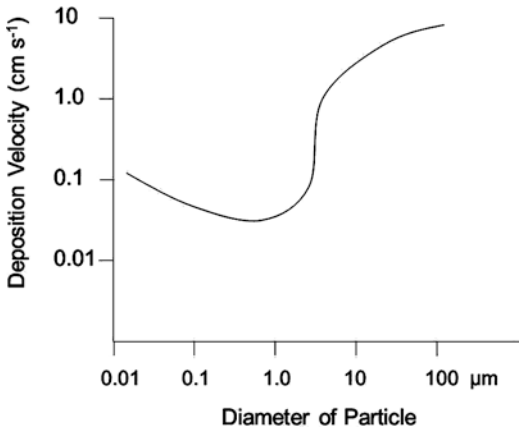

Fig. 6.4 Non-linear variation in deposition velocity as a function of molecular size and particle diameter. Based on Chamberlain, AC. The movement of particles in plant communities. pp. 155–203 in Vegetation and the Atmosphere. I Principles. Monteith, J.L. (ed). ©1975 by Academic Press (Elsevier)

across the size distribution (Fig. 6.4); and (iii) the residence time of elements in the atmosphere may vary as a function of the size fraction in which the element occurs.

What are the implications of these observations for atmospheric deposition? At the heavier end of the size spectrum illustrated in Fig. 6.3, dust and salt particles tend to be enriched in elements such as Ca, Mg, Al, Si, Na, and K. Because the larger particles are subject to rapid gravitational settling, the elements associated with that size fraction tend to have shorter atmospheric residence times and relatively higher atmospheric deposition rates in environments influenced by dust sources and marine salts.

At the other end of the size spectrum (in the sub-micrometer range), gases such as sulfur dioxide, nitrogen oxides, and nitric acid vapor tend to exhibit longer atmospheric residence times, and are subject to **long-range transport** from emission sources to downwind receptor areas. Ultimately, these molecules are transferred via diffusion or impaction from the atmosphere to various surfaces such as forest canopies, or are washed from the atmosphere in wet precipitation. Dry deposition of these gases is enhanced when vegetation surfaces are moist.

In between the gaseous and large particle size fractions is a class of microscopic aerosols that ranges from roughly 0.1 to 1.0 μm in diameter and includes components such as ammonium sulfate particles and lead (Pb) aerosols. Because these particles are too small to experience rapid gravitational settling and are too large to exhibit rapid deposition by diffusion, theoretical deposition velocities for that size class are expected to be less than those observed for smaller and larger size classes (see non-linear relationship in Fig. 6.4). In reality, however, deposition of sub-micrometer aerosols can be

increased considerably by impaction processes that result from the interaction of wind-borne aerosols impinging on the large surface area of vegetation in the landscape.

Atmospheric Emissions and Deposition of Sulfur and Nitrogen

Nitrogen and sulfur provide useful illustrations of the relationships between atmospheric emissions and deposition. Sulfur and nitrogen oxides are two important **acid-forming precursors** that contribute to **acidic deposition** and other air quality problems. Sulfur oxide (SO_x) emissions are primarily derived from combustion of fossil fuels containing reduced or elemental sulfur and from smelting of metal sulfides such as iron, lead, zinc, and copper sulfide. Nitrogen oxides (NO_x) are formed and released to the atmosphere during high temperature combustion associated with transportation, electrical generation, and heating. Sulfur oxides include the chemical species SO_2, SO_3^{2-}, and SO_4^{2-}, whereas nitrogen oxides include NO, N_2O, NO_2, and NO_3^-. Emissions of SO_x and NO_x increased greatly in the U.S. during the twentieth century of economic growth, reaching peak annual values of 28–30 million metric tons for SO_x and 23 million metric tons for NO_x (Fig. 6.5). After the 1980's, U.S. emissions of SO_x declined steadily in response to federal Clean Air Act regulations, whereas emissions of NO_x remained relatively unchanged.

What is the environmental fate of SO_x and NO_x emissions? After entering the atmosphere, sulfur oxides can be oxidized (often in the presence of hydrogen peroxide) and **hydrolyzed** in water to form sulfuric acid. Both the H_2SO_4 and remaining SO_2 may be carried by long-range transport to areas far downwind of the original SO_x emission source. During atmospheric transport, sulfuric acid may cycle back to the Earth's surface as acidic deposition, or it may undergo further reactions in the atmosphere. For example, sulfuric acid can react with ammonia gas derived from agricultural sources to form ammonium sulfate, a neutral but **acid-forming salt**. Sulfuric acid can also be neutralized by reaction with atmospheric dust particles to form various sulfate salts of calcium, magnesium, potassium, or sodium. SO_x emitted to the atmosphere eventually returns to Earth through atmospheric deposition processes. As shown in Fig. 6.6, there is a strong relationship between anthropogenic SO_2 emissions and sulfur deposition. In this case, as emissions in the Northeast regional **airshed** declined in response to regulations in the Clean Air Act, deposition of sulfur in downwind locations decreased in a nearly linear fashion.

The environmental fate of NO_x is somewhat different from that of SO_x. After NO_x compounds are released from stationary or mobile sources, nitrogen oxides contribute to four major atmospheric processes: (i) acidic deposition, (ii) formation of tropospheric ozone, (iii) greenhouse warming, and (iv) depletion of stratospheric ozone. In terms of atmospheric deposition, evidence indicates that much of the NO_x released to the atmosphere is quickly oxidized to nitric acid, HNO_3, which may remain as nitric acid vapor, may dissolve in cloud droplets as aqueous nitric acid, or may react with dust or ammonia gas to form nitrate salts. Ultimately, most of this N returns to Earth through wet or dry deposition processes.

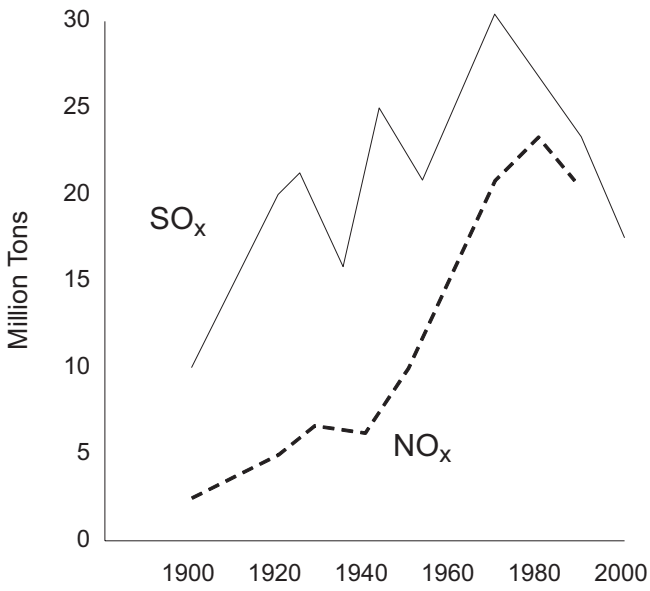

Fig. 6.5 Annual emissions of sulfur dioxide and nitrogen oxides in the U.S. from 1900 to 2000 (Data from NAPAP, Washington D.C)

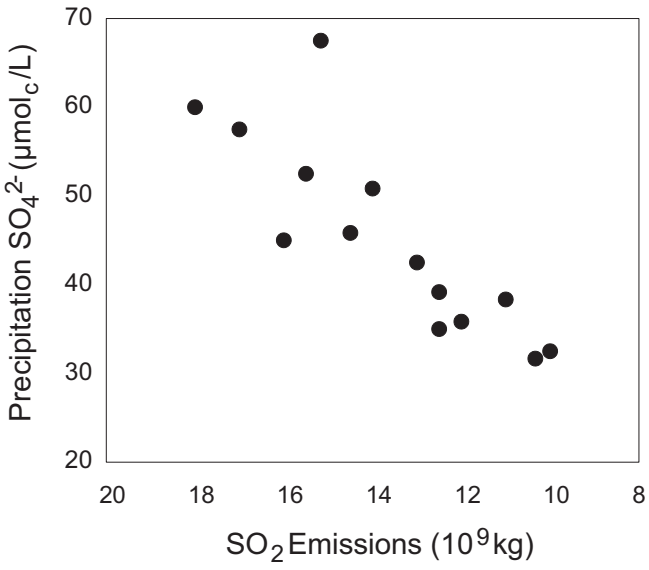

Fig. 6.6 Relationship between volume-weighted concentrations of sulfate ion in bulk precipitation at Hubbard Brook Experimental Forest, NH versus annual sulfur emissions in the regional source area. From Likens, G.E., T.J. Butler, and D.C. Buso. Long- and short-term changes in sulfate deposition: effects of the 1990 Clean Air Act Amendments. Biogeochemistry 52:1–11 ©2001 by Springer with permission of Springer

Measurement and Analysis of Atmospheric Deposition

Wet Deposition

Wet deposition is routinely monitored by sampling networks in North America, Europe, China, and at various other locations around the globe. Results from those monitoring networks are generally reported in terms of ion concentrations (e.g., μmol L^{-1} or mg L^{-1}) and wet deposition fluxes of ions or elements (e.g., kg ha^{-1}, g m^{-2}, mol_c ha^{-1}, or mol ha^{-1}). Most networks have adopted a standard automated "wet-only" inert collector to sample precipitation volume and chemistry (NADP 1994). This sampler excludes dust and dryfall materials from the collection bucket between rain or snow events, and opens only during wet precipitation events. Unfortunately, the sampler is not an efficient collector of fog, cloud water, or dew, so that other methodologies are required to sample those inputs in regions where their contribution to wet deposition is significant (Lovett 1994).

Historically, precipitation was sampled with **bulk precipitation** collectors composed of an open plastic funnel and collection bottle that sampled wet precipitation plus an undetermined amount of **dryfall** (Likens et al. 1977). However, Richter and Lindberg (1988) demonstrated at Walker Branch Watershed in Tennessee that mean concentrations of ions can differ significantly in wet-only versus bulk precipitation collectors located at the same site (Table 6.1). Potential discrepancies such as these between collector designs unfortunately introduce uncertainties into historical or contemporary comparisons of precipitation chemistries and deposition estimates involving both wet-only and bulk precipitation collectors. Hence, investigators must be cautious in noting the collector design associated with a given wet deposition data set.

Dry Deposition

Compared with precipitation inputs, dry deposition is a much more difficult process to quantify, because there is no consistent way to sample the heterogeneous gases and dry particles that enter an ecosystem. Consequently, investigators often try to bracket dry deposition through a combination of estimation techniques (Lovett and Lindberg 1986). One standard method involves using an air sampler to collect particles and gases on multiple filter packs, eluting and analyzing the trapped chemical constituents, and calculating mean air concentrations based on the volume of air that passed through the sampler. Then, the investigator must calculate or select a reasonable theoretical deposition velocity for each substance, and multiply mean air concentration times the deposition velocity of the gas or particle to obtain an estimate of the dry deposition flux of that chemical to a given receptor surface (Lovett and Lindberg 1986).

Dry deposition has also been estimated with a variety of other techniques. Lindberg and Lovett (1985) placed artificial surfaces in a forest canopy for fixed time periods, eluted the trapped chemical species, and estimated dry deposition per unit area. Graustein and Armstrong (1983) used strontium (Sr) isotopes as geochemical tracers to estimate cation deposition to a montane ecosystem in the southwestern U.S. Lovett et al. (1992), Rustad et al. (1994), and others have used watershed mass balance budgets to estimate dry deposition as a difference term where other elemental inputs and outputs are relatively well characterized. Finally, some investigators have used the forest canopy as an integrative collector of wet plus dry deposition of certain elements such as sulfur and chloride that have been shown, in many cases, to move conservatively through the canopy without significant enrichment or depletion. The strength of this estimation approach for sulfur deposition was demonstrated by Lindberg and Lovett (1992), who reported a strong 1:1 correlation between total annual flux of sulfate in **throughfall** plus **stemflow** versus total annual atmospheric deposition of sulfate estimated by other independent means. In a later paper, however, Rustad et al. (1994) questioned the reliability of this approach for mixed forests with heterogeneous conifer cover.

Two comparative field studies in Maine and Tennessee provide examples of the difficulty we face trying to estimate dry deposition to forest ecosystems. In their study at Walker Branch Watershed at Oak Ridge, TN, Lovett and Lindberg (1986) used three separate methods to estimate dry deposition of nitrate to a deciduous forest. Estimates of the annual dry deposition flux ranged from 1.8 to 9.1 kg NO_3^--N ha^{-1} among the different methods, with a mean value of 4.8 kg NO_3^--N ha^{-1}. This dry deposition flux estimate represented almost half of the total annual nitrogen input of 10.1 kg N ha^{-1} to the watershed.

In a separate study at Bear Brook Watershed in Maine, Rustad et al. (1994) compared estimates of sulfur and chloride dry deposition using a watershed mass balance approach versus measurements of net **canopy throughfall** enrichment for each element. For the mass balance approach, the authors assumed that annual streamflow outputs of each element minus wet deposition inputs to the watershed provide an

Table 6.1 Comparison of element inputs estimated with bulk precipitation versus wet-only collectors at Walker Branch Watershed, Oak Ridge, TN (Richter and Lindberg 1988)

	SO_4^{2-}	NO_3^-	Ca^{2+}	H^+
Mean concentration[a], μmol_c L^{-1}				
Wet-only	58.8	16.6	10.5	56.8
Bulk precipitation	67.8	11.3	25.6	59.2
Annual ion deposition, $kmol_c$ ha^{-1} yr^{-1}				
Wet-only	0.79	0.22	0.14	0.76
Bulk precipitation	0.91	0.15	0.34	0.79

[a]Volume-weighted concentration; μmol_c = micromoles of ionic charge; $kmol_c$ = kilomoles of ionic charge

estimate of unmeasured dry deposition. For their second approach, the authors assumed that element fluxes measured beneath the forest canopy as throughfall represent wet deposition plus dry deposition washed from the foliar surfaces. By subtracting wet deposition chemistry from canopy throughfall fluxes and assuming that sulfate and chloride are not depleted or enriched by the canopy, the authors were able to use net throughfall flux as an estimate of dry deposition. Their estimates in a mixed northern hardwood forest indicated that mean annual dry deposition of sulfate ranged from 320 $mol_c\ ha^{-1}$ (throughfall method) to 616 $mol_c\ ha^{-1}$ (mass balance method), whereas mean annual dry deposition of chloride varied from 261 $mol_c\ ha^{-1}$ (throughfall) to 380 $mol_c\ ha^{-1}$ (mass balance).

Total atmospheric deposition is estimated as the sum of wet plus dry deposition. Depending upon the element or ion of interest and the geographic location, the uncertainty of wet, dry, and total deposition estimates can be substantial or relatively small. Because dry deposition typically represents 25–50% of total deposition for most elements, large errors in estimating dry deposition can translate into large uncertainties in total atmospheric deposition. Likewise, in areas where cloud water or fog are important components of wet deposition, errors in their measurement can again introduce large uncertainties into estimates of total deposition. Finally, it is important to note that analytical measurements of chemical species in wet and dry deposition require careful quality control protocols to avoid further uncertainties. In a landscape analysis of variations in deposition rates in the Catskill Mountains, NY, Weathers et al. (2000) found that deposition to "hotspots" such as coniferous forest edge zones at high elevation could be 300% greater than deposition to lower elevation forests on the same mountain. Thus deposition heterogeneity can be impressive!

Analysis of Precipitation Chemistry

How do investigators characterize and interpret the chemistry of wet deposition? Once a sample of precipitation has been collected, it is normally analyzed for complete anion and cation chemistry (Table 6.2). Results can then be expressed in units of **equivalent charge** (e.g., $\mu mol_c\ L^{-1}$) in order to check cation-anion **charge balance** to determine if the sample analysis meets the test of **electrical neutrality**. If sums of cation and anion charge equivalents balance within the limits of analytical error (Fig. 6.7), there is reasonable assurance that major ion chemistry has been adequately quantified. Alternatively, if there is a significant discrepancy between positive and negative ions, this would generally indicate that one or more ions have been over-estimated, underestimated, or ignored. In cases where there is measurable dissolved organic carbon (DOC) in a sample, there may be an "anion deficit" that can be attributed to charged organic anions that have not been analyzed (Cronan and Aiken 1985).

Table 6.2 Analysis of precipitation chemistry for a sample collected in New Hampshire, USA (Data from Cronan and Reiners 1983). Units are $\mu mol_c\ L^{-1}$

Cations	Concentration	Anions	Concentration
H^+	86	Cl^-	5
Ca^{2+}	11	NO_3^-	25
Mg^{2+}	5	SO_4^{2-}	98
K^+	2	PO_4^{3-}	<1
Na^+	3	HCO_3^-	<1
NH_4^+	22		
Fe^{2+}	1		
Al^{3+}	1		
Sum (+)	131	Sum (−)	128

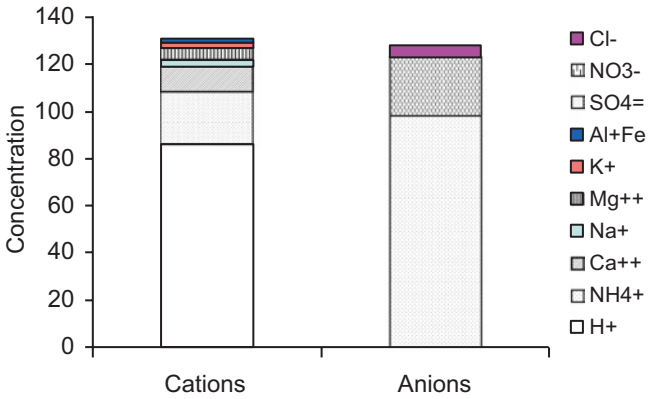

Fig. 6.7 Example of a cation-anion charge balance analysis for precipitation collected in the mountains of New England (Data from Cronan 1980a). Units = $\mu mol_c\ L^{-1}$

Table 6.3 Precipitation chemistry in Wisconsin expressed in mass units versus charge equivalents

	Concentration	
Element or chemical parameter	$mg\ L^{-1}$	$\mu mol_c\ L^{-1}$
H^+ (based on pH = 4.0)		100
Ca^{2+}	0.84	42
Mg^{2+}	0.10	8
K^+	0.30	8
Na^+	0.39	17
NH_4-N	0.52	37
NO_3-N	0.36	26
SO_4-S	0.74	46
Cl^-	0.48	14
Sum of cations (+)		**212**
Sum of anions (−)		**86**

To illustrate how the principle of electrical neutrality can serve as a powerful tool for geochemical analysis of water samples, we can examine chemical data for precipitation collected during a field study in Wisconsin (Table 6.3). In the original journal article (*Ecology* 65, 1984), the authors

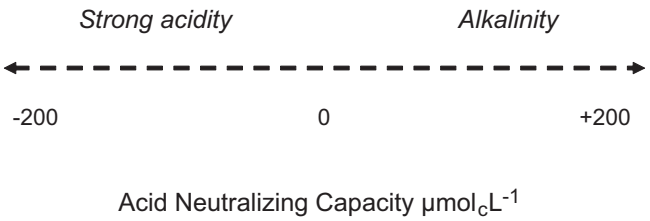

Fig. 6.8 Conceptual illustration showing a gradient of acid neutralizing capacity ranging from negative to positive values

reported results in mass concentration units of mg L^{-1}. For one of our class exercises, my students converted the pH and ion chemistry values to equivalent charge units and compared the cation-anion balance. To our surprise, mean rain chemistry reported for the Wisconsin site had a huge imbalance between measured cations (212 $\mu mol_c\ L^{-1}$) and anions (86 $\mu mol_c\ L^{-1}$), implying that there was an analytical error or omission in the chemical data (Table 6.3). This oversight might have been avoided with a simple charge balance computation.

Acid neutralizing capacity or ANC is one chemical parameter that is very useful in tracing the evolution and transformation of water chemistry during transport of wet deposition through watershed ecosystems. This term is defined as the concentration difference in molar charge equivalents between the sum of **basic cations** minus the sum of strong acid anions, $C_B - C_A$. As shown in Fig. 6.8, ANC is a continuous function that ranges from negative values (indicating net strong acidity), to zero, and on up to positive values (indicating net acid neutralizing capacity or **alkalinity**). A sample of precipitation that contains net strong acidity and a negative ANC is, by definition, **acidic precipitation** (although other definitions are also recognized). ANC will be discussed in further detail in Chap. 9.

Ion ratios are often calculated for precipitation samples in order to discriminate regions affected by different element sources. For example, at sites near the ocean, the Na:Cl molar ratio in precipitation is similar to the Na:Cl ratio of 0.86 in seawater (Broecker 1974). Proceeding inland, Na:Cl ratios can change considerably as the influence of marine sodium chloride diminishes and there is an increased contribution of Na-rich continental dust (Yuretich et al. 1981; Munger and Eisenreich 1983). Similarly, the sulfate:nitrate ratio in acidic precipitation can range from >1.0 in areas where atmospheric strong acids are dominated by industrial SO_2 emissions from fossil fuel combustion to ion ratios of <1.0 in areas such as southern California where nitric acid derived from transportation emissions of NO_x dominates precipitation acidity.

Mean concentrations of ions in precipitation or deposition may be reported as **volume-weighted** or unweighted values, and it is important to understand how and why these estimates can differ. In general, concentrations of ions in precipitation are inversely related to cumulative volume of precipitation. Thus, successive rain events or prolonged rain showers exhibit higher concentrations in the early stages of rainfall and decreasing concentrations in later stages of rainfall, after the atmosphere has experienced washout of most gases, particles, and ions. The effects of these relationships on the calculation of mean rainfall chemistry can be illustrated with the following example, where the **weighted mean** of 48.7 μmol L^{-1} is much less than the **unweighted mean** of 80 μmol L^{-1}, a value that does not account for the dilute chemistry of high volume rain events.

	Successive rain events		
Example	1	2	3
Sample volume (liter)	0.25	0.10	1.20
Ion concentration (μmol L^{-1})	50	150	40
Unweighted mean	= (50 + 150 + 40 μmol L^{-1})/3 = 80 μmol L^{-1}		
Weighted mean[a]	= [Sum Vol_i * $Conc_i$]/[Sum Vol]		
	= (0.25*50 + 0.1*150 + 1.2*40)/1.55 = 48.7 μmol L^{-1}		

[a]Where volumes and concentrations are summed over rain events i = 1 to n

Have you ever seen the term "excess sulfate" used in a description of deposition chemistry? Investigators will sometimes make a "sea-salt" correction with atmospheric deposition data in order to distinguish between ions derived from marine aerosols versus ions associated with other sources such as anthropogenic emissions. Cogbill and Likens (1974) used Na^+ ion as a basis for this correction, since its dominant source is the ocean. Using the ratio of Na^+ to other ions in seawater, one can predict the equivalent amounts of sulfate, chloride, magnesium, calcium, and potassium expected to originate from the sea (Granat 1972). Remaining "excess ions" above sea-salt are assumed to originate from terrestrial or anthropogenic sources. At Hubbard Brook Experimental Forest, NH, Cogbill and Likens (1974) found that marine sulfate represented ~5% of total sulfate in precipitation; excess sulfate from fossil fuel emissions represented the remaining 95% of the total for that anion. These proportions have since changed somewhat in response to federal regulations requiring decreases in sulfur emissions from power plants and industry.

Environmental Patterns of Precipitation Chemistry and Atmospheric Deposition

Precipitation chemistry and atmospheric deposition vary – sometimes dramatically – as a function of time and space. One of the challenges in biogeochemistry is to be able to discern the environmental patterns of wet and dry deposition, to understand the processes controlling those variations, and to assess the consequences of variable elemental inputs from the atmosphere for ecosystem structure and function.

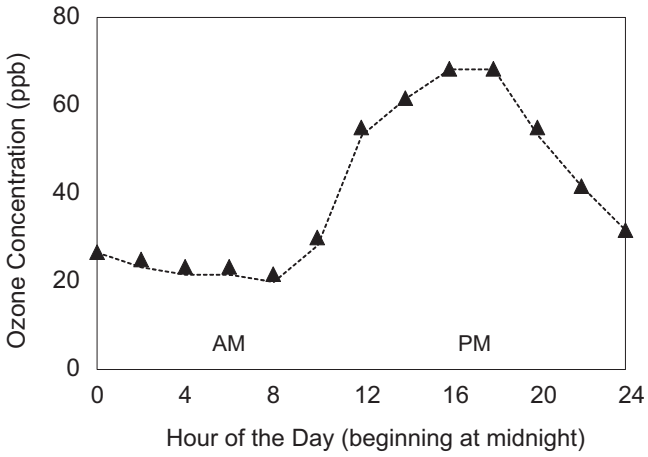

Fig. 6.9 Mean hourly air concentrations of ozone over a diurnal cycle at Oak Ridge, TN. Data from G.E. Taylor and P.J. Hanson, Oak Ridge National Laboratory – used with permission

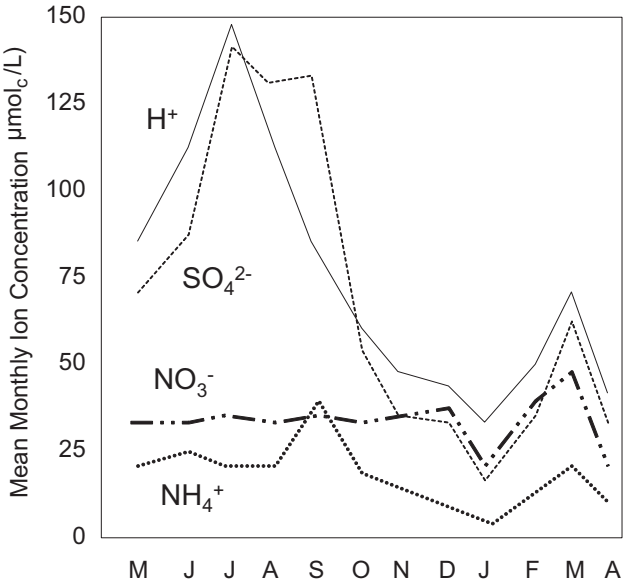

Fig. 6.10 Monthly variations in precipitation chemistry in the Adirondack Mountains, NY (Johannes et al. 1981)

Daily Patterns

Temporal variations occur at a variety of scales and include cyclic, episodic, stochastic, and directional patterns. As an example, Fig. 6.9 illustrates the diurnal changes in mean hourly tropospheric ozone (O_3) concentrations recorded at a low-elevation site in eastern Tennessee. For that location, ambient concentrations of ground-level ozone are lowest at night, build up during the morning (as moisture, NO_x, and volatile hydrocarbons react in the presence of sunlight to form O_3), and reach peak values during the afternoon. Since ozone deposition to plants is greatest when foliar stomata are open, this pattern implies that plants are at greatest risk for ozone exposure and associated oxidant stress on sunny afternoons in eastern Tennessee (Taylor and Hanson 1992).

Monthly Patterns

Monthly variations in the concentrations of sulfate, nitrate, ammonium, and hydrogen ions in precipitation from the Adirondack region of New York are illustrated in Fig. 6.10. At this time scale, it is apparent that mean monthly weighted concentrations of sulfate and hydrogen ions vary considerably over an annual cycle, with lowest concentrations generally observed in winter and highest levels recorded in summer. How can we account for these large fluctuations in precipitation chemistry? Some of the important interacting factors are changes in prevailing seasonal storm tracks, differences in the **scavenging efficiency** of winter snowfall versus wet precipitation, and variations in regional emissions and long-range transport patterns.

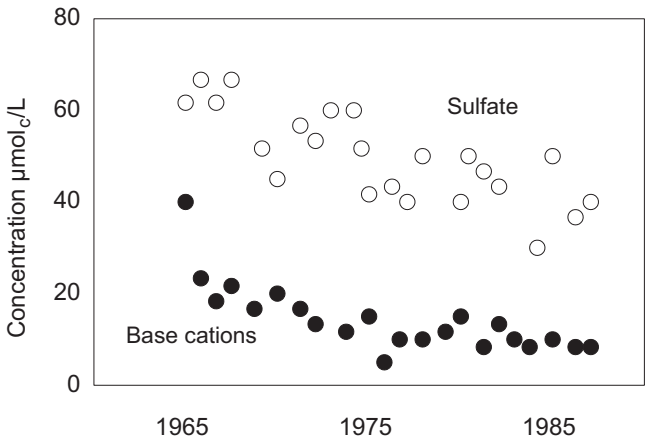

Fig. 6.11 Bulk precipitation trends at Hubbard Brook Experimental Forest, NH based on volume-weighted concentration data. Reprinted with permission from Driscoll, C.T., G.E. Likens, L.O. Hedin, J.S. Eaton, and F.H. Bormann. Changes in the chemistry of surface waters. Environmental Science and Technology 23:137–143. ©1989 American Chemical Society

Multi-year Trends in Precipitation Chemistry

An example of a 25 yr trend in precipitation chemistry is illustrated in Fig. 6.11 based on data collected by Gene Likens and co-workers at Hubbard Brook Experimental Forest in New Hampshire (Driscoll et al. 1989; Likens et al. 2001). At that location, concentrations of sulfate and **base cations** in bulk precipitation exhibited erratic, but significant declines from the early 1960's to the late 1980's. Precipitation pH followed an even more erratic pattern over the same period, but generally increased in concert with decreasing concentrations of

strong acid sulfate anions in precipitation. The decline of sulfate ion in precipitation was presumably a reflection of declining sulfur emissions in response to the Clean Air Act and modernization of electrical generation. Decreases of base cations in precipitation were largely a reflection of regulations requiring electrostatic precipitators to remove dust and fly ash from smokestack emissions. What other factors may have introduced complexity into the pH pattern?

Long-Term Historical Trends in Atmospheric Deposition of Mercury

Investigators have used historical evidence derived from wetlands, lake sediments, and ice cores to reconstruct long-term trends in atmospheric deposition of different elements and compounds of interest. For example, several groups have examined peat profiles to determine how inputs of mercury (Hg) to wetlands have changed over the course of human civilization. When mercury is used in smelting and manufacturing, it enters the atmosphere as volatile elemental Hg and is ultimately deposited back to Earth via atmospheric deposition processes. Martinez-Cortizas et al. (1999) analyzed peat from a Spanish bog and found evidence that metallurgical advances from the early Celtic and Roman periods, through the Middle Ages, and into the modern era produced increasing emissions of Hg that were recorded as increasing Hg concentrations in the dated layers of peat (Fig. 6.12).

Spatial Patterns: Deposition in North America

Deposition patterns across North America exhibit strong differences and gradients that reflect regional variations in air emission sources, meteorology, geography, and the relative importance of different deposition processes. Summary data collected by the National Atmospheric Deposition Program in 2000 are illustrated in Fig. 6.13 showing wet deposition fluxes for sulfate, ammonium, and calcium for the U.S. In the example of sulfate, we see that most of the eastern U.S. received more than 10–15 kg ha^{-1} of wet sulfate deposition in 2000, whereas the western U.S. received about one quarter of that amount or <4 kg ha^{-1} yr^{-1}. How can we account for the regional differences illustrated for SO_4^{2-}, Ca, and NH_4^+ in the figure?

Specific examples of wet deposition chemistry from different locations in the U.S. are shown in Table 6.4. These field sites span a geographic range from the eastern to the western U.S. and exhibit 5–30-fold differences for the various chemical parameters. For example, solution pH is as low as 4.3–4.4 at two sites, but is an order of magnitude higher at the two western sites. In Washington, rainfall exhibits low Ca, reflecting minimal sources of Ca-rich dust in the region; yet, the Na concentration in precipitation at the Olympic Park is the highest of all five sites, reflecting the influence of marine aerosols blown in from the Pacific Ocean. The mid-western site at Argonne, IL exhibits precipitation chemistry that reflects the influence of agricultural dust (elevated Ca), emissions from manure or feedlots (elevated NH_4^+), and S emissions from fossil fuel combustion (elevated SO_4^{2-}). What other patterns are evident?

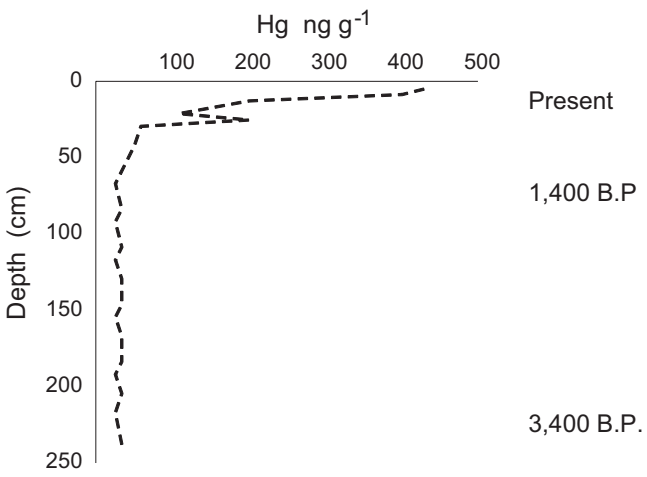

Fig. 6.12 Historical reconstruction of Hg inputs from atmospheric deposition based on Hg accumulation in a peat bog From Martinez-Cortizas, A., X. Pontevedra-Pombal, E. Garcia-Rodeja, J.C. Novoa-Munoz, and W. Shotyk. 1999. Mercury in a Spanish peat bog: archive of climate change and atmospheric metal deposition. Science 284: 939–942. Reprinted with permission from AAAS

Spatial Patterns: Influence of Vegetation and Canopy Structure on Atmospheric Deposition

Atmospheric deposition inputs to terrestrial ecosystems are strongly influenced by the composition and distribution of vegetation, foliage surface area, and plant canopy roughness. This effect occurs because dry deposition of gases and aerosols is greatly enhanced by impaction, absorption, and adsorption processes in the exposed surface area of the plant canopy. Field experiments by Grennfelt (1987) in Sweden provide a graphic illustration of the forest canopy effect on deposition of sulfate and nitrate. As shown in Fig. 6.14, wet deposition was sampled in the open and at points along a gradient from the edge of a pine forest into the forest interior. At the forest edge, sulfate deposition collected as canopy throughfall was more than twice as high as deposition to the open field. Proceeding away from the exposed forest edge and into the forest, sulfate deposition declined, but remained at least 50% higher than deposition to the field. A similar pattern was also observed for nitrate deposition. These patterns are consistent with the prediction that plant canopy surface area in a watershed increases dry deposition inputs of elements, and that an exposed forest edge may have even higher rates of dry deposition. **Canopy washout** of any dry deposition accumulated on foliar surfaces prior to a precipitation

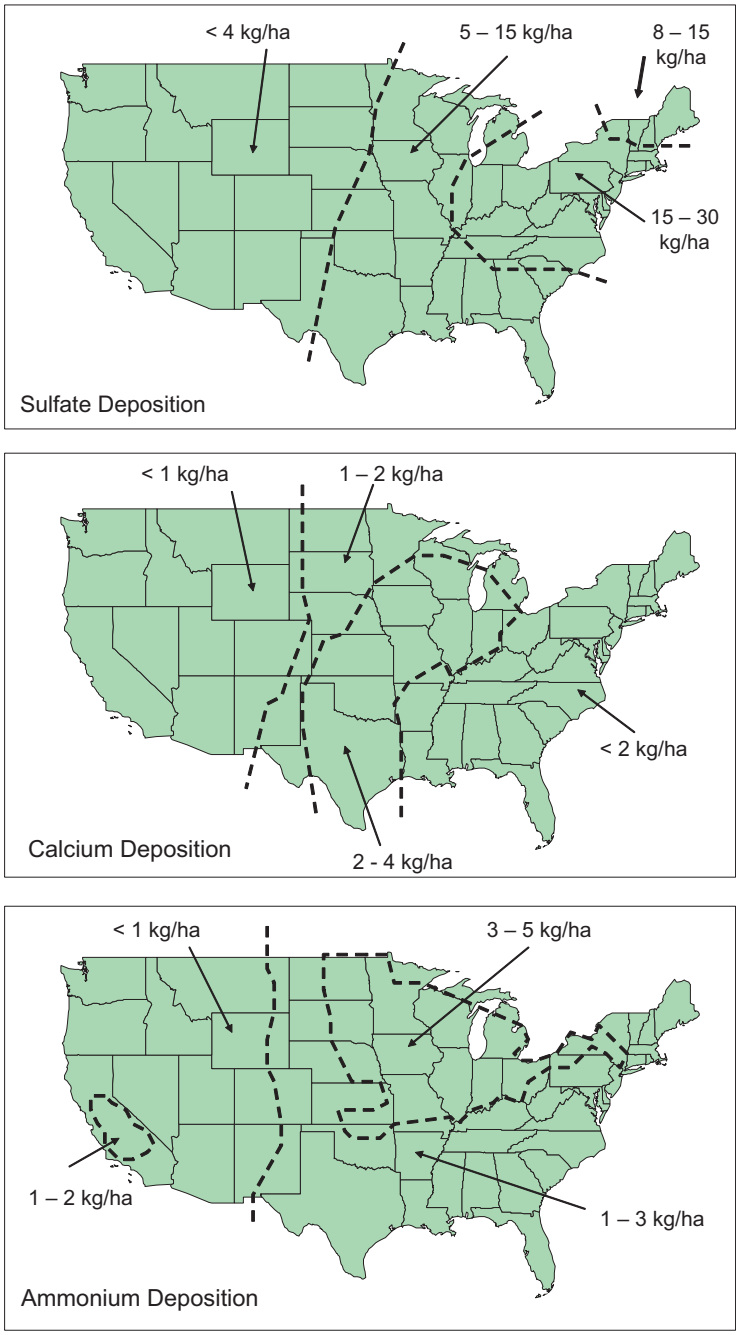

Fig. 6.13 Patterns of wet deposition in kg ha^{-1} yr^{-1} for sulfate, ammonium, and calcium (NADP 2000). *Dashed lines* delineate regions characterized by the indicated ranges of deposition

Table 6.4 Annual weighted mean concentrations of selected ions in wet deposition for several contrasting locations in the United States. (Source: NADP 1982). Units = mg L^{-1}

Site	Rainfall (cm)	pH	Ca	Na	NH_4^+	NO_3^-	SO_4^{2-}
Huntington Forest, NY	104	4.4	0.10	0.05	0.25	1.35	2.30
Coweeta Forest, NC	183	4.7	0.06	0.15	0.10	0.60	1.25
Argonne, IL	107	4.3	0.25	0.10	0.35	1.55	3.10
Davis, CA	83	5.5	0.05	0.20	0.45	0.85	0.60
Olympic Park, WA	367	5.4	0.05	0.50	0.02	0.05	0.35

event results in enrichment of throughfall beneath the forest canopy.

It should be noted that nitrate deposition to a forest canopy can be more complicated than might be implied by Grennfelt's data. In some cases, nitrate in wet deposition (or dry-deposited N) may be absorbed by foliage or canopy epiphytes during moisture movement through the canopy. When this happens, canopy throughfall may contain less

nitrate than that observed in a wet-only collector located in the open, implying perhaps that the canopy does not enhance deposition of nitrate-N. In reality, however, a complete mass balance would likely show that the sum of nitrate absorbed in the canopy plus nitrate in canopy throughfall is greater than nitrate collected in the open.

In comparing chemistries of canopy throughfall and wet deposition, it is important to understand that the amount of an element sampled in canopy throughfall is the result of multiple potential enrichment and depletion processes. Wet deposition inputs to the forest canopy may be supplemented by cloudwater or fog inputs to the canopy, may be enriched by foliar leaching of solutes or washout of dry deposition, may be concentrated by evaporation processes, and may be altered by absorption or adsorption processes occurring during moisture passage through the canopy. For example, protons in acidic deposition are often adsorbed by foliage via cation exchange reactions that result in the neutralization of canopy throughfall, accompanied by the enrichment of throughfall with cations (Cronan and Reiners 1983; Lovett and Lindberg 1984). These differential patterns of throughfall enrichment and depletion are illustrated in Fig. 6.15.

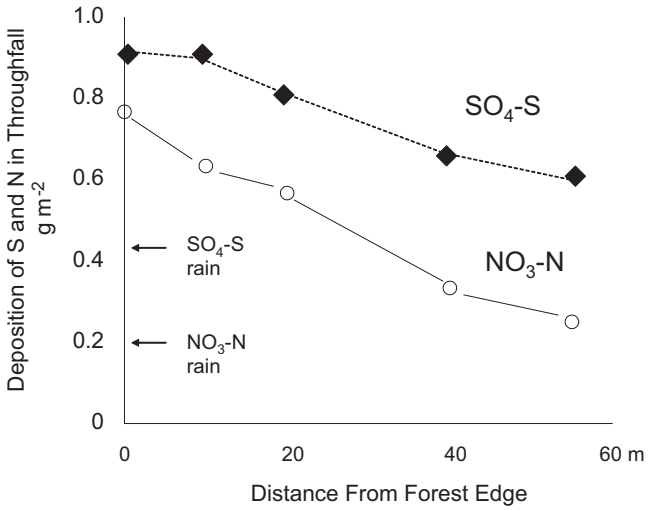

Fig. 6.14 Comparison of sulfate-S and nitrate-N collected in canopy throughfall along a sampling gradient proceeding from the edge to the interior of a pine forest in southern Sweden. *Arrows* show concentrations in rainfall collected in an open field at the study site. From Grennfelt, P. 1987. Deposition processes for acidifying compounds. Environmental Technology Letters 8:515–527. Reprinted by permission of the publisher, Taylor & Francis Ltd

Spatial Patterns: Comparison of Atmospheric Deposition at Different Forest Sites

Results from the Integrated Forest Study (Johnson and Lindberg 1992) provide a rich database for comparative analysis of the patterns of variation in atmospheric deposition across North America. Annual atmospheric sulfur deposition fluxes are presented in Fig. 6.16 for several North American forested sites sampled during the period 1986–1989. As shown in the graph, total sulfate deposition varied more than four-fold among sites, ranging from <500 mol_c ha^{-1} yr^{-1} in a Douglas-fir forest in Washington (DF) to >2000 mol_c ha^{-1} yr^{-1} at a high-elevation spruce-fir site in the Great Smoky Mountains (ST). Comparing the contributions of wet, dry, and cloud deposition to total sulfate inputs, there is further variation among sites – at the Turkey Lakes (TL) site in Ontario, wet deposition of S is the dominant input; at the loblolly pine (LP) site at Oak Ridge, TN, S deposition is split 50:50 between wet and dry deposition; and at the Great Smoky Mountains, TN (ST) and Whiteface Mountain, NY (WF) sites, there is a large S input from cloud water deposition.

A similar range of variation is evident looking at the N deposition data shown in Fig. 6.17. Again, we see a four to

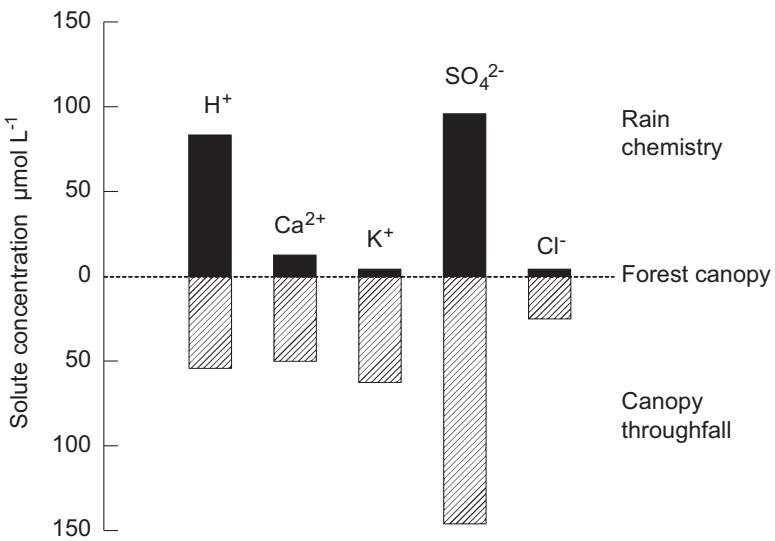

Fig. 6.15 Comparison of wet deposition (above *horizontal line*) versus canopy throughfall chemistry for a northern hardwood forest in New Hampshire, USA. Concentrations of calcium, potassium, sulfate, and chloride ions are enriched in transit through the canopy, whereas H^+ ion is diminished. Data from Cronan and Reiners (1983)

five-fold difference between sites with the lowest inputs (e.g., Douglas-fir forest in Washington (DF) @ 400 mol N ha^{-1} yr^{-1}) and sites with the highest inputs (e.g., Great Smoky Mountains spruce-fir (ST) @ almost 2000 mol N ha^{-1} yr^{-1}). Differences are also clearly apparent in terms of the relative contributions of wet, dry, and cloud water deposition to total N inputs to the watersheds. Based on the principles that have been discussed in this chapter, think about how you can account for the differences in atmospheric deposition of S and N among these field sites.

Another intriguing example of spatial contrasts in atmospheric deposition can be found in high elevation ecosystems. At elevations above 1000 m in the humid north temperate zone, it is not uncommon for cloud water deposition to account for 30–50% of the moisture input to forest ecosystems (Lovett et al. 1982; Dingman 1994). What is also interesting is the fact that cloud water chemistry differs considerably from the chemistry of wet precipitation. As shown with data from the White Mountains of New Hampshire, solutes in cloud water can be almost five times more concentrated compared to precipitation (Fig. 6.18). When the large inputs of concentrated cloud water are added to moisture inputs derived from **orographic precipitation**, one finds that total atmospheric deposition of strong acids and other ions to high elevation forest ecosystems is greatly enhanced compared to lower elevation systems. Indeed, that is why the Great Smoky Mountain and Whiteface Mountain sites represent such extreme endpoints in the preceding graphs from the IFS investigation. In their study of atmospheric deposition of nitrogen in southern Chile, Weathers and Likens (1997) reported that cloud water concentrations of ammonium ion were up to 80 times higher than volume-weighted mean concentrations in rainfall collected nearby.

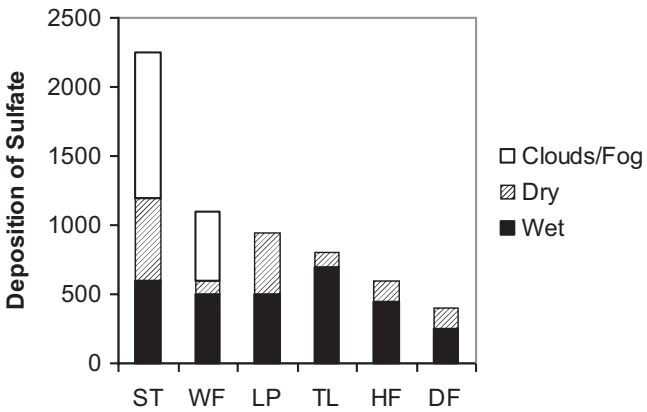

Fig. 6.16 Annual atmospheric deposition of sulfate by each input process for field sites in the Integrated Forest Study, 1986–1989. Abbreviations for field sites are: DF-Douglas-fir, WA; HF-mixed hardwood, NY; LP-loblolly pine, TN; ST-spruce, high elevation in Smoky Mts.; TL-mixed hardwood, Ontario; WF-spruce-fir, Whiteface Mt., NY. From Mitchell, M.J. and S.E. Lindberg. Sulfur chemistry, deposition, and cycling in forests. pp. 72–149 in Johnson, D.W. and S.E. Lindberg (eds). Atmospheric Deposition and Forest Nutrient Cycling: A Synthesis of the Integrated Forest Study. Ecological Studies Vol. 91 Springer-Verlag, NY. ©1992 and used with permission of Springer Units of deposition = mol_c ha^{-1} yr^{-1}

Modeling Atmospheric Deposition Patterns

Despite the complexity of atmospheric deposition, there have been ongoing efforts to incorporate current understanding into models that can be used to predict patterns of deposition at various spatial scales and time steps. One such model is the Regional Atmospheric Deposition Model (RADM) that predicts air concentrations and deposition for various trace gases monitored by NAPAP, the National Acid Precipitation Assessment Program (Chang 1991). Another example is the spatial model of atmospheric deposition for the northeastern U.S. developed by Ollinger et al. (1993). In that modeling effort, regression relationships for deposition chemistry

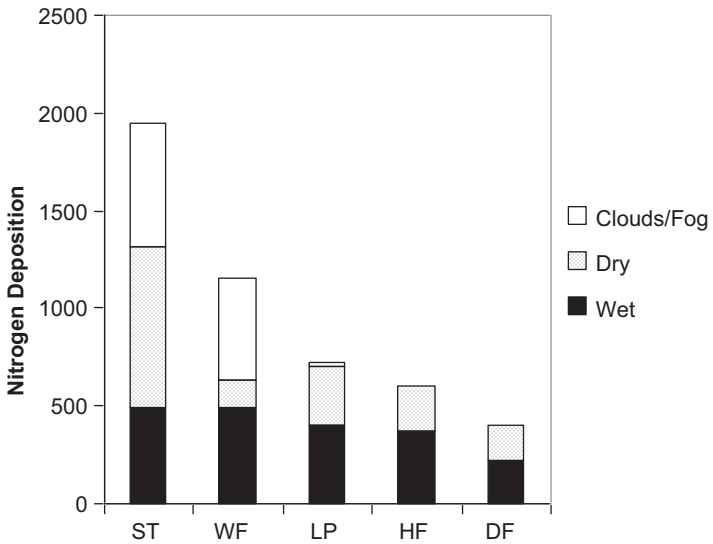

Fig. 6.17 Annual atmospheric deposition of nitrogen by each input process for field sites in the Integrated Forest Study, 1986–1989. From Cole, D.W. Nitrogen chemistry, deposition, and cycling in forests. pp. 150–213 in Johnson, D.W. and S.E. Lindberg (eds). Atmospheric Deposition and Forest Nutrient Cycling: A Synthesis of the Integrated Forest Study. Ecological Studies Vol. 91 Springer-Verlag, NY. ©1992 and used with permission of Springer. Units of deposition = mol ha^{-1} yr^{-1}

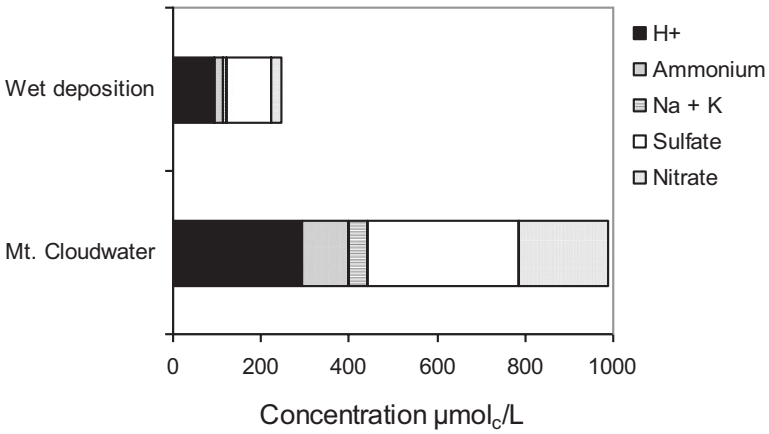

Fig. 6.18 Comparison of chemistry in cloud water versus bulk precipitation for high elevation sites in the White Mts., NH. Ion concentrations from left to right in *bar graphs* are: H^+, NH_4^+, Na^+, K^+, SO_4^{2-}, and NO_3^- (Data from Lovett et al. 1982)

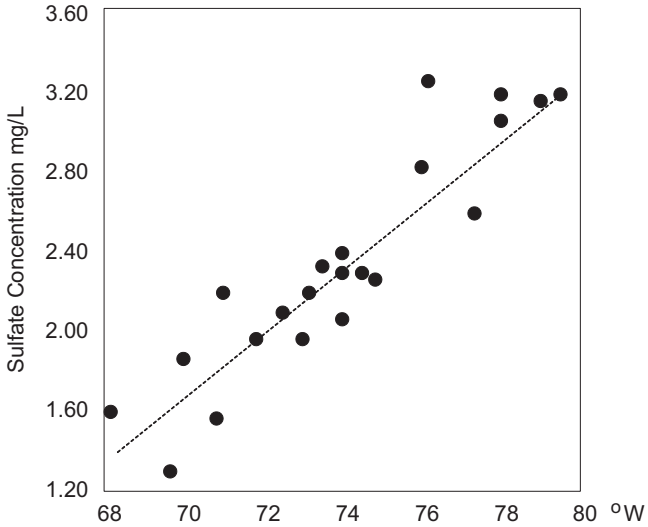

Fig. 6.19 Regression plot of mean annual sulfate ion concentration versus longitude for precipitation in the northeastern U.S. From Ollinger, S.V., J.D. Aber, G.M. Lovett, S.E. Millham, R.G. Lathrop, and J.M. Ellis. A spatial model of atmospheric deposition for the northeastern United States. Ecological Applications 3:459–472. ©1993 by the Ecological Society of America

(Fig. 6.19) were combined with a GIS spatial database in order to predict annual wet deposition inputs for a variety of elements across the northeastern landscape as a function of latitude, longitude, and elevation. Dry deposition was estimated in their study by combining atmospheric concentrations of each element with assumed deposition velocities for each chemical substance.

A Case Study of Deposition Inputs to a Forest Ecosystem

Measuring and estimating atmospheric inputs of elements to a forested watershed is a complex process that requires empirical measurements, modeling, and considerable expertise with plant processes and environmental physics. Walker Branch Watershed in Oak Ridge, TN is one of the few field sites in the U.S. where intensive efforts have been made to assemble detailed estimates of total atmospheric deposition to a forested catchment. Table 6.5 presents a summary of the annual ion deposition estimates developed by Lindberg et al. (1986) for an oak forest at Walker Branch Watershed. These data illustrate for a single ecosystem in one climatic region the relative contributions of different deposition components to the inputs of sulfate, nitrate, H^+, ammonium, calcium, and potassium ions. The authors noted in their report that the overall uncertainty for wet deposition flux estimates is about ±20 percent, whereas the uncertainty for dry deposition fluxes is roughly ±50 percent for sulfate, calcium, potassium, and ammonium ions, and approximately ±75 percent for nitrate and H^+ ions.

Table 6.5 Total annual atmospheric deposition of major ions to an oak forest at Walker Branch Watershed based on 2 yr of data reported by Lindberg et al. (1986)

	Atmospheric deposition ($mmol_c\ m^{-2}\ yr^{-1}$)					
Process	SO_4^{2-}	NO_3^-	H^+	NH_4^+	Ca^{2+}	K^+
Precipitation	70	20	69	12	12	0.9
Dry deposition						
Fine particles	7	0.1	2.0	3.6	1.0	0.1
Coarse particles	19	8.3	0.5	0.8	30	1.2
Vapors	62	26	85	1.3	0	0
Total deposition	160	54	160	18	43	2.2

In summary, the cycling of elements through the atmosphere and back to receptors in the biosphere is a complex phenomenon that is critically important for biogeochemical patterns and processes observed in watershed ecosystems. As one example, the cycling of toxic methyl mercury described in Chap. 3 begins with emissions of volatile Hg from industrial combustion sources, long-range transport of this contaminant, and subsequent atmospheric deposition of Hg to watersheds where methylation occurs. Thus, a thorough understanding of Hg biogeochemistry requires a detailed consideration of major atmospheric transport and deposition processes affecting this element. Likewise, most other elements have important atmospheric cycling pathways that are integral to a comprehensive analysis of ecosystem biogeochemistry.

Mineral Weathering

7

Introduction

Mineral weathering is a process characterized by chemical and physical breakdown of geologic materials, accompanied by the generation of dissolved solutes plus relatively stable new mineral phases. Weathering is important as a (i) source of nutrients such as calcium, magnesium, potassium, sodium, iron, silica, and a variety of trace metals; (ii) source of **acid neutralizing capacity** or **alkalinity**; (iii) source of phosphorus and sulfur in certain types of geologic formations; and (iv) vital process contributing to formation of clay colloids or secondary minerals. In watershed ecosystems, mineral weathering represents a crucial process of replenishment (Fig. 7.1) that helps to offset cation losses resulting from leaching and forest harvesting, and it restores alkalinity consumed by acidic deposition and soil acidification processes. At any given time in the landscape, weathering processes may involve minerals with different chemistries, different rates of reaction, and different locations in the soil profile, surficial geologic overburden, or bedrock geology of a watershed.

Ecosystem Context

To gain an initial perspective on the role of weathering in terrestrial ecosystems, we can consider the calcium cycle at Walker Branch Watershed in Oak Ridge, TN (Johnson and Henderson 1989). In that forested ecosystem, annual loss of dissolved Ca in stream water equals 147 kg ha^{-1}, compared to annual atmospheric inputs of 16 kg ha^{-1}. By comparison, the exchangeable Ca pool in the upper 60 cm of soil is just 710 kg ha^{-1}. Clearly, net leaching loss of Ca from the Walker Branch Watershed cannot be explained by depletion of soil exchangeable Ca, because that pool is too small to supply Ca for more than 5–6 years. The evidence indicates, instead, that primary mineral weathering in this watershed supplies much of the Ca for stream exports and replenishment of exchangeable Ca in the soil profile. In this example, it is dolomitic limestone bedrock enriched in Ca and Mg that is weathering and exerting a strong influence on Ca cycling.

Mineral Weathering Processes

Chemical weathering occurs as rocks or mineral soil particles are subjected to aqueous **hydrolysis** reactions, oxidation, **complexation**, and dissolution by acids derived from microbial metabolism, plant roots, or acidic

C.S. Cronan, *Ecosystem Biogeochemistry*, Springer Textbooks in Earth Sciences, Geography and Environment, DOI 10.1007/978-3-319-66444-6_7

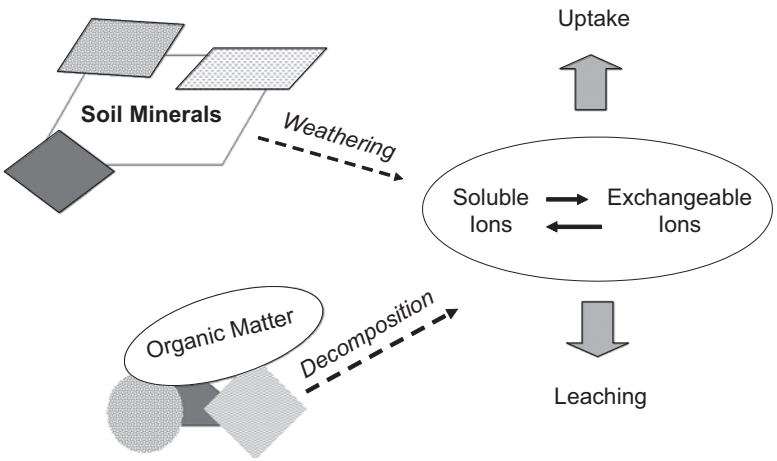

Fig. 7.1 Mineral weathering is a key nutrient cycling pathway that contributes to pools of soluble and exchangeable ions in watershed ecosystems

precipitation. As a result of these processes, the crystal structures of minerals break down and release soluble elements into the surrounding aqueous medium. Two examples of weathering reactions involving a **primary mineral** (feldspar) and a **secondary mineral** (kaolinite) are shown below:

Weathering of a Primary Mineral, Calcium Feldspar

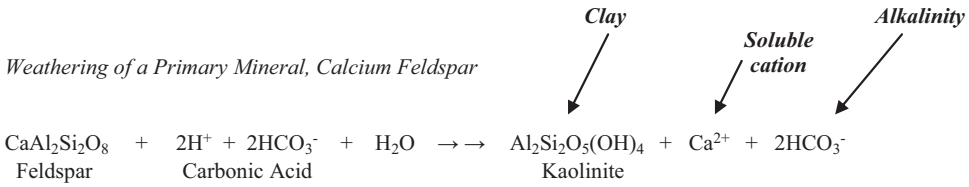

Weathering of a Secondary Mineral, Kaolinite

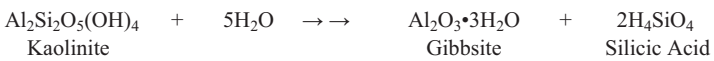

In the first example illustrated above, the weathering reaction involving feldspar, water, and carbonic acid consumes H^+, releases the nutrient calcium plus bicarbonate (which can act as an acid buffer), and generates a kaolinite clay crystal that contributes to the cation exchange capacity of the soil. In the second example, kaolinite decomposes to form soluble silicic acid plus residual solid-phase gibbsite. Weathering reactions such as these examples are referred to as **incongruent dissolution** reactions, because they yield both soluble ions and a residual secondary mineral phase as reaction products.

Alternatively, chemical weathering may involve **congruent dissolution**, which occurs when a mineral completely dissolves without leaving any residual secondary mineral phase clays or metal oxides. Two examples of this type of weathering reaction are the dissolution of calcite (calcium carbonate), which occurs relatively rapidly, and the dissolution of quartz (Table 7.1), which is generally a very slow reaction. Additional examples of both types of weathering reactions are also presented in Table 7.1.

Heterogeneous Mineral Weathering at Different Scales

Evidence from visual and microscopic analysis indicates that chemical weathering processes are heterogeneous in the environment. If you examine an igneous or metamorphic rock from your garden, you may see small cavities or pits that

Table 7.1 Examples of congruent and incongruent mineral dissolution reactions (Garrels and Christ 1965)

Congruent	
Weathering of calcite	$CaCO_3 + H_2CO_3 + H_2O \rightarrow \rightarrow Ca^{2+} + 2HCO_3^- + H_2O$
Weathering of quartz	$SiO_2 + 2H_2O \rightarrow \rightarrow H_4SiO_4$
Dissolution of gibbsite	$Al(OH)_3 + 3H^+ \rightarrow \rightarrow Al^{3+} + 3H_2O$
Dissolution of goethite	$FeOOH + 3H^+ \rightarrow \rightarrow Fe^{3+} + 2H_2O$
Incongruent	
$\underset{\text{albite}}{NaAlSi_3O_8} + H_2CO_3 + 4.5H_2O \rightarrow\rightarrow Na^+ + HCO_3^- + 2H_4SiO_4 + 0.5\underset{\text{kaolinite}}{Al_2Si_2O_5(OH)_4}$	
$\underset{\text{biotite}}{KMg_3AlSi_3O_{10}(OH)_2} + 7H_2CO_3 + 0.5H_2O \rightarrow\rightarrow K^+ + 3Mg^{2+} + 7HCO_3^- + 2H_4SiO_4 + 0.5\,\text{kaolinite}$	

Fig. 7.2 Cavity formed through preferential mineral dissolution in a rock matrix

likely originated through preferential dissolution of an easily weathered mineral within the overall rock matrix (Fig. 7.2). At a finer scale, examination of soil mineral grains with scanning electron microscopy often shows etch pits where physical strain or imperfections in crystal structure have allowed preferential dissolution in an otherwise homogeneous mineral (Velbel 1986).

At a larger scale, mineral weathering in a soil profile or watershed catchment is almost always characterized by spatial heterogeneity. In other words, we can be assured that the bulk soil and bedrock are not evenly weathering at a uniform rate. Rather, weathering is likely concentrated in zones characterized by (i) more weatherable minerals, (ii) conditions of elevated acidity (e.g., upper soil and rhizosphere), (iii) smaller mineral grain sizes with high surface areas, (iv) enhanced exposure to water infiltration, or (v) prolonged hydrologic contact between minerals and acidic drainage water (e.g., groundwater zone).

Evidence for spatial differences in weathering rates can be found in research results from a variety of geographic settings. In a comparative study of soil weathering in three contrasting forest ecosystems in the northeastern U.S., the author found that unit weathering rates were roughly three times higher in upper mineral horizons compared to lower mineral horizons. The A horizon of a fine textured Inceptisol exhibited a weathering rate of 3.3 $mmol_c\ kg^{-1}\ yr^{-1}$ versus a rate of 1.0 $mmol_c\ kg^{-1}\ yr^{-1}$ in the B horizon. A sandy loam Spodosol in the same study exhibited a weathering rate of 0.7 $mmol_c\ kg^{-1}\ yr^{-1}$ in the upper mineral horizon, compared to a rate of 0.2 $mmol_c\ kg^{-1}\ yr^{-1}$ for the B horizon (Cronan 1985b).

In their study of mineral weathering in the Catoctin Mountains of Maryland, Katz et al. (1985) found further evidence illustrating the remarkable heterogeneity of weathering processes. High exports of soluble Ca from their watershed could not be accounted for by dissolution of the major minerals in the soils and geologic materials. The authors concluded that much of the soluble Ca in stream water originated from preferential dissolution of small calcite lenses scattered through the porous geologic overburden. Similar results from Horton et al. (1999) and Price et al. (2013b) have emphasized how weathering of small amounts of calcite within a matrix of resistant granitic bedrock can greatly increase Ca exports in stream runoff.

Controls on Mineral Weathering Rates

Under most conditions, mineral weathering is a rate-limited process that proceeds rather slowly towards an elusive theoretical equilibrium state. It is thus important to ask what factors control weathering rates and under what circumstances faster or slower rates of mineral dissolution would be expected.

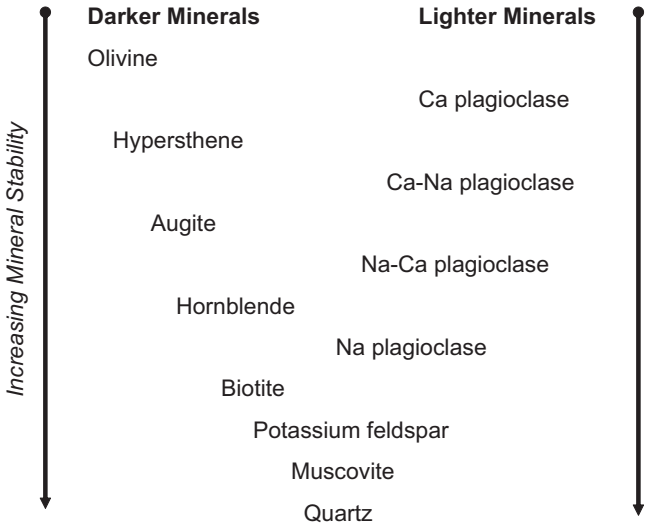

Fig. 7.3 Ranking of minerals in terms of relative stability and resistance to weathering; olivine is relatively unstable and highly weatherable, whereas quartz is stable

Mineralogical Controls

One of the major factors governing rates of weathering in watershed ecosystems is the **mineralogy** of surficial and bedrock geologic materials. Some minerals such as quartz and muscovite mica are very stable at the Earth's surface and are consequently highly resistant to chemical weathering (Fig. 7.3). In contrast, minerals such as olivine, calcite, and calcium plagioclase are thermodynamically more unstable, making them more susceptible to chemical weathering processes (Fig. 7.3). In between these examples are many other **mafic** and **felsic** minerals that exhibit intermediate stability and weatherability.

Geologic formations and surficial deposits in many terrestrial ecosystems are dominated by silicate and aluminosilicate minerals; consequently, these types of minerals exert a strong influence on watershed weathering rates. Variations in weathering rates among silicate minerals can be accounted for in part by the degree of SiO_2 polymerization in the crystal structure (Johnson 1984), as well as by the stoichiometry of base cations in a particular mineral formula. As illustrated in Table 7.2, silicate minerals range from those that contain isolated silica tetrahedra with low Si/O ratios (e.g., forsterite) to those characterized by silica double chains, sheets, and frameworks with high percentages of Si-O-Si linkages and larger Si/O ratios (e.g., tremolite, talc, and quartz). In general, the rate of mineral dissolution in a field setting is inversely related to the percentage of Si-O-Si linkages within the geologic substrate, with quartz exhibiting 100% Si-O-Si linkages and the slowest weathering rate under acidic environmental conditions.

Table 7.2 Structure and polymerization of silicate minerals (from Johnson 1984). In general, minerals with increasing percentages of Si-O-Si linkages are more resistant to acid hydrolysis and less likely to dissolve in the field

SiO_2 polymer configuration	Si-O-Si linkages	Anion formula	Si/O ratio	Example
Isolated tetrahedra	0	SiO_4	1/4	Mg_2SiO_4 (forsterite)
Tetrahedra doublet	25%	Si_2O_7	1/3.5	$Ca_2Al_3O(SiO_4)(Si_2O_7)$ OH. (epidote)
Single chain	50%	SiO_3	1/3	$MgSiO_3$ (enstatite)
Closed chain	50%	$(SiO_3)_n$	1/3	$Be_3Al_2(SiO_3)_3$ (beryl)
Double chain	69%	Si_4O_{11}	1/2.75	$Ca_2Mg_5(Si_4O_{11})_2(OH)_2$ (tremolite)
Sheet	75%	Si_4O_{10}	1/2.5	$Mg_3(Si_4O_{10})(OH)_2$ (talc)
Framework	100%	SiO_2	1/2	SiO_2 (quartz)

The potential influence of mineralogy on weathering rates can be illustrated with results from lab dissolution experiments using pure samples of different minerals. For example, Manley and Evans (1986) compared dissolution of two feldspars – anorthite ($CaAl_2Si_2O_8$) and albite ($NaAlSi_3O_8$) – in carbonic acid, and reported that release of silica and aluminum was 3–4 times faster from the Ca-rich mineral compared to the Na-rich feldspar. Schott et al. (1981) examined lab dissolution rates for diopside ($CaMg[Si_2O_6]$) versus tremolite ($Ca_2Mg_5Si_8O_{22}(OH)_2$) and found that silica release from tremolite was only 10% as fast as silica dissolution from diopside. This striking difference was largely attributed to the presence of double chain polymerization in tremolite (an amphibole), making it less weatherable than diopside (a pyroxene).

Influence of Acidity and Complexing Ligands on Weathering Rates

Strong and weak acids are important chemical weathering agents, acting as a potential source of protons and **complexing ligands**. In solution, H^+ ions promote mineral dissolution by displacing metallic cations in the mineral crystal lattice, whereas complexing ligands bind to metallic atoms on mineral surfaces or in solution, resulting in a lower chemical activity and increased solubility of the cation. The end result of these processes is enhanced chemical weathering through cation depletion of the mineral lattice. Examples of complexing ligands include fluoride, sulfate, citrate, and humic acid anions.

Many weathering reactions exhibit a pH-dependence, with dissolution rate increasing in proportion to the **free acidity** or H^+ ion activity in solution. Based on laboratory studies, it has been suggested that feldspar dissolution varies as a function of the H^+ ion activity raised to the power of 0.3–0.8 (Wollast 1967; Wollast and Chou 1985). Thus, a weathering reaction

rate for feldspar could be written as Rate = $k_*[H^+]^{0.33}$. The overall extent of mineral dissolution from weathering reactions can be influenced by the **total acidity** or acid supply rate of the system; this reserve acidity insures that as protons are consumed in weathering reactions, there is constant replenishment of H^+ ions for further acid attack.

Carbonic acid, which forms when CO_2 dissolves in water, is one of the primary **weak acids** contributing to chemical weathering in the biosphere (Garrels and Christ 1965). Carbon dioxide occurs in the atmosphere at a concentration of approximately 400 ppm (parts per million) and reaches concentrations in soils that are 10–100 times higher than atmospheric pCO_2 as a result of root and microbial respiration, coupled with diffusion limitations within the soil matrix. When CO_2 dissolves in a raindrop or into a film of soil moisture, the following equilibria are established:

$$CO_2 + H_2O \leftrightarrow H_2CO_3 \leftrightarrow H^+ + HCO_3^- \qquad (7.1)$$

If CO_2 is added to soil water from respiration, more carbonic acid will be formed, resulting in increased dissociation to protons and bicarbonate on the right side of the reaction. Similarly, if the temperature declines, more CO_2 will partition into solution, causing a shift toward the right side of the equilibrium. If the system is acidified by an external input of strong acid, the reaction will be pushed to the left, with the result that more of the total CO_2 will remain undissociated and some of the CO_2 may degas from solution. Because of the temperature-dependent solubility of CO_2, a rise in temperature will produce a similar shift to the left and a degassing of CO_2.

In a simple aqueous system dominated by carbonic acid, solution pH can be computed as a function of the pCO_2 or partial pressure of CO_2. From Eq. (7.1) above, we can write two equilibrium expressions representing CO_2 dissolution to form carbonic acid and dissociation of carbonic acid at 25 °C:

$$\left[H_2CO_3\right] / pCO_2 = K_1 = 3.4 \times 10^{-2} \qquad (7.2)$$

$$\left[H^+\right] * \left[HCO_3^-\right] / \left[H_2CO_3\right] = K_2 = 4 \times 10^{-7} \qquad (7.3)$$

Re-arranging Eq. (7.2), we get $[H_2CO_3] = pCO_2 * 3.4 \times 10^{-2}$

Re-arranging Eq. (7.3) and substituting for $[H_2CO_3]$ in the denominator, we have the following:

$$\left[H^+\right] * \left[HCO_3^-\right] = \left(4 \times 10^{-7}\right) * \left(pCO_2\right) * \left(3.4 \times 10^{-2}\right) = \left(1.36 \times 10^{-8}\right) * \left(pCO_2\right) \qquad (7.4)$$

Case 1 Solution pH at Ambient Atmospheric pCO_2

If we use an atmospheric pCO_2 of 380 ppm, solution pH is calculated from expression (7.4) as follows:

$$pCO_2 = 0.000380 = 10^{-3.42}$$

$$\left[H^+\right] * \left[HCO_3^-\right] = 1.36 \times 10^{-8} \times pCO_2 = 4.94 \times 10^{-12} \qquad (7.5)$$

Assuming that $[H^+] = [HCO_3^-]$ at equilibrium and knowing that pH = −log $[H^+]$, we take the negative log of the square root of the product in Eq. (7.5) to get pH = 5.65.

Case 2 Solution pH at Elevated pCO_2

If we now assume an elevated soil pCO_2 equal to 100 times the atmospheric concentration in the previous example, we similarly calculate the following solution pH in a simple carbonic acid and water system:

$$pCO_2 = 10^{-1.42}\,\text{atm.}$$

$$\left[H^+\right] * \left[HCO_3^-\right] = 4.94 \times 10^{-10}$$

$$pH = -\log\left[H^+\right] = 4.65$$

This example thus illustrates how elevated pCO_2 in the soil or groundwater environment can theoretically drive solution pH below 5, producing an aggressive weathering solution.

Organic acids, which are characterized by carboxylic (−COOH) and hydroxyl (−OH) weak acid functional groups, are a second major source of acidity for weathering reactions in the biosphere. These acids vary widely in structural complexity from simple **aliphatic** acids such as the 2-carbon acetic and 4-carbon malic acids derived from plant and microbial metabolism to large polycyclic **fulvic** and **humic acids** produced during the decay of organic detritus. Organic acids are important sources of protons plus complexing ligands. An example is the dicarboxylic acid shown below which can ionize to release two protons, leaving an oxalate anion capable of forming a **bidentate chelate** with a cation such as Ca^{2+}.

$$\underset{\text{oxalic acid}}{H_2C_2O_4} \leftrightarrow \quad H^+ + HC_2O_4^- \leftrightarrow \quad \underset{\text{oxalate ligand}}{2H^+ + C_2O_4^{2-}}$$

In this example, the proton dissociation constant for the first ionization step is $10^{-1.23}$, and the equilibrium reaction can be written as follows:

$$\left[H^+\right] * \left[HC_2O_4^-\right] / \left[H_2C_2O_4\right] = K_1 = 10^{-1.23}$$

We can use this expression to emphasize an important insight regarding weak acids. When the first carboxyl group on this acid is half dissociated, the ratio of $[HC_2O_4^-]/[H_2C_2O_4]$ equals 1 and the equilibrium expression simplifies to $[H^+] = K_1$. Taking the -log of both sides, we get pH = −log $(10^{-1.23})$ = 1.23. From this, it is apparent that the pH at which the organic acid is half-dissociated is equivalent to the pK or

−log of the dissociation constant. In this example, the first carboxylic acid group will be more than 50% ionized above pH 1.23. As such, this is considered a very strong "weak acid". In comparison, a weaker organic acid such as acetic acid has a pK around 4.75 and is mostly un-ionized below pH 3.5 and only 50% dissociated at pH 4.75.

Strong mineral acids, which comprise the third group of acidic substances contributing to chemical weathering, include familiar compounds such as sulfuric, nitric, and hydrochloric acids. These reactive acids ionize rapidly and completely to release protons and the free inorganic anions SO_4^{2-}, NO_3^-, and Cl^-. In contrast to many of the organic anions or ligands that complex easily with metallic cations, these inorganic anions tend to form weaker complexes with metals and thus exert most of their influence through direct H^+ attack. Sulfate does, however, form potentially important complexes with aluminum, calcium, and several other metals.

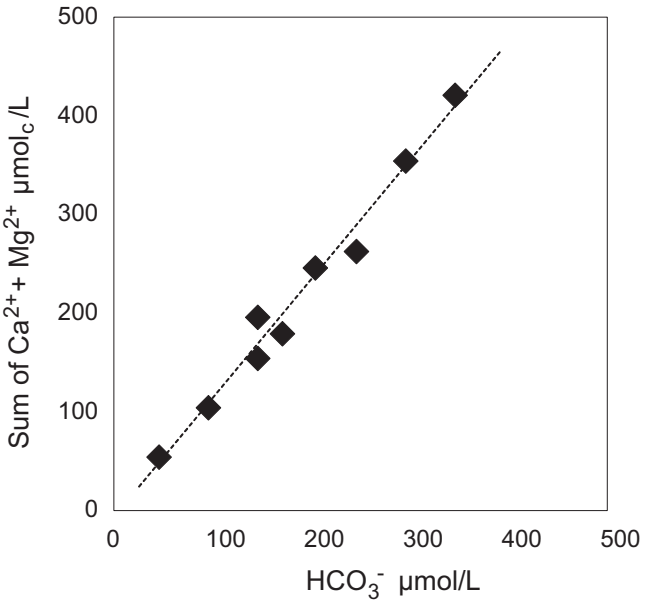

Fig. 7.5 Relationship between bicarbonate and divalent cation (Ca + Mg) concentrations for waters flowing from the weathering zone in the South Cascade Glacier watershed. From Reynolds, R.C. and N.M. Johnson. 1972. Chemical weathering in the temperate glacial environment of the northern Cascade Mountains. Geochimica Cosmochimica Acta 36:537–554, with permission from Elsevier

Experimental Effects of Acidity on Weathering Rates

The potential influence of acidity and complexation reactions on rates of mineral weathering have been demonstrated by a number of investigators using dissolution experiments with pure mineral samples. For example, Chou and Wollast (1984) reported that dissolution of albite ($NaAlSi_3O_8$) increased about 10-fold as treatment pH decreased from pH 5.5 to 2.5. In another series of experiments, Manley and Evans (1986) compared feldspar weathering rates for equimolar concentrations of carbonic, organic, and mineral acids under controlled laboratory conditions. As shown in Fig. 7.4, dissolution rates were lowest for weak carbonic acid, higher for the strong acid HCl, and highest for citric acid, an organic acid that forms complexes with Al and Ca, thereby increasing their solubilities and release rates during weathering. In other words, the organic acid generated the highest weathering rate, because it not only supplied protons for acid attack, but also enhanced dissolution through complexation reactions.

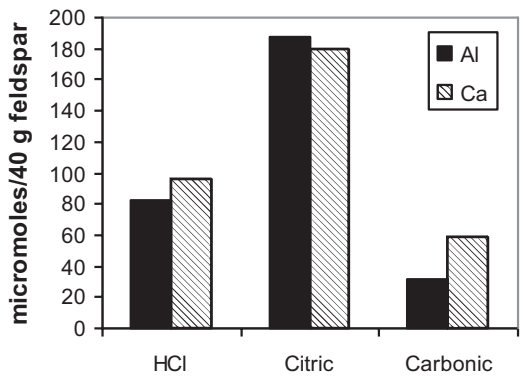

Fig. 7.4 Rates of release of Ca and Al ions from calcic plagioclase during 10 weeks of dissolution in 10^{-4} M mineral, organic, and carbonic acids (Data from Manley and Evans 1986)

In their study of chemical weathering in a North American montane glacier, Reynolds and Johnson (1972) found that carbonation reactions were the most important mechanism driving high rates of mineral dissolution. The importance of carbonic acid weathering was reflected by the fact that cations exported in streamwater at their study site were tightly correlated with bicarbonate ion concentrations derived from carbonic acid (Fig. 7.5). Evidently, other sources of acidity such as mineral or organic acids were not present or abundant in that glacial environment.

Physical Influences on Weathering Rates

Weathering rates of minerals can vary greatly as a function of physical characteristics (e.g., particle sizes and surface areas) and in response to variable climatic and hydrological conditions (in terms of annual precipitation, temperature, water contact time, and flushing rates). Schalscha et al. (1967) examined the influence of particle size and surface area on dissolution rates of granodiorite exposed to salicylic acid and found that Fe release from the finest size fraction (<0.07 mm) was 16 times higher than Fe released from the

coarsest size fraction (0.25–0.50 mm). Helgeson et al. (1984) independently confirmed the strong effects of mineral surface area on weathering reaction rates. Lanyon and Hall (1979) demonstrated that weathering rates of minerals in the laboratory increase with higher temperature, and White and Blum (1995) reported that weathering release of SiO_2 and Na^+ increased with precipitation and temperature in a wide range of field studies. Investigators have found that soils on south-facing slopes in the northern hemisphere have higher mean annual temperatures and more highly weathered soil profiles than nearby soils on north-facing slopes (Losche et al. 1970; Franzmeier et al. 1969). It should be noted, however, that temperature relationships can be complicated by the fact that carbon dioxide is more soluble at lower temperatures (increasing the weathering potential of the solution) and soil organic acids tend to be more abundant in cooler humid regions (again increasing the weathering potential of the soil solution). Nevertheless, as a general rule, weathering rates are expected to increase with decreased particle sizes, increased mineral surface area, increased hydrologic flushing (Velbel 1985,1986), and increased temperature (Fig. 7.6).

Biotic Influences on Mineral Weathering Rates

Plants, lichens, fungi, and bacteria exert a prodigious influence on mineral weathering rates in the field through their contributions to acid production and release of organic complexing compounds. As an example, April and Keller (1990) examined weathering in the rhizosphere of forest soils and observed evidence of more intense mineral weathering and clay mineral alteration in the rhizoplane adjacent to plant roots. Hiebert and Bennett (1992) reported that feldspar minerals colonized by indigenous bacteria in the groundwater zone at a site in Minnesota exhibited higher rates of weathering, presumably because of the high concentrations of organic acids formed by the bacteria. Burghelea et al. (2015) reported that mineral weathering and associated nutrient release were enhanced by plant processes and associated arbuscular mycorrhizae in mesocosm experiments with porous assemblages of minerals planted with buffalo grass.

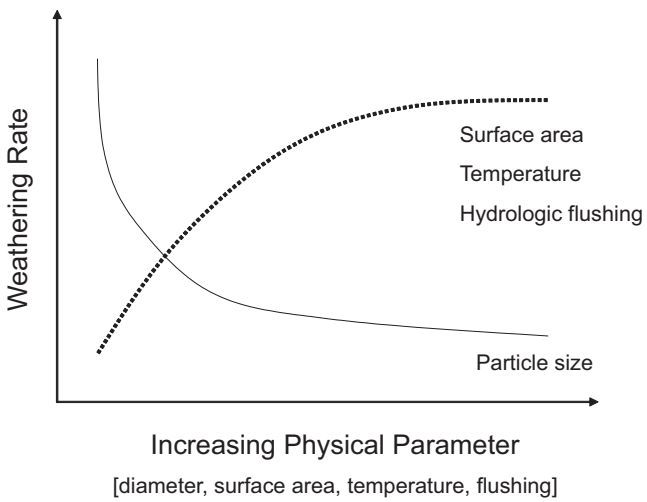

Fig. 7.6 General relationships between weathering rate and physical factors

Influence of Mineral Dissolution on the Solution Chemistry of Natural Waters

Water chemistry evolves and changes as precipitation or snowmelt drains through a watershed and moves down a river drainage system. Along this pathway, the signature of weathering reactions is inscribed in the ionic composition of the evolving parcel of water. As a consequence, water chemistry can be used to make inferences about weathering processes in a watershed ecosystem.

The diagrams in Fig. 7.7 provide a conceptual basis for considering how individual minerals can impart distinctive characteristics to a weathering solution in a watershed. In an ecosystem where potassium feldspar is a major source of weathering products, dissolution of this mineral in carbonic acid would release soluble SiO_2 plus potassium bicarbonate in the mole ratios shown in Fig. 7.7. In comparison, the Na-feldspar, albite, weathers to produce a sodium bicarbonate solution plus SiO_2. Calcium plagioclase feldspar, on the other hand, yields a solution dominated by calcium bicarbonate and SiO_2. In the absence of feldspar minerals, we might observe an example of a weathering solution containing calcium bicarbonate, with little or no accompanying SiO_2; this evidence could imply the weathering of calcite (Fig. 7.7). The final two examples in Fig. 7.7 illustrate that dark minerals such as pyroxene and biotite (black mica) decompose during weathering to yield their own distinctive mixtures of dissolved silica, Na^+, K^+, Mg^{2+}, and Ca^{2+}.

In a field setting, of course, natural waters often reflect the complex geochemical signatures of many different weathering, ion exchange, and absorption reactions, so that it is difficult to see the pure signal of one particular mineral dissolution reaction. In one of our biogeochemical studies, we sampled soil solution chemistry and found the calcium and sodium-rich cation stoichiometry depicted in the left-hand bar of Fig. 7.8. The question was: did the **base cation** molar concentrations in soil drainage water reflect the dominant influence of mineral weathering or other alternative processes? When we determined base cation stoichiometry of the bulk soil mineral phase, we found that K^+ and Na^+ were the dominant cations on a molar basis, whereas Ca^{2+} was rela-

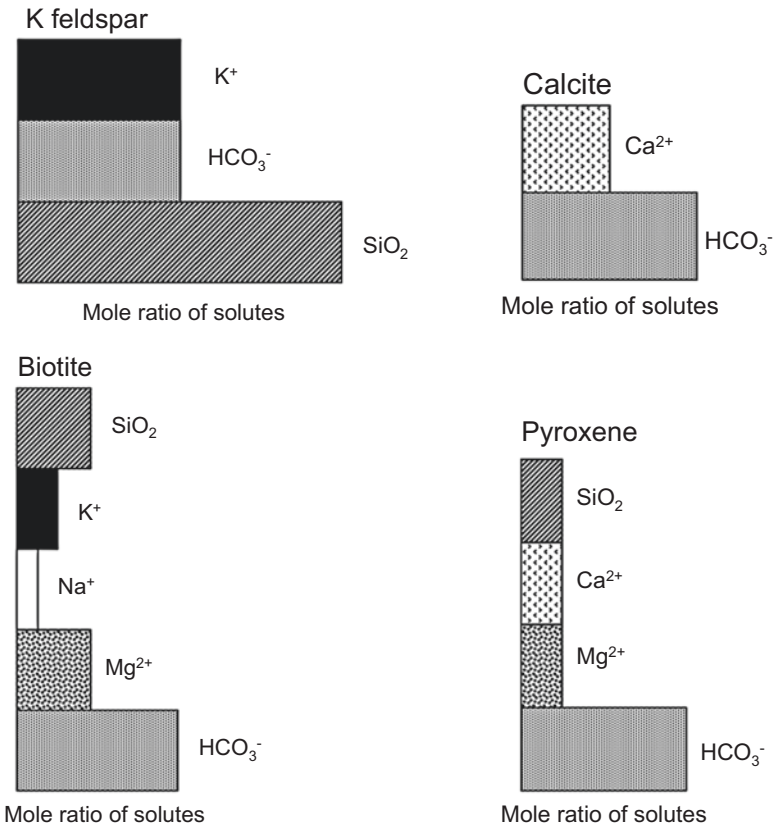

Fig. 7.7 Calculated compositions of solutions resulting from dissolution of single pure minerals. *Bars* show mole ratios of solutes relative to HCO_3^- (Data from Garrels 1967)

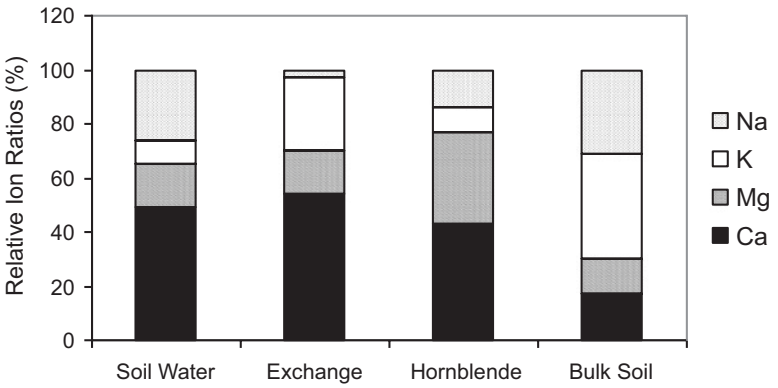

Fig. 7.8 Relative molar proportions of base cations in soil drainage water, the soil exchange complex, hornblende minerals, and the bulk soil chemistry of a forested watershed in the Adirondack Park, NY (Data from Cronan 1985a)

tively depleted or deficient in the bulk soil (Fig. 7.8). By comparison, cation chemistry of the major weatherable heavy mineral in the watershed – hornblende – was dominated by Ca^{2+} and Mg^{2+} (Fig. 7.8). In a final step, we examined the cation exchange pool as a critical geochemical buffer linking mineral weathering reactions and solution chemistry, and observed that exchangeable cation chemistry was dominated on a molar basis by Ca^{2+} and K^+, but was deficient in Na^+.

We were forced to conclude that soil water chemistry at the study site is a complex mixture from multiple sources, rather than a simple solution derived from a specific weathering reaction. In part, soil solution chemistry seemed to reflect the relative abundances of Ca^{2+} and Mg^{2+} in the cation exchange reservoir and in hornblende; however, the relative abundance of Na^+ in the soil solution was more of a reflection of the Na^+ enrichment of the bulk soil mineralogy shown in Fig. 7.8. Apparently, there was a mineral source such as albite within the bulk soil matrix that served as a weathering source for Na.

Genesis and Weathering of Clays

Weathering processes are important for the formation of two major classes of soil colloids: silicate clays and hydrous oxides. In the early to intermediate stages of

primary mineral weathering (e.g., younger soils), 2:1 aluminosilicate clays such as illite, vermiculite, and montmorillonite are likely to predominate in the soil environment. However, in advanced stages of weathering, it is expected that 1:1 kaolinite clay and oxides of iron and aluminum will become more abundant as the final products of the weathering breakdown of primary minerals and 2:1 secondary minerals (Brady 1984). These general trends are evident when soils are compared from different geographic regions. Where soil profiles have developed over long periods in warm, humid climates (e.g., southeastern U.S. and Central America), we tend to find highly weathered, deep soils containing high concentrations of kaolinite clay and oxides of iron and aluminum. In contrast, younger soils that have been less heavily impacted by long-term weathering generally contain lower concentrations of clays, with higher proportions of illite, vermiculite, and/or montmorillonite 2:1 clays. Examples of these contrasting conditions can be found by comparing Camp Branch watershed in Tennessee, where the Ultisol soil contains >22% clay and is dominated by kaolinite and vermiculite, versus a northern watershed at Big Moose, New York, where the Spodosol soil contains <3% clay and is dominated by vermiculite with minor amounts of kaolinite and mixed layer clays (Cronan et al. 1990).

Methods of Estimating Weathering Contributions to Ecosystem Element Budgets

Weathering is the dominant long-term source of cations and acid neutralizing capacity for most terrestrial ecosystems; thus, efforts to understand element cycling patterns and processes in watershed ecosystems require rigorous estimates of mineral weathering rates. Unfortunately, there is no simple acceptable way to estimate field weathering rates. For example, estimates of mineral dissolution in the laboratory are on the order of 10^{-11} moles m^{-2} s^{-1}, but these rates are as much as three orders of magnitude faster than field estimates of rock weathering (Velbel 1986; Schnoor 1990). Thus, one cannot simply extrapolate from controlled experimental studies in the laboratory to whole system weathering rates.

Mass Balance Estimation

One standard approach for estimating watershed weathering rates involves the use of element **mass balance** calculations (Katz et al. 1985; Paces 1986; Clayton 1988). If we represent a watershed as a series of pools and transfers, we can express the mass balance of each weatherable cation as follows:

$$\begin{aligned}&\textbf{Weathering} = \textbf{Outputs}\,(\text{in streamflow})\\ &-\textbf{Inputs}\,(\text{in atmospheric deposition})\\ &\pm\textbf{Storage}\,(\text{as exchangeable cations or secondary minerals})\\ &\pm\textbf{Storage}\,(\text{in biomass})\end{aligned}$$

This relationship implies that if one estimates, over a fixed time interval, the streamflow outputs of a cation, atmospheric inputs of the cation in wet + dry deposition, net increases or decreases in storage of the cation on the soil exchange complex, and net increases or decreases in storage of the cation in biomass, one can compute the weathering rate of the cation by solving the difference equation shown above and in Fig. 7.9. In order to include silica and aluminum in a weathering calculation, one could simply modify the mass balance to account for transfer of these elements from primary minerals to secondary minerals formed during specific weathering reactions in the watershed.

Although this approach provides a powerful tool for use in watershed studies, there are potentially large uncertainties associated with the technique. Ecosystem mass balance weathering estimates for a variety of study sites have been found to range from roughly 300 to 3000 mol_c ha^{-1} yr^{-1} for the sum of Ca + Mg + K + Na. How confident can we be with the accuracy of these values? Part of the mass balance depends on the stability or fluctuation of the cation exchange storehouse over time. Because of the large size of a typical cation exchange reservoir in a forested watershed, a 10% error in the mass balance estimate for net storage of cations in the exchange-

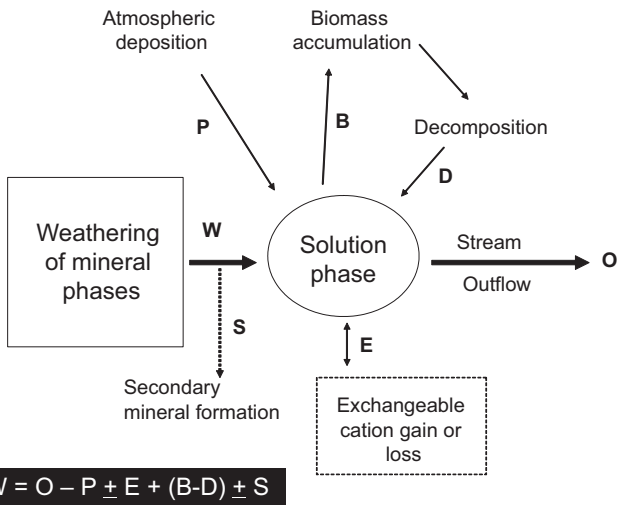

Fig. 7.9 Conceptual diagram of an ecosystem mass balance for mineral weathering. *Bold letters* (e.g., W = Weathering) in the diagram are used in the mass balance equation to represent each process

able pool can translate into an uncertainty of several hundred $mol_c\ ha^{-1}\ yr^{-1}$. Similarly, net accumulation of Ca, Mg, and K in forest biomass can range from negative values (in a degrading forest) to positive values as high as several thousand $mol_c\ ha^{-1}\ yr^{-1}$. Thus, errors in estimates for changes in storage of exchangeable cations or biomass increments of cations can be large enough to produce uncertainties of ±100% in ecosystem mass balance weathering estimates.

One way to constrain ecosystem mass balance estimates is to combine them with a consideration of weathering reaction stoichiometries. Clayton (1988) provided an excellent example of this approach in his study of weathering rates of orthoclase and plagioclase feldspars in three forested watersheds in the Idaho batholith. The author estimated rates of chemical weathering for three intensive study watersheds at Silver Creek in southwestern Idaho, where mean annual temperature is 4 °C and annual precipitation is 100 cm (65% snow). Soils at the site are Entisols <1 m thick and bedrock is a uniform quartz monzonite, with equal amounts of quartz, orthoclase feldspar, and plagioclase feldspar. Using mineralogical analyses, bulk rock chemistry, and stream chemistry, the investigator inferred reaction stoichiometries for dissolution of the two feldspar minerals and predicted masses of soluble cations, silicic acid, and residual solid-phase kaolinite clay expected for weathering of each mole of orthoclase or plagioclase. The author then applied a watershed mass balance approach involving atmospheric inputs, vegetation accumulation, runoff exports, and secondary mineral storage to estimate annual weathering of base cations, which ranged from 1480 to 1700 $mol_c\ ha^{-1}\ yr^{-1}$ for his three study sites (Table 7.3). As an independent check on his computations, he tested to see if observed fluxes of silica and base cations in stream exports were consistent with the mineral weathering stoichiometries he had assumed for his watersheds. Since predicted SiO_2 fluxes were 94–99% of the measured fluxes, the author concluded that stream exports of cations and silica could be accounted for by mineral hydrolysis of the two feldspars and formation of residual kaolinite clay in the soil profile. It was a remarkable final outcome with very close agreement between predicted and observed fluxes!

Table 7.3 Mass balance fluxes for Idaho watershed SC-2 described by Clayton (1988). Data show net weathering release of cations, H^+ consumed in feldspar hydrolysis, feldspar weathering predicted from cation flux, and predicted SiO_2 flux from weathering reaction stoichiometry (which closely matched observed SiO_2 flux)

	Mass transferred		
Process	kg $ha^{-1}\ yr^{-1}$	mol $ha^{-1}\ yr^{-1}$	$mol_c\ ha^{-1}\ yr^{-1}$
Field measurements			
Net Na flux	13.3	579	579
Net Ca flux	18.1	452	904
Net K flux	1.7	44	44
Net SiO_2 flux	79.6	1321	–
Sum Na + Ca + K	–	–	1527
H^+ consumed	–	–	1527
Weathering predictions			
Albite weathered	152	580	–
Anorthite weathered	126	453	–
Orthoclase weathered	12	44	–
Kaolinite formed	197	765	–
SiO_2 release	167	2772	–
SiO_2 consumed	92	1526	–
Predicted net SiO_2 flux	75	1246	–

Element Tracers as Indicators of Weathering Rates

Some investigators have used sodium or silica exports from a watershed as a means of estimating rates of ecosystem mineral weathering (Paces 1983). If it is assumed that Na^+ released by primary mineral dissolution is not strongly accumulated in plant biomass or retained on cation exchange surfaces, then one can measure the annual flux of Na^+ in stream outflow and can back-calculate how much of the bulk mineral phase or a specific **sodic mineral** such as albite must have dissolved to release the observed amount of Na^+. Knowing element chemistry of the bulk mineral phase or the presumed sodic primary mineral, one can use that information to estimate total moles of each cation (including Na^+) released by the weathering process. Unfortunately, this approximation of weathering depends on simplifying assumptions that are a potentially large source of uncertainty.

Other investigators, assuming that silica concentrations in streamwater can only be derived from mineral dissolution processes, have used silica output fluxes from watersheds to estimate weathering rates or minimum weathering rates. For this procedure, one can either (i) back-calculate the amounts of cations plus silica released from the bulk soil mineral phase to account for streamwater silica, or (ii) assume that weathering is dominated by a specific mineral and take into account the amount of weathering required to account for both the silica in streamwater and the amount of silica retained in secondary clay formation. Knowing the silica/cation ratios in the original mineral phases, it is then possible to estimate the total base cation release from the weathering process. Clayton (1988) demonstrated that over half the silica released by primary mineral weathering at his sites in Idaho was ultimately stored in secondary mineral formation, thus emphasizing the importance of knowing reaction stoichiometries for a given watershed and accounting for silica immobilized in residual weathering products such as kaolinite.

Some investigators have used isotopic tracers to estimate mineral weathering rates in watershed ecosystems. Miller et al. (1993) focused on natural strontium (Sr) isotopes to estimate relative contributions of soil exchangeable cation depletion versus mineral weathering to observed streamwater outputs of base cations in a high-elevation ecosystem at

Whiteface Mt., NY. In their analysis, the authors identified two "end-member" sources of Sr exhibiting contrasting $^{87}Sr/^{86}Sr$ ratios: atmospheric deposition, with a ratio of 0.70931, and local bedrock and till, with much lighter ratios of 0.705160 and 0.706585. These isotopic ratios were compared to ratios in the soil exchange complex, vegetation, and streamwater exports from the ecosystem. Qualitatively, they found that Sr isotopic ratios in streamwater were depleted in the heavy isotope and thus were more similar to ratios in the geologic end-members, rather than ratios in atmospheric deposition or the soil exchange complex. Their quantitative analysis showed that roughly 70% of Sr exported in streamwater originated from new primary mineral weathering reactions. They extrapolated cation weathering rates by assuming that cations weather from the bedrock and till in proportion to cation/Sr ratios in the geologic matrix. Again, this method of extrapolation may be problematic, because of various untested assumptions.

Weathering Estimation with Mineral Depletion Techniques

April and Newton (1985) described a technique for estimating long-term weathering rates based on the concept of mineral depletion through the soil profile. They assumed that surficial parent material in a watershed originates as a relatively homogeneous, well-mixed geologic deposit; thus, weathering processes should progressively deplete weatherable minerals from the surface downward under the influence of gravitational water flow. Accordingly, they sampled mineral phases at depth increments from the surface and observed the depletion curves for Ca, K, Mg, and Na depicted in Fig. 7.10. When they integrated the depletion curves, they were able to estimate the total loss of base cations from the upper soil profile since the initiation of soil formation at the end of the last glacial retreat 14,000 yr before the present. Dividing base cation losses by the time

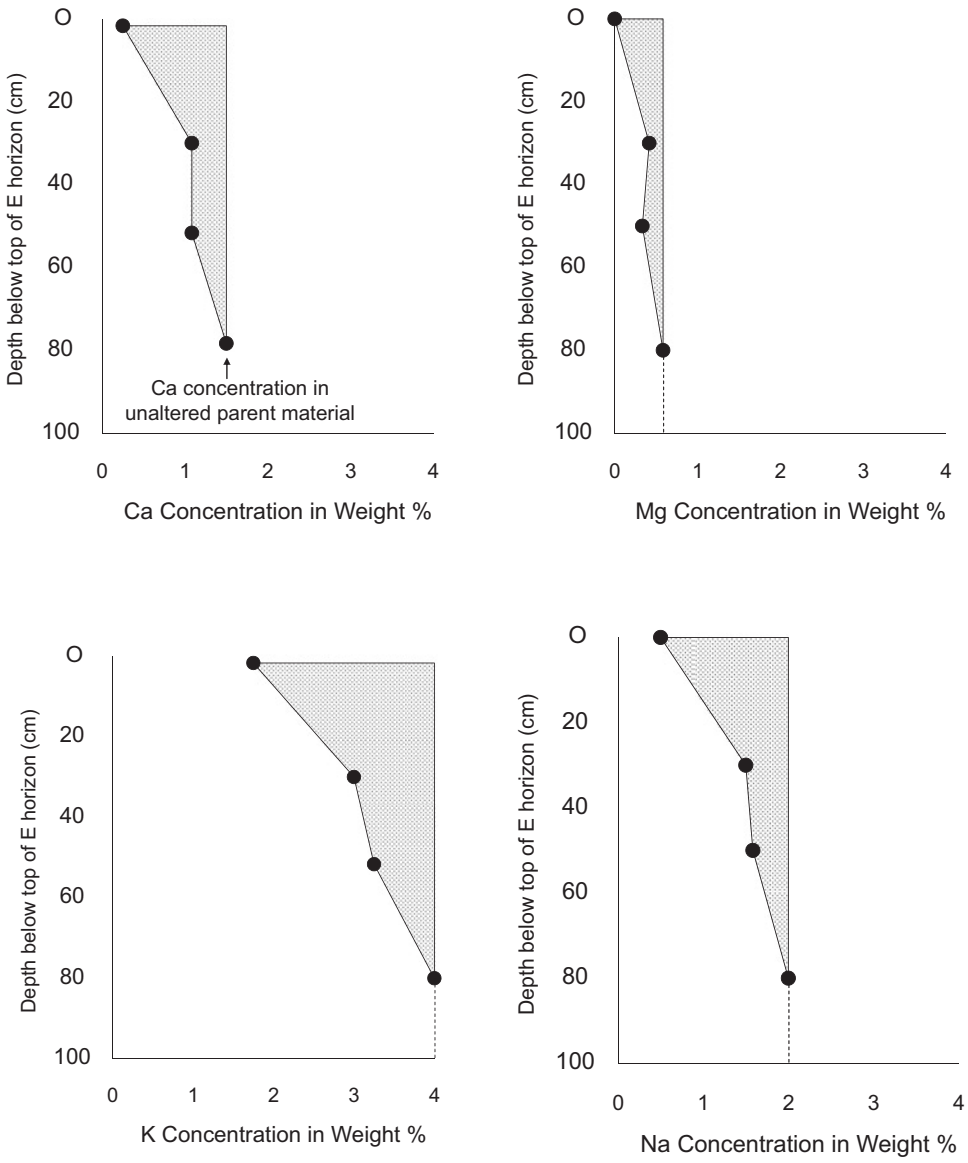

Fig. 7.10 Mineral depletion curves for a cool temperate Spodosol in the Adirondack Mountains, NY. Connected dots show the weight percent of each cation by depth in the soil. Hatched areas show the amounts of each cation lost to weathering over the centuries. Reproduced with permission of Springer from April, R. and R.M. Newton. Influence of geology on lake acidification in the ILWAS watersheds. Water, Air, and Soil Pollution 26:373–386. ©1985 by D. Reidel Publishing Company

interval, they developed an approximation of the long-term weathering rate since deglaciation amounting to 500–620 $mol_c\ ha^{-1}\ yr^{-1}$. Land et al. (1999) applied a similar mineral depletion technique to estimate historical weathering rates in northern Sweden, and reported that over the last 8700 years, mineral weathering has released 360 $mol_c\ ha^{-1}\ yr^{-1}$ of the cations Ca + Mg + K + Na.

Comparison of Weathering Estimates

How do different weathering estimation procedures compare when applied collectively to a single study system? In an intensive study of three contrasting forest soils, the author examined the extent of convergence of multiple independent techniques for estimating weathering rates. The experiments involved exposure of undisturbed plant-free soil columns to simulated rainfall, analysis of cation leaching losses, and measurement of changes in the soil exchangeable cation reservoirs. As illustrated with a Becket Spodosol from the Adirondack Park, NY in Table 7.4, the mass balance estimate of weathering in the 50 cm soil column was 1510 $mol_c\ ha^{-1}\ yr^{-1}$. However, an alternative minimum mass balance estimate of 80 $mol_c\ ha^{-1}\ yr^{-1}$ was also calculated by assuming that a large fraction of the base cation loss from the soil column could be accounted for by statistically undetectable depletion of the soil cation exchange complex (i.e., without much of a contribution from fresh mineral dissolution). This approximation was computed by knowing the 95% confidence interval error bars on the estimates of exchangeable cation concentrations. Using both the Na^+ flux tracer approach and the silica flux ratio procedure described earlier, additional independent estimates of 1030 and 250 $mol_c\ ha^{-1}\ yr^{-1}$ were obtained. A fifth estimate of long-term weathering (620 $mol_c\ ha^{-1}\ yr^{-1}$) was provided by April and Newton's (1985) calculation of mineral depletion for that specific soil. Finally, a watershed mass balance budget for the site where the Becket soil columns originated indicated that ecosystem weathering rates for base cations amounted to 1480 $mol_c\ ha^{-1}\ yr^{-1}$.

In spite of considerable variation in the results, there were indications of convergence among some procedures. Based on the silica flux ratio and mineral depletion estimates, it appears that the minimum long-term weathering rate for the soil and watershed is in the range of 200–600 $mol_c\ ha^{-1}\ yr^{-1}$. On the other hand, results from the soil mass balance, sodium flux ratio, and watershed mass balance calculations suggest that the soil profile is currently weathering at a rate between 1000 and 1500 $mol_c\ ha^{-1}\ yr^{-1}$. Overall, it is apparent that quantifying rates of mineral weathering in watershed ecosystems is very challenging!

Table 7.4 Comparison of weathering estimates for a forest Becket Spodosol based on several independent estimation techniques (Cronan 1985b). Weathering is taken to be the sum of Ca + Mg + K + Na released from primary minerals, expressed in $mol_c\ ha^{-1}\ yr^{-1}$

Soil column mass balance	1510
Soil column mass balance (minimum)[a]	80
Sodium ion flux ratio[b]	1030
Silica flux ratio[c]	250
Soil mineral depletion[d]	620
Watershed mass balance[e]	1480

[a]Half of the 95% confidence interval on the exchangeable cation pool size estimate was subtracted from the soil column mass balance estimate of 1510 $mol_c\ ha^{-1}\ yr^{-1}$ (first entry in column) to account for the possibility of undetectable changes in exchangeable cation reserves during the experiment

[b]Because sodium is considered to be relatively conservative, the solution Na flux and bulk XRF soil chemistry were used to calculate the release of Ca + Mg + K necessary to account for the observed Na flux

[c]This technique assumes that solution silica flux is directly related to the rate of release of Si + Ca + Mg + K + Na from primary minerals

[d]This estimate from April and Newton (1985) is based on a long-term weathering rate determined from mineral depletion in the Becket soil profile

[e]This estimate is based on data from the ILWAS watersheds where the Becket soil was obtained. The flux estimate combines annual stream export of cations from Woods Lake watershed with an estimate of annual biomass increment of cations. Soil exchangeable cation pools were assumed to be steady-state

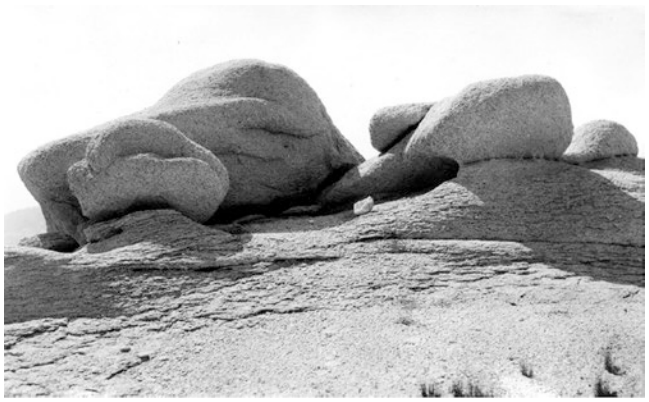

Yosemite granite, F.E. Matthes, US Geological Survey, 1913

Comparison of Weathering in Different Ecosystems

Many of the older studies of weathering were conducted by geologists who reported results expressed as a surface **denudation rate** or rate of removal of the surface of rock minerals. Velbel (1985) indicated that the average denudation rate for the southern Appalachian Mts. was 4 cm per 1000 yr. In comparison, Paces (1986) found that forested watersheds in Czechoslovakia exhibited denudation rates in the range of 0.9–1.4 cm per 1000 yr and agricultural basins were as high as 3.2 cm per 1000 yr. In Rhodesia, Owens and Watson (1979) estimated denudation rates of 0.5–1.5 cm per 1000 yr.

Table 7.5 Comparison of weathering export fluxes ($mol_c\ ha^{-1}\ yr^{-1}$) for different study watersheds

Author	Location	Weathering rate
Reynolds and Johnson (1972)	Alpine glacier, WA	9300[b]
Likens et al. (1977)	Temperate hardwoods, NH	2000
Rosen (1982)	Temperate conifer, Sweden	640
April and Newton (1985)	Temperate hardwoods, NY	500–620[a]
Cronan (1985b)	Temperate hardwoods, NY	1480
Katz et al. (1985)	Temperate hardwoods, MD	2200
Paces (1986)	Temperate forest, Czech Rep.	6400
Baron et al. (1990)	Loch Vale watershed, CO	390[b]
Miller et al. (1993)	Boreal conifer, NY	1500
Land et al. (1999)	Northern forest, Sweden	360[a]
Horton et al. (1999)	Yellowstone River, WY	2100[b]

[a]Long-term weathering rate over thousands of years
[b]Weathering rate is based on cation denudation in runoff, without a consideration of storage in biomass or soils. The estimate from Horton et al. (1999) represents granitic weathering in the Yellowstone River watershed, corrected to exclude the enormous Ca flux derived from calcite dissolution in the watershed. The same authors estimated that cation exports from carbonate-rich sedimentary rocks amounted to an astounding 65,900 $mol_c\ ha^{-1}\ yr^{-1}$

Other investigators have focused on the release of base cation equivalents in weathering (Table 7.5). Reynolds and Johnson (1972) estimated that weathering in the South Cascade Glacier watershed, WA was as high as 9300 $mol_c\ ha^{-1}\ yr^{-1}$. In comparison, Likens et al. (1977) reported a watershed mass balance weathering rate of 2000 $mol_c\ ha^{-1}\ yr^{-1}$ at Hubbard Brook Experimental Forest, NH; Miller et al. (1993) estimated a weathering rate of 1500 $mol_c\ ha^{-1}\ yr^{-1}$ for a high-elevation conifer forest at Whiteface Mt., NY; Rosen (1982) reported a weathering rate of 640 $mol_c\ ha^{-1}\ yr^{-1}$ in a conifer watershed in central Sweden; Paces (1986) estimated that weathering of a highly acidified forested basin in the Czech Republic amounted to 6400 $mol_c\ ha^{-1}\ yr^{-1}$; and Cronan (1985b) presented a watershed mass balance estimate of weathering for a mixed northern hardwood watershed in the Adirondack Park, NY of 1480 $mol_c\ ha^{-1}\ yr^{-1}$. Let's look at the details of some of these examples of weathering analyses.

Reynolds and Johnson (1972) investigated mineral weathering in a temperate glacier environment at an altitude of 1970 m in the Cascade Mountains, WA. Preliminary analysis indicated that local bedrock was composed of phlogopite-actinolite schists, quartz diorite metamorphosed into greenstone, unaltered diorite, and basaltic dikes. Associated with these bedrocks were distinct clay mineral assemblages composed of vermiculite and smectites that provided clear evidence of ongoing mineral weathering. Using hydrologic discharge data combined with flow-dependent stream runoff chemistry, the authors computed an estimated **chemical denudation rate** of 9300 $mol_c\ ha^{-1}\ yr^{-1}$ based on the summed annual exports of Ca + Mg + Na + K. Because their watershed lacked significant vegetation, they were able to ignore biomass accumulation in their mass balance. Furthermore, by focusing on chemical denudation rate, rather than the more inclusive chemical weathering rate, the authors were able to avoid the difficult and uncertain task of estimating cation storage in secondary minerals and exchangeable cation pools. Overall, the authors documented an enormous cation denudation rate that reflects the combined influences of a high annual water flux (runoff = 409 cm) and rapid mineral dissolution driven by vigorous carbonic acid weathering.

Katz et al. (1985) investigated chemical weathering in the Catoctin Mountains, MD, where mean precipitation is 112 cm and mean annual temperature is 12 °C. The site is underlain by metabasalt bedrock that largely appears to weather to kaolinite. The authors used a watershed mass balance analysis, combined with measurements of stream runoff chemistry, to estimate annual net base cation exports of 2194 $mol_c\ ha^{-1}\ yr^{-1}$. They then used a series of simultaneous equations to match the observed net exports of cations, silica, and bicarbonate ion to predicted weathering stoichiometries of the four major weatherable minerals – albite, calcite, chlorite, and actinolite. They concluded that observed solute exports from the watershed could be accounted for by the annual weathering of 316 moles of albite, 249 moles of calcite, 115 moles of chlorite, and 23 moles of actinolite per hectare. In their final analysis, strong acids from atmospheric deposition contributed 40% and carbonic acid contributed 60% of the H^+ ions for mineral weathering in their system. A more recent study in the Catoctin Mountains by Price et al. (2013b) indicated that 90% of Ca^{2+} export in stream runoff was derived from calcite in bedrock fractures, rather than from the more abundant silicate minerals in the watershed.

In the Loch Vale watershed within the Rocky Mountain National Park, CO, two other studies have provided insights regarding weathering patterns of granitic watersheds that contain calcite inclusions within the bedrock matrix. Baron et al. (1990) reported a relatively low cation denudation rate of 390 $mol_c\ ha^{-1}\ yr^{-1}$ for the granitic basin, and estimated that 40% of the exported cations were derived from calcite weathering. In a subsequent study, Price et al. (2013a) examined 24 years of stream mass balance data, and estimated that calcite dissolution contributed 40–65% of the Ca^{2+} in stream waters, oligoclase contributed 25%, and apatite contributed 10–35%.

A number of investigators have raised concerns that stream exports of cations may provide an inflated estimate of primary mineral weathering under circumstances where soil exchangeable cation pools are being depleted by modern acidification processes and the desorbed cations are leaching into streams.

Two different studies have provided a bit of perspective on this question. Paces (1986) concluded from his studies of a forested basin subjected to intense acidification in the Czech Republic that 84% of the Ca ion in runoff was derived from depletion of exchangeable cation reserves. Thus, environmental conditions were tipping toward a serious imbalance between leaching loss and weathering replenishment of exchangeable cations. In contrast to that study, Miller et al. (1993) used Sr isotope analysis to infer that cation exchange reactions contributed 30% of the Sr exported in streamwater and 80% of annual Sr uptake by the plant community in a high elevation site with an annual weathering rate of 1500 $mol_c\ ha^{-1}\ yr^{-1}$.

In concluding this chapter, we can appreciate that chemical weathering processes are a significant driving force in the biogeochemical cycles of many elements. There is even recent evidence that weathering of certain sedimentary rocks can yield measurable releases of N (Holloway and Dahlgren 2002). Yet, our ability to measure and to predict weathering rates in watershed ecosystems is somewhat limited. Given current uncertainties associated with most quantitative estimates of field mineral weathering rates, there is a continuing need for new creative research approaches aimed at improving our understanding of this core area of biogeochemistry.

Watershed Hydrology

8

Ecosystem and Landscape Perspectives

Picture a summer thunderstorm in a southern hardwood forest and consider how the ecosystem might respond to this sudden precipitation input. How much of this rainfall event will appear as storm water runoff in the stream channel and how quickly will streamflow respond to the thunderstorm? In what ways might this precipitation event influence biogeochemical processes and nutrient cycling in this ecosystem? Do we expect this rain event to produce changes in stream chemistry, perhaps causing episodic acidification of the stream? In this chapter, we will focus on understanding basic principles of watershed hydrology and the influences of hydrologic patterns and processes on element cycling in watershed ecosystems.

Figure 8.1 provides a general conceptual diagram for considering watershed hydrology. As shown, water movement through a watershed can include vertical **infiltration** into the soil or groundwater zones, **evaporation** and **transpiration** of moisture into the atmosphere, lateral transport along shallow or deeper **flow paths** into surface water, and water export as stream runoff. Inputs of precipitation may be partially stored as **canopy interception**, soil moisture, surface water, winter snowpack, or groundwater. Each of these storage reservoirs varies in size and exhibits a different **residence time** for water moving through that ecosystem compartment.

On a map of the landscape, it is evident how individual streams and rivers are parts of branching **drainage networks** composed of small tributaries draining small watersheds (Fig. 8.2), which combine to form larger streams and rivers draining larger drainage basins. Each stream or river can be described in terms of **stream order** (i.e., its position in the hierarchy of tributaries). As illustrated in Fig. 8.3, first-order streams are those that have no tributaries. Second-order streams are those that have as tributaries only first-order channels, and so on as shown in the diagram. Thus, a small mountain stream might typically be considered a first or second-order stream, whereas a large river might be classified as a fifth-order or larger system. For each stream or river, there is an upstream **catchment** or **watershed** that collects precipitation and delivers drainage water to the stream system (Fig. 8.2).

Influence of Geology and Soils on Storage and Movement of Water

Patterns of water movement and storage in the landscape are strongly influenced by climate, soil conditions, topography, **surficial geology**, and bedrock geology, although the importance of each factor can vary significantly among watersheds

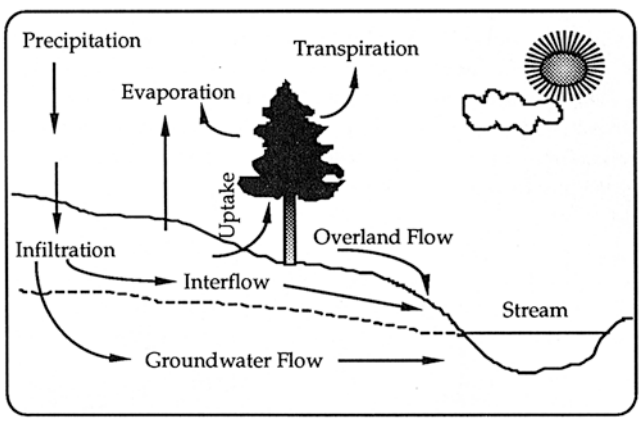

Fig. 8.1 Components of hydrologic transfers in a watershed ecosystem

C.S. Cronan, *Ecosystem Biogeochemistry*, Springer Textbooks in Earth Sciences, Geography and Environment, DOI 10.1007/978-3-319-66444-6_8

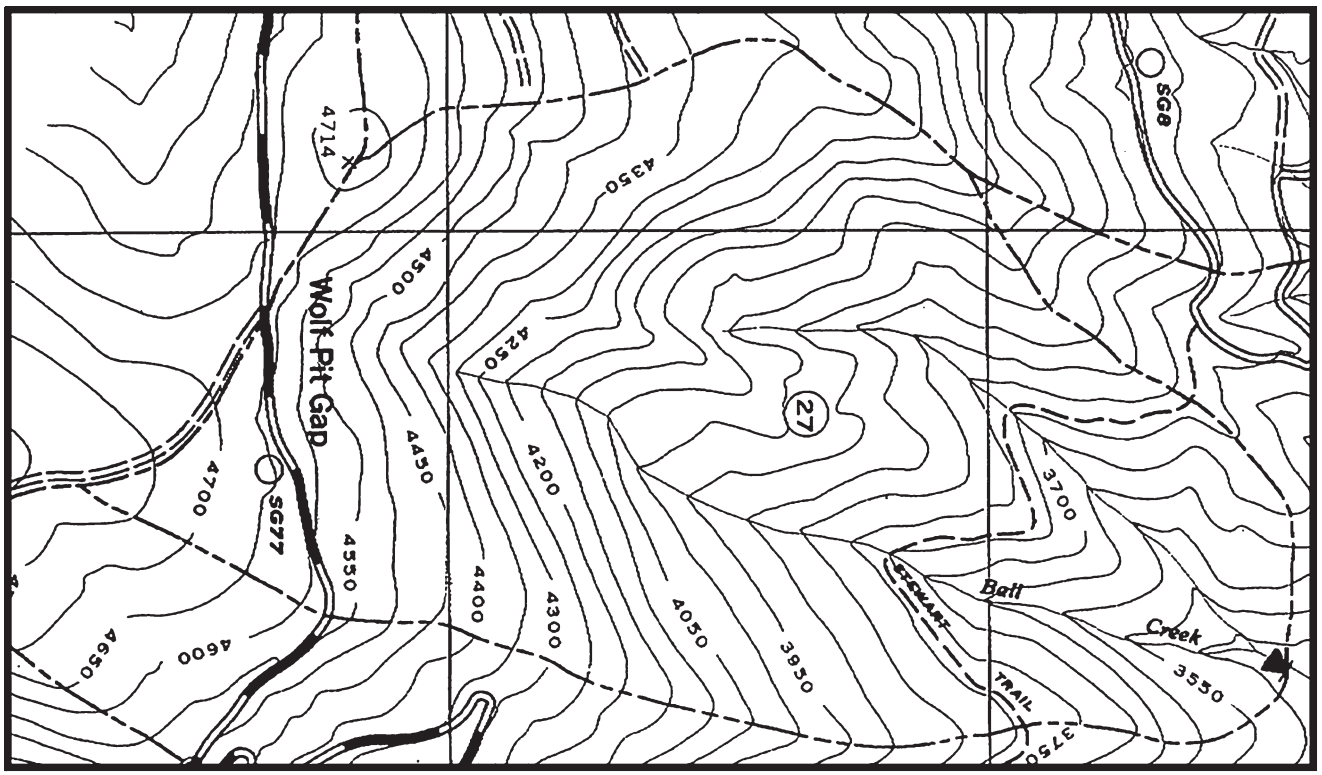

Fig. 8.2 Topographic map showing (i) a watershed delineated by a perimeter drainage divide (*dashed lines*) and (ii) a stream drainage network. The stream system drains from left to right

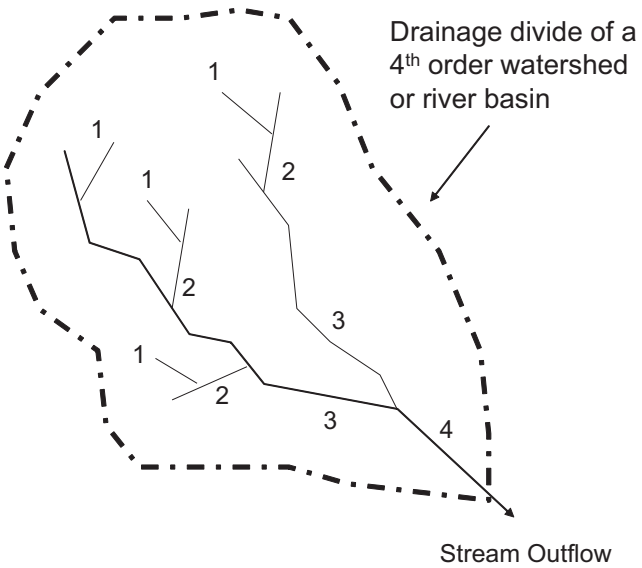

Fig. 8.3 Illustration of 1st through 4th order streams in a drainage network

and regions. Because bedrock throughout much of the biosphere is buried beneath soils, deposits of unconsolidated sediments, or the weathered overburden of **saprolite**, it is these porous geologic materials that often directly influence local hydrology. Besides weathered saprolite, other major types of surficial geologic deposits include volcanic ash, **alluvial** sediments, **colluvial** debris, **aeolian** silt, marine sediments, **lacustrine** silts and clays, and glacial deposits of **till** and outwash sand. The **flow path** of water through each of these different kinds of geologic settings affects the residence time of water, discharge patterns of runoff, solid phases that water contacts and reacts with in its passage through the system, and the chemistry of surface waters and groundwater in the watershed (Fig. 8.4).

Figure 8.5 provides an example of a surficial geologic map and cross-section for a small watershed in the Adirondack Mountains of New York State. In this illustration, surficial geology of the watershed is characterized by four major features: a thick deposit of glacial till >1-3 m in depth; a wetland peat deposit; an area of thin glacial till plus bedrock; and areas dominated by exposed bedrock outcrop. In cross-section, granitic gneiss bedrock is exposed in parts of the upper hillslope, but the lower basin surrounding the lake is covered with one or two layers of glacial till. The surficial glacial deposits in the diagram are composed of rock cobbles and stones distributed through a matrix of quartz and feldspar sand and silt-sized particles. An analysis of the size distribution of particles within the glacial till deposit would show a pattern resembling the one shown in

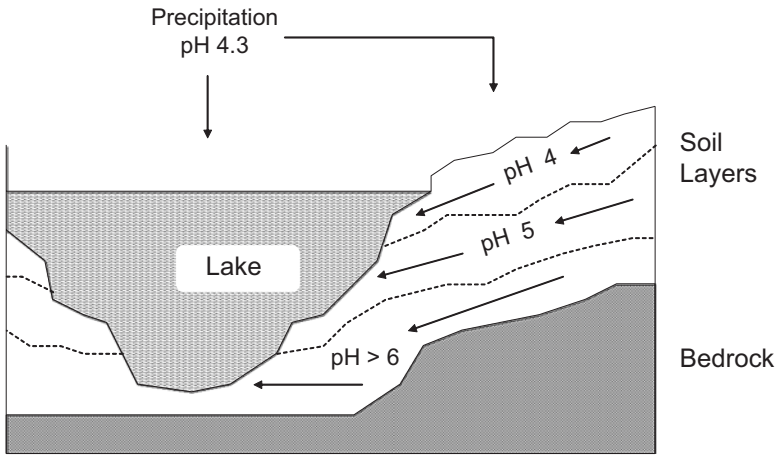

Fig. 8.4 The flow path of infiltrating precipitation can influence the resulting chemistry and acidity of drainage water moving laterally into streams and lakes. In this example, deeper flow paths correspond to drainage water characterized by higher pH values and ANC. Reproduced with permission of Springer from Gherini, S.A., L. Mok, R.J.M. Hudson, G.F. Davis, C.W. Chen, and R.A. Goldstein. The ILWAS Model: formulation and applications. Water, Air, Soil Pollution 26: 425–459. ©1985 by D. Reidel Publishing Company

Fig. 8.5 Conceptual diagram illustrating a map view and geologic cross-section of bedrock and surficial geology in a small watershed located in a glaciated landscape

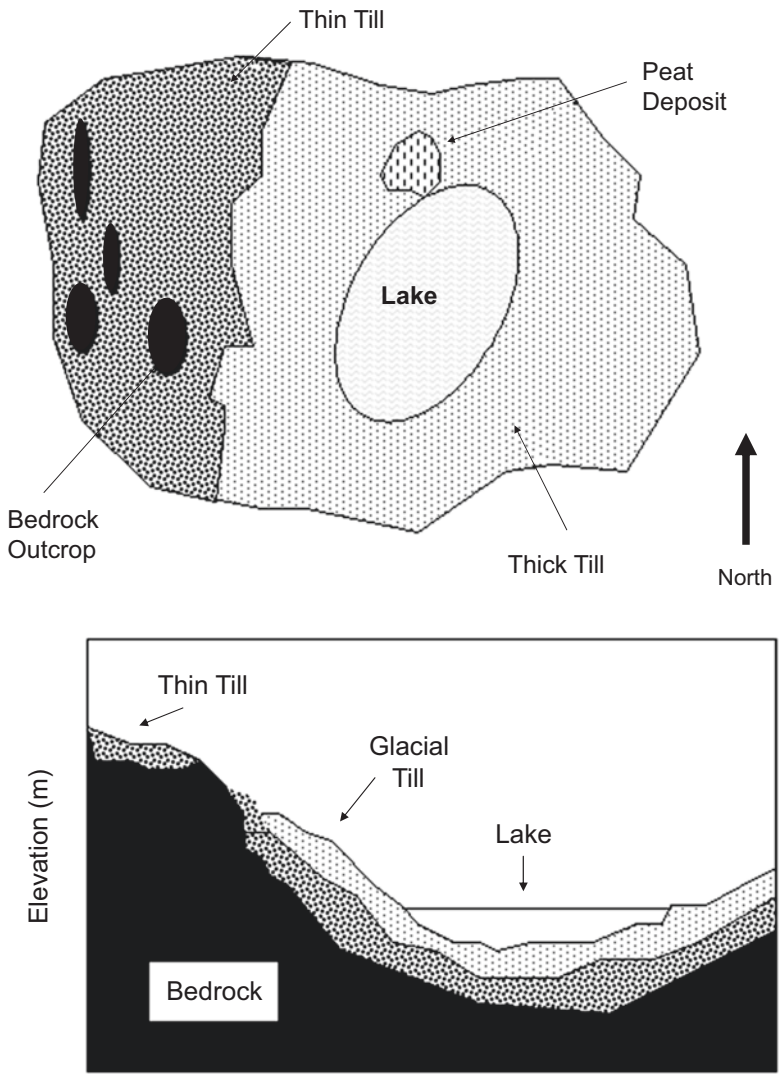

Fig. 8.6. The question a biogeochemist might ask is: "how does this pattern of surficial geology affect hydrologic and biogeochemical processes?" Indeed, whether we focus on a watershed such as the example in Fig. 8.5 or a completely different catchment, it is important to consider how differences in the distribution, thickness, texture, and mineralogy of surficial deposits can influence storage, movement, and the chemistry of water in a watershed.

Soil Hydrologic Properties

The water infiltration and moisture retention characteristics of a soil are largely controlled by the combined influences of soil texture, structure, organic matter content, and the nature and distribution of **micropores** and **macropores** within the soil matrix. These multiple variables determine whether water infiltrates rapidly through the soil profile, pools on the soil surface, or is absorbed and retained by soil colloids. In a soil with good texture, structure, and organic matter content, water drains from larger pores and is retained in the smaller pores, giving a balance of water availability and aeration.

The moisture-holding characteristics of different soils can be compared if we know the amount of water held by the soils at **field capacity** (soil tension of −0.03 MPa) and at the **wilting point** (soil tension of −1.5 MPa), where one mega-Pascal (MPa) = 10 bars = 10.13 atm (Fig. 8.7). The difference between these two measurements is the quantity of **available water** that can be stored in the soil between rain events. As you can recall from Fig. 2.7, there is considerable variation in the water retention characteristics of soils with different textures. Whereas sandy soils tend to have low field capacities and small reserves of available water, loamy soils exhibit higher more optimal field capacities and reservoirs of available water.

The potential water infiltration rate varies widely among soils and separate soil horizons, and can be quantified using estimates of **saturated soil hydraulic conductivity**. In the examples shown in Table 8.1, we see that the sandy Wisconsin and Missouri clay loam soil horizons differ by three orders of magnitude in terms of predicted soil water conductivity. This is a striking contrast! What are the implications of these

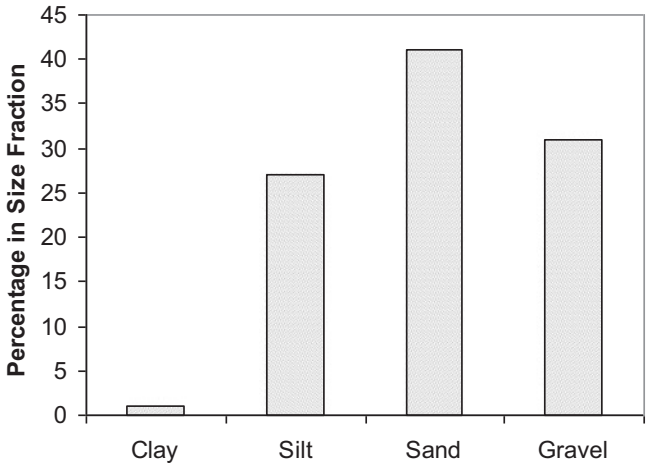

Fig. 8.6 Grain-size distribution for a soil formed on a glacial till in New England (data from Dingman 1994)

Table 8.1 Comparison of hydraulic conductivity for fine-textured and coarse soil horizons (R. Newton unpub. data)

Soil type	Sand	Silt	Clay	Gravel	Conductivity
	(%)	(%)	(%)	(%)	cm s^{-1}
B Horizon, Missouri	3	64	33	0	2×10^{-5}
B_s Horizon, New York	67	23	2	8	1×10^{-3}
B_2 Horizon, Wisconsin	92	4	0	4	1×10^{-2}

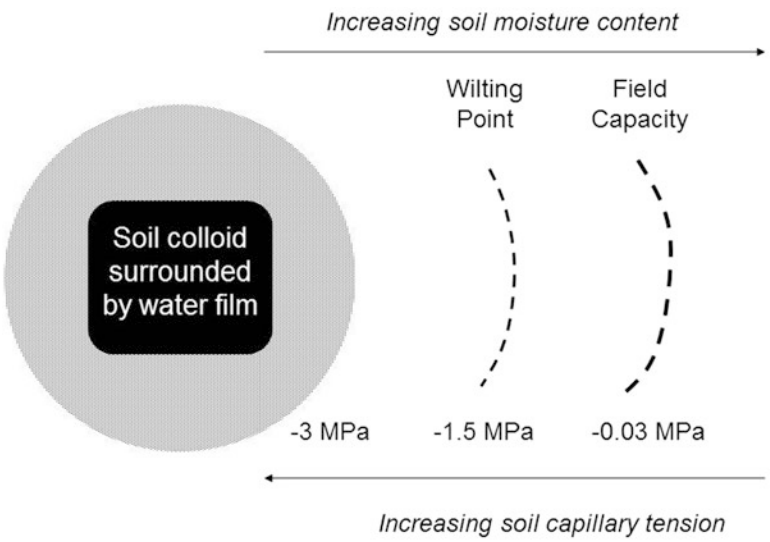

Fig. 8.7 Capillary tension increases as soils dry from a saturated condition (where gravitational water drains freely through macropores), to field capacity at –0.03 MPa, and down to the thin water film corresponding to the wilting point at –1.5 MPa. The gray shaded area represents unavailable hygroscopic water held at tensions greater than –3.1 MPa. Data from Dingman (1994)

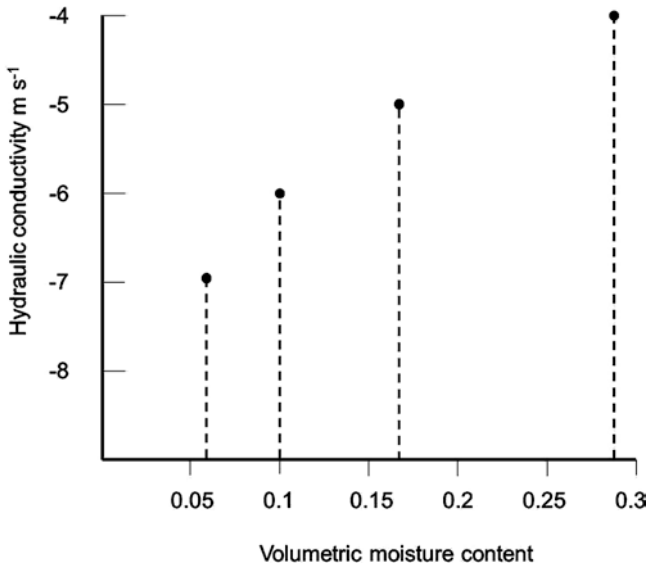

Fig. 8.8 Variation of hydraulic conductivity, K, versus volumetric moisture content for a fine sand. Values on ordinate are expressed as log K (e.g., –8 corresponds to 10^{-8} m s^{-1}) (data from Hornberger et al. 1998).

differences in hydraulic conductivity among soils? What happens when the rate of moisture inputs from rainfall or snowmelt exceeds the infiltration rate of a given soil horizon?

Not only does hydraulic conductivity vary among soils with different textures, but it also changes in a given soil as the volumetric moisture content increases or decreases. In Fig. 8.8, we see that a five-fold change in volumetric moisture content, Θ, of a fine-textured sandy soil is accompanied by a 1000-fold change in hydraulic conductivity, K. Thus, the potential rate of infiltration drops dramatically as a soil dries. During periods between moisture inputs, an **unsaturated zone** develops in the upper soil as drying occurs; in contrast, a **saturated zone** commonly occurs near the depth of the water table.

Water Movement and Streamflow Generation in a Watershed

One of the fundamental challenges in hillslope and watershed hydrology is to understand the flow paths of water movement within catchments (Kampf and Burges 2007), patterns of streamflow generation that result from moisture inputs to a given watershed (Barthold and Woods 2015), and the interplay of biogeochemical and hydrologic processes within a watershed ecosystem. If we sample water chemistry along a drainage gradient from precipitation inputs, through soils and surficial deposits, and into a stream channel, we find that the chemistry of water evolves and changes dramatically in response to various biogeochemical transformation processes during drainage through the catchment. Furthermore, if we sample at different times during the

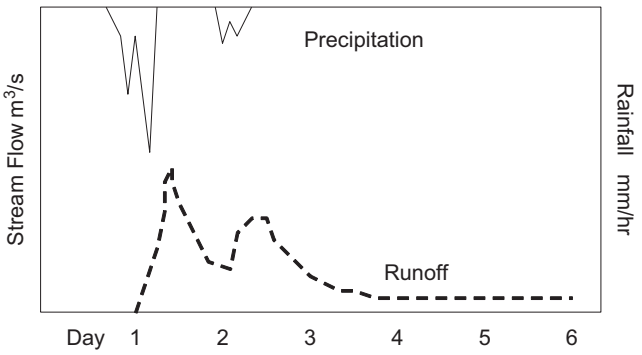

Fig. 8.9 Conceptual diagram showing sequential precipitation inputs (*solid line*) and stream discharge for a small forested watershed in New England

annual hydrologic cycle, we are likely to observe important temporal differences in stream chemistry. These changes and seasonal differences in stream water quality are determined by dynamic interactions between hydrologic flow paths and spatially distributed biogeochemical processes within a drainage basin. Because of this, it is important to understand the hydrologic source compartments and drainage pathways that control runoff patterns and processes in watershed ecosystems (Raymond and Saiers 2010).

Measurements of precipitation inputs and streamflow outputs in a watershed ecosystem are often plotted on rainfall **hyetograph**s and runoff **hydrograph**s as a means of analyzing relationships between the timing and magnitude of water inputs and outputs in a drainage basin (Fig. 8.9). Graphs such as these are intriguing, because they raise so many important questions as to how observed stream output responses are related to the internal physical properties and hydrogeologic parameters in a given watershed. In many watersheds, streamflow response to a storm event is rapid and pronounced, implying that rainfall is routed quickly to streams, rather than slowly infiltrating through the soil matrix and into the stream channel. In other catchments, episodic stormflow responses may be relatively rare, only occurring after the most severe precipitation events. How do these observations fit together? An answer to this apparent enigma requires the integration of hydrologic processes across different time and spatial scales.

As water moves through a watershed ecosystem and emerges as streamflow, some fraction of the moisture follows **preferred pathways** through soil **macropores**, whereas other drainage water infiltrates more slowly through capillary pores in the soil matrix. The relative importance of preferred pathways is determined by local topography, soil characteristics, vegetation, animal burrows, and geologic conditions; movement through these pathways generally occurs only under conditions of **saturated flow** observed during a rain event or at snowmelt. We can also envision preferential water movement occurring when infiltrating water backs up above

a layer of impervious sediments or bedrock, and flows laterally through a more porous overlying soil horizon. In general, we would expect preferred pathways to dominate (1) over short time scales when moisture inputs to the watershed are relatively high and (2) at small spatial scales, particularly where the depth to bedrock is shallow, the slope is steeper, the incidence of root channels and burrows is higher, or near stream channels where saturated moisture conditions are more common. Beckers and Alila (2004) developed a model for streamflow generation in a temperate rain forest located in British Columbia, and concluded that subsurface matrix flow is the largest contributor to streamflow (67% of time), but preferential flow through macropore networks begins to dominate streamflow during peak periods when discharge exceeds 2.8 mm $hr.^{-1}$.

Figure 8.10 provides an illustration of the dynamic influence of preferential flow paths on stream discharge during spring snowmelt in the Adirondack Mountains, NY. In this example, the groundwater table rises rapidly to a plateau during early snowmelt, coincident with a slow gradual increase in stream discharge. During this period, the rising hydraulic gradient produces a gradual increase in water infiltration through the deep soil and a steady increase in **baseflow** contribution to stream runoff. The next day, there is a larger snowmelt event, a hydrologic threshold is apparently reached, and both groundwater level and streamflow rise together in rapid succession. How can we account for this unusual sequence of events? The evidence suggests that on the second day of melting (late March 14th), the cumulative infiltration of meltwater has expanded the groundwater table upward into a more porous zone that permits rapid lateral flow into the stream channel. With the water-table now intersecting more permeable upper soil layers, the soil hydrologic

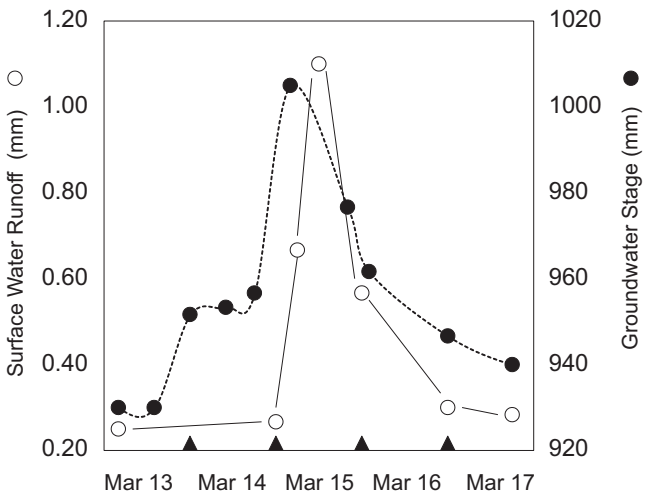

Fig. 8.10 Relationship between groundwater stage (*black circles*) and stream runoff (*open circles*) during a March snowmelt event in the Adirondack Mountains, NY (based on unpublished data from R.M. Newton – used with permission)

connection to the stream opens up as if a macropore faucet has been turned on. The rise in streamflow now reflects combined inputs of groundwater baseflow plus a large preferential flow component derived from near-surface soil horizons.

One of the dominant concepts in stormflow generation is the idea that water contributing to storm runoff in streams largely originates in **variable source areas** that quickly become saturated by rainfall or snowmelt and serve as sources for rapid interflow or saturated overland flow of water to the adjacent stream channel. These easily saturated zones are typically in or near the stream **riparian zone** and represent only a portion of the entire watershed area. According to a conceptual model defined by Dunne and Black (1970), the hydrologic source area contributing to stream runoff will expand or contract, depending on the moisture status of catchment soils, the variable height of the water-table within the system, and the antecedent and current inputs of precipitation and/or meltwater. In the illustration depicted in Fig. 8.11, we see that the saturated variable source area covers 50% of a particular catchment in the left panel, but shrinks to 30% of the catchment in the right-hand panel, 1 week later. Nippgen et al. (2015) applied a spatially distributed hydrologic model to a watershed in the Rocky Mountains of Montana, and reported that the variable source area for that catchment ranged from <1% during the fall and winter base flow period to 71% of the entire watershed during snowmelt.

Attempts to understand hydrology and drainage pathways in small watersheds have used concepts of **new** versus **old** water and **quickflow** versus **baseflow** (Hornberger et al. 1998). Geochemical tracer studies have shown that stream water runoff during precipitation events or snowmelt periods is composed of a mix of "newer" water from current moisture inputs and "older" water that has previously infiltrated the soil and has reacted with the soil matrix. The "new" water is presumed to move as **quickflow** through near-surface macropores or as overland flow from saturated variable source areas. The older water apparently moves as a mixture of quickflow from variable source areas and as **interflow** or groundwater baseflow. The hydraulic pressure of new moisture inputs is thought to generate movement of subsoil older water via **piston-flow displacement** (Fig. 8.12). Beven and Kirkby (1979) incorporated this type of dichotomous view into their watershed hydrologic simulation model, TOPMODEL, and assumed that streamflow is the sum of subsurface flow plus overland or near-surface quickflow from saturated variable source areas. In a study of hydrologic flow paths and sources in a montane watershed in Scotland, Soulsby et al. (2015) used isotopic records to infer that "old" water was a prominent component of stream water in their catchment. The average age of stream water was 1.8 years, but ages ranged from

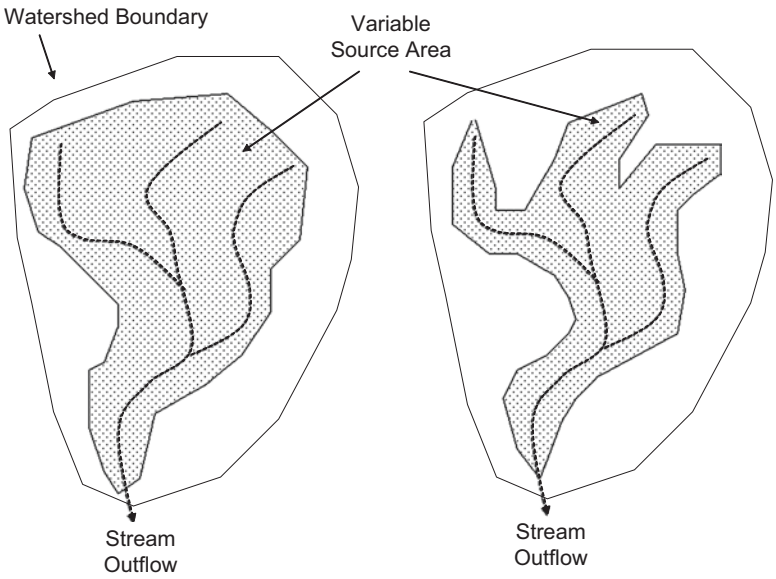

Fig. 8.11 Illustration of variable source areas during (*left panel*) and after (*right panel*) a storm or melt event. Shaded zones are the portion of total watershed area that is saturated as a result of sub-surface impediments to drainage. Substantial stream flow (*dashed lines*) originates in these source areas

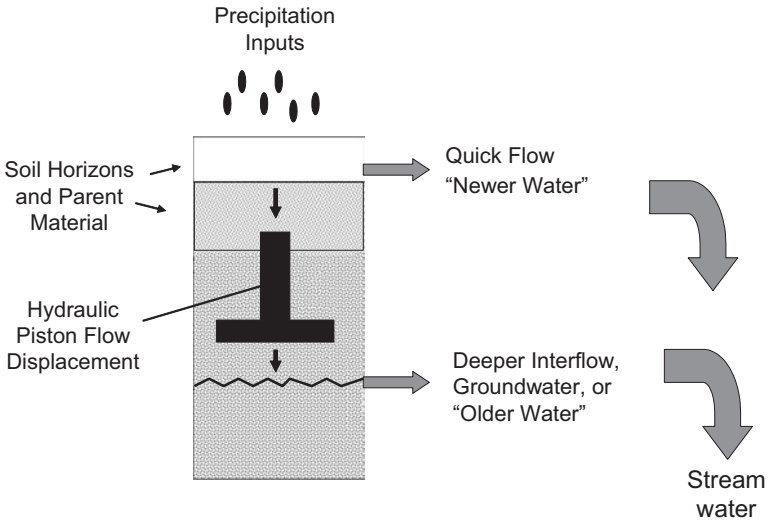

Fig. 8.12 Conceptual illustration of the potential contributions to stream runoff from "newer" quickflow stormwater and "older" ground-water derived from vertical piston-flow displacement

1 month (during storm events) to 4 years (in dry periods when flow is sustained by groundwater).

What happens in a forested catchment between precipitation events? In between episodic rainfall and snowmelt periods, hydrologic conditions are characterized by drainage of soil moisture, water removals via evaporation and transpiration, adjustments in moisture storage reservoirs, occasional low intensity precipitation events, and baseflow runoff in the stream channel. During these intervals, **unsaturated flow** conditions will tend to predominate in upper soil horizons as water moves via diffusion or infiltrates as matrix flow through soil micropores. Over long time scales, these unsaturated soil moisture conditions will tend to even out some of the small-scale spatial heterogeneity of biogeochemical conditions generated by episodic stormflow and macropore drainage at a given moment and location in a watershed.

Inferring Stream Hydrology from Stream Chemistry in Small Watersheds

A number of investigators have used chemical tracers or episodic changes in stream chemistry to make inferences about the hydrology of small watersheds. For instance, Elwood and Turner (1989) reported that concentrations of calcium in stream water at Walker Branch Watershed, TN decline abruptly during large precipitation events (Fig. 8.13). They concluded that as stream discharge increases during a storm, the contribution of groundwater baseflow (which has a long contact time with calcium-rich bedrock) decreases as a proportion of streamflow and is diluted by precipitation reaching the channel via quickflow pathways. Because drainage water in the upper soil profile is characterized by minimal calcium enrichment, transport of that water into the

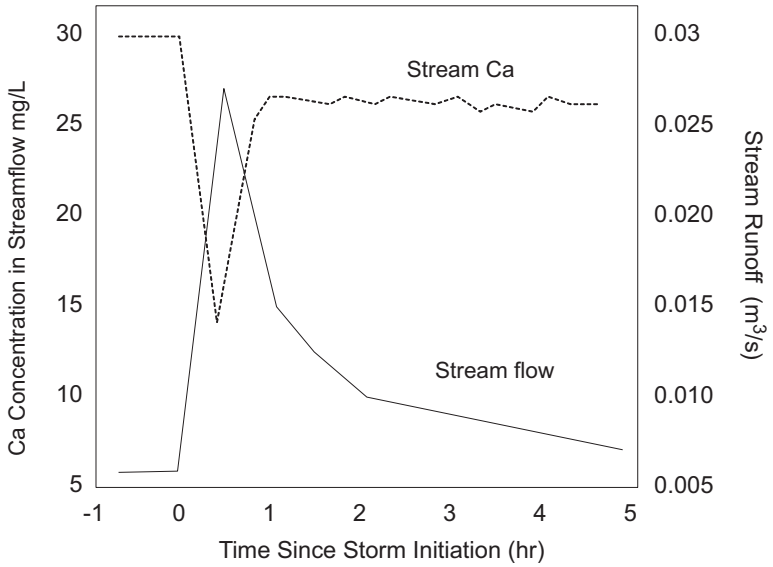

Fig. 8.13 Illustration of a storm event at Walker Branch Watershed, TN showing an abrupt decrease in stream water calcium ion concentration coincident with peak stream discharge. From Henderson, G.S., A. Hunley, and W. Selvidge. 1977. Nutrient discharge from Walker Branch Watershed. pp. 307–320 in D.L. Correll (ed) Watershed Research in Eastern North America: A Workshop to Compare Results. Chesapeake Bay Center for Environmental Studies, Edgewater, MD

stream channel produces a sharp decline in stream water Ca concentration. As the storm flow recedes, the proportion of groundwater increases, raising the stream Ca concentration.

Several studies have used chemical approaches to infer how much of stream runoff at a given time is derived from baseflow versus other flow paths (Neill et al. 2011). In theory, if one knows the chemistry of streamwater, precipitation, canopy throughfall, soil water at various soil depths, and groundwater, it should be possible to account for stream chemistry as a mixture of different proportions of water derived from one or more different source compartments within the watershed. Hooper et al. (1990) applied this conceptual approach to watersheds in Georgia and Norway, using end-member mixing analysis (EMMA) to predict stream chemistry and to infer the dominant flow paths of water contributing to runoff. For their analysis, it was assumed that streamwater over the course of an annual hydrograph represents a changing mixture of shallow soil water, deeper soil water, and groundwater. In drier periods, stream chemistry contained higher ANC and Ca concentrations (reflecting a larger contribution from groundwater), whereas episodic storm events coincided with rising concentrations of acidity, soluble Al, and dissolved organic matter (indicative of solution chemistry in upper soil layers). The investigators were able to use their model in combination with field measurements of solution chemistry to predict changes over time in the apparent relative contributions of interflow and baseflow to observed stream runoff.

Mulder et al. (1990) used Cl^- ion and soluble Al as geochemical tracers to infer the contributions of shallow and deeper soil water to stream runoff during a large precipitation event at Birkenes watershed in southern Norway. The authors sampled during a storm event containing a high concentration of marine salt and found that much of the chloride signal observed in the stream came from shallow interflow originating in the saturated O horizon of the upper soil profile. Deeper soil layers exhibited much lower chloride concentrations during the storm and therefore could not have been the major source of water for stream runoff during peak flow. The authors also found that runoff chemistry during peak discharge was depleted in ionic Al and enriched in H^+ ion, a pattern similar to that found in the O horizon, but unlike the chemistry of water sampled in the deeper soil layers. Thus, the investigators concluded that hydrologic flow paths are more heavily dominated by near-surface interflow during peak runoff events, but that stream discharge is sustained between large rainfall and snowmelt events by baseflow from deeper soil layers and ground-water.

Cronan et al. (1999) examined relationships between seasonal hydrology and stream chemistry in 20 small watersheds in the Aroostook River Basin in northern Maine. Results indicated that during low flow, stream chemistry reflected the dominant influence of groundwater inputs characterized by high Ca concentrations and low concentrations of dissolved organic matter. In contrast, stream chemistry during peak runoff periods exhibited much lower concentrations of Ca and much higher concentrations of soluble C (Fig. 8.14). This change in stream chemistry presumably resulted from shifting flow paths of water movement into streams during high flow. When runoff was high, there was an increased contribution of shallow interflow from surface soil horizons enriched in soluble C and depleted in Ca in comparison to groundwater.

Water Balance of a Watershed Ecosystem

One simple, but powerful approach for understanding the hydrologic cycle is to think in terms of the **water balance** or **water budget** of a given natural system. This approach can

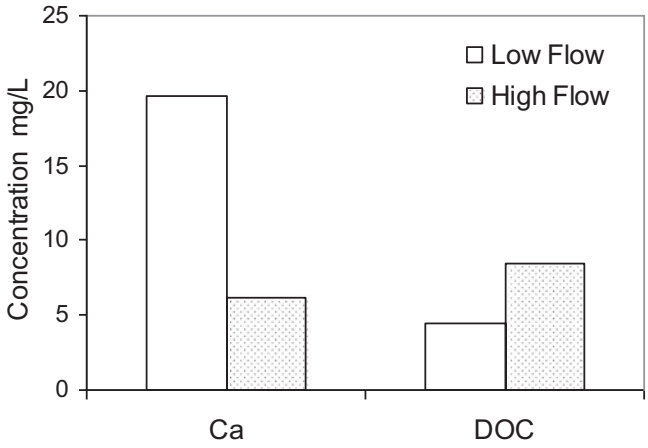

Fig. 8.14 Comparison of stream chemistry during low and high flow periods in the Aroostook River basin, Maine. DOC = dissolved organic carbon (Cronan et al. 1999)

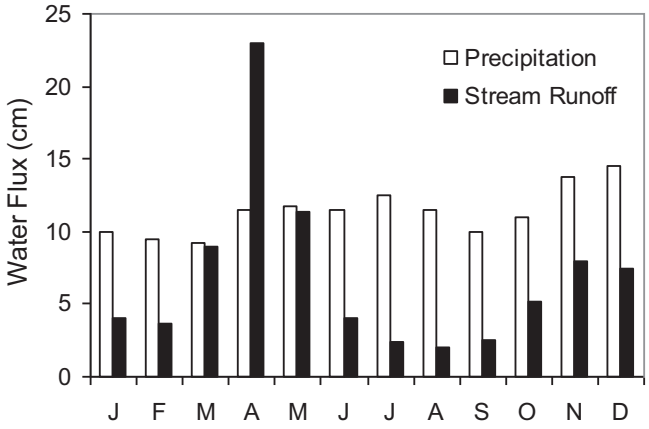

Fig. 8.15 Average monthly precipitation inputs and streamflow outputs for a small watershed in the northeastern United States

be readily applied to an individual leaf, a single organism, or to an entire ecosystem, at either shorter or longer time scales. The general mass balance equation for a hydrologic budget can be written as follows:

Water Inputs = Water Outputs ± Storage Changes

In other words, you can account for the fate of water inputs to an organism or an ecosystem by summing the loss of water plus or minus the change in storage of water. If outputs exceed inputs, then the organism or system experiences a negative water balance that depletes stored reserves, and may lead to water stress. For a watershed ecosystem, the water budget is written as follows:

Precipitation = Runoff + Evapotranspiration + Δ Storage

Here, water inputs (P) as precipitation, fog, or cloudwater are balanced by water losses as stream runoff (R) and **evapotranspiration** (abbreviated ET) plus increases or decreases in storage of water (S) in soil moisture, biota, groundwater, or snowpack. In a lake-watershed ecosystem, changes in lake storage would also be taken into account. It should be noted that generating a reliable water budget requires a reasonable assurance that there is little or no groundwater loss from the watershed via deep bedrock fractures.

By re-arranging the hydrologic mass balance equation, it is possible to estimate unknowns in the water balance. For example, if annual precipitation and runoff are measured and annual change in storage is assumed to be negligible, one can estimate annual ET (which is difficult to measure) by difference as the following expression: **ET = P – R**.

Seasonal adjustments in water budgets are easily understood in the framework of a water balance equation. During periods of low precipitation, runoff and ET are sustained to some extent by removal of stored water. However, below a given threshold of water depletion, runoff and ET decline or cease until the system is **recharged** by precipitation. During winter in the cool temperate zone, much of the precipitation input accumulates as snowpack, ET decreases or ceases completely, and runoff is sustained by release of stored groundwater and occasional wet deposition or melting events.

In Fig. 8.15, an illustration is presented showing the dynamic hydrologic variations that occur in a northern forested watershed. In August, for example, streamflow outputs are much less than precipitation inputs, because most of the monthly rainfall is removed from the system by summer evapotranspiration. In contrast, stream runoff greatly exceeds precipitation during April, because rainfall inputs combine with a large pulse of runoff from spring snowmelt to generate peak discharge conditions for the year.

Measurement Techniques for Ecosystem Water Budgets

Before proceeding with our analysis of water budgets, we should briefly review some of the basic methods that are used to estimate inputs, outputs, and storage of water in studies of watershed ecosystems. Collections of wet deposition volumes are generally made using a standard U.S. Weather Bureau rain gage equipped with wind shield protectors and positioned at a height of 2 m in a suitable open area away from the influence of surrounding vegetation and structures (Likens and Bormann 1995). Forest throughfall volumes are typically sampled beneath the forest canopy with 20 cm diameter plastic funnels located at a height of ~1.5 m above the forest floor (Olson et al. 1981). Snowpack storage in temperate, alpine, and boreal climates is often sampled with snow core surveys involving successive collections of snowpack along marked survey lines; at each sample point, a plastic tube is used to collect a complete vertical snow core that

is later melted to determine water content. Soil moisture can be sampled gravimetrically or can be monitored with a non-destructive technique known as Time Domain Reflectometry (TDR) that has been described by Topp and Davis (1985) and others. Changes in groundwater storage can be monitored with wells consisting of a plastic or metal pipe inserted into a drilled hole in the ground, screened at the lower end to permit water entry, and capped at the surface to minimized contamination and evaporation.

Analysis of runoff patterns requires a means of quantifying and visualizing streamflow or river discharge over time. In most watershed studies, stream discharge is routinely monitored at a gauging station similar to the example in Fig. 8.16. A stage height graph generated by a continuous recorder is converted using a rating curve into a discharge hydrograph similar to the illustration in Fig. 8.17. This information can then be used to understand stream hydrologic patterns (Hornberger et al. 1998).

Although ecosystem evapotranspiration rates are often calculated by difference in a water budget, rates of evaporation and transpiration can be estimated independently using other techniques (Shimizu et al. 2015). Potential evaporation can be estimated with empirical pan evaporation methods or with models based on physical measurements and meteorological relationships (Montieth 1965; Dingman 1994; Ershadi et al. 2015). Transpiration can be estimated with measurements of sap flux density using a Granier-type flow meter composed of heated and unheated thermocouple pairs and applying a heat balance equation to the flow of xylem water (Cermak et al. 1984; Oren et al. 1998).

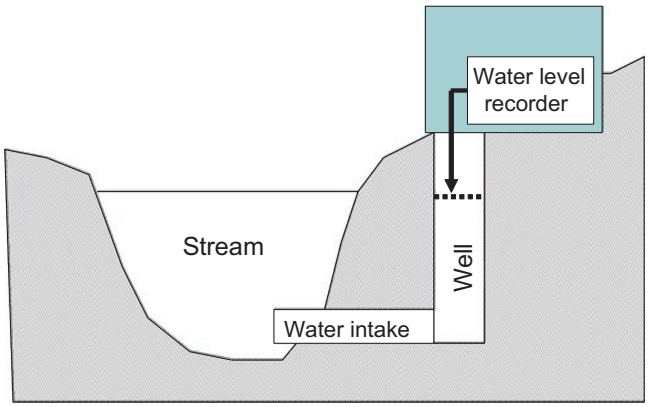

Fig. 8.16 Schematic diagram of a stream gauging station used to record streamflow depth or stage height as a function of time

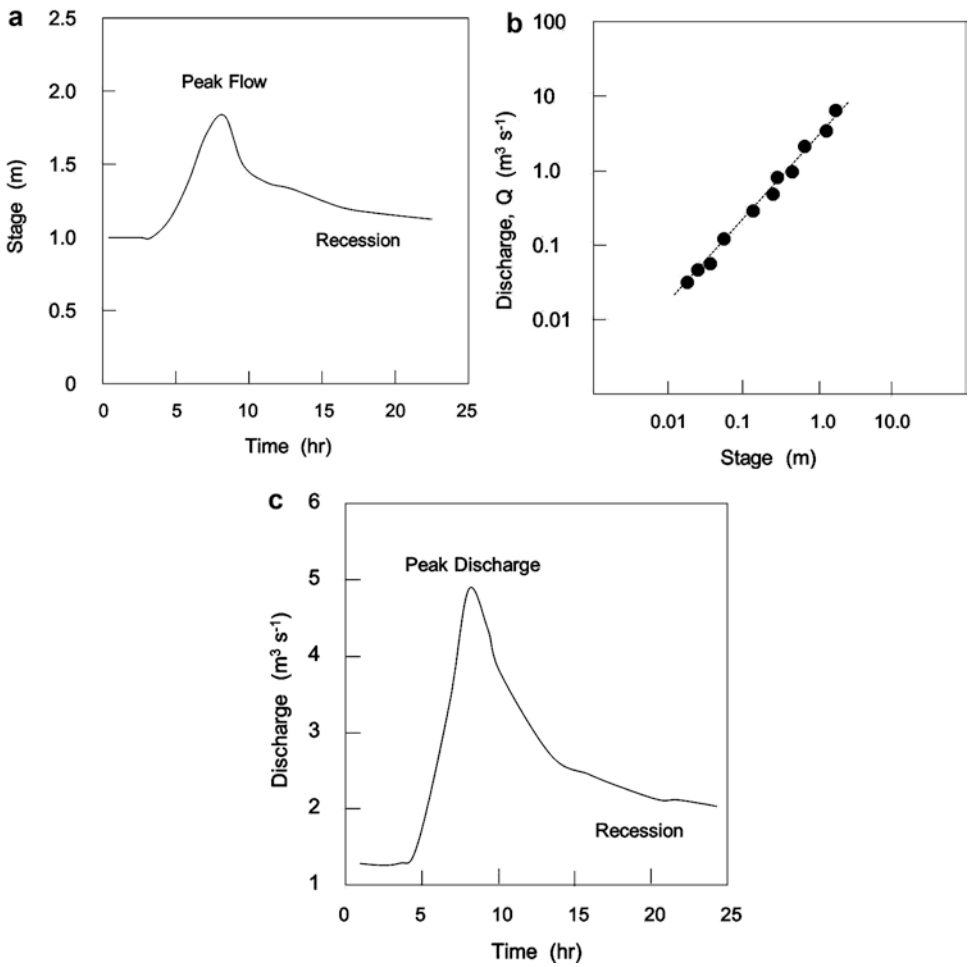

Fig. 8.17 Examples of (**a**) a stage hydrograph for a stream or river; (**b**) a rating curve relating stage height to stream discharge (Q) for that catchment; and (**c**) a discharge hydrograph for a stream during a single precipitation event

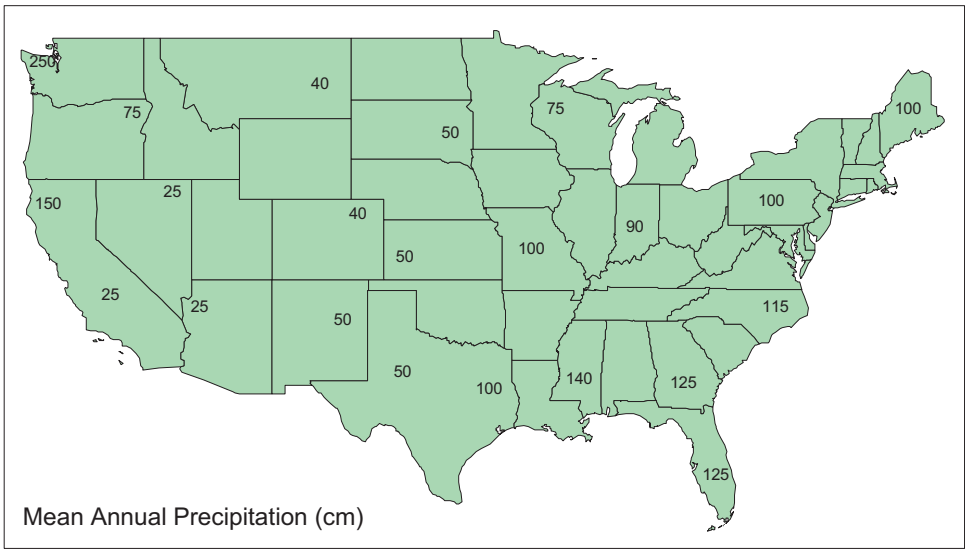

Fig. 8.18 Regional examples of mean annual precipitation in the continental U.S

Components of a Water Budget: Precipitation Inputs

One of the important sources of variation in water budgets among watersheds is the spatial and temporal variability of precipitation inputs. Looking at the map of precipitation patterns across the U.S. shown in Fig. 8.18, it is apparent that continents exhibit pronounced gradients of annual precipitation. For example, moving from the eastern seaboard to the central plains in the U.S., precipitation decreases by ~50% from 100 cm yr^{-1} (40 in yr^{-1}) to less than 50 cm yr^{-1} (20 in yr^{-1}). Another major gradient can be found along the Pacific coast, where rainfall ranges from 250 cm yr^{-1} (100 in yr^{-1}) in the Olympic Peninsula, WA to 20–40 cm yr^{-1} (~15 in yr^{-1}) in southern California.

In many geographic regions, there are ecologically important elevational gradients in precipitation. At the high elevations of mountains, water vapor cools, condenses, and produces **orographic precipitation** above and beyond the regional precipitation norm. Moreover, the increased precipitation resulting from orographic influence is often supplemented with moisture from cloud water deposited on the stems and foliage of high elevation plants. Combined inputs of orographic precipitation and cloud water deposition can yield total precipitation at upper elevations that is two times the regional average at lower elevations.

In the Green Mountains, VT, Siccama (1974) reported that precipitation increases with elevation at a rate of 2.9 cm/100 m, and maximum snow depth increases from about 60 cm at 550 m elevation to 115 cm at an elevation of 1160 m. In the White Mountains of New Hampshire, mean annual precipitation increases from about 130 cm yr^{-1} at 250 m elevation (Likens and Bormann 1995) to roughly 180 cm yr^{-1} at 1200 m (Dingman 1981). Furthermore, Lovett et al. (1982) estimated that gross cloud water deposition adds an additional 80 cm yr^{-1} of moisture to subalpine forests at 1200 m in the White Mountains of central New Hampshire. Thus, atmospheric inputs of water to high elevation ecosystems can be greatly enhanced by orographic and cloud deposition processes.

Ollinger et al. (1993) used a regression model to predict mean annual precipitation as a function of latitude, longitude, and elevation in the northeastern U.S. For locations below 400 m, the regression model contains the following form: Precipitation = 670.20 – (7.02 * latitude) – (3.62 * longitude) + (0.013 * elevation). Above 400 m, the regression is as follows: Precipitation = 643.43 – (7.02 * latitude) – (3.62 * longitude) + (0.090 * elevation). These elevation coefficients represent a precipitation increase of 13 cm/1000 m below 400 m elevation and a precipitation increase of 90 cm/1000 m at elevations above 400 m.

As shown in Fig. 8.19, there are also important temporal variations in precipitation regimes across the continental U.S. In the Mediterranean climate around San Diego, CA, most of the limited rainfall occurs in winter. By contrast, there is an ample, even distribution of rainfall in New England, and a summer wet season in Florida. Temporal variations in precipitation may also include seasonal shifts in the mix of rain and snow (Fig. 8.20).

Components of a Water Budget: Evapotranspiration (ET)

Evapotranspirational losses of water from a watershed ecosystem vary as a function of season, climate, topography, soils, and vegetative cover. At a fundamental level, both

evaporation and transpiration are strongly influenced by the temperature and vapor pressure relationships illustrated in Fig. 8.21. As shown by the solid line in the diagram, air has a finite, temperature-dependent capacity for water vapor. Below the dewpoint or saturation level, dry or unsaturated air draws water from its surroundings through the processes of evaporation and plant transpiration. The rate of evapotranspiration increases as a function of the **water vapor pressure deficit** (where **vpd** = the difference between the present air concentration of water vapor and the maximum concentration of water vapor expected at the dewpoint for that air temperature). If temperature increases, air can hold more water vapor (Fig. 8.21). Conversely, cooling a parcel of air will reduce its capacity for holding water vapor, will lower the vapor pressure deficit, and will lower the potential for ET.

As indicated in the earlier chapter on plant processes, the driving force for plant uptake and transpiration of water is a gradient termed the **water potential**. A water potential gradient develops in response to the plant water deficit created by water loss to the dry atmosphere. When there is a

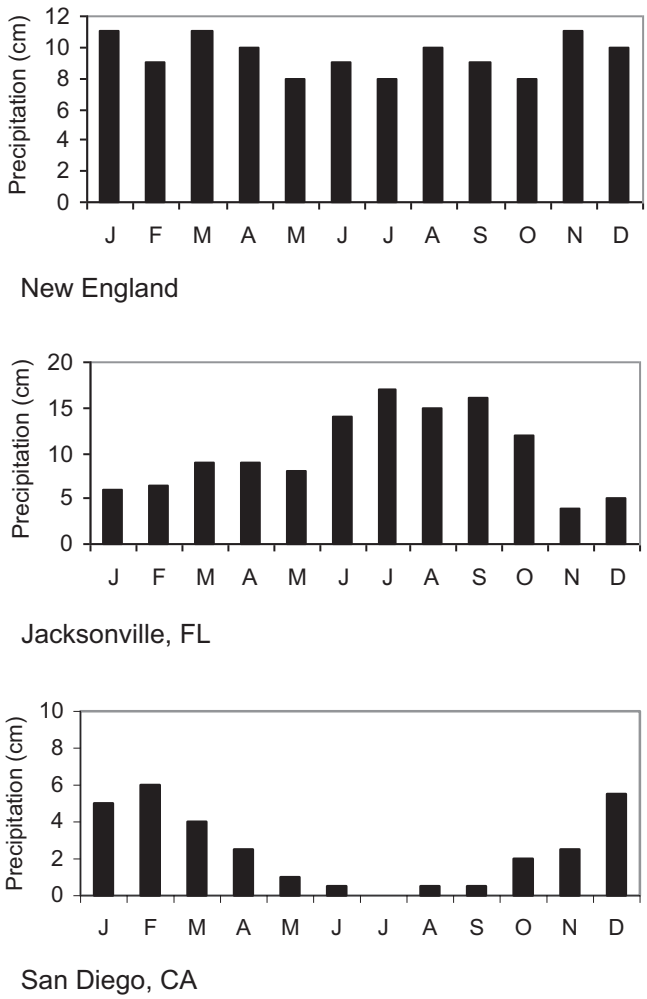

Fig. 8.19 Seasonal rainfall regimes in North America; bar graphs show mean monthly precipitation

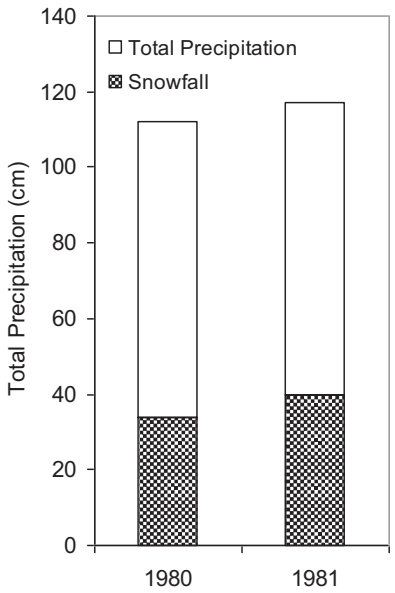

Fig. 8.20 Proportions of rain and snow in precipitation for 2 years in the Adirondack Mts., NY (Data from Johannes et al. 1985)

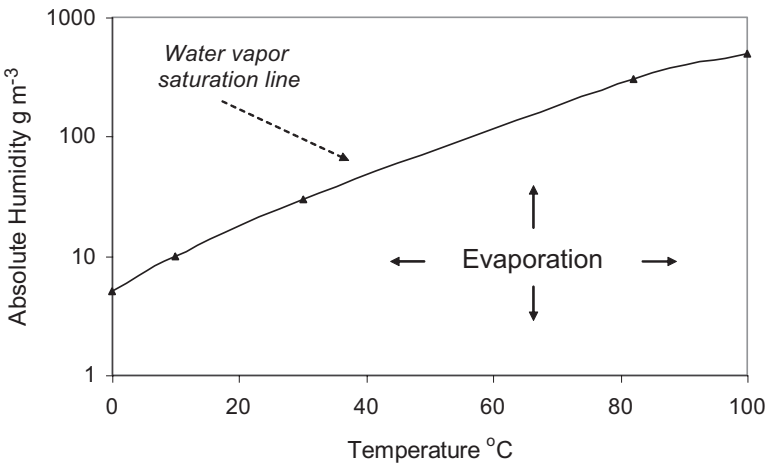

Fig. 8.21 Water saturation vapor pressure as a function of temperature; below the line, air is under-saturated, which promotes evaporation of water

water potential difference between the plant and soil, moisture in the soil responds to the water potential gradient like a ball rolling down a hill in response to gravity (Fig. 8.22). Thus, soil moisture moves from a zone of greater abundance (the soil matrix) to a zone of lesser abundance (inside the plant). Likewise, free water inside the plant responds to the vapor pressure deficit of the atmosphere, with increasing plant water loss as the atmosphere warms and relative humidity declines. The process of plant water uptake will continue as long as there is a sufficient water potential gradient to extract water from the soil.

Plant control over transpiration is exerted through the dynamic process of **stomatal conductance**, which is mediated by guard cells that respond to changes in sunlight, leaf-to-air vapor pressure deficit, leaf water potential, leaf temperature, and internal CO_2 concentration. Maximum leaf conductances for forest tree species range from roughly 0.11 cm s^{-1} in red pine to 0.29 cm s^{-1} in red maple to 0.83 cm s^{-1} in Douglas fir (Lee 1980 in Dingman 1994).

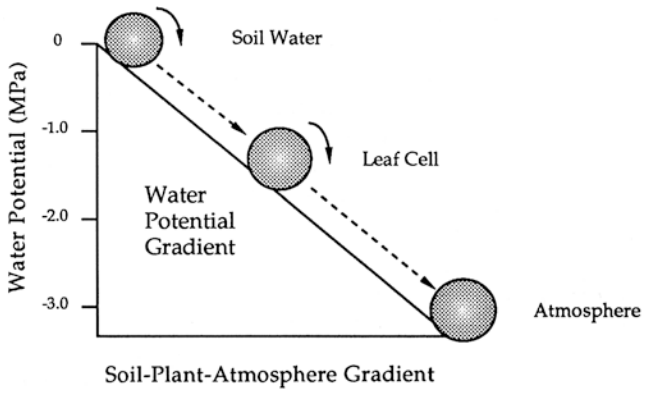

Fig. 8.22 Conceptual representation of a water potential gradient from a moist soil, to a leaf cell (with a negative water potential), and finally into the atmosphere (with the most negative water potential along the gradient)

The impact of evapotranspiration on the water budget of a terrestrial ecosystem is closely coupled to the **phenology**, leaf area, and activity of the plant community. When leaves or needles unfold or emerge from dormancy at the beginning of the growing season, there is a rapid increase in foliar surface area and a concomitant increase in canopy interception, canopy evaporation of intercepted water, leaf conductance, and transpirational water loss through stomata. As illustrated for a southern deciduous forest in Fig. 8.23, transpiration rises from negligible levels in early spring to tremendous levels observed during summer when high temperatures, high vapor pressure deficits, and maximum leaf area index occur simultaneously.

Results from an experiment conducted at Coweeta Hydrologic Lab in North Carolina by Swank and Douglass (1974) provide an example of the powerful influence of changes in ET on ecosystem water budgets. The authors reported that 15 years after two experimental watersheds were converted from mature hardwood forest to successional white pine forest, annual streamflow was reduced 20 cm below that expected for the same watersheds covered with mature hardwood forest. The implication of these findings is that, compared to the previous southern hardwood forest cover, transpiration increased significantly in evergreen white pines, because of their larger leaf area index and a year-round canopy.

Working with loblolly pine (*Pinus taeda*) stands at the Duke Forest in North Carolina, Phillips and Oren (2001) estimated that mean summertime transpiration rates ranged from 1.5 to 2.5 mm d^{-1}, single day maximum transpiration

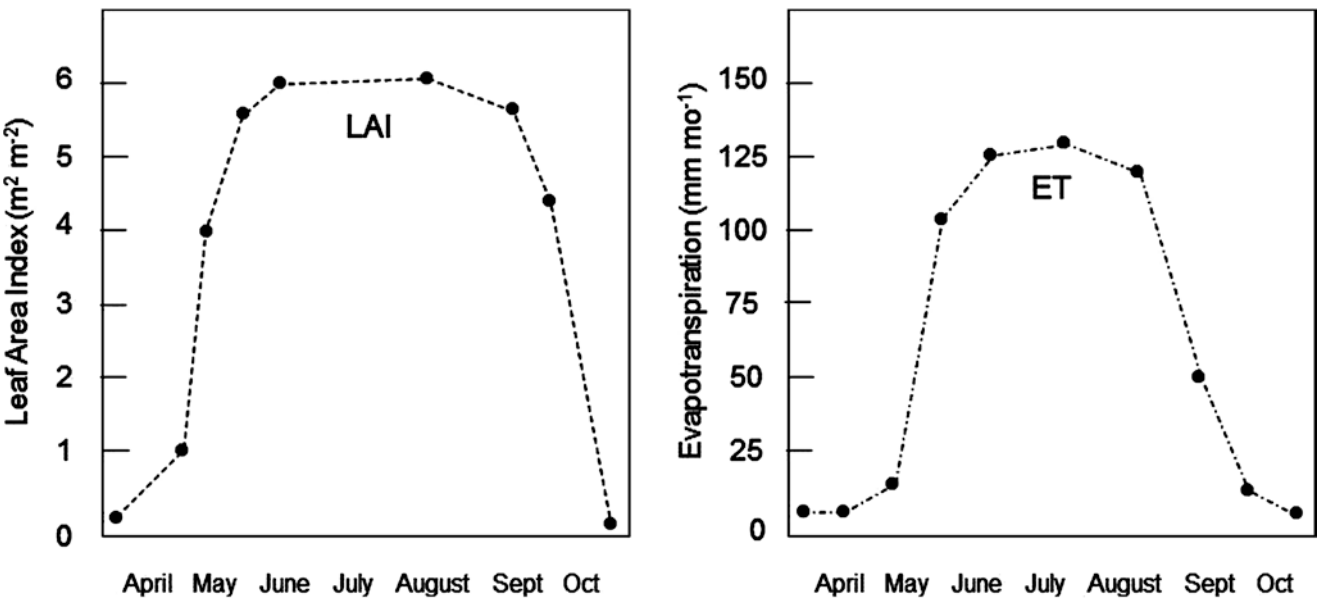

Fig. 8.23 Seasonal phenology of canopy foliar development (left panel) and ET (right panel) in a Tennessee deciduous forest. Reproduced with permission of Springer from Luxmore, R.J. and D.D. Huff. Water pp. 164–196 in D.W. Johnson and R.I. Van Hook (eds) Analysis of Biogeochemical Cycling Processes in Walker Branch Watershed. Springer-Verlag, NY. ©1989 by Springer

rates reached 2.9 mm d^{-1}, and mean total evapotranspiration amounted to 1.6 mm d^{-1} (Oren et al. 1998). Curiously, extrapolation of this mean ET rate to a growing season of 200 days amounts to only 32 cm, which is low compared with many estimates of annual ET in forested regions. Other authors have reported estimates of total evapotranspiration in various pine stands ranging from 0.9 to 3.8 mm d^{-1} (Roberts et al. 1980; Granier et al. 1990; Cermak et al. 1995).

Components of a Water Budget: Hydrologic Storage

The major parameters controlling hydrologic storage patterns in watersheds are seasonal climatic factors and physical characteristics of the drainage basin related to topography and geomorphology. Water storage in a drainage basin can include winter snowpack, lake storage, and watershed storage in the form of groundwater, soil moisture, biomass moisture content, or water retained in surface depressions or vernal pools. In a watershed that lacks winter snowfall, contains no lake or pond for water storage, or is covered by a shallow overburden of sediments, the significance of water storage would be diminished. Where storage reservoirs exist, short-term or seasonal changes in water storage can be an important quantitative component of a water budget. However, over longer time periods of one or more years, net changes in hydrologic storage are often assumed to cancel out as a zero term.

Canopy interception is one of the hydrologic storage terms that becomes evident when rainfall collected in the open is compared with canopy throughfall beneath a forest overstory. In general, throughfall volumes are less than gross precipitation inputs, because 1–2 mm of moisture from incident precipitation is intercepted and is stored on the foliage, branches, and bark of a forest community (Helvey and Patric 1965). Intercepted water is stored briefly and then evaporates into the atmosphere. Interception has been estimated to account for 10 to 40% of annual precipitation in different forest types and climates (Waring and Schlesinger 1985; Dingman 1994). For example, interception represented 9% of gross precipitation in an Amazonia rain forest and 34% of gross precipitation in a mature Douglas-fir forest in the northwestern U.S. (Dingman 1994).

Soil moisture storage is one of the most dynamic components of an ecosystem water budget, varying from saturated conditions during rainy seasons and snowmelt periods to much drier conditions characteristic of summer. At field capacity, a fine-textured loamy soil may hold 20–25 cm of water in the upper 1 m of the profile, whereas a sandy soil may hold a water equivalent as low as 6 cm (Singer and Munns 1996). Between periods of water recharge, soil moisture decreases from the combined influences of plant transpiration, diffusion and evaporation, and gravitational water losses. Simulated seasonal patterns of soil water recharge and withdrawal are illustrated in Fig. 8.24 for a Scots pine forest in Sweden investigated by Jansson and Halldin (1979). The authors used models to predict dramatic variations in soil moisture content at shallow depth, but found more subdued fluctuations at a depth of 100 cm. In their examination of soil moisture depletion in trembling aspen stands in Minnesota, Mital and Sucoff (1983) reported that patterns of depletion followed the relative density of roots (i.e., higher near-surface root densities corresponded with higher rates of moisture removal), which is consistent with the pattern in Fig. 8.24. At Duke Forest, Oren et al. (1998) estimated that >90% of the water used in evapotranspiration by loblolly pines came from the upper 35 cm of the soil profile; in a loblolly pine stand in Oklahoma, Stogsdill et al. (1992) reported that water uptake occurred to a depth of at least 1.2 m.

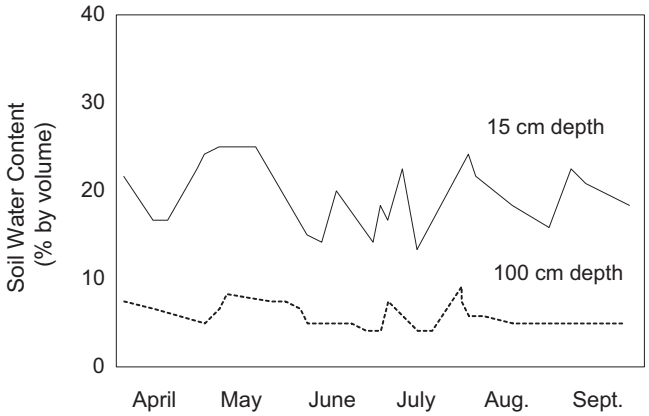

Fig. 8.24 Simulated patterns of soil water withdrawal by ET (valleys) and recharge from precipitation (peaks) in a Scots pine forest. Reprinted from Jansson, P.E. and S. Halldin. 1979. Model for annual water and energy flow in a layered soil. pp. 145–163 in Developments in Agricultural and Managed Forest Ecology, with permission from Elsevier

Groundwater storage, which is difficult to estimate, can be monitored with wells located within a drainage basin. During an annual cycle, the groundwater reservoir may experience periods of recharge by infiltrating precipitation and snowmelt, followed by periods of depletion when the continuous process of groundwater outflow is not offset by adequate moisture recharge. In summer, strong ET demand can divert water from infiltrating to recharge groundwater, thereby imposing pronounced temporal changes in the amount of groundwater storage. Fig. 8.25 depicts the patterns of water-table recession observed in a Maine forested wetland, where a steep water-table decline from August to September was estimated to represent the removal of 12 cm of stored water from each square meter of catchment.

Seasonal snow pack development in cool temperate and high-elevation watersheds can retain and store precipita-

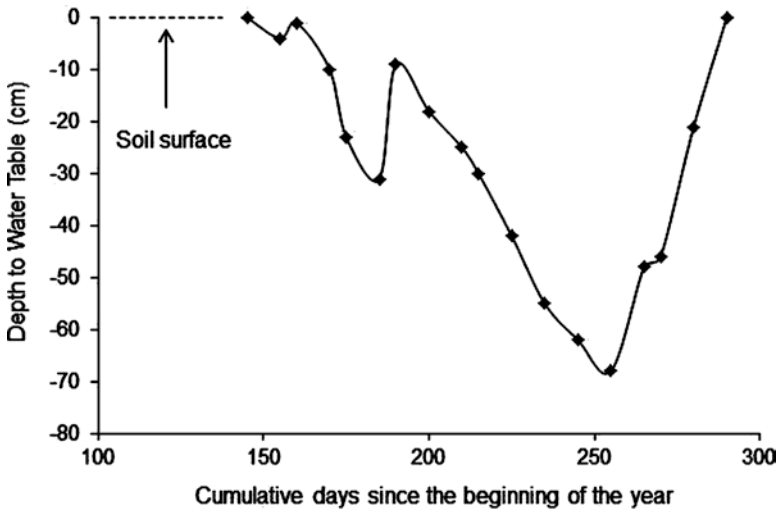

Fig. 8.25 Weekly mean water-table depth in a forested wetland at Penobscot Experimental Forest, Maine, USA. Each point is the mean of 15 wells (Data from Cronan et al. 1998)

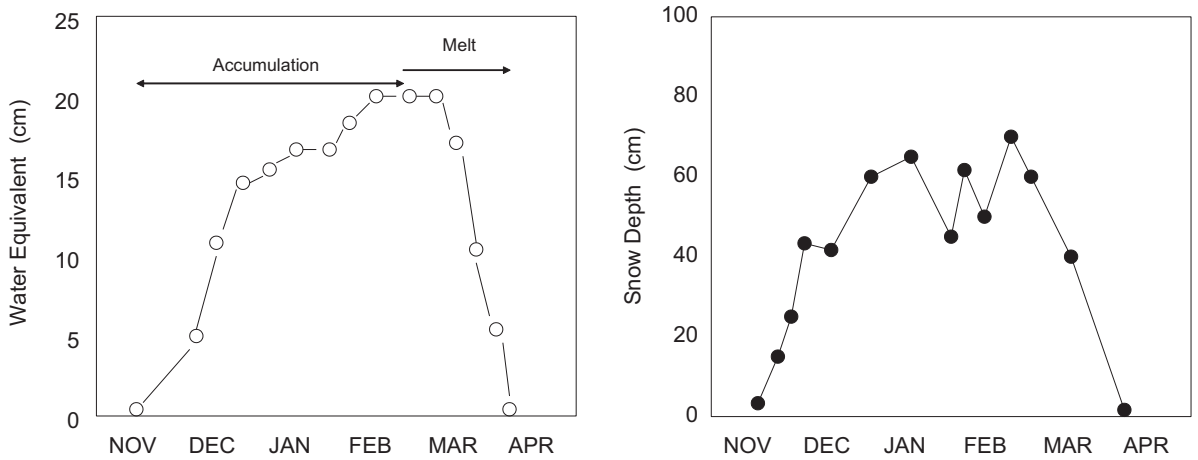

Fig. 8.26 Snow pack water equivalents (*left*) and snow depth (*right*) at Sleepers River Watershed, Danville, VT during a single year (data from Anderson et al. 1977)

tion inputs amounting to 10–30 cm of water during mid-winter. Later, during snowmelt, that moisture storage reservoir can release meltwater as a substantial internal input to groundwater recharge and spring runoff. At Sleepers River Watershed, VT, Anderson et al. (1977) found that cumulative snow pack reached a maximum depth of 70 cm and a water equivalent of 20 cm in February (Fig. 8.26). In a study of climatic conditions along an elevational gradient in the Green Mountains, VT, Siccama (1974) reported that maximum snow depth ranged from 60 cm at 550 m elevation to 115 cm at 1160 m, and snow pack duration ranged from 22 weeks at the lowest elevation to 30 weeks at 1160 m.

One of the striking aspects of snow pack hydrology is the unusual biogeochemical behavior of ions released during snowmelt. As a snow pack ages, freeze-thaw processes lead to the expulsion of ions from ice crystals and accumulation of solutes at the grain boundaries within the snow pack. This sets the stage for ionic enrichment of meltwater during the first period of spring melt. Typically, 50–80% of the original ions contained in the snow pack are released in the first 20–30% of meltwater (Dingman 1994). In their study of snowmelt chemistry in Quebec, Stein et al. (1986) found that snowmelt pH was as low as 3.5 in early spring and increased to >4.5 at the end of the melting period. The implications of this snowmelt pattern is that streams and sensitive organisms may be exposed to a concentrated slug of ions and acidity during the early stages of spring melt; this may represent an important transient ecological stress.

Components of a Water Budget: Stream Runoff

In most watershed studies, stream discharge is routinely monitored at a gauging station, so that runoff can be estimated on an instantaneous, daily, weekly, monthly, or annual basis.

Streamflow data can then be used to understand water and nutrient transport patterns in a given drainage basin.

Although runoff data can be presented and analyzed in a number of numerical formats, it is most common to express these values in units of volumetric discharge ($m^3\ s^{-1}$ or $ft^3\ s^{-1}$) or cm of runoff from a given area of ground surface. Being able to convert between these units can be helpful in comparing data from different studies and in expressing fluxes normalized to a common watershed area. As an example, we can look at a river in Maine – the Aroostook River – which has a drainage area of 6440 km^2 (644,000 ha) and a mean annual total flow of 3.54 x 10^9 $m^3\ yr^{-1}$. In order to compare this river with another one, we could normalize the flow to a unit area of watershed and ask how much of the annual water input to a hectare of drainage basin leaves as runoff. Dividing through to get the depth of water exported from each hectare as streamflow, we can estimate that annual runoff amounts to 55 cm of water per hectare. Data comparing river runoff for some of the largest watersheds in the world are shown in Table 8.2.

Table 8.2 Comparison of runoff patterns for world rivers (data from Dingman 1994)

	Drainage area	Discharge		Runoff
River	(10^3 km^2)	($km^3\ yr^{-1}$)	cm yr^{-1}	Ratio[a]
Amazon	7180	6000	83	0.47
Congo	3822	1330	34	0.25
Orinoco	1086	915	84	0.46
Brahmaputra	589	630	107	0.65
Mississippi	3224	560	17	0.21
Ganges	1073	490	45	0.42
Saint Lawrence	1030	330	31	0.33

[a]Ratio of the mean annual discharge divided by mean annual precipitation

Stream runoff represents an integrated watershed response to geologic conditions in the drainage basin, climate, variable water inputs, seasonal variations in storage and evapotranspiration, and dynamic changes in the relative contributions from baseflow and quickflow to stream discharge. Two contrasting **hydrographs** are presented in Fig. 8.27 to illustrate how stream runoff patterns can vary in space and time for different drainage basins. We see that both streams exhibit dramatic **peak flows** associated with precipitation or snowmelt events, as well as troughs representing low flow or **base flow** conditions. Comparing the two streams, we see that the hydrograph for WS II is more "flashy" and exhibits greater extremes between high and low flows, despite the fact that both streams are located close to each other and have similar precipitation inputs. In this particular example, the dissimilar runoff patterns for the two watersheds can be accounted for by differences in geomorphology and groundwater storage in the two catchments. In the upper watershed (WS I), a thick overburden of glacial till holds a large groundwater reservoir that acts as a hydrologic buffer, absorbing some of the water during peak flow periods and releasing water during base flow conditions. As a result, even during drier periods, minimum flows from watershed WS I are much higher than those observed in watershed WS II, which lacks thick surficial deposits and contains a much smaller groundwater storage reservoir.

Another way of visualizing differences in runoff characteristics among watersheds is to plot stream discharge using a flow duration or flow exceedence graph as shown in Fig. 8.28. A graph such as this illustrates the percentage of time a given streamflow occurs over an annual cycle in a given watershed. We see that peak storm flows are plotted in the upper left corner of the graph, and that high runoff levels occur less than 10–20% of the time, whereas flows equal to

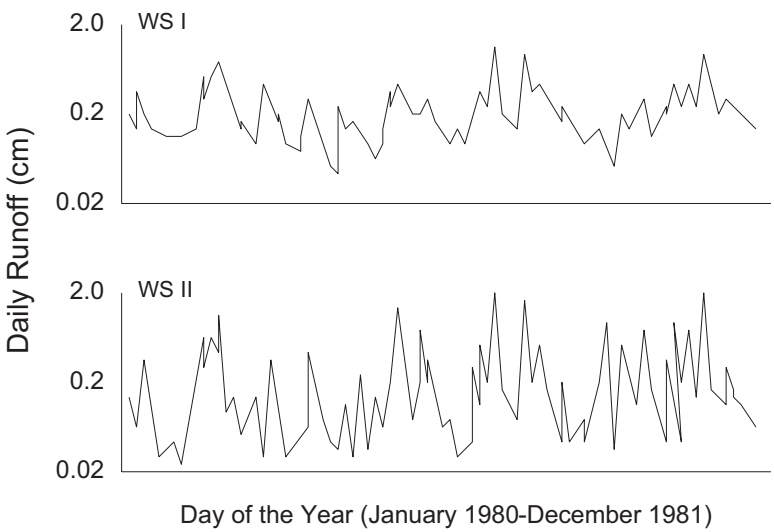

Fig. 8.27 Hydrographs for two forested Adirondack watersheds, NY. Reproduced by permission of Springer with data from Peters, N.E. and P.S. Murdoch. Hydrogeologic comparison of an acidic lake basin with a neutral lake basin in the west-central Adirondack Mountains, New York. Water, Air, and Soil Pollution 26: 387–402. ©1985 by D. Reidel Publishing Company

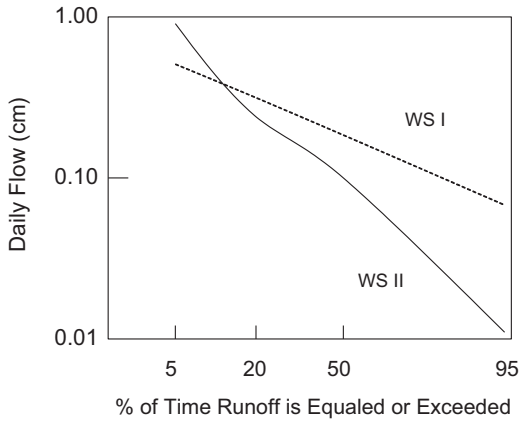

Fig. 8.28 Flow duration curves for the two small watersheds (WS I and II) shown in the previous figure. Reproduced with permission of Springer with data from Peters, N.E. and P.S. Murdoch. Hydrogeologic comparison of an acidic lake basin with a neutral lake basin in the west-central Adirondack Mountains, New York. Water, Air, and Soil Pollution 26:387–402. ©1985 by D. Reidel Publishing Company

Table 8.3 Monthly water budgets for a small lake-watershed in the Adirondack Park, NY (Peters and Murdoch 1985). Values are expressed in cm of water. P is precipitation, ΔS_s is the change in snowpack storage, R is runoff, ET is evapotranspiration calculated by the vapor-pressure method, ΔS_L is the change in lake storage, and ΔS_w is the change in watershed storage during the 1980 water year

Month	P	ΔS_s	R	ET	ΔS_L	ΔS_w
January	8.1	+3.8	4.2	0.0	−2.2	+0.4
February	3.3	+2.7	1.0	0.0	−0.4	+0.0
March	11.4	−3.1	7.9	0.0	+1.1	+5.6
April	10.7	−3.4	13.9	3.6	−0.5	−2.8
May	7.1	–	2.4	6.8	+0.2	−2.4
June	9.6	–	3.5	8.5	−0.6	−1.9
July	16.0	–	3.0	10.8	+0.4	+1.9
August	7.0	–	1.3	9.6	+0.2	−4.1
September	11.3	–	2.3	5.5	+0.2	+3.2
October	13.1	–	6.4	2.1	+0.1	+4.5
November	12.8	–	10.8	0.0	+0.1	+1.9
December	10.5	+8.0	6.9	0.0	−0.2	−4.1
Yearly	120.9	+8.0	63.6	46.9	−1.6	+2.2

or exceeding base flow conditions occur 90–95% of the time (lower right hand corner). In this type of graph, watersheds with flashier hydrographs and less hydrologic buffering (e.g.,WS II) tend to have steeper negative slopes, whereas streams draining watersheds with significant groundwater contributions generally exhibit flatter slopes and have higher minimum flows.

Integrated Analysis of a Water Budget

The data summarized in Table 8.3 provide an opportunity to examine the integrated components of a water budget over a 12 month sampling period in a small northern watershed in the Adirondack Mts., NY. In the first column, we see that precipitation inputs varied from 3.3 to 16.0 cm per month and added up to a total of 120.95 cm for the year. In the next column, the data show that snowpack storage rose in January and February, declined in March and April, and rose again in December, giving an annual net balance of +8.0 cm of water equivalent stored in snowpack. Stream runoff ranged from a minimum of 1.0 cm in February (when precipitation was low and snowpack storage was high) to a maximum of 13.9 cm in April (when precipitation and snowmelt were both high), and totaled 63.6 cm for the year. Evapotranspiration was essentially zero during the winter months, increased to a maximum of 10.8 cm of water in July, and summed to 46.9 cm for the year. Changes in lake storage and watershed groundwater storage are also shown in the table.

For the same watershed, simplified water budgets calculated over a period of 4 years show that precipitation ranged from 117.2 to 136.5 cm/yr and averaged 125 cm/yr, stream runoff varied from 62.7 to 87.8 cm/yr and averaged 73.7 cm/yr, and evapotranspiration ranged from 35.6 to 73.8 cm/yr and averaged 51.3 cm/yr Changes in storage were assumed to be negligible over that multi-year period. Expressing those results in terms of percentages, we find that roughly 40% of precipitation inputs returned to the atmosphere as evapotranspiration and 60% of moisture inputs left the watershed as stream runoff.

Aqueous Chemistry

9

Introduction

Many of the important inputs, outputs, and internal transfers of elements in watershed ecosystems occur through the medium of water. As water moves through the drainage gradient in a watershed, solution chemistry evolves and changes in response to the differential influences of biogeochemical processes. By tracking changes in aqueous chemistry, it is possible to infer what processes control aqueous concentrations and transfers of elements. The aqueous chemistry of a watershed essentially provides a "window on the world" of biogeochemical processes that are otherwise invisible and difficult to detect. In many respects, the analysis of solution chemistry in a watershed ecosystem is similar to the testing of blood chemistry in a human body. In both cases, concentrations of solutes and gases provide important indicators of the internal functions of the system.

Solution chemistry in a watershed ecosystem can be examined conceptually in the context of the simplified hydrologic source compartments depicted in Fig. 9.1. In a given watershed ecosystem, each of the hydrologic reservoirs or pools represents a potential source or sink for dissolved solutes and gases. Outputs of water from each compartment often exhibit distinctive patterns of aqueous chemistry that differ from other compartments and reflect the influence of specific biogeochemical processes and environmental conditions characteristic of that reservoir. One compartment may be a source of internal acidity, decreasing solution pH, whereas another compartment may be a sink for acidity and a source of **ANC**, thus raising pH.

The intent of this chapter is to examine patterns of solution chemistry in watershed ecosystems and to discuss the major physical, biological, and chemical factors and processes controlling the chemistry and fluxes of elements in natural waters. We shall explore how and why aqueous chemistry varies in space and over time in a watershed. It will become evident that elements do not simply "flush down the drainage pipe" via mass flow and gravity in a watershed ecosystem. Our ultimate goal will be to develop a basis for understanding the individual behavior of different types of ions and solutes in natural waters.

An Example of Soil Solution Chemistry: Analysis and Interpretation

What kinds of observations and insights can be obtained from analysis of aqueous chemistry data? In one of our research studies, we examined how acidic precipitation influences leaching and ion transport in forest soil columns in a controlled greenhouse setting. The columns were undisturbed cylinders of soil that had no plants growing on them, but were otherwise representative of natural soils found in forested ecosystems of the northeastern U.S. Simulated rainfall of known chemistry was applied to each column and soil drainage water was sampled beneath the surface O horizon, E horizon, and lower B horizon. Results from a sandy Adams

C.S. Cronan, *Ecosystem Biogeochemistry*, Springer Textbooks in Earth Sciences, Geography and Environment, DOI 10.1007/978-3-319-66444-6_9

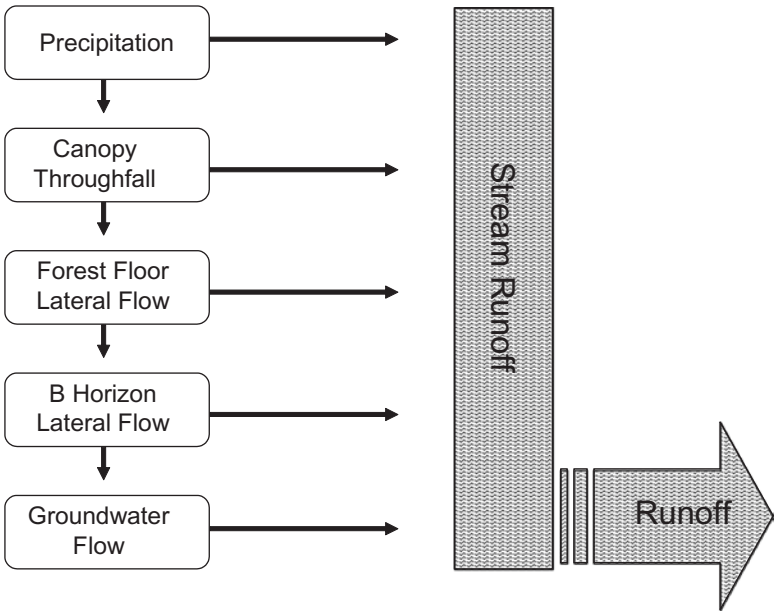

Fig. 9.1 Hydrologic source compartments exhibit distinctive solution chemistries and changing contributions to stream runoff as hydrologic conditions vary

Table 9.1 Changes in solution chemistry of precipitation during infiltration through O, E, and B horizons of Adams soil columns[a] from a pine-oak forest ecosystem in New Hampshire (Cronan 1985b). Concentrations in $\mu mol_c\ L^{-1}$

Parameter	Precipitation	O Horizon outflow	E Horizon outflow	B Horizon
pH	3.52	4.30	4.55	5.50
Ca	20	39	61	169
Mg	10	13	42	47
SO_4^{2-}	330	428	444	18
NO_3^-	30	61	76	368
DOC (mmol/L)	0	5.3	2.0	0.33

[a]Replicated undisturbed soil columns lacking living plants

series Spodosol were especially striking, as reflected with the trends for pH, sulfate, nitrate, and dissolved organic carbon (DOC) shown in Table 9.1. Precipitation inputs of pH 3.5 increased two full pH units to pH 5.5 in transit through the 50 cm deep soil column. Sulfate concentration in precipitation was 330 $\mu mol_c\ L^{-1}$, increased to 428 $\mu mol_c\ L^{-1}$ in O horizon **leachate**, but then plunged to 18 $\mu mol_c\ L^{-1}$ in soil water draining from the B horizon. Nitrate concentration increased progressively from an initial value of 30 $\mu mol_c\ L^{-1}$ in precipitation to 368 $\mu mol_c\ L^{-1}$ in soil water beneath the B horizon. Finally, DOC was absent from precipitation, increased dramatically to >5 mmol C L^{-1} in O horizon leachate, but then diminished to <0.5 mmol C L^{-1} in soil water at 50 cm in the B horizon.

How can we account for these variable patterns and order of magnitude changes in aqueous chemistry? Clearly, the soil profile was a sink for acidity, and the rise in solution pH was the result of some combination of processes contributing to ANC generation (e.g., mineral weathering, cation exchange, and anion adsorption). The behavior of sulfate suggests that the O horizon was a source for sulfate, but the B horizon was a sink for soluble sulfate. Presumably, removal of sulfate from solution was dominated by sulfate adsorption on iron or aluminum oxides in the B horizon. In the case of nitrate ion, the entire soil profile was a source for this **mobile anion**. Apparently, mineralization and nitrification of organic N in the soil profile exceeded microbial demand, resulting in a large flux of soluble nitrate into soil drainage water. It is interesting to note that the process of nitrification may have acidified the soil and increased the anion exchange capacity, thus enhancing the adsorption and retention of sulfate. Finally, the pattern of DOC concentrations indicated that the O horizon was a strong source for soluble organic C, but the B horizon was an effective sink for this material. As expected in a podzolized soil, soluble carbon leached from decaying organic matter in the O horizon, but was removed from solution in the illuvial B horizon by a combination of microbial mineralization and adsorption/precipitation reactions.

Stepping back from this example, we can see a number of themes emerging concerning aqueous chemistry of natural waters: (i) individual elements and ions can exhibit very different patterns of solution chemistry and transport; (ii)

changes in the chemistry of natural waters reflect the influence of multiple different biogeochemical processes; and (iii) by focusing on solution chemistry, it is possible to detect the signals or evidence of dynamic biogeochemical processes that are otherwise very difficult to observe based on monitoring of soil solid phase properties. With this introduction, let us now proceed to develop a framework for understanding the aqueous chemistry of watershed ecosystems.

General Concepts of Aqueous Chemistry

Sample Collection and Analysis

Solution chemistry parameters in natural waters are typically measured at very low concentration ranges of μmol L^{-1}, mmol L^{-1}, parts per million (ppm), or parts per billion (ppb). Thus, it is crucial that protocols for sample handling and analysis follow rigorous **QA/QC** standards for quality control and quality assurance, so as to maximize the accuracy of measurements and to minimize data artifacts and uncertainty. Solution chemistry data sets should always be screened to verify that acceptable methods have been used for sample collection, processing, filtration, preservation, storage, analysis, replication, and QA/QC.

Selection of Analytical Parameters

The choices of parameters to be measured in a water sample depend upon the study objectives and research design, the availability of funds and instrumentation for analysis, and the time budget for a project. In many studies of natural waters, efforts are made to characterize all major cations (Ca, Mg, Na, K, and NH_4^+) and anions (SO_4^{2-}, NO_3^-, Cl^-, F^-, and PO_4^{3-}), ANC, pH, dissolved inorganic carbon (DIC), and a variety of trace elements such as Fe, Mn, or Zn. Other studies may focus on soluble organic C, N, and P, or specific contaminants such as pesticides, aromatic hydrocarbons, or heavy metals such as Hg. For some parameters, the measurement of an element may be based on an operational definition. For example, ionic aluminum (Al) may be defined as the fraction of total aluminum that binds to a cation exchange column at a specified pH. In an effort to distinguish different fractions or species of an element or ion, investigators may use different separation techniques or analytical probes to quantify each component. For example, **DOC** may be fractionated into hydrophobic and hydrophilic classes of compounds using ion exchange and reverse phase chromatography, followed by infrared analysis of the DOC concentration in separate column effluents (Cronan and Aiken 1985). In studies of Al chemistry, ionic Al may be separated from uncharged Al using ion exchange chromatography, followed by quantitative speciation of ionic Al using a thermo-dynamic equilibrium model (e.g., Driscoll 1984).

Alkalinity or Acid Neutralizing Capacity (ANC)

Alkalinity can be quantified by titration as the sum of proton acceptors in a solution, expressed as ALKALINITY = $HCO_3^- + 2CO_3^{2-} + OH^- + RCOO^- - H^+$ and where $RCOO^-$ refers to organic anions. An example would be a solution of sodium bicarbonate that contains an alkalinity equal to the concentration of HCO_3^-. Alternatively, alkalinity or ANC can be defined using solution chemistry data and the principle of **electrical neutrality**. For instance, a typical water sample might include the following charge balance components (where each ion is expressed in moles L^{-1} and each polyvalent ion is multiplied by its charge):

$$\text{Cations} = H^+ + 2Ca^{2+} + 2Mg^{2+} + K^+ + Na^+ + NH_4^+ + 2Fe^{2+} + nAl^{n+}$$

$$\text{Anions} = 2SO_4^{2-} + NO_3^- + Cl^- + F^- + HCO_3^- + 2CO_3^{2-} + OH^- + RCOO^-$$

Based on electrical neutrality, **sum of cations = sum of anions**

This expression can be re-arranged as follows:

$$[2Ca^{2+} + 2Mg^{2+} + K^+ + Na^+ + NH_4^+ + 2Fe^{2+} + nAl^{n+}] - [2SO_4^{2-} + NO_3^- + Cl^- + F^-]$$

$$= HCO_3^- + 2CO_3^{2-} + OH^- + RCOO^- - H^+ = \text{ALKALINITY}$$

If we then substitute C_B for the *sum of base-forming cations* listed above and C_A for the *sum of strong acid anions* shown above, the equations simplify to the following equivalent expressions:

$$\mathbf{C_B - C_A = HCO_3^- + 2CO_3^{2-} + OH^- + RCOO^- - H^+ = ALKALINITY = ANC}$$

As demonstrated by Schofield et al. (1985), these two expressions for charge balance ANC and titration alkalinity have previously been found to agree closely using empirical titration and charge balance data. We should note briefly here that a hydroxy-metal such as $AlOH^{2+}$ can act both as a proton acceptor in a calculation of titration alkalinity and can also be considered a component of C_B, but we will not pursue that particular rabbit hole any further in this discussion.

Let's consider several examples of solutions with different values of ANC or alkalinity. In a dilute solution of nitric acid at 0.0001 M, the concentration of base cations is zero and the concentration of strong acid anions is 0.0001 M or 0.1 mmol L^{-1}. Substituting into the relationship $C_B - C_A$, we calculate that the solution has a negative ANC of 0.1 mmol

L^{-1} (which equals a free acidity of 100 μmol L^{-1} with a pH of 4.0). In contrast, a solution of 0.01 M KCl has an ANC of $C_B - C_A = 0.01$ M $K^+ - 0.01$ M $Cl^- = 0$.

Similarly, a solution of 0.001 M carbonic acid, has an ANC or alkalinity of zero, because $H^+ = HCO_3^-$; therefore, the expression ALKALINITY = $HCO_3^- - H^+$ is equal to zero. Finally, the ANC of a solution containing 0.01 M $NaHCO_3$ can be calculated as $C_B - C_A = Na^+ - 0 = 0.01$ M. This is equivalent to the expression: ALKALINITY = $HCO_3^- - H^+ = HCO_3^- - 0 = 0.01$ M. Based on these examples, would you expect a solution to gain ANC from the addition of $CaCl_2$ or KNO_3?

Acidity and pH

Free acidity is measured with an electrode as pH = −log [H^+], where the brackets indicate the **ion activity** of H^+ ion in solution. **Bound acidity** can be determined by titration of undissociated weak acid protons with dilute NaOH to an operational endpoint (e.g., 7.0) or an empirical equivalence point (pH where the concentration of added base cation is equal to the concentration of the weak acid anion). In estimating acidity, it is important to note that measurement of solution pH requires careful technique, because the pH probe is sensitive to temperature, ionic strength, sample stirring, and the partial pressure of carbon dioxide, pCO_2. If CO_2 degasses from a super-saturated sample or from a cool field sample that has warmed, the measured pH may be higher than the original field pH.

Conductivity

Measurement of **electrical conductivity** provides a way to estimate the total ionic contributions to electrical conductance in a water sample. Conductivity of an electrolyte solution is inversely proportional to its resistance and increases with total ion concentration; hence, dilute, deionized water has a very low conductivity and a high resistance. As shown in Table 9.2, individual ions have equivalent conductance values that vary from 350 μmho or μS for H^+ ion to 51 μmho or μS for Na^+ ion. The contributions from individual ions in a water sample can be summed to estimate the molar conductivity of an electrolyte solution at a specified temperature (Table 9.3).

Table 9.2 Equivalent conductances @25 °C of selected ions expressed in μS or μmho (from CRC Handbook 1978)

Ion	H^+	Na^+	K^+	Ca^{2+}	Cl^-	NO_3^-	SO_4^{2-}
Conductance	350	51	75	60	76	71	79

Table 9.3 Molar conductivities of electrolytes at 25 °C in water expressed in μmho cm^{-1} or μS cm^{-1}

NaCl	123.7[a]
KCl	146.9
NaI	124.3
HCl	421.4
$AgNO_3$	130.5

[a]From Daniels and Alberty (1975)

In sampling Maine rivers, we have found striking variations in conductivity at different collection times. For example, the lower Kennebec River had a conductivity of 335 μS cm^{-1} during a high tide cycle versus a value of 43 μS cm^{-1} at low tide, when freshwater dominated discharge. The Penobscot River had a conductivity of 37μS cm^{-1} during high flow associated with a storm, but values increased twofold to 78 μS cm^{-1} under low flow conditions when groundwater inputs dominated river discharge.

Since the relationship between molarity and specific conductance is known for most ionic species, the measured conductivity of water samples can be used as an internal check on both the accuracy and completeness of analytical measurements of ionic species. After the conductivity of a sample has been measured, the expected conductivity is calculated as the sum of the products of the ionic molarities and the equivalent conductance values for each of the measured ions in solution (U.S. EPA 1988), corrected for concentration effects using the Debye-Huckel-Onsager equation (Atkins 1978). Then, the measured and calculated values of conductivity are compared. Application of this cross-checking technique to streams sampled by U.S. EPA in the Mid-Atlantic and Southeastern U.S. indicated excellent agreement ($r^2 = 0.987$) between expected and observed conductivity values (Fig. 9.2). This implies that there were no systematic errors in the analysis of ionic species for those stream water samples. However, suppose there was a sample plotted at coordinates x = 100 and y = 200 on Fig. 9.2, what would you conclude about the chemical analysis of that stream sample?

Ionic Strength and Ion Activity

The term **ionic strength** provides another way of describing the solution concentration range for a natural water sample. Aqueous ionic strength can be quantified using the following relationship:

$$I = 0.5 * \sum m_i * z_i^2, \text{ where } m_i = \text{molarity of ion}_i \text{ and } z_i = \text{charge of ion}_i$$

As an example, the ionic strength of a 0.001 M solution of $CaCl_2$ is $I = 0.5 * [(0.001 * 4) + (0.002 * 1)] = 0.003$ M.

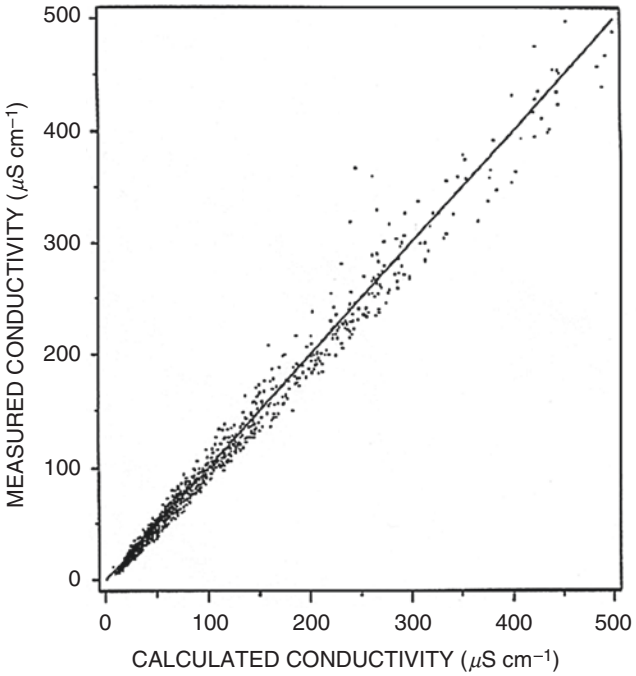

Fig. 9.2 Measured versus calculated conductivity for stream samples (US EPA 1988)

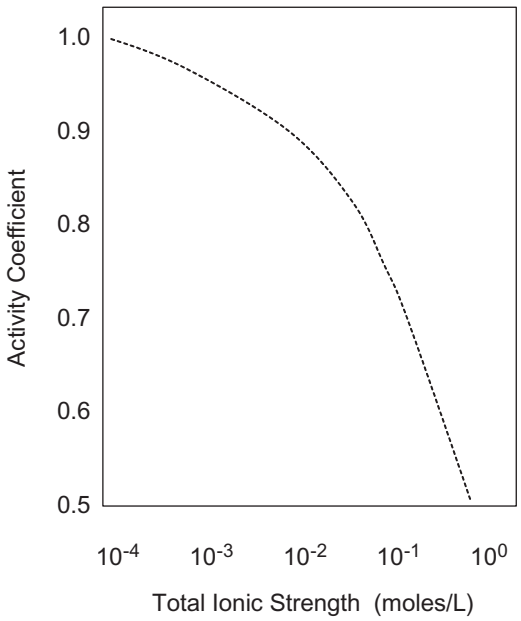

Fig. 9.3 Ionic activity of fluoride as a function of total ionic strength

In discussions of solution chemistry, we often use the term **concentration** as a simplification for **ion activity** – which is the ***effective concentration*** in solution. Ionic activity is roughly equal to molar concentration in very dilute solutions, but becomes less than concentration as ionic strength increases. This distinction can be important when we consider geochemical processes of dissolution and precipitation in natural waters. As waters become more concentrated with ions, interactions among solutes decrease the ion activities in solution, lowering the numbers of ions that can effectively participate in chemical reactions. Ion activity is calculated as the product of an ion activity coefficient of a chemical species (γ_i) times its molarity (m_i), or $a_i = \gamma_i * m_i$. With increasing concentration, the activity coefficient diminishes and the ion activity also decreases accordingly (Fig. 9.3).

Most analytical methods measure concentrations of ions, rather than ion activities. However, the glass pH electrode and other ion selective electrodes provide estimates of ion activities. In order to convert concentration data to ion activities, one can estimate the ion activity coefficient as follows:

$$\log \gamma_i = -(A * z_i^2 * \sqrt{I})/(1 + å * B * \sqrt{I})$$

where $\varepsilon = 2727.586 + 0.6224107 * T - 466.9151 * \ln T - 52000.87/T$

$A = 1.82 * 10^6 * (\varepsilon * T)^{-3/2}$

$B = 50.3 * (\varepsilon * T)^{-1/2}$

T = absolute temperature å = ionic radius

I = ionic strength z_i = ionic charge

Influence of Temperature on Solution Equilibria

Changes in temperature have important effects on reaction rates and thermodynamic equilibria in natural waters. For example, the solubilities of $Al(OH)_3$ and gaseous CO_2 in water are higher at cool versus warm temperatures. In seawater, CO_2 solubility increases from 32 moles m^{-3} at 24 °C to 65 moles m^{-3} at 0 °C (Broecker 1974). Dissolution of gibbsite in an acidic stream channel can be described as $Al(OH)_3 + 3H^+ = Al^{3+} + 3H_2O$, where $K_{eq} = [Al^{3+}] / [H^+]^3$. For this dissolution reaction, the log K at 25 °C is 8.77, but the log K at 10 °C is almost an order of magnitude greater at 9.66, reflecting the increased solubility of Al-trihydroxide at lower temperature. In contrast to these examples, other processes such as metabolic reactions and cation adsorption on clays (Walker et al. 1988) tend to increase with temperature.

Hydrolysis and Chemical Speciation as a Function of pH

Many elements occur in natural waters as different aqueous chemical species, depending upon pH and redox conditions. For example, the orthophosphate ion in phosphoric acid, H_3PO_4, is protonated in acidic solutions ($H_2PO_4^-$ or HPO_4^{2-}) and only dissociates to free PO_4^{3-} at higher pH. Soluble iron occurs in the ferrous form (Fe^{2+}) under conditions of lower

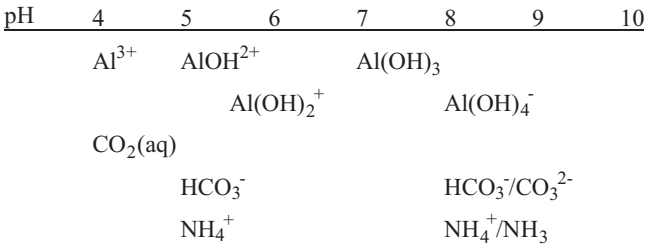

Fig. 9.4 Examples of chemical speciation as a function of solution pH. For instance, HCO_3^- occurs above pH 4.5 whereas carbonate ion occurs above pH 7; trivalent Al occurs below pH 4.5, but hydrolyzes to hydroxyl-Al above that pH

pH and redox, but oxidizes to the less soluble ferric form (Fe^{3+}) as pH and redox potential increase. Soluble inorganic aluminum occurs as trivalent Al^{3+} in acidic solutions below pH 4 to 5, but hydrolyzes to form hydroxides such as $AlOH^{2+}$ and $Al(OH)_2^+$ as the pH rises above pH 4.5. Aluminum **hydrolysis** results from the reaction of trivalent Al with water as shown below:

1. $Al^{3+} + H_2O = AlOH^{2+} + H^+$
2. $Al^{3+} + 2H_2O = Al(OH)_2^+ + 2H^+$

From a biogeochemical perspective, it is important to note that the different chemical species of elements may vary in their biological availability and chemical behavior. For example, some evidence indicates that Al^{3+} ion is more toxic to plant roots than the hydroxy-Al ions (Cronan and Grigal 1995). In the carbonate system, the monovalent bicarbonate ion is very soluble, whereas divalent carbonate ion tends to form insoluble precipitates with Ca and other metals. Fig. 9.4 provides a general overview of several elements that exhibit pH-dependent chemical species.

Rate-Limited Versus Equilibrium Conditions

Solute concentrations and element fluxes in watershed ecosystems are influenced by both equilibrium processes and rate-limited reactions that may or may not reach equilibrium in the time frame of water movement along a hydrologic flow path. Examples of equilibrium processes are acid dissociation and ion exchange in the soil matrix. In contrast, rate-limited reactions include mineral dissolution, gaseous and solute diffusion, and biotic uptake. The rates at which these reactions proceed in a given environmental setting help to determine the extent of depletion or enrichment of natural waters with certain solutes or ions that are subject to kinetic controls. For example, a soil water sample collected in a cultivated watershed during spring might exhibit higher nitrate concentrations if low temperature conditions inhibit rapid plant uptake of nitrate ions from solution.

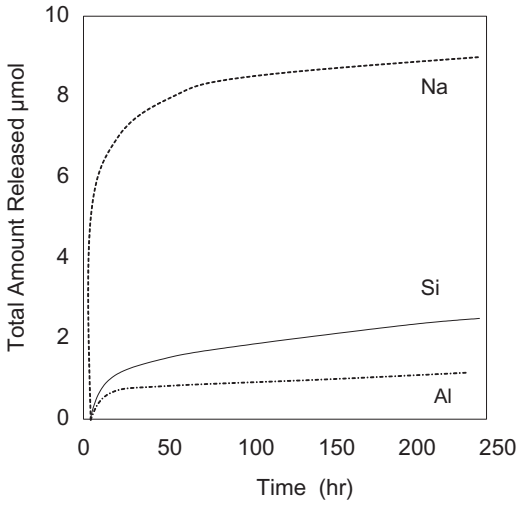

Fig. 9.5 Cation release from albite during a mineral weathering experiment in water at pH 5.6. From Wollast, R. and L. Chou. Kinetic study of the dissolution of albite with a continuous flow-through fluidized bed reactor. pp. 75-96 in J.I. Drever (ed) The Chemistry of Weathering. ©1985 by D. Reidel Publishing Company, with permission of Springer

The influence of kinetic limitations can be visualized with mineral weathering data. In their investigation of albite dissolution at pH 5.6, Wollast and Chou (1985) reported that it took hours or days for the release of soluble Si, Al, and Na to reach an asymptote approaching an equilibrium state (Fig. 9.5). This implies that natural waters affected by this type of dissolution process will exhibit changes in solution chemistry over time as weathering inputs of Si, Al, and Na progressively enrich the water parcel. Similar kinetic constraints on water chemistry are evident when we examine ions such as K^+ that are strongly controlled by root uptake processes. In soils where root absorption is limited by cold temperatures or low O_2 concentrations, these constraints on uptake of K^+ ion relative to the rate of K^+ supply may translate into varying soil solution concentrations of K^+ in response to this rate-limited cation removal process.

Differential Anion Mobility

Johnson and Cole (1980) summarized a large body of literature indicating that nutrient transport in forest ecosystems is strongly regulated by the availability and mobility of anions in soil solutions. Each of the major anions in drainage waters has distinct properties that affect its production and movement through a watershed. For example, production of bicarbonate is regulated by soil pCO_2 and solution pH. Mobility of phosphate is greatly affected by soil adsorption reactions, with secondary control by biological uptake. The mobility of nitrate ion is regulated almost solely by biological processes (plant uptake, nitrification, denitrification, microbial immobilization), whereas chloride ion is relatively unaffected by either

biological or chemical retention mechanisms. Sulfate mobility is controlled by multiple processes such as biological uptake, sulfate reduction, soil adsorption, and chemical precipitation reactions. Fluoride ion mobility is largely controlled by rates of geologic inputs, and is relatively unaffected by retention mechanisms. Finally, organic anions are controlled by biological production processes and a combination of removal processes involving biological mineralization, surface adsorption on soil colloids, and chemical precipitation with metals. Knowing the factors controlling the differential mobilities of anions, it is possible to predict general patterns of cation and anion transport in watershed ecosystems.

Effects of Ecosystem Processes on Solution Chemistry

Returning to the analogy of human blood chemistry, it is important to emphasize that the solution chemistry of water moving through a watershed ecosystem provides a sensitive assay of dynamic nutrient cycling processes. As water enters an ecosystem in precipitation and moves through the plant canopy, soil, and watershed drainage basin, solution chemistry progressively changes in response to the influences of multiple biogeochemical processes. For each of these processes, we can predict the changes expected in solution chemistry (Table 9.4). Similarly, the characteristics of aqueous chemistry observed at a given time or place in a watershed ecosystem can be used to infer the presence or potential importance of a particular biogeochemical process.

Table 9.4 Effects of biogeochemical processes on aqueous chemistry

Process	Effects on solution chemistry
Mineral weathering	May release Ca, Mg, K, Na, Si, Fe, Al, P, ANC, and consume H^+
Biological mineralization	May enrich solution with soluble elements and CO_2
Biological immobilization	Adds elements to microbial biomass and removes ions from solution
Plant absorption	Removes elements from solution and may contribute H^+, OH^-, HCO_3^-, or organic ligands (R-COOH)
Soil respiration	Increases pCO_2 and may acidify solution chemistry
Organic acid release	May acidify solution and increase soluble C concentration
Foliar uptake	May selectively remove elements from wet deposition inputs to canopy
Canopy leaching or washout	May enrich particular elements and may alter solution pH
Nitrification	Consumes NH_4^+, releases NO_3^-, and produces H^+ ions
Denitrification	Causes removal of NO_3^- and possible addition of dissolved N_2O
Mineral dissolution/ precipitation	May enrich or deplete specific elements in solution
Cation adsorption/ ion exchange	May have equivalent removals and releases of competing cations
Anion adsorption/ion exchange	May have anion removal accompanied by release of OH^-
Evaporation/dilution	Produces general increase or decrease in ionic concentrations

Case Studies: Analysis and Interpretation of Aqueous Chemistry in Natural Waters

Controls on the Chemistry of Forest Floor Leachates

In this section, we shall examine a number of case studies in an effort to understand how and why aqueous chemistry changes during water movement through watershed ecosystems. To begin with a simple example, imagine a cool rainy morning high in the mountains of New England and consider how solution chemistry might change as water drips off the canopy and infiltrates through the thick forest floor horizon at the soil surface. Now, take a look at the data from a high-elevation balsam fir forest in New Hampshire shown in Table 9.5. On the left side of the table, the mean chemistry of canopy throughfall water is shown, along with mean ion concentrations in forest floor leachate solutions sampled in the field over a growing season. In contrast, numerical data on the right side of the table show results from an experiment in which undisturbed forest floors were removed from the same field site and were exposed to simulated rainfall events in a controlled environmental chamber. These data summarize the mean chemical composition of (i) artificial throughfall solutions applied to intact forest floor **microcosms** and (ii) leachate solutions collected beneath the forest floor micro-

Table 9.5 Comparative solution chemistry of forest floor inputs and outputs for a balsam fir forest in New Hampshire (data from Cronan 1980a, b). Concentrations are expressed in $\mu mol_c\ L^{-1}$; $RCOO^-$ represents organic anions.

	Field system		Laboratory microcosms	
	Canopy Throughfall	Forest Floor Leachate	Canopy Throughfall	Forest Floor Leachate
pH	4.02	4.04	4.00	4.01
Ca^{2+}	36	25	25	17
Mg^{2+}	14	15	10	10
K^+	37	16	20	36
NH_4^+	6	5	5	81
SO_4^{2-}	143	137	125	160
NO_3^-	12	8	20	22
Cl^-	13	16	19	27
$RCOO^-$	28	52	0	63

cosms. In comparing the two data sets, the major factor that distinguishes the field (left-hand) from the lab (right-hand) systems is the absence of living plant roots and active plant uptake processes in the lab microcosm forest floor cores.

Two major questions arise concerning the data in Table 9.5: (i) how can we account for changes in solution chemistry as canopy throughfall infiltrates the forest floor, and (ii) how is forest floor solution chemistry affected by field versus lab conditions? In terms of solution acidity, it is apparent that input and output pH values are similar in both field and lab systems, suggesting that these forest floor horizons exert minimal net influence on the free acidity of canopy throughfall solutions in the pH range of 4.0. However, Ca-ion concentrations in forest floor solutions are only two-thirds as large as throughfall inputs in both systems, indicating net removal of dissolved Ca in transit through the O horizon. Given the lack of active plant processes in the lab system, this evidence implies that the major net retention of Ca-ion in these forest floors occurs through abiotic cation exchange processes. In contrast to Ca, the concentration of divalent Mg-ion exhibits little net change between inputs and outputs for either the field or lab systems.

The behavior of K^+ ion is striking in that K^+ concentration drops by more than 50% in transit through the field O horizon, but increases by more than 75% in passage through the lab forest floors. This pattern implies that there is strong biological retention of K^+ ion in the field system where plant uptake processes are active. However, in the lab microcosms that lack plants, the forest floor solution is actually enriched in K^+ ion through mineralization or ion exchange processes. A similar pattern is evident for ammonium ion, with elevated concentrations of this ion in leachate solutions from lab forest floors that lack active plant uptake and have N mineralization rates in excess of microbial immobilization. Look at the patterns exhibited by sulfate, chloride, and organic acid anions ($RCOO^-$) in Table 9.5 and consider how you can account for these observations.

Comparison of Stream Chemistry Along a Hydrologic Flow Gradient

Aqueous chemistry evolves and changes in response to biogeochemical processes and hydrologic routing as water moves down a stream drainage gradient. Hence, we see a changing chemical signature in samples collected from upper to lower reaches of a stream system. As an example, Hauhs (1985) reported that stream chemistry in the uplands of a watershed in the Harz Mountains of Germany contrasted sharply with stream water collected several hundred meters downstream in the lower catchment (Table 9.6). In this particular case, there was a dramatic downstream increase in pH from 4.3 to 6.3. This decline in acidity was accompanied by a sharp rise in concentrations of Ca^{2+} ion and Mg^{2+} ion, and a decrease in the strong acid anions, SO_4^{2-} and NO_3^-. As such, these data imply that there was a downstream increase in ANC that was driven by two major influences: (i) watershed release of divalent cations from soil ion exchange and mineral weathering, and (ii) watershed retention of sulfate and nitrate ions through adsorption, absorption, or precipitation reactions. Why did these processes only manifest themselves in the lower reaches of the stream? Apparently, hydrologic sources for stream water in the lower elevations of the watershed were dominated by drainage water that followed a deeper flow path that permitted more extensive chemical transformation of aqueous chemistry.

Table 9.6 Comparison of stream chemistries in headwater and downstream reaches of Lange Bramke watershed in the Harz Mountains, Germany (Hauhs 1985). Upper and lower sample locations are ~500 m apart along the drainage gradient. Concentration units are $\mu mol_c\ L^{-1}$

Parameter	Headwater	Downstream	Change
pH	4.32	6.34	+2.02
Ca^{2+}	105	178	+73
Mg^{2+}	87	158	+71
K^+	24	24	0
Na^+	66	69	+3
SO_4^{2-}	288	242	−46
NO_3^-	97	70	−27
Cl^-	100	99	−1

Changes in Solution Chemistry and ANC Generation Along a Watershed Drainage Gradient

In an earlier study, our research team compared patterns of aqueous chemistry and solute transport in two forested watersheds located in Tennessee and New York (Cronan et al. 1990). As illustrated in Table 9.7 and Fig. 9.6, the northern and southern study watersheds exhibited strong differences in aqueous chemistry. Soil and stream drainage waters in the northern ecosystem were more acidic and contained higher concentrations of base cations, soluble aluminum, sulfate, nitrate, and organic carbon than waters in the southern watershed. What ecosystem processes might account for these differences?

The major differences in solution chemistry between the two watersheds were related to different patterns of alkalinity generation and mobile anion transport in these contrasting systems. In the northern watershed, atmospheric inputs of acidity were partially neutralized through the release of mixed cations (Ca, Al, Mg, K, and Na) from soils and detritus. Because of the high mobility of sulfate and nitrate in the northern watershed, there was significant transport of Al and base cations through the soil profile and into stream water. At the southern watershed, atmospheric inputs of strong acid produced a different outcome. In that ecosystem, soil sulfate

Table 9.7 Mean soil water and stream water chemistries in northern and southern watersheds (units = μmol L^{-1})

	Camp Branch WS, TN				*Big Moose WS, NY*			
	O[a]	B2	C	Stream	O	B2	BC	Stream
pH	4.43	5.10	5.22	5.15	4.24	4.55	4.79	4.65
Ca	18	14	7	7	36	44	56	44
Mg	18	26	15	18	8	10	14	10
K	44	12	14	14	37	11	14	10
Na	18	25	16	24	18	33	45	33
Al	16	3	2	3	42	72	61	33
SO_4^{2-}	48	47	18	24	60	88	108	73
NO_3^-	2	0	0	0	80	67	49	38
Cl^-	17	20	23	24	14	12	12	11
DOC	1140	175	65	115	1170	620	235	320

[a]Soil solutions in O, B, and C horizons were sampled with subsurface lysimeters (Cronan et al. 1990)

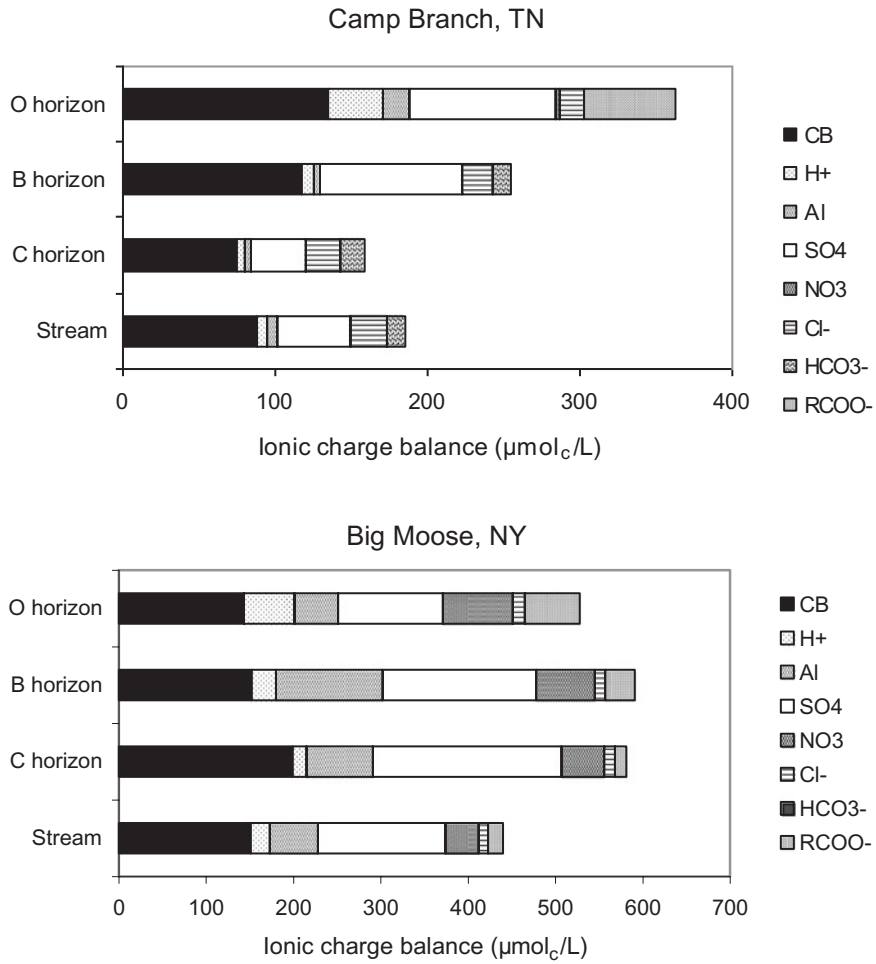

Fig. 9.6 Comparison of charge balance contributions of different ions in water samples collected along drainage gradients from O horizons to streams in southern and northern hardwood forest watersheds (Cronan et al. 1990)

adsorption, biological retention of nitrate, and base cation release were the major sources of acid neutralizing capacity for soil drainage waters and surface waters. Because these processes resulted in the release of alkalinity and the removal of mobile strong acid anions, solutions were dilute, only slightly acidic, and concentrations of soluble Al remained relatively low throughout most of the drainage profile in the southern watershed.

As a means of integrating the overall changes in aqueous chemistry, ANC budgets were prepared for the northern and southern watersheds using solution chemistry data and estimates of hydrologic transfers between ecosystem compartments (Fig. 9.7). In both watersheds, there was a gain of 1400 to 1500 mol_c ANC ha^{-1} comparing precipitation inputs to leachate outputs from the O horizon. ANC gain in the southern ecosystem was the result of base

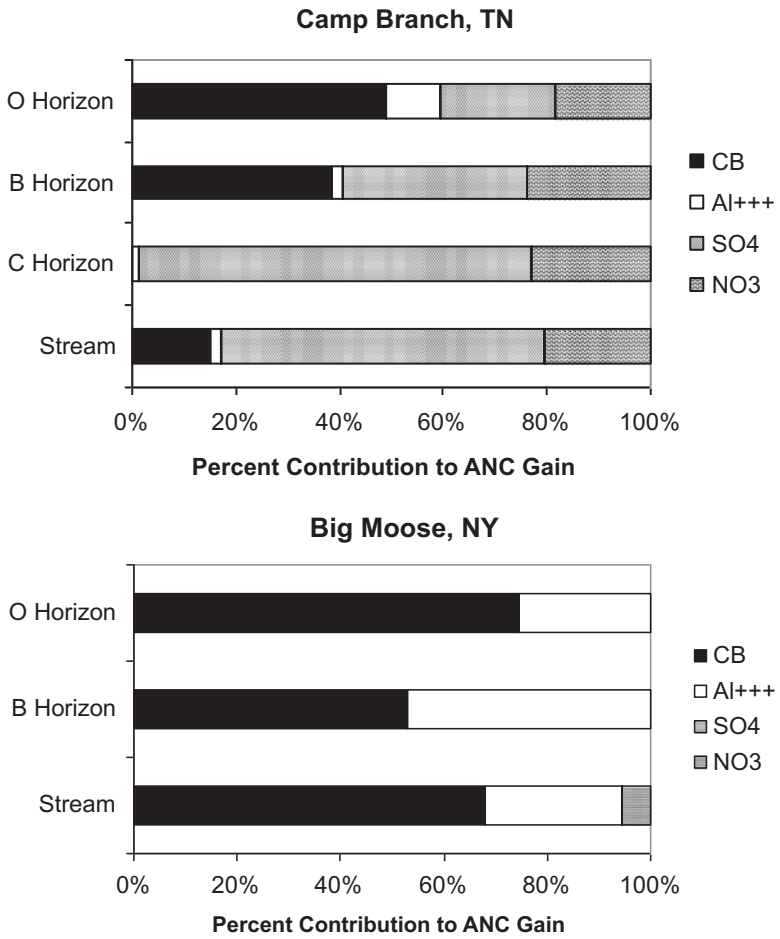

Fig. 9.7 Components of ANC generation in southern and northern watersheds. For each ecosystem level, the bar graph indicates the percentage of net ANC contributed by base cation release (C_B), release of ionic Al, sulfate adsorption, and nitrate uptake relative to rainfall inputs (Cronan et al. 1990)

cation release and strong acid anion removals, whereas ANC generation in the northern system was dominated by the release of base cations and soluble Al. Moving through the soil profile and down the hydrologic gradient to a comparison of stream water outputs for the two ecosystems (Fig. 9.7), there was a striking contrast in the relative sources of alkalinity. Analysis of stream water indicated that ANC generation in the southern site averaged roughly 1200 mol_c ANC ha^{-1} and this process was dominated by sulfate and nitrate retention in the watershed. In comparison, ANC gain in the northern watershed averaged 1900 mol_c ANC ha^{-1} and was dominated by the release of base cations and soluble Al.

Effects of Land Use on Watershed Exports of Nutrients in Stream Runoff

Land use activities, disturbance, and forest succession in a watershed can potentially affect the aqueous chemistry of drainage and stream waters. In the Aroostook River basin in Maine, we found that stream water concentrations of nitrate-N and Ca were positively correlated with the percentage of farming in a watershed (Fig. 9.8), whereas concentrations of dissolved organic carbon (DOC) were inversely correlated with the proportion of agricultural land in the surrounding watershed (Cronan et al. 1999). These patterns imply that the forested landscape is a relatively strong sink for N in the Aroostook River basin, but that increasing amounts of farming in a watershed lead to conditions of N enrichment, diminished retention of soluble N, and increased leaching of NO_3-N. The striking pattern of Ca exports suggests that streams draining cultivated watersheds are either enriched by leaching of agricultural lime amendments or by the weathering of richer geologic substrates that have been preferentially selected for farming activities. In contrast to these patterns, concentrations of DOC declined with increasing percentage of farming in a watershed, implying that agricultural systems are weaker sources for generation of DOC or are stronger sinks for DOC consumption or retention compared with watersheds dominated by forest and wetland cover.

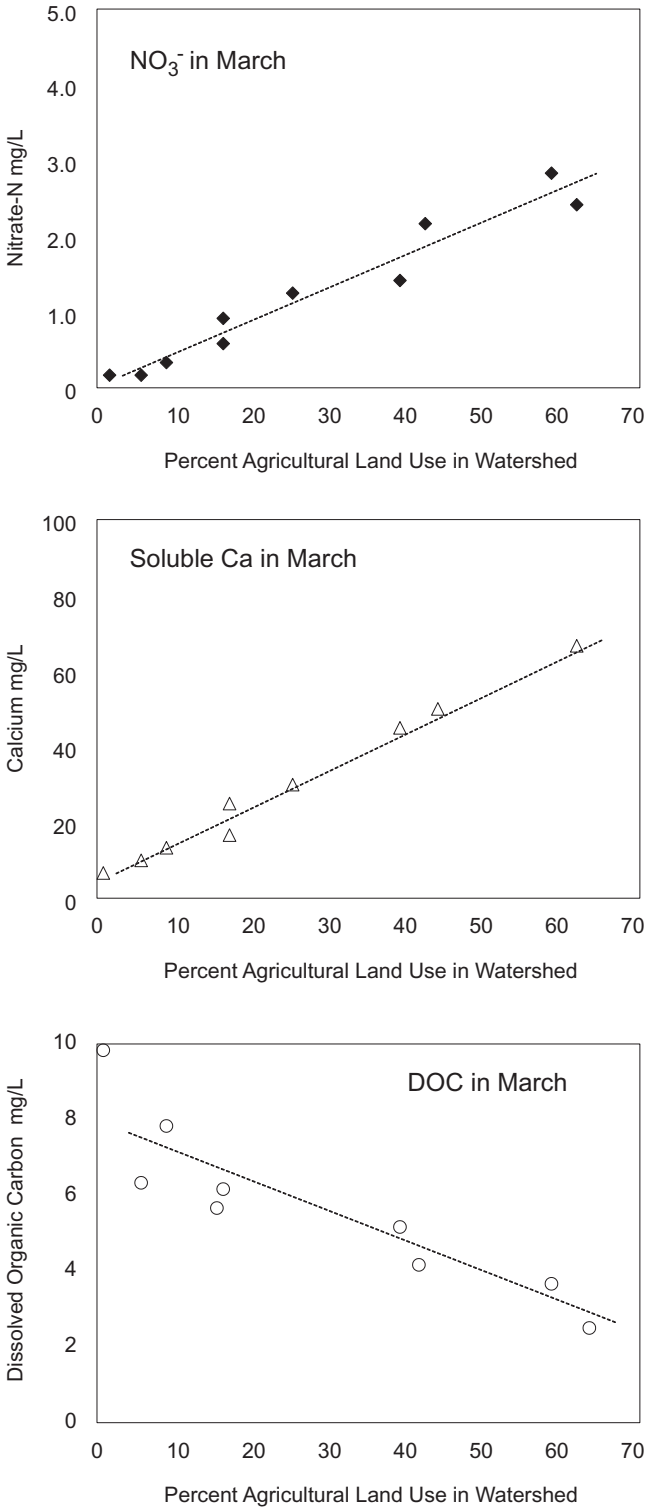

Fig. 9.8 Stream concentrations vary as a function of increasing farmland area in the Aroostook River Watershed, Maine (Cronan et al. 1999)

Integrated Element Cycling

10

Introduction

Previous chapters largely focused on the component biogeochemical processes and pathways that contribute to the structure and function of terrestrial ecosystems. This chapter integrates those processes to examine system-level cycling of nutrients and other elements at scales ranging from local forest stands to regional drainage basins, and includes a final section on global-scale cycling. Examples will illustrate the different ways in which elements accumulate and cycle under varying environmental conditions.

Element cycling is a simple concept that describes a vast and complex set of interacting processes that govern the distribution and movement of elements in the biosphere. Using the schematic diagram in Fig. 10.1, we can discuss some of the general principles of element cycling in a forest ecosystem (often referred to as *nutrient cycling*). For any given nutrient or element, it is possible to describe **pools** where the element is stored or accumulated and **fluxes** or transfers of the element between storage compartments or pools. In the figure, element pools include living biomass, geologic substrates, soil organic matter, and the soil exchange complex. Element fluxes include transfers in leaf litter, canopy leaching, soil leaching, stream export, and atmospheric deposition. It is also possible to discuss element cycling in terms of ecosystem **sources** and **sinks** for nutrients and other elements. For example, major sources for soluble N in a terrestrial ecosystem could include atmospheric deposition inputs and decomposition and mineralization of organic matter, whereas major sinks for soluble N could include plant and microbial biomass.

General Concepts of Element Cycling

In any given analysis of an element cycle or budget, investigators try to assemble their best estimates of the important pools, transfers, and increments of change in storage compartments. Depending upon the intensity and priorities of the study and the specific elements of interest, a biogeochemical analysis of an element cycle may include some or all of the major pools and processes listed in Table 10.1.

Although element cycling processes occur at a variety of time scales, many of the data sets for element cycles and budgets are reported as mean annual values. This time step is convenient in terms of providing a consistent measurement unit and requiring a reasonable level of sampling effort. However, the emphasis on annual estimates tends to limit our understanding of natural variations in element cycling that are associated with seasonal and phenological changes over shorter time periods.

Terminology

In discussions of element cycling, investigators sometimes use the terms uptake, requirement, and annual increment to quantify the behavior of a given nutrient. **Nutrient uptake**

C.S. Cronan, *Ecosystem Biogeochemistry*, Springer Textbooks in Earth Sciences, Geography and Environment, DOI 10.1007/978-3-319-66444-6_10

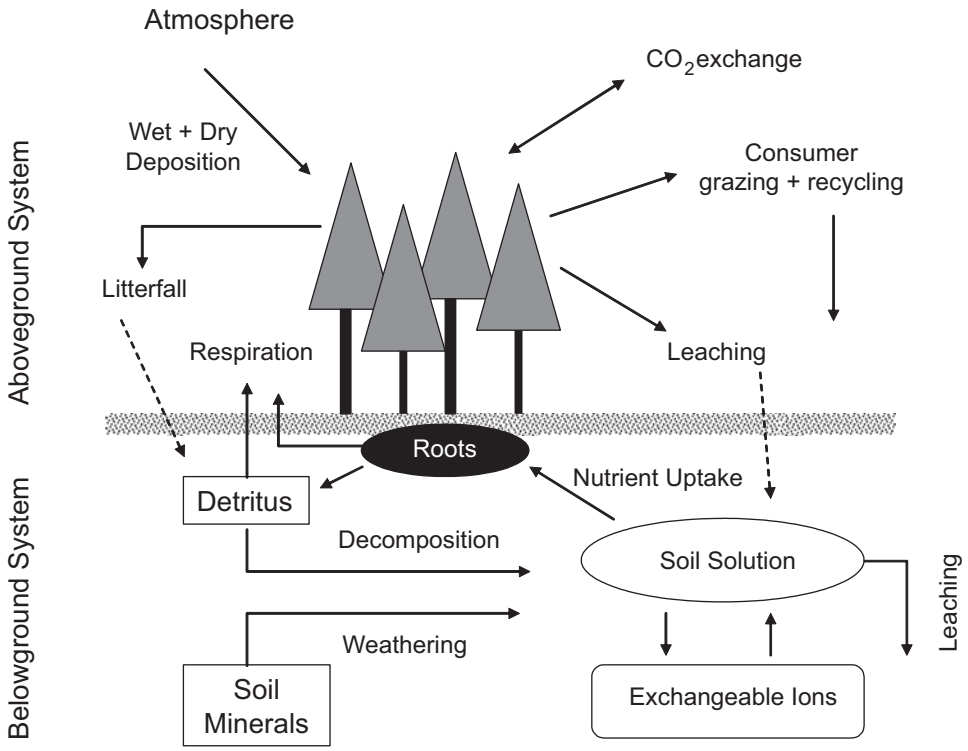

Fig. 10.1 Conceptual diagram of element cycling pools and fluxes in a forest

Table 10.1 Potential pools and processes for consideration in an element cycle or budget

Pools
Plant Biomass (foliage, branches, stem wood, woody roots, fine roots)
Microbial biomass
Forest floor detritus
Soil organic matter
Coarse woody debris
Soil solution
Soil minerals
Soil exchangeable ions
Transfers
Atmospheric wet and dry deposition
Plant uptake
Foliar resorption
Litterfall – foliage, branches, wood
Canopy leaching of inorganic and organic solutes
Mortality and turnover of roots (fine and coarse)
Microbial mineralization
Microbial immobilization
Gaseous transfers
Mineral weathering
Soil leaching of inorganic and organic solutes
Stream runoff of inorganic and organic solutes
Increments or Decrements for the Element
Net primary production by tissue type and aboveground versus belowground
Net microbial biomass increment via immobilization
Net accumulation or loss in forest floor or SOM
Changes in soil exchangeable ions
Tree mortality resulting in changes in live biomass and coarse woody debris pools

can be defined as the annual plant increment of an element accumulated in new woody tissues plus annual losses of that element through litterfall, root turnover, leaching, and net stemflow. The **nutrient requirement** for a forest stand is the annual **element increment** associated with production of new shoot and root tissues plus current year foliage. Depending upon the element of interest and site conditions, annual uptake of a given nutrient may be more or less than the nutrient requirement. For a nutrient such as nitrogen, a forest may meet part of the annual requirement by using previously resorbed and stored N, while the remaining requirement for N is taken up by the root system or is absorbed directly by foliage exposed to atmospheric deposition inputs. In contrast, uptake of potassium by a forest ecosystem may be much greater than annual requirement, because K^+ is readily leached from foliage and therefore must be replaced continuously during the year.

Comparison of Element Cycles in Terrestrial Ecosystems

Patterns of element cycling vary among elements and are also influenced by differences in species composition and site conditions among contrasting ecosystems. In this section, element cycles for nitrogen, calcium, and aluminum will be examined using comparative data from the literature.

Nitrogen Cycle

Despite the central importance of nitrogen cycling in terrestrial ecosystems, the literature contains few detailed and complete nitrogen budgets for forested watershed ecosystems. Nevertheless, we can use the examples in Table 10.2 to explore some of the general patterns of N cycling in forested ecosystems. To begin, we might ask how much N is required to meet the annual demand or requirement for a growing mature forest. In the northern hardwood forest at Hubbard Brook, NH, the annual N requirement for above and belowground plant production is roughly 120 ± 20 kg N ha^{-1}. Of this total requirement, perhaps 25% of the N demand is supplied from recycled N derived from foliar resorption in the previous year. Another 7–8% of the N demand can be accounted for by atmospheric deposition. Thus, roughly two-thirds of the N required for production of foliage, woody tissues, and roots in this hardwood forest must originate via mineralization of detritus and soil organic matter by soil microbes. This estimate of 80 kg N ha^{-1} yr^{-1} represents about 7% of the pool of forest floor N and 1.5–2.0% of the combined forest floor and mineral soil pool of N. As shown in Table 10.2, total annual N mineralization at the Hubbard Brook forest may actually be as much as 50% higher than that estimate, or roughly 120 kg N ha^{-1} yr^{-1}. In other studies, annual N mineralization rates have been reported to be approximately 115 kg N ha^{-1} yr^{-1} in a western conifer forest at HJ Andrews Forest, OR (Sollins et al. 1980) and 90 kg N ha^{-1} yr^{-1} in northern hardwood stands in Michigan (Fisk et al. 2002).

Table 10.2 Annual nitrogen budgets for four North American forested watersheds: northern hardwoods at Hubbard Brook Experimental Forest, NH (HBEF), chestnut oak at Walker Branch Watershed, TN (WBW), western conifers at HJ Andrews Forest, OR (HJA), and sugar maple stands in Michigan (SMMI)

Component	HBEF[a]	WBW	HJA	SMMI
Pools (kg N ha^{-1})				
Biomass				
Aboveground	350	430	–	600
Belowground	180	100	–	–
Forest Floor	1100	300	–	500
Mineral Soil	3600	4700	–	–
Transfers + Transformations (kg N ha^{-1} yr^{-1})				
Atmospheric Deposition	8	13	2	13.5
Mineralization	70–120	–	117	90
Plant uptake	80–105	62	42	16–40
Foliar resorption	35–40	38	18	–
Litterfall	45–55	34	18	19
Root Turnover	6–60	–	22	–
Canopy Throughfall + SF	9	3	1	0
Denitrification	–	–	–	–
Microbial immobilization	–	–	–	–
Stream Runoff export	4	3	1.5	–
Annual Increments or Changes (kg N ha^{-1} yr^{-1})				
Plant Biomass Increment	9	25	–	0–16

[a]From Likens et al. (1977), Johnson and Henderson (1989), Sollins et al. (1980), Fisk et al. (2002)

Mineral soil organic matter (SOM) is generally the largest pool of stored N, followed by forest floor detritus and plant biomass (Table 10.2). Johnson and Turner (2014) estimated that the overall median N content of litter plus SOM is 5900 kg N ha^{-1}. They also noted that the vast majority of forest ecosystems contain less N than would be expected from even modest cumulative inputs from atmospheric deposition and N fixation. They suggested that the reason for this is periodic fire, which can remove large amounts of N by volatilization, even in humid ecosystems when they experience droughts.

As illustrated in Table 10.2, nitrogen fluxes associated with litterfall, foliar resorption, and fine root turnover are generally of the same magnitude, ranging from about 20–60 kg N ha^{-1} yr^{-1}. Much smaller fluxes (on the order of 0–9 kg N ha^{-1} yr^{-1}) are associated with leaching and washout of N in canopy throughfall and stemflow (Table 10.2). In these undisturbed forest ecosystems, stream exports of N (1–4 kg N ha^{-1} yr^{-1}) are smaller than N inputs from atmospheric deposition. Assuming that denitrification outputs of gaseous N are low in these ecosystems, the N budgets imply that these forested watersheds are acting as sinks for N retention.

Forests generally act as effective sinks for moderate N additions, although watershed losses of N are stimulated by chronically elevated N inputs. In the northeastern U.S., 50–100% of atmospheric inputs of inorganic N are retained on an annual basis by forested watersheds (Aber et al. 2003). Christ et al. (1995) added up to 520 kg N ha^{-1} yr^{-1} for 2 yr to an American beech stand at Hubbard Brook Forest, NH using ammonium sulfate, and found that plots retained >95% of added N. In the Netherlands, Koopmans et al. (1996) studied the fate of ^{15}N added to N-saturated Douglas fir and Scots pine forests receiving addition rates of 5 and 50 kg N ha^{-1}. In low N-input plots, 95% of the isotope was retained, while high N-input plots retained 80–90% of the ^{15}N. Gundersen (1998) reported that a 75-yr-old Norway spruce stand in Denmark exposed to chronic annual additions of 35 kg N ha^{-1} as ammonium nitrate retained 92% of added N inputs. A comparison of European watersheds by Dise et al. (1998) suggested an average retention rate of nearly 65%, with higher retention in systems receiving more ammonium than nitrate. It should be noted that retention of added N in forest soils tends to narrow C:N ratios over time, which can lead to increased rates of net nitrification by soil microbes and increased potential for nitrate export.

Table 10.3 Annual calcium budgets for North American forest ecosystems, including northern hardwoods at Hubbard Brook, NH (HBEF), oak forest at Walker Branch Watershed, TN (WBW), western conifers at HJ Andrews Forest, OR (HJA), eastern hardwoods at Coweeta Hydrologic Lab, NC (CW), slash pine in FL (SP), loblolly pine in MS (LP), and high elevation forest, NY (HEF).

Component	HBEF[a]	WBW	HJA	CW	SP	LP	HEF
Pools (kg Ca ha^{-1})							
Biomass Ca	480	980	750	830	–	90	350
Forest Floor Ca	370	430	570	130	–	80	390
Soil exchangeable Ca	510	710	4450	940	–	–	515
Total soil Ca	9600	3800	–	2500	–	–	–
Transfers + Transformations (kg Ca ha^{-1} yr^{-1})							
Atmospheric deposition	2	16	4	–	5	5	3
Litterfall	41	55	41	44	20	–	–
Canopy leaching/washout	7	14	8	8	7	3	3
Plant uptake	62	100	45	75	23	–	–
Mineralization of detritus	42	–	64	–	–	7	–
Woody increment	8	31	0	23	–	–	–
Root turnover	3	–	25	–	–	–	–
Mineral weathering	21	–	119	–	–	–	9
Stream export	14	147	123	–	–	–	7

[a]Data from Likens et al. (1998), Johnson and Henderson (1989), Sollins et al. (1980), Henderson et al. (1978), Gholz et al. (1985), Switzer and Nelson (1972), Friedland and Miller (1999)

Calcium Cycle

There are few comprehensive examples of Ca budgets for forested watersheds in the literature, but the data compiled in Table 10.3 provide a basis for examining general patterns of Ca cycling. On an annual time step, plant uptake of Ca by forest communities is relatively large, ranging from ~45 to 100 kg ha^{-1}. Much of the annual demand for Ca is met by microbial mineralization of detritus and mineral weathering, whereas atmospheric deposition is generally a much smaller source of available Ca. As an example, annual transfers of available Ca at Hubbard Brook Experimental Forest, NH are dominated by mineralization (42 kg ha^{-1} yr^{-1}) and weathering (21 kg ha^{-1} yr^{-1}), with a small contribution from atmospheric deposition of Ca (2 kg ha^{-1} yr^{-1}). In comparison, Ca demand at HJ Andrews Forest, OR is largely met by solution transfers from weathering (119 kg ha^{-1} yr^{-1}) and mineralization (64 kg ha^{-1} yr^{-1}), with atmospheric inputs amounting to only ~4 kg ha^{-1} yr^{-1} (Table 10.3). Annual recycling of Ca by forest communities includes a large flux of Ca in litterfall (up to 50–60 kg ha^{-1} yr^{-1}), a smaller transfer of Ca in canopy leaching and washout (<10–15 kg ha^{-1} yr^{-1}), and small to medium Ca transfers in root turnover. In contrast to the element N, Ca is virtually immobile in plants and is therefore not recycled internally via foliar resorption processes. Stream exports of Ca vary as a function of geologic conditions and mobile anions in a given watershed, but range from lower values on the order of 5 to 15 kg ha^{-1} yr^{-1} at sites such as HBEF in New Hampshire up to larger fluxes approaching 150 kg ha^{-1} yr^{-1} at WBW in Tennessee.

In most watersheds, soil and bedrock minerals contain the largest pool of stored Ca, and it is this reservoir that slowly replenishes ecosystem Ca through mineral weathering processes. At HBEF and WBW, the pools of total Ca in the soil profile are estimated to be approximately 9600 and 3800 kg ha^{-1}, respectively. By comparison, plant biomass and soil exchangeable cation pools of Ca generally range from 500 to 1000 kg ha^{-1}. A final important storage pool for Ca is the forest floor horizon, which typically contains roughly 100 to 500 kg ha^{-1} of organically bound and mineral particulate Ca.

Aluminum Cycle

Aluminum is a nonessential element for living organisms, but is a critical geochemical component of most forest ecosystems. As such, the cycling of aluminum provides an interesting contrast with nutrients such as nitrogen or calcium. In those watersheds where Al has been examined, it is estimated that the biomass pool of Al ranges from roughly 10 to 75 kg ha^{-1}. This small accumulation of Al in forest biomass is consistent with the expected behavior of an element that is not readily taken up or recycled within plants. Although Al uptake rates have not been examined in most field studies, the data in Table 10.4 indicate that very little Al is recycled in litterfall (generally <1.5 kg ha^{-1} yr^{-1}) and combined canopy leaching + washout (<3 kg ha^{-1} yr^{-1}). Thus, we do not generally observe a strong direct plant influence on the cycling of Al in forest ecosystems.

With Al cycling, we are forced to look belowground at the forest floor and mineral soil in order to see the major sources, sinks, and transfers of this element (Fig. 10.2). Most soils contain large amounts of Al that can be selectively extracted or digested into various operationally-defined pools. For example, amorphous Al hydroxides and oxides occur in soils at 12,000 to 73,000 kg ha^{-1}, Al adsorbed to organic humic substances ranges from roughly 2000 to 7000 kg ha^{-1}, and KCl-exchangeable ionic Al ranges from approximately 500 to 4500 kg ha^{-1} (Table 10.4). In comparison, forest floor horizons have been shown to contain smaller amounts of Al ranging from 100 to 850 kg ha^{-1}.

The transfer of aqueous Al in soil drainage waters and streamflow varies among watersheds as a function of biogeochemical conditions. Although many soils exhibit elevated fluxes of soluble Al moving through surface organic horizons (on the order of 2 to 9 kg ha^{-1} yr^{-1}), Al transfers through mineral subsoils can range widely from values <0.2 kg ha^{-1} yr^{-1} to fluxes of >50 kg ha^{-1} yr^{-1} (Table 10.4). These differences in Al transfers are largely controlled by the acidity and anion chemistry of each soil. Similarly, the export of Al in stream water can vary considerably from less than 1 to more than 7 kg Al ha^{-1} yr^{-1}, depending on the hydrologic sources and ANC of stream runoff (Table 10.4 and Fig. 10.2).

Table 10.4 Annual budgets for aluminum cycling at Big Moose, NY (BMW), Camp Branch, TN (CBW), Tunk Mt., ME (TMW), Findley Lake, WA (FLW), Pine Barrens, NJ (PBW), and Solling, Germany (SP)

	BMW[a]	CBW	TMW	FLW	PBW	SP
Pools (kg Al ha^{-1})						
Biomass	–	–	17	74	8	–
Forest Floor	–	–	840	255	110	370
Soil						
Exchangeable Al	1510	4670	–	–	530	–
Humic Al	6880	2290	–	–	–	–
Amorphous Al hydroxides	72,900	11,800	–	–	–	–
Transfers (kg Al ha^{-1} yr^{-1})						
Atmospheric deposition	–	–	0.2	–	–	–
Litterfall	0.4	4.7	0.7	1.2	2	–
Canopy leaching/ washout	–	–	0.1	0.3	1.4	2.9
Plant uptake	–	–	–	–	–	–
Mineralization	–	–	0	–	–	–
Woody increment	–	–	–	–	–	–
Root turnover	–	–	0.6	59	–	–
Mineral weathering	–	–	–	–	–	–
Soil solution by horizon						
O/A	8.6	1.8	2.1	–	3.1	–
B	17	0.5	–	–	3.6	51.5
C	0.5	0.2	–	–	3.6	–
Stream export	7.3	0.5	2.6	–	–	–

[a]Data for all sites from Cronan (1994)

Nutrient Cycling in Relation to Ecosystem Succession

One of the central ecological paradigms proposed by Odum (1969) and echoed in other subsequent publications is the proposition that terrestrial ecosystems exhibit greater conservation of nutrients and more closed nutrient cycles as they proceed through succession toward maturity (often termed old-growth or "climax" conditions). Woodwell (1974a) expressed similar views, stating that "mature systems are tight; disturbance causes leakage of nutrients" and noting

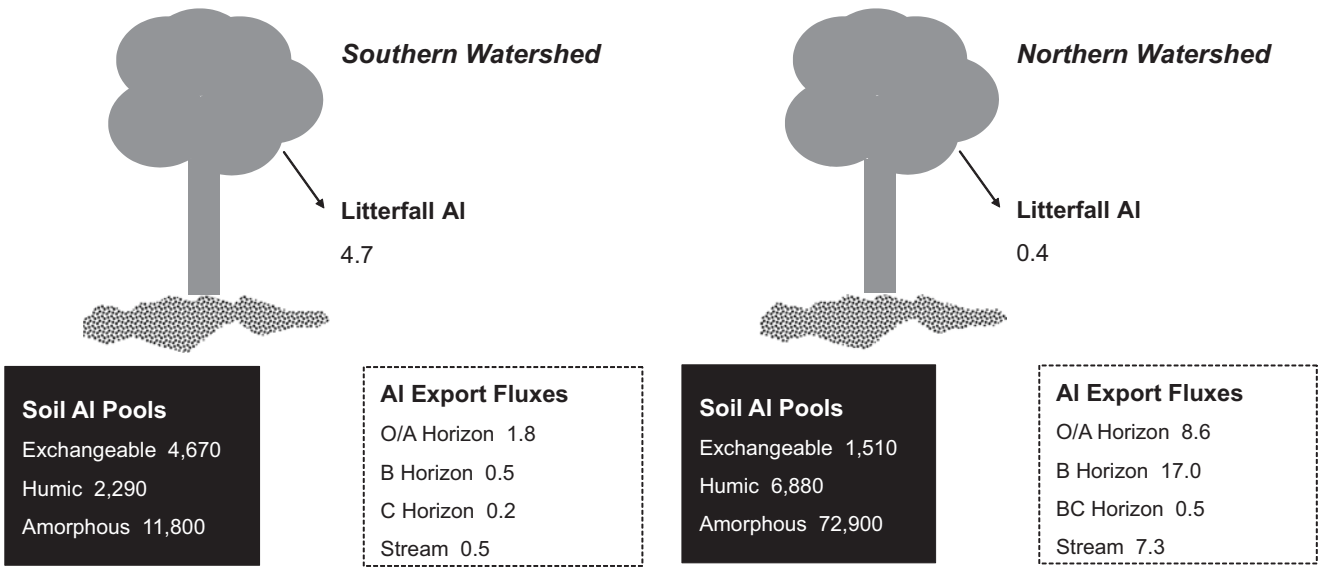

Fig. 10.2 Comparison of Al pools and cycling in northern (Big Moose, NY) and southern (Camp Branch, TN) watersheds (Cronan et al. 1990). Units are kg Al ha^{-1} for pools and kg Al ha^{-1} yr^{-1} for fluxes

elsewhere that "more mature stages use nutrients and energy more efficiently". As these themes were tested and challenged, investigators began to refine our understanding of the relationships between succession and patterns of element cycling in watersheds.

In their conceptual analysis of ecosystem succession and nutrient retention, Vitousek and Reiners (1975) hypothesized that changes in **net ecosystem production (NEP)** are a major determinant of element export fluxes in terrestrial ecosystems. The authors argued that during primary succession, element outputs in stream runoff are initially high (roughly equal to inputs) and then decline to a minimum as elements are accumulated in biomass and detritus during mid-succession when NEP is highest. Their model also predicted that output rates eventually rise again in late succession when NEP approaches zero and inputs are roughly balanced by outputs. A major part of their paradigm shift focused on the notion that steady-state conditions (where inputs equal outputs) are to be expected in more mature non-aggrading ecosystems. The authors noted that secondary succession is often accompanied by negative NEP immediately following disturbance, so that output rates can exceed input rates during early succession. In a follow-up to that publication, the authors revised their hypothesis somewhat to clarify the point that absolute inputs and outputs of elements can both vary considerably from the beginning to the end of ecosystem succession, and that output patterns will depend on the element under consideration, the nature of the parent material, and interactions among multiple ecosystem processes (Gorham et al. 1979).

During the same time period, Bormann and Likens (1979) wrote about this subject and questioned Odum's contention that ecosystem development is accompanied by a trend toward tighter nutrient cycles. They argued that the greatest regulation over watershed nutrient export occurs in the "Aggradation Phase" of second-growth forest recovery (first 100 yr or so), and that increased nutrient loss is observed as a forest approaches and enters the "Shifting-Mosaic Steady-State". They agreed with Vitousek and Reiners (1975) that there "is little doubt that total biomass storage plays a major role in regulating nutrient export from the northern hardwood ecosystem". Similarly, they agreed with Gorham et al. (1979) that other factors besides biomass storage may change with time and affect patterns of element inputs and outputs. Since that period of dynamic debate, ecosystem ecologists have tended to reject the original nutrient conservation hypothesis proposed by Odum (1969) in favor of the interpretation of Vitousek and Reiners (1975) and others.

Chemical Input-Output Budgets for Watershed Ecosystems

Watershed ecosystems are often analyzed and are compared using chemical budgets based on inputs in atmospheric deposition and outputs in stream runoff (Gorham et al. 1979). When the budget is expressed as the annual input of an element (I) minus annual output in runoff (O), the resulting net difference (I – O) indicates whether the watershed is acting as a **source** or a **sink** for that element. If outputs are less than inputs (I > O), the difference term is positive and the ecosystem is assumed to be accumulating that element in biotic or abiotic storage pools. In contrast, if outputs are greater than inputs (I < O), the negative difference term implies that the ecosystem serves as a source for exports of that element. Finally, if element inputs are equivalent to outputs (I = O), a watershed is assumed to be in a more or less **steady-state** condition with respect to that element.

For illustration, we can compare chemical budgets for two different forested watersheds in the eastern U.S.: Hubbard Brook Experimental Forest, NH (HBEF) and Walker Branch Watershed, TN (WBW). HBEF is a mature northern hardwoods forest underlain by glacial till and igneous/metamorphic rocks, whereas WBW is a mature southern hardwoods forest underlain by soils and residuum derived from dolomitic limestone. As shown in Table 10.5, both watersheds exhibit similar general patterns of export of magnesium, potassium,

Table 10.5 Comparison of chemical budgets for selected elements at Hubbard Brook Experimental Forest, NH and Walker Branch Watershed, TN (Likens et al. 1977; Johnson and Henderson 1989). Units are in kg ha^{-1} yr^{-1}.

Element	Inputs	Outputs	Inputs – Outputs
Magnesium (Mg)			
Hubbard Brook	0.6	3.3	−2.7
Walker Branch	2.1	77.1	−75.0
Calcium (Ca)			
Hubbard Brook	2.2	13.9	−11.7
Walker Branch	14	148	−134
Potassium (K)			
Hubbard Brook	0.9	2.4	−1.5
Walker Branch	3.1	6.8	−3.7
Sodium (Na)			
Hubbard Brook	1.6	7.5	−5.9
Walker Branch	3.9	4.5	−0.6
Sulfate-S			
Hubbard Brook	18.8	17.6	+1.2
Walker Branch	18.8	11.3	+7.5
Nitrogen (N)			
Hubbard Brook	20.7	4.0	+16.7
Walker Branch	8.7	1.8	+6.9

calcium, and sodium, and accumulation of sulfur and nitrogen. However, the magnitude of these source and sink patterns differ, because of underlying differences in environmental conditions. The export of base cations from both watersheds suggests that mineral weathering provides a net source of cations to stream runoff. Yet, the very large export of Ca and Mg from WBW implies that the carbonate bedrock is a much stronger source for divalent cations, compared to the glacial till and resistant bedrock of the northern site. On the other hand, soil minerals and bedrock at HBEF are a larger source of Na for stream runoff as compared with the dolomitic limestone that dominates the southern ecosystem.

How do we account for the positive chemical budgets for N and S in the two watersheds? At WBW, the strong retention of sulfate-S is largely the result of sulfate adsorption in the Ultisol soils of this southern watershed. At HBEF, the relatively small net retention of sulfate-S may be the result of biotic and abiotic retention mechanisms or may be an insignificant difference resulting from estimation inaccuracies. In effect, the HBEF watershed may currently be in a near steady-state condition with respect to sulfate-S, although studies by Likens et al. (2002) suggest that net exports of sulfate-S are increasing. Based on the striking retention of N in each watershed, there is a clear indication of the presence of strong biotic sinks for N at HBEF and WBW.

Investigators have also applied chemical budgets to watersheds in an effort to examine the fate of strong acids derived from atmospheric deposition. For example, Paces (1985) reported that inputs of H^+ ion in wet deposition at four Czechoslovakian watersheds ranged from 37 to 46 mmol m^{-2} yr^{-1}, whereas exports of H^+ ion were negligible. Thus, the study watersheds acted as very strong sinks for H^+ ion, which was consumed in weathering and soil cation exchange reactions.

Element Cycling at the Landscape Scale: Exports of N and P from Large Watersheds

David and Gentry (2000) examined large scale patterns of nutrient cycling across the agricultural, suburban, and urban landscapes of Illinois, USA. The authors calculated net anthropogenic inputs of N and P as inputs of fertilizer, atmospheric deposition, and N_2 fixation minus net exports of N or P in grain or animal products. Estimated net anthropogenic inputs of N were roughly 32 kg N ha^{-1} yr^{-1}, whereas N export fluxes for major river systems in Illinois ranged from 5 to 24 kg N ha^{-1} yr^{-1} and averaged 17 kg N ha^{-1} yr^{-1}. Thus, riverine export flux of N was >50% of estimated anthropogenic inputs. Over the study period from 1979 to 1996, the net input of N to Illinois was estimated at >8.6 million Mg N (Mg = 10^6 g), compared with riverine exports of 4.4 million Mg N. The authors assumed that the majority of the 4.2 million Mg N retained by the Illinois landscape was actually recycled to the atmosphere via denitrification. They also described a huge internal cycle of ammonia, where perhaps 50% of the N in manure was volatilized as NH_3 over the Illinois landscape.

Phosphorus exhibited a more conservative pattern of cycling in the Illinois landscape. The authors reported that net annual anthropogenic P inputs were high through the year 1990, but declined to minimal levels after that time period. Annual P exports in river runoff ranged from 0.7 to 1.1 kg ha^{-1} yr^{-1}, with 38% in dissolved forms and 62% of total P in particulate forms. Over the period from 1979 to 1996, cumulative P inputs to the landscape were 739,000 Mg P, whereas riverine exports in Illinois amounted to 255,000 Mg P. The authors assumed that soil sorption of P helped to conserve roughly two-thirds of anthropogenic P inputs to the Illinois landscape. Elsewhere, rising exports of riverine P have been reported for watersheds in China containing intensive agriculture or high population densities (Chen et al. 2015; Zhang et al. 2015).

Castro et al. (2000) conducted a broad landscape analysis involving 34 watersheds in the eastern U.S. Net anthropogenic inputs of N were calculated as the sum of fertilizer inputs, N_2 fixation, atmospheric deposition of nitrate-N, net import of N in food, and net import of N in livestock feed. Annual N inputs ranged from 6 to 71 kg N ha^{-1} yr^{-1} among the 34 watersheds, with a mean net anthropogenic input of 28 kg N ha^{-1} yr^{-1}. Major sources of N inputs varied among regions. In the northeastern U.S., net food import and atmospheric deposition of nitrate-N accounted for 49% and 22% of total N inputs, respectively. In contrast, N fertilization (29%) and net food import (24%) dominated net N inputs to the watershed of Delaware Bay, whereas net livestock feed import (31%) and N fertilization (26%) were the dominant inputs to watersheds draining into Chesapeake Bay. Overall, the authors estimated that watershed retention of anthropogenic N [(inputs – outputs)/inputs] ranged from 18 to 80% among watersheds, with a mean annual retention of 62%.

Element Cycling at the Global Scale

Global Nitrogen Cycle

Nitrogen cycles at the watershed and landscape levels are all linked to a dynamic global nitrogen cycle involving atmospheric, terrestrial, freshwater, and marine compartments and fluxes. For example, the increasing local use of fertilizer

Table 10.6 Global nitrogen cycle based on estimates from Vitousek et al. (1997) and Schlesinger (1991)

Nitrogen Pools	Units = Tg = 10^{12} g
Atmosphere	3.8 billion
Soils	95,000
Plant biomass	3500
Annual Inputs to Reactive N Pool	
Lightning fixation	<10
Natural biological N_2 fixation	
Terrestrial	140
Marine	>30
Anthropogenic fixation	140
Annual Transfers of N	
Denitrification	240
River runoff to oceans	40
Burial in ocean sediments	10
Internal Cycling of N in Biosphere	
Terrestrial	1200
Marine	6000

Table 10.7 Global carbon cycle based on estimates from Schlesinger (1991). Units = 10^{15} g C = gigaton = billion metric tons = Pg (petagrams)

Carbon pools	
Atmosphere	720
Land plants	560
Soils	1500[a]
Oceans	38,000
Fossil fuels and shale	5000
Annual Transfers into Atmospheric Pool	
Respiration	
Terrestrial	122
Marine	105
Fossil fuel combustion	5
Annual Uptake from Atmospheric Pool	
Photosynthesis	
Terrestrial	120
Marine	107
Annual increase in Atmospheric CO_2	3

[a]Upper 1 m of soil

in Chinese agriculture has greatly enhanced global microbial emissions of nitrous N_2O (nitrous oxide), a greenhouse gas that contributes to increased global warming potential in the atmosphere. Thus, local and regional changes in nitrogen cycling have potential implications for global biogeochemical processes.

As indicated by the data summarized in Table 10.6, the global N budget is dominated by a huge pool of **unreactive** N_2 gas in the atmosphere. Much smaller quantities of reactive or biologically available N are found circulating through the biosphere. Compared with the atmospheric pool of N (3.8 billion Tg), soils contain roughly 95,000 Tg of N and terrestrial plant biomass contains approximately 3500 Tg N. It is estimated that natural background levels of N fixation from lightning, terrestrial biological N_2 fixation, and marine N_2 fixation have historically amounted to as much as 150 to 200 Tg yr^{-1} (Table 10.6). However, human production of fertilizers, combustion of fossil fuels, and expansion of agriculture have contributed an additional 140 Tg N to annual inputs of reactive N in the global N budget (Vitousek et al. 1997). Thus, the influence of human activities has roughly doubled annual sources of reactive N in the biosphere.

What are the major cycling pathways for reactive N inputs in the global N budget? As shown in Table 10.6, there is a vigorous internal circulation of N in the biosphere involving the recycling of perhaps 1200 Tg N yr^{-1} in terrestrial systems and 6000 Tg N yr^{-1} in marine systems. In addition, roughly 240 Tg N is returned to the atmosphere each year via microbial denitrification from terrestrial, aquatic, and marine systems. Another 40 Tg of N is exported from terrestrial systems to the oceans in river runoff, and approximately 10 Tg N is buried in ocean sediments. Remaining annual inputs of reactive N accumulate in living biomass and contribute to enrichment of the atmosphere with trace gases such as N_2O, NO, and NO_2.

Global Carbon Cycle

In recent years, there has been intense interest in understanding the global carbon budget, because of interactions between rising concentrations of atmospheric CO_2, global warming, and climate changes. The modern trend of atmospheric enrichment with CO_2 stems from an imbalance in the relative rates of CO_2 release from respiration plus combustion versus the offsetting rates of CO_2 absorption and storage in the biosphere. Currently, the enhanced CO_2 release from fossil fuel combustion and land clearing activities exceeds the assimilation and sequestration of CO_2 in biomass, new detritus, and ocean systems.

As indicated in Table 10.7, the major storage reservoirs in the global carbon budget include the following pools: oceans (38,000 Pg), fossil fuels and shale (5000 Pg), soils (1500 Pg), atmosphere (720 Pg), and land plants (560 Pg). Annual transfers of C into the atmospheric reservoir include large fluxes from terrestrial (122 Pg) and marine (105 Pg) respiration, plus a smaller but significant flux from fossil fuel combustion amounting to approximately 5 Pg C yr^{-1}. This annual

transfer of 232 Pg C yr^{-1} is largely offset by annual photosynthetic uptake from the atmospheric pool by terrestrial (120–122 Pg) and marine (107 Pg) systems. Residual C that is not absorbed and sequestered in terrestrial or ocean pools contributes to annual increases in atmospheric CO_2 amounting to about 3 Pg C yr^{-1}.

At present, the global C budget contains various degrees of certainty and uncertainty. While we are reasonably confident of estimates of annual C emissions associated with fossil fuel combustion and annual increases in mean global CO_2 concentration, many other parts of the budget are less certain. In particular, scientists are continually trying to improve estimates of C transfer rates between the atmospheric pool and C reservoirs in biomass, soils, and the oceans. For example, the source-sink behavior of forested land in different regions of the biosphere is under investigation to determine the extent to which net C sequestration in forests can account for observed rates of CO_2 increase in the atmosphere.

Biogeochemical Models

11

Introduction

Part of our insatiable quest for scientific understanding is really an effort to assemble an integrated knowledge base that allows us to extrapolate and to make predictions about the behavior of living systems and the environment. Although some natural systems are relatively simple, many others are complex and contain intricate relationships and feedbacks. Whatever the level of complexity, it can be very useful to have a framework or a model for integrating current understanding about a particular system of interest. In scientific terms, a **model** can be defined as a qualitative conceptual or quantitative numerical representation of a process, pattern, or system. According to Levin (1999), models provide a tool for making connections between observations and the mechanisms responsible for those phenomena. Biogeochemical models range in scale and complexity from rudimentary exponential decay equations describing the loss of leaf mass in decomposing litter (Fig. 11.1) to large integrated ecosystem models capable of simulating the dynamic patterns of energy flow, nutrient cycling, and hydrologic routing in a watershed. In this chapter, we will examine how biogeochemical models provide valuable tools for integrating knowledge and synthesizing new insights regarding element cycling patterns and processes.

There are a number of compelling reasons why models are valuable tools in biogeochemistry. Whenever a model is designed and developed, the investigators are forced to define what is known about the ecological patterns or processes in the model framework and to identify the key interactions controlling changes in the ecological system of interest. Not only is this process of synthesis and integration important by itself, but it also helps investigators to identify information gaps in our understanding and to target areas for further empirical or experimental investigation. Biogeochemical models are most effective when they are used as a synergistic tool to complement the efforts of empirical or experimental research; in this interactive role, models can contribute to achieving the major goals listed in Table 11.1.

Considerations in the Development of a Biogeochemical Model

Suppose we wished to design a numerical model to simulate carbon cycling processes in a forested watershed. How would we organize a strategy to accomplish this task? To begin, it would be important to state the objectives of the modeling exercise and to list the kinds of biogeochemical or ecological questions that would be addressed by the carbon cycling model. At every step, it would be necessary to determine which assumptions would be incorporated into the model in terms of key variables, processes, interactions, and simulation time steps. For example, would it be acceptable to assume that tissue respiration varies with temperature according to a Q_{10} relationship? It would also be important to ask what kinds of scales and aggregation would be incorporated into the model and how these choices would affect resolution, accuracy, and efficiency. Decisions would also have to be made as to how system components or processes

C.S. Cronan, *Ecosystem Biogeochemistry*, Springer Textbooks in Earth Sciences, Geography and Environment, DOI 10.1007/978-3-319-66444-6_11

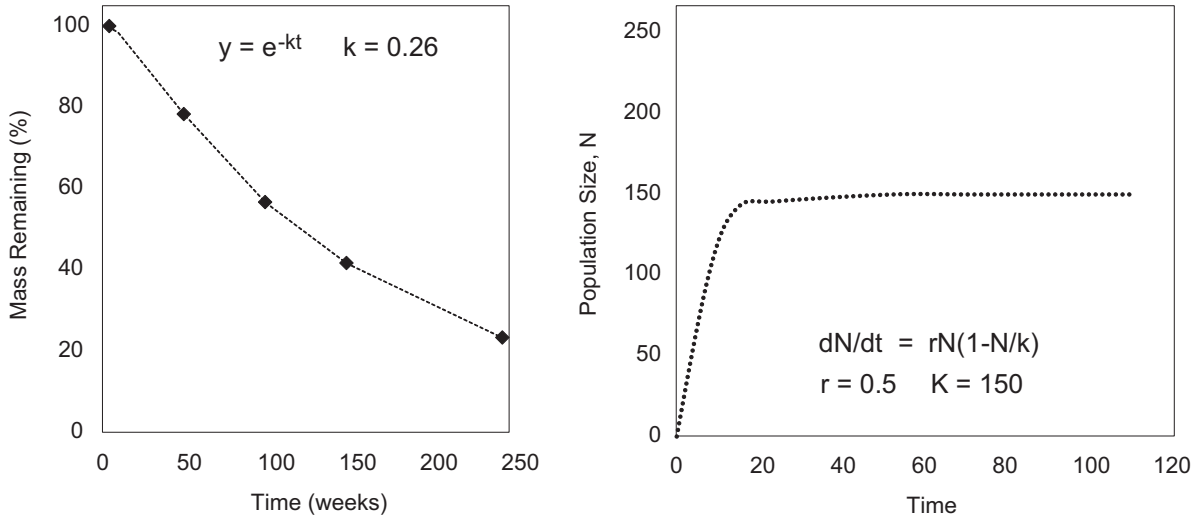

Fig. 11.1 Examples of models for (**a**) leaf litter decomposition as a function of elapsed time, t, and a species-specific decay constant, k, and (**b**) density-dependent population growth based on rate of growth, r, and carrying capacity, K

Table 11.1 Objectives of biogeochemical models

1.	Compile and integrate information and current understanding
2.	Identify gaps in our knowledge base and current understanding
3.	Explore feedbacks and interactions among multiple variables in a study system
4.	Generate questions and hypotheses for empirical testing
5.	Evaluate apparent sensitivity of biogeochemical relationships and variables
6.	Make predictions and simulate outcomes of new scenarios (with due caution)

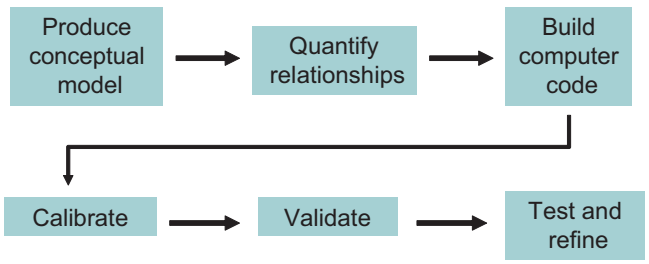

Fig. 11.2 General sequence of activities in the development of a model

would be represented in terms of a balance between simplicity and realism. For instance, would we select a generic type of tree for our forest or would the model include a realistic variety of species that might differ in carbon cycling characteristics? It would then be necessary to determine how these choices would affect run times, cost, data requirements, and applicability of the model to other systems or sites.

Design and development of a model require specific decisions about the kinds of data inputs and model outputs to be included. Will both the input parameters and model outputs be easily measured, so as to permit reliable execution, **calibration**, and **validation** of the biogeochemical model? In a carbon cycling model, this might require specifying whether plant moisture status would be determined by soil water potential or by another more readily measured parameter. Likewise, model simulations of carbon fixation could potentially require more simple (e.g., mean daily solar radiation flux) or more complex input data (e.g., hourly solar flux and vapor pressure deficit). Finally, it must be clear how the model will be tested and validated to determine its ability to represent a real biogeochemical system.

Steps in Building a Biogeochemical Model

There are a number of sequential steps that occur in the design and implementation of a model (Fig. 11.2). After identifying the objectives of a new biogeochemical model, an investigator produces a conceptual representation of the system or process showing **state variables**, interactions, or transfers (Fig. 11.3). This qualitative framework is then transformed into a quantitative description of initial conditions, state variables, transfer functions, and the various interactions, relationships and processes prescribed in the conceptual model. For example, in a carbon cycling model, one might prepare a function describing soil efflux of carbon dioxide in terms of temperature, moisture, and substrate conditions.

Once a model has reached the quantitative design stage, the model structure is translated into computer code using a PC spreadsheet or programming language. Next, the investigator uses baseline data to define all variables and initial parameters, so that the model can be tested and calibrated.

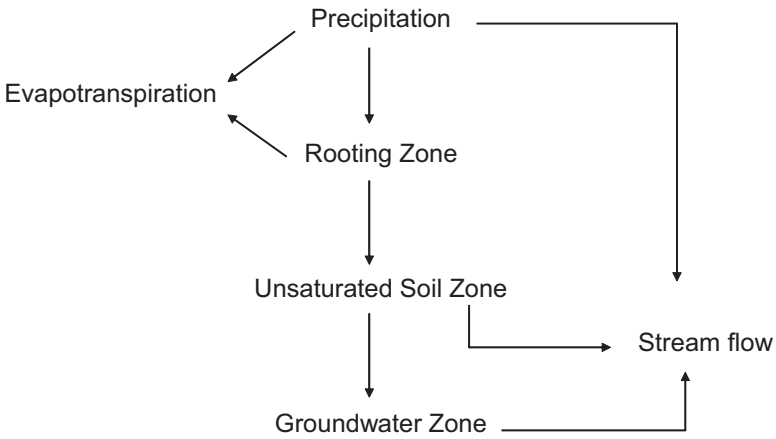

Fig. 11.3 Example of a simple conceptual model showing major storage compartments and water transfers in the forest hydrology model, BROOK, developed by Federer and Lash (1978)

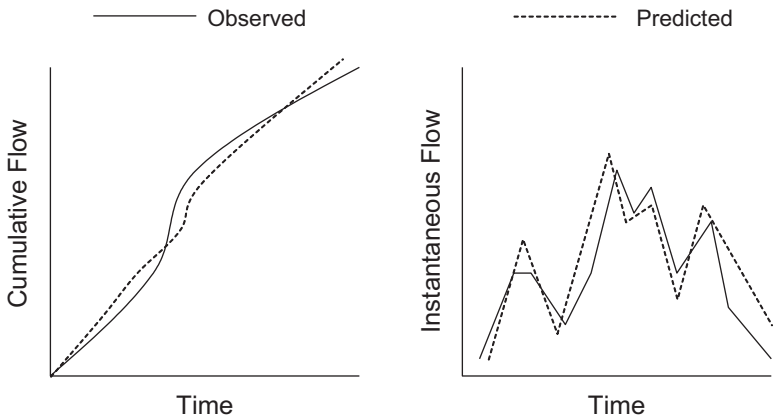

Fig. 11.4 Observed and predicted hydrologic flows can be compared at two different time scales as a means of calibrating a hydrologic model. In the *left panel*, predicted cumulative stream runoff over a period of 12 months departs somewhat from measured runoff; in the *right panel*, predicted storm runoff peaks are close to observed streamflow patterns, but are not identical

The calibration procedure involves checking the model to determine if it can reproduce the general behavior of a reference system. During this tuning or tweaking phase, faulty relationships may become apparent in the model and adjustments may be required to address shortcomings of the model design. As an example, calibration of a watershed hydrology model may require comparison of observed and predicted cumulative annual flows and instantaneous flows (Fig. 11.4), followed by iterative model adjustments (e.g., Gherini et al. 1985).

Ultimately, when a model has been shown to reproduce the observations of a calibration data set, a **validation** test is performed to determine if the model can reproduce the behavior of a new independent set of observations. For instance, a hydrology model might be calibrated with data from the 1999 to 2003 water years, but the validation test might involve checking model predictions against stream flow and climatic data for the 2004–2006 water years. As a final test, models are often subjected to a **sensitivity analysis** to determine which variables have the greatest effect on model outputs and which conceptual uncertainties or problematic input data may exert a strong adverse effect on the model (e.g., McCormack et al. 2015). Thereafter, most models are refined and are improved through iterative steps involving hypothesis testing and feedback from empirical studies.

When calibration and validation stages have been completed, the thrill and anticipation of running model simulations can finally be experienced. At this stage, models can be used to generate hypotheses and to make predictions that can be evaluated against experimental results. In some cases, models are used to explore scenarios that cannot easily be tested in the field or lab. Under these conditions, scientists have to find alternative ways of determining the relative veracity of the predictions. As an example, efforts have been made to use general circulation models (GCM's) to predict the influence of rising atmospheric carbon dioxide on global surface temperatures. Unfortunately, it is not possible to test whether a GCM model is accurate or not in predicting a specific rise in mean

temperature by the year 2070. In an effort to examine uncertainty in that type of long-range prediction, inter-laboratory calibration studies have been conducted comparing predictions from multiple separate independent GCM models developed in labs around the world. Results reported by Cess et al. (1993) showed that predictions for mean global temperature increases ranged from <2° C to >5° C, largely as a result of different assumptions incorporated in the model designs (Fig. 11.5). This implies that there is at least a two-fold range of uncertainty in this type of prediction.

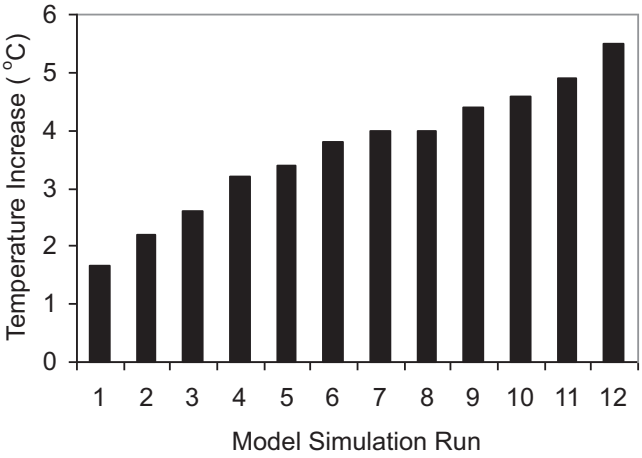

Fig. 11.5 Comparison of global warming predictions from multiple GCM (general circulation models) under conditions equal to twice current atmospheric CO_2 concentration. Mean predicted global temperature increase = 3.8 °C and CV = 26% From Cess, R.D. et al (29 co-authors). 1993. Uncertainties in carbon dioxide radiative forcing in atmospheric general circulation models. Science 262:1252–1255. Reprinted with permission from AAAS

An Introductory Model of Watershed Nitrogen Cycling

One of the simplest platforms to use in constructing a biogeochemical model is a PC spreadsheet based on EXCEL (Verburg and Johnson 2001). My students and I have used this approach to investigate the general behavior of the nitrogen cycle in a northern hardwood forest in New England. Our objective was to explore the ways in which we could potentially account for the nitrate losses in stream water that are characteristic of forested watersheds experiencing "nitrogen saturation" (Aber et al. 1989). In nitrogen saturated watersheds, stream export of nitrate-N is elevated above background levels, because the forest ecosystem cannot retain all of the nitrogen that is supplied from atmospheric inputs and internal recycling. For this exercise, we developed a simple N cycling model and performed a sensitivity analysis to test how small changes in state variables or rates of processes could translate into measurable increases or decreases in stream exports of nitrogen.

In designing the conceptual model of N cycling, we aggregated the forest ecosystem into a limited number of major compartments and transfers (Fig. 11.6). The forest was broken into aboveground and belowground vegetation pools, with each compartment containing major tissue types such as leaves, branch wood, bole wood, fine roots, and large roots. For each tissue category, there was a mean N concentration, a mean biomass, and an estimate of annual primary production. Major transfers included annual plant uptake of N, annual N resorption, and detrital cycling of N in litterfall, branch loss, and fine root turnover.

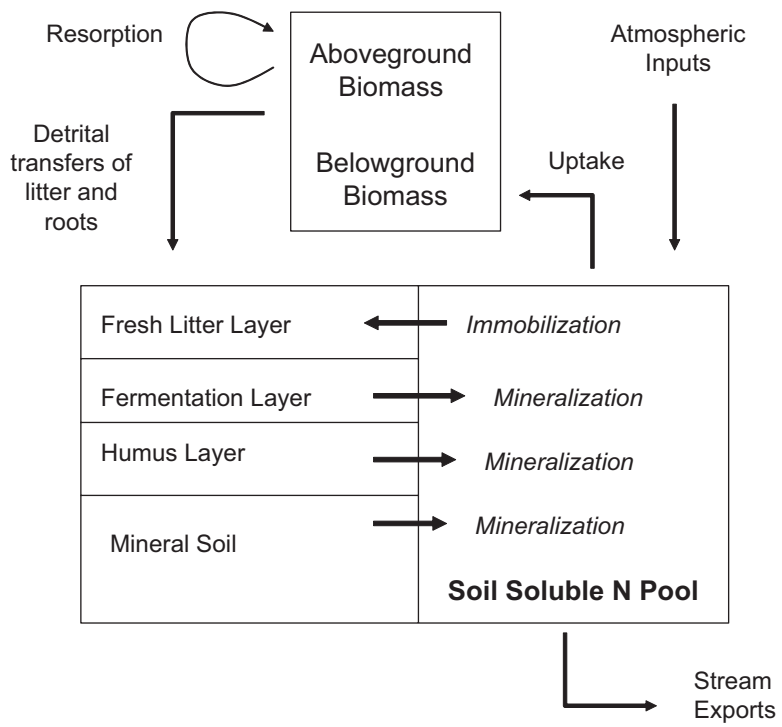

Fig. 11.6 Conceptual model of a simple N cycle in a forested ecosystem

Table 11.2 Pool sizes and NPP for an N cycle model based on northern hardwood forests (Sheldon 2003)

	Biomass (kg ha^{-1})	Biomass N (kg ha^{-1})	NPP (kg ha^{-1} yr^{-1})	NPP N (kg ha^{-1} yr^{-1})
Aboveground				
Foliage	2800	67.2	2800	67.2
Live branches	41,820	154.7	2255	8.3
Sapwood + heartwood	92,780	92.8	2391	2.4
Stem bark	9350	58.9	268	1.7
Total aboveground	151,750	373.6	7714	79.6
Belowground				
Root crowns	11,650	31.5	321	0.9
Lateral roots (<10 mm)	9745	42.9	974	4.3
Lateral roots (2.5–10 mm)	5150	45.8	515	4.6
Fine roots (1–2.5 mm)	1519	14.4	945	9.0
Fine roots (<1 mm)	4103	74.1	2555	46.1
Total belowground	32,167	208.7	5310	64.9
Total Forest	**183,917**	**582**	**13,024**	**144**

The soil was treated as a forest floor or O horizon containing three layers and a single aggregated subsoil or mineral soil horizon. Each soil compartment was characterized by a mass of N, a C/N ratio, and a variable N mineralization rate. The major transfers in the soil were N removals in plant uptake, microbial immobilization of N, and N release through microbial mineralization and nitrification. Soil microbes were considered to immobilize N in fresh litter with a C/N > 25, whereas soil organic N was mineralized when the C/N ratio was below 25. Finally, atmospheric inputs of N were specified for the watershed and all parts of the model were connected with mass balance relationships.

In order to parameterize the model with field data, we selected Watershed 6 at Hubbard Brook Experimental Forest as our reference condition, and used published data from that site to quantify the pools and transfer rates of N. Mean pool sizes of above and belowground biomass and N were defined as shown in Table 11.2. In addition, estimates of annual net primary production and annual N demand in plant NPP were obtained from the literature. Because most of the biological data were based on annual estimates, this limited the resolution of the model to predictions of annual N fluxes and transfers. As shown in Table 11.2, the reference watershed was estimated to contain roughly 580 kg N ha^{-1} in above- and belowground plant biomass, and annual demand for N in NPP was approximately 144 kg N ha^{-1} yr^{-1}. The largest sinks for N in the annual N cycling budget were identified as new foliage production and fine root production.

Major annual transfers in the forest N cycle (Table 11.3) were coded as dynamic variables in the EXCEL spreadsheet model. Foliar N resorption was initially set at 55.8%

Table 11.3 Annual transfers for the Base Case Scenario in the N cycle model (Sheldon 2003)

Foliar N resorption rate (% of foliar N pool)	55.8
Aboveground litterfall (kg N ha^{-1} yr^{-1})	
Foliage	29.7
Branches and limbs	10.5
Stemwood	0.6
Other	5.5
N immobilization in decaying litter (kg N ha^{-1} yr^{-1})	14.4
Soil and forest floor N mineralization (kg N ha^{-1} yr^{-1})	123

and aboveground N uptake was calculated as the annual N demand in aboveground NPP minus the amount of N resorbed in the prior year. Belowground roots were assumed to turnover at different rates according to size classes, and the N uptake required to replace those roots was added to the net N uptake associated with aboveground NPP. Annual N return in detrital cycling of aboveground litter and belowground root turnover was also estimated in the model. Nitrogen immobilized by microbes during the first 12 mo of fresh litter decay was based on annual foliar litter mass and litter decay data from Hubbard Brook Forest, NH. Nitrogen release from microbial mineralization of detritus and soil organic matter was estimated using seasonal estimates of mineralization rates obtained for different soil horizons at Hubbard Brook Forest. Each mineralization rate was applied to the mass of soil in that horizon and cumulative mineralization fluxes were estimated based on a growing season of 150 days divided into spring, summer, and fall seasons.

Annual ecosystem transfers of N were tabulated with mass balance relationships to determine the extent to which inputs and outputs to the soil available pool of soluble inor-

Table 11.4 Mass balance relationships incorporated in the N cycle model

Biomass N Pool = Foliage N + Branch N + Stem Wood N + Stem Bark N + Root N by size classes
N Increment in NPP = Sum of N in foliage NPP + Branch NPP + Stem NPP + Root NPP
Detrital Inputs to Soil = Foliar N Pool * (1-% resorption) + Root N Pool * % Turnover + Branch/Stem litter N
N Immobilization in Decaying Litter = (0.75 * Litterfall Mass/50) – (Litterfall Mass * 0.5 * N/C Ratio)
N Mineralization = Sum of N Mineralization rate * Mass * Days for each forest floor and soil layer by season
Annual Plant N Demand = Annual N Pool in NPP of branches/wood/roots + foliar N Pool * (1-% resorption)
Annual DIN Supply Rate = Atmospheric N Deposition + N Mineralization
Annual Watershed Export of DIN = Annual DIN Supply Rate – N Immobilization – Plant N Demand

Note: *DIN* dissolved inorganic N; *NPP* net primary production

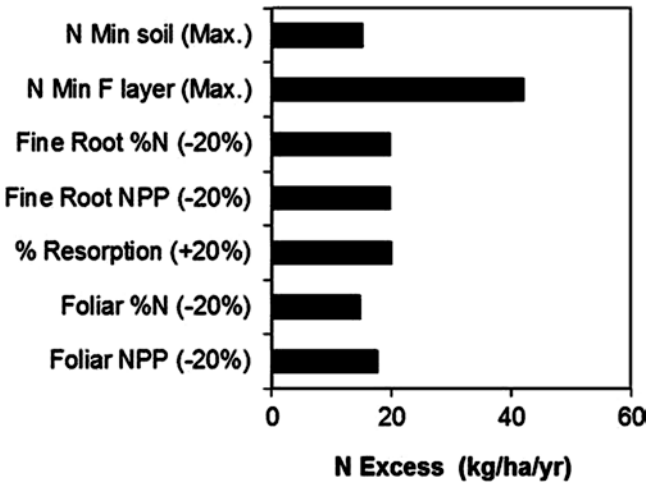

Fig. 11.7 Results of a sensitivity analysis of the forest N cycle model. Bars show predicted changes in excess soluble nitrate-N under conditions where a specific forest N cycle parameter is changed to the minimum or maximum value reported in the literature or is raised or lowered by 20% compared to a base case. N excess in the base case scenario was ~9 kg ha^{-1} yr^{-1}. As an example, a 20% reduction in foliar NPP doubled the N excess available for stream export to 17.5 kg ha^{-1} yr^{-1} (see above)

ganic N (DIN) were balanced in the N cycle of the reference watershed (Table 11.4). Inputs of DIN to the soil water pool were estimated as the sum of atmospheric deposition (7 kg N ha^{-1} yr^{-1}) plus N mineralization in the forest floor (91.5 kg N ha^{-1} yr^{-1}) and mineral subsoil (31.5 kg N ha^{-1} yr^{-1}), for a total annual N supply rate of 130 kg N ha^{-1} yr^{-1}. In comparison, removals or outputs of DIN from the soil pool amounted to 107 kg N ha^{-1} yr^{-1} in net plant uptake plus 14 kg N ha^{-1} yr^{-1} in microbial immobilization during fresh litter decay, for a total annual N demand of 121 kg N ha^{-1} yr^{-1}. Thus, calibration of the N cycle model with empirical data from watershed 6 at HBEF indicated that annual DIN supply could exceed N demand by 9 kg N ha^{-1} yr^{-1}. If this excess N was nitrified and subsequently leached from the system, the watershed could exhibit an annual stream water export of nitrate amounting to 9 kg N ha^{-1} yr^{-1}. For perspective, the actual stream water exports of nitrate-N at that watershed have ranged from <1 to >7 kg N ha^{-1} yr^{-1} over the last 30 yr

With the N cycle model reasonably calibrated for baseline conditions, it was possible to ask how N supply, demand, and stream export might change if assumptions or input data were changed to reflect the range of natural variations observed in ecosystem properties and cycling rates. In order to examine model sensitivity to these parameters, a literature survey was conducted to determine the ranges of minimum and maximum values reported for each variable in the model. These parameters included N concentrations in plant tissues, foliar resorption rates, N mineralization and immobilization rates, plant NPP estimates, length of the growing season, and root turnover rates.

Substitution of these data into sequential runs of the N cycle model demonstrated that relatively small realistic changes in individual parameters in the ecosystem N cycle could potentially shift the input-output balance of the N cycle, resulting in marked increases or decreases in the excess nitrate-N available for export in stream water (Fig. 11.7). For example, dropping the mean foliar N concentration from 2.4% to 1.9% would lower the size of the plant sink, thereby increasing the N available for stream export from 9 kg N ha^{-1} yr^{-1} (base case) to >14 kg N ha^{-1} yr^{-1}. Alternatively, an increase in foliar N to 2.9% would increase the sink strength and would diminish potential N exports to <3 kg N ha^{-1} yr^{-1}. In comparison, assuming that annual fine root production was 20% higher or lower than the baseline condition could potentially decrease predicted nitrate-N exports to −25 kg N ha^{-1} yr^{-1} (with more root production and a larger fine root N sink) or increase stream exports to 19.5 kg N ha^{-1} yr^{-1} (with less root production). Results also illustrated that changes in assumed N mineralization rates and length of the growing season can potentially exert large influences on the ecosystem N balance and the amounts of N available for export.

Applications of Biogeochemical Models

The literature contains a fascinating collection of ecological and biogeochemical models spanning physiological, population, community, ecosystem, landscape, and global scales of resolution. In the section that follows, selected examples of models are briefly summarized to illustrate a cross-section of these research efforts.

TREGRO: A Model to Simulate Plant Responses to Interacting Stresses

The simulation model TREGRO was developed by Weinstein et al. (1991) to analyze the response of red spruce trees to multiple stresses such as drought, nutrient deficiency, and exposure to pollutants. The intent of the model is to predict patterns of growth and carbon allocation for individual trees as a function of growing conditions. In the model, a tree is divided into the following compartments: a canopy of conifer needles grouped by age class, branch wood, stem wood, and two root size classes (coarse and fine) in each of three soil horizons. In each compartment, three carbon pools are tracked by the model: living structure, dead structure or wood, and total non-structural carbohydrates. During a simulation, TREGRO monitors plant carbon balance by (i) calculating photosynthesis of an entire red spruce tree each hour as a function of ambient environmental conditions and the availability of light, water, and nutrients; (ii) allocating daily redistribution of carbon throughout the plant; and (iii) accounting for the loss of carbon via respiration and senescence. To accomplish this task, the model tracks the flow of CO_2 to the sites of fixation at the needles, the availability of light in the canopy, supply of water and nutrient resources in each of the soil horizons, and the amounts of these resources absorbed by the tree. Soil and plant water potentials, photosynthesis, and leaf respiration are simulated in the model each hour, whereas nutrient uptake, C allocation, and growth are computed on a daily basis. Figure 11.8 illustrates the sequence of events simulated during a daily time-step by TREGRO.

Following its initial development, the TREGRO model was used by Retzlaff et al. (1996) to examine the potential effects of elevated atmospheric ozone concentrations on a mature sugar maple tree. The authors reported that after 3 years of simulated exposure to twice ambient ozone concentrations, the 160 year old tree experienced a 14% reduction in carbon gain compared to unexposed trees (Fig. 11.9). This simulated reduction occurred in the TNC (total non-structural carbohydrate) storage pool of the simulated tree, with the majority of the reduction located in the coarse woody roots. A response such as this might be expected to compromise the competitive ability and stress tolerance of a tree growing in a forest community.

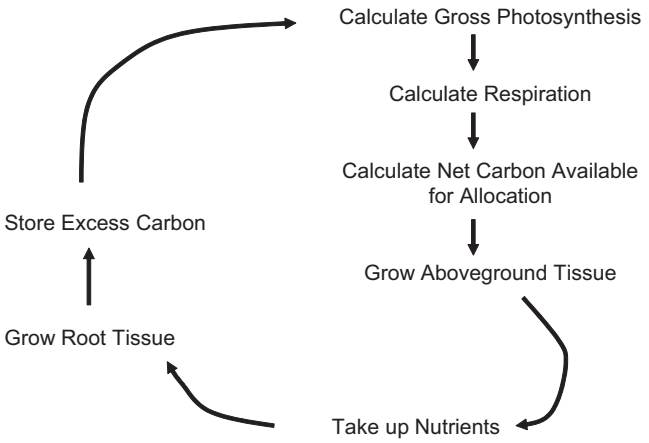

Fig. 11.8 Conceptual diagram showing processes linked in the TREGRO model

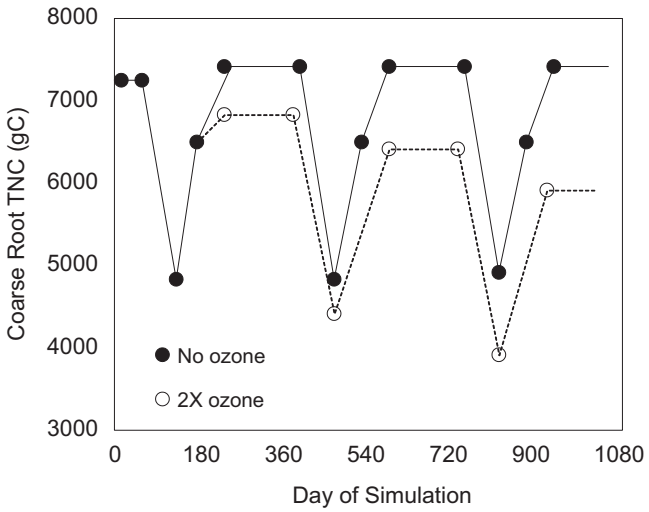

Fig. 11.9 Seasonal patterns of coarse root TNC pools predicted by TREGRO in a sugar maple tree growing with and without elevated ozone exposure From Retzlaff, W.A., D.A. Weinstein, J.A. Laurence, and B. Gollands. 1996. Simulated root dynamics of a 160-year-old sugar maple (*Acer saccharum* Marsh) tree with and without ozone exposure using the TREGRO model. Tree Physiology 16:915–921 by permission of Oxford University Press

TEM: A Global Model of Net Primary Productivity

Raich et al. (1991) designed a mechanistic terrestrial ecosystem simulation model (TEM) that used spatially referenced information on soils, vegetation, and climate to estimate pool sizes and fluxes of C and N and monthly primary production at continental to global spatial scales. Their objective was to describe the spatial and temporal patterns of net primary productivity in South America as a function of a limited set of environmental variables. As shown in Fig. 11.10, the conceptual model for TEM was based on five state variables and a number of transfer fluxes and ecosystem parameters associated with C and N pools in vegetation and soil. The authors combined a highly aggregated and simplified model of plant/soil processes affecting NPP with a grid-cell based GIS model of environmental conditions and plant production. Model predictions of NPP in each grid cell were driven by calculations of gross primary productivity (GPP) based on solar energy inputs, atmospheric CO_2, moisture availability, air temperature, nitrogen availability, and relative photosynthetic

capacity of the vegetation. Monthly estimates of NPP were then computed for each grid cell as GPP minus rough estimates for autotrophic respiration.

Predictions from the TEM model were used to produce GIS maps of potential annual NPP for South America and monthly estimates of NPP for major vegetation cover types in South America (Fig. 11.11). The authors reported that their estimated annual NPP values were generally within the range of values described by other authors for the major vegetation types in the region. The TEM estimate of total potential NPP for non-wetland areas of South America was 26.3 Pg organic matter yr^{-1}, compared with a range of 24.4 to 28.8 Pg yr^{-1} reported by Box (1978) for all of South America.

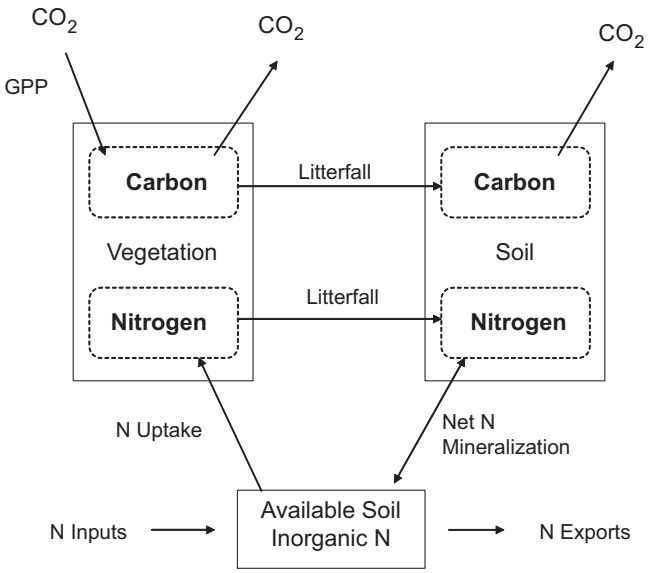

Fig. 11.10 Conceptual diagram of the TEM simulation model From Raich, J.W., E.B. Rastetter, J.M. Melillo, D.W. Kicklighter, P.A. Steudler, B.J. Peterson, A.L. Grace, B. Moore, and C.J. Vorosmarty. Potential net primary productivity in South America: application of a global model. Ecological Applications 1:399–429. ©1991 by the Ecological Society of America

The CENTURY Soil Organic Matter Model

The CENTURY model was developed by Parton et al. (1987) to simulate carbon and nutrient dynamics over time scales of months to millennia in a variety of ecosystems, including native grasslands and agricultural lands. Modeling objectives were to (i) simulate the effects of climatic gradients on soil organic matter and productivity over large areas (in order to predict the effects of climate change), and (ii) identify key soil properties controlling SOM differences among soils within a given climatic zone.

The CENTURY model is composed of a soil organic matter/decomposition submodel, a water budget model, a grassland/crop submodel, a forest production submodel, and functions related to environmental changes and management events. When calibrated for a study system, the model computes the flow of carbon, nitrogen, phosphorus, and sulfur through ecosystem compartments. The simulation model is designed with a monthly time-step and requires the following driving variables as input: monthly average maximum and minimum air temperature, monthly precipitation, soil texture, plant N, P, and S content, lignin content of plant material, atmospheric and soil inputs of N, and initial soil C, N, P, and S.

As shown in Fig. 11.12, the SOM submodel in CENTURY contains three soil organic matter fractions: (i) an active fraction (active SOM) of soil C and N consisting of microbes, microbial products, and soil organic matter with a short turnover time (1–5 yr); (ii) a pool of C and N (slow SOM) that is physically protected or occurs in chemical forms that are slowly decomposed with an intermediate turnover time (20–40 yr); and (iii) a fraction that is chemically recalcitrant and often physically protected (passive SOM) with a long

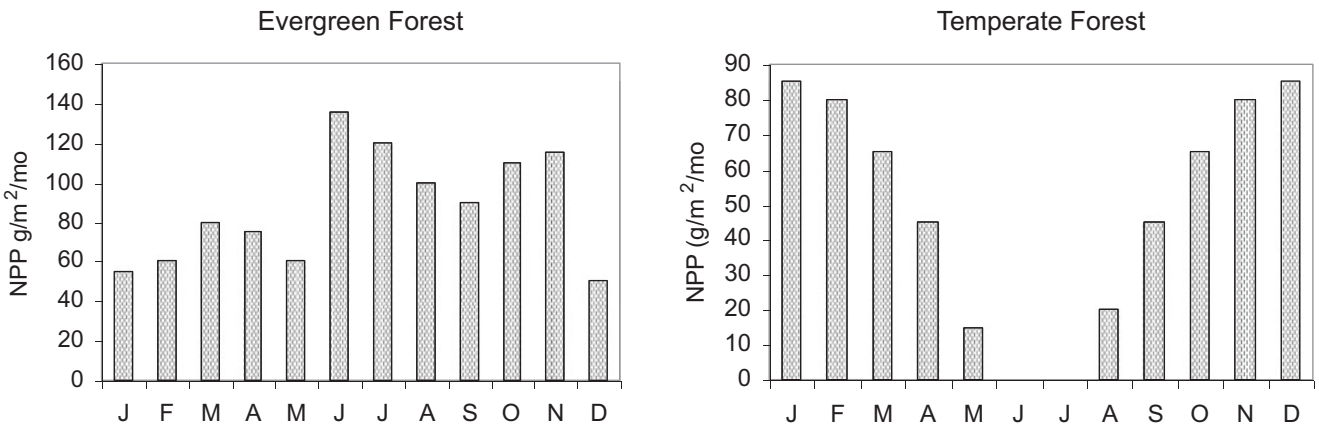

Fig. 11.11 Estimated monthly NPP for two major cover types – Evergreen Forest and Temperate Forest – In South America as predicted by TEM From Raich, J.W., E.B. Rastetter, J.M. Melillo, D.W. Kicklighter, P.A. Steudler, B.J. Peterson, A.L. Grace, B. Moore, and C.J. Vorosmarty. Potential net primary productivity in South America: application of a global model. Ecological Applications 1:399–429. ©1991 by the Ecological Society of America

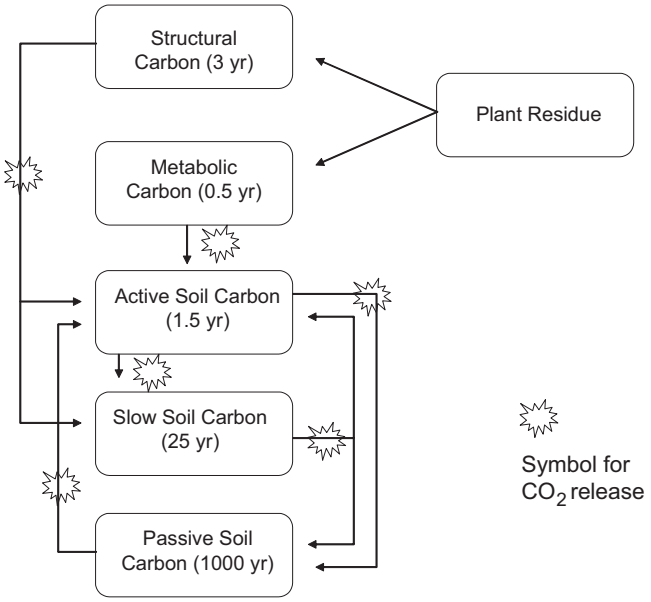

Fig. 11.12 Flow diagram showing compartments and carbon flows in the CENTURY model Republished with permission of the Soil Science Society of America from Parton, W.J., D.S. Schimel, C.V. Cole, and D.S. Ojima. 1987. Analysis of factors controlling soil organic matter levels in grasslands. Soil Science Society of America J. 51:1173–1179. Permission conveyed through the Copyright Clearance Center Inc.

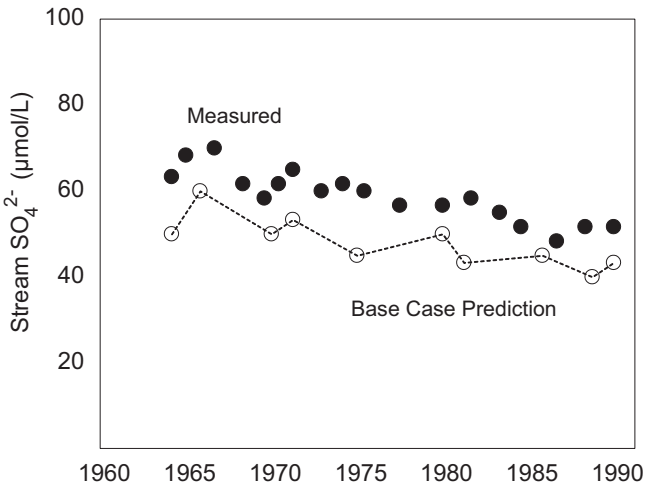

Fig. 11.13 Simulated and observed concentrations of sulfate in streamwater runoff at Watershed 6 at Hubbard Brook Experimental Forest, NH From Gbondo-Tugbawa, S.S., C.T. Driscoll, M.J. Mitchell, J.D. Aber, and G.E. Likens. A model to simulate the response of a northern hardwood forest ecosystem to changes in S deposition. Ecological Applications 12:8–23. ©2002 by the Ecological Society of America

turnover time (200–1500 yr). Plant residue composed of shoot and root biomass is divided in the model into structural pools that have 1–5 yr turnover times and metabolic pools that have 0.1 to 1 yr turnover times prior to transfer into SOM pools.

PnET-BGC: An Integrated Biogeochemical Model

The detailed long-term data set generated by investigators at Hubbard Brook Experimental Forest, NH inspired the development of three successive ecosystem modeling efforts – PnET, PnET-BGC, and PnET-CN. In its original formulation, PnET was designed as a generalized lumped-parameter model to predict photosynthesis, evapotranspiration, and NPP in forest ecosystems (Aber and Federer 1992). Afterwards, Driscoll, Aber, and colleagues developed PnET-BGC as an integrated biogeochemical model to evaluate the effects of atmospheric deposition on forest and aquatic ecosystems (Gbondo-Tugbawa et al. 2001, 2002). A subsequent model, PnET-CN, was produced to predict cycling of carbon, nitrogen, and water in temperate forest ecosystems (Thorn et al. 2015).

In their version of PnET-BGC, Gbondo-Tugbawa et al. (2002) included representations of major biogeochemical processes that were assumed to influence watershed cycling and export of sulfur derived from atmospheric deposition. Atmospheric deposition was estimated from relationships between known S emission patterns and bulk deposition, and from observed ratios of dry to bulk deposition fluxes of S. Small amounts of internal S release from weathering were included, along with biotic cycling of S by plants and soil microbes. Finally, a soil chemistry module was incorporated to simulate chemical processes such as sulfate adsorption and buffering of acidity.

When the authors compared simulated annual volume-weighted concentrations of sulfate in stream water at Hubbard Brook Experimental Forest with measured values for the period 1964–1992, it was found that the PnET-BGC model under-predicted actual stream concentrations by an average of 9 µmol L^{-1} (Fig. 11.13). In an effort to account for this discrepancy, the authors examined other possible sources for S inputs to the watershed. Their analysis showed that increasing estimated inputs from dry deposition, internal weathering of a sulfur-bearing mineral, or net mineralization of organic S contributed to improved model predictions that were more consistent with observed stream chemistry.

Watershed Acidification Models

The ILWAS model was developed to predict changes in surface water acidity and chemistry as a function of atmospheric deposition inputs, hydrologic conditions, and a suite of biogeochemical processes controlling alkalinity production and consumption in lakes and their surrounding watersheds (Gherini et al. 1985; Munson and Gherini

1991). The model was configured to represent each watershed as a collection of subcatchments with specific vegetation, snowpack, and soil compartments. Drainage from subcatchments within the overall watershed flowed into a lake ecosystem that contained multiple layers in the water column. Lake water chemistry was predicted as a function of hydrologic flow routing in combination with detailed relationships describing forest canopy processes, decompo sition/mineralization patterns, soil chemical reactions, mineral weathering processes, carbon dioxide equilibria, and acid-base chemistry. After calibration, this **deterministic** model was able to simulate a variety of dynamic ecosystem indicators on a daily time-step, including the lake outflow hydrograph, lake pH, and lake outlet alkalinity. An alternative modeling approach for examining watershed acidification was developed by Cosby et al. (1985, 2001), who used the steady-state MAGIC model to simulate historical and potential future stream runoff chemistry.

Nutrient Cycling Models

Boyer et al. (2006) reviewed and summarized a number models focused on denitrification and N cycling in terrestrial and aquatic ecosystems. DAYCENT is described as a daily version of the CENTURY model that simulates contributions from nitrification and denitrification to N gas fluxes from soils. INCA is a mass balance simulation model for water and N that quantifies plant uptake, nitrification, denitrification, mineralization, and immobilization within specific land use types and watershed subcatchments in order to predict stream N exports. SPARROW is a hybrid statistical and process-based model that estimates sources and transport of N in watersheds and surface waters. Finally, Boyer and coauthors described HSPF as a complex water quality simulation model that operates on a daily time-step and includes major processes related to N cycling in soils, shallow groundwater, and aquatic systems.

Other modelers have addressed a range of questions in forested watersheds. Karama et al. (2013) combined the LANDIS-II landscape model of forest dynamics with an extension module, NuCycling-Succession, which focuses on the interactions of nutrient cycling and successional processes in response to forest management practices and global change. The core emphasis of the model was to simulate pools and fluxes of N, P, and C in forest ecosystems. In a related study, Wang et al. (2014) used a multi-model comparative approach to simulate the long-term effects of harvesting on NPP and the cycling of C and N in aspen forests. Five different models – Biome-BGC, CENTURY, FORECAST, PnET-CN, and LANDIS-II – were compared in their ability to simulate biogeochemical responses to seven sequential forest harvesting events. At Harvard Forest, MA, Tonitto et al. (2014) used a modified version of PnET to simulate the effects of long-term N additions on soil organic matter dynamics. Finally, Tipping et al. (2012) designed the N14C model to simulate the biogeochemical responses of plant-soil systems to anthropogenic N deposition. The model operates with four plant functional types and includes a range of details on C and N cycling, NPP, and SOM dynamics.

Models in Watershed Hydrology

Hydrologic models have been used extensively to integrate current understanding and to identify gaps in our knowledge of water relations and hydrological processes in watershed ecosystems. Models of water relations and evapotranspiration patterns in forest communities have been reviewed by Whitehead and Hinckley (1991), and include the basic Penman-Monteith model (Monieith 1965; Ershadi et al. 2015), the FOREST-BGC model (Running and Coughlan 1988; Running et al. 1989; Running and Gower 1991), and the PROSPER model (Luxmore et al. 1978). Three examples of models focused on watershed runoff and whole system water budgets include: TEHM, the Terrestrial Ecosystem Hydrology Model (Huff et al. 1977; Luxmore 1989), TOPMODEL (Beven and Kirkby 1979; Wolock 1993), and BROOK (Federer and Lash 1978). Building on those earlier studies, Beckers and Alila (2004) developed a hydrologic model to predict rapid preferential hillslope runoff contributions to peak flow generation in a temperate rain forest watershed. Nippgen et al. (2015) designed the spatially-distributed Watershed ECOHydrology model to examine variations in runoff source areas over space and time. Finally, Soulsby et al. (2015) used an isotopic mixing model to investigate temporal variations in the ages of water contributing to runoff.

Ecosystem Disturbance and Stress

12

Introduction

Ecosystems are influenced by a wide variety of persistent or acute **forcing factors** (White 1979; Foster et al. 1997; Groffman et al. 2004), including stochastic disturbances, cyclic or chronic environmental stresses, and human management activities (Table 12.1). A **disturbance** can be defined as an event that removes or damages organisms, generates openings in a community, or abruptly alters environmental conditions, leading to changes in ecosystem structure or function. As an example, there was a major ice storm across northern New England in 1998 that caused major tree damage, opened canopy gaps, and introduced a large pulse of coarse woody debris into forested watersheds in the region. What kinds of broad ecological and biogeochemical consequences would you expect from this type of winter disturbance?

In comparison with an ecological disturbance, a **stress** can be viewed as any biotic (e.g., pathogen) or abiotic (e.g., drought) constraint or influence that adversely affects critical life processes for organisms. A winter time stress might include an unusual period of severe subfreezing conditions or a mid-winter thaw that exceeds normal tolerances of cold-adapted organisms. When ecosystems are exposed to disturbance events, stresses, or other forcing factors, there may be dynamic changes in multiple interrelated processes and system properties (Table 12.2). One of the exciting challenges in biogeochemistry and ecology is to be able to predict ecosystem responses to diverse anthropogenic or natural forcing factors. In the chapter that follows, selected examples are presented to illustrate the varied nature of ecosystem disturbances, stresses, and biogeochemical responses.

Disturbance and Recovery in the Context of Ecological Succession

When a forest ecosystem is disturbed by a windstorm, an insect outbreak, logging, or other forcing factors, the biogeochemical response of the system unfolds over multiple time scales ranging from days to decades, all within the context of ecological succession. **Succession** is a process that occurs during the progressive sequential stages of maturation and ecological development following disturbance (Fig. 12.1). Succession is typically characterized by (i) changes in species composition, (ii) changes in community structure, and (iii) changes in ecosystem properties and functions. One unusual example of ecological succession is observed in the high elevations of New England, where subalpine balsam fir forests exhibit repeating bands of mortality that have been termed "fir waves". The interior of a fir wave contains a forest structure dominated by dead mature balsam fir trees in the overstory, coupled with an understory of vigorous balsam fir regeneration (Fig. 12.2). In this curious example, the dominant species does not change through succession, but the forest community cycles through changing age classes and stand structures that set the stage for altered nutrient source-sink relationships and biogeochemical cycling.

C.S. Cronan, *Ecosystem Biogeochemistry*, Springer Textbooks in Earth Sciences, Geography and Environment, DOI 10.1007/978-3-319-66444-6_12

Table 12.1 Examples of disturbances, stresses, and management activities that may affect terrestrial ecosystems

Forest harvesting(logging)	Atmospheric pollution
Windstorm	Ice storm
Drought	Flooding
Insect outbreak	Herbicide/pesticide applications
Mass movements of sediments	Lava flows
Sludge or wastewater applications	Fire (wildfire versus prescribed burning)
Vegetation/land conversion	Wetland drainage
Beaver impoundment	Fertilization
Intensive grazing	Human recreation
Urbanization	Soil liming

Table 12.2 Examples of ecosystem parameters that respond to disturbance, stress, and human management

Atmospheric inputs	Soil chemistry and fertility
Organic matter cycling	Ecosystem nutrient cycling
Plant nutrition and nutrient circulation	Soil solution chemistry and leaching
Microbial processes	System hydrology
Surface water chemistry	Erosion and sediment transport
Weathering	Gaseous fluxes
Input-output budgets	Biodiversity
Biotic composition and structure	Biomass, productivity, and energy flow

Effects of Forest Harvesting on Watershed Ecosystems

In previous chapters, we discussed how the plant community serves an integral role in the energy flow and nutrient cycling of a forested ecosystem. The growing plant community acts as a nutrient pump, a nutrient sink or storehouse, and as a powerhouse for energy production. What happens in biogeochemical terms when the plant community is disturbed by deforestation and harvesting? This question has been addressed in a number of field experiments, with results varying as a function of environmental, ecological, and treatment conditions. To illustrate some of the potential ways in which deforestation can disturb the biotic integrity and biogeochemical functions of a forested watershed, we can examine results from an experimental clear-cut harvest conducted at Hubbard Brook Experimental Forest, NH in the 1960s by Herb Bormann and Gene Likens (Bormann et al. 1974). This experimental treatment was executed using a number of techniques that suited the experimental design criteria of the investigators, but which differed considerably from approaches used in conventional commercial logging operations at the time.

The Hubbard Brook experimental clear-cut was implemented in a mixed northern hardwood forest in central New Hampshire, USA. Prior to the harvest, the experimental watershed (WS 2) was monitored and compared with a reference watershed (WS 6) for a period of 2 years. In 1966, a winter harvest was conducted and all the woody

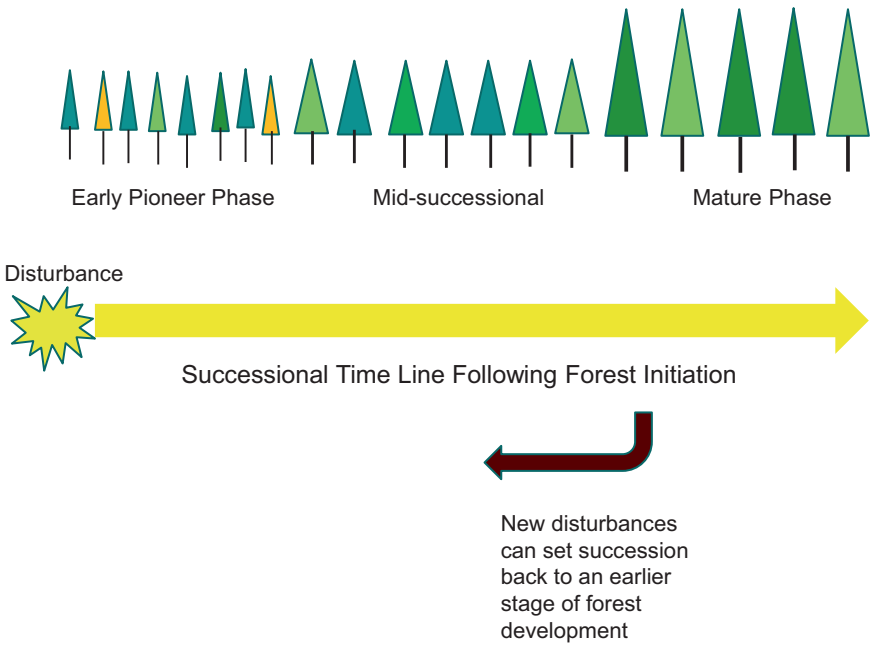

Fig. 12.1 General conceptual model of ecological succession showing ecosystem maturation moving to the *right* and disturbance shifting the forest system toward the *left*

boles and branches were left in place to minimize disturbance to the soil from skidding activity. For the next 3 years, vegetation re-growth was prevented on WS 2 using herbicide applications. In retrospect, the experimental disturbance was in some respects rather gentle (e.g., leaving the woody stems and branches in place) as well as extreme (e.g., using herbicide to inhibit plant re-growth).

Fig. 12.2 Fir waves (*light gray* patches on mountainside) represent one of the mortality, disturbance, and successional patterns observed in high-elevation subalpine conifer forests of northern New England

The implicit null hypothesis for the experiment was that *there is no significant watershed impact from clear-cut harvesting of the forest*. So, what was the outcome of this watershed manipulation experiment?

Biotic impacts were rather pronounced in the clear-cut watershed (Fig. 12.3). The living plant community was removed and re-growth was prevented, causing a virtual cessation of plant uptake and the temporary elimination of a major nutrient sink. In effect, plant uptake was absent from the watershed for a period of 3 years. When herbicide treatment was terminated at the end of 3 years, the ecosystem was rapidly transformed into an early successional state characterized by progressive increases in nutrient accumulation in re-growing vegetation. In the aftermath of logging, soil microbes responded to the fresh inputs of root and woody detritus, the lack of plant competitors, and the altered forest micro-climate with dramatic increases in rates of decomposition and nitrogen mineralization. One of the major impacts was a large increase in soil nitrification that occurred in response to the experimental clear-cut.

With removal of the living forest plant community, there was a pronounced re-adjustment in the water budget for Watershed 2. Although precipitation inputs continued unchanged, moisture outputs as ET dropped substantially because of the lack of plant transpiration. As a consequence,

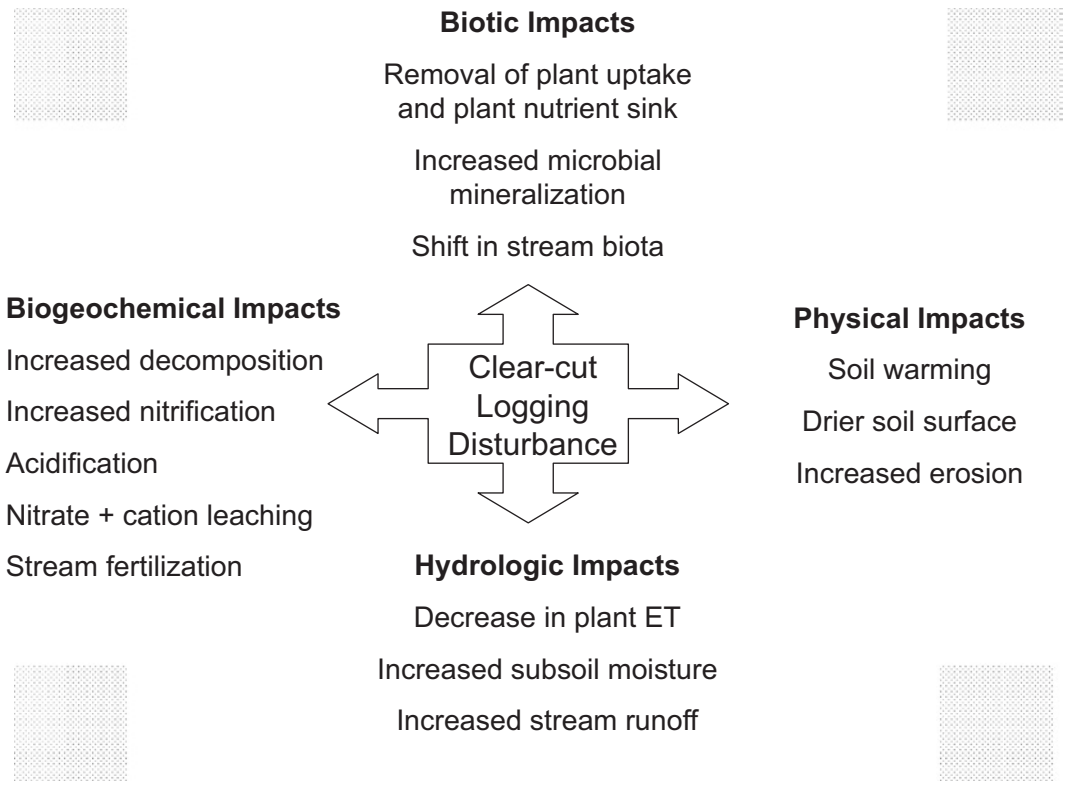

Fig. 12.3 Summary of major ecological and biogeochemical responses to forest clear-cutting on Watershed 2 at Hubbard Brook Experimental Forest, NH

there was more water available for recharge of subsoil moisture and for stream runoff. On average, ET declined by two-thirds, whereas annual streamflow increased 26–40%. The increase in stream discharge contributed to accelerated export of nutrients and erosion of sediments from the watershed. In the absence of a forest overstory, the exposed soil surface also experienced greater solar inputs and warming in summer, thus enhancing rates of microbial decomposition. In addition, subsurface soil moisture increased in the clear-cut watershed.

Element cycling processes responded to the harvest disturbance with a variety of striking patterns. The vigorous increase in soil nitrification generated a prolonged pulse of nitric acid leaching through soils and into the stream channel. This process depleted soil nitrogen, enhanced cation leaching from soils, and contributed to soil and stream acidification (with stream pH declining from 5.1 to 4.3). Annual watershed export of nitrate-N rose from <10 to nearly 600 kg ha^{-1} in the first one to two years after the harvest. There was also an intriguing decline in stream water sulfate ion concentrations that probably resulted from two principle factors: a decline in dry deposition to the leafless watershed and increased soil sulfate adsorption and retention resulting from soil acidification associated with elevated nitrification rates. Overall, the large increases in nutrient export from the watershed were interpreted as evidence that plants play a major role in nutrient conservation in forested watersheds.

The Hubbard Brook clear-cut experiment also emphasized the strong linkages between aquatic and terrestrial ecosystems. As noted earlier, changes in the terrestrial system were accompanied by a variety of important aquatic impacts such as acidification and nutrient loading to the stream draining Watershed 2. In addition, tree harvesting allowed increased light penetration to the stream channel. In combination, these factors produced changes in element cycling, energy flow, and food web composition in the stream.

Twenty Years of Recovery Following Harvesting at Hubbard Brook Forest, NH

Reiners (1992) conducted periodic sampling campaigns to quantify biomass and nutrient cycling patterns during the first 20 yr of ecosystem recovery after deforestation of the northern hardwoods forest in Watershed 2 at Hubbard Brook Experimental Forest (HBEF). After two decades of vegetation regrowth, the successional forest at HBEF had achieved a biomass of 52,000 kg ha^{-1}, which was equivalent to 38% of the biomass in the adjacent uncut reference forested watershed (WS 6). At that point in time, annual forest aboveground net primary production was roughly 20,000 kg ha^{-1} yr^{-1}, implying that the rapidly growing forest in WS 2 was a substantial sink for nutrients. Nutrient accumulation over the 20 yr period produced element pools in aboveground biomass of 107 kg N ha^{-1}, 16 kg P ha^{-1}, 119 kg Ca ha^{-1}, and 81 kg K ha^{-1}.

Effects of Wildfire and Prescribed Burning

Fires are a common natural disturbance feature in many forested regions of the world, with burn recurrence intervals ranging from a few years to several centuries (Franklin et al. 1987; Reich et al. 2001). Considering the potential landscape impacts of fire disturbance, what kinds of ecosystem responses would you expect to observe in burned forested watersheds? How might plants, microbes, soils, nutrient cycling, and hydrologic patterns be affected by a fire?

Wildfires

In the early 1970s, after a wildfire burned through a conifer forest at Entiat, WA, Grier (1975) investigated the effects of burning on nutrient losses resulting from volatilization and ash convection. By comparing burned and unburned forest plots in the study area in the immediate aftermath of the wildfire, the author estimated that losses of soil and forest floor nutrients amounted to roughly 900 kg N ha^{-1}, 75 kg Ca ha^{-1}, 30 kg Mg ha^{-1}, 300 kg K ha^{-1}, and 700 kg Na ha^{-1}. These losses from volatilization and convection were estimated to represent the following percentages of soil nutrient pools: 39% for N, 11% for Ca, 15% for Mg, 35% for K, and 83% for Na. As such, this example illustrated how an intense fire can significantly alter soil storage reservoirs for several essential nutrients.

Other investigations have since confirmed that hot wildfires such as the one at Entiat, WA can indeed have large impacts on selected nutrients. In a broad survey and meta-analysis of data from burned ecosystems, Wan et al. (2001) found that reduction in forest floor N is linearly related to fuel consumption percentage. Thus, with more intense burning of the forest floor and higher fire temperatures, there is an increased loss of stored N. Kurth et al. (2014) examined the biogeochemical effects of stand-replacing wildfires in ponderosa pine (*Pinus ponderosa*) forests of the southwestern U.S. Their evidence suggested that wildfires in ponderosa pine stands can act as a "press" type of disturbance that triggers a multi-decadal shift in N cycling characterized by high nitrification rates and elevated N availability.

Prescribed Burning as a Management Practice

Prescribed burning is a fire management tool that is used to lessen the potential for severe wildfire and to minimize adverse ecological impacts from burning. Do results from biogeochemical assessments of prescribed burns confirm

Table 12.3 Comparison of soil N losses associated with wildfires (W) and prescribed burning (P) in different regions

Study and location	Nitrogen loss kg ha^{-1}
W – Grier (1975), WA	885
P – Debano and Conrad (1978), CA	146
P – Richter et al. (1982), SC	40
P – Schoch and Binkley (1986), NC	0
P – Caldwell et al. (2002), CA	56–524

that these frequent low intensity fires actually minimize disturbance impacts? Richter et al. (1982) examined prescribed fires in loblolly pine (*Pinus taeda*) stands in South Carolina, and reported limited adverse effects on soils and nutrient cycling. Releases of N and S from the forest floor to the atmosphere via volatilization and ash dispersal varied up to a maximum of 40 kg N ha^{-1} and 8 Kg S ha^{-1}. In the same study, releases of forest floor P, Ca, Mg, and K to the atmosphere were small. Similar findings were reported by Schoch and Binkley (1986), who examined the effects of prescribed burning in North Carolina loblolly pine ecosystems and found no significant reduction in N content of the forest floor. They reported, however, that in the first growing season after a burn, the decomposition rate of the forest floor increased more than two-fold, releasing 60 kg ha^{-1} more inorganic N than that observed in unburned plots.

Comparing results from the western U.S. with the southeastern U.S. (Table 12.3), we find that the evidence appears more equivocal or incomplete regarding biogeochemical responses to fire management practices. Caldwell et al. (2002) reported that prescribed fires stimulate potentially large losses of C and N from forest floors of semiarid pine forests in the eastern Sierra Nevada Mountains. The authors found that C losses ranged from 6000 to 24,000 kg C ha^{-1} and N losses ranged from 56 to 524 kg N ha^{-1} (Table 12.3). Compared with normal deposition and soil leaching rates in these forests, the losses of N as a result of prescribed burning were relatively large and significant. Debano and Conrad (1978) also reported N losses in California forests that were well above values from the Southeast. Thus, it would seem that there is a need for further investigation of this topic.

Effects of Forest Fire Smoke on Radiative Forcing

Another important ecological impact of fires is the contribution of soot and smoke to changes in air quality and regional air chemistry. Hobbs et al. (1997) examined the effects of smoke from biomass burning on atmospheric **radiative forcing** in the tropics, where 80% of all burning takes place. They found that the global mean direct radiative forcing due to smoke from biomass burning worldwide is no more than about −0.3 watt/m^2 of cooling, compared with +2.45 watts/m^2 of warming due to anthropogenic greenhouse gases. However, they concluded that smoke can exert a potentially large cooling effect on regional climate in areas subjected to enhanced burning associated with drought and human activities.

Randerson et al. (2006) reported that a boreal forest fire in Alaska generated an increase in radiative forcing during the first year after burning, largely though emissions of greenhouse gases and black carbon. However, when the authors modeled the long-term impacts of burning over an 80-year fire cycle, they concluded that, despite a short-term increase in radiative forcing, there was a net long-term decrease in radiative forcing as a result of increases in surface albedo of the canopy.

Disturbance and Stress Resulting from Chronic N Inputs to Forest Ecosystems

One of the major enigmas concerning N cycling is the phenomenon of **nitrogen saturation** that has been observed in forested watersheds in North America and northern Europe (Aber et al. 1989). Nitrogen has historically been regarded as one of the key nutrients limiting forest and crop productivity. At lower levels of soil fertility, N amendments are expected to stimulate increased productivity. However, higher levels of N enrichment or chronic inputs of elevated N can potentially destabilize and stress terrestrial ecosystems, creating a condition of N saturation characterized by multiple adverse changes in ecosystem structure and function (Nihlgard 1985; Aber et al. 1989; Fenn et al. 1998). The impacts of N saturation result from over-supply of N relative to the retention or storage capacity of ecosystem sinks.

A primary indicator of N enrichment and saturation in forested watersheds is the leaching of nitrate-N in soil drainage water and export of nitrate in stream water (Fig. 12.4), especially during the growing season. These symptoms have been described for watersheds in the Adirondack and Catskill Mountains of New York (Cronan 1985a; Murdoch and Stoddard 1993; Lovett et al. 2000), the White Mountains of New Hampshire (Goodale et al. 2000), Lead Mountain in Maine (Kahl et al. 1999), and at numerous other locations in North America and northern Europe. Loss of NO_3^- ions from watersheds implies that forest N sinks have reached a threshold of nitrogen saturation and that watersheds may be at increased risk of soil cation depletion, stream acidification, and other negative impacts associated with over-supply of N (Driscoll et al. 2003).

Modern trends of accelerated N cycling and N enrichment in the biosphere (Vitousek et al. 1997; Driscoll et al. 2003) have generated great interest in understanding forest ecosystem responses to chronic inputs of reactive N

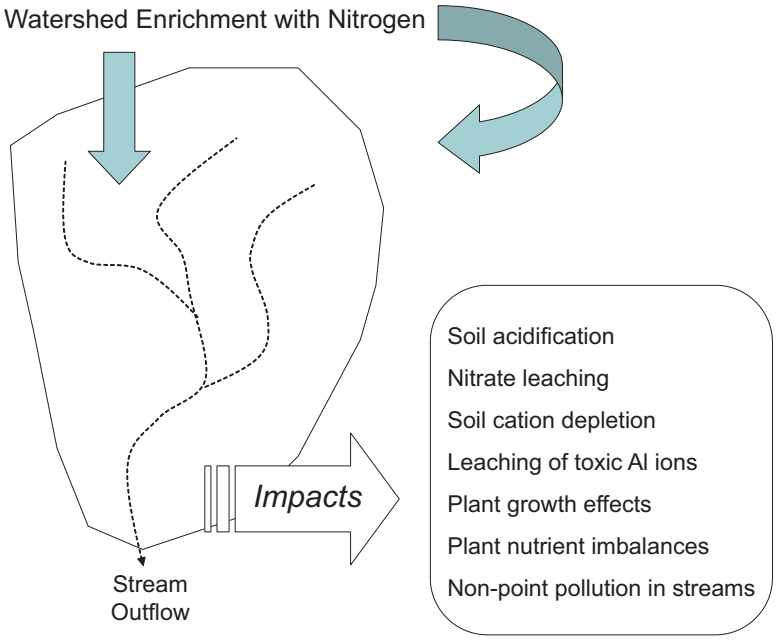

Fig. 12.4 Conceptual diagram showing common symptoms of N saturation

(Galloway et al. 2003). Using a variety of experimental approaches, investigators have attempted to determine the N retention capacities of ecosystems, the major sinks where added N inputs accumulate, and the ways in which nutrient cycling and forest production are affected by N enrichment.

At Harvard Forest, a team of investigators established a field experiment to test the responses of a 70 yr old red pine stand and a 50 yr old mixed hardwood forest to simulated increases in chronic N deposition. Treatments included a control @ 8 kg N ha^{-1} yr^{-1}, a low N amendment @ 50 kg N ha^{-1} yr^{-1}, and a high N treatment @ 150 kg N ha^{-1} yr^{-1}. In summarizing results, Magill et al. (2000) reported that soil leaching losses of NO_3^- progressively increased over 9 yr in treated pine stands, and eventually became significant after 8 years of chronic N additions in adjacent mixed hardwood plots. Forest growth responses were inconsistent, with increased wood production in the hardwood stand, but diminished wood growth in the fertilized pine stand. Overall, N retention was generally very high in all plots, ranging from 85% to 99% of annual inputs. Evidence suggested that 50 to 83% of retained N was stored in soil N pools.

Investigators implemented a paired catchment approach at Bear Brook Watershed, ME to compare ecosystem responses to chronic N inputs and soil acidification associated with experimental applications of ammonium sulfate fertilizer (Kahl et al. 1993; Norton et al. 1999). After a period of baseline monitoring in the East and West Bear Brook watersheds, annual loading of N was artificially increased four-fold in the treatment catchment from reference levels of 8.4 kg N ha^{-1} yr^{-1} to treatment levels of 33.6 kg N ha^{-1} yr^{-1}.

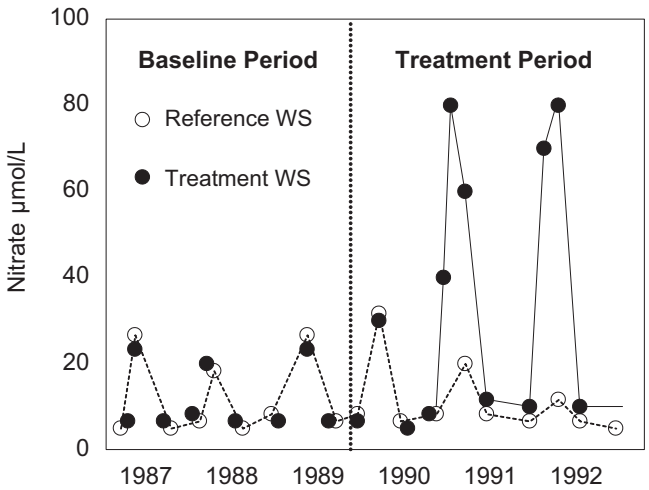

Fig. 12.5 Bear Brook Watershed responses to N enrichment (data from Norton et al. 1999). After N inputs increased, the treatment watershed exhibited elevated concentrations of nitrate-N in stream runoff

By the third year after treatment, stream water nitrate concentrations in the treatment watershed had more than tripled (Fig. 12.5), and N retention in the watershed had declined from reference levels of 94–74% retention of annual N inputs. These responses indicated that added inputs of N in the experimental treatment had exceeded the watershed capacity to retain N in various soil and biomass sinks.

Despite their impressive role as N sinks, forest ecosystems tend to respond to N enrichment with increased N exports in runoff, potentially accompanied by soil cation depletion, stream acidification, and other adverse impacts

associated with over-supply of N. One important consequence of N deposition to forests is the acidification of soils and the associated effects of this process on soil cation depletion and mobilization of ionic aluminum (Lawrence et al. 1999; Fernandez et al. 2003). Soil acidification may be further enhanced as declining soil C:N ratios promote increased nitrification rates, resulting in additional proton generation in the soil. As concentrations of nitrate ion increase in acidic forest soils, there is an increased potential for mobilization of soluble ionic Al^{3+} from soil minerals, which can interfere with divalent cation uptake and root growth (Cronan and Grigal 1995). At Harvard Forest, Aber et al. (1995) reported decreased Mg:N and Ca:Al ratios and declining tree growth and vigor in pine stands exposed to chronic N additions. In studies at Fernow Experimental Forest, WV, Gilliam et al. (1996) found that mixed hardwoods exposed to 4 yr of experimental amendments of N and S exhibited significantly lower tissue Ca concentrations compared to controls. Both of these examples are consistent with stress responses associated with soil acidification and Al antagonism of nutrient cation uptake.

Given current rates of atmospheric deposition, many temperate forests are gaining roughly 50–100 kg N ha^{-1} in aggrading biomass and soil organic matter each decade. As such, an important question for the future is whether these forests will respond to further N enrichment with growth stimulation or inhibition. Although evidence from the literature is somewhat equivocal on this topic, several studies have shown that forest growth is inhibited by chronically elevated N additions, especially in evergreen species (McNulty et al. 1996; Aber et al. 1998; Magill et al. 2000). Where this occurs, conditions of N saturation have the potential to diminish the strength of the plant sink in forest ecosystems, further de-stabilizing the N cycle.

Elevated N additions to forest ecosystems can potentially change microbial decomposition, N mineralization, nitrification, trace gas emissions, and N immobilization. Magill and Aber (1998) examined decomposition of red pine and mixed hardwoods litter for 6 yr at Harvard Forest, and reported that masses of litter remaining and lignin content of litter were significantly greater after 4 yr in N treated plots compared to controls. Berg et al. (1998) examined long-term decomposition of litter and humus in an N-saturated Scots pine stand in the Netherlands and found that enhanced atmospheric N deposition aggravates carbon limitation for microbial degradation processes. This contributes to strong reductions in long-term decomposition rates and increased accumulations of detrital C. Makipaa (1995) reported that 30 yr of cumulative additions of 596–926 kg N ha^{-1} to Scots pine and Norway spruce stands in Finland increased the carbon content of the humus layer by 14–87% and mineral soil by 15–167%. In contrast, Gundersen et al. (1998) compiled data from five coniferous NITREX sites in Europe and reported that forest floor mass decreased with increased N status of sites. There is thus some variability in the responses of organic matter cycles to N enrichment.

The fate of N additions to forest ecosystems is largely determined by interactions among plant, microbial, and soil organic matter N sinks. Investigators have shown that the strength and temporal influence of these sinks can vary somewhat among different study sites. Koopmans et al. (1996) followed the fate of ^{15}N added to N-saturated Douglas-fir and Scots pine forest plots in the Netherlands, and reported that up to 33% of the ^{15}N accumulated in tree biomass and up to 65% of the isotope was retained in the upper 70 cm of soil (with organic soil layers accounting for 60% of the total soil retention). Tietema et al. (1998) examined the fate of ^{15}N added as ammonium and nitrate to coniferous forests in the NITREX project. Up to 30% of the added isotope was taken up by trees and as much as 15% was retained in the mineral soil at all treatment levels. Sjoberg and Persson (1998) studied the fate of $^{15}NH_4^+$ added to mor humus samples from N-poor and N-rich plots in a Swedish Scots pine forest and concluded that the major mechanisms of immobilization were microbial N assimilation, followed by incorporation of nitrogen into soil organic matter. Nadelhoffer et al. (1999) examined sinks for ^{15}N additions to chronic N treatment plots at Harvard Forest and reported that forest floors and soils were the dominant sinks for N deposition. Mature trees accumulated <5% of ^{15}N added to reference plots and 20 to 24% of ^{15}N added to fertilized plots. In an old-growth temperate forest in southern Chile, Perakis and Hedin (2001) used ^{15}N to demonstrate that inputs of ammonium and nitrate are both retained by rapid assimilation and turnover through microbial biomass, and subsequent N transfer from microbial biomass into plant and soil organic matter pools.

Although forests are currently experiencing N enrichment in North America and Europe, a number of experiments have examined how forests might respond to simulated reductions in atmospheric N inputs. Gundersen et al. (1998) reported that nitrate leaching at N-saturated NITREX sites decreased almost to background levels after removal of N inputs with deposition exclusion roofs. Johannisson et al. (1999) reported that leaching of nitrate-N from a forest receiving annual additions of 108 kg N ha^{-1} rapidly decreased when N additions were stopped. Quist et al. (1999) examined the reversibility of N saturation in a 46-yr old Scots pine stand in northern Sweden exposed to 2 decades of annual inputs of 108 kg N ha^{-1}. After treatments were stopped, most of the symptoms of N saturation were largely reversed within 7 yr after the treatments ended.

Biogeochemical Implications of Rising Atmospheric CO_2 and Climate Change

The global climate system provides a fascinating template for thinking about biogeochemical feedbacks, especially when we consider the potential influence of anthropogenic CO_2 originating from combustion of fossil fuels and human land clearing activities. During the industrial period since 1850, concentrations of the atmospheric greenhouse gas, CO_2, have increased over 40% from roughly 280 ppm to roughly 400 ppm. How is the climate system responding to this change and what are the potential implications of this upturn in gaseous CO_2 for biogeochemical phenomena in watershed ecosystems?

As a starting point for our assessment, we can examine the fundamental interacting components of the climate system that govern the thermal regime of the earth. To state the obvious, the ultimate source of energy driving the climate system is the sun; the flux of this solar irradiance reaching the outer atmosphere varies as a function of sunspots, solar flare activity, and fluctuations in the Earth's orbit. In the atmosphere and at the surface of the earth, a major factor controlling the fate of solar inputs is the **albedo** or variable reflectivity of atmospheric dust and aerosols, snow cover, ice, open ocean water, contrasting land cover types, and clouds. Albedo represents a negative forcing factor in the global heat budget, offsetting the warming potential of solar irradiance. A higher albedo promotes cooler conditions, because more solar energy is reflected back into space. In contrast, a low albedo implies less reflectivity and more absorption of heat. Black carbon particles in the atmosphere, exposed dark soil, and ice-free ocean water all have a low albedo and tend to absorb solar radiation, thus contributing to warming of the planet.

The influence of albedo is counter-balanced to varying degrees by the presence of greenhouse gases (GHG) such as CO_2, N_2O, water vapor, chlorofluorocarbons (CFCs) and methane, which absorb infrared (IR) radiation that would otherwise reflect or radiate from the earth back into space. Human activities have had an especially strong modern influence on emissions of CO_2 and other anthropogenic GHG, thus increasing the warming potential of the climate system. With increased concentrations of these gases in the atmosphere, more IR radiation is trapped and more net heat energy is added to the dynamic climate system.

One potential positive feedback loop that accompanies the warming influence of rising CO_2 is an increase in evapotranspiration, which produces higher levels of atmospheric water vapor and associated warming by this greenhouse gas. In contrast, absorption and storage of atmospheric CO_2 by photosynthetic autotrophs or cool ocean water can slow the warming that would otherwise be expected to accompany rising emissions of this gas.

Clouds continue to be somewhat of an enigma in the climate system in that they can represent positive or negative forcing factors. Thinner clouds tend to contribute to warming of the atmosphere and earth as a result of the IR-absorbing behavior of water vapor. In contrast, thicker clouds contribute to albedo and act to cool the earth by reflecting incoming solar radiation. Thus, depending on the nature of cloud cover – whether thin and wispy or thick and cottony – the heat balance in a given region can be tipped toward warmer or cooler conditions.

Overall, evidence indicates that the earth is warming, and the stage is set for potentially dramatic changes in global weather patterns and climate. The rise in mean global temperature since 1850, the onset of drought conditions in Australia and the western U.S., the decrease in summer arctic sea ice cover, the recession of alpine glaciers, and the increased frequency and intensity of extreme weather events are all consistent with a warming and more active global climate system. How might these changes influence the biogeochemical patterns and processes we have discussed in earlier chapters?

Building a Conceptual Framework

Think about the hypotheses you would propose in an effort to build a conceptual framework for understanding the potential influences of global warming and climate change on biogeochemical patterns and processes. You might start by working your way through different system components such as soils, plants, microbes, and food webs, or perhaps you might be more interested in thinking about integrative concepts and processes such as disturbance or hydrologic coupling. Before reading any further, take some time to generate your own thoughts about this intellectual challenge – what are your predictions?

If we begin with soils, one might predict that some soils will experience important changes in thermal regime and/or moisture conditions, with possible implications for soil organic matter turnover. For soils that experience warming with adequate moisture, decomposition rates for surface litter and SOM may accelerate and this alone could lead to a decrease in soil organic carbon storage pools. The unknowns in this scenario are (i) to what degree is the soil heavy fraction "protected" from enhanced decomposition in response to warming; (ii) to what extent is modern nitrogen enrichment of soils likely to stabilize SOM and to retard the stimulatory influence of warming; and (iii) are there compensating inputs from biota that will offset carbon losses from accelerated decay of litter and SOM?

In a warming scenario, some soils may experience more soil freeze-thaw activity as insulating snow cover becomes less massive or less common. Two potential impacts of this

change could include a change in winter hydrology and flow paths, and a microbial response involving increased cell turnover or stimulation of carbon and nitrogen metabolism. These processes could combine to generate a winter spike in soil nitrate leaching from soils to adjacent streams. On the other hand, we might simply observe a time shift in an existing phenomenon. Currently, winter snow melt in the northeastern U.S. generates a pulse of nitrate leaching derived from snowpack and organic soil horizons. Conceivably, in a future warming scenario with less winter snowpack and more freeze-thaw activity, much of the vernal nitrate pulse may be replaced by spikes of nitrate leaching during winter precipitation and melting events.

How do we expect plants to respond to a climate change scenario characterized by warming and possible changes in moisture regime? For plants with access to adequate light, water, and nutrients, we might postulate that rising concentrations of CO_2 will stimulate increased plant productivity. Furthermore, we might expect plants to exhibit increased water use efficiency in response to elevated CO_2, and this could mean that moderate regional decreases in precipitation associated with climate change could be offset by the productivity gains of plants that are able to use water more efficiently. On the other hand, water stress may become more common in some areas where warming is accompanied by decreased precipitation during the growing season. Plant allocation patterns may well change as CO_2, nutrient, and water resources de-couple or shift in response to climate changes. In a scenario where water or nutrients become limiting, plants may allocate relatively more growth to belowground root production, which could influence the source-sink behavior of SOM. If plants respond to climate changes with altered competitive interactions and progressive shifts in geographic ranges, the resulting differences in community composition across the landscape could potentially affect the stoichiometry or magnitude of plant nutrient sinks, with implications for coupled processes involving soil microbes, SOM turnover, and watershed exports of nutrients.

If we envision a future scenario of climate change that is characterized by increased frequency and intensity of extreme weather events such as hurricanes, droughts, ice storms, or tornadoes, how might those changes translate into biogeochemical responses? From a simple conceptual perspective, we would expect that these events will generate disturbances of various magnitudes to the plant community, the soil system, and watershed-level water and nutrient cycles. Damage to the plant community will open a "window of opportunity" for short-term nutrient and sediment exports to streams, rivers, and even coastal waters. As a result, an increase in extreme weather events may create pulses of soil erosion and downstream nutrient export that may have cumulative measurable effects on the source watersheds and downstream receptors. At the same time, these disturbances will likely generate a pulse of woody detrital inputs to soils that may enhance SOM pools. In addition, in the aftermath of the disturbances, gaps in the forest landscape will be colonized by young successional vegetation that will act as a strong nutrient sink that minimizes the chances of further nutrient exports.

What about other possible interactions involving climate change and disturbance processes such as wildfire, insect outbreaks, and forest harvesting? One possible synergy that could occur in the future is that regional warming and drying could generate sufficient plant stress that trees become more susceptible to insect pest outbreaks. These combined stresses could increase tree mortality and fuel loads, and this could set the stage for new wildfire disturbances, with associated impacts on successional status, soil nutrients, and runoff chemistry. What we do not know is whether this type of scenario will contribute to expansion of the overall area subject to recurring wildfires, or whether we can expect a geographic shift in the locations of frequent wild fire disturbances.

How will wetland ecosystems respond to climate changes and how will these effects translate into biogeochemical impacts? Warming and loss of permafrost in boreal wetlands could stimulate emissions of CO_2 and methane from belowground stored carbon pools, producing a positive forcing effect on global warming processes. Yet, if warming is accompanied by increased evapotranspiration and decomposition in wetlands, the decline in soil waterlogging and increase in nutrient supply may promote increased plant productivity and carbon capture that offset some of the impacts of greenhouse gas release from peat and SOM. If water table recession is substantial in a warmer or drier future scenario, enhanced decomposition in wetland soils and peats may be accompanied by acidification processes (as S and N are oxidized) that contribute to surface water acidification.

The Rest of the Journey

In closing this final chapter, we have reached both an end and a beginning. Hopefully, you are now poised to begin a much more detail exploration of the amazing interrelationships and intriguing mysteries in this interdisciplinary field of science. May your path lead you to important new discoveries and insights regarding biogeochemical patterns and processes in the biosphere.

Biographical Sketch

The author is a Professor in the School of Biology and Ecology at the University of Maine, Orono, ME. He wrote a previous introductory textbook entitled *Introduction to Ecology and Ecosystems Analysis*, and has published over 70 peer-reviewed scientific articles in journals such as *Bioscience, Science, Nature, Water Resources Research, Environmental Science and Technology, Ecological Modeling, Landscape Ecology, Tree Physiology, Biogeochemistry, Analytical Chemistry, Soil Science Society of America Journal, Geochimica Cosmochimica Acta*, and *Environmental Management*. He is former director of the School of Biology and Ecology and founding director of the Graduate Program in Ecology and Environmental Science at the University of Maine. The author earned a B.A. in Ecology at the University of Pennsylvania and a Ph.D. in Biological Sciences at Dartmouth College.

C.S. Cronan, *Ecosystem Biogeochemistry*, Springer Textbooks in Earth Sciences, Geography and Environment, DOI 10.1007/978-3-319-66444-6

Epilogue

Biogeochemical processes are part of an amazing *complex adaptive system* in the biosphere that is characterized by diverse interconnections and feedbacks, coupled with remarkable emergent patterns and properties expressed in the form of biological and ecological diversity, ecosystem services, and human creativity and culture. At present, the biosphere and its inhabitants represent a system in transition. We are in a time of dynamic changes and adjustments in the world economy, in the social fabric of human cultures, and in the interconnected life systems of the biosphere. Arctic summer sea ice expanse has reached another historic minimum, greenhouse gas emissions from human activities are ever increasing, biodiversity is at risk from multiple stresses, water tables are declining in many regions, and the evidence of biogeochemical imbalances and disturbances is apparent across the globe. In a human population that has grown to over 7 billion persons, we have the seeds of a future teetering on the edge of disaster, famine, and stress, but we also have a rising wave of incredible human creative energy and intellectual capital. Both fear and hope seem to be in constant struggle in the minds and lives of many.

So, what are the options? Is it reasonable to think that human knowledge, ingenuity, compassion, and cooperation can provide a means of confronting and overcoming these global challenges? Certainly, it is reasonable, but is it likely? Perhaps one meaningful way to answer this question is to say that solutions to these challenges will be more likely to arise if we can forge a shared vision based on sustainable principles and actions. The challenge then becomes one of defining a working approach by which human society makes more efficient use of resources, reduces consumption, minimizes the human footprint of development and waste generation, and embraces a sea change in the current rules of the marketplace.

By some means, we must articulate and implement a vision of stewardship, human development, and global commerce that measures up to the standards of sustainability. This is the global challenge we face – to transform knowledge into wisdom and wisdom into sustainable decisions and actions that support and maintain the creative potential and health of human civilization and the entire biosphere.

C.S. Cronan, *Ecosystem Biogeochemistry*, Springer Textbooks in Earth Sciences, Geography and Environment, DOI 10.1007/978-3-319-66444-6

Problem Sets

Sample Problems in General Chemistry

1. A rock sample contains 15% Al_2O_3 by weight. What is the concentration of Al in mg kg^{-1}?
2. A leaf contains 2.0% nitrogen on a dry weight basis. What is the N concentration in ppm (parts per million)? If the fresh leaf contains 75% water, what is the N concentration on a fresh weight or wet weight basis?
3. How do you prepare a 5×10^{-3} M solution of phosphate using KH_2PO_4?
4. What is the H^+ ion activity in moles L^{-1} of a water sample at pH 4.73?
5. What is the pH of a water sample containing 0.000165 moles H^+ L^{-1}?
6. What mass of NaOH would be required to neutralize 3000 L of pH 4.5 rainwater?
7. The isotopic ratio $^{87}Sr/^{86}Sr$ for an ocean water standard is 0.70923
   (a) If the $^{87}Sr/^{86}Sr$ ratio for atmospheric aerosols in New York is 0.70931, what is the delta value ($\delta\ ^{87}Sr$) of this sample *permil* relative to the ocean standard?
   (b) If the $^{87}Sr/^{86}Sr$ ratio for feldspar minerals in New York is 0.70516, what is the delta value ($\delta\ ^{87}Sr$) of this sample *permil* relative to the ocean standard?
8. Rain begins to fall from an air mass whose initial $\delta^{18}O$ value is −9.0‰; the fractionation factor ($\alpha_{\text{liquid-vapor}}$) is 1.0092 at the condensation temperature.
   (a) Apply the Raleigh Distillation Equation to compute the isotopic composition of the air mass after 60% of the water vapor has recondensed. Express your answer as $\delta^{18}O$.
   (b) Compute the isotopic composition of the resulting rainwater as a value of $\delta^{18}O$.

Sample Problems in Soil Chemistry

9. You have a mineral soil with a moisture content of 50% and a bulk density of 1.5 g cm^{-3}. You want to determine the concentrations of exchangeable cations and the percent base saturation. You extract 5.0 g of field-moist soil with 100 ml of 1 M NH_4Cl and a separate 5.0 g of soil with 100 ml of 2 M KCl. You centrifuge and filter the supernatants of each soil extraction and use an AAS instrument to estimate the following concentrations of cations in each supernatant:

Cation	Concentration in Extract, mg L^{-1}
H^+	0.25
Al^{3+}	22.5
Ca^{2+}	5.0
Mg^{2+}	0.30
K^+	0.78
Na^+	0.06

   (a) What are the exchangeable cation concentrations in cmol(+) kg^{-1}?
   (b) What is the effective cation exchange capacity (CEC)? [Effective CEC = sum of all exchangeable cations at field pH]
   (c) What is the percent base saturation (% B.S.) for the soil?
   (d) What is the pool of exchangeable Ca in the uppermost 20 cm of this soil (expressed in moles (+) ha^{-1})?

10. For the soil in the previous problem, it is known from laboratory titration that this soil has a pH of 4.5 at 10% base saturation and a pH of 5.5 at 40% base saturation. How much limestone ($CaCO_3$) would theoretically be required to increase the base saturation from 10% to 40% in the uppermost 20 cm of soil?

Sample Problems in Atmospheric Deposition

11. The precipitation sample shown below was collected on a mountain in New England and was rushed to the laboratory for immediate analysis. How would the chemistry and pH change if nitrification by microbial contaminants occurred in the water sample prior to analysis and all of the NH_4^+ was nitrified? The ion concentrations are expressed in µmol L^{-1}. Indicate final pH and concentrations of ammonium and nitrate.

C.S. Cronan, *Ecosystem Biogeochemistry*, Springer Textbooks in Earth Sciences, Geography and Environment, DOI 10.1007/978-3-319-66444-6

	H_2O (cm)	pH	Ca	Mg	NH_4^+	SO_4^{2-}	NO_3^-
Rain Sample	2	4.10	11	5	22	98	25

12. Listed below are data for monthly mean precipitation amounts and sulfate ion concentrations at one location in the southeastern United States.

Month	Precipitation (cm)	Sulfate (mg L^{-1})
1	31.8	3.5
2	18.7	3.9
3	38.7	3.4
4	23.4	3.8
5	19.5	2.9
6	5.1	3.2
7	2.9	3.0
8	2.1	2.4
9	4.6	2.6
10	1.8	3.2
11	9.8	2.7
12	20.4	3.0

(a) Compare the unweighted and volume-weighted annual mean sulfate concentrations.
(b) Calculate the annual wet deposition of sulfate (SO_4^{2-}) in mol_c ha^{-1} yr^{-1} and sulfate-S in kg S ha^{-1} yr^{-1}.
(c) If the mean annual volume-weighted pH of precipitation is 4.3 at this site, what is the approximate annual H^+ ion deposition in mol_c ha^{-1} yr^{-1}?

Sample Problem in Hydrology

13. Visit the Water Resources of Maine website at http://me.water.usgs.gov and use the data base to survey hydrologic runoff records for the Aroostook River at Masardis (site number 01015800). You can use this USGS data base to find all kinds of historical and real-time data for streamflow conditions. I have previously asked students to find specific peak flow records in the online data base, but the USGS keeps changing the site and updating the runoff numbers, which means that the problem answer keeps changing to match changes in the data base. As a result, I am providing the runoff value below that is required to answer the problem.
(a) During the period 1978–1998, the highest daily runoff flow occurred on 4/19/83 and reached a value of 23,100 cfs. For this watershed, the drainage area is 892 square miles. Express that peak flow in the following two different units: cubic meters per second (m^3/s), and cm of flow per day from the drainage basin. The last term expresses peak flow on a unit area basis similar to the measurement of precipitation inputs (e.g., so many cm of rainfall per 24-h day).
(b) Retrieve the daily mean discharge data for the same river site during the period September 1, 1999 to September 30, 1999. Prepare a flow duration or exceedence graph for the September data using a log scale on the y-axis labeled Daily Runoff (cfs) and an arithmetic scale on the x-axis labeled Frequency of Runoff this High.

Sample Problems in Mineral Weathering

14. You have been hired to analyze data from a U.S. Forest Service watershed to determine the relative contributions of atmospheric deposition and weathering to stream cation exports. A previous vegetation study indicated that net annual biomass increment in the watershed is 1000 kg dry matter ha^{-1} yr^{-1} with mean weighted cation concentrations for the biomass increment of 0.5% Ca, 0.5% Mg, and 1.0% K (with no detectable Na). The hydrologic budget shows 100 cm of precipitation, 40 cm of evapotranspiration, and 60 cm of stream runoff. Estimate weathering in mol_c ha^{-1} yr^{-1} for each of the four major cations; show your work and state your assumptions.

	Ca	Mg	K	Na
Precipitation Chemistry				
Weighted mean, mg L^{-1}	0.20	0.06	0.20	0.12
Stream Chemistry				
Weighted mean, mg L^{-1}	2.00	0.30	0.78	1.15

15. Most experimental studies of weathering indicate that dissolution of feldspars increases as a function of solution acidity. Which solution would produce a faster initial rate of weathering: a solution of an organic acid such as fulvic acid at pH 4.85 or an aqueous solution of carbonic acid in equilibrium with a pCO_2 of 1.5%? Show your work and explain your answer.
16. How much acid neutralizing capacity (ANC) is released during the weathering of 15.0 g of anorthite, a calcium feldspar (as illustrated below)? Show your computational steps, your ANC expression, and present your answer in $mmol_c$.

$$CaAl_2Si_2O_8 + 2H_2CO_3 + H_2O \rightarrow Ca^{2+} + 2HCO_3^- + Al_2Si_2O_5(OH)_4$$

Sample Problems in Element Cycling and Aqueous Chemistry

17. A forest calcium budget shows an annual Ca uptake by plants of 56 kg ha^{-1}. Focusing only on Ca and assuming that Ca^{2+} uptake is coupled with proton release from the plant root to the soil rhizosphere, what is the potential

H^+ ion release associated with the annual uptake of Ca? Show your work and express your answer in mol_c ha^{-1} yr^{-1}. How does this estimate compare with the average annual atmospheric wet deposition of H^+ ion in New England (assuming mean pH = 4.3 and annual precipitation = 100 cm)?

18. Consider a watershed where the weighted annual mean concentration of chloride ion in precipitation is 25 μmol(−) L^{-1}, the average annual stream runoff is 65% of precipitation inputs, and water storage is stable (i.e., steady-state on an annual basis). If you assume that chloride moves "conservatively" through the system without enrichment or depletion of mass (from uptake, mineralization, adsorption, or weathering), what is the final weighted annual mean concentration of Cl^- ion in stream water?
19. Consider a forest with an annual N uptake of 50 kg N ha^{-1} yr^{-1}, rainfall equivalent to 100 cm, and transpiration equivalent to 25% of rainfall. If we assumed that the forest acquires all of its N via passive bulk flow of transpirational water, what concentration of N in the soil water (as dissolved inorganic N) is necessary to allow the forest to take up 50 kg N ha^{-1} yr^{-1}? Express your answer as the solution concentration of inorganic N in mg L^{-1}. [Note that concentrations of inorganic N in field soil solutions are commonly <10% of the mean value you have calculated; this suggests that plants must use energy-dependent active uptake to meet their N demand].

Sample Problems in Organic Matter Cycling

20. Data are presented below indicating the chemical composition of fresh leaf litter from three **northern tree species**. Use the data to predict which litter substrate would decay fastest. Rank the species from highest to lowest in order of their expected rates of decay. Show your logic or computations, and indicate the literature reference(s) upon which your rationale is based.

Species	%N	%Ca	%K	%Lignin
A	1.6	0.05	0.12	12.0
B	1.6	0.07	0.18	16.0
C	2.4	0.10	0.22	18.0

21. What is the estimated annual CO_2 release from microbial decomposition of organic matter in the forest floor (O horizon) of an ecosystem under the following conditions? State any assumptions and express CO_2 release in g CO_2 m^{-2} yr^{-1}
    - The forest floor is assumed to be in steady-state
    - Forest floor mass is 50,000 kg organic matter ha^{-1}
    - Annual inputs of detritus to the forest floor from litterfall + root mortality + throughfall DOM = 2500 kg organic matter ha^{-1} yr^{-1}
22. Does leaf decay generate acidity or alkalinity? Consider a gram of decaying leaf with the composition shown below. Estimate the net ANC production that will likely result from complete microbial mineralization of this leaf with an initial mass of 1.0 g. Show three possible outcomes for this decomposition process based on the following assumptions: (1) assume that all of the N is only subject to ammonification, (2) assume that all of the N is subject to ammonification followed by 100% nitrification, and (3) assume all of the mineralized N is ultimately denitrified to dinitrogen, N_2. Remember to consider the other elements as well.

Foliar concentrations (shown below) in parts per thousand in a leaf weighing 1.0 g

Carbon = 480	Nitrogen = 7	Sulfur = 2
Calcium = 8	Potassium = 4	Magnesium = 1

Sample Problems on Element Budgets

23. Use the data below to estimate how much calcium is exported from this watershed in a 1-year time period. Express your answer in moles of charge (mol_c yr^{-1}) and indicate any assumptions you made. (note that cfs = cubic feet per second)

Month	Mean daily flow (cfs)	Mean Daily Ca concentration mg L^{-1}
J	1000	3
F	1500	3
M	1200	3
A	4000	2
M	6000	2
J	3000	3
J	500	5
A	500	6
S	2000	3
O	4000	3
N	7000	2
D	1000	2

24. Consider a forest soil where the subsurface pool of soil organic matter contains 150,000 kg C ha^{-1} and decays at an annual rate of 0.5% yr^{-1}. What is the mean residence time of this carbon pool and how much carbon as root detritus and DOM must be transferred into this pool each year (in units of g C m^{-2} yr^{-1}) to maintain it at steady-state? How does this estimate compare with reported values of fine root biomass and turnover?

Problem Answers

Sample Problems in General Chemistry

1. A rock sample contains 15% Al_2O_3 by weight. What is the concentration of Al in mg kg^{-1}?

   Answer:

   Formula Weight of $Al_2O_3 = (2 \times 27) + (3 \times 16) = 102$ g

   Aluminum represents 54/102 or 52.9% of the formula weight

   The rock sample contains 15 g Al_2O_3 per 100 g of total rock

   The aluminum content equals 52.9% of the Al_2O_3 or 0.529×15 g $Al_2O_3 = 7.935$ g

   Thus, the rock contains 7.935 g Al per 100 g rock

   Multiply numerator and denominator by 10 to scale up to a kg

   This gives 79.35 g Al per 1000 g rock

   Multiply the numerator by 1000 mg per g to get (79.35 g Al/ kg rock) × (1000 mg/g)

   This yields 79,350 mg Al kg^{-1} rock

2. A leaf contains 2.0% nitrogen on a dry weight basis. What is the N concentration in ppm (parts per million)? If the fresh leaf contains 75% water, what is the N concentration on a fresh weight or wet weight basis?

   Answer:

   2% N = 2 mg N per 100 mg dry leaf

   1 ppm = 1 mg per 1000,000 mg, so we must multiply by 10,000 to get the nitrogen mass associated with one million mg of dry leaf material

   Multiply (2 mg N / 100 mg dry leaf) × $10^4/10^4$ = 20,000 mg N / 1000,000 mg dry leaf

   This is equivalent to 20,000 ppm N

   On a fresh weight basis with 75% water, you have 1 part dry mass per 4 parts total mass

   20,000 ppm N × (1 part dry mass / 4 parts dry mass + water) = 5000 ppm N

3. How do you prepare a 5×10^{-3} M solution of phosphate using KH_2PO_4?

   Answer:

   The formula weight for this compound is 39 + 2 + 31 + 64 = 136 g

   The final concentration is 0.005 M

   0.005 M × 136 g / mole = 0.68 g KH_2PO_4

4. What is the H^+ ion activity in moles L^{-1} of a water sample at pH 4.73?

   Answer:

   Since pH is the negative log of hydrogen ion activity, to compute molar H^+ ion activity from pH, take the value of 10^{-pH} or $10^{-4.73}$, which equals 1.86×10^{-5} M L^{-1}

5. What is the pH of a water sample containing 0.000165 moles H^+ L^{-1}?

   Answer:

$$pH = -\log(0.000165) = 3.78$$

6. What mass of NaOH would be required to neutralize 3000 L of pH 4.5 rainwater?

   Answer:

   Rainwater acidity = $10^{-pH} = 10^{-4.5} = 0.0000316$ moles H^+ L^{-1}

   3000 L × 0.0000316 moles H^+ L^{-1} = 0.0948 moles H^+

   This must be balanced by an equivalent amount of NaOH (formula weight = 40 g)

   0.0948 mole NaOH × 40 g / mole NaOH = 3.79 g NaOH to neutralize acidity

7. The isotopic ratio $^{87}Sr/^{86}Sr$ for an ocean water standard is 0.70923

   (a) If the $^{87}Sr/^{86}Sr$ ratio for atmospheric aerosols in New York is 0.70931, what is the delta value ($\delta\ ^{87}Sr$) of this sample *permil* relative to the ocean standard?

   Answer:

$$\delta = \left(\left(R_{sample} - R_{standard}\right) / R_{standard}\right) * 1000$$

$$= \left[\left(0.70931 - 0.70923\right) / 0.70923\right] \times 1000 = +0.1128‰$$

C.S. Cronan, *Ecosystem Biogeochemistry*, Springer Textbooks in Earth Sciences, Geography and Environment, DOI 10.1007/978-3-319-66444-6

(b) If the $^{87}Sr/^{86}Sr$ ratio for feldspar minerals in New York is 0.70516, what is the delta value ($\delta\,^{87}Sr$) of this sample *permil* relative to the ocean standard?

Answer:

$$\left[\left(0.70516-0.70923\right)/0.70923\right]\times 1000=-5.7386‰$$

8. Rain begins to fall from an air mass whose initial $\delta^{18}O$ value is −9.0‰; the fractionation factor ($\alpha_{\text{liquid-vapor}}$) is 1.0092 at the condensation temperature.

(a) Apply the Raleigh Distillation Equation to compute the isotopic composition of the air mass after 60% of the water vapor has recondensed. Express your answer as $\delta^{18}O$.

Answer:

$$\delta^{18}O_{\text{air mass}}=\left[\left(\delta^{18}O_{o}\right)+1000\right]f^{(\alpha-1)}-1000$$
$$=\left[\left(-9.0‰\right)+1000\right]\times\left(0.4\right)^{(1.0092-1)}-1000$$
$$=-8.92445+991.60556-1000$$
$$=-17.32‰$$

(b) Compute the isotopic composition of the resulting rainwater as a value of $\delta^{18}O$.

Answer:

$$\delta^{18}O_{\text{rainwater}}=\alpha\left(\delta^{18}O_{\text{vapor}}+1000\right)-1000$$
$$=1.0092\left(-17.32‰+1000\right)-1000$$
$$=-17.48‰+1009.2-1000$$
$$=-8.28‰$$

Sample Problems in Soil Chemistry

9. You have a mineral soil with a moisture content of 50% and a bulk density of 1.5 g cm^{-3}. You want to determine the concentrations of exchangeable cations and the percent base saturation. You extract 5.0 g of field-moist soil with 100 ml of 1 M NH_4Cl and a separate 5.0 g of soil with 100 ml of 2 M KCl. You centrifuge and filter the supernatants of each soil extraction and use an AAS instrument to estimate the following concentrations of cations in each supernatant:

Cation	Concentration in Extract, mg L^{-1}
H^+	0.25
Al^{3+}	22.5
Ca^{2+}	5.0
Mg^{2+}	0.30
K^+	0.78
Na^+	0.06

(a) What are the exchangeable cation concentrations in cmol(+) kg^{-1}?

Answer:

The general principle is that you must convert extract concentrations to centimoles of ionic charge and then transform this value to $cmol_c$ per kg of dry soil. If a mol_c of Al^{3+} has a mass of 9.0 g (based on a formula weight of 27 g / valence of 3+), then a $cmol_c$ of Al^{3+} has 1/100th of that mass or 0.09 g or 90 mg. In the example above, you extract 5.0 g of moist soil that has 50% moisture content, so you actually have 2.5 g dry soil. You are extracting the soil in 100 ml of salt solution, which is one-tenth of a liter. This means that the absolute value of extracted cation in the 100 ml volume is 10% of the extract concentration listed above in mg L^{-1}.

Let's look at an example for Ca^{2+} from the list of extracted cations.

Convert the supernatant extract concentration to $cmol_c\ L^{-1}$

5 mg $Ca^{2+}\ L^{-1}$ × 1 $cmol_c$ / 200 mg Ca^{2+} = 0.025 $cmol_c$ $Ca^{2+}\ L^{-1}$

Scale the ion concentration in the 100 ml extract to a concentration per mass of dry soil

0.025 $cmol_c$ $Ca^{2+}\ L^{-1}$ × (0.1 L extract volume / 2.5 g dry soil) = 0.0025 $cmol_c$ / 2.5 g dry soil

Then, scale to 1 kg dry soil

(0.0025 $cmol_c$ / 2.5 g dry soil) × (1000 g / kg) = 1.0 $cmol_c$ $Ca^{2+}\ kg^{-1}$ dry soil

Using that approach, the exchangeable cation concentrations in cmol(+) kg^{-1} are as follows:

$$H^+=1, Al^{3+}=10.0, Ca^{2+}=1.0, Mg^{2+}$$
$$=0.1, K^+=0.08, \text{and } Na^+=0.008.$$

(b) What is the effective cation exchange capacity (CEC)?

[Effective CEC = sum of all exchangeable cations at field pH]

Answer:

$$\text{Effective CEC} = \text{sum of exchangeable } H^+ + Al^{3+} + Ca^{2+} + Mg^{2+} + K^+ + Na^+$$
$$=1+10+1+0.1+0.08+0.008=12.19\,\text{cmol}(+)\,kg^{-1}$$

(c) What is the percent base saturation (% B.S.) for the soil?

Answer:

The percent base saturation equals the sum of base forming cations as a percentage of the CEC.

$$\%\text{B.S.}=\left[\frac{\left(\text{Sum of Exchangeable Ca}+\text{Mg}+\text{K}+\text{Na}\right)}{\text{CEC}}\right]\times 100$$
$$=\left(1.188/12.19\right)\times 100=9.74\%$$

(d) What is the pool of exchangeable Ca in the uppermost 20 cm of this soil (expressed in moles (+) ha^{-1})?

Answer:

The volume of soil per square meter = 20 cm depth × 10^4 cm^2 m^{-2} = 2 × 10^5 cm^3 m^{-2}

Multiply by soil bulk density to get 1.5 g cm^{-3} × 2 × 10^5 cm^3 m^{-2} = 3 × 10^5 g m^{-2}

Divide by 1000 to convert soil mass to kg basis = 300 kg soil m^{-2}

Given a soil exchangeable concentration of 1.0 $cmol_c$ Ca^{2+} kg^{-1} dry soil, compute the following:

Exchangeable Ca^{2+} = 1.0 $cmol_c$ Ca^{2+} kg^{-1} × 300 kg soil m^{-2} = 300 $cmol_c$ Ca^{2+} m^{-2}

Convert to moles: 300 $cmol_c$ Ca^{2+} m^{-2} × (1 mol_c Ca^{2+} / 100 $cmol_c$ Ca^{2+}) = 3 mol_c Ca^{2+} m^{-2}

Scale to one hectare, where 1 ha = 10^4 m^2

3 mol_c Ca^{2+} m^{-2} × 10^4 m^2 ha^{-1} = 30,000 moles(+) ha^{-1}

10. For the soil in the previous problem, it is known from laboratory titration that this soil has a pH of 4.5 at 10% base saturation and a pH of 5.5 at 40% base saturation. How much limestone ($CaCO_3$) would theoretically be required to increase the base saturation from 10% to 40% in the uppermost 20 cm of soil?

Answer:

From earlier steps, we know that CEC = 12.2 $cmol_c$ kg^{-1}, exchangeable Ca^{2+} = 1.0 $cmol_c$ kg^{-1}, and the exchangeable pool of Ca^{2+} in the upper 20 cm of soil = 30,000 mol_c ha^{-1}

Compute the CEC per hectare as follows:

(12.2 $cmol_c$ CEC kg^{-1} / 1.0 $cmol_c$ Ca^{2+} kg^{-1}) × 30,000 mol_c Ca^{2+} ha^{-1} = 366,000 mol_c CEC ha^{-1}

10% base saturation = 0.10 × 366,000 mol_c CEC ha^{-1} = 36,600 mol_c ha^{-1}

40% base saturation = 0.40 × 366,000 mol_c CEC ha^{-1} = 146,400 mol_c ha^{-1}

To increase the base saturation from 10% to 40% requires the addition of exchangeable bases equal to:

146,400–36,600 = 109,800 mol_c ha^{-1}

One mol_c of $CaCO_3$ = formula weight / valence of 2^+ = 100 g /2 = 50 g = 0.050 kg

(0.05 kg $CaCO_3$ / mol_c) × (109,800 mol_c / ha) = 5490 kg $CaCO_3$ per hectare

Sample Problems in Atmospheric Deposition

11. The precipitation sample shown below was collected on a mountain in New England and was rushed to the laboratory for immediate analysis. How would the chemistry and pH change if nitrification by microbial contaminants occurred in the water sample prior to analysis and all of the NH_4^+ was nitrified? The ion concentrations are expressed in µmol L^{-1}. Indicate final pH and concentrations of ammonium and nitrate.

	H_2O	pH	Ca	Mg	NH_4^+	SO_4^{2-}	NO_3^-
	(cm)						
Rain Sample	2	4.10	11	5	22	98	25

Answer:

Use a basic equation for nitrification as follows: $NH_4^+ + 2O_2 \rightarrow NO_3^- + H_2O + 2H^+$

Substitute in the stoichiometric values shown above for the rain sample

$22NH_4^+ + 44O_2 \rightarrow 22NO_3^- + 22H_2O + 44H^+$

Final NH_4^+ = 0 µmol L^{-1}

Final NO_3^- = 25 + 22 = 47 µmol L^{-1}

Initial H+ = $10^{-4.1}$ = 0.000079 M L^{-1} = 79 µmol L^{-1}

Final H^+ = 79 + 44 = 123 µmol L^{-1} = 0.000123 M L^{-1}

pH = − log [0.000123] = 3.91

12. Listed below are data for monthly mean precipitation amounts and sulfate ion concentrations at one location in the southeastern United States.

Month	Precipitation (cm)	Sulfate (mg L^{-1})
1	31.8	3.5
2	18.7	3.9
3	38.7	3.4
4	23.4	3.8
5	19.5	2.9
6	5.1	3.2
7	2.9	3.0
8	2.1	2.4
9	4.6	2.6
10	1.8	3.2
11	9.8	2.7
12	20.4	3.0

(a) Compare the unweighted and volume-weighted annual mean sulfate concentrations.

Answer:

The unweighted mean concentration is the sum of the 12 monthly sulfate values divided by 12.

= 3.13 mg SO_4^{2-} L^{-1}

The volume-weighted mean is calculated by weighting each monthly sulfate concentration by the monthly precipitation value in cm, using the following relationship:

Σ (concentration$_i$ × cm of precipitation$_i$) / Σ cm of precipitation = 3.34 mg SO_4^{2-} L^{-1}

(b) Calculate the annual wet deposition of sulfate (SO_4^{2-}) in mol_c ha^{-1} yr^{-1} and sulfate-S in kg S ha^{-1} yr^{-1}.

Answer:

3.34 mg L^{-1} × 178.8 cm × (10^4 cm^2 / m^2) × (1 L / 10^3 cm^3) × (10^4 m^2 / ha) × (1 kg / 10^6 mg)

= 59.7 kg SO_4^{2-} ha^{-1}

Convert to moles$_c$ = 59.7 kg SO_4^{2-} ha^{-1} × (1 mol$_c$ / 0.048 kg SO_4^{2-}) = 1244 mol$_c$ SO_4^{2-} ha^{-1}

Sulfate-S deposition = 59.7 kg SO_4^{2-} ha^{-1} × (32 g S / 96 g SO_4) = 19.9 kg S ha^{-1}

Here is a shortcut for step 1

You can make a 10^6 jump from mg L^{-1} to kg ha^{-1} or from μmol$_c$ L^{-1} to mol$_c$ ha^{-1} with the following:

(annual weighted concentration) × (annual precipitation) / 10

e.g., 3.34 mg SO_4^{2-} L^{-1} × 178.8 cm / 10 = 59.7 kg SO_4^{2-} ha^{-1}

[Note that the units do not carry through in the computation above, so you have to know the final units]

(c) If the mean annual volume-weighted pH of precipitation is 4.3 at this site, what is the approximate annual H^+ ion deposition in mol$_c$ ha^{-1} yr^{-1}?

Answer:

H^+ ion activity = $10^{-4.3}$ = 0.00005 mol H^+ L^{-1} = 5 × 10^{-5} mol L^{-1} = 50 μmol$_c$ L^{-1}

Using the scaling relationship shown in the previous shortcut,

(50 μmol$_c$ H^+ L^{-1}) × 178.8 cm / 10 = 894 mol$_c$ H^+ ha^{-1}

Sample Problem in Hydrology

13. Visit the Water Resources of Maine website at http://me.water.usgs.gov and use the data base to survey hydrologic runoff records for the Aroostook River at Masardis (site number 01015800). I have previously asked students to find specific peak flow records in the online data base, but the USGS keeps changing the site and updating the runoff numbers, which means that the problem answer keeps changing to match changes in the data base. As a result, I am providing the runoff value below that is required to answer the problem.

(a) During the period 1978–1998, the highest daily runoff flow occurred on 4/19/83 and reached a value of 23,100 cfs. For this watershed, the drainage area is 892 square miles. Express that peak flow in the following two different units: cubic meters per second (m^3/s), and cm of flow per day from the drainage basin. The last term expresses peak flow on a unit area basis similar to the measurement of precipitation inputs (e.g., so many cm of rainfall per 24-h day).

Answer:

The highest annual flow occurred on 4/19/83 and reached a value of 23,100 cfs

23,100 cfs × (0.0283 m^3 / ft^3) = 654 m^3 s^{-1}

To compute the cm of flow, first calculate the drainage area in cm^2

Drainage area = 892 mi^2 × (2.59 km^2 / mi^2) = 2310 km^2

2310 km^2 × (10^6 m^2 / km^2) × (10^4 cm^2 / m^2) = 2.31 × 10^{13} cm^2

Now, convert the peak flow to cubic centimeters for a 24 hr. period

654 m^3 s^{-1} × (10^6 cm^3 / m^3) × (60 s / min) × (60 min / hr) × (24 hr. / day) = 5.65 × 10^{13} cm^3 d^{-1}

Divide the volume of discharge by the area of the watershed

(5.65 × 10^{13} cm^3 d^{-1}) / (2.31 × 10^{13} cm^2) = 2.45 cm d^{-1} per unit of watershed area

(b) Retrieve the daily mean discharge data for the same river site during the period September 1, 1999 to September 30, 1999. Prepare a flow duration or exceedence graph for the September data using a log scale on the y-axis labeled Daily Runoff (cfs) and an arithmetic scale on the x-axis labeled Frequency of Runoff this High.

Answer:

Use Fig. 8.28 in Chap. 8 as an example for this problem.

Sample Problems in Mineral Weathering

14. You have been hired to analyze data from a U.S. Forest Service watershed to determine the relative contributions of atmospheric deposition and weathering to stream cation exports. A previous vegetation study indicated that net annual biomass increment in the watershed is 1000 kg dry matter ha^{-1} yr^{-1} with mean weighted cation concentrations for the biomass increment of 0.5% Ca, 0.5% Mg, and 1.0% K (with no detectable Na). The hydrologic budget shows 100 cm of precipitation, 40 cm of evapotranspiration, and 60 cm of stream runoff. Estimate weathering in mol$_c$ ha^{-1} yr^{-1} for each of the four major cations; show your work and state your assumptions.

	Ca	Mg	K	Na
Precipitation Chemistry				
Weighted mean, mg L^{-1}	0.20	0.06	0.20	0.12
Stream Chemistry				
Weighted mean, mg L^{-1}	2.00	0.30	0.78	1.15

Answer:

Assume that (i) weathering = sum of cations in runoff – cations in precipitation + cations in biomass increment, and

(ii) dry deposition and changes in stored soil cations are negligible.

Cations in the biomass increment of 1000 kg ha^{-1} yr^{-1} are

Ca = 0.005 × 1000 kg ha^{-1} yr^{-1} = 5 kg Ca ha^{-1} yr^{-1} × (1 mol_c / 0.02 kg Ca^{2+}) = 250 mol_c ha^{-1} yr^{-1}

Mg = 0.005 × 1000 kg ha^{-1} yr^{-1} = 5 kg Mg ha^{-1} yr^{-1} × (1 mol_c / 0.01215 kg Mg^{2+}) = 411 mol_c ha^{-1} yr^{-1}

K = 0.01 × 1000 kg ha^{-1} yr^{-1} = 10 kg K ha^{-1} yr^{-1} × (1 mol_c / 0.039 kg K^+) = 256 mol_c ha^{-1} yr^{-1}

Cations in precipitation can be computed using the shortcut from Problem 12b.

Ca = 0.2 mg L^{-1} × 100 cm / 10 = (2 kg ha^{-1} yr^{-1}) × (1 mol_c / 0.02 kg Ca^{2+}) = 100 mol_c Ca^{2+} ha^{-1} yr^{-1}

Mg = 0.06 mg L^{-1} × 100 cm / 10 = (0.6 kg ha^{-1} yr^{-1}) × (1 mol_c / 0.01215 kg Mg^{2+}) = 49 mol_c Mg^{2+} ha^{-1} yr^{-1}

K = 0.2 mg L^{-1} × 100 cm / 10 = (2 kg ha^{-1} yr^{-1}) × (1 mol_c / 0.039 kg K^+) = 51 mol_c K^+ ha^{-1} yr^{-1}

Na = 0.12 mg L^{-1} × 100 cm / 10 = (1.2 kg ha^{-1} yr^{-1}) × (1 mol_c / 0.023 kg Na^+) = 52 mol_c Na^+ ha^{-1} yr^{-1}

Cations in stream runoff can also be computed using the shortcut from Problem 12b.

Ca = 2 mg L^{-1} × 60 cm / 10 = (12 kg ha^{-1} yr^{-1}) × (1 mol_c / 0.02 kg Ca^{2+}) = 600 mol_c Ca^{2+} ha^{-1} yr^{-1}

Mg = 0.3 mg L^{-1} × 60 cm / 10 = (1.8 kg ha^{-1} yr^{-1}) × (1 mol_c / 0.01215 kg Mg^{2+}) = 148 mol_c Mg^{2+} ha^{-1} yr^{-1}

K = 0.78 mg L^{-1} × 60 cm / 10 = (4.68 kg ha^{-1} yr^{-1}) × (1 mol_c / 0.039 kg K^+) = 120 mol_c K^+ ha^{-1} yr^{-1}

Na = 1.15 mg L^{-1} × 60 cm / 10 = (6.9 kg ha^{-1} yr^{-1}) × (1 mol_c / 0.023 kg Na^+) = 300 mol_c Na^+ ha^{-1} yr^{-1}

Solving for W = RO – P + B for each element

Ca = 600–100 + 250 = 750 mol_c Ca^{2+} ha^{-1} yr^{-1}

Mg = 148–49 + 411 = 510 mol_c Mg^{2+} ha^{-1} yr^{-1}

K = 120–51 + 256 = 325 mol_c K^+ ha^{-1} yr^{-1}

Na = 300–52 + 0 = 248 mol_c Na^+ ha^{-1} yr^{-1}

The total estimated cation weathering rate = 1833 mol_c ha^{-1} yr^{-1}

15. Most experimental studies of weathering indicate that dissolution of feldspars increases as a function of solution acidity. Which solution would produce a faster initial rate of weathering: a solution of an organic acid such as fulvic acid at pH 4.85 or an aqueous solution of carbonic acid in equilibrium with a pCO_2 of 1.5%? Show your work and explain your answer.

Answer:

Use the carbonate equilibria in Chap. 7, substitute in the pCO_2 value given above, and solve the equations as follows:

$$\left[H^+\right]\times\left[HCO_3^-\right]=1.36\times10^{-8}\times pCO_2$$
$$=1.36\times10^{-8}\times0.015$$
$$=2.04\times10^{-10}$$

Take the square root of the preceding value = 1.428×10^{-5}

Take the negative log of this value = − log $[H^+]$ = pH = 4.85

Based on this computation, both the carbonic acid and fulvic acid solutions have the same pH of 4.85. However, the fulvic acid would be expected to produce faster weathering, because fulvic acids not only provide H^+ ions for proton attack, but also contribute to chelation or complexation reactions that enhance chemical breakdown of minerals (see Chap. 7).

16. How much acid neutralizing capacity (ANC) is released during the weathering of 15.0 g of anorthite, a calcium feldspar (as illustrated below)? Show your computational steps, your ANC expression, and present your answer in $mmol_c$.

$$CaAl_2Si_2O_8 + 2H_2CO_3 + H_2O$$
$$\rightarrow Ca^{2+} + 2HCO_3^- + Al_2Si_2O_5\left(OH\right)_4$$

Answer:

$ANC = C_B - C_A$ or Sum of proton acceptors – H^+

$= Ca^{2+} - 0$ or $2HCO_3^-$

Formula weight of anorthite = 40 + 54 + 56 + 128 = 278 g

The percent Ca in anorthite = 40 / 278 = 0.143 = 14.3%

15 g anorthite × 0.143 = 2.145 g Ca = 2145 mg Ca

2145 mg Ca × (1 $mmol_c$ / 20 mg Ca) = 107.25 $mmol_c$ Ca^{2+}

If ANC = Ca^{2+} − 0, then ANC = 107.25 $mmol_c$

Sample Problems in Element Cycling and Aqueous Chemistry

17. A forest calcium budget shows an annual Ca uptake by plants of 56 kg ha^{-1}. Focusing only on Ca and assuming that Ca^{2+} uptake is coupled with proton release from the plant root to the soil rhizosphere, what is the potential H^+ ion release associated with the annual uptake of Ca? Show your work and express your answer in mol_c ha^{-1} yr^{-1}. How does this estimate compare with the average annual atmospheric wet deposition of H^+ ion in New England (assuming mean pH = 4.3 and annual precipitation = 100 cm)?

Answer:

56 kg Ca^{2+} ha^{-1} yr^{-1} × (1000 mol_c / 20 kg Ca) = 2800 mol_c Ca^{2+} ha^{-1} yr^{-1}

Uptake of Ca^{2+} requires an equivalent release of H^+ for charge balance = 2800 mol_c ha^{-1} yr^{-1}

H^+ ion in wet deposition = $10^{-4.3}$ = 0.000050 M L^{-1} = 50 μmol_c L^{-1}

Annual wet deposition can be computed with the shortcut in Problem 12b.

($50\ \mu mol_c\ H^+\ L^{-1}$) × 100 cm / 10 = $500\ mol_c\ ha^{-1}\ yr^{-1}$

Proton release from root uptake of Ca^{2+} is over five times greater than estimated wet deposition of protons.

18. Consider a watershed where the weighted annual mean concentration of chloride ion in precipitation is 25 μmol(−) L^{-1}, the average annual stream runoff is 65% of precipitation inputs, and water storage is stable (i.e., steady-state on an annual basis). If you assume that chloride moves "conservatively" through the system without enrichment or depletion of mass (from uptake, mineralization, adsorption, or weathering), what is the final weighted annual mean concentration of Cl^- ion in stream water?

Answer:

ET concentrates 1.0 L of precipitation to 0.65 L of runoff. Thus, 25 $\mu mol_c\ Cl^-\ L^{-1}$ in rainwater becomes 25 $\mu mol_c\ Cl^-$ per 0.65 L in runoff. We compute the new concentration as follows:

25 $\mu mol_c\ Cl^-\ L^{-1}$ × (1.0 L / 0.65 L) = 38.5 $\mu mol_c\ Cl^-\ L^{-1}$

19. Consider a forest with an annual N uptake of 50 kg N $ha^{-1}\ yr^{-1}$, rainfall equivalent to 100 cm, and transpiration equivalent to 25% of rainfall. If we assumed that the forest acquires all of its N via passive bulk flow of transpirational water, what concentration of N in the soil water (as dissolved inorganic N) is necessary to allow the forest to take up 50 kg N $ha^{-1}\ yr^{-1}$? Express your answer as the solution concentration of inorganic N in mg L^{-1}. [Note that concentrations of inorganic N in field soil solutions are commonly <10% of the mean value you have calculated; this suggests that plants must use energy-dependent active uptake to meet their N demand].

Answer:

25% of 100 cm = 25 cm × ($10^4\ cm^2$ / m^2) × (1 L / $1000\ cm^3$) = 250 L $H_2O\ m^{-2}$

Plant uptake = 50 kg N $ha^{-1}\ yr^{-1}$ × (10^6 mg / kg) × (1 ha / $10^4\ m^2$) = 5000 mg N $m^{-2}\ yr^{-1}$

Divide the nitrogen mass by the transpirational water volume

(5000 mg N $m^{-2}\ yr^{-1}$) / (250 L m^{-2}) = 20 mg N L^{-1}

Sample Problems in Organic Matter Cycling

20. Data are presented below indicating the chemical composition of fresh leaf litter from three **northern tree species**. Use the data to predict which litter substrate would decay fastest. Rank the species from highest to lowest in order of their expected rates of decay. Show your logic or computations, and indicate the literature reference(s) upon which your rationale is based.

Species	%N	%Ca	%K	%Lignin
A	1.6	0.05	0.12	12.0
B	1.6	0.07	0.18	16.0
C	2.4	0.10	0.22	18.0

Answer:

Using the ratio of % lignin: % nitrogen, which Melillo et al. (1982) found is inversely related to litter decay rate, one would predict that A and C (with ratios of 7.5) would decay faster than B (ratio of 10.0).

21. What is the estimated annual CO_2 release from microbial decomposition of organic matter in the forest floor (O horizon) of an ecosystem under the following conditions? State any assumptions and express CO_2 release in g $CO_2\ m^{-2}\ yr^{-1}$

- The forest floor is assumed to be in steady-state
- Forest floor mass is 50,000 kg organic matter ha^{-1}
- Annual inputs of detritus to the forest floor from litterfall + root mortality + throughfall DOM = 2500 kg organic matter $ha^{-1}\ yr^{-1}$

Answer:

If the forest floor is assumed to be in steady state, then inputs and outputs of detritus to this compartment are approximately equivalent.

Annual detrital inputs of 2500 kg organic matter $ha^{-1}\ yr^{-1}$ = 250 g $m^{-2}\ yr^{-1}$.

Assuming that detritus is roughly 50% carbon, we calculate that inputs and outputs are as follows:

250 g organic matter $m^{-2}\ yr^{-1}$ × (0.5 g C / 1 g organic matter) = 125 g C $m^{-2}\ yr^{-1}$

Annual carbon dioxide release is 125 g C $m^{-2}\ yr^{-1}$ × (44 g CO_2 / 12 g C) = 458 g $CO_2\ m^{-2}\ yr^{-1}$

22. Does leaf decay generate acidity or alkalinity? Consider a gram of decaying leaf with the composition shown below. Estimate the net ANC production that will likely result from complete microbial mineralization of this leaf with an initial mass of 1.0 g. Show three possible outcomes for this decomposition process based on the following assumptions:

(1) assume that all of the N is only subject to ammonification, (2) assume that all of the N is subject to ammonification followed by 100% nitrification, and (3) assume all of the mineralized N is ultimately denitrified to dinitrogen, N_2. Remember to consider the other elements as well.

Foliar concentrations (shown below) in parts per thousand in a leaf weighing 1.0 g

Carbon = 480	Nitrogen = 7	Sulfur = 2
Calcium = 8	Potassium = 4	Magnesium = 1

Answer:

Charge associated with each element in its ionic form:
7 mg N × (1 $mmol_c$ / 14 mg) = 0.5 $mmol_c$
2 mg S × (1 $mmol_c$ / 16 mg) = 0.125 $mmol_c$
8 mg Ca × (1 $mmol_c$ / 20 mg) = 0.4 $mmol_c$
4 mg K × (1$mmol_c$ / 39 mg) = 0.1025 $mmol_c$
1 mg Mg × (1 $mmol_c$ / 12.15 mg) = 0.08 $mmol_c$
Use ANC = $C_B - C_A$

Case 1 with ammonification
(0.5 $mmol_c$ NH_4^+ + 0.4 $mmol_c$ Ca^{2+} + 0.1025 $mmol_c$ K^+ + 0.08 $mmol_c$ Mg^{2+})
– (0.125 $mmol_c$ SO_4^{2-})
= 0.96 $mmol_c$ ANC

Case 2 with nitrification
(0.4 $mmol_c$ Ca^{2+} + 0.1025 $mmol_c$ K^+ + 0.08 $mmol_c$ Mg^{2+}) – (0.5 $mmol_c$ NO_3^-
+ 0.125 $mmol_c$ SO_4^{2-})
= – 0.04 $mmol_c$ ANC

Case 3 with denitrification
(0.4 $mmol_c$ Ca^{2+} + 0.1025 $mmol_c$ K^+ + 0.08 $mmol_c$ Mg^{2+})
– (0.125 $mmol_c$ SO_4^{2-})
= 0.46 $mmol_c$ ANC

Sample Problems on Element Budgets

23. Use the data below to estimate how much calcium is exported from this watershed in a 1-year time period. Express your answer in moles of charge (mol_c yr^{-1}) and indicate any assumptions you made. (note that cfs = cubic feet per second)

Month	Mean daily flow (cfs)	Mean Daily Ca concentration mg L^{-1}
J	1000	3
F	1500	3
M	1200	3
A	4000	2
M	6000	2
J	3000	3
J	500	5
A	500	6
S	2000	3
O	4000	3
N	7000	2
D	1000	2

Answer:

Convert each mean daily flow to metric using cfs × (0.0283 m^3 / ft^3) and scale this to a monthly value by multiplying by (60 s / min) × (60 min / hr) × (24 hr. / day) × days in the month. Convert this value to liters per month, multiplying m^3 mo^{-1} by 1000 L / m^3, convert mean Ca concentrations to charge equivalents by multiplying mg Ca L^{-1} × (1 mol_c / 20,000 mg), and calculate monthly Ca export by multiplying monthly discharge in liters per month times Ca concentration in mol_c L^{-1}. Finally, sum up the 12 monthly values for Ca export to obtain an estimate of annual Ca export of 2.96 × 10^8 mol_c yr^{-1}. Use a spreadsheet to simplify this computation.

24. Consider a forest soil where the subsurface pool of soil organic matter contains 150,000 kg C ha^{-1} and decays at an annual rate of 0.5% yr^{-1}. What is the mean residence time of this carbon pool and how much carbon as root detritus and DOM must be transferred into this pool each year (in units of g C m^{-2} yr^{-1}) to maintain it at steady-state? How does this estimate compare with reported values of fine root biomass and turnover?

Answer:
150,000 kg C ha^{-1} × 0.005 = 750 kg C ha^{-1} yr^{-1}
Mean residence time = Pool size / loss rate = 150,000 / 750 = 200 yr
Annual detrital input = 750 kg C ha^{-1} yr^{-1} × (1000 g / kg) × (1 ha / 10^4 m^2) = 75 g C m^{-2} yr^{-1}
As shown in Chap. 5, live root biomass at a depth of 10–40 cm can be in the range of 100 to 150 g m^{-2} and turnover rates can be as high as 100% per year.

Glossary

Acid a proton donor capable of acidifying an aqueous solvent

Acid, Strong an acid that ionizes readily to release virtually all of its protons

Acid, Weak an acid that ionizes partially to produce an equilibrium between bound and free protons

Acid, Mineral an acid that contains no hydrocarbons (e.g., sulfuric acid)

Acid, Organic an acid containing hydrocarbons (e.g., citric acid)

Acid-Forming Precursor a compound that can be readily converted to an acid

Acid-Forming Salt a substance such as ammonium sulfate that can be metabolized by microbes to form a strong acid (in this case, nitric acid generated by nitrification)

Acid Ionization Constant an equilibrium constant describing the extent of proton dissociation characteristic of a specific acid

Acid Neutralizing Capacity (ANC) the capacity of a substance or mixture to react with an acid to form a neutral salt (ANC is often referred to as alkalinity)

Acidic Deposition the transfer of acids and acid-forming compounds from the atmosphere to Earth

Acidic Precipitation precipitation with a pH below the carbonic acid equilibrium of roughly pH 5.6

Acidity (Free and Bound) free acidity is the activity of H^+ ions in solution, whereas bound acidity is the quantity of titratable protons in a compound

Actinorhizal N fixing bacteria of the genus *Frankia* that associate with roots of woody plants

Active Transport the movement of an element or substance across a membrane with the assistance of an energy input, usually in the form of ATP

Activity the effective concentration of ions in a solution corrected for the influence of ionic strength

Adsorption the electrostatic attraction of a charged cation or anion to a surface with an opposite charge

Aeolian a deposit of fine sediments originating from wind-borne transport

Aerobic conditions with suitable oxygen present that electrons can be passed to oxygen as the terminal acceptor during metabolism

Aerosol an airborne microscopic particle

Airshed the area that contributes atmospheric emissions to downwind receptor watersheds

Alicyclic hydrocarbon molecules in which carbon chains link to form rings

Aliphatic hydrocarbon compounds composed of chains of carbon atoms

Alkali Metal a monovalent cation found in the first column of the Periodic Table

Alkaline Earth Metal a divalent cation in the second column of the Periodic Table

Alkalinity the sum of proton acceptors in solution (concentration of substances capable of neutralizing acidity)

Alkaloid a heterocyclic compound containing nitrogen that is produced by secondary metabolism in plants and acts as a toxin against herbivores

Alkane hydrocarbon containing only single bonds between carbon atoms

Alkene a hydrocarbon with one or more double bonds between carbon atoms

Alkyne a hydrocarbon containing one or more triple bonds between carbon atoms

Allelopathic Substance a potentially toxic organic substance released by plants to inhibit other competitors

Alluvial transported and deposited by water

Ambient Ozone the prevailing background concentration of ozone in the environment

Ammonification transformation of organic nitrogen (e.g., amino N) into NH_3

ANC see the definition for acid neutralizing capacity

Anaerobic in the absence of oxygen

Anion ion with negative charge

Anion Adsorption the attraction of a negatively charged ion toward a surface with a positive charge

Anoxic lacking oxygen

C.S. Cronan, *Ecosystem Biogeochemistry*, Springer Textbooks in Earth Sciences, Geography and Environment, DOI 10.1007/978-3-319-66444-6

Apoplast the continuum of cell walls and extracellular spaces in a plant

Aridisol soils found in arid regions where moisture is limiting for plant growth and soil development

Aromatic hydrocarbon molecules containing six-membered rings each with three C-C double bonds

Ash-Free Organic Matter an estimate of the organic matter content of a sample, excluding the mineral ash remaining after high temperature combustion

Assimilation conversion or incorporation of nutrients into living cells or tissues

Assimilatory Nitrate Reduction metabolic reduction of nitrate within an organism to permit assimilation of the nitrogen into amino-N for protein synthesis

Assimilatory Sulfate Reduction metabolic reduction of sulfate ions within an organism to permit assimilation of the resulting reduced S into amino acids and proteins

Atmospheric Deposition the transfer of wet, dry, or gaseous substances from the atmosphere to the surface of the Earth

Atmospheric Residence Time the time period during which a substance remains in the atmosphere before returning to Earth

Atomic Radius a measure of the size of an atom with its electron cloud

Available Water the amount of water held in a soil between the field capacity and the wilting point

Base Cation cation (other than H^+ or ionic aluminum) capable of combining with OH^- to form a base

Baseflow river or stream runoff sustained by groundwater in the absence of precipitation or snowmelt

Base Saturation percentage of cation exchange capacity (CEC) filled with nutrient base cations (i.e., Ca, Mg, K, Na)

Bidentate Chelate a complex in which a ligand binds through two donor atoms to a metal ion

Biogenic Gas a gas that is produced or generated by a living organism

Biogeochemistry analysis of the patterns and processes by which nutrients and other biologically active elements and compounds interact with living organisms and circulate in the biosphere

Bound Acidity protons on weakly acidic functional groups that are not dissociated at ambient pH

Brown Rot a type of wood decay caused by Basidiomycete fungi that causes wood to become brittle

Bulk Precipitation precipitation collected in an open plastic funnel that includes wet deposition plus an undetermined amount of dryfall particles

C-3 Plant a plant such as a maple that is adapted to mesic conditions and forms two 3-carbon products as a result of the initial stage of carbon fixation

C-4 Plant a plant such as maize that is adapted to sunny drier environments and forms a 4-carbon compound as the initial product of carbon dioxide uptake

C:N Ratio an ecological indicator calculated by dividing the carbon mass or molar concentration by the nitrogen mass or molar concentration

Calibration a phase of model building in which model parameters are adjusted to improve the accuracy of outputs and predictions

Calvin Cycle the dark reaction in photosynthesis that consumes ATP and NADPH in order to fix CO_2

Canopy Interception the interception and retention of wet precipitation by foliage in the forest canopy

Canopy Leaching the removal of nutrient ions or solutes from foliage by rainwater passing over the leaves or needles

Canopy Throughfall the solution that results as precipitation washes through the foliage and branches of a forest canopy

Canopy Washout removal of dry deposited substances from a forest canopy by wet deposition

Carbon-Bonded Sulfur atoms of sulfur that are bonded directly to carbon in a molecule

Carbon: Element Ratio the relative proportions of carbon and any other element in a sample

Carbonic Acid an acid formed from the dissolution of CO_2 in water to form H_2CO_3

Carboxyl a functional group composed of COOH

Catchment the drainage area that collects water feeding into a stream, river, or lake

Cation ion with a positive charge

Cation Adsorption attraction of a positively charged ion to a surface with a negative charge

Cation Exchange the reversible interchange between a cation in solution and a cation adsorbed on the surface of a negatively charged colloid or cellular structure

Cation Exchange Capacity the amount of adsorbed cations that can be retained by a solid phase exchanger (expressed in cmol(+)/kg)

CEC see the definition for cation exchange capacity, which is abbreviated CEC

Charge Balance the equivalence between cations and anions in a system

Charge Density the density of ionic charge relative to ionic radius

Charge Equivalents moles of charge in a sample

Chelate a stable type of coordination complex in which a metal binds to multiple functional groups in a single multidentate ligand

Cheluviation a soil leaching process in which metallic ions are mobilized and are transported by organic acids that form chelates with the metals

Chemical Denudation Rate the rate at which solutes are removed from a watershed in stream runoff

Chemical Ecology a field of science focused on the influence of chemical interactions on ecology

Chemoautotroph a microorganism that uses carbon dioxide as a source of carbon and reduced inorganic substances as an energy source

Chlorosis yellowing of a leaf or needle as a result of plant stress

Clay (1:1 and 2:1) an aluminosilicate mineral composed of tetrahedral and octahedral sheets

Cloud Condensation formation of a moisture droplet around a nucleus such as a microscopic particle

Coarse Woody Debris (CWD) woody detritus such as branches and tree boles

Colloid a microscopic particle such as clay or a humus particle that may have a surface electric charge

Colluvial material moving downslope under the influence of gravity

Complexation a process by which a monodentate or multidentate ligand binds covalently to a cation

Complexing Ligand an anionic molecule that donates electrons to form a coordination complex with a metal

Concentration moles of a substance per unit volume or mass

Conductivity a measure of the electrical conductance of a water sample; conductivity increases with the total concentration of ions in solution

Congruent Dissolution mineral dissolution in which the solid phase is transformed completely to solutes

Conservative Ion an ion that moves without significant retention or enrichment through a watershed

Coordinate Bond a covalent bond in which a ligand donates electrons to an electron-deficient cation

Coordination Complex a compound containing a metal ion bonded to surrounding molecules or ions that act as ligands

Coulombic Attraction attraction based on electrical charges and electrostatic forces

Counter Ion an ion that balances the opposite charge of an adjacent ion

Covalent Bond a chemical bond in which electrons are shared between nuclei of adjacent atoms

Crown Leaching removal of dissolved solutes from plant foliage in a forest by precipitation moisture

Cucurbitacin a plant defensive compound that deters herbivores by imparting a bitter taste to leaves

Cynaogenic Glycoside a nitrogenous plant toxin that is metabolized by insects to form hydrogen cyanide

Decay Constant an estimate (k) of the fractional rate of decay per year

Decomposition the decay of organic matter or detritus as a result of physical leaching and microbial metabolism

Degree Days sum of daily temperatures above freezing (0 °C) for the year

Denitrification the reduction of nitrate by microbial organisms; complete denitrification produces N_2 gas

Denudation Rate the rate at which weathering processes remove mineral elements from a watershed

Depleted (in Heavy Isotope) the composition of an element is deficient in heavy isotope compared to a standard reference material, resulting in a "light" isotopic signature

Deposition (Dry and Wet) the transfer of wet, dry, or gaseous substances from the atmosphere to the surface of the Earth

Deposition Velocity the rate of transfer of material from the atmosphere to surfaces on Earth

Deterministic Model a mathematical model in which quantitative relationships and variables are specified, rather than being based on probabilities

Detritus dead organic matter

Diffusion movement of molecules from a region of higher to a region of lower concentration

Dissimilatory Nitrate Reduction anaerobic reduction of nitrate ion to ammonium ion by microbes that use nitrate as an electron sink during metabolism

Dissimilatory Sulfate Reduction anaerobic reduction of sulfate ion to sulfide ion by microbes that use sulfate as a terminal electron acceptor during metabolism

Dissolution transformation of a solid phase substance into solutes

Disturbance an event that removes or damages organisms and opens colonization space in an ecosystem

DOC dissolved organic carbon that may give a yellow or brown hue to natural waters

DOM dissolved organic matter (includes DOC and other components of soluble organic matter)

Drainage Network the branching dendritic system of streams and rivers in a drainage basin

Dry Deposition the transfer of dry particles, aerosols, or gases to receptors on Earth

Dryfall particles that fall from the atmosphere under the influence of gravity

Ecological Biochemistry study of the influence of secondary metabolites on ecological interactions

Ecosystem a functional ecological unit composed of interacting organisms and their environmental surroundings. The boundaries that define an ecosystem can be relatively sharp – as in the case of a watershed or a lake ecosystem – or they may be more subtle or subjective in nature (e.g., an estuarine ecosystem with fluctuating tidal ranges and salinity gradient). In hierarchical terms, an ecosystem represents a high-level organizational unit that incorporates population-based and community-based processes into an environmental framework. Within a given ecosystem, we can distinguish structural and functional patterns and processes involving linked biotic and abiotic components.

E_h the redox potential of a system measured with a platinum electrode

Eddy Covariance a biophysical technique based on concentration gradients and wind parameters that is used to estimate gas exchanges between the atmosphere and surfaces on Earth

Effective CEC cation exchange capacity estimated as the sum of exchangeable cations in a field soil, rather than the potential exchange capacity measured by ammonium adsorption at pH 7 or greater.

Electrical Conductivity a measure of the electrical conductance of a water sample; conductivity increases with the total concentration of ions in solution

Electrical Neutrality the principle dictating that opposite charges in a system must balance

Electronegative elements such as oxygen that attract bonding electrons and become negatively charged

Element Increment the annual increase in element mass incorporated into new biomass production

Element ratio ratio of one element to another expressed in mass or molar units

Eluviation removal of metal ions from a soil horizon under the influence of acid leaching

Enriched (with Heavy Isotope) the composition of an element is isotopically "heavy" and contains a higher proportion of heavy isotope than a reference standard

Equlibrium a condition in which rates of forward and backward reactions are equivalent

Equlibrium Constant the value of the ratio of equilibrium concentrations of products to equilibrium concentrations of reactants, each raised to a power equal to its stoichiometric coefficient

Equivalent Charge moles of charge associated with a particular ion

Equivalent Weight the mass of an element or substance that will displace or otherwise react with one mole of hydrogen (1.008 g) or one half mole of oxygen (8.00 g)

Ester a hydrocarbon in which a side group bonds to the oxygen atom of a carbonyl group

Evaporation transfer of water from the liquid phase to the vapor phase in response to heat input

Evapotranspiration a term describing the combined processes of evaporation and plant transpiration that account for water transfer from a watershed to the atmosphere

Exchangeable Acidity the protons adsorbed to the soil exchange complex that act as a reservoir of acidity

Facultative a generalist micro-organism that can switch between aerobic respiration and fermentation as a function of redox conditions

Felsic rock minerals that are rich in aluminum and silica

Fermentation occurs under conditions of lower redox when the process of glycolysis terminates in the formation of lactic acid or ethanol as the end-product of pyruvate synthesis

Field Capacity the amount of water held by a soil at a tension of –0.03 MPa, after the soil has been saturated and free gravitational water has drained from the pores

Fine Roots the smallest plant roots (usually less than 1 mm diameter) that are most active in absorption of water and nutrients

Fine Root Production annual growth of new fine roots (generally less than 1 mm in diameter)

First Order a chemical reaction for which the rate is proportional to a reactant concentration raised to the power of 1 (e.g., the exponent is 1)

Flavonoid family of flower pigments based on the flavone skeleton and containing a phenolic-OH group

Flow Path the pathway followed by water as it drains through a watershed and into groundwater or surface water

Flux refers to the transfer of mass into or out of a system

Fly Ash residual ash material resulting from coal combustion that emits from a power plant stack

Foliar Stipling necrotic spots that develop on plant leaves or needles

Forcing Factor in terms of the heat budget of the Earth, a forcing factor contributes either to a warming or cooling of the atmosphere by either reinforcing or offsetting the input of solar energy

Forest Floor the uppermost soil horizon or O horizon in a forest that is primarily composed of leaf litter and decaying organic matter

Fragipan a soil layer that is very dense and acts as a barrier to root and moisture penetration

Free Acidity the acidity resulting from proton dissociation by strong acids or acidic functional groups; this is the acidity measured by a pH probe

Fulvic Acid a polycarboxylic organic acid that is soluble in basic and acidic solutions, contains a mixture of aliphatic and aromatic structures, and has a molecular weight of < 2000 daltons

Functional Group an atom or group of atoms that imparts specific chemical properties to an organic compound

Glacial Till a glacial deposit composed of unsorted sediments and rocks

Gleying soil formation under saturated conditions and poor drainage, resulting in reducing conditions and limited differentiation of soil horizons

Gravitational Settling vertical transfer of particles from the atmosphere or a water column to a solid surface

Gross Mineralization the total microbial conversion of organic N to ammonium-N over a given time period

Gross Production total fixation of carbon by primary producers in a given time period

Groundwater water that is stored beneath the ground surface in a watershed, ultimately contributing to stream base flow

Heavy Fraction a dense soil fraction composed of organic matter aggregated with mineral material

Heavy Metal a metal such as lead, mercury, or cadmium with a large atomic mass and a potential for biological toxicity

Henry's Law Constant describes the solubility of a gas in water as a function of the partial pressure of that gas

Hill Reaction the light reaction in photosynthesis that combines the photolysis of water with the production of ATP and NADPH

Histosol a soil composed primarily of organic matter such as peat

Humic characterized by or derived from partially decomposed organic matter that is generally acidic

Humic Acid an aromatic polycarboxylic organic acid that is soluble in base, but is insoluble below pH 1

Humic Colloid a microscopic soil particle composed of decayed or humified organic matter

Humus organic detritus that has undergone decomposition and has a high surface area to volume ratio

Hydrogen Bonding a chemical bond that occurs when an electronegative atom serves as an electron donor and partially shares its nonbonding electrons with a polarized hydrogen atom

Hydrograph a graphical representation of the variable water discharge over time by a stream or river

Hydrolysis reaction of a molecule or compound with water

Hydrolyzed a compound or molecule that has reacted with water to dissolve or to ionize

Hydrophilic a polar substance, molecule, or functional group that is "water loving" and is readily soluble in water

Hydrophobic a non-polar substance, molecule, or functional group that is not readily soluble in water

Hydroxyl an OH functional group or OH^- ion

Hyetograph a graphical representation of rainfall patterns over time at a particular location

Hyphae the filaments that comprise the body of a fungus

Illuviation a soil process in which leached solutes and colloids accumulate in subsoil mineral horizons

Immobile Nutrient a nutrient that is not readily transported from one tissue to another by the phloem

Immobilization this occurs when a soluble ion is assimilated into microbial biomass

Impaction occurs when a moving particle or aerosol encounters a surface, loses momentum, and deposits on the surface

Inceptisol a soil formed in fine parent material where conditions do no permit sufficient leaching and translocation to generate distinctive subsurface horizons

Incongruent Dissolution transformation of a mineral into solutes plus a residual solid phase

Infiltration movement of water into and through a soil or geologic deposit

Interception the retention or storage of precipitation by plant foliage, prior to generation of throughfall

Interflow water moving horizontally through soil layers toward a downslope drainage channel

Ion Activity the "effective" concentration of an ion in solution calculated as a function of ionic strength using an ion activity coefficient

Ion Exchange the reversible movement of ions between an aqueous solution and a solid phase charged surface such as an aluminosilicate clay

Ion Ratio the abundance or concentration of one ion compared to another in a ratio or fraction

Ionic Bond a bond between oppositely charged ions

Ionic Strength a measure of the total concentration of ions in solution based on molarity and ionic charge

Isoelectric Point the pH at which an amphoteric substance is electrically neutral and exhibits no net positive or negative charge

Isomorphic Substitution a process by which an ion substitutes for another ion of similar size in the lattice of a clay; the new ion may have a different electrical charge than the original ion

Isotope Dilution an experimental technique using stable isotopes in which a reaction rate is estimated by adding a heavy isotope tracer to a system and measuring the rate at which that isotope is diluted by background generation of a molecule containing the light isotope of that element.

Kinetic refers to the rate of a chemical process

Lacustrine sediments derived from a lake environment

Leachate a solution that has contacted a solid phase and has gained solutes as a result of that interaction

Leaching removal of ions and other solutes from solid phases by water

Leaf Area Index ratio of projected leaf area per unit of ground area beneath a forest canopy

Ligand an ion or molecule that shares electrons with a metal atom

Light Fraction a low density mineral-free soil fraction composed of decayed plant material and microbial biomass

Lithic Element an element that occurs in minerals and rock

Litterfall recycling of foliage and branches from a plant community back to the soil surface

Long-Range Transport transport of substances such as pollutants over long distances in the atmosphere

Lysimeter a sampling device intended to collect soil water for chemical analysis

Macronutrient a chemical that an organism must acquire in relatively large amounts for nutrition

Macropore a large soil pore through which gravitational water moves

Mafic rock minerals that are rich in magnesium and iron

Mass Balance a systematic analysis of the inputs and outputs of elements to a system based on mass

Mass Fractionation separation or discrimination of isotopes based on differences in mass

Methanogenesis the production or generation of methane by microbes known as methanogens

Methanotroph a microbial organism that consumes and oxidizes methane as an energy source

Methylation addition of a methyl group ($-CH_3$) to an atom or molecule (as in mercury methylation)

Microcosm a small bench-top sized replica of an ecological system

Micronutrient a chemical that an organism requires in small amounts for nutrition

Micropore a small or microscopic soil pore through which capillary water moves

Mineral Acid an acid such as nitric, hydrochloric, or sulfuric that lacks carboxylic functional groups

Mineralogy the mineral composition (e.g., quartz or biotite) of soil, surficial material, or bedrock

Mineral Soil usually refers to the subsoil that is composed almost entirely of mineral grains and clays

Mineral Weathering chemical breakdown of solid phase minerals to release weathering products

Mineralization (Gross and Net) transformation of organically bound elements to inorganic forms that are available for biological uptake

Mobile Anion a negatively charged ion that moves relatively freely through the soil without major retention by biotic or abiotic mechanisms

Model a qualitative conceptual or quantitative numerical representation of a process, pattern, or system

Monodentate Ligand a molecule containing a single functional group capable of sharing electrons with a metal ion

Multidentate Ligand a molecule containing two or more functional groups capable of sharing electrons with a metal ion through coordinate bonds

Mycorrhizal Fungi fungal species that form symbiotic associations with plant roots

Necromass the mass of dead tissue

Necrosis death of tissue through disease or stress

Net Ecosystem Production (NEP) the amount of gross primary production remaining after subtracting autotrophic and heterotrophic respiration

Net Mineralization microbial gross mineralization minus microbial immobilization of ammonium-N

Net Primary Production (NPP) gross primary production minus autotrophic respiration

New water water that has recently entered a watershed as precipitation, moves laterally as quickflow, and rapidly appears as stream runoff

Nitrate Reduction (assimilatory and dissimilatory) reduction of nitrate ion to a less oxidized state such as NO or N_2

Nitrification oxidation of ammonium ion to nitrate by micro-organisms

Nitrogen Fixation transformation of atmospheric dinitrogen (N_2) to ammonia (NH_3)

Nitrogen Saturation a condition in which the supply of inorganic N exceeds biological demand for N

Nitrogenase the enzyme that catalyzes the process of N fixation

Non-polar a molecule that lacks strong electronegative or electropositive attributes and is consequently insoluble or poorly soluble in water

Nuclide a nucleus of a specific isotope of an element

Nutrient Requirement annual element increment associated with the production of new shoots, roots, and current foliage

Nutrient Uptake annual plant increment of an element accumulated in new woody tissues plus annual losses of that element through litterfall, root turnover, leaching, and net stemflow.

Nutrient Use Efficiency amount of biomass produced per unit of a given nutrient

Obligate an organism that is a specialist in terms of only surviving under a specified set of conditions

Old water water that has infiltrated the soil over a period of time and has reacted with the soil matrix

Operational Definition a definition that is not unique, but which is established by a particular set of operating procedures

Order of Reaction the power to which the concentration of a reactant is raised in a rate law

Organic Acid a hydrocarbon that contains at least one acidic carboxyl group

Orographic Precipitation enhanced precipitation resulting from adiabatic cooling associated with high elevation mountains

Osmosis movement or diffusion of water across a semipermeable membrane

Osmotic Potential a component of water potential that is proportional to the concentration of solutes in a solution

Oxidation donation of an electron from an atom

Oxisol a tropical soil that is highly weathered and contains a large accumulation of iron oxides

Parent Material the geologic material in which soil formation occurs

Peak Flow the period of runoff when water level and velocity are elevated by stormflow or snowmelt

Pedogenesis soil formation

Periodic Table a chart showing relationships among elements based on mass and electron shells

Permanent Charge electrical charge on a clay colloid that results from isomorphic substitution in the lattice and is independent of changes in pH

pH-dependent a process that varies as a function of the acidity or pH conditions in the environment

Phenology study of seasonal changes in the morphology, physiology, and behavior of living organisms

Piston Flow Displacement movement of water through soils in response to hydrostatic pressure from above

Plasmalemma membrane surrounding the cytoplasm of a plant cell

Platinum Electrode a probe that is used to estimate redox potential

Podzolization a soil forming process that occurs in well-drained temperate forest soils where climatic conditions are cool and mesic and organic acid leaching is a major driver of pedogenesis

Polar Covalent Bond a covalent bond in which the shared electrons are preferentially attracted toward a more electronegative atom

Pool a reservoir or storage compartment in an ecosystem containing accumulated elements or substances

Precipitation removal of ions from solution through bonding and formation of insoluble colloids

Precipitation (Wet) liquid water transferred to a watershed from the atmosphere via gravity

Preferred Pathway a pathway followed by drainage water moving through macropores in the soil

Primary Mineral a mineral such as quartz, feldspar, or hornblende that originates from magma

Primary Production energy assimilation and biomass production by plants; gross primary production (GPP) is the total energy assimilated by plants, whereas net primary production (NPP) is the plant biomass remaining after subtracting plant respiration

Priming Effect the vigorous response of microbial decomposers to an input of fresh organic detritus

Production Efficiency the ratio of plant net primary production (NPP) divided by GPP

Products in a chemical reaction, products occur on the right side of the reaction

Proficient Plant a plant that lowers its concentrations of N and P to very low levels through resorption

QA/QC this abbreviation refers to quality assurance and quality control in measurements and analysis

Quickflow water that moves quickly through a watershed and into a stream channel or lake

Quinone an aromatic hydrocarbon that contains an oxygen atom double-bonded to a carbon atom

Radiative Forcing the extent to which a substance or process acts to cool or to warm the heat budget of the Earth

Rainout removal of gases and particles from a cloud during rain droplet formation and deposition

Reactants in a chemical reaction, reactants occur on the left side of the reaction

Reaction Rate a measure of the rate at which reactants interact to form products in a chemical reaction

Recharge a process by which infiltrating water replenishes groundwater

Redox a measure of the oxidation or reduction status of a system

Reduction addition of an electron to an atom

Residence Time an estimate of the time an atom of a substance remains in a system before being replaced or removed

Resorption removal or retranslocation of an element from foliage to woody tissues prior to leaf drop

Retranslocation movement of an element from one plant sink to another sink via the phloem

Rhizosphere the soil zone immediately surrounding a plant root system and its associated mycorrhizae

Riparian Zone terrestrial zone located immediately adjacent to or on the banks of a stream, river, or other water body and subjected to periodic flooding

Root Free Space the apoplast on the exterior of a plant root into which ions diffuse from the rhizosphere

Root Turnover the processes of death, decay, and replacement of roots in a plant community

Rubisco an enzyme in the Calvin Cycle (ribulose bisphosphate carboxylase) that catalyzes CO_2 fixation

Sand soil particles with diameters ranging from 0.05 to 2.0 mm

Saprolite a type of soil parent material composed of highly weathered and crumbling bedrock

Saturated Flow movement of gravitational water through soil macropores

Saturated Soil Hydraulic Conductivity the rate of vertical water infiltration into a soil under saturated conditions

Saturated Zone the soil horizons and surficial deposits in a watershed that are saturated with water

Saturation Index ratio of the ion activity product of two ions divided by the solubility product of the ions

Scavenging Efficiency the extent to which different forms of precipitation absorb or remove substances from the atmosphere

Second Order Reaction a chemical reaction for which the rate is proportional to a reactant concentration raised to the power of 2 (e.g., the exponent is 2)

Secondary Compounds usually refers to metabolites produced by secondary metabolism related to defense of the organism

Secondary Mineral a mineral such as a clay or metal oxide that is generated from the weathering products of primary minerals

Senescence the inherent aging and deterioration of foliage that precedes leaf or needle drop by perennial plants

Sensitivity Analysis a procedure used to test which parameters in a computer model are most or least influential in determining overall outputs or predictions

Siderophore a soluble organic substance released by plants that helps to increase the solubility of key plant nutrients such as iron in the soil

Silt soil particles with diameters ranging from 0.002 to 0.05 mm

Sink a system at any scale that acts as a place of accumulation for nutrients, matter, or energy

Site Quality the ability of a plot of land to provide resources to support the growth of organisms

Sodic Mineral a mineral containing appreciable amounts of the element sodium

Soft Rot the soft consistency of wood decayed by fungi that break down cell walls

Soil Buffer Capacity the ability of a soil horizon to resist changes in pH in response to added acid or base

Soil Colloid a microscopic soil particle such as a clay, metal oxide, or humus particle

Soil Heavy Fraction soil organic matter that is adsorbed onto mineral surfaces or sequestered in micro-aggregates

Soil Horizon a horizontal layer in a soil profile with distinctive physical and chemical features

Soil Hydraulic Conductivity the rate at which soil moisture moves through soil pores

Soil Leaching movement of solutes through soils in response to water infiltration

Soil Light Fraction fraction of soil organic matter that is relatively free of mineral material and includes plant and microbial detritus

Soil Order a major soil group such as an Oxisol that is defined by physical-chemical properties and climatic conditions

Soil Organic Matter (SOM) the detrital remains of plant, animal, and microbial biomass in soils

Soil Respiration efflux of carbon dioxide from soils that is derived from respiration by plant roots, soil animals, and microbes

Soil Texture a description of the relative proportions of sand, silt, and clay particles in a soil

Source place of origin for materials moving to a sink

Spodosol a major soil order characterized by a subsurface spodic B horizon

Stable Isotope an atom characterized by a specific number of protons and neutrons that is stable and does not normally disintegrate through radioactive decay

State Variable a parameter in a computer model describing the quantitative condition of a system component

Steady State a condition in which inputs and outputs are approximately equal in a system

Stemflow precipitation moisture that has moved from the forest canopy downward toward the ground following the stem or bole of the tree

Stoichiometry a description of the ratios of elements in cells, tissues, or organisms

Stoichiometric Coefficient in chemical notation, this integer precedes each reactant or product and indicates the relative numbers of moles of each molecule involved in a reaction

Stomatal Conductance the rate at which gas or water vapor is exchanged through stomatal pores; this varies with the size of the stomatal aperture

Stream Order the position of a stream in the hierarchy from small headwater streams to large rivers

Stress a biotic or abiotic constraint or influence that adversely affects critical life processes for organisms

Strong Acid a compound that readily dissociates in water to release acidifying protons

Strong Mineral Acid an acid such as nitric, hydrochloric, hydrofluoric, or sulfuric acid that generates extreme acidity

Succession an ecological process that occurs during the successive stages of maturation and ecological development following disturbance in a biological community

Sulfate Reduction (Assimilatory and Dissimilatory) reduction of sulfate ions to sulfide or other reduced species of sulfur as a result of electron transfers mediated by living organisms

Surficial Deposit usually refers to an accumulation of sediments or residuum overlying bedrock

Surficial Geology the study of surficial sedimentary deposits or residuum overlying bedrock

Symplast the pathway in plants for movement of water from cell to cell within the cytoplasm

Throughfall moisture derived from atmospheric deposition that passes through plant foliage in a forest canopy and drips to the ground

Till unsorted glacial debris that forms a specific type of surficial deposit with sandy features

Total Acidity the sum of free and titratable bound acidity in a compound with acidic functional groups

Trace Metal an element that occurs in low concentrations and belongs to the transition metal group in the Periodic Table

Transpiration transfer of water vapor from plant stomata to the atmosphere in response to a water potential gradient

Ultisol a major soil order found in warm humid climates, with a subsurface accumulation of clay

Unreactive N_2 the triple-bonded dinitrogen gas that occurs at a concentration of 78% in the atmosphere

Unsaturated Flow movement of soil moisture in response to capillary forces and soil matric potential

Unsaturated Zone portion of soil profile and surficial deposits in a watershed where moisture content is below field capacity

Unweighted Mean the average computed as the sum of data points divided by the number of data points

Validation a process in which a model is independently confirmed or validated using new data

Vapor Pressure Deficit difference between the current air concentration of water vapor and the concentration of water vapor predicted at the dewpoint for that air temperature

Variable Source Area a zone in a watershed that quickly becomes saturated by rainfall or snowmelt and serves as a source for rapid interflow or saturated overland flow to a stream channel

Volume Weighted Mean a mean calculated by taking into account differences in sample volumes

Washout removal of dry deposition from a plant canopy by wet deposition; this term also refers to below-cloud scavenging of chemical substances

Water Balance or Budget an analysis of water inputs, outputs, and storage in a watershed

Water Potential a physical property that explains the movement of water in plants, other organisms, and soils; in plants, water potential is the sum of pressure potential and osmotic potential

Watershed the topographically defined area that collects wet deposition and drains into a stream or surface water system

Water Stress a condition characterized by a low water potential and water deficiency that may be accompanied by adverse physiological symptoms

Weak Acid a compound with a small acid dissociation constant that partially ionizes in water to release protons (an example is acetic acid or carbonic acid)

Weathering the physical or chemical breakdown of minerals

Weighted Mean a mean value that is calculated using differences in sample amounts to weight the proportional contribution of each sample concentration to the overall average

Wet Deposition the transfer of water droplets and solutes to receptors on Earth

White Rot a decay process caused by Basidiomycete and some Ascomycete fungi, giving wood a bleached appearance

Wilting Point the soil water potential (–1.5 MPa) at which water scarcity causes wilting in plants

Zero Point of Charge the pH at which a colloid has not net positive or negative electrical charge

References

Aber JD, Federer CA (1992) A generalized lumped-parameter model of photosynthesis, evapotranspiration, and net primary production in temperate and boreal forest ecosystems. Oecologia 92:463–474

Aber JD, Melillo JM (1991) Terrestrial ecosystems. Saunders College Publishing, Philadelphia

Aber JD, Nadelhoffer KJ, Steudler P, Melillo JM (1989) Nitrogen saturation in northern forest ecosystems. Bioscience 39:378–386

Aber JD, Magill A, McNulty SG, Boone RD, Nadelhoffer KJ, Downs M, Hallett R (1995) Forest biogeochemistry and primary production altered by nitrogen saturation. Water Air Soil Pollut 85:1665–1670

Aber JD, McDowell W, Nadelhoffer KJ, Magill A, Bernston G, Kamakea SG, McNulty S, Currie W, Rustad L, Fernandez I (1998) Nitrogen saturation in temperate forest ecosystems. Bioscience 48:921–934

Aber JD, Goodale CL, Ollinger SV, Smith ML, Magill AH, Martin ME, Hallett RA, Stoddard JL (2003) Is nitrogen deposition altering the nitrogen status of northeastern forests? Bioscience 53:375–389

Adams MWW, Stiefel EI (1998) Biological hydrogen production: not so elementary. Science 282:1842–1843

Anderson EA, Greenan HJ, Whipkey RZ, Machell CT (1977) NOAA-ARS cooperative snow research project: watershed hydroclimatology and data for water years 1960–1974. U.S. NOAA and ARS, Washington, DC

Anderson TR, Groffman PM, Walter MT (2015) Using a soil topographic index to distribute denitrification fluxes across a northeastern headwater catchment. J Hydrol 522:123–134

April R, Keller D (1990) Mineralogy of the rhizosphere in forest soils of the eastern United States: mineralogic studies of the rhizosphere. Biogeochemistry 9:1–18

April R, Newton RM (1985) Influence of geology on lake acidification in the ILWAS watersheds. Water Air Soil Pollut 26:373–386

Atkins PW (1978) Physical chemistry. W.H. Freeman Co., San Francisco

Axelsson E, Axelsson B (1986) Changes in carbon allocation patterns in spruce and pine trees following irrigation and fertilization. Tree Physiol 2:189–204

Baisden WT, Parfitt RL, Ross C, Schipper LA, Canessa S (2011) Evaluating 50 years of time-series soil radiocarbon data: towards routine calculation of robust C residence times. Biogeochemistry. doi:10.1007/s10533-011-9675-y

Bardgett RD, Streeter TC, Bol R (2003) Soil microbes compete effectively with plants for organic nitrogen inputs to temperate grasslands. Ecology 84:1277–1287

Barford CC, Wofsy SC, Goulden ML, Munger JW, Pyle EH, Urbanski SP, Hutyra L, Saleska SR, Fitzjarrald D, Moore K (2001) Factors controlling long and short-term sequestration of atmospheric CO_2 in a mid-latitude forest. Science 294:1688–1691

Barkmann J, Schwintzer CR (1998) Rapid N_2 fixation in pines? Results of a Maine field study. Ecology 79:1453–1457

Barnes RT, Raymond PA, Casciotti KL (2008) Dual isotope analyses indicate efficient processing of atmospheric nitrate by forested watersheds in the northeastern U.S. Biogeochemistry 90:15–27

Baron J, Drever JI, Mast MA (1990) Chemical weathering in the Loch Vale watershed, Rocky Mountain National Park, Colorado. Water Resour Res 26:2971–2978

Barry RG, Chorley RJ (1970) Atmosphere, weather, and climate. Holt, Rinehart, and Winston, New York, 320 p

Barthold FK, Woods RA (2015) Stormflow generation: a meta-analysis of field evidence from small, forested catchments. Water Resour Res 51:3730–3753

Bashkin MA, Binkley D (1998) Changes in soil carbon following afforestation in Hawaii. Ecology 79:828–833

Beckers J, Alila Y (2004) A model of rapid preferential hillslope runoff contributions to peak flow generation in a temperate rain forest watershed. Water Resour Res 40, W03501, doi:10.1029/2003WR002582

Berg B, Staaf H (1981) Leaching, accumulation, and release of nitrogen in decomposing forest litter. Ecol Bull 33:163–178

Berg MP, Kniese JP, Zoomer R, Verhoef HA (1998) Long-term decomposition of successive organic strata in a nitrogen saturated Scots pine forest soil. For Ecol Manag 107:159–172

Berg B, Davey MP, De Marco A, Emmett B, Faituri M, Hobbie SE, Johansson M-B, Liu C, McClaugherty C, Norell L, Rutigliano FA, Vesterdal L, Virzo De Santo A (2010) Factors influencing limit values for pine needle litter decomposition: a synthesis for boreal and temperate pine forest systems. Biogeochemistry 100:57–73

Beven KJ, Kirkby MJ (1979) A physically-based variable contributing area model of basin hydrology. Hydrol Sci Bull 24:43–69

Binkley D (1981) Nodule biomass and acetylene reduction rates of red alder and Sitka alder on Vancouver Island, B.C. Can J For Res 11:281–286

Binkley D, Richter D (1987) Nutrient cycles and H^+ budgets of forest ecosystems. Adv Ecol Res 16:1–51

Bloom AJ, Chapin FS, Mooney HA (1985) Resource limitation in plants – an economic analogy. Annu Rev Ecol Syst 16:363–392

Booth MS, Stark JM, Rastetter E (2005) Controls on nitrogen cycling in terrestrial ecosystems: a synthetic analysis of literature data. Ecol Monogr 75:139–157

Bormann FH, Likens GE (1979) Pattern and process in a forested ecosystem. Springer, New York

Bormann FH, Likens GE, Siccama TG, Pierce RS, Eaton JS (1974) The export of nutrients and recovery of stable conditions following deforestation at Hubbard Brook. Ecol Monogr 44:255–277

Bormann FH, Likens GE, Melillo JM (1977) Nitrogen budget for an aggrading northern hardwood forest ecosystem. Science 196:981–983

Bowden RD, Nadelhoffer KJ, Boone RD, Melillo JM, Garrison JB (1993) Contributions of aboveground litter, belowground litter, and

C.S. Cronan, *Ecosystem Biogeochemistry*, Springer Textbooks in Earth Sciences, Geography and Environment, DOI 10.1007/978-3-319-66444-6

root respiration to total soil respiration in a temperate mixed hardwood forest. Can J For Res 23:1402–1407
Bowden RD, Rullo G, Stevens GR, Steudler PA (2000) Soil fluxes of carbon dioxide, nitrous oxide, and methane at a productive temperate deciduous forest. J Environ Qual 29:268–276
Bowen HJM (1966) Trace elements in biochemistry. Academic Press, New York
Bowen HJM (1979) Environmental chemistry of the elements. Academic Press, New York
Box E (1978) Geographical dimensions of terrestrial net and gross primary production. Radiat Environ Biophys 15:305–322
Boyer EW, Alexander RB, Parton WJ, Li C, Butterbach-bahl K, Donner SD, Skaggs W, DelGrosso SJ (2006) Modeling denitrification in terrestrial and aquatic ecosystems at regional scales. Ecol Appl 16:2123–2142
Brady NC (1984) The nature and properties of soils. Macmillan Publishing Co., New York, 750 p
Bray JR, Gorham E (1964) Litter production in forests of the world. Adv Ecol Res 2:101–157
Bremner JM (1997) Sources of nitrous oxide in soils. Nutr Cycl Agroecosyst 49:7–16
Broecker WS (1974) Chemical oceanography. Harcourt, Brace. Javanovich, Inc., New York, 214 p
Buchmann N (2000) Biotic and abiotic factors controlling soil respiration rates in *Picea abies* stands. Soil Biol Biochem 32:1625–1635
Bünemann EK (2015) Assessment of gross and net mineralization rates of soil organic phosphorus: a review. Soil Biol Biochem 89:82–98
Burghelea C, Zaharescu DG, Dontsova K, Maier R, Huxman T, Chorover J (2015) Mineral nutrient mobilization by plants from rock: influence of rock type and arbuscular mycorrhiza. Biogeochemistry 124:187–203
Caldwell TG, Johnson DW, Miller WW, Qualls RG (2002) Forest floor carbon and nitrogen losses due to prescription fire. Soil Sci Soc Am J 66:262–267
Castro MS, Driscoll CT, Jordan TE, Reay WG, Boynton WR, Seitzinger SP, Styles RV, Cable JE (2000) Contribution of atmospheric deposition to the total nitrogen loads to thirty-four estuaries on the Atlantic and Gulf coasts of the United States. In: Valigura RM et al (eds) An assessment of nitrogen loads to United States estuaries with an atmospheric perspective. American Geophysical Union, Washington, DC, pp 77–106
Cermak J, Jenik J, Kucera J, Zidek V (1984) Xylem water flow in a crack willow tree (*Salix fragilis* L.) in relation to diurnal changes of environment. Oecologia 64:145–151
Cermak J, Cienciala E, Kucera J, Lindroth A, Bednajova E (1995) Individual variation of sap-flow rate in large pine and spruce trees and stand transpiration: a pilot study at the central NOPEX site. J Hydrol 168:17–27
Cess RD et al, 29 co-authors (1993) Uncertainties in carbon dioxide radiative forcing in atmospheric general circulation models. Science 262: 1252–1255
Chamberlain AC (1975) The movement of particles in plant communities. In: Monteith JL (ed) Vegetation and the atmosphere. I principles. Academic Press, London, pp 155–203
Chang JS (1991) Report 4 – the regional acidic deposition model and engineering model. In: Irving PM (ed) Acidic deposition: state of science and technology. Summary Report of the U.S. National Acid Precipitation Assessment Program, Washington, DC, pp 49–55
Chapin FS, Van Cleve K (1989) Approaches to studying nutrient uptake, use, and loss in plants. In: Pearcy RW et al (eds) Plant physiological ecology – field methods and instrumentation. Chapman and Hall, New York, pp 185–207
Chappelka A, Skelly J, Somers G, Renfro J, Hildebrand E (1999a) Mature black cherry used as a bioindicator of ozone injury. Water Air Soil Pollut 116:261–266
Chappelka A, Somers G, Renfro J (1999b) Visible ozone injury on forest trees in great Smoky Mountains National Park, USA. Water Air Soil Pollut 116:255–260
Chen D, Hu M, Guo Y, Dahlgren RA (2015) Influence of legacy phosphorus, land use, and climate change on anthropogenic phosphorus inputs and riverine export dynamics. Biogeochemistry 123:99–116
Chou L, Wollast R (1984) Study of the weathering of albite at room temperature and pressure with a fluidized bed reactor. Geochim Cosmochim Acta 48:2205–2218
Christ M, Zhang Y, Likens GE, Driscoll CT (1995) Nitrogen retention capacity of a northern hardwood forest soil under ammonium sulfate additions. Ecol Appl 5:802–812
Clayton JL (1988) Some observations on the stoichiometry of feldspar hydrolysis in granitic soil. J Environ Qual 17:153–157
Cogbill CV, Likens GE (1974) Acid precipitation in the northeastern United States. Water Resour Res 10:1133–1137
Cole DW (1992) Nitrogen chemistry, deposition, and cycling in forests. In: Johnson DW, Lindberg SE (eds) Atmospheric deposition and forest nutrient cycling: a synthesis of the integrated forest study, Ecological Studies, vol 91 . Springer, New York, pp 150–213
Coleman DC, Crossley DA (1996) Fundamentals of soil ecology. Academic Press, New York
Cosby BJ, Hornberger GM, Galloway JN, Wright RF (1985) Modeling the effects of acid deposition: assessment of a lumped parameter model of soil water and streamwater chemistry. Water Resour Res 21:51–63
Cosby BJ, Ferrier RC, Jenkins A, Wright RF (2001) Modelling the effects of acid deposition: refinements, adjustments, and inclusion of nitrogen dynamics in the MAGIC model. Hydrol Earth Syst Sci 5:499–517
Covington WW (1981) Changes in forest floor organic matter and nutrient content following clear cutting in northern hardwoods. Ecology 62:41–48
CRC (1978) CRC handbook of chemistry and physics, 59th ed. Weast RC, Astle MJ (eds). CRC Press, W. Palm Beach
Crill PM, Bartlett B, Harriss RC, Gorham E, Verry ES, Sebacher DI, Mazdar L, Sanner W (1988) Methane flux from Minnesota peatlands. Glob Biogeochem Cycles 2:317–384
Cromack K, Monk CD (1975) Litter production, decomposition, and nutrient cycling in a mixed hardwood watershed and a white pine watershed. In: Howell FG et al. (eds) Mineral cycling in southeastern ecosystems. CONF-740513. National Technical Information Service, pp 609–624
Cronan CS (1980a) Solution chemistry of a New Hampshire subalpine ecosystem: a biogeochemical analysis. Oikos 34:272–281
Cronan CS (1980b) Controls on leaching from coniferous forest floor microcosms. Plant Soil 56:301–322
Cronan CS (1985a) Biogeochemical influence of vegetation and soils in the ILWAS watersheds. Water Air Soil Pollut 26:355–371
Cronan CS (1985b) Chemical weathering and solution chemistry in acid forest soils: differential influence of soil type, biotic processes, and H^+ deposition. In: Drever JI (ed) Chemistry of weathering. D. Reidel Publishing Co., Boston, pp 175–195
Cronan CS (1990) Patterns of organic acid transport from forested watersheds to aquatic ecosystems. In: Perdue EM, Gjessing ET (eds) Organic acids in aquatic ecosystems. Wiley, New York, pp 245–260
Cronan CS (1994) Aluminum biogeochemistry in the ALBIOS forest ecosystems: the role of acidic deposition in aluminum cycling. In: Godbold DL, Huttermann A (eds) Effects of acid rain on forest processes. Wiley-Liss, New York, pp 51–81
Cronan CS (2003) Belowground biomass, production, and carbon cycling in mature Norway spruce, Maine, USA. Can J For Res 33:339–350
Cronan CS, Aiken GR (1985) Chemistry and transport of soluble humic substances in forested watersheds of the Adirondack Park, NY. Geochim Cosmochim Acta 49:1697–1705

Cronan CS, Grigal DF (1995) Use of calcium/aluminum ratios as indicators of stress in forest ecosystems. J Environ Qual 24:209–226
Cronan CS, Reiners WA (1983) Canopy processing of acid precipitation by coniferous and hardwood forests in New England. Oecologia 59:216–223
Cronan CS, Reiners WA, Reynolds RC, Lang GE (1978) Forest floor leaching: contributions from mineral, organic, and carbonic acids in New Hampshire subalpine forests. Science 200:309–311
Cronan CS, Driscoll CT, Newton RM, Kelly JM, Schofield CL, Bartlett RJ, April R (1990) A comparative analysis of aluminum biogeochemistry in a northeastern and southeastern forested watershed. Water Resour Res 26:1413–1430
Cronan CS, Lytle D, Piampiano J (1998) Influence of seasonal drought on water-table levels and hydrochemistry in two forested wetlands, Maine. Northeast Nat 5:313–322
Cronan CS, Piampiano JT, Patterson HH (1999) Influence of land use and hydrology on exports of carbon and nitrogen in a Maine river basin. J Environ Qual 28:953–961
Cumming JR (1993) Growth and nutrition of nonmycorrhizal and mycorrhizal pitch pine (*Pinus rigida*) seedlings under phosphorus limitation. Tree Physiol 13:173–187
Currie WS, Aber JD (1997) Modeling leaching as a decomposition process in humid montane forests. Ecology 78:1844–1860
Cusack DF, Chadwick OA, Ladefoged T, Vitousek PM (2012) Long-term effects of agriculture on soil carbon pools and carbon chemistry along a Hawaiian environmental gradient. Biogeochemistry. doi:10.1007/s10533-012-9718-z
Dai S, Schwendtmayer C, Schurmann P, Ramaswamy S, Eklund H (2000) Redox signaling in chloroplasts: cleavage of disulfides by an iron-sulfur cluster. Science 287:655–658
Daniels F, Alberty RA (1975) Physical chemistry, 4th ed. Wiley, New York, 687 p
David MB, Gentry LE (2000) Anthropogenic inputs of nitrogen and phosphorus and riverine export for Illinois, USA. J Environ Qual 29:494–508
Davidson EA, Hart SC, Shanks CA, Firestone MK (1991) Measuring gross nitrogen mineralization, immobilization, and nitrification by ^{15}N isotopic pool dilution in intact soil cores. J Soil Sci 42:335–349
Davidson EA, Hart SC, Firestone MK (1992) Internal cycling of nitrate in soils of a mature coniferous forest. Ecology 73:1148–1156
Davidson EA, Matson PA, Vitousek PM, Riley R, Dunkin K, Garcia-Mendez G, Maass JM (1993) Processes regulating soil emissions of NO and N_2O in a seasonally dry tropical forest. Ecology 74:130–139
Davidson EA, Potter CS, Schlesinger P, Klooster SA (1998) Model estimates of regional nitric oxide emissions from soils of the southeastern United States. Ecol Appl 8:748–759
Dawson TE (1996) Determining water use by trees and forests from isotopic, energy balance and transpiration analyses: the roles of tree size and hydraulic lift. Tree Physiol 16:263–272
Dawson TE, Ehleringer JR (1993) Isotopic enrichment of water in the woody tissues of plants: implications for plant water source, water uptake, and other studies which use the stable isotopic composition of cellulose. Geochim Cosmochim Acta 57:3487–3492
Day ME (2000) Influence of temperature and leaf-to-air vapor pressure deficit on net photosynthesis and stomatal conductance in red spruce (*Picea rubens*). Tree Physiol 20:57–63
Debano LF, Conrad CE (1978) The effect of fire on nutrients in a chaparral ecosystem. Ecology 59:489–497
DeBoer W, Kowalchuck GA (2001) Nitrification in acid soils: micro-organisms and mechanisms. Soil Biol Biochem 33:853–866
DeHayes DH, Schaberg PG, Hawley GJ, Strimbeck GR (1999) Acid rain impacts calcium nutrition and forest health. Bioscience 49:789–800
Dingman SL (1981) Elevation: a major influence on hydrology of New Hampshire and Vermont, USA. Hydrol Sci Bull 26:399–413
Dingman SL (1994) Physical hydrology. Macmillan Publishing Co., New York, 575 p
Dise NB, Matzner E, Gundersen P (1998) Synthesis of nitrogen pools and fluxes from European forest ecosystems. Water Air Soil Pollut 105:143–154
Dornbush ME, Isenhart TM, Raich JW (2002) Quantifying fine root decomposition: an alternative to buried litterbags. Ecology 83:2985–2990
Driscoll CT (1984) A procedure for the fractionation of aqueous aluminum in dilute acidic waters. Int J Environ Anal Chem 16:267–284
Driscoll CT, Likens GE, Hedin LO, Eaton JS, Bormann FH (1989) Changes in the chemistry of surface waters. Environ Sci Technol 23:137–143
Driscoll CT, Lawrence GB, Bulger AJ, Butler TJ, Cronan CS, Eager C, Lambert KF, Likens GE, Stoddard JL, Weathers KC (2001) Acidic deposition in the northeastern United States: sources and inputs, ecosystem effects, and management strategies. Bioscience 51:180–198
Driscoll CT, Whital D, Aber J, Boyer E, Castro M, Cronan C, Goodale C, Groffman P, Hopkinson C, Lambert K, Lawrence G, Ollinger S (2003) Nitrogen pollution in the northeastern United States: sources, effects, and management options. Bioscience 53:357–374
Dunne T, Black RD (1970) Partial area contributions to storm runoff in a small New England watershed. Water Resour Res 6:1296–1311
Edwards NT, Harris WF (1977) Carbon cycling in a mixed deciduous forest floor. Ecology 58:431–437
Ehleringer JR, Buchmann N, Flanagan LB (2000) Carbon isotope ratios in belowground carbon cycle processes. Ecol Appl 10:412–422
Ellsworth DS, Reich PB (1992) Water relations and gas exchange of *Acer saccharum* seedlings in contrasting natural light and water regimes. Tree Physiol 10:1–20
Ellsworth DS, Reich PB (1993) Canopy structure and vertical patterns of photosynthesis and related leaf traits in a deciduous forest. Oecologia 96:169–178
Elser JJ, Dobberfuhl DR, MacKay NA, Schampel JH (1996) Organism size, life history, and N:P stoichiometry. Bioscience 46:674–684
Elwood JW, Turner RR (1989) Streams: water chemistry and ecology. In: Johnson DW, Van Hook RI (eds) Analysis of biogeochemical cycling processes in Walker Branch Watershed. Springer, New York, pp 301–350
Ershadi A, McCabe MF, Evans JP, Wood EF (2015) Impact of model structure and parameterization on Penman-Monteith type evaporation models. J Hydrol 525:521–535
Fahey TJ (1983) Nutrient dynamics of aboveground detritus in lodgepole pine (*Pinus contorta ssp. latifolia*) ecosystems, southeastern Wyoming. Ecol Monogr 53:51–72
Fahey TJ, Siccama TG, Driscoll CT, Likens GE, Campbell J, Johnson CE, Battles JJ, Aber JD, Cole JJ, Fisk MC, Groffman PM, Hamburg SP, Holmes RT, Schwarz PA, Yanai RD (2005) The biogeochemistry of carbon at Hubbard Brook. Biogeochemistry 75:109–176
Federer CA, Lash D (1978) BROOK: a hydrologic simulation model for eastern forests. Water Resources Research Center, University of New Hampshire, Durham
Fenn ME, Poth MA, Aber JD, Baron JS, Bormann BT, Johnson DW, Lemly AD, McNulty SG, Ryan DF, Stottlemyer R (1998) Nitrogen excess in North American ecosystems: predisposing factors, ecosystem responses, and management strategies. Ecol Appl 8:706–733
Fernandez IJ, Rustad LE, Norton SA, Kahl JS, Cosby BJ (2003) Experimental acidification causes soil base cation depletion at the Bear Brook Watershed in Maine. Soil Sci Soc Am J 67:1909–1919
Field C, Merino J, Mooney HA (1983) Compromises between water use efficiency and nitrogen use efficiency in five species of California evergreens. Oecologia 60:384–389
Findley DA, Keever GJ, Chappelka AH, Eakes DJ, Gilliam GH (1996) Sensitivity of red maple cultivars to acute and chronic exposures of ozone. J Arbori 22:264–269

Firestone MK, Firestone RB, Tiedje JM (1980) Nitrous oxide from soil denitrification: factors controlling its biological production. Science 208:749–751

Fisk MC, Zak DR, Crow TR (2002) Nitrogen storage and cycling in old and second-growth northern hardwood forests. Ecology 83:73–87

Foster JR, Lang GE (1982) Decomposition of red spruce and balsam fir boles in the White Mountains of New Hampshire. Can J For Res 12:617–626

Foster DR, Aber JD, Melillo JM, Bowden RD, Bazzaz FA (1997) Forest response to disturbance and anthropogenic stress. Bioscience 47:437–445

Franklin JF, Shugart HH, Harmon ME (1987) Tree death as an ecological process. Bioscience 37:550–556

Franzmeier DP, Pederson EJ, Longwell TJ, Byrne JG, Losche CK (1969) Properties of some soils of the Cumberland plateau as related to slope aspect and position. Soil Sci Soc Am J 33:755–761

Frey SD, Ollinger S, Nadelhoffer K, Bowden R, Brzostek E, Burton A, Caldwell BA, Crow S, Goodale CL, Grandy AS, Finzi A, Kramer MG, Lajtha K, LeMoine J, Martin M, McDowell WH, Minocha R, Sadowsky JJ, Templer PH, Wickings K (2014) Chronic nitrogen additions suppress decomposition and sequester soil carbon in temperate forests. Biogeochemistry 121:305–316

Friedland AJ, Miller EK (1999) Major element cycling in a high-elevation Adirondack forest: patterns and changes, 1986–1996. Ecol Appl 9:958–967

Fuentes JD, Wang D (1999) On the seasonality of isoprene emissions from a mixed temperate forest. Ecol Appl 9:1118–1131

Gabrielli CP, McDonnell JJ, Jarvis WT (2012) The role of bedrock groundwater in rainfall–runoff response at hillslope and catchment scales. J Hydrol 450–451:117–133

Galloway JN, Aber JD, Erisman JW, Seitzinger SP, Howarth RW, Cowling EB, Cosby BJ (2003) The nitrogen cascade. Bioscience 53:341–356

Garrels RM (1967) Genesis of some groundwaters from igneous rocks. In: Abelson PH (ed) Researches in geochemistry, vol 2. Wiley, New York, pp 405–420

Garrels RM, Christ CL (1965) Solutions, minerals, and equilibria. Harper Publishers, New York

Garrison VH, Shinn EA, Foreman WT, Griffin DW, Holmes CW, Kellogg CA, Majewski MS, Richardson LL, Ritchie KB, Smith GW (2003) African and Asian dust: from desert soils to coral reefs. Bioscience 53:469–480

Gaudinski JB, Trumbore SE, Davidson EA, Zheng S (2000) Soil carbon cycling in a temperate forest: radiocarbon-based estimates of residence times, sequestration rates, and partitioning fluxes. Biogeochemistry 51:33–69

Gbondo-Tugbawa SS, Driscoll CT, Aber JD, Likens GE (2001) Evaluation of an integrated biogeochemical model (PnET-BGC) at a northern hardwood forest ecosystem. Water Resour Res 37:1057–1070

Gbondo-Tugbawa SS, Driscoll CT, Mitchell MJ, Aber JD, Likens GE (2002) A model to simulate the response of a northern hardwood forest ecosystem to changes in S deposition. Ecol Appl 12:8–23

Gherini SA, Mok L, Hudson RJM, Davis GF, Chen CW, Goldstein RA (1985) The ILWAS model: formulation and applications. Water Air Soil Pollut 26:425–459

Gholz HL, Fisher RF, Pritchett WL (1985) Nutrient dynamics in slash pine plantation ecosystems. Ecology 66:647–659

Gholz HL, Hendry LC, Cropper WP (1986) Organic matter dynamics of fine roots in plantations of slash pine (*Pinus elliotti*) in north Florida. Can J For Res 16:529–538

Giardina CP, Ryan MG (2000) Evidence that decomposition rates of organic carbon in mineral soil do not vary with temperature. Nature 404:858–860

Gilliam FS, Adams MB, Yurish BM (1996) Ecosystem nutrient responses to chronic nitrogen inputs at Fernow Experimental Forest, WV. Can J For Res 26:196–205

Gilmour CC, Henry EA, Mitchell R (1992) Sulfate stimulation of mercury methylation in freshwater sediments. Environ Sci Technol 26:2281–2287

Gonzalez G, Seastedt TR (2001) Soil fauna and plant litter decomposition in tropical and subalpine forests. Ecology 82:955–964

Goodale CL, Aber JD, McDowell WH (2000) Long-term effects of disturbance on organic and inorganic nitrogen export in the White Mountains, NH. Ecosystems 3:433–450

Gordon WS, Jackson RB (2000) Nutrient concentrations in fine roots. Ecology 81:275–280

Gorham E, Vitousek PM, Reiners WA (1979) The regulation of chemical budgets over the course of terrestrial ecosystem succession. Annu Rev Ecol Syst 10:53–84

Gosz JR, Likens GE, Bormann FH (1972) Nutrient content of litterfall on the Hubbard Brook Experimental Forest, NH. Ecology 53:769–784

Gosz JR, Likens GE, Bormann FH (1973) Nutrient release from decomposing leaf and branch litter in the Hubbard Brook Forest, NH. Ecol Monogr 43:173–191

Gosz JR, Likens GE, Bormann FH (1976) Organic matter and nutrient dynamics of the forest and forest floor in the Hubbard Brook Forest. Oecologia 22:305–320

Goulden ML, Munger JW, Fan SM, Daube BC, Wofsy SC (1996) Exchange of carbon dioxide by a deciduous forest: response to interannual climate variability. Science 271:1576–1578

Gower ST, Reich PB, Son Y (1993) Canopy dynamics and aboveground production of five tree species with different leaf longevities. Tree Physiol 12:327–345

Gower ST, Krankina O, Olson RJ, Apps M, Liner S, Wang C (2001) Net primary production and carbon allocation patterns of boreal forest ecosystems. Ecol Appl 11:1395–1411

Granat L (1972) On the relation between pH and the chemical composition in atmospheric precipitation. Tellus 24:550–560

Granier A, Bobay V, Gash JHC, Gelpe J, Saugier B, Shuttleworth WJ (1990) Vapor flux density and transpiration rate comparisons in a stand of maritime pine (*Pinus pinaster* Ait.) in Les Landes forest. Agric For Meteorol 51:309–319

Graustein WC, Armstrong RL (1983) The use of strontium-87/strontium-86 ratios to measure atmospheric transport into forested watersheds. Science 219:289–292

Grennfelt P (1987) Deposition processes for acidifying compounds. Environ Technol Lett 8:515–527

Grier CC (1975) Wildfire effects on nutrient distribution and leaching in a coniferous ecosystem. Can J For Res 5:599–607

Grier CC, Vogt KA, Keyes MR, Edmonds RL (1981) Biomass distribution and above- and belowground production in young and mature *Abies amabilis* zone ecosystems of the Washington Cascades. Can J For Res 11:155–167

Groffman PM, Driscoll CT, Likens GE, Fahey TJ, Holmes RT, Eager C, Aber JD (2004) Nor gloom of night: a new conceptual model for the Hubbard Brook Ecosystem study. Bioscience 54:139–148

Gundersen P (1998) Effects of enhanced nitrogen deposition in a spruce forest at Klosterhede, Denmark, examined by moderate NH_4NO_3 addition. For Ecol Manag 101:251–268

Gundersen P, Emmett BA, Kjonaas OJ, Koopmans CJ, Tietema A (1998) Impact of nitrogen deposition on nitrogen cycling in forests: a synthesis of NITREX data. For Ecol Manag 101:37–55

Gunthardt-Goerg MS, McQuattie CJ, Maurer S, Frey B (2000) Visible and microscopic injury in leaves of five deciduous tree species related to current critical ozone levels. Environ Pollut 109:489–500

Hamilton EW, Frank DA (2001) Can plants stimulate soil microbes and their own nutrient supply? Evidence from a grazing tolerant grass. Ecology 82:2397–2402

Harborne JB (1982) Introduction to ecological biochemistry. Academic Press, New York, 278 p

Harmon ME, Franklin JF, Swanson FJ, Sollins P, Gregory SV, Lattin JD, Anderson NH, Cline SP, Aumen NG, Sedell JR, Lienkaemper GW, Cromack K, Cummins KW (1986) Ecology of coarse woody debris in temperate ecosystems. Adv Ecol Res 15:133–276

Harris WF, Sollins P, Edwards NT, Dinger BE, Shugart HH (1975) Analysis of carbon flow and productivity in a temperate deciduous forest ecosystem. In: Reichle DE, Franklin JF (eds) Productivity of world ecosystems. National Academy of Sciences, Washington, DC, pp 116–122

Hart SC (1999) Nitrogen transformations in fallen tree boles and mineral soil of an old-growth forest. Ecology 80:1385–1394

Hart SC, Firestone MK (1989) Evaluation of three *in situ* soil nitrogen availability assays. Can J For Res 19:185–191

Hatch AB (1937) The physical basis of mycotrophy in the genus *Pinus*. Black Rock For Bulln 6:1–168

Haug A (1984) Molecular aspects of aluminum toxicity. CRC Critil Rev Plant Sci 1:345–373

Hauhs M (1985) Wasser- und stoffhaushalt im einzugsgebiet der Langen Bramke (Harz). Berichte des Forschungszentrums Waldokosysteme/ Waldsterben, Bd. 17

Haynes BE, Gower ST (1995) Belowground carbon allocation in unfertilized and fertilized red pine plantations in northern Wisconsin. Tree Physiol 15:317–325

Hedin LO, Granat L, Likens GE, Buishand TA, Galloway JN, Butler TJ, Rodhe H (1994) Steep declines in atmospheric base cations in regions of Europe and North America. Nature 367:351–354

Hedin LO, von Fischer JC, Ostrom NE, Kennedy BP, Brown MG, Robertson GP (1998) Thermodynamic constraints on nitrogen transformations and other biogeochemical processes at soil-stream interfaces. Ecology 79:684–703

Heilman P, Ekuan G (1982) Nodulation and nitrogen fixation by red alder and Sitka alder on coal mine spoils. Can J For Res 12:992–997

Helgeson HC, Murphy WM, Aagaard P (1984) Thermodynamic and kinetic constraints on reaction rates among minerals and aqueous solutions. II. Rate constants, effective surface area, and the hydrolysis of feldspar. Geochim Cosmochim Acta 48:2405–2432

Helvey JD, Patric JH (1965) Canopy and litter interception of rainfall by hardwoods of eastern United States. Water Resour Res 1:193–206

Henderson GS, Hunley A, Selvidge W (1977) Nutrient discharge from Walker Branch Watershed. In: Correll DL (ed) Watershed research in eastern North America: a workshop to compare results. Chesapeake Bay Center for Environmental Studies, Edgewater, pp 307–320

Henderson GS, Swank WT, Waide JB, Grier CC (1978) Nutrient budgets of Appalachian and Cascade region watersheds: a comparison. For Sci 24:385–397

Hiebert FK, Bennett PC (1992) Microbial control of silicate weathering in organic-rich ground water. Science 258:278–281

Hildebrand E, Skelly JM, Fredericksen TS (1996) Foliar response of ozone-sensitive hardwood tree species from 1991 to 1993 in the Shenandoah National Park, VA. Can J For Res 26:658–669

Hobbie SE (1996) Temperature and plant species control over litter decomposition in Alaskan tundra. Ecol Monogr 66:503–522

Hobbie SE (2015) Plant species effects on nutrient cycling: revisiting litter feedbacks. Trends Ecol Evol 30:357–363

Hobbie EA, Colpaert JV (2003) Nitrogen availability and colonization by mycorrhizal fungi correlate with nitrogen isotope patterns in plants. New Phytol 157:115–126

Hobbie EA, Ouimette AP (2009) Controls of nitrogen isotope patterns in soil profiles. Biogeochemistry 95:355–371

Hobbs PV, Reid JS, Kotchenruther RA, Ferek RJ, Weiss R (1997) Direct radiative forcing by smoke from biomass burning. Science 275:1776–1778

Högberg MN, Blaško R, Bach LH, Hasselquist NJ, Egnell G, Näsholm T, Högberg P (2014) The return of an experimentally N-saturated boreal forest to an N-limited state: observations on the soil microbial community structure, biotic N retention capacity and gross N mineralization. Plant Soil 381:45–60

Hogsett WE, Weber JE, Tingey D, Herstrom A, Lee EH, Laurence JA (1997) An approach for characterizing tropospheric ozone risk to forests. Environ Manag 21:105–120

Holloway JM, Dahlgren RA (2002) Nitrogen in rock: occurrences and biogeochemical implications. Global Biogeochem Cycles 16:65-1–65-17

Holmes WE, Zak DR (1994) Soil microbial biomass dynamics and net nitrogen mineralization in northern hardwoods. Soil Sci Soc Am J 58:238–243

Holmes WE, Zak DR (1999) Soil microbial control of nitrogen loss following clear-cut harvest in northern hardwood ecosystems. Ecol Appl 9:202–215

Honeycutt CW, Zibilske LM, Clapham WM (1988) Heat units for describing C mineralization and predicting net N mineralization. Soil Sci Soc Am J 52:1346–1350

Hooper RP, Christophersen N, Peters NE (1990) Modeling streamwater chemistry as a mixture of soilwater end-members – an application to the Panola Mountain catchment, Georgia, USA. J Hydrol 116:321–343

Hornberger GM, Raffensperger JP, Wiberg PL, Eshleman KN (1998) Elements of physical hydrology. Johns Hopkins University Press, Baltimore, 302 p

Horton TW, Chamberlain CP, Fantle M, Blum JD (1999) Chemical weathering and lithologic controls of water chemistry in a high-elevation river system: Clark's Fork of the Yellowstone River, Wyoming and Montana. Water Resour Res 35:1643–1655

Horwath WR, Pregitzer KS, Paul EA (1994) ^{14}C allocation in tree-soil systems. Tree Physiol 14:1163–1176

Huff DD, Luxmore RJ, Mankin JB, Begovich CL (1977) TEHM: a terrestrial ecosystem hydrology model. ORNL/NSF/EATC-27. Oak Ridge National Laboratory, Oak Ridge

Huntington TG, Ryan DF, Hamburg SP (1988) Estimating soil nitrogen and carbon pools in a northern hardwood forest ecosystem. Soil Sci Soc Am J 52:1162–1167

Ingestad T (1971) A definition of optimum nutrient requirements in birch seedlings. II Physiol Plant 24:118–125

Ingestad T, Agren GI (1991) The influence of plant nutrition on biomass allocation. Ecol Appl 1:168–174

IPCC (1992) Climate change 1992 – supplemental report. Cambridge University Press, New York

IPCC (2007) Climate change 2007 – the physical science basis. Working group I. Intergovernmental Panel on Climate Change, Cambridge University Press, New York

Jacinthe PA, Groffman PM, Gold AJ, Mosier A (1998) Patchiness in microbial nitrogen transformations in groundwater in a riparian forest. J Environ Qual 27:156–164

Jackson RB, Mooney HA, Schulze ED (1997) A global budget for fine root mass, surface area, and nutrient contents. Proc Natl Acad Sci USA 94:7362–7366

Jansson PE, Halldin S (1979) Model for annual water and energy flow in a layered soil. In: Halldin S (ed) Comparison of forest water and energy exchange models. International Society for Microbial Ecology, Copenhagen, pp 145–163

Jenny H (1941) Factors of soil formation – a system of quantitative pedology. McGraw-Hill Book Company, New York

Jobbagy EG, Jackson RB (2000) The vertical distribution of soil organic carbon and its relation to climate and vegetation. Ecol Appl 10:423–436

Jobbagy EG, Jackson RB (2001) The distribution of soil nutrients with depth: global patterns and the imprint of plants. Biogeochemistry 53:51–77

Johannes AH, Altwicker ER, Clesceri NL (1981) Characterization of acidic precipitation in the Adirondack region. Report EA-1826. Electric Power Research Institute, Palo Alto

Johannes AH, Altwicker ER, Clesceri NL (1985) The Integrated Lake-Watershed Acidification Study: atmospheric inputs. Water Air Soil Pollut 26:339–353

Johannisson C, Myrold DD, Hogberg P (1999) Retention of nitrogen by a nitrogen-loaded Scots pine forest. Soil Sci Soc Am J 63:383–389

Johnson NM (1984) Acid rain neutralization by geologic materials. In: Bricker OP (ed) Geological aspects of acid deposition. Butterworth Publ, Boston, pp 37–53

Johnson DW (1992) Nitrogen retention in forest soils. J Environ Qual 21:1–12

Johnson DW, Cole DW (1977) Sulfate mobility in an outwash soil in western Washington. Water Air Soil Pollut 7:489–495

Johnson DW, Cole DW (1980) Anion mobility in soils: relevance to nutrient transport from forest ecosystems. Environ Int 3:79–90

Johnson DW, Henderson GS (1989) Terrestrial nutrient cycling. In: Johnson DW, Van Hook RI (eds) Analysis of biogeochemical cycling processes in Walker Branch Watershed. Springer, New York, pp 233–300

Johnson DW, Lindberg SE (eds) (1992) Atmospheric deposition and forest nutrient cycling – a synthesis of the Integrated Forest Study. Ecological Studies, vol 91. Springer, New York, 707 p

Johnson DW, Turner J (2014) Nitrogen budgets of forest ecosystems: a review. For Ecol Manag 318:370–379

Johnson DW, Van Hook RI (eds) (1989) Analysis of biogeochemical cycling processes in Walker Branch Watershed. Springer, New York, 401 p

Johnson NM, Driscoll CT, Eaton JS, Likens GE, McDowell WH (1981) "Acid rain", dissolved aluminum and chemical weathering at the Hubbard Brook Experimental Forest, NH. Geochim Cosmochim Acta 45:1421–1437

Johnson CE, Driscoll CT, Siccama TG, Likens GE (2000) Element fluxes and landscape position in a northern hardwood forest watershed ecosystem. Ecosystems 3:159–184

Johnsson L, Berggren D, Karen O (1999) Content and bioavailability of organic forms of nitrogen in the O horizon of a podzol. Eur J Soil Sci 50:591–600

Joslin JD, Henderson GS (1987) Organic matter and nutrients associated with fine root turnover in a white oak stand. For Sci 33:330–346

Kahl JS, Norton SA, Fernandez IJ, Nadelhoffer KJ, Driscoll CT, Aber JD (1993) Experimental inducement of nitrogen saturation at the watershed scale. Environ Sci Technol 27:565–568

Kahl J, Norton S, Fernandez I, Rustad L, Handley M (1999) Nitrogen and sulfur input-output budgets in the experimental and reference watersheds, Bear Brook Watershed in Maine (BBWM). Environ Monit Assess 55:113–131

Kampf SK, Burges SJ (2007) A framework for classifying and comparing distributed hillslope and catchment hydrologic models. Water Resour Res 43:W05423, doi:10.1029/2006WR005370

Karama SL, Weisberg PJ, Scheller RM, Johnson DW, Miller WW (2013) Development and evaluation of a nutrient cycling extension for the LANDIS-II landscape simulation model. Ecol Model 250:45–57

Katz BG, Bricker OP, Kennedy MM (1985) Geochemical mass balance relationships for selected ions in precipitation and stream water, Catoctin Mountains, Maryland. Am J Sci 285:931–962

Kaye JP, Burke IC, Mosier AR, Guerschman JP (2004) Methane and nitrous oxide fluxes from urban soils to the atmosphere. Ecol Appl 14:975–981

Kerin EJ, Gilmour CC, Roden E, Suzuki MT, Coates JD, Mason RP (2006) Mercury methylation by dissimilatory iron-reducing bacteria. Appl Environ Microbiol 72:7919–7921

Keyes MR, Grier CC (1981) Above and belowground net production in 40 yr old Douglas-fir stands on low and high productivity sites. Can J For Res 11:599–605

Killingbeck KT (1996) Nutrients in senesced leaves: keys to the search for potential resorption and resorption proficiency. Ecology 77:1716–1727

Killingbeck KT, May JD, Nyman S (1990) Foliar senescence in an aspen (*Populus tremuloides*) clone: the response of element resorption to interramet variation and timing of abscission. Can J For Res 20:1156–1164

King GM (1996) *In situ* analyses of methane oxidation associated with the roots and rhizomes of a bur reed, *Sparganium eurycarpum*, in a Maine wetland. Appl Environ Microbiol 62:4548–4555

Kohl L, Laganiere J, Edwards KA, Billings SA, Morrill PL, Van Biesen G, Ziegler SE (2015) Distinct fungal and bacterial $\partial^{13}C$ signatures as potential drivers of increasing $\partial^{13}C$ of soil organic matter with depth. Biogeochemistry 124:13–26

Kolb TE, Fredericksen TS, Steiner KC, Skelly JM (1997) Issues in scaling tree size and age responses to ozone: a review. Environ Pollut 98:195–208

Koopmans CJ, Tietema A, Boxman AW (1996) The fate of ^{15}N enriched throughfall in two coniferous forest stands at different nitrogen deposition levels. Biogeochemistry 34:19–44

Kulkarni MV, Burgin AJ, Groffman PM, Yavitt JB (2014) Direct flux and ^{15}N tracer methods for measuring denitrification in forest soils. Biogeochemistry 117:359–373

Kurth VJ, Hart SC, Ross CS, Kaye JP, Fule PZ (2014) Stand-replacing wildfires increase nitrification for decades in southwestern ponderosa pine forests. Oecologia 175:395–407

Lajtha K, Michener RH (1994) Stable isotopes in ecology and environmental science. Blackwell Scientific Publications, Boston

Lambert RL (1980) The biomass, coverage, and decay rates of dead boles in terrace forests, South Fork Hoh River, Olympic National Park. In: Second conference on scientific research in the national parks, AIBS, San Francisco, pp 64–79

Lambert RL, Cromack K (1982) Mass, nutrient content, and decay rate of dead boles in rain forests of Olympic National Park. Can J For Res 12:511–521

Lambert RL, Lang GE, Reiners WA (1980) Loss of mass and chemical change in decaying boles of a subalpine balsam fir forest. Ecology 61:1460–1473

Land M, Ingri J, Oehlander B (1999) Past and present weathering rates in northern Sweden. Appl Geochem 14:761–774

Lang GE, Knight DH (1979) Decay rates for boles of tropical trees in Panama. Biotropica 11:316–317

Lang GE, Cronan CS, Reiners WA (1981) Organic matter and major elements of the forest floors and soils in subalpine balsam fir forests. Can J For Res 11:388–399

Lanyon LE, Hall GF (1979) Dissolution of selected rocks and minerals in dilute salt solution as influenced by temperature regime. Soil Sci Soc Am J 43:192–195

Laurence JA, Amundson RG, Kohut RJ, Weinstein DA (1997) Growth and water use of red spruce (*Picea rubens* Sarg.) exposed to ozone and simulated acidic precipitation for four growing seasons. For Sci 43:355–361

Lawrence GB, David MB, Lovett GM, Murdoch PS, Burns DA, Stoddard JL, Baldigo BP, Porter JH, Thompson AW (1999) Soil calcium status and the response of stream chemistry to changing acidic deposition rates in the Catskill Mountains of New York. Ecol Appl 9:1059–1072

Levin SA (1999) Fragile dominion – complexity and the commons. Perseus Publications, Cambridge, 250 p

Likens GE, Bormann FH (1995) Biogeochemistry of a forested ecosystem. Springer, New York, 159 p

Likens GE, Bormann FH, Pierce RS, Eaton JS, Johnson NM (1977) Biogeochemistry of a forested ecosystem. Springer, New York

Likens GE, Driscoll CT, Buso DC, Siccama TG, Johnson CE, Lovett GM, Fahey TJ, Reiners WA, Ryan DF, Martin CW, Bailey SW (1998) The biogeochemistry of calcium at Hubbard Brook. Biogeochemistry 41:89–173

Likens GE, Butler TJ, Buso DC (2001) Long- and short-term changes in sulfate deposition: effects of the 1990 Clean Air Act Amendments. Biogeochemistry 52:1–11

Likens GE, Driscoll CT, Buso DC, Mitchell MJ, Lovett GM, Bailey SW, Siccama TG, Reiners WA, Alewell C (2002) The biogeochemistry of sulfur at Hubbard Brook. Biogeochemistry 60:235–316
Lindberg SE, Lovett GM (1985) Field measurements of dry deposition rates of particles to inert and foliar surfaces in a forest. Environ Sci Technol 19:228–244
Lindberg SE, Lovett GM (1992) Deposition and canopy interactions of airborne sulfur: results from the Integrated Forest Study. Atmos Environ 26A:1477–1492
Lindberg SE, Lovett GM, Richter DD, Johnson DW (1986) Atmospheric deposition and canopy interactions of major ions in a forest. Science 231:141–145
Lindroth A, Klemedtsson L, Grelle A, Weslien P, Langvall O (2008) Measurement of net ecosystem exchange, productivity, and respiration in three spruce forests in Sweden shows unexpectedly large soil carbon losses. Biogeochemistry 89:43–60
Losche CK, McCracken RJ, Davey CB (1970) Soils of the steeply sloping landscapes in the southern Appalachian Mountains. Soil Sci Soc Am J 34:473–478
Lovett GM (1994) Atmospheric deposition of nutrients and pollutants in North America: an ecological perspective. Ecol Appl 4:629–650
Lovett GM, Goodale CL (2011) A new conceptual model of nitrogen saturation based on experimental nitrogen addition to an oak forest. Ecosystems 14:615–631
Lovett GM, Lindberg SE (1984) Dry deposition and canopy exchange in a mixed oak forest as determined by analysis of throughfall. J Appl Ecol 21:1013–1028
Lovett GM, Lindberg SE (1986) Dry deposition of nitrate to a deciduous forest. Biogeochemistry 2:137–148
Lovett GM, Reiners WA, Olson RK (1982) Cloud droplet deposition in subalpine balsam fir forests: hydrological and chemical inputs. Science 218:1303–1304
Lovett GM, Likens GE, Nolan SS (1992) Dry deposition of sulfur to the Hubbard Brook Experimental Forest: a preliminary comparison of methods. In: Schwartz SE, Slinn WGN (eds) Precipitation scavenging and atmosphere-surface exchange, vol 3. Hemisphere, Washington, DC, pp 1391–1402
Lovett GM, Weathers KC, Sobczak WV (2000) Nitrogen saturation and retention in forested watersheds of the Catskill Mountains, NY. Ecol Appl 10:73–84
Lovett GM, Arthur MA, Weathers KC, Fitzhugh RD, Templer PH (2013) Nitrogen addition increases carbon storage in soils, but not in trees, in an eastern U.S. deciduous forest. Ecosystems 16:980–1001
Luxmore RJ (1989) Modeling chemical transport, uptake, and effects in the soil-plant-litter system. In: Johnson DW, Van Hook RI (eds) Analysis of biogeochemical cycling processes in Walker Branch Watershed. Springer, New York, pp 351–384
Luxmore RJ, Huff DD (1989) Water. In: Johnson DW, Van Hook RI (eds) Analysis of biogeochemical cycling processes in Walker Branch Watershed. Springer, New York, pp 164–196
Luxmore RJ, Huff DD, McConathy RK, Dinger BE (1978) Some measured and simulated plant water relations of yellow-poplar. For Sci 24:327–341
Lyford WH, Wilson BF (1964) Development of the root system of *Acer rubrum* L. Harvard Forest paper no. 10, Harvard Forest, Petersham
Magill AH, Aber JD (1998) Long-term effects of experimental nitrogen additions on foliar litter decay and humus formation in forest ecosystems. Plant Soil 203:301–311
Magill AH, Aber JD, Berntson GM, McDowell WH, Nadelhoffer KJ, Melillo JM, Steudler P (2000) Long-term nitrogen additions and nitrogen saturation in two temperate forests. Ecosystems 3:238–253
Makipaa R (1995) Effect of nitrogen input on carbon accumulation of boreal forest soils and ground vegetation. For Ecol Manag 79:217–226
Manley EP, Evans LJ (1986) Dissolution of feldspars by low molecular weight aliphatic and aromatic acids. Soil Sci 141:106–111
Manzoni S, Trofymow JA, Jackson RB, Porporato A (2010) Stoichiometric controls on carbon, nitrogen, and phosphorus dynamics in decomposing litter. Ecol Monogr 80(1):89–106
Martinelli LA, Piccolo MC, Townsend AR, Vitousek PM, Cuevas E, McDowell W, Robertson GP, Santos OC, Treseder K (1999) Nitrogen stable isotopic composition of leaves and soil: tropical versus temperate forests. Biogeochemistry 46:45–65
Martinez-Cortizas A, Pontevedra-Pombal X, Garcia-Rodeja E, Novoa-Munoz JC, Shotyk W (1999) Mercury in a Spanish peat bog: archive of climate change and atmospheric metal deposition. Science 284:939–942
Matson PA, Naylor R, Ortiz-Monasterio I (1998) Integration of environmental, agronomic, and economic aspects of fertilizer management. Science 280:112–115
Mayer LM, Xing B (2001) Organic carbon-surface area-clay relationships in acid soils. Soil Sci Soc Am J 65:250–258
McCormack LM, Crisfield E, Raczka B, Schnekenburger F, Eissenstat DM, Smithwick EAH (2015) Sensitivity of four ecological models to adjustments in fine root turnover rate. Ecol Model 297:107–117
McDowell WH, Likens GE (1988) Origin, composition, and flux of dissolved organic carbon in the Hubbard Brook Valley. Ecol Monogr 58:177–195
McFarlane KJ, Torn MS, Hanson PJ, Porras RC, Swanston CW, Callaham MA Jr, Guilderson TP (2012) Comparison of soil organic matter dynamics at five temperate deciduous forests with physical fractionation and radiocarbon measurements. Biogeochemistry. doi:10.1007/s10533-012-9740-1
McLaughlin SB, Anderson CP, Edwards NT, Roy WK, Layton PA (1990) Seasonal patterns of photosynthesis and respiration of red spruce saplings from two elevations in declining southern Appalachian stands. Can J For Res 20:485–495
McNulty SG, Aber JD, Newman SD (1996) Nitrogen saturation in a high elevation spruce-fir stand. For Ecol Manag 84:109–121
Medhurst JL, Beadle CL (2002) Sapwood hydraulic conductivity and leaf area – sapwood area relationships following thinning of a *Eucalyptus nitens* plantation. Plant Cell Environ 25:1011–1019
Meentenmeyer V (1978) Macroclimate and lignin control of litter decomposition rates. Ecology 59:465–472
Melillo JM, Aber JD, Muratore JF (1982) Nitrogen and lignin control hardwood leaf litter decomposition dynamics. Ecology 63:621–626
Melillo JM, Aber JD, Linkins AE, Ricca A, Fry B, Nadelhoffer KJ (1989) Carbon and nitrogen dynamics along the decay continuum: plant litter to soil organic matter. Plant Soil 115:189–198
Melillo JM, Steudler PA, Aber JD, Newkirk K, Lux H, Bowles FP, Catricala C, Magill A, Ahrens T, Morrisseau S (2002) Soil warming and carbon cycle feedbacks to the climate system. Science 298:2173–2176
Mildner M, Bader MK-F, Baumann C, Korner C (2015) Respiratory fluxes and fine root responses in mature *Picea abies* trees exposed to elevated atmospheric CO concentrations. Biogeochemistry 124:95–111
Miller EK, Blum JD, Friedland AJ (1993) Determination of soil exchangeable cation loss and weathering rates using Sr isotopes. Nature 362:438–441
Mital D, Sucoff E (1983) Predicting soil moisture depletion beneath trembling aspen. Can J For Res 13:45–52
Mitchell MJ, Lindberg SE (1992) Sulfur chemistry, deposition, and cycling in forests. In: Johnson DW, Lindberg SE (eds) Atmospheric deposition and forest nutrient cycling: a synthesis of the Integrated Forest Study, Ecological Studies, vol 91. Springer, pp 72–149
Mitchell MJ, Driscoll CT, Kahl JS, Likens GE, Murdoch PS, Pardo LH (1996) Climatic control of nitrate loss from forested watersheds in the northeast United States. Environ Sci Technol 30:2609–2612
Mitchell MJ, Lovett G, Bailey S, Beall F, Burns D, Buso D, Clair TA, Courchesne F, Duchesne L, Eimers C, Fernandez I, Houle D, Jeffries DS, Likens GE, Moran MD, Rogers C, Schwede D, Shanley

J, Weathers KC, Vet R (2011) Comparisons of watershed sulfur budgets in southeast Canada and northeast US: new approaches and implications. Biogeochemistry 103:181–207
Montieth JL (1965) Evaporation and environment. In: Proceedings of 19th symposium Society for Experimental Biology, Cambridge University Press, New York, pp 205–233
Montieth DT, Henrys PA, Evans CD, Malcolm I, Shilland EM, Pereira MG (2015) Spatial controls on dissolved organic carbon in upland waters inferred from a simple statistical model. Biogeochemistry 123:363–377
Moore TR, Knowles R (1989) The influence of water table levels on methane and carbon dioxide emissions from peatland soils. Can J Soil Sci 69:33–38
Moran-Zuloaga D, Dippold M, Glaser B, Kuzyakov Y (2015) Organic nitrogen uptake by plants: re-evaluation by position-specific labeling of amino acids. Biogeochemistry 125:359–374
Morse JL, Durán J, Groffman PM (2015) Soil denitrification fluxes in a northern hardwood forest: the importance of snowmelt and implications for ecosystem N budgets. Ecosystems 18:520–532
Mueller KE, Hobbie SE, Chorover J, Reich PB, Eisenhauer N, Castellano MJ, Chadwick OA, Dobies T, Hale CM, Joagodzinski AM, Kalucka I, Kieliszewska-Rokicka B, Modrzynski J, Rozen A, Skorupski M, Sobczyk L, Stasinska M, Trocha LK, Weiner J, Wierzbicka A, Oleksyn J (2015) Effects of litter traits, soil biota, and soil chemistry on soil carbon stocks at a common garden with 14 tree species. Biogeochemistry 123:313–327
Mulder J, Christophersen N, Hauhs M, Vogt RD, Andersen S, Andersen DO (1990) Water flow paths and hydrochemical controls in the Birkenes catchment as inferred from a rainstorm high in seasalts. Water Resour Res 26:611–622
Munger JW, Eisenreich SJ (1983) Continental-scale variations in precipitation chemistry. Environ Sci Technol 17:32A–42A
Munson RK, Gherini SA (1991) Processes influencing the acid-base chemistry of surface waters. In: Charles DF (ed) Acidic deposition and aquatic ecosystems. Springer, New York, pp 9–34
Murdoch PS, Stoddard JL (1993) Chemical characteristics and temporal trends in eight streams of the Catskill Mountains, NY. Water Air Soil Pollut 67:367–396
Murphy KL, Klopatek JM, Klopatek CC (1998) The effects of litter quality and climate on decomposition along an elevational gradient. Ecol Appl 8:1061–1071
Murphy CJ, Baggs EM, Morley N, Wall DP, Paterson E (2015) Rhizosphere priming can promote mobilization of N-rich compounds from soil organic matter. Soil Biol Biochem 81:236–243
Nadelhoffer KJ, Downs MR, Fry B (1999) Sinks for ^{15}N-enriched additions to an oak forest and a red pine plantation. Ecol Appl 9:72–86
NADP – National Atmospheric Deposition Program (NRSP-3) (1982) NADP Program Office, Illinois State Water Survey, 2204 Griffith Dr., Champaign, IL 61820
NADP – National Atmospheric Deposition Program (NRSP-3) (1992) NADP Program Office, Illinois State Water Survey, 2204 Griffith Dr., Champaign, IL 61820
NADP – National Atmospheric Deposition Program (NRSP-3) (1994) NADP Program Office, Illinois State Water Survey, 2204 Griffith Dr., Champaign, IL 61820
NADP – National Atmospheric Deposition Program (NRSP-3) (2000) NADP Program Office, Illinois State Water Survey, 2204 Griffith Dr., Champaign, IL 61820
NAPAP. National acid precipitation assessment program, Washington, DC
Nasholm T, Ekblad A, Nordin A, Giesler R, Hogberg M, Hogberg P (1998) Boreal forest plants take up organic nitrogen. Nature (London) 6679:914–916
Nasto MK, Alvarez-Clare S, Lekberg Y, Sullivan BW, Townsend AR, Cleveland CC (2014) Interactions among nitrogen fixation and soil phosphorus acquisition strategies in lowland tropical rain forests. Ecol Lett 17:1282–1289
Neill C, Chaves JE, Biggs T, Deegan LA, Elsenbeer H, Figueiredo RO, Germer S, Johnson MS, Lehmann J, Markewitz D, Piccolo MC (2011) Runoff sources and land cover change in the Amazon: an end-member mixing analysis from small watersheds. Biogeochemistry 105:7–18
Neu V, Neill C, Krusche AV (2011) Gaseous and fluvial carbon export from an Amazon forest watershed. Biogeochemistry 105:133–147
Nihlgard B (1985) The ammonium hypothesis – an additional explanation to the forest dieback in Europe. Ambio 14:2–8
Nippgen F, McGlynn BL, Emanuel RE (2015) The spatial and temporal evolution of contributing areas. Water Resour Res 51:4550–4573
Norton S, Kahl J, Fernandez I, Haines T, Rustad L, Nodvin S, Schofield J, Strickland T, Erickson H, Wigington P, Lee J (1999) The Bear Brook Watershed, Maine (BBWM), USA. Environ Monit Assess 55:7–51
Odum EP (1969) The strategy of ecosystem development. Science 164:262–270
Ollinger SV, Aber JD, Lovett GM, Millham SE, Lathrop RG, Ellis JM (1993) A spatial model of atmospheric deposition for the northeastern United States. Ecol Appl 3:459–472
Ollinger SV, Aber JD, Reich PB (1997) Simulating ozone effects on forest productivity: interactions among leaf, canopy, and stand-level processes. Ecol Appl 7:1237–1251
Olmsted J, Williams GM (1997) Chemistry – the molecular science. Wm. C. Brown Publ, Boston, 1056 p
Olson JS (1963) Energy storage and the balance of producers and decomposers in ecological systems. Ecology 44:322–331
Olson RK, Reiners WA (1983) Nitrification in subalpine balsam fir soils: tests for inhibitory factors. Soil Biol Biochem 15:413–418
Olson RK, Reiners WA, Cronan CS, Lang GE (1981) The chemistry and flux of throughfall and stemflow in subalpine balsam fir forests. Holarct Ecol 4:291–300
Oren R, Ewers BE, Todd P, Phillips N, Katul G (1998) Water balance delineates the soil layer in which moisture affects canopy conductance. Ecol Appl 8:990–1002
Owens LB, Watson JP (1979) Rates of weathering and soil formation on granite in Rhodesia. Soil Sci Soc Am J 43:160–166
Paces T (1983) Rate constants of dissolution derived from the measurements of mass balance in hydrological catchments. Geochim Cosmochim Acta 47:1855–1863
Paces T (1985) Sources of acidification in central Europe estimated from elemental budgets in small basins. Nature 315:31–36
Paces T (1986) Weathering rates of gneiss and depletion of exchangeable cations in soils under environmental acidification. J Geol Soc Lond 143:1–5
Pan Y, Birdsey RA, Fang J, Houghton R, Kauppi PE, Kurz WA, Phillips OL, Shvidenko A, Lewis SL, Canadell JG, Ciais P, Jackson RB, Pacala SW, McGuire AD, Piao S, Rautiainen A, Sitch S, Hayes D (2011) A large and persistent carbon sink in the world's forests. Science 333:988–993
Panek JA, Matson PA, Ortiz-Monasterio I, Brooks P (2000) Distinguishing nitrification and denitrification sources of N_2O in a Mexican wheat system using ^{15}N. Ecol Appl 10:506–514
Parton WJ, Schimel DS, Cole CV, Ojima DS (1987) Analysis of factors controlling soil organic matter levels in grasslands. Soil Sci Soc Am J 51:1173–1179
Perakis SS, Hedin LO (2001) Fluxes and fates of nitrogen in soil of an unpolluted old-growth temperate forest, southern Chile. Ecology 82:2245–2260
Peterjohn WT, Melillo JM, Steudler PA, Newkirk KM, Bowles FP, Aber JD (1994) Responses of trace gas fluxes and N availability to experimentally elevated soil temperatures. Ecol Appl 4:617–625

Peters NE (1984) Hydrologic analysis of Woods and Panther Lake basins in the west-central Adirondack Mountains, NY. In: Goldstein RA, Gherini SA (eds) The Integrated Lake-Watershed Acidification Study, ch 5, vol 4: Summary of major results. EPRI, Palo Alto

Peters NE, Murdoch PS (1985) Hydrogeologic comparison of an acidic lake basin with a neutral lake basin in the west-central Adirondack Mountains, New York. Water Air Soil Pollut 26:387–402

Phillips N, Oren R (2001) Intra- and inter-annual variation in transpiration of a pine forest. Ecol Appl 11:385–396

Prescott CE (2010) Litter decomposition: what controls it and how can we alter it to sequester more carbon in forest soils? Biogeochemistry 101:133–149

Price JR, Peresolak K, Brice RL, Tefend KS (2013a) Temporal variability in the chemical weathering of Ca^{2+}-bearing phases in the Loch Vale watershed, Colorado, USA: a mass-balance approach. Chem Geol 342:151–166

Price JR, Rice KC, Szymanski DW (2013b) Mass-balance modeling of mineral weathering rates and CO_2 consumption in the forested, metabasaltic Hauver Branch watershed, Catoctin Mountain, Maryland, USA. Earth Surf Process Landf 38:859–875

Pulliam WM (1993) Carbon dioxide and methane exports from a southeastern floodplain swamp. Ecol Monogr 63:29–53

Putney JW (1998) Calcium signaling: up, down, up, down….what's the point? Science 279:191–192

Qualls RG, Haines BL, Swank WT (1991) Fluxes of dissolved organic nutrients and humic substances in a deciduous forest. Ecology 72:254–266

Quist ME, Nasholm T, Lindeberg J, Johannisson C, Hogbom L, Hogberg P (1999) Responses of a nitrogen saturated forest to a sharp decrease in nitrogen input. J Environ Qual 28:1970–1977

Raich JW, Nadelhoffer KJ (1989) Belowground carbon allocation in forest ecosystems: global trends. Ecology 70:1346–1354

Raich JW, Rastetter EB, Melillo JM, Kicklighter DW, Steudler PA, Peterson BJ, Grace AL, Moore B, Vorosmarty CJ (1991) Potential net primary productivity in South America: application of a global model. Ecol Appl 1:399–429

Randerson JT et al., 16 co-authors (2006) The impact of boreal forest fire on climate warming. Science 314 (5802):1130–1132

Raymond PA, Saiers JE (2010) Event controlled DOC export from forested watersheds. Biogeochemistry 100:197–209

Rebbeck J (1996) Chronic ozone effects on three northeastern hardwood species: growth and biomass. Can J For Res 26:1788–1798

Redfield AC (1958) The biological control of chemical factors in the environment. Am Sci 46:205–221

Reich PB, Walters MB, Ellsworth DS (1992) Leaf life-span in relation to leaf, plant, and stand characteristics among diverse ecosystems. Ecol Monogr 62:365–392

Reich PB, Grigal DF, Aber JD, Gower ST (1997) Nitrogen mineralization and productivity in 50 hardwood and conifer stands on diverse soils. Ecology 78:335–347

Reich PB, Peterson DW, Wedin DA, Wrage K (2001) Fire and vegetation effects on productivity and nitrogen cycling across a forest-grassland continuum. Ecology 82:1703–1719

Reiners WA (1986) Complementary models for ecosystems. Am Nat 127:59–73

Reiners WA (1992) Twenty years of ecosystem reorganization following experimental deforestation and regrowth suppression. Ecol Monogr 62:503–523

Retzlaff WA, Weinstein DA, Laurence JA, Gollands B (1996) Simulated root dynamics of a 160-year-old sugar maple (*Acer saccharum* Marsh) tree with and without ozone exposure using the TREGRO model. Tree Physiol 16:915–921

Reuss JO (1983) Implications of the calcium-aluminum exchange system for the effect of acid precipitation on soils. J Environ Qual 12:591–595

Reuss JO, Walthall PM (1990) Soil reaction and acidic deposition. In: Norton SA et al (eds) Acidic precipitation volume 4. Springer, New York, pp 1–33

Reynolds RC, Johnson NM (1972) Chemical weathering in the temperate glacial environment of the northern Cascade Mountains. Geochim Cosmochim Acta 36:537–554

Richardson SM, McSween HY (1989) Geochemistry – pathways and processes. Prentice-Hall, Englewood Cliffs, 488 p

Richter DD, Lindberg SE (1988) Wet deposition estimates from long-term bulk and event wet-only samples of incident precipitation and throughfall. J Environ Qual 17:619–622

Richter DD, Markewitz D (1995) How deep is soil? Bioscience 45:600–609

Richter DD, Ralston CW, Harms WR (1982) Prescribed fire: effects on water quality and forest nutrient cycling. Science 215:661–663

Richter DD, Markewitz D, Wells CG, Allen HL, April R, Heine PR, Urrego B (1994) Soil chemical change during three decades in an old-field loblolly pine (*Pinus taeda* L.) ecosystem. Ecology 75:1463–1473

Richter DD, Markewitz D, Trumbore SE, Wells CG (1999) Rapid accumulation and turnover of soil carbon in a re-establishing forest. Nature 400:56–58

Roberts J, Pymar CF, Wallace JS, Pitman RM (1980) Seasonal changes in leaf area, stomatal and canopy conductances, and transpiration from bracken below a forest canopy. J Appl Ecol 17:409–422

Rosen K (1982) Supply, loss, and distribution of nutrients in three coniferous forest watersheds in central Sweden. Reports in forest ecology and forest soils, 41, Uppsala.

Roskowski JP (1975) Differential nitrogen fixation in wood litter. Bull Ecol Soc Am 56(2):12

Roskowski JP (1980) Nitrogen fixation in hardwood forests of the northeastern United States. Plant Soil 54:33–44

Rothstein DE (2009) Soil amino-acid availability across a temperate-forest fertility gradient. Biogeochemistry 92:201–215

Rudd JWM (1995) Sources of methyl mercury to freshwater ecosystems: a review. Water Air Soil Pollut 80:697–713

Running SW, Coughlan JC (1988) A general model of forest ecosystem processes for regional applications. I. Hydrologic balance, canopy gas exchange and primary production processes. Ecol Model 42:125–154

Running SW, Gower ST (1991) FOREST-BGC. A general model of forest ecosystem processes for regional applications. II. Dynamic carbon allocation and nitrogen budgets. Tree Physiol 9:147–160

Running SW, Nemani RR, Peterson DL, Band LE, Potts DF, Pierce LL, Spanner MA (1989) Mapping regional forest evapotranspiration and photosynthesis by coupling satellite data with ecosystem simulation. Ecology 70:1090–1101

Rustad LE (1994) Element dynamics along a decay continuum in a red spruce ecosystem in Maine, USA. Ecology 75:867–879

Rustad LE, Cronan CS (1988) Element loss and retention during litter decay in a red spruce stand in Maine. Can J For Res 18:947–953

Rustad LE, Cronan CS (1989) Cycling of aluminum and nutrients in litterfall of a red spruce (*Picea rubens* Sarg.) stand in Maine. Can J For Res 19:18–23

Rustad LE, Kahl JS, Norton SA, Fernandez IJ (1994) Underestimation of dry deposition by throughfall in mixed northern hardwood forests. J Hydrol 162:319–336

Ryan MG (1991) Effects of climate change on plant respiration. Ecol Appl 1:157–167

Salisbury FB, Ross CW (1985) Plant physiology, 3rd ed. Wadsworth Publishing Co., Belmont

Santoro AE (2016) The do-it-all nitrifier. Science 351:342–343

Schaberg PG, DeHayes DH, Hawley GJ, Strimbeck GR, Cumming JR, Murakami PF, Borer CH (2000) Acid mist, soil Ca, and Al alter the mineral nutrition and physiology of red spruce. Tree Physiol 20:73–85

Schaefer SC, Hollibaugh JT, Alber M (2009) Watershed nitrogen input and riverine export on the west coast of the US. Biogeochemistry 93:219–233

Schalscha EB, Appelt H, Schaltz A (1967) Chelation as a weathering mechanism. I. Effect of complexing agents on the solubilization of iron from minerals and granodiorite. Geochim Cosmochim Acta 31:587–596

Schier GA (1970) Seasonal pathways of ^{14}C-photosynthate in red pine labeled in May, July, and October. For Sci 16:2–13

Schlesinger WH (1977) Carbon balance in terrestrial detritus. Annu Rev Ecol Syst 8:51–81

Schlesinger WH (1991 and 1997) Biogeochemistry – an analysis of global change. Academic Press, New York, 443 p

Schnoor JL (1990) Kinetics of chemical weathering: a comparison of laboratory and field weathering rates. In: Stumm W (ed) Aquatic chemical kinetics: reaction rates of processes in natural waters. Wiley, New York, pp 475–504

Schoch P, Binkley D (1986) Prescribed burning increased nitrogen availability in a mature loblolly pine stand. For Ecol Manag 14:13–22

Schofield CL, Galloway JN, Hendry GR (1985) Surface water chemistry in the ILWAS basins. Water Air Soil Pollut 26:403–423

Schott J, Berner RA, Sjoberg EL (1981) Mechanism of pyroxene and amphibole weathering – I. Experimental studies of iron-free minerals. Geochim Cosmochim Acta 45:2123–2135

Schwarze FWMR, Engels J, Mattheck C (1999) Fungal strategies of wood decay in trees. Springer, New York

Schwintzer CR, Tjepkema JD (1994) Factors affecting the acetylene to $^{15}N_2$ conversion ratio in root nodules of *Myrica gale* L. Plant Physiol 106:1041–1047

Sexstone AJ, Revsbech NP, Parkin TB, Tiedje JM (1985) Direct measurement of oxygen profiles and denitrification rates in soil aggregates. Soil Sci Soc Am J 49:645–651

Sheen J (1996) Ca^{2+} – dependent protein kinases and stress signal transduction in plants. Science 274:1900–1902

Sheldon JF (2003) Sensitivity analysis of a nitrogen cycling model for a northern hardwood forest. Unpublished honors thesis, University of Maine. Honors advisor: C.S. Cronan

Shimizu T, Kumagai T, Kobayashi M, Tamai K, Iida S, Kabeya N, Ikawa R, Tateishi M, Miyazawa Y, Shimizu A (2015) Estimation of annual forest evapotranspiration from a coniferous plantation watershed in Japan (2): comparison of eddy covariance, water budget, and sap-flow plus interception loss. J Hydrol 522:250–264

Siccama TG (1974) Vegetation, soil, and climate on the Green Mountains of Vermont. Ecol Monogr 44:325–349

Silver WL, Herman DJ, Firestone MK (2001) Dissimilatory nitrate reduction to ammonium in upland tropical forest soils. Ecology 82:2410–2416

Singer MJ, Munns DN (1996) Soils – an introduction, 3rd ed. Prentice-Hall, Upper Saddle River, 480 p

Sinsabaugh RL, Follstad Shah JJ (2011) Ecoenzymatic stoichiometry of recalcitrant organic matter decomposition: the growth rate hypothesis in reverse. Biogeochemistry 102:31–43

Sjoberg RM, Persson T (1998) Turnover of carbon and nitrogen in coniferous forest soils of different N-status and under different $^{15}NH_4$-N application rates. Environ Pollut 102:385–393

Sobota DJ, Harrison JA, Dahlgren RA (2009) Influences of climate, hydrology, and land use on input and export of nitrogen in California watersheds. Biogeochemistry 94:43–62

Sollins P, Grier CC, McCorison FM, Cromack K, Fogel R, Fredriksen RL (1980) The internal element cycles of an old-growth Douglas-fir ecosystem in western Oregon. Ecol Monogr 50:261–285

Soong JL, Parton WJ, Calderon F, Campbell EE, Cotrufo MF (2015) A new conceptual model on the fate and controls of fresh and pyrolized plant litter decomposition. Biogeochemistry 124:27–44

Soulsby C, Birkel C, Geris J, Dick J, Tunaley C, Tetzlaff D (2015) Stream water age distributions controlled by storage dynamics and nonlinear hydrologic connectivity: modeling with high-resolution isotope data. Water Resour Res 51:7759–7776

Staaf H, Berg B (1982) Accumulation and release of plant nutrients in decomposing Scots pine needle litter. Long-term decomposition in a Scots pine forest II. Can J Bot 60:1561–1568

Stein J, Jones HG, Roberge J, Sochanska W (1986) The prediction of both runoff quality and quantity by the use of an integrated snowmelt model. In: Morris EM (ed) Modeling snowmelt-induced processes. IAHS Publ. No. 155. IAHS Press, Wallingford

Stevenson FJ (1982) Humus chemistry: genesis, composition, reactions. Wiley-Interscience, New York

Stevenson FJ (1985) Geochemistry of soil humic substances. In: Aiken GR et al (eds) Humic substances in soil, sediment, and water. Wiley, New York, pp 13–52

Stevenson FJ (1986) Cycles of soil. Wiley, New York

Stogsdill WR, Wittwer RF, Hennessey TC, Dougherty PM (1992) Water use in thinned loblolly pine plantations. For Ecol Manag 50:233–245

Strader RH, Binkley D, Wells CG (1989) Nitrogen mineralization in high-elevation forests of the Appalachians. I Regional patterns in southern spruce-fir forests. Biogeochemistry 7:131–145

Strickland TC, Sollins P (1987) Improved method for separating light and heavy-fraction organic material from soil. Soil Sci Soc America J 51:1390–1393

Sucoff E, Thornton FC, Joslin JD (1990) Sensitivity of tree seedlings to aluminum: I. Honeylocust. J Environ Qual 19:163–171

Sullivan BW, Smith WK, Townsend AR, Nasto MK, Reed SC, Chazdon RL, Cleveland CC (2014) Spatially robust estimates of biological nitrogen (N) fixation imply substantial human alteration of the tropical N cycle. PNAS 111:8101–8106

Sun B, Griffin BM, Ayala-del-Rio HL, Hashsham SA, Tiedje JM (2002) Microbial dehalorespiration with 1,1,1-trichloroethane. Science 298:1023–1025

Swank WT, Douglass JE (1974) Streamflow greatly increased by converting deciduous hardwood stands to pine. Science 185:857–859

Switzer GL, Nelson LE (1972) Nutrient accumulation and cycling in loblolly pine (*Pinus taeda* L.) plantation ecosystems: the first twenty years. Soil Sci Soc Am J 36:143–147

Talbot JM, Martin F, Kohler A, Henrissat B, Peay KG (2015) Functional guild classification predicts the enzymatic role of fungi in litter and soil biogeochemistry. Soil Biol Biochem 88:441–456

Taylor GE, Hanson PJ (1992) Forest trees and tropospheric ozone: role of canopy deposition and leaf uptake in developing exposure-response relationships. Agric Ecosyst Environ 42:255–273

Taylor GE, Johnson DW, Andersen CP (1994) Air pollution and forest ecosystems: a regional to global perspective. Ecol Appl 4:662–689

Thompson MV, Vitousek PM (1997) Asymbiotic nitrogen fixation and litter decomposition during long-term soil development in Hawaiian montane rain forest. Biotropica 29:134–144

Thorn AM, Xiao J, Ollinger SV (2015) Generalization and evaluation of the process-based forest ecosystem model PnET-CN for other biomes. Ecosphere 6(3):1–27

Tiedje JM, Sexstone AJ, Myrold DD, Robinson JA (1982) Denitrification: ecological niches, competition, and survival. Antonie van Leeuwenhock 48:569–583

Tietema A, Boxman AW, Bredemeier M, Emmett BA, Moldan F, Gundersen P, Schleppi P, Wright RF (1998) Nitrogen saturation experiments (NITREX) in coniferous forest ecosystems in Europe: a summary of results. Environ Pollut 102:433–437

Tipping E, Rowe EC, Evans CD, Mills RTE, Emmett BA, Chaplow JS, Hall JR (2012) N14C: a plant–soil nitrogen and carbon cycling model to simulate terrestrial ecosystem responses to atmospheric nitrogen deposition. Ecol Model 247:11–26

Tonitto C, Goodale CL, Weiss MS, Frey SD, Ollinger SV (2014) The effect of nitrogen addition on soil organic matter dynamics: a model analysis of the Harvard Forest Chronic Nitrogen Amendment Study and soil carbon response to anthropogenic N deposition. Biogeochemistry 117:431–454

Toon OB, Pollock JB (1976) A global average model of atmospheric aerosols for radiative transfer calculations. J Appl Meteorol 15:225–246

Topp GC, Davis JL (1985) Measurement of soil water content using time-domain reflectometry (TDR): a field evaluation. Soil Sci Soc Am J 49:19–24

Trumbore S (2000) Age of soil organic matter and soil respiration: radiocarbon constraints on belowground C dynamics. Ecol Appl 10:399–411

Trumbore SE, Gaudinski JB (2003) The secret lives of roots. Science 302:1344–1345

Trumbore SE, Chadwick OA, Amundson R (1996) Rapid exchange between soil carbon and atmospheric carbon dioxide driven by temperature change. Science 272:393–396

Turner J, Singer MJ (1976) Nutrient distribution and cycling in a subalpine coniferous forest ecosystem. J Appl Ecolo 13:295–301

Turner BL, Yavitt JB, Harms KE, Garcia MN, Wright SJ (2015) Seasonal changes in soil organic matter after a decade of nutrient addition in a lowland tropical forest. Biogeochemistry 123:221–235

Ugolini FC, Dahlgren RA (1987) The mechanism of podzolization as revealed by soil solution studies. In: Righi D, Chauvel A (eds) Podzols et Podzolisation. AFES et INRA, Plaisir et Paris, pp 195–203

US EPA (1988) Chemical characteristics of streams in the mid-Atlantic and southeastern United States (national stream survey – phase I). Volume I: population descriptions and physico-chemical relationships. EPA/600/3-88/021a, Washington, DC

USDA Soil Conservation Service (1975) Soil taxonomy – a basic system of soil classification for making and interpreting soil surveys. Wiley, New York, 754 p

Velbel MA (1985) Geochemical mass balances and weathering rates in forested watersheds of the southern Blue Ridge. Am J Sci 285:904–930

Velbel MA (1986) Influence of surface area, surface characteristics, and solution composition on feldspar weathering rates. In: Davis JA, Hayes KF (eds) Geochemical processes at mineral surfaces, ACS symposium series no. 323, pp 615–634

Veldekampe E (1994) Organic carbon turnover in three tropical soils under pasture after deforestation. Soil Sci Soc Am J 58:175–180

Venterea RT, Lovett GM, Groffman PM, Schwarz PA (2003) Landscape patterns of net nitrification in a northern hardwood-conifer forest. Soil Sci Soc Am J 67:527–539

Verburg PSJ, Johnson DW (2001) A spreadsheet-based biogeochemical model to simulate nutrient cycling processes in forest ecosystems. Ecol Model 141:185–200

Vitousek PM (1982) Nutrient cycling and nutrient-use efficiency. Am Nat 119:553–572

Vitousek PM, Reiners WA (1975) Ecosystem succession and nutrient retention: a hypothesis. Bioscience 25:376–381

Vitousek PM, Walker LR (1989) Biological invasion by *Myrica faya* in Hawaii: plant demography, nitrogen fixation, ecosystem effects. Ecol Monogr 59:247–265

Vitousek PM, Aber JD, Howarth RW, Likens GE, Matson PA, Schindler DW, Schlesinger WH, Tilman DG (1997) Human alteration of the global nitrogen cycle: sources and consequences. Ecol Appl 7:737–750

Vogt KA, Grier CC, Vogt DJ (1986) Production, turnover, and nutrient dynamics of above- and belowground detritus of world forests. Adv Ecol Res 15:303–377

Volin JC, Reich PB, Givnish TJ (1998) Elevated carbon dioxide ameliorates the effects of ozone on photosynthesis and growth: species respond similarly regardless of photosynthetic pathway or plant functional group. New Phytol 138:315–325

Walker WJ, Cronan CS, Patterson HH (1988) A kinetic study of aluminum adsorption by aluminosilicate clay minerals. Geochim Cosmochim Acta 52:55–62

Wan S, Hui D, Luo Y (2001) Fire effects on nitrogen pools and dynamics in terrestrial ecosystems: a meta-analysis. Ecol Appl 11:1349–1365

Wang F, Mladenoff DJ, Forrester JA, Blanco JA, Scheller RM, Peckham SD, Keough C, Lucash MS, Gower ST (2014) Multimodel simulations of forest harvesting effects on long-term productivity and CN cycling in aspen forests. Ecol Appl 24(6):1374–1389

Waring RH, Schlesinger WH (1985) Forest ecosystems – concepts and management. Academic Press, Orlando

Weand MP, Arthur MA, Lovett GM, Sikora F, Weathers KC (2010) The phosphorus status of northern hardwoods differs by species but is unaffected by nitrogen fertilization. Biogeochemistry 97:159–181

Weathers KC, Likens GE (1997) Clouds in southern Chile: an important source of nitrogen to nitrogen-limited ecosystems? Environ Sci Technol 31:210–213

Weathers KC, Lovett GM, Likens GE, Lathrop R (2000) The effect of landscape features on deposition to Hunter Mountain, Catskill Mountains, NY. Ecol Appl 10:528–540

Weinstein DA, Beloin RM, Yanai RD (1991) Modeling changes in red spruce carbon balance and allocation in response to interacting ozone and nutrient stresses. Tree Physiol 9:127–146

Weintraub SR, Russell AE, Townsend AR (2014) Native tree species regulate nitrous oxide fluxes in tropical plantations. Ecol Appl 24:750–758

Wenner NG, Merrill W (1998) Pathological anatomy of needles of *Pinus strobus* exposed to charcoal-filtered air or three times ambient ozone concentrations or infected by *Canavirgella banfieldii*. Can J Bot 76:1331–1339

Werner C, Schnyder H, Cuntz M, Keitel C, Zeeman MJ, Dawson TE, Badeck F-W, Brugnoli E, Ghashghaie J, Grams TEE, Kayler ZE, Lakatos M, Lee X, Máguas C, Ogée J, Rascher KG, Siegwolf RTW, Unger S, Welker J, Wingate L, Gessler A (2012) Progress and challenges in using stable isotopes to trace plant carbon and water relations across scales. Biogeosciences 9:3083–3111

White PS (1979) Pattern, process, and natural disturbance in vegetation. Bot Rev 45:229–299

White AF, Blum AE (1995) Effects of climate on chemical weathering in watersheds. Geochim Cosmochim Acta 59:1729–1747

Whitehead D, Hinckley TM (1991) Models of water flux through forest stands: critical leaf and stand parameters. Tree Physiol 9:35–57

Whittaker RH, Likens GE, Bormann FH, Eaton JS, Siccama TG (1979) The Hubbard Brook Ecosystem Study: forest nutrient cycling and element behavior. Ecology 60:203–220

Winner WE (1994) Mechanistic analysis of plant responses to air pollution. Ecol Appl 4:651–661

Wofsy SC, Goulden ML, Munger JW, Fan SM, Bakwin PS, Daube BC, Bassow SL, Bazzaz FA (1993) Net exchange of CO_2 in a mid-latitude forest. Science 260:1314–1317

Wollast R (1967) Kinetics of the alteration of K-feldspar in buffered solutions at low temperature. Geochim Cosmochim Acta 31:635–648

Wollast R, Chou L (1985) Kinetic study of the dissolution of albite with a continuous flow-through fluidized bed reactor. In: Drever JI (ed) The chemistry of weathering. D. Reidel Publishing Co., Boston, pp 75–96

Wolock DM (1993) Simulating the variable source area concept of streamflow generation with the watershed model TOPMODEL. U.S. Geological Survey Open File Report, Earth Science Information Center, Box 25286, MS 517, Denver

Woodwell GM (1974a) Success, succession, and Adam Smith. Bioscience 24:81–87

Woodwell GM (1974b) Variation in the nutrient content of leaves of *Quercus alba*, *Quercus coccinea*, and *Pinus rigida* in the Brookhaven Forest from bud-break to abscission. Am J Bot 61:749–753

Woodwell GM, Botkin DB (1970) Metabolism of terrestrial ecosystems by gas exchange techniques: the Brookhaven approach. In: Reichle DE (ed) Analysis of temperate forest ecosystems. Springer, New York, pp 73–85

Yang L, Chang S-W, Shin H-S, Hur J (2015) Tracking the evolution of stream DOM source during storm events using end member mixing analysis based on DOM quality. J Hydrol 523:333–341

Yavitt JB, Fahey TJ (1982) Loss of mass and nutrient changes of decaying woody roots in lodgepole pine forests, southeastern Wyoming. Can J For Res 12:745–752

Yavitt JB, Fahey TJ, Sherman RE, Groffman PM (2015) Lumbricid earthworm effects on incorporation of root and leaf litter into aggregates in a forest soil, New York state. Biogeochemistry 125:261–273

Yun SC, Laurence JA (1999) The response of sensitive and tolerant clones of *Populus tremuloides* to dynamic ozone exposure under controlled environmental conditions. New Phytol 143:305–313

Yuretich RF, Crerar DA, Kinsman DJJ, Means JL, Borcsik MP (1981) Hydrogeochemistry of the New Jersey coastal plain. 1. Major element cycles in precipitation and river water. Chem Geol 33:1–21

Zhang W, Swaney DP, Hong B, Howarth RW, Han H, Li X (2015) Net anthropogenic phosphorus inputs and riverine phosphorus fluxes in highly populated headwater watersheds in China. Biogeochemistry 126:269–283

Zogg GP, Zak DR, Pregitzer KS, Burton AJ (2000) Microbial immobilization and the retention of anthropogenic nitrate in a northern hardwood forest. Ecology 81:1858–1866

Index

C.S. Cronan, *Ecosystem Biogeochemistry*, Springer Textbooks in Earth Sciences, Geography and Environment, DOI 10.1007/978-3-319-66444-6

Z